ASSESSMENT OF PASSIVE TREATMENT AND BIOGEOCHEMICAL REACTORS FOR AMELIORATING ACID MINE DRAINAGE AT STOCKTON COAL MINE

A thesis submitted in partial fulfilment of the requirements for the

Degree of Philosophy of Doctor in Civil and Natural Resources Engineering in the University of Canterbury

by C. A. McCauley

University of Canterbury

2011

Table of Contents

List of Figures

List of Tables

List of Symbols and Acronyms

Basic Dimensions
[L] = length
[M] = mass
[t] = time
[T] = temperature

Nomenclature (English)
A = area [L^2]
B = channel width (in v-notch weir channel) [L]
C_{Al} = ferrous Al concentration [M/L^3 or mol/L^3]
$C_{BM(Br)}$ = benchmark Br concentration [M/L^3 or mol/L^3]
C_{Br} = Br concentration [M/L^3 or mol/L^3]
$C_{Br}(t)$ = Br concentration at time t [M/L^3 or mol/L^3]
C_{Ca} = Ca concentration [M/L^3 or mol/L^3
C_{Cu} = Cu concentration [M/L^3 or mol/L^3]
C_d = the coefficient of discharge [dimensionless] or downstream concentration [M/L^3 or mol/L^3]
C_{in} = inlet concentration [M/L^3 or mol/L^3]
C_{Fe}^{2+} = ferrous Fe concentration [M/L^3 or mol/L^3]
C_{Fe}^{3+} = ferric Fe concentration [M/L^3 or mol/L^3]
C_{Mg} = Mg concentration [M/L^3 or mol/L^3]
C_{Mn} = Mn concentration [M/L^3 or mol/L^3]
$C_{Mn(in)}$ = influent Mn concentration [M/L^3 or mol/L^3]
$C_{Mn(out)}$ = effluent Mn concentration [M/L^3 or mol/L^3]
$C_{NaBr(dose)}$ = concentration of sodium bromide dose solution [M/L^3]
C_{Ni} = Ni concentration [M/L^3 or mol/L^3]
C_{out} = outlet concentration [M/L^3 or mol/L^3]
C_s = saturation concentration [M/L^3 or mol/L^3]
C_u = upstream concentration [M/L^3 or mol/L^3]
C_{Zn} = Zn concentration [M/L^3 or mol/L^3]
D = dispersion coefficient [L^2/t]
D = thickness of a limestone leaching bed [L]
E = oxygen transfer efficiency [dimensionless or percentage]
e_{DTD} = detention time distribution efficiency [dimensionless]
e_V = volumetric efficiency [dimensionless]
f(t) = detention time distribution function at time t [t^{-1}]
$f(t)_{TIS}$ = detention time distribution function at time t for TIS model [t^{-1}]
g = gravitational acceleration [L/t^2]
G_s = particle density [M/L^3]
h= head of water or depth of water above the bottom of a v-notch weir [L]
H = water hardness [M/L^3 (as $CaCO_3$)]
HMTV = hardness modified trigger value [M/L^3]
k = reaction rate constant [units dependent on reaction order; 1/t for first order]
K = hydraulic conductivity [L/t]
L = length [L]
m = mass [M]
m_{Br} = mass of Br [M]
$m_{Br(i)}$ = mass of Br introduced with inflow[M]
$m_{Br(o)}$ = mass of Br measured exiting with outflow[M]
m_{NaBr} = mass of sodium bromide[M]
m_s = mass of substrate (including moisture)[M]
$m_{s(dry)}$ = mass of dried substrate [M]
$m_{s(sat)}$ = mass of saturated substrate [M]
$m_{s(wet)}$ = mass of wet substrate [M]
m_{sa} = surface area of limestone[L^2]
m_v = bed volume [L^3]

m_w = mass of water [M]
$m_{w(air)}$ = mass of water that freely drains from substrate [M]
n = number of observations [dimensionless]
N = typical sedimentation efficiency [dimensionless]
N = number of tanks (tanks in series reactor model) [dimensionless]
p = probability
P = the apparent number of tanks in series [dimensionless]
P = the distance from the bottom of the v-notch weir to the bottom of the channel [L]
pH_{act} = actual pH [-log [mol/L^3]]
pH_{eq} = equilibrium pH [-log [mol/L^3]]
Q = discharge or volumetric flowrate [L^3/t]
Q_{20^oC} = discharge or volumetric flowrate at 20°C [L^3/t]
Q_{E4} = volumetric flowrate of influent in E4 containers (bench-scale treatability tests) [L^3/t]
Q_{perm} = flowrate of influent in permeameter containers (bench-scale treatability tests) [L^3/t]
R – correlation coefficient [dimensionless]
R^2 – coefficient of determination [dimensionless]
SA = surface area [L^2]
SI = saturation index [-log [mol/L^3]]
SSQE = sum of squared errors [units dependent on measurement]
t = time [t]
Δt = time between sampling events or time increment [t]
t_d = time delay
t_p = tracer peak time [t]
TV = standardised trigger value at a hardness of 30 mg/L as $CaCO_3$ [M/L^3]
V = volume [L^3]
V_{bm} –volume of bedding material [L^3]
V_{pp} –volume of post peel [L^3]
V_{sub} –volume of substrate [L^3]
V_{sw} –volume of surface water [L^3]
V_w –volume of water in voids or pore-water volume [L^3]
$V_{w(BGCR)}$ – pore-water volume within all components of the BGCRs [L^3]
V_v – volume of voids [L^3]
$V_{v(air)}$ – free draining void volume (for computing air porosity) [L^3]
$V_{v(tot)}$ – total void volume (for computing total porosity) [L^3]
X – loading rates or concentrations [mol/t or M/t]

Nomenclature (Greek)

ε = porosity (or fraction of volume occupied by voids (or water if saturated)) [L^3/L^3]
ε_{air} = air porosity (or specific yield) [L^3/L^3]
ε_{bm} = air porosity of bedding material [L^3/L^3]
ε_{pp} = air porosity of post peel [L^3/L^3]
ε_{sub} = air porosity of substrate [L^3/L^3]
ε_{sw} = air porosity of surface water = 1 [L^3/L^3]
ε_{whc} = water-holding capacity [L^3/L^3]
$\Gamma(N)$ = gamma function [dimensionless]
λ = hydraulic efficiency [dimensionless]
μ = dynamic viscosity [M/Lt]
μ_{20^oC} = dynamic viscosity [M/Lt]
θ = theoretical (or nominal) resident-time distributions (or cumulative pore-water volumes) [t/t]
θ_{BGCR} = theoretical (or nominal) resident-time distribution in BGCRs [t/t]
ρ = fluid density [M/L^3]
ρ_{NaBr} = density of sodium bromide tracer dose solution [M/L^3]
ρ_d = dry bulk density [M/L^3]
ρ_s = substrate bulk density [M/L^3]
ρ_{sat} = saturated bulk density [M/L^3]

ρ_{wet} = wet bulk density [M/L^3]
Σ = summation of [dimensionless]
σ = variance [t^2]
σ_θ^2 = dimensionless variance [dimensionless]
τ = mean tracer hydraulic residence time in BGCR [t]
τ_{BGCR} = theoretical (or nominal) hydraulic residence time in BGCR [t]
τ_{bm} = theoretical (or nominal) hydraulic residence time in bedding material within BGCRs [t]
τ_{pp} = theoretical (or nominal) hydraulic residence time in post peel within BGCRs [t]
τ_{sub} = theoretical (or nominal) hydraulic residence time in substrate mixture within BGCRs [t]
τ_{sw} = theoretical (or nominal) hydraulic residence time in surface water layer of BGCRs [t]
ω = moisture content [M/M]
ω_s = substrate moisture content [M/M]
ω_{sat} = saturated substrate moisture content [M/M]
ω_{wet} = wet substrate moisture content [M/M]

Acronyms and Abbreviations (Symbols and Greek Letters)
↓ - precipitate
> - greater than
>> - much greater than
< - less than
>> - much less than
= - equals
≈ - approximately

Acronyms and Abbreviations (English Letters)
AAS - atomic absorption spectrometry
ALD - anoxic limestone drain
AMD – acid mine drainage
ANOVA – analysis of variance
amsl – above mean sea level
Apatite II^{TM} – $Ca_{10-x}Na_x(PO_4)_{6-x}(CO_3)x(OH)_2$
ARD – acid rock drainage
AS - acid soluble
BCRs - biochemical reactors
BGCRs - biogeochemical reactors
BOD – biochemical oxygen demand
BSE – back scatter electron
C/N – carbon to nitrogen ratio
CANZ - Coal Association of New Zealand
CCA - chromated copper arsenate
CCC - criteria continuous concentration
CFR – U.S. Code of Federal Regulations
CMC - criteria maximum concentration
CMFR – completely mixed flow reactor
CSTR – continuously stirred tank reactor
DO – dissolved oxygen
DOC – dissolved organic carbon
EDAX – energy dispersive spectroscopy
EDS - electron dispersive spectrophotometry
EPA – U.S. Environmental Protection Agency
FRST - Foundation for Research Science and Technology
HDPE – high-density polyethylene
HRT – hydraulic residence time (or hydraulic retention time)
HTO – tritium oxide
IANZ – International Accreditation New Zealand
IC- ion chromatography

ICP-MS – inductively coupled plasma – mass spectrometry
ICP-OES - inductively coupled plasma – optical emission spectrometry
ID - insufficient data
IMPs - inorganic media passive systems
ISO - International Organisation for Standardization
LDPE – low-density polyethylene
LLB - limestone leaching bed
MIW – mine-impacted water
mol - moles
NA - non applicable
n/d - not defined
NMD – neutral mine drainage
NOAA – National Oceanic and Atmospheric Administration (U.S.)
NPDES - National Pollutant Discharge and Eliminations System
NSD – nodulated stack dust
NTUs - nephelometric turbidity units
OLC - open limestone channel
OLD – oxic limestone drain
P – analysis of variance (ANOVA) probability
PCR - polymerise chain reaction
PFR – plug flow reactor
ppm – parts per million
ppt – precipitate
PQL – practical quantitation limit
PVC – polyvinyl chloride
QA/QC – quality assurance/quality control
R&D – research and development
RAPS - reducing and alkalinity producing system
ReRAPS – recirculating- reducing and alkalinity producing system
RTD - residence time distribution
SAPS - successive and alkalinity producing system
SCOOFI - surface catalyzed oxidation of ferrous iron
SEM – scanning electron microscopy
SI – saturation index
SRB – sulphate reducing bacteria
SRBR – sulphate-reducing bioreactor
SSQE - sum of squared errors
T - total
TA – total acidity (pH 8.3)
TC – total carbon
TDS – total dissolved solids
TIC – total inorganic carbon
TIF - Technology for Industry Fellowship
TIS – tanks in series
TKN - total kjeldahl nitrogen
TN – total nitrogen
TOC – total organic carbon
TON – total oxidised nitrogen
TP – total phosphorous
TR - total recoverable
TSS – total suspended solids
UK – United Kingdom
U.S. – United States
USA – United States of America
VALD – vertical anoxic limestone drain
VFW – vertical flow wetland
WET - whole effluent toxicity

WHO – World Health Organization

Chemical Elements (including Cations and Anions)

Al – aluminium
As - arsenic
As^{3+} - arsenite
As^{5+} - arsenate
Au - gold
B - Boron
Br - bromine
Ca - calcium
Cd - cadmium
Cl - chloride
Cl^- – chlorine ion (used in chlorination)
Co - cobalt
Cr – chromium
Cr^{3+} – trivalent chromium or Cr (III)
Cu - copper
Fe – iron
Fe^{2+} - ferrous iron
Fe^{3+} - ferric iron
H^+ - hydrogen cation (or proton acidity)
$[H^+]$ - hydrogen cation molar concentration (in units mol/L)
K - potassium
Li - lithium
Mg - magnesium
Mn - manganese
Mn^{2+} - divalent manganese
Mn^{4+} - tetravalent manganese
Mo – molybdenum
N - nitrogen
Na - sodium
Ni – nickel
P - phosphorous
Pb - lead
S - Sulfur
S^{2-} - sulphide (elemental sulphur)
Se – selenium
Si - silica
Tl - Thallium
U^{6+} - uranium (hexavalent)
Zn – zinc

Chemical Compounds and Ions (excluding Metals)

$C_3H_5O_3Na$ – sodium lactate
$C_3H_5(OH)_3$ - glycerol
$C_6H_{12}O_6Na$- sodium glucose or sodium gluconate
$C_{12}H_{22}O_{11}$ - sucrose
CaO – calcium oxide (or calcia or lime)
$Ca(OH)_2$ – calcium hydroxide or lime
CH_2O – organic carbon
CH_3CH_2COOH – propionic acid
CH_3COONa – sodium acetate
CH_4 - methane
CO_2 – carbon dioxide
CO_3^{2-} - carbonate
H_2 - hydrogen

H_2CO_3 – carbonic acid
H_2O – water
H_2O_2 – hydrogen peroxide
H_2S – hydrogen sulphide
H_2SO_4 – sulphuric acid
H_4SiO_4 – silicic acid
HCl – hydrochloric acid
HCO_3^- bicarbonate
HNO_3 – nitric acid
KBr – potassium bromide
KCl – potassium chloride
LiBr – lithium bromide
MgO – magnesium oxide or magnesia
MgOH – magnesium hydroxide
Na_2CO_3 - sodium bicarbonate or soda ash
NaBr – sodium bromide
NaCl – sodium chloride
NaOH – sodium hydroxide
NH_3 – ammonia
NH_4^+ - ammonium
NH_4Cl – ammonium chloride
O_2 - oxygen
O_3 – ozone (used in ozonation)
OH^- - hydroxide
PO_4^{3-} - phosphate
SF_6 – sulphur hexafluoride
SO_4^{2-} - sulphate

Minerals (including Metal Precipitates and Ions)
Al_2O_3 - alumina
$Al(OH)_3$ – aluminium hydroxide or gibbsite
$Al_2Si_2O_5(OH_4)$ – kaolinite
$Ca(Al, Mg)_6(Si_4O_{10})_3(OH)_6$ *nH_2O - montmorillonite
$CaAl_2Si_2O_8$ - anorthite
$CaCO_3$ – calcium carbonate
$CaSiO_3$ - calcium metasilicate (slag)
$CaSO_4$ – anhydrite
$CaSO_4$*$2H_20$ - gypsum
Fe_2O_3 - hematite
Fe_2O_3*$2H_20$ - ferrihydrite
$FeAsO_4$*$xFe(OH)_3$ – ferric arsenate
$(Fe, Mg, Al)_6(Si, Al)_4O_{10}(OH)_8$ - chlorite
$(Fe,Ni)_{1+x}S$ (where x=0-0.11) - mackinawite
$Fe(OH)_2$ – ferrous hydroxide
$Fe(OH)_3$ – ferric hydroxide
FeO(OH) – iron oxyhydroxide or goethite
$FeHS^+$ – iron hydrogen sulphide cation
FeS – iron sulphide
FeS_2 – pyrite
$FeSO_4$*7H2O - melanterite
$KAl_2(AlSi_3O_{10})(F,OH)_2$ - microcline
$KAlSi_3O_8$ – potassium feldspar
$KAl_3(SO_4)_2(OH)_6$ - alunite
$KFe^{3+}(OH)_6(SO_4)_2$ - jarosite
$(K,H_3O)(Al,Mg,Fe)_2(Si,Al)_4O_{10}[(OH)_2$*$H_2O$ - illite
$(Mg,Fe)_3Si_2O_5(OH)_4$ - chrysotile
$Mg_3Si_4O_{10}(OH)_2$ - talc

$Mg_4Si_6O_{15}(OH)_2$*6H2O - sepiolite
$Mn^{2+}Mn^{3+}2O_4$ - hausmannite
$Mn(OH)_2$ - pyrochroite
MnO(OH) - manganite
MnO_2 – manganese dioxide or pyrolox or pyrolusite
$NaAlSi_3O_8$ - albite
NO_2^- - nitrite
NO_3^- - nitrate
SiO_2 – chalcedony, quartz, silica, silicon dioxide
(Zn, Fe)S - sphalerite
$Zn(OH)_2$ - zinc hydroxide
Zn_2SiO_4 – willemite

Acknowledgments

This research was made possible through financial support from Solid Energy New Zealand Limited, a Technology for Industry Fellowship awarded by Technology New Zealand (New Zealand Government) and a grant awarded by the Coal Association of New Zealand. Additional financial support was received through numerous research grants and a conference travel grant awarded by the University of Canterbury Department of Civil and Natural Resources Engineering. A New Zealand Postgraduate Study Abroad Award administered by Education New Zealand was also granted.

Technical and logistical support by various university technicians, especially Peter McGuigan, Ian Sheppard and Bob Wilsea-Smith, and operational staff at Stockton Mine was much appreciated. Mentoring from Dr. Paul Weber, Dave Trumm and Andrew Brough was valuable. Advice and support from my academic supervisors, Dr. Aisling O'Sullivan and Dr. Mark Milke was very useful. Advice from Dr. Peter Robinson, Environmental Client Services Manager for RJ Hill Laboratories Limited, benefited this research. Lab assistance and sampling by Nicola McHaffie, Jenna Hutchinson and Julia Valigore was much valued.

PPCS Ltd. donated Bioblend® compost, which was appreciated. Sea Products, Ltd. in Christchurch donated mussel shells used for the project. Peter McGuigan and I will always be appreciative of the tasty steamed mussels they served us while we were shoveling mussel shells into containers.

Most importantly, I would like to thank family, friends and past colleagues who have supported and encouraged me throughout my life. I am especially indebted to my soul mate and wife, Penny McCauley, who has always been there for me. My experiences at the University of Alaska-Fairbanks with many field-oriented colleagues helped divert my career interests into a more meaningful direction. I am particularly indebted to my former boss, David Nyman, whose incredible knowledge base, positive persona and shared passion for adventure helped shape my understanding of environmental systems and developing methodology for "getting the job done." I am also grateful for the many socially and environmentally conscious friends I have developed over the years whose efforts have contributed to the many "baby steps" required to change the world for the better. Finally, life is an adventure: work hard, play harder, but keep your bike on the track.

Abstract

Acid mine drainage (AMD) at Stockton Coal Mine, located near Westport, New Zealand, is generated from the oxidation of pyrite within sedimentary overburden exposed during surface mining. The pyrite oxidation releases significant acidity, Fe, and sulphate together with trace metals to the receiving environment. Aluminium is also elevated in drainage waters due to acid leaching from overburden materials. Thirteen AMD seeps emanating from waste rock dumps, and associated sediment ponds were monitored at Stockton Coal Mine to characterise water chemistry, delineate their spatial and temporal variability, and quantify metal loads. Dissolved metal concentrations ranged from 0.05-1430 mg/L Fe, 0.200-627 mg/L Al, 0.0024-0.594 mg/L Cu, 0.0052-4.21 mg/L Ni, 0.019-18.8 mg/L Zn, <0.00005-0.0232 mg/L Cd, 0.0007-0.0028 mg/L Pb, <0.001-0.154 mg/L As and 0.103-29.3 mg/L Mn and the pH ranged from 2.04-4.31. Currently this AMD is treated further downstream by a number of water treatment plants employing a combination of ultra fine limestone and calcium hydroxide; however, in the interest of assessing more cost-effective technologies, passive treatment systems were investigated for their treatment and hydraulic efficacy and as potential cost-effective options.

Biogeochemical reactors (BGCRs) were selected as the most appropriate passive treatment system for ameliorating AMD at Stockton Coal Mine. Results of mesocosm-scale treatability tests showed that BGCRs incorporating mussel shells, *Pinus radiata* bark, wood fragments (post peel), and compost increased pH to ≥6.7 and sequestered ≥98.2% of the metal load from the Manchester Seep located within the Mangatini Stream catchment. The following design criteria were recommended for BGCRs incorporating 20-30 vol. % mussel shells as an alkalinity amendment: 1) 0.3 mol sulphate /m^3 substrate/day for sulphate removal (mean of 94.1% removal (range of 87.6-98.0%)); 2) 0.4 mol metals/m^3/day for metal (mean of 99.0% removal (range of 98.5-99.9%)) and partial sulphate (mean of 46.0% removal (range of 39.6-57.8%)) removal; and 3) 0.8 mol metals/m^3/day for metal (mean of 98.4% removal (range of 98.2-98.6%) and minimal sulphate (mean of 16.6% removal (range of 11.9-19.2%)) removal. At the maximum recommended loading rate of 0.8 mol total metals/m^3/day an average of 20.0 kg/day (7.30 tonnes/year) of metals and 85.2 kg acidity as $CaCO_3$/day could be removed from the Manchester Seep AMD by employing BGCRs. The design hydraulic residence time (HRT) would be 3.64 days. On an acidity areal loading basis, a design criterion of 65 g/m^2/day was recommended.

Tracer studies conducted on the BGCRs indicated ideal flow characteristics for cylindrical drum-shaped reactors and non-ideal flow conditions for trapezoidal-shaped reactors indicative of short-circuiting, channelised flow paths and internal recirculation. Consequently, this resulted in compromised treatment performance in the trapezoidal-shaped reactors. The relaxed tanks in series (TIS) model could be successfully applied to model the treatment performance of drum-shaped reactors; however, the model was unsuccessful for trapezoidal-shaped reactors. Because most pilot

and full-scaled vertical flow wetlands (VFWs) have consisted of trapezoidal-prism basins excavated into the ground, the rate-removal methods previously recommended (e.g. mol metals/m^3/day) should be applied to BGCR design, evaluation and operation rather than results of hydraulic and reactor modelling.

Overall, a staged passive treatment approach is recommended. The first stage should consist of a sedimentation basin to remove sediment, the second stage a BGCR to remove acidity and metals and the third an aerobic wetland to provide oxygenation and tertiary treatment of metals (primarily Fe) from BGCR effluent. Preliminary analysis indicates that BGCRs are potentially a more cost-effective means of treating AMD at Stockton Coal Mine compared with the current active lime-dosing plant by over $125/tonne of acidity ($197/tonne for BGCRs versus $324/tonne for lime dosing (60% efficient)); however, their successful implementation would need to recognise current treatment goals, required areal footprint and inherent maintenance requirements.

Introduction

Purpose

Acid mine drainage (AMD) has impacted an estimated 125 km of freshwater streams throughout the West Coast of the South Island, New Zealand (James, 2003). This thesis focuses on passive treatment options for ameliorating acidity and metals associated with AMD at Stockton Coal Mine, located on the West Coast of the South Island in New Zealand approximately 35 km north of the township of Westport. The research findings are also applicable internationally where coal mining has negatively impacted thousands of kilometres of streams and rivers in Europe (PIRAMID Consortium, 2003) and nearly 8300 km of streams in the Eastern U.S.A. from over 500 abandoned mine sites (U.S. EPA, 2008).

Funding and Industrial Sponsorship

This research was sponsored by Technology New Zealand through the Technology for Industry Fellowships (TIF) programme funded by the Foundation for Research Science and Technology (FRST), the Government funding research agency. The TIF programme enables research and development (R&D) projects to be conducted bilaterally between University and industrial partners. Financial sponsors included Solid Energy New Zealand Limited, the Coal Association of New Zealand (CANZ) and the Department of Civil and Natural Resources Engineering at the University of Canterbury. Industrial partners included Solid Energy New Zealand Limited, CRL Energy Ltd. and Pattle Delamore Partners Ltd. Because of the prescribed R&D and applied focus of the TIF programme, this research was focused towards application of its results and outcomes for implementation by the industry partners.

Research Objectives and Scope

The primary objective of this research was to assess whether AMD from Stockton Coal Mine could be effectively treated passively with biogeochemical reactors (BGCRs) utilising industrial waste products, including mussel shells, as substrate media and to what capacity. The research progressed systematically with results from each stage of the research applied in a progressive manner to develop experimental designs and analysis thereof for subsequent experiments. Biogeochemical reactors are essentially anaerobic vertical flow wetlands where treatment occurs via a complex array of biogeochemical mechanisms. The specific biogeochemical mechanisms of contaminant removal were not assessed during this study but are discussed in the literature review chapter of this thesis (Chapter 1).

Chapter 1 ("Literature Review") details the impacts of AMD in New Zealand, the generation and water chemistry of AMD, different types of passive treatment systems employed in treating mine-impacted waters (MIWs) including AMD, mechanisms for contaminant removal within treatment

systems and their treatment effectiveness and flow hydraulics within passive treatment systems. The objective of the literature review was to comprehensively evaluate various biogeochemical mechanisms associated with the creation of AMD and its treatment via passive methods. It primarily assesses previous research efforts detailing challenges and mechanisms for passive treatment of MIWs, primarily AMD.

The primary objective of content discussed in Chapter 2 ("Variability of Stockton Coal Mine Acid Mine Drainage Chemistry and its Feasibility for Passive Treatment") was to evaluate the spatial and temporal variability of water chemistry from AMD seeps throughout Stockton Coal Mine. Inverse geochemical modelling was also performed to assess the origin of AMD and minerals that could precipitate following treatment. Another objective was to evaluate the feasibility of implementing passive treatment systems at each seep location. This was performed so that a candidate site could be selected. Subsequent research efforts focused on passively treating this AMD water using BGCRs.

Chapter 3 ("Biogeochemical Reactor Substrate Geotechnical Properties and Chemistry") includes primarily analysis of the geotechnical properties of BGCR substrate mixtures consisting mostly of organic and alkaline industrial waste products. The primary objectives of this analysis included establishing weight-volume relationships and to ensure adequate flow capacity of the substrate mixtures. This information was used for converting substrate mixtures from a volume basis to a weight basis, and vice-versa, and subsequent analysis of the hydraulic residence time (HRT) and flow characteristics of the BGCRs. Other objectives involved analysis of the chemical composition of the substrate materials to determine if any deleterious substances were present that could potentially leach from them and to quantify the theoretical alkalinity generation potential from the substrate mixtures.

Chapter 4 ("Acidity, Metal and Sulphate Removal from Mesocosm-Scale Biogeochemical Reactor Treatability Tests") discusses the laboratory-based mesocosm-scale treatability tests performed on BGCRs treating the candidate site AMD water. The objectives of this analysis were to evaluate the treatment effectiveness and capacity of different substrate mixtures, including the novel use of mussel shells as an alkalinity amendment, determine the effect of reactor shape on treatment performance and establish rate removal design criteria .

The primary objective of analysis discussed in Chapter 5 ("Use of pH and Alkalinity as Surrogate Measurements for Assessing the Iron and Aluminium Concentrations in Biogeochemical Reactor Effluent") was to examine the potential use of pH and alkalinity as surrogate parameters for estimating Fe and Al concentrations in BGCR effluent. Sample pH and alkalinity are more cost-effective and easily measured parameters than metal concentrations so are more practical for instantaneous treatment assessment. This analysis was performed using results of the mesocosm-scale treatability tests discussed in Chapter 4.

Chapter 6 (“Tracer Testing to Determine the Hydraulic Characteristics of Mesocosm-Scale Biogeochemical Reactors and Their Application to Reactor Modelling”) evaluates the results of tracer studies conducted on the two-different shaped (cylindrical and trapezoidal prism) reactors. The objectives were to analyse differences in flow hydraulics from the different shaped reactors, apply these results to reactor modelling techniques, calculate reaction rate kinetics and determine the applicability of these methods for design purposes.

Minimal research has examined the scaling-up processes from lab to full-scale field application of passive treatment systems for mine-water treatment. The objective of Chapter 7 (“Advancing Scaling Challenges Associated with Passive Acid Mine Drainage Treatment Systems”) was to develop an approach to bridge the research gap of the laboratory results (discussed in Chapters 3-6) with performance of proposed pilot-scale systems operating *in-situ*. The approach includes a comprehensive physical and experimental model for designing, testing and validating operational field-scale systems. Results from pilot-scale treatability tests can provide useful information relevant to full-scale design that may not be possible to assess in laboratory studies such as treatment performance at variable climatic conditions so a reliable scaling-up methodology is recommended.

Conclusions generated from this research are discussed in Chapter 8 (“Conclusions and Recommendations”) and publications arising from this research to date are summarised in Chapter 9.

The content of this thesis has important implications in the management and treatment of AMD and other MIWs. It contributes extensively to the knowledge of AMD characteristics in New Zealand. Experimental results contribute new knowledge of optimal BGCR designs utilising waste substrate products facilitated by passive treatment. In particular, the use of mussel shell waste proved a novel and more effective substitute for conventionally used limestone as an alkalinity source.

1. Literature Review

The objective of this literature review is to provide background information regarding the generation of AMD (and other MIWs) in the New Zealand context, the biogeochemistry associated with metal and acidity removal processes in passive treatment systems, their design criteria and treatment performance, flow hydraulics and application of reactor modelling to passive mine-water treatment system performance.

1.1 Acid Mine Drainage Impacts to New Zealand Stream Health

Numerous catchments in New Zealand are impacted from unabated acid mine drainage (AMD), which negatively influences stream health. As a result, stream biodiversity and ecological health have been significantly altered (Harding and Boothryd, 2004; Harding, 2005). Numerous processes contribute to this. Increased acidity reduces stream water pH, which results in increased concentrations of dissolved metals. Increased turbidity and suspended solids (as a result of unrehabilitated mine site erosion) and precipitated metals smother streambeds with sediment, ferric hydroxide ($FeOH_3$) and other metal oxyhydroxides. Additionally, hydrological alterations and synergistic effects resulting from these chemical and physical impacts cause perturbations to stream ecological function. Anthony (1999) and Winterbourn et al. (2000) reported severely reduced taxonomic richness of invertebrate communities in AMD-impacted streams in New Zealand. Vascular plants are usually not present in acidic streams, but acid-tolerant algae such as *Ulothrix* sp., *Microspora* and *Tribonema* can be abundant (Harding and Boothroyd, 2004). Most fish species are negatively impacted by AMD as well due primarily to low pH and metal toxicity (Harding and Boothroyd, 2004). Such effects can be acute, resulting in death, or chronic, causing impaired health including mucous secretion on fish gills, which impairs gas exchange, or causing physiological stress that reduces fish condition (Harding and Boothroyd, 2004). Treatment of AMD is therefore essential to mitigate or avoid further impacts on New Zealand Streams.

1.2 Regional Geology, Site Characteristics and Coal Mining History Relevant to Acid Mine Drainage Generation – West Coast, South Island, New Zealand

Coal mining in New Zealand began in the 1830s with mining districts becoming established in the 1870s for commercial purposes (Pattrick, 2004; Solid Energy New Zealand Limited, 2005). The majority of coal mining regions with potential to generate AMD are located on the West Coast of the South Island within the Brunner Coal Measures. Historical coal mining regions located within the Brunner Coal Measures include, for instance, the Denniston and Stockton Plateaus located 25-35 km north of Westport (Figure 1.1). Terrain is rugged, undulating and typically situated 500-1100 m above sea level overlooking the Tasman Sea. Average precipitation exceeding 6000 mm annually is common (Trumm et al., 2005; Solid Energy New Zealand Limited, 2007). The Brunner Coal Measures were formed in estuarine or marginal marine environments where repeated reworking of sediments resulted in unfavourable conditions for preserving carbonate-bearing minerals and

favourable conditions for the formation of pyrite (Pope et al., 2006; 2010). They contain carbonaceous mudstones and abundant sulphide minerals (pyrite) and subsequently high acid generating capabilities (Black et al., 2005; Trumm et al., 2005; Pope et al., 2006; 2010).

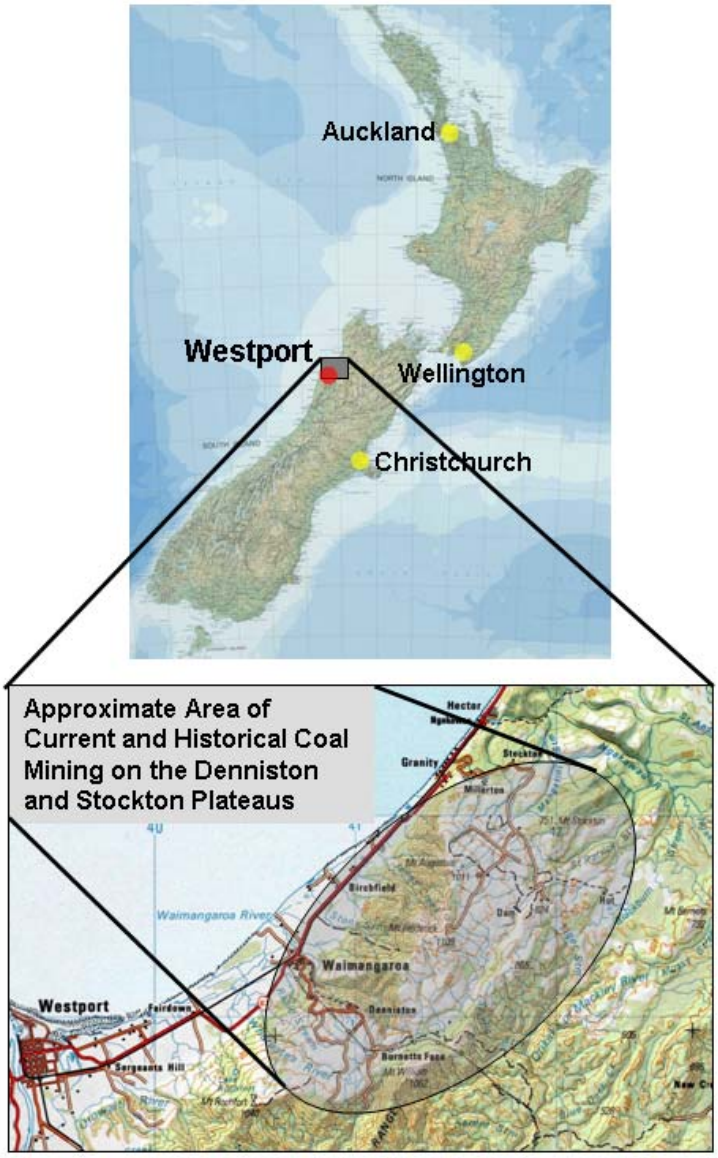

Figure 1.1. Current and historical coal mining regions on the Denniston and Stockton Plateaus (from MapToaster Topo (2007)).

1.2.1 Stockton Coal Mine

Stockton Coal Mine represents New Zealand's largest opencast coal mine. Coal mining operations commenced in the 1950s, and leachate from acid-generating waste rock has impacted the Waimangaroa, Mangatini and Ngakawau catchments (Lindsay et al., 2003; Black et al., 2005). Historical coal mining within the Ngakawau River catchment has been documented since 1872. Some of these relic coal mines still contribute to AMD discharges downgradient of Stockton Coal Mine (Lindsay et al., 2003; Black et al., 2005).

The Ngakawau catchment comprises an area of 20,500 hectares with surface exposure consisting of 25% Brunner Coal Measures, 30% carbonaceous mudstones (Kaiata mudstone) and 35% other basement materials including granites, gneiss, greywacke and argillites (Black et al., 2005). The Mangatini Stream (Figure 1.2) drains north into the Ngakawau River, and its catchment consists of predominately Brunner Coal Measures and Kaiata mudstone (Black et al., 2005), which have the capacity to produce AMD.

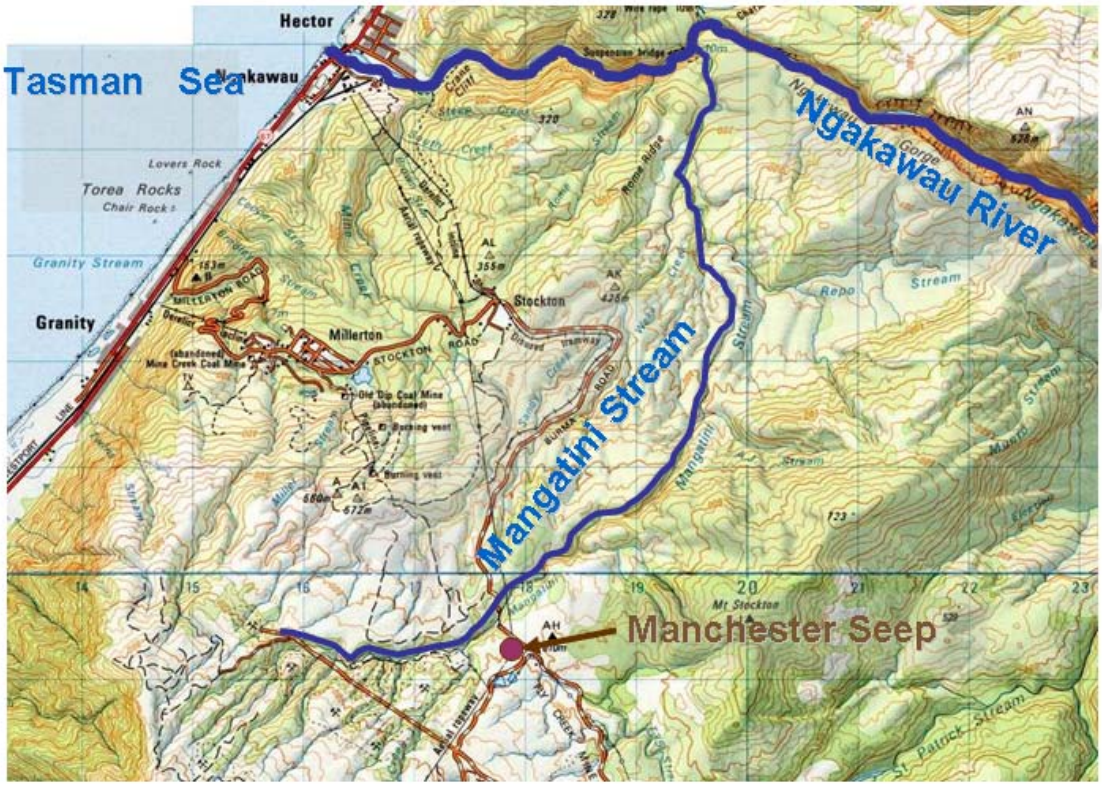

Figure 1.2. Topographic map of the Mangatini and Ngakawau catchments (from MapToaster Topo (2007)).

Black et al. (2005) reported background pH values from non-AMD impacted streams within the Mangatini and Ngakawau catchments often ranged between 3.5 and 4.5. The maximum pH measured was 6.9 at the Ngakawau River upstream from any known AMD impacts. A comparison of water chemistry from the upper and lower Ngakawau River and Mangatini Stream is shown in Table 1.1 as discussed by Black et al. (2004). Samples from the lower Ngakawau River were collected at the confluence of Mangatini Stream and the Ngakawau River (Figure 1.2). Results suggest that the Lower Ngakawau River was impacted from the Mangatini Stream AMD as shown by increased metal and acidity concentrations. Subsequent to this analysis, Solid Energy New Zealand Limited has implemented treatment of AMD within the Mangatini catchment via the Mangatini ultrafine limestone dosing plant and the Black Water Treatment Plant that employs calcium hydroxide ($Ca(OH)_2$)

treatment. This achieves company and community environmental goals of pH >4.0 and <1 mg/L Al 99% of the time.

Table 1.1: Mean water chemistry from the upper and lower Ngakawau River and Mangatini Stream collected from 1998-2004 (Black et al., 2005). Metal concentrations represent the dissolved fraction (passes through a 0.45 μm filter).

	Upper Ngakawau River	Lower Ngakawau River	Mangatini Stream
pH	6.9	4.8	3.5
Acidity to pH 8.3 (mg/L as $CaCO_3$)	6	17	248
Sulphate (mg/L)	3	19	126
Diss. Fe (mg/L)	0.1	0.3	6.2
Diss. Al (mg/L)	0.10	1.08	22.3
Diss. Ni (mg/L)	<0.001	0.007	0.120
Diss. Zn (mg/L)	0.057	0.129	0.611
TSS (mg/L)	12	33	61

1.2.2 Denniston Plateau

Water chemistry analysed from Rapid Stream on the Denniston Plateau demonstrates AMD impacts and natural low pH upgradient of these impacts. Trumm et al. (2003; 2005; 2006) and Trumm and Watts (2010) evaluated AMD chemistry emanating from two abandoned mine adits from Sullivan Mine. They found that a 5 km stretch of the nearby Rapid Stream was impacted with elevated acidity, metal and sulphate concentrations. A summary of water chemistry reported by Trumm et al. (2005; 2006) and Trumm and Watts (2010) is shown in Table 1.2. The low background (unimpacted by AMD) pH of 4.5 reported is not uncommon in streams within the Brunner Coal Measures as natural acid rock drainage (ARD) is generated due to weathering of natural carbonaceous mudstone and coal outcrops (Black et al., 2005). Additionally, the leaching of organic acids can result in natural brown water streams in the South Island of New Zealand that contain low pH (Winterbourn et al., 2000).

Table 1.2: Average water chemistry from Rapid Stream background and Sullivan Mine AMD between February 2001 and June 2002 (Trumm et al., 2005; 2006; Trumm and Watts, 2010).

	Rapid Stream Background	Sullivan Mine AMD
pH	4.5	2.9
Acidity to pH 3.7 (mg/L as $CaCO_3$)	<1	214
Sulphate (mg/L)	4.9	366
Diss. Fe (mg/L)	0.04	47
Diss. Al (mg/L)	0.09	14
Diss. Ni (mg/L)	0.001	0.13
Diss. Zn (mg/L)	0.009	0.72
Diss. As (mg/L)	<0.001	0.012
Diss. Mn (mg/L)	0.01	0.51

1.3 Acid Mine Drainage Chemistry – Brunner Coal Measures

Acidity is initially generated from the oxidation of pyrite (FeS_2; Section 1.3.1) in disturbed overburden where sulphuric acid (H_2SO_4) is created. de Joux (2003) conducted acid-generating column tests from coal and overburden collected on the Denniston Plateau. He found that coal and mudstone generated leachate containing the lowest pH at 2.8 and 2.5-2.7, respectively. Sandstone leachate contained pH values between 5.3 and 5.5.

The primary metals associated with AMD within the Brunner Coal Measures are Fe and Al. Iron is released during the decomposition of pyrite as a result of the acid production and drop in pH. Aluminium leaches from the ubiquitous micaceous and feldspathic-rich rocks within the carbonaceous mudstones and sandstone (Black et al., 2005). Other metals including Cu, Ni, Zn, Cd, As, Pb and Mn also dissolve from minerals within the parent bedrock and overburden when exposed to acidity. Weber et al. (2006) found that the most likely source of Ni was from pyrite within the Kaiata mudstone.

Numerous factors including site-specific geology, geochemistry and mining practices (e.g. opencast versus underground mining) influence AMD chemistry. Pope et al. (2006) showed variable AMD chemistry generated within the Brunner Coal Measures (pH 2.41-3.78). Pope et al. (2006) also delineated water chemistry from opencast and underground mines and as a function of their geology. There was generally a higher Al:Fe molar concentration ratio in opencast mines (Al/Fe = 1.02-25.91) compared with underground mines (Al/Fe = 0.22-4.06). This was attributed to the greater disturbances of overburden and sediments in open mine pits, which allow greater reaction time of sulphuric acid (H_2SO_4) produced from pyrite oxidation with Al-containing minerals (Pope et al. 2006; 2010). Newman (1988) and Pope et al. (2006; 2010) also report that sediment surrounding coal seams is often feldspar depleted and contains less Al compared with sediments stratigraphically further from the coal seams. During underground mining, most sediment disturbance occurs near the coal seam(s), whereas overburden extracted during open-pit mining includes sediment stratigraphically further from the coal seam(s).

Sediment, typically quantified in the aqueous matrix as total suspended solids (TSS) and/or turbidity, is also a common contaminant associated with AMD. Sediment transport occurs during erosion of disturbed land, especially during high intensity rainfall events. During the mining process, vegetation which otherwise stabilises soil is removed. Rock fragments are also created during blasting, which are removed to overburden dumps and can be prone to erosion, especially on steep slopes. Minimising erosion and subsequent sediment transport via advection in surface water runoff poses a substantial challenge for the mining industry. Jack (2006) showed that erosion can be reduced and better managed by slope reduction of stockpiles at Stockton Coal Mine, although natural armouring significantly reduced sediment loss over a short-time frame.

1.3.1 Iron Chemistry

Equations 1.1-1.4 summarise the commonly accepted chemical reactions associated with pyrite oxidation and Fe hydrolysis (Skousen, 1996; Rose and Cravotta, 1998; Pennsylvania Department of Environmental Protection, 1999; Ford, 2003; Watzlaf et al., 2004).

$$2\ FeS_2 + 7\ O_2 + 2\ H_2O \rightarrow 2\ Fe^{2+} + 4\ SO_4^{2-} + 4\ H^+ \quad \textbf{(1.1)}$$

pyrite + oxygen + water → ferrous iron + sulphate + hydrogen cations (proton acidity)

$$4\ Fe^{2+} + O_2 + 4\ H^+ \rightarrow 4\ Fe^{3+} + 2\ H_2O \quad \textbf{(1.2)}$$

ferrous iron + oxygen + hydrogen cations (acidity) → ferric iron + water

$$4\ Fe^{3+} + 12\ H_2O \leftrightarrow 4\ Fe(OH)_3\downarrow + 12\ H^+ \quad \textbf{(1.3)}$$

ferric iron + water → ferric hydroxide (ppt) + hydrogen cations (proton acidity)

$$FeS_2 + 14\ Fe^{3+} + 8\ H_2O \rightarrow 15\ Fe^{2+} + 2\ SO_4^{2-} + 16\ H^+ \quad \textbf{(1.4)}$$

pyrite + ferric iron + water → ferrous iron + sulphate + hydrogen cations (proton acidity)

Equation 1.1 denotes the weathering of pyrite, which is oxidised once exposed to oxygen and water. This results in the release of proton acidity in the form of H^+ ions. Two moles of H^+ ions are released for every mole of pyrite oxidised during this reaction.

Equation 1.2 represents the rate-determining step where ferrous iron (Fe^{2+}) is oxidized to ferric iron (Fe^{3+}) in the presence of oxygen (Singer and Stumm, 1970; Lowson, 1982). One mole of proton acidity is consumed for every mole of Fe^{2+} oxidised. The reaction rate is pH dependent and occurs more readily at pH≥3.5 where the reaction can readily proceed abiotically. At lower pH values (commonly <4.0), iron-oxidizing bacteria such as *Acidithiobacillus ferrooxidans* (formerly called *Thiobacillus ferrooxidans*) contribute significantly to the oxidative process and can increase reaction rates by a factor up to 1E6 (Singer and Stumm, 1970; Kleinmann and Crerar, 1979; Kirby et al., 1999; Watzlaf et al., 2004).The Fe^{3+} formed as a result of Fe^{2+} oxidation can either react to form ferric hydroxide (Equation 1.3) or act as a strong oxidising agent causing further dissolution of pyrite and release of proton acidity (Equation 1.4).

Iron hydrolysis occurs in Equation 1.3. By-products of this reaction include one mole of ferric hydroxide precipitate and three moles of proton acidity for every mole of Fe^{3+} hydrolysed. Not all Fe^{3+} formed in Equation 1.2 precipitates as ferric hydroxide in Equation 1.3, especially at pH<4. Under these conditions, Equation 1.3 is most accurately written as an equilibrium reaction proceeding both forward and reverse. These reactions typically occur relatively rapidly in mine workings due to low pH so solubility equilibrium is often achieved.

The presence of ferric hydroxide was observed in AMD-impacted streams in the vicinity of the Brunner Coal Measures at pH values as low as 2.5. The presence of acid-tolerant algae at these locations may potentially contribute to ferric hydroxide formation at such low pHs. Microenvironments are possibly created at and near the algae-water interface where algae supersaturates the water with dissolved oxygen (DO) and some alkalinity may also be produced during algae photosynthesis via consumption of carbon dioxide (CO_2) from carbonic acid (H_2CO_3; Kadlec and Knight, 1996; Kadlec and Wallace, 2009). The mechanisms of the physiological operation of algae at such low pHs are uncertain but it is suspected that they are somehow able to process free carbon dioxide (Harding and Boothryd, 2004). The self-catalytic nature of biologically mediated ferric hydroxide precipitation also likely contributes to the ongoing formation of ferric hydroxide.

Ferric Fe that does not precipitate as ferric hydroxide in Equation 1.3 acts as the oxidising reactant in Equation 1.4. The oxidation of pyrite by Fe^{3+} occurs very rapidly and is considered the fast step in pyrite dissolution (Lowson, 1982). Ferric Fe acts as a stronger oxidising agent than DO (Younger et al., 2002). As a result, pyrite oxidation by Fe^{3+} shown in Equation 1.4 proceeds quicker than pyrite oxidation via DO shown in Equation 1.1. For every mole of pyrite oxidized by Fe^{3+}, 16 moles of proton acidity are released.

Equations 1.1, 1.2 and 1.4 are cyclic, self propagating and will proceed until pyrite, Fe^{3+} or other oxidizing metals or oxygen are used up. An overall reaction summary of the pyrite oxidation process is shown in Equation 1.5.

$$4\ FeS_2 + 15\ O_2 + 14\ H_2O \rightarrow 4\ Fe(OH)_3\downarrow + 8\ SO_4^{2-} + 16\ H^+ \qquad \textbf{(1.5)}$$

pyrite + oxygen + water → ferric hydroxide (ppt) + sulphate + hydrogen cations (proton acidity)

Overall, four moles of H^+ cations are generated for every mole of pyrite oxidised in the net sequence of reactions.

1.3.2 Aluminium Chemistry

The primary sources of Al at Stockton Coal Mine include potassium feldspar or microcline ($KAlSi_3O_8$), muscovite ($KAl_2(AlSi_3O_{10})(F,OH)_2$) and kaolinite ($Al_2Si_2O_5(OH)_4$) (Black et al., 2005). When potassium feldspar is exposed to proton acidity, silicic acid (H_4SiO_4) and kaolinite are produced as shown in Equation 1.6 (Younger et al., 2002; Watzlaf et al., 2004). Kaolinite is further degraded in the presence of proton acidity, resulting in trivalent Al ions as shown in Equation 1.7. Precipitation of Al^{3+} as aluminium hydroxide ($AlOH_3$), which typically occurs at a pH of 4.7 or greater, releases proton Lewis acidity in the form of hydrogen ions as shown in Equation 1.8.

$$2\ KAlSi_3O_8 + 2H^+ + 9\ H_2O \rightarrow 4\ H_4SiO_4 + Al_2Si_2O_5(OH_4) + 2\ K^+ \quad \textbf{(1.6)}$$

potassium feldspar + hydrogen ions (proton acidity) + water → silicic acid + kaolinite

$$Al_2Si_2O_5(OH_4) + 6\ H^+ \rightarrow 2\ Al^{3+} + 2\ H_4SiO_4 + H_2O \quad \textbf{(1.7)}$$

kaolinite + hydrogen ions (proton acidity) → aluminium ions + silicic acid + water

$$Al^{3+} + 3\ H_2O \rightarrow Al(OH)_3\downarrow + 3\ H^+ \quad \textbf{(1.8)}$$

aluminium ions + water → aluminium hydroxide (ppt) + hydrogen ions (proton acidity)

Iron and Al dissolution are typically more complicated than depicted in the reactions presented in Equations 1.1-1.8. Additional elements such as Ca, Mg, Na, K and Si and lattice structure influence mineral dissolution and mechanisms for releasing and neutralising proton acidity (Weber, 2003).

1.3.3 Acidity

Acidity is defined as the ability of a water to neutralise a base (Watzlaf et al., 2004; American Public Health Association (APHA), 2005). It is most often reported in units mg/L as calcium carbonate ($CaCO_3$) since the formation of bicarbonate (HCO_3^-) from calcium carbonate dissolution (Section 1.5.1.1) represents the most common mechanism for creating alkalinity and neutralising acidity in nature (Tchobanoglous and Schroeder, 1985). Acidity can be measured empirically via titration with a sodium hydroxide (NaOH) solution following Standard Method 2310B (APHA, 2005) to a pH endpoint of 3.7, which represents acidity (pH 3.7), or to a pH endpoint of 8.3, which represents total acidity (pH 8.3). Acidity can also be calculated by summing metal and proton acidity as shown in Equation 1.9 where C_{Fe}^{2+}, C_{Fe}^{3+}, C_{Al}, C_{Cu}, C_{Ni} and C_{Zn} represent their respective dissolved metal concentrations in mg/L (modified from Hedin et al., 1994a; Younger et al., 2002; PIRAMID Consortium, 2003; Watzlaf et al., 2004).

$$\text{Acidity}_{calc}\ (\text{mg/L as } CaCO_3) = 50.045(2\ C_{Fe}^{2+}/55.85 + 3\ C_{Fe}^{3+}/55.85 + 3\ C_{Al}/26.98 + 2\ C_{Cu}/63.55 + 2\ C_{Ni}/58.71 + 2\ C_{Zn}/65.38 + 1000(10^{-pH})) \quad \textbf{(1.9)}$$

Equation 1.9 can also be modified to include acidity contributions from additional metals that may be present in MIWs such as Mn and As. Cravotta and Kirby (2004) concluded that measured acidity can be used to avoid calculation discrepancies related to the speciation of metals in the dissolved or precipitated state and the ionic state of Fe as Fe^{3+} and Fe^{2+}. Cravotta and Kirby (2004) also reported that at pH>2.2, Fe^{3+} complexes with hydroxide anions (OH^-), thus, it may be appropriate to modify Equation 1.9 further such that all Fe in a mine water is represented as Fe^{2+}, avoiding the reliance on speciating between the two Fe cationic states. Cravotta and Kirby (2004) and Hedin (2006b) found that calculated acidity (Equation 1.9) and total acidity (pH 8.3) values were comparable and could be used as a reliable quality assurance/quality control (QA/QC) check; however, Means and Hilton (2004) found poor association between calculated acidity and total acidity (pH 8.3) for three of four

MIWs evaluated. Magnesium hydrolysis during analysis for two of the samples contributed to higher acidity measured from titration compared with calculated values. Incomplete hydrolysis of Mn during titration contributed to biased low total acidity (pH 8.3) compared to calculated acidity for one of the samples. This demonstrates how site specific mine-water chemistry can influence the relationship between calculated and measured acidities.

1.4 Active Treatment Overview

Active treatment represents proven and reliable technology for ameliorating AMD (Brown et al., 2002; Younger et al., 2002; Waters et al., 2003; Aube et al., 2006). It will not be discussed in detail because the focus of this research pertains to passive treatment with an emphasis on systems incorporating sulphate reduction. Nonetheless, a brief synopsis of commonly employed active treatment processes is discussed in Appendix A, but it is recommended to consult such sources as Brown et al. (2002), Younger et al. (2002), Tchobanoglous et al. (2003), Waters et al. (2003), Aube et al. (2006) and Trumm (2008; 2010) for detailed information and design criteria regarding conventional active treatment processes with application to MIWs. Additionally, the computer programme AMDTreat can be used to aid in the selection, design and costing of active-treatment systems (Means et al., 2003; U.S. Department of the Interior, 2010). In AMD treatment, a process involving dosing with lime (applied as calcium oxide (CaO) or as a slurry of hydrated calcium hydroxide ($Ca(OH)_2$)) is most commonly employed to neutralise the AMD and, consequently, precipitate metals as hydroxides.

1.5 Passive Treatment Options for Ameliorating Acid Mine Drainage

Passive wastewater treatment relies on natural and/or waste materials and biogeochemical processes to create favourable conditions for sequestering contaminants of concern such as metals. Reactive media is commonly comprised of industrial or other waste products that can be sourced for free or cheaply, so most of their cost is associated with transport and construction. Although not maintenance free, passive treatment does not require the continual costs associated with chemical dosing and energy requirements incurred in operating process equipment in active treatment. Mine water is typically gravity fed into passive treatment systems so pumps are not required.

Advantages of passive treatment over conventional active treatment include lower operating costs, low capital costs if waste materials are used, development of ecological niches such as wildlife habitat in wetland-type systems, potential to be integrated into the natural landscape and are more aesthetically appealing than a chemical-treatment plant. Disadvantages include potential for high initial capital and construction costs, large land area requirements, especially for high flows and waters containing high contaminant concentrations, less control of effluent characteristics compared to active-treatment processes and the inability to adequately treat some of the most concentrated waters or sequester difficult contaminants such as those within the broader spectrum of total dissolved solids (TDS) including Na (and sometimes sulphate).

Passive treatment technologies for ameliorating AMD have evolved quite substantially over the past two decades and numerous installations have proven their reliability; however, treatment longevity is typically expected at 25 years or less (Younger et al., 2002; Wildeman et al., 2006). Passive treatment should be considered if MIW chemistry and flow are well understood, there is adequate land area available and future site disturbances that may alter MIW contaminant loadings can be mitigated without damage to the system (Wildeman et al., 2006). Decommissioned or abandoned sites are often more suitable for passive treatment (Wildeman et al., 2006; Trumm, 2010).

Numerous passive treatment options and design criteria specific to mine-water treatment are well documented in overseas literature (e.g. Younger et al., 2002; PIRAMID Consortium, 2003; Watzlaf et al., 2004; Wildeman and Schmiermund, 2004; Johnson and Hallberg, 2005). Examples of different passive-treatment systems including their respective acronyms are summarised in Table 1.3. A more descriptive explanation of each system is presented in subsequent sections. Anaerobic (reducing) systems, excluding compost wetlands, are generally quite similar and their functional application only differs in name. To reduce the convolution associated with these various names and acronyms, they will subsequently be referred to as vertical flow wetlands (VFWs) under most circumstances. The main exception is that VFWs examined during this thesis research will be referred to as biogeochemical reactors (BGCRs). Vertical flow wetlands in mine-water treatment have been reported to operate under the premises of a complex array of biogeochemical reactions so referring to them as BGCRs may be the most appropriate alternative, albeit, the specific biogeochemical mechanisms were not analysed as part of this study.

Hybrid or semi-passive systems that utilise many of the principals typical in passive treatment also exist. These systems typically utilise an active component that requires energy use such as a recirculation pump in recirculating-reducing and alkalinity producing systems (ReRAPS) or an organic feed such as ethanol or lactate; however, they rely on passive biogeochemical reactions for MIW treatment (Garret et al., 2002; Kaksonen et al., 2004).

Choosing the appropriate passive treatment technology is largely dependent on water chemistry. Passive treatment typically involves an oxidising or reducing strategy. Design flowcharts/keys have been developed to aid in choosing the appropriate passive treatment system typically based on key parameters such as acidity and alkalinity, Fe, Al and/or other metal concentrations, Fe^{2+} to Fe^{3+} ratio, DO and topography (Hedin et al., 1994a; Gusek, 2002; PIRAMID, 2003; Watzlaf et al., 2004; Ziemkiewicz et al., 2003; Skousen, 2006; Trumm, 2006a; 2010; Wildeman et al., 2006; Trumm, 2007b; Gusek, 2009a; 2009b). In many cases (e.g. Labar and Nairn, 2009; Nairn et al., 2009), passive treatment involves multiple treatment stages in series with each cell designed to remove a specific contaminant. Most passive treatment systems include a sedimentation basin as the first treatment stage to remove sediment that could potentially clog subsequent treatment stages (Gusek, 2002;

Watzlaf et al., 2004; Wildeman et al., 2006). An oxidation stage is often incorporated as the final treatment, or "polishing," stage to further treat the MIW and add DO, especially for reducing systems including VFWs and anoxic limestone drains (ALDs) (Gusek, 2009).

Table 1.3: A summary of different types of passive treatment systems utilised in treatment of MIWs including commonly used acronyms.

Passive System Name	Acronym
Aerobic (Oxidation) Systems (Wetland Types)	
Natural Wetland	
Sedimentation Pond	
Aerobic Wetland	
Anaerobic (Reducing) Systems (Substrate Based Wetland Types)	
Vertical Flow Wetland	VFW
Sulphate Reducing Bioreactor	SRBR
Biochemical Reactor	BCR
Biogeochemical Reactor	BGCR
Successive and Alkalinity Producing System	SAPS
Reducing and Alkalinity Producing System	RAPS
Recirculating Reducing and Alkalinity Producing System	ReRAPS
Compost (Anaerobic) Wetland	
Limestone Based Systems	
Oxic Limestone Drain	OLD
Anoxic Limestone Drain	ALD
Vertical Anoxic Limestone Drain	VALD
Open Limestone Channel	OLC
Limestone Leaching Bed	LLB
Horizontal Flow Leaching Bed	HFLB
Diversion Well	
Other Inorganic Based Systems	
Slag Leaching Bed	
Surface Catalysed Oxidation of Ferrous Iron	SCOOFI
Inorganic Media Passive System	IMP

Limited research has been conducted on passive treatment systems for ameliorating AMD in New Zealand. O'Sullivan (2005) summarised AMD chemistry and potential passive-treatment options viable in New Zealand. Trumm et al. (2005; 2006; 2007), Trumm (2006b) and Trumm and Watts (2010) have reported results from bench-scale trials of VFWs and limestone leaching beds (LLBs) for treating AMD from Herbert Stream and Rapid Stream within the Brunner Coal Measures. Mackenzie (2010) investigated the use of VFWs, LLBs and open limestone channels (OLCs) for treating AMD emanating from Fanny Creek within the Brunner Coal Measures.

1.5.1 Metal Removal Mechanisms

The primary metal removal mechanisms utilised in passive treatment systems are summarised in Sheoran and Sheoran (2006). Mechanisms differ depending on water chemistry and the passive-treatment option employed. Metals can be removed by either oxidising or reducing strategies, abiotically or biotically. Mechanisms contributing to metal removal include formation of hydroxides

via oxidation and hydrolysis reactions, precipitation and co-precipitation, sorption (including absorption and adsorption), settling and sedimentation and biogeochemical formation of metal carbonates and sulphides during sulphate reduction (Sheoran and Sheoran, 2006). Alkalinity generation is a major component of most passive treatment systems since acidity requires neutralisation and pH needs to be increased in most MIWs to precipitate metals.

1.5.1.1 Alkalinity Generation Methods

Alkalinity is required to neutralise proton acidity in AMD and the Lewis acidity generated from metal hydrolysis, primarily Fe and Al. Limestone has been the most common alkaline material utilised in passive treatment systems, primarily because it is typically cost effective, has suitable dissolution rates, and is relatively abundant near mine sites (Waybrant et al.; 1998; Thomas and Romanek, 2002a and 2002b; Younger et al., 2002; Watzlaf et al., 2004; Wildeman et al., 2006). Mukhopadhyay et al. (2007) suggest limestone dissolution, at least during the initial stages of passive treatment operation, follow pseudo first-order kinetics. Calcium carbonate purity in the limestone, its reactive surface area, and its subsequent dissolution rate also contributes to its effectiveness to treat MIWs (Mukhopadhyay et al., 2007). Therefore, limestone of high calcium carbonate purity (e.g. >90%) is recommended for use in passive mine-water treatment applications (Watzlaf et al., 2004).

Limestone dissolution (Equation 1.10) proceeds quicker under anoxic conditions than oxic because solubility rates of calcium carbonate are greater as carbon dioxide (CO_2) partial pressure increases. (Cravotta et al., 2004; Mukhopadhyay et al., 2007).

$$CaCO_3 + H^+ \rightarrow Ca^{2+} + HCO_3^- \quad \textbf{(1.10)}$$

calcium carbonate + hydrogen cations (proton acidity) → calcium + bicarbonate

Carbon dioxide partial pressure is greater in closed (e.g. anoxic) systems so more alkalinity is generated compared with an open system (Turner and McCoy, 1990; Stumm and Morgan, 1996). Watzlaf et al. (2004) summarise equilibrium alkalinity concentrations at different carbon dioxide partial pressures. The partial pressure of carbon dioxide under atmospheric conditions is approximately 0.0003 atm with 60 mg/L as $CaCO_3$ of alkalinity capable of being generated (Watzlaf et al., 2004). Younger et al. (2002) report that 150-350 mg/L as $CaCO_3$ of alkalinity is commonly generated when mine waters are exposed to limestone in closed systems, which corresponds to carbon dioxide partial pressures of about 0.006-0.05 atm. Therefore, closed systems are sometimes employed for maximising limestone dissolution for efficient alkalinity generation.

Additional alkaline materials used in passive mine-water treatment include shells from bivalves (Cubillas et al., 2005; this study), seafood processing wastes such as fish bones and proprietary blends such as Apatite II^{TM} containing fish bones (Lapointe, 2006; McCloskey, 2006; Ross et al., 2006; PIMS

nw, 2007), chitin derived from crabs (Korte, 2008; Robinson-Lora, 2008; Venot, 2008a; 2008b; Newcombe and Brennan, 2009; Robinson-Lora and Brennan, 2009; Robinson-Lora and Brennan, 2010), Bauxsol^{TM} (Davies-McConchie, 2002 and steel slag (Simmons et al., 2002; Younger et al., 2003; Bowden et al., 2006). Cubillas et al. (2005) summarise dissolution rates and the influence of surface geometry of calcite, aragonite, mussel shells, clams and cockles exposed to a pH 4 hydrochloric acid (HCl) solution and found that they increase with increased exposure due to changes in mineralogical lattice structure. Chitin is a carbohydrate derived from the exoskeletons of anthropods including crabs and typically requires processing. Slag (calcium alumino-silicate oxides) is a waste product generated from steel production and contains good alkalinity generating qualities (Simmons et al., 2002). It contains a high reactive surface area, which enhances oxidation of Fe^{2+} to Fe^{3+} and, subsequently, promoting Fe removal via ferric hydroxide formation and precipitation (Simmons et al., 2002; Younger et al., 2003; Bowden et al., 2006). More details pertaining to slag and its production are discussed in Simmons et al. (2002). Apatite II^{TM} ($Ca_{10-x}Na_x(PO_4)_{6-x}(CO_3)x(OH)_2$) consists mostly of fish bones that can be used to buffer waters between pH 6.5 and 7.0 via phosphate (PO_4^{3-}), hydroxide (OH^-) and substituting carbonate (CO_3^{2-}) groups, but, like chitin, requires extensive pre-processing (PIMS nw, 2007). Bauxsol^{TM} consists of a mixture of "red mud" from alumina production with sea water of salts/brines comprised of Ca and Mg (Davies-McConchie, 2002; Lapointe, 2006).

Bicarbonate alkalinity is also produced during sulphate reduction during bacterial metabolism (Neculita et al., 2007) as shown in Equation 1.11 (Stumm and Morgan, 1981).

$$2\ CH_2O + SO_4^{2-} \rightarrow H_2S + 2\ HCO_3^- \qquad \textbf{(1.11)}$$

organic carbon + sulphate → hydrogen sulphide + bicarbonate

Sufficient labile organic carbon and sulphate are required to maintain and optimise the process (Waybrant et al., 1998; Cocos et al., 2002; Gibert et al., 2004; Kaksonen et al., 2004; Gibert et al., 2005a; Hemsi et al., 2005; Doshi, 2006; Place et al., 2006). This is an important mechanism of alkalinity generation in VFWs. An additional alkalinity source such as limestone is often augmented with the organic carbon source to improve bicarbonate generation and MIW treatment performance (Gusek and Wildeman, 2002; Rose and Dietz, 2002; Watzlaf et al., 2004; Wildeman et al., 2006).

1.5.1.2 Oxidation and Hydrolysis (Metal Precipitation) in Aerobic Systems

Iron and Al represent the most common metals found in MIWs including most AMD at Stockton Coal Mine. The precipitation of ferric hydroxide is typically abiotic and dependent on both pH and DO. Precipitation of Fe^{2+} as a hydroxide proceeds as shown in Equation 1.12.

$$4\ Fe^{2+} + 4\ O_2 + 10\ H_2O \rightarrow 4\ Fe(OH)_3\downarrow + 8\ H^+ \quad \textbf{(1.12)}$$

ferrous iron + oxygen + water → ferric hydroxide (ppt) + hydrogen cations (acidity)

Lowry (1982) provides a thorough review of pyrite (including Fe^{2+}) oxidation. Singer and Stumm (1970) described the oxidation of Fe^{2+} under pH conditions between 4 and 8 by the following rate expression in Equation 1.13 where t represents time, k represents the rate expression and [element, compound or ionic species] represents molar concentration.

$$d[Fe^{2+}] / dt = -k\ [Fe^{2+}][O_2] / [H^+]^2 \quad \textbf{(1.13)}$$

Oxidation of Fe^{2+} is highly dependent on pH (the rate-limiting parameter) since it is second order, while Fe^{2+} and oxygen (O_2) are first order. Ferrous Fe typically does not readily form a hydroxide until pH>8 when the reaction rate rapidly increases.

Microbiological oxidation of Fe^{2+} is not well understood, especially with respect to kinetics. The process tends to occur when pH<5 but is more evident between pH 2 and 3 when abiotic oxidation is very slow or nonexistent (Kleinmann and Drerar, 1979; Younger et al., 2002).

If sufficient alkalinity is present in a mine water, Fe^{2+} can be oxidised to Fe^{3+} via aeration and precipitated as ferric hydroxide; however, two moles of H^+ are generated for each mole of Fe^{2+} oxidised and precipitated. Therefore, as dissolved Fe concentrations decrease as a result of hydroxide precipitation, pH declines. For every 1.0 mg/L of Fe precipitate, alkalinity is reduced by 1.8 mg/L as $CaCO_3$ (Watzlaf et al., 2004; Hedin, 2008a; 2008b).

Removal of Al as a hydroxide is highly dependent on pH and readily precipitates as a low density gelatinous hydroxide at pH≥4.7 that can potentially clog passive treatment systems (Younger et al., 2002). A large settling pond is recommended to allow sufficient settling time of aluminium hydroxide, and agitation must be minimised to avoid floc resuspension (Younger et al., 2002). Therefore, oxidising strategies to precipitate aluminium hydroxide are typically not recommended for MIWs containing high Al concentrations, but coprecipitation with Fe flocs can improve settling efficiency.

Sequestering other metals such as Cu, Ni, Zn, Cd, Pb and Mn via passive oxidising strategies is typically much less effective since achieving the required pH (e.g. pH>8) is not feasible or easily attained to promote hydrolysis (Wildeman et al., 2006). Passive Mn removal can be difficult because Fe oxidation kinetics out compete those of Mn, a pH>6 is required and Fe and Al must be reduced to concentrations less than about 2 mg/L prior to targeting Mn removal (Rose et al., 2003; Bamforth et

al., 2006). When both Mn and Fe are present, the following chemical reaction occurs resulting in Fe^{2+} reducing MnO_2 causing it to redissolve.

$$MnO_2 + 2\ Fe^{2+} + 4\ H_2O \rightarrow 2\ Fe(OH)_3\downarrow + Mn^{2+} + 2\ H^+ \quad \textbf{(1.14)}$$

manganese dioxide + ferrous iron + water → ferric hydroxide (ppt) + divalent manganese + hydrogen cations (proton acidity)

In the absence of Fe, oxidation and precipitation of Mn can readily occur by the reactions shown in Equations 1.15 and 1.16.

$$Mn^{2+} + 0.5\ O_2 + 2\ H^+ \rightarrow Mn^{4+} + H_2O \quad \textbf{(1.15)}$$

divalent manganese + oxygen + hydrogen cations (proton acidity) → tetravalent manganese + water

$$Mn^{4+} + 2\ H_2O \rightarrow MnO_2 + 4\ H^+ \quad \textbf{(1.16)}$$

tetravalent manganese + water → manganese dioxide + hydrogen cations (proton acidity)

The use of dolomite already containing manganite (MnOOH), manganese dioxide (MnO_2) or other manganese hydroxide precipitate helps catalyse Mn oxidation (Younger et al., 2003; Bamforth et al., 2005; Bamforth et al., 2006). Algal mats have also successfully increased Mn oxidation and hydrolysis rates by supersaturating water with DO and creating microenvironments of higher pH (Knauer et al., 1999; Hallberg and Johnson, 2005). Algal photosynthesis consumes carbonic acid from solution, therefore increasing pH; however, the opposite occurs during non-daylight hours where carbon dioxide is produced via respiration, which reacts with H^+ cations to form carbonic acid (H_2CO_3).

1.5.1.3 Precipitation, Coprecipitation and Sorption

Precipitation, coprecipitation and sorption processes are metal removal mechanisms commonly employed to settle or sequester metals. Removal of metals such as Pb, Cu, Zn, Ni and Cd can occur by coprecipitation with or sorption to Fe and Al precipitates (Rose and Ghazi, 1998; Lee et al., 2002) or adsorption onto organic substrates (Sheoran and Sheoran, 2006). Precipitation and coprecipitation processes improve settlement rates due to formation of larger, and consequently, denser metal flocs. Settlement rates of ferric hydroxide and aluminium hydroxide flocs are improved during complexation with water or hydroxide to form oxyhydroxides and also during additional complexation with sulphate to form hydroxysulphates. Benjamin (2002) describes metal complexation in greater detail.

Sorption of metals in passive mine-water treatment occurs onto sediment, metal precipitates and organic surfaces primarily via adsorptive processes including physisorption and chemisorption. Cation exchange processes such as metals adhering to a sediment surface or a highly anionic surface

such as zeolites by weak intermolecular (Van der Waal's) attractions represents a physisorption mechanism. Chemisorption mechanisms involve chemical bonding at surfaces, hence co-precipitation and can occur for various metals on surfaces of ferric hydroxide and iron oxyhydroxide (FeOOH) complexes. These complexes typically become less amorphous and form stable mineralogical complexes as they age due to metal diffusion into internal bonding sites where they become incorporated into the crystal structure (Cornell and Schwertmann, 1996). This process "frees up" sorption sites at the mineral surface. The processes of metal physisorption and chemisorption can continue until all reactive surface sites are saturated; however, sorption processes are dynamic with hydroxyl groups typically occupying unused sorption sites where they are available for reaction (Cornell and Schwertmann, 1996). Partition coefficients for metals binding to sediment (K_d) and organic carbon (K_{oc}) compared to the aqueous phase are dependent on water chemistry (especially pH) and sorptive properties of sediment or organic carbon.

The primary mechanism of trace metal sorption onto surfaces of Fe and Al hydroxide and oxyhydroxide precipitates involves ligand exchange of surface hydroxyl groups whose charges are influenced by pH (Jong and Parry, 2004). Lee et al. (2002) found that sorption onto precipitates formed during neutralisation of AMD was pH dependent, which governed the abundance of the primary sorbent (e.g. Fe (pH<4), Al (pH≈5) and Mn (pH≈8). Zanker et al. (2003) discuss colloid complexes comprised of predominately Fe and Al sorbing nearly 100% of As and Pb and 70% of Cu in near neutral adit water. Adsorption of Pb and Cu on particulate matter in a wetland was strong, whereas Zn, Ni and Cd were weak making their risk for bioavailability greater (Alloway, 1990; Sheoran and Sheoran, 2006). Kairies et al. (2005) found sorption affinities of metals on goethite (α-FeO(OH)), an iron oxyhydroxide, decreased with increasing crystallinity in the effluent water of ALDs and VFWs containing pH values from 5.89-7.42. Sorption preferences were in the order of Zn>Co≈Ni>Mn with Co and Ni showing sorption preference on Mn oxides when present. Dzombak and Morel (1990) also observed a greater sorption affinity for Zn compared to Ni with sorption preferences on goethite surfaces in the order of Cr>Pb>Cu>Zn>Ni>Ca. Gerth (1990) and Cornell and Schwertmann (1996) found sorption preferences of Cu>Pb>Zn>Co>Ni>Mn>Ca>Mg on a synthetic goethite. Inoculation of an aqueous metal solution with an isolated rhizosphere bacterial consortium facilitated precipitation of metals with a preference Cr>>Cd>Ni (Chen and Cutright, 2003), which may have application for trace metal removal in vegetated wetlands where hydrophytic roots and rhizomes are known to support active microbial communities (Kadlec and Knight, 1996; Kadlec and Wallace, 2009).

Sorption of metals onto biogenic metal sulphides (e.g. created during sulphate reduction) is not well documented. Jong and Parry (2004) found Pb^{2+}, Cu^{2+}, Cd^{2+}, Zn^{2+}, Ni^{2+}, Fe^{2+} and As^{5+} removal from aqueous solution and adsorption onto biogenic metal sulphides. Adsorption effectiveness was

dependent on initial aqueous metal concentrations, pH and adsorbent dosage with pH, which was most influential.

Sorption of metals onto organic substrates in organic-based passive treatment systems occurs more readily during system start-up (Neculita et al., 2007). Gibert et al. (2005a) estimated 40% of Zn was removed in a compost-based system by sorption until saturation of all reactive sorption sites. Sorption of metals onto organic media occurs more readily at higher pHs because of less competition with H^+ cations (Gibert et al., 2005b). Once sorption sites of organic substrates reach saturation, additional metals can not be sequestered by sorption and other processes are required for their effective immobilisation.

1.5.1.4 Sedimentation and Particle Settling

Sedimentation and particle settling represent the simplest processes employed for treating MIWs. Particle settling rates and efficiency are primarily influenced by particle size with larger particle sizes settling quicker than smaller particles as commonly demonstrated with sedimentation theory and Stoke's Law (Das, 1998; Building Industry Authority, 2001; Tchobanoglous et al., 2003). Other factors that influence settling rates include fluid viscosity, particle density, particle shape and the presence of films (e.g. biofilm, oil or organic carbon) adhered to particles that can reduce particle density. Sedimentation can be improved by maximising hydraulic efficiency including reduction of influent velocity, preventing short circuiting and dead zones/eddies, minimising bioturbation, reducing wave action and extending flow pathways (e.g. through baffles).

Sedimentation is frequently required for removal and storage of sediment and/or, metal flocs in mine-water treatment. Opencast mining, in particular, causes land disturbances that commonly result in erosion and sediment transport. Sediment size and composition vary within and across mine sites. Therefore, it is important to design sediment retention systems appropriate for known and expected conditions. Younger et al. (2003) states that design for settling 4 μm shale particles (typically 3-4 hour retention time) is robust enough for most mining applications. Ferric hydroxide flocs (initially <2.5 μm in diameter) require up to eight times the retention time of sediment. A general treatment design given by Watzlaf et al. (2004) recommends 8-24 hour retention time. Sedimentation theory utilising Stoke's Law for particle settling can be used as a more precise method for sizing sedimentation basins since it takes into account such variables as particle size, particle density and typical sedimentation efficiency as well as fluid density and viscosity (Tchobanoglous et al., 2003).

1.5.1.5 Sulphate Reduction

Sulphate reducing conditions provide an environment for precipitating dissolved divalent metals into immobile minerals and metal sulphides (Waybrant et al., 1998; Gusek, 2002; Gibert et al., 2003; Watzlaf et al., 2004; Doshi, 2006; Wildeman et al., 2006; Zagury et al, 2006; Neculita et al., 2007).

The primary mechanism of sequestering metals as a sulphide is shown in Equation 1.17 (Stumm and Morgan, 1981).

$$Me^{2+} + H_2S \rightarrow MS\downarrow + 2\ H^+ \quad \textbf{(1.17)}$$

divalent cationic metal + hydrogen sulphide → metal sulphide + hydrogen cations (proton acidity)

Examples of divalent metals commonly found in AMD include Fe^{2+}, Cd, Cu, Ni and Zn.

Numerous organic substrates, some of which have been amended with alkalinity sources, have been utilised as electron donors in sulphate reduction (Equation 1.11) research and VFWs (Table 1.4). A detailed list of references reporting research associated with these organic substrates and alkalinity amendments are summarised in Table A.1 in Appendix A. Many organic substrates utilised for mine-water treatment applications include readily available waste products (Gusek, 2002; Younger et al., 2002; Watzlaf et al., 2004).

Table 1.4: Substrate materials used in sulphate-reduction research and VFWs employed in mine-water treatment.

Substrate Category	Individual Substrate Materials
Compost	General (Unspecified) Compost, Conifer Compost, Leaf Compost
Manure	General (Unspecified) Animal Manure, Cow Manure, Dairy Manure, Horse Manure, Poultry Manure and Sheep Manure
Plant Derived (Excluding Wood Products)	Alfalfa, Corn Stover, Hay, Leaf Mulch, Oak Leaf, Rice Hulls, Sphagnum Peat Moss, Walnuts and Walnut Shells
Wood Products	Cellulose, Conifer Sawdust, Decayed Wood, Sawdust, Spent Oak Chips and Wood Chips/Waste
Sludges	Anaerobic Digester Fluid, Sewage and Wastepaper Recycling Plant
Simple Liquid Organics and Oils	Ethanol (C_2H_5OH), Sodium Lactate ($C_3H_5O_3Na$), Sodium Acetate (CH_3COONa), Propionic Acid (CH_3CH_2COOH), Glycerol ($C_3H_5(OH)_3$), Sodium Glucose ($C_6H_{12}O_6Na$), Sucrose ($C_{12}H_{22}O_{11}$), Molasses and Soybean Oil
Organic Mixtures	Organic Substrates, Organic Substrates Augmented with Limestone, Municipal Compost and Calcite
Other Sources	Fly Ash, Magnetite Sand (Fe_3O_4), Organic-Rich Soil, Manganese Dioxide (MnO_2; Pyrolox) and Zero-Valent Fe

There is no consensus on the best substrate (or substrate mixture) to use for treating MIWs with VFWs due to the interactions and complexities affiliated with microbial degradation of organic materials. Pereyra et al. (2005) and Zagury et al. (2006) found that sulphate reduction was most effective when incorporating a mixture of labile and long-term organic substrates as opposed to using an individual substrate. Buccambuso et al. (2007b) found slightly better sulphate reduction, and subsequently metal removal, in VFWs containing ethanol compared with a consortium of lignocellulose organic materials; however, the lower cost and maintenance required for systems incorporating lignocellulose organic

materials typically make them a more feasible long-term choice. It may be beneficial to include an organic source already inoculated with sulphate-reducing bacteria such as compost or manure (Wildeman et al., 2006); however, studies have shown that this is not compulsory for effective MIW treatment (Figueroa et al., 2007) and there is risk of faecal coliform and biochemical oxygen demand (BOD) release by inclusion of manure sources (Blumenstein et al., 2008).

The proven success and increased application of microbial-mediated sulphate reduction processes has resulted in increased interest in understanding the role of microorganisms and sulphate-reducing bacteria (SRB) in mine-water treatment (Ledin and Pedersen, 1996). Sulphate reduction occurs in environments where sulphate-reducing bacteria (SRB) can survive, metabolise and proliferate. Such environmental conditions include: anaerobic conditions, abundance of sulphate, Eh typically between 0 and -150 mV (or less) and sufficient labile organic carbon and micronutirents (Doshi, 2006; Sheoran and Sheoran, 2006; Neculita et al., 2007).

Sufficient labile organic carbon and sulphate are required as an energy source and terminal electron acceptor, respectively, for SRB in VFWs (Waybrant et al., 1998; Cocos et al., 2002; Gibert et al., 2004; Kaksonen et al., 2004; Gibert et al., 2005a; Hemsi et al., 2005; Zagury et al., 2006). Logan et al. (2003; 2005) found that cellulose degradation was the rate-limiting step in sulphate reduction, which emphasises the importance of choosing appropriate labile and recalcitrant organic sources. Pruden et al. (2005) also found that the rate-limiting step is not the population of SRB, which accounts for <2% of microbial communities in bioreactors (Pruden et al., 2006). Buccambuso et al. (2007a) concluded that despite the low percentage of SRB in a field VFW, their systems have a high capacity for sulphate reduction. A better understanding of the decomposition of organic substrates and their effect on sulphate reduction is still needed. Use and calibration of reactive transport models based on Contois kinetics, such as those employed by Hemsi et al. (2010), offer promise, but their application to longer-term field data sets still needs to be proven successful.

Sulphate-reducing bacterial activity is important in VFW treatment performance, in conjunction with their symbiotic relationship with cellulolytic microbes responsible for providing more labile carbon to SRB (Buccambuso et al., 2007a). Logan et al. (2005) demonstrated microbial processes involved in cellulose degradation from cellulose to lactate and acetate, which can be used by SRB as electron donors. Results from their series of batch experiments using a mixture of organic materials mixed with limestone indicated that: 1) cellulose availability was never limited, but its degradation and the subsequent availability of substrate SRB can utilise as electron donors (e.g. lactate and acetate) was limited; 2) fermentative and respiratory microbial communities were highly active, even during periods of decline in sulphate reduction; 3) SRB populations preferred lactate over acetate; 4) methanogenesis likely did not limit SRB activity since methanogens showed a preference for acetate, whereas SRB showed a preference for lactate; and 5) nutrient and sulphate availability, metal toxicity

and pH played only minor roles in limiting SRB activities. Chang et al. (2000) found that products of cellulose degradation, including fatty acids and alcohols, were utilised as electron donors during sulphidogenesis.

The pH also influences SRB proliferation. Ross et al. (2003) stated SRB thrive best at pH values between 5.5 and 9.0. Jong and Parry (2006) measured sulphate reduction rates ranging from 0.553-1.052 mol/m^3/day when influent pH was dropped from 6.0 to 4.0 in a porous media reactor comprised of sand with a lactate feed. Sulphate reduction declined to 0.00335 mol/m^3/day (1% of sulphate feed) when influent pH was further lowered to 3.5. Elliot et al. (1998) found that SRB could withstand a pH of 3.0 in a sodium lactate medium. Sulphate-reducing bacteria were most active at pH>4.0 with sulphide production decreasing when influent pH was lowered to 3.5. Tsukamoto et al. (2004) found SRB survival at pH 2.5 in ethanol-fed systems but less tolerant compared to pH>3.0.

Reaction kinetics in biologically-mediated systems are also increased exponentially with increasing temperatures as commonly modelled using the Arrhenius equation (Equation 1.17) where k represents the rate constant, A represents the pre-exponential rate factor, E_{act} is the activation of energy, R is the gas constant and T is temperature (Tchobanoglous et al., 2003).

$$k = Ae^{(-Eact/RT)} \quad \textbf{(1.18)}$$

Eliot et al. (1998) found that metal removal from VFWs tended to occur most efficiently at more circumneutral pHs (5.0-8.0) and at higher temperatures (Elliot et al., 1998). Neculita et al. (2007) reported that sulphate reduction was most effective at temperatures >6^{o}C. Therefore, it can be expected that such systems operating under cold climatic conditions will achieve less effective treatment performance (Gusek, 2004; Wildeman et al., 2006; Spangler et al., 2008).

Results from chemical modelling performed by Rose (2007) indicated that acidity removal in VFWs is limited by a complex association with mine-water influent pH, carbon dioxide partial pressure, Fe^{3+} and Al (and other metal) concentrations, sulphate reduction and limestone dissolution. Modelling results were generally consistent with empirical data and also indicated that greater acidity removal was possible in more acidic mine-waters. Zipper and Skousen (2010) confirmed this trend with empirical data.

Sulphate-reducing bacteria are also more effective when established within a solid porous media environment since this provides binding sites for the bacteria to attach (Glombitza, 2001). A balance needs to be established for optimal pore size to minimize potential for system plugging but still have adequate surface area for SRB proliferation (Tsukamoto et al., 2004).

Investigation of the microbiological diversity within sulphate reducing systems employed in mine-water treatment applications is complex and not well understood (Webb et al., 1998). Pruden et al. (2006) found by polymerise chain reaction (PCR) cloning that individual SRB species account for a minor number of microorganisms (<2% in three of four samples analysed) in two VFWs comprised of a mixture of organic substrates. Pruden et al. (2005) earlier evaluated bacteria present in laboratory columns containing a variety of organic and inert materials fed a simulated mine water (1000 mg/L sulphate). Bacteria belonging predominately to the *Clostridium* group, which includes cellulose degraders, fermenters and sulphate reducers, were most prevalent; however, PCR analysis indicated that a decrease in sulphate reduction activity does not necessarily correlate with a decrease in SRB populations. Prieto et al. (2008) compared microbial communities via PCR analysis on substrate material from a VFW consisting of ethanol and two comprised of lignocellulose organic materials (e.g. hay and woodchips and corn stover and woodchips). Sulphate-reducing bacteria were more abundant in the ethanol-containing reactor, whereas there was a more diverse consortium of microorganisms prevalent in the BCRs containing lignocellulose organic substrates. This increased biodiversity may make them more resilient to system stress. Pereyra et al. (2005) concluded from laboratory experiments that microbial activity, and consequently metal removal, was greatest from one of two reactors inoculated with a consortium of organic substrates (e.g. compost and manure) obtained from field VFWs treating MIWs as opposed to individual organic substrates.

Ingvorsen et al. (2003) found a biphasic pattern in SRB growth in activated sludge samples with a five-hour period of linear growth followed by exponential growth when exposed to anoxic conditions (SRB numbers ranged from 2.1E5-1.1E6 cells/mL). Sulphate-reducing bacterial growth reached maximum numbers in about four days where numbers remained relatively constant. VFWs are, therefore, expected to undergo a lag period prior to obtaining a quasi-equilibrium state. Lloyd et al. (2004) also noted a similar biphasic trend in sulphate reduction for systems stimulated with sucrose and ammonium chloride (NH_4Cl). They postulated that N was limited based on the presence of N-fixating bacteria. Kaksonen et al. (2004) found that a reactor fed ethanol as the organic electron donor yielded a more diverse culture of microorganisms compared with the system fed lactate.

Neculita et al. (2007) summarise some of the inhibitory conditions that affect SRB. Although a carbon to nitrogen (C/N) ratio of about 10 was reported as appropriate for degradation of complex organic materials (Reinertsen et al., 1984; Bechard et al., 1994), Zagury et al. (2006) reported that it was not a good indicator of sulphate-reducing activity for the six natural organic materials they tested. Inhibition of SRB can occur due to metal toxicity or exposure to high concentrations of oxygen or dissolved hydrogen sulphide, although these effects are reversible (Reis et al., 1992; Nagpal et al., 2000). Toxic effects of hydrogen sulphide were reported at concentrations ranging from 477-617 mg/L (1346-1742 mg/L equivalent sulphate), concentrations typically not encountered in passive sulphate-reducing systems employed for mine-water treatment (Okabe et al., 1992; Reis et al., 1992;

Al-Ani, 1994; Kolmert et al., 1997; Neculita et al., 2007). The inhibitory effects of hydrogen sulphide could also be related to the precipitation of metal sulphides, which are reported to inhibit SRB by direct deposition on bacterial cells (Utgikar et al., 2002).

1.5.2 Natural Wetlands and Brief History in Mine Water Treatment

The ability of natural wetlands to improve water quality is well documented with applications for a wide range of municipal, residential and industrial pollutants (Kadlec and Knight, 1996; Kadlec and Wallace, 2009). Primary removal mechanisms are biogeochemical and physical-chemical in nature including: 1) plant uptake (e.g. nutrient removal); 2) physical settling (e.g. sedimentation, settling of metal precipitates, filtration by vegetation and retention in plant rhizophere); 3) sorption (e.g. absorption and adsorption onto organic matter and sediment and metals such as arsenic adsorbing to ferric hydroxide surfaces); 4) precipitation and coprecipitation as hydroxides, carbonates or metal sulphides); and 5) other microbiological processes (Kadlec and Knight, 1996; Kadlec and Wallace, 2009).

Seidel and Kickuth at the Max Planck Institute in Plon, Germany are typically credited with the initial research efforts for development of treatment wetland technology when they conducted bench-scale research on the ability of wetlands and wetland vegetation to remove organic pollutants from waste water beginning in 1952 (Kadlec and Knight, 1996; Younger et al., 2002; Kadlec and Wallace, 2009). Howard T. Odum and fellow researchers examined wetland processes and mechanisms for ameliorating municipal wastewater in the United States beginning in 1967 as the ability of wetlands to purify water was gaining recognition (Kadlec and Knight, 1996; Kadlec and Wallace, 2009). Wetland treatment technology for municipal wastewater, stormwater and agricultural runoff was well established prior to recognition that the technology could also be applied to ameliorate mine waters. Sobolewski (2007) lists a number of documented cases of natural wetlands improving mine drainage. Boyle (1965) documented zinc removal of 40 parts per million (ppm) from a bog wetland in Canada. Sheoran (2005) documented increase in pH and reduction in Cu, Fe, Co, Zn, Pb, Ni and Mn concentrations from circumneutral discharge from a Cu mine tailing impoundment. Development of current engineered-wetland technology for treating mine waters evolved from observations that water quality of coal mine drainage improved once passing through *Sphagnum* bogs (Huntsman et al., 1978; Wieder and Lang, 1982). Since these observations, passive treatment systems have been designed and constructed to simulate more of an engineering design and approach incorporating efficiency and reduction in land-area requirements (Wildeman et al., 2006).

1.5.3 Oxidising Passive Treatment Systems

Oxidising passive-treatment strategies are typically designed to generate alkalinity and precipitate metals as hydroxides. These include OLCs, LLBs, aerobic wetlands, sedimentation ponds, slag leaching beds (e.g. surface catalysed oxidation of ferrous iron (SCOOFIs) and other inorganic media passive systems (IMPs). System type is typically chosen based on MIW chemical signature,

topography and availability of system components such as limestone, topsoil, wetland vegetation, liners, etc.

1.5.3.1 Cascades

Cascades are the most commonly employed passive aeration technique but require sufficient land availability and hydraulic gradient to successfully implement. Aeration increases oxygenation rates of Fe^{2+} to Fe^{3+} and, consequently, the formation of ferric hydroxide and oxyhydroxide precipitates. Cascades are typically employed for oxygenating neutral mine drainage (NMD) or neutralised AMD. Ferric hydroxide precipitates are settled and stored in a subsequent pond and/or aerobic wetland.

Cascades are typically designed to provide enough DO to oxidise 50 mg/L Fe^{2+} (Younger et al., 2002; Watzlaf et al., 2004), although 30 mg/L is sometimes used as a more conservative goal (PIRAMID, 2003). Watzlaf et al. (2004) state that 55 mg/L of Fe^{2+} is oxidised if the DO concentration is 8 mg/L. Maximising oxygen transfer efficiency is critical in cascade design. Koduri and Barkdoll (2004) tested predicative models for oxygen transfer efficiency versus cascading aeration structures of four-water treatment plants. Although some of the models predicted oxygen transfer within 2-13% of empirically measured values, they should be used with caution since most are derived from empirical data employing different flow and hydraulic structures. The oxygenation process is also dependent on temperature and DO concentrations so most predictive models incorporate correction factors for these parameters.

Entrained air bubbles created by cascades should disperse the full depth of the water body to maximise oxygen transfer efficiency. Baylar and Bagatur (2000) compared oxygen transfer of different weir types under different flow regimes and hydraulic drop heights. The v-notch weir containing a drop height of 0.9 metres provided the best oxygen transfer. Drop heights >0.9 metres were less efficient since the nappe tends to break apart. The efficiency of oxygen transfer decreased as flow rate increased. The tailwater depth, or depth water bubbles penetrate below the upper water surface, was consistently 0.6 times the hydraulic drop height for all weirs, which is consistent with results reported by Avery and Novak (1978). Younger et al. (2002) and PIRAMID (2003) recommend that cascade design ensures thin sheet flow in simple ‘flights’ of steps 100 mm wide for every L/s of flow. Four to six steps are typical, ensuring 500-800 mm drop height. They also recommend depth of “plunge pools” at least as deep and wide as the water drop height to allow sufficient oxygen ingress.

1.5.3.2 Open Limestone Channels / Oxic Limestone Drains

Open limestone channels, sometimes referred to as oxic limestone drains (OLDs), consist of a trench filled with limestone designed to add alkalinity and promote precipitation of ferric and aluminium hydroxides. Their application is most effective for treating mine waters with Fe and Al concentrations of 10-20 mg/L and acidity <90 mg/L as $CaCO_3$ (Cravotta and Trahan, 1999). Zipper and Skousen (2010) found that alkalinity generation was directly proportional to influent acidity; therefore, more

alkalinity generation can be expected with higher influent acidity. The recommended design criterion is three hours hydraulic residence time (HRT; Cravotta and Trahan, 1999). Minimum velocity recommended is 0.1 m/min to reduce Fe fouling limestone (Younger et al., 2002; PIRAMID, 2003). Systems should also be constructed on a slope >12% to minimise clogging and reduce fouling (Ziemkiewicz et al., 2003). Armouring of limestone by ferric hydroxide results in decreased dissolution rates (Ziemkiewicz, 1997; Mukhopadhyay et al., 2007). Limestone dissolution is reduced 20-50% compared with unarmoured limestone (Pearson and McDonnell, 1975; Ziemkiewicz et al., 1994). The feasibility of implementing OLCs at Stockton Coal Mine is limited due to high Fe and Al concentrations. Performance examples of OLCs are summarised in Appendix A.

1.5.3.3 Limestone Leaching Beds

Limestone leaching beds are essentially horizontal flow reactors or VFWs filled with limestone. Skousen and Ziemkiewicz (2005) reported that LLBs were among the most successful passive treatment systems they evaluated in mine-water treatment. In 17 systems analysed, acidity removal averaged 17.6 g/day/US tonne of limestone (range of 0.4-40 g/day/US tonne of limestone). Zipper and Skousen (2010) showed that alkalinity generation generally increased with increased influent acidity. Black et al. (1999) recommended LLBs to treat water containing little or no alkalinity and low dissolved metal concentrations. Watzlaf et al. (2004) suggest that LLBs are most appropriate for targeting Mn removal subsequent to Fe removal from MIWs since Mn will not oxidise effectively in the presence of Fe. Rose et al. (2003) concluded that Mn could successfully be removed from MIWs with LLBs but recommended influent pH>6 and influent Fe and Al concentrations ≤2 mg/L. Manganese removal rates were typically 2-3 g Mn/m^2/day with removal rates of 8-17 g Mn/m^2/day reported in some systems. Denholm et al. (2002) found Mn removal of up to 30 mg/L in similar systems called horizontal flow limestone beds (HFLB). Furthermore, Denholm et al. (2008) were able to successfully recover Mn bearing material from an HFLB for use as a "glaze colourant" by local ceramic artists with potential application in brick manufacturing. Although LLBs have potential application for treating some AMD at Stockton Coal Mine (as Trumm (2006b) and Trumm et al. (2007b; 2008) demonstrated), they were not a focus of this study due to excessive Fe and Al concentrations at the primary seep evaluated during this study.

1.5.3.4 Ponds and Aerobic Wetlands

Ponds and wetlands are proven and recommended technologies for remediating net-alkaline ferruginious mine waters (Hedin et al., 1994a; Gusek, 2002; PIRAMID, 2003; Ziemkiewicz et al., 2003; Watzlaf et al., 2004; Wildeman et al., 2006). Ponds are often designed to remove and store sediment but are also utilised to allow sufficient HRT for formation and settlement of iron flocs. Aerobic wetlands provide final polishing or tertiary treatment of residual Fe and, when applicable, provides some Mn removal. Wetland vegetation enhances ecological niches, uptakes some metals, filters fine sediments, provides a surface for periphyton growth, which sorbs metals, and creates microzones of oxidising conditions through radial oxygen loss (e.g. plant roots in the rhizosphere)

enhancing hydroxide formation (Kadlec and Knight, 1996; Younger et al., 2002; Kadlec and Wallace, 2009). Aerobic wetlands also provide ancillary benefits including wildlife habitat and aesthetic appeal (Kadlec and Knight, 1996; Kadlec and Wallace, 2009).

Overloading aerobic wetlands with sediment can result in system failure and expensive maintenance relative to sedimentation ponds due to added costs associated with topsoil and wetland vegetation. It is also common practice (e.g. in the United Kingdom (UK)) to precede aerobic wetlands with a sedimentation pond (Sapsford et al., 2007). Ponds are the recommended first stage of any passive treatment system receiving NMD containing about 50 mg/L Fe by the government's Coal Authority in the UK (Younger et al., 2002). A general treatment design given by Watzlaf et al. (2004) is an initial aeration stage including cascades or a waterfall, followed by a 1.2-2.4 metre deep pond designed for 8-24 hour retention time followed by an ~0.15 m deep vegetated wetland. An advantage of utilising the staged approach of ponds followed by aerobic wetlands is the potential to "harvest" ferric hydroxide precipitate from the ponds (dependent on product purity) as a saleable product for industrial applications (Hedin, 1999; 2003; 2006a; 2008a; 2008b).

Current design criteria for ponds and aerobic wetlands for Fe removal are 10-20 g/m^2/day (Hedin et al., 1994; Younger et al., 2002; PIRAMID, 2003; Watzlaf et al., 2004). Hedin (2008a; 2008b) reported an average Fe removal rate of 26 g/m^2/day in a pond array and an average residual Fe removal rate of 4 g/m^2/day in the subsequent aerobic wetland "final polishing" stage for treating a circumneutral Fe laden MIW. Ponds and aerobic wetlands could provide a similar function as a "final polishing" stage at Stockton Coal Mine.

Design criteria commonly employed for Mn removal are 0.5-1.0 g/m^2/day (Hedin et al., 1994a; Younger et al., 2002; Watzlaf et al., 2004); however, Mn removal does not occur in aerobic wetlands if Fe concentrations are >1 mg/L (Nairn and Hedin, 1993). Oxidation of Fe, and subsequent precipitation of ferric hydroxide, is thermodynamically more favourable than Mn oxidation as demonstrated in Equation 1.14 (Bamforth et al., 2005). Therefore, Fe must be removed from mine waters prior to targeting Mn removal. Additional information regarding Mn removal via passive treatment by utilisation of algal mats, rock filters (utilising dolomite), Mn oxidising bacteria and the importance of Mn carbonates and oxyhydroxides in promoting Mn precipitation by alkalination and oxygen supersaturation are reported elsewhere (Knauer et al., 1999; Rousch and Sommerfeld, 1999; Sikora et al., 2000; Johnson, 2002; Johnson, 2003; Rose et al., 2003; Bamforth et al., 2005; Hallberg and Johnson, 2005; Sheoran and Bhandari, 2005; Bamforth et al., 2006).

1.5.3.5 Slag Leaching Beds and Surface Catalysed Oxidation of Ferrous Iron Reactors

Slag has been successfully applied in treating AMD because of its high surface area and ability to generate alkalinity within short HRTs. Younger et al. (2002) describes SCOOFIs, which incorporate slag. Sorption occurs on the slag and oxidation of Fe^{2+} to Fe^{3+} occurs in circumneutral mine water. The authors report Fe removal rates of hundreds of grams of Fe/m^3/day (equivalent to 25 g/m^2/day) in saturated flow reactors and 12 g/m^3/day (0.05 g/m^2/day) in unsaturated flow reactors (Jarvis and Younger, 2001). Hydraulic residence times reported in the unsaturated reactors were much shorter compared to those employed in other passive treatment systems (ranging between 70 and 360 seconds). The use of slag at Stockton Coal Mine is not feasible due to the lack of supply in the region and the prohibitive costs to ship it to site. Performance examples of slag leaching beds and SCOOFIs are summarised in Appendix A.

1.5.4 Reducing Passive Treatment Systems

There are predominately three types of passive systems which utilise reducing conditions to generate alkalinity and sequester metals. These include ALDs, VFWs and compost wetlands. Anoxic limestone drains rely on increased abiotic dissolution rates of limestone due to the build up of carbon dioxide partial pressures, whereas VFW reducing systems rely on sulphate reduction and a complex array of biogeochemical transformations for alkalinity generation and metal sequestration. Since treatment effectiveness of surface flow compost (sometimes referred to as anaerobic) wetlands relative to VFWs is quite low (e.g. acidity removal of 3.5-7.0 g $CaCO_3$/m^2/day (Younger et al., 2002; Watzlaf et al., 2004)), they will not be discussed. The primary application for compost wetlands pertains to sites where a VFW is also appropriate.

1.5.4.1 Anoxic Limestone Drains

Anoxic limestone drains are essentially OLCs (or OLDs) except the MIW saturates and flows through limestone that is capped with clay and/or a synthetic plastic, thus preventing the ingress of oxygen and, subsequently, maximising internal carbon dioxide partial pressure. When considering implementation of an OLC/OLD versus an ALD, additional capital costs incurred by capping the system with an impermeable membrane and maintenance requirements must be considered along with whether or not the topography is steep enough to flush out metal precipitates.

Anoxic limestone drains should only aim to increase pH and alkalinity when Fe is present in the reduced state of Fe^{2+}. Recommended influent water chemistry is <1.0 mg/L Fe^{3+}, Al and DO, pH>5 and calculated acidity <150 mg/L as $CaCO_3$ (Watzlaf et al., 2004). PIRAMID (2003) state that Fe^{3+} and Al concentrations ≤2 mg/L are suitable. Anoxic limestone drains exposed to MIW exceeding these conditions will likely fail prematurely due to system clogging or limestone armouring with ferric hydroxide and/or aluminium hydroxide. Watzlaf et al. (2004) proposed designing ALDs with a HRT

of 15 hours when ≥85% of maximum achievable alkalinity is attained. Limestone should contain >82% $CaCO_3$ to generate sufficient alkalinity, although >90% is preferred. Anoxic limestone drains are unfeasible for treating AMD at Stockton Coal Mine because water chemistry parameters exceed those recommended. Additional information pertaining to the rate models of limestone dissolution in ALDs and performance examples of ALDs are summarised in Appendix A.

1.5.4.2 Vertical Flow Wetlands

Vertical flow wetlands have been successfully implemented and are an attractive method of simultaneously sequestering a wide range of metals including Fe, Al, Cu, Ni, Zn, Pb, Cd, Co, Hg, Se and Tl (Gusek, 2002; Gusek and Wildeman, 2002; Rose and Dietz, 2002; Younger et al., 2002; Gusek, 2004; Watzlaf et al., 2004; Skousen and Ziemkiewicz, 2005; Neculita et al., 2007; Blumenstein et al., 2008; Blumenstein and Gusek, 2009). They are commonly employed for treating AMD containing high concentrations of Al, which can be difficult to remove and settle in aerobic treatment systems (Gusek and Wildeman, 2002; Younger et al., 2002; PIRAMID, 2003; Watzlaf et al., 2004). Vertical flow wetlands were thus chosen as the primary focal point of this thesis due to their ability to remove a wide range of metals including Al. Most VFWs in mine-water treatment operate as downflow reactors where flow enters from the top and discharges from a piping network in the bottom.

Thomas and Romanek (2002a; 2002b) used back-scatter electron (BSE) imaging and an energy dispersive spectroscopy (EDAX) detector to determine the mineralogy in VFWs comprised of 75 vol.% compost and 25 vol.% limestone (1.22 mm nominal diameter). Results showed three distinct mineralogical zones throughout the columns, transitioning from an oxide zone where Fe oxyhydroxides predominate, a transitional zone consisting mostly of Al hydroxysulphates and a reduced zone consisting of ubiquitous sulphides (>95% Fe sulphide (FeS)).

Various substrate mixtures and flow configurations have been employed in VFWs. Many reducing and alkalinity producing systems (RAPS) have utilised a 0.15-0.61 m layer of compost (or a mixture of compost and limestone) overlying 0.6-1.2 m of limestone (Watzlaf et al., 2004). Most VFWs have utilised a wide range of organic substrates (summarised in Table A.1) and have sometimes included limestone in their mixtures (Gusek, 2004; Doshi, 2006; Neculita et al., 2007). Hydraulic head recommended for systems comprised of compost as the sole carbon source is 1.5-2.0 m to allow sufficient hydraulic throughput (PIRAMID, 2003; Watzlaf et al., 2004). Therefore, it may be advantageous to include bulking material in the organic mixture to increase hydraulic conductivity, thus reducing hydraulic head requirements and the potential of substrate clogging.

Design criteria recommended for VFWs have been typically reported on a molar volumetric loading basis or an acidity areal loading basis. Wildeman et al. (2006) recommended a design criterion of 0.3 mol of metal removal/m^3 of substrate/day. They also indicated that removal efficiencies are reduced about 25% in cold climates. Watzlaf et al. (2004) recommended applying areal removal rates of 25-30

g acidity as $CaCO_3/m^2$ surface area/day. Gusek (2002) reported sulphate removal of about 0.30 mol/m^3/day could be expected from VFWs comprised of a mixture of organic materials and crushed limestone.

Numerous studies have evaluated the performance of VFWs for removing sulphate, acidity and metals, which are summarised in Tables 1.5, 1.6 and 1.7, respectively. The studies chosen have generally incorporated limestone or other alkalinity amendment in the organic substrate mixture, since this is becoming standard practice in passive mine-water treatment (Watzlaf et al., 2004; Wildeman et al., 2006). Results are variable and dependent on numerous characteristics including mine-water chemistry, substrate mixture, limestone purity, contaminant loading rates and HRT. Manganese is typically the most difficult metal to remove, since it is rather soluble as a sulphide, followed by Fe. Other metals including Al, Cu, Ni, Zn, Cd, Co and Pb are readily removed.

Table 1.5: Sulphate removal reported in VFWs.

Reference	Scale	Substrate	Sulphate Removal Rates
Gibert et al. (2004)	Bench	Sheep manure and limestone substrate	1) 0.44 mol/m^3/day (27% removal) with HRT=9.0 days. 2) 0.17 mol/m^3/day (18% removal) with HRT=2.4 days.
Thomas and Romanek (2002a)	Bench	75% compost and 25% limestone overlaying 150 mm of coarse limestone.	1) From 0.25-0.35 mol/m^3/day (20% removal).
Dvorak et al. (1992)	Pilot	Manure, hay, straw, corn cobs, wood chips, gypsum and limestone	1) 0.214-0.333 mol/m^3/day (17-20% removal).

Table 1.6: Acidity removal reported in VFWs.

Reference	Scale	Substrate	Acidity Removal Rates and Key Results
Skousen and Ziemkiewicz (2005)	Full	Typically mushroom compost and limestone	1) >200 g/m^2/day (n=2); 39-87 g/m^2/day (n=5); 2-17 g/m^2/day (n=8); and no removal (n=1).
Rose (2004)	Full	Typically mushroom compost and limestone	1) Update from Rose and Dietz (2002). 2) Typical removal rates declined from 40 g $CaCO_3$/m^2/day to 34 g $CaCO_3$/m^2/day. 3) Systems incorporating fine limestone in the compost mixture yielded about twice this acidity removal.
Ziemkiewicz et al. (2003)	Full	Typically mushroom compost and limestone	1) Preceded results from Skousen and Ziemkiewicz (2005). 2) Average removal of 62.3 g $CaCO_3$/m^2/day.
Rose and Dietz (2002)	Full	Typically mushroom compost and limestone	1) 25-50 g $CaCO_3$/m^2/day (n=12)
Thomas and Romanek (2002a)	Bench	75 vol.% mixture of compost and 25 vol.% limestone (nominal grain size of 1.23 mm limestone)	1) Average removal of 87.8 g $CaCO_3$/m^2/day; however, average feed rate for the experiments was 57.8 g $CaCO_3$/m^2/day. 2) This indicates higher alkalinity generation rates when influent acidity loading was high, likely due to increased dissolution of limestone as supported by Zipper and Skousen (2010). 3) This corresponds with findings by Rose and Dietz (2002) and Rose (2007), which showed positive correlations between influent retention time, H^+ and Fe concentrations with alkalinity generation.

Table 1.7: Metal removal reported in VFWs.

Reference	Scale	Substrate	Metal Removal Rates and Key Results
Gusek et al. (2008)	Pilot	Woodchips, rice hulls, cow manure, hay, ash and limestone sand	1) 96.1% average metal (Fe, Al, Cu, Zn, Cd, Co, Pb and Mn) removal. 2) A period of system overloading required a two-month period to completely recover. 3) Iron removal was poor (53%) during one sampling period potentially due to decreased microbial activity as a result of colder temperatures. 4) Possible dissolution and export of Mn from organic substrate materials.
Reisman et al. (2008)	Pilot	Wood chips, dairy manure, hay and limestone fines	1) Cu, Cd, Pb and Zn concentrations reduced by >95%. 2) Iron and Mn likely leached from substrate (average 1% Fe and 12 % Mn removal). 3) Remote monitoring, data acquisition and sampling equipment not cost effective due to unanticipated expenditures accrued to mitigate malfunction and problems.
Venot et al. (2008a; 2008b)	Mesocosm (in field)	Peas gravel, sand and ChitoRem^{TM} SC-20 comprised of 20% chitin, 40% $CaCO_3$, 30% protein, 9% N and <1% P	1) Effluent alkalinity elevated (typically between 5000-10,000 mg/L as $CaCO_3$) due primarily to the release of ammonia (NH_3) (220-450 mg/L) and Ca (commonly >1000 mg/L). 2) Manganese reduced from 21.5 mg/L to 3 mg/L (86% removal). 3) Iron reduced from 41.2 mg/L to 0.04 mg/L. 4) Copper reduced from 0.03 mg/L to 0.0003 mg/L.
Figueroa et al. (2007)	Bench	Corn stover and walnut shells	1) Second treatment stage following a limestone reactor. 2) <0.1 mg/L Zn in effluent reduced from 45-55 mg/L in one system and 1-2 mg/L in the other
Trumm et al. (2005; 2006); Trumm and Watts (2010)	Mesocosm (in field)	150 mm layer of limestone overlain by a 130 mm layer of mushroom compost	1) Removal efficiencies of 97% Fe, 100% Al and 66% Ni from influent 59 mg/L Fe and 14 mg/L Al (HRT=5 hours). 2) At another site, removal efficiencies were 99% Fe, 96% Al, 95% Ni , 99% Zn and 51% Mn from average influent concentrations of 34 mg/L Fe, 1.6 mg/L Al, 0.12 mg/L Ni, 1.1 mg/L Zn and 0.35 mg/L Mn with a (HRT=20 hours)
Gusek and Wildeman (2002)	Bench	Various organics and crushed limestone	1) <0.1 mg/L Al in effluent.

1.6 Passive Treatment Flow Hydraulics, Tracer Studies and Application to Ideal-Reactor Models

1.6.1 Flow Hydraulics

Flow hydraulics are important when designing and operating any passive treatment system (Younger et al., 2002; PIRIMID, 2003; Gusek, 2004; Wildeman et al., 2006). Studies have reported that flow hydraulics impact treatment performance and have also provided conceptual design recommendations to achieve efficient flow hydraulics whilst minimising undesirable flow characteristics such as short circuiting, scouring and stagnant zones (Busler et al., 2002; Younger et al., 2002; PIRIMID, 2003; Gusek, 2004; Wildeman et al., 2006; Panuvatvanich et al., 2009). Despite this knowledge, there have been limited studies that quantify flow characteristics and discrepancies between theoretical and "real" HRTs in passive treatment systems for mine-water treatment.

Design of flow distribution structures (or flow-distribution arrangement) for any passive treatment system is important to achieve the most efficient flow through the system (e.g. minimise the difference between theoretical and "real" HRT by preventing eddies and dead zones). Uniform water distribution across the inlet of passive treatment systems can help achieve this. In surface flow vegetated wetland systems, vegetation must line the entire width of the system to prevent short circuiting. In systems incorporating porous media, development of preferential flow paths must be prevented. Means to achieve this include maintaining surface water levels above the porous media (especially in systems with low to moderate hydraulic conductivities (e.g. $\leq 10^{-4}$ m/s), designing the system to contain high hydraulic conductivities (e.g. $\geq 10^{-3}$ m/s) and/or placing a layer of material on top of the primary porous media/substrate that contains a higher hydraulic conductivity. Although much literature states that adequate hydraulic head (e.g. 2.0 m (Watzlaf et al., 2004)) is necessary in many VFWs, bulking agents such as woodchips can be mixed with the substrate to increase hydraulic conductivity, thus reducing the minimum hydraulic head required and minimising the potential of short circuiting.

1.6.2 Tracer Studies

Tracer study analysis is commonly employed to analyse the flow characteristics of reactors and other treatment systems. Bench and pilot-scale studies are an important time to conduct these since they provide an opportunity to assess how flow hydraulics may change during the scaling-up process. Levenspiel (1999) and Kadlec and Wallace (2009) provide detailed recommendations on methods for conducting tracer studies and analysing results. The most common method employed involves spiking a reactor with an inert tracer as an instantaneous pulse with influent flow. Numerous chemical tracers have been employed to ascertain reactor and treatment system hydraulics in surface flow and subsurface porous media systems (Kadlec and Wallace, 2009). Various tracers including their advantages and disadvantages are summarised in Table 1.8. Inert tracers such as sodium bromide (NaBr), potassium bromide (KBr) and lithium bromide (LiBr) are typically recommended and most commonly applied since they are relatively inexpensive, non- reactive so good mass recoveries can be

achieved, non-toxic at concentrations used and Br is typically present at low background concentrations. The most commonly used is sodium bromide because it is often the least expensive, readily available and non-toxic. Chemical dyes are typically not recommended in systems containing organic matter due to sorption and incomplete mass recovery (Line et al., 2003; Weaver et al., 2003) and retardation such as flow three to four times slower compared with an inert Br or Li tracer (Harden et al., 2003). Kadlec and Wallace (2009) evaluated the tracer recovery from surface flow and subsurface flow wetlands. Their results indicated an average mass recovery of 85±16% (range of 37-112%) in 28 surface flow wetlands and an average mass recovery of 92±20% (range of 45-160%) in 32 subsurface flow wetlands for inert tracers (Br and Li). For the rhodamine WT (RWT) dye tracer, mass recovery averaged 75±13% (range of 60-83%) in three surface flow wetlands but was not reported for subsurface flow wetlands).

Tracer studies have not commonly been conducted on passive treatment system in mine-water treatment. Watzlaf et al. (2004) reported some channelling and dead zones or back-mixing within two ALDs based on tracer studies using sodium bromide. Busler et al. (2002) performed a series of tracer studies utilising iridescent dyes on VFWs, which indicated that the systems may be plugging. Robinson-Lora and Brennan (2009) used sodium chloride as a tracer on microcosm VFWs incorporating ChitoRem^{TM} SC-20 (20% chitin). Their reactors behaved as ideal (plug flow) reactors with low dispersion (<0.015); however, they were tubular (38.1 mm diameter X 1219 mm length) and if applied on a larger scale, would likely employ a different shape and configuration that would achieve less efficient flow.

Table 1.8: Advantages and disadvantages of tracers employed in passive mine-water treatment systems, reactors and engineered wetlands.

Tracer	Advantages	Disadvantages	Reference(s)
Chemical Dyes			
Rhodamine WT (RWT)	Relatively inexpensive; non-toxic; concentrations can be measured *in-situ* with a portable spectrophotometer	Sorption to organic matter retards its mass transport compared to water molecules and yields low mass recoveries; biodegradation and photodegradation can occur.	Harden et al. (2003); Lin et al. (2003); Holland et al. (2004); Crohn et al. (2005); Kadlec and Wallace (2009)
Fluorescein	Relatively inexpensive, typically better mass recoveries than rhodamine; concentrations can be measured *in-situ* with a portable spectrophotometer	Sorption to organic matter retards its mass transport and yields low mass recoveries; spectrophotometer required for quantification; biodegradation and photodegradation can occur.	Harden et al. (2003)
Other Iridescent Dyes	Relatively inexpensive; non-toxic; visually discernible and can be used to detect obvious short-circuiting; not present in background source water.	More qualitative than quantitative; can adsorb to gravel and organic matter retarding its mass transport and yielding low mass recoveries; biodegradation and photodegradation can occur.	Busler et al. (2002); Weaver et al. (2003); Kadlec and Wallace (2009)
Other Chemical and Biological Tracers			
Sodium Bromide (NaBr)	Relatively inexpensive; quantitative; inert so good mass recoveries typically obtained; non-toxic at concentrations used in tracer studies; typically low background Br concentrations present in waters.	Costs associated with analysis via either a bromine (Br) specific ion probe or, more quanititatively and reliably, ion chromatography (IC) or inductively coupled plasma–mass spectrometry (ICP-MS); potential density stratification.	Lin et al. (2003); Watzlaf et al. (2004); Kadlec and Wallace (2009)
Potassium (KBr or Lithium Bromide (LiBr)	Similar to NaBr; with LiBr; Li ion can also be measured (via inductively coupled plasma-optical emission spectrometry (ICP-OES) or atomic absorption spectrometry (AAS)) since it is typically inert and present at low background concentrations.	More expensive than NaBr; otherwise, similar to NaBr.	Martinez and Wise (2003); Kadlec and Wallace (2009)
Sulphur Hexafluoride (SF_6)	Quantitative; inert so good mass recoveries typically obtained	Its use under any circumstances is typically inadvisable; global warming potential in the atmosphere up to 23,900 times that of CO_2 and an estimated lifetime within the atmosphere of 3200 years	Harden et al. (2003); FLIR Systems, Inc. (2007)
Sodium Chloride (NaCl)	Cheap; can be detected with a conductivity probe	Must typically be used in high concentrations that can harm plants or bacteria (such as SRB); may be less effective in waters containing moderate to high conductivity (such as AMD or VFW effluent); density stratification likely.	Chazarenc et al. (2003); Kadlec and Wallace (2009)
Bacteriophage PRD-1 (a viral tracer)	Quantitative, inert so good mass recoveries typically obtained	Input of microorganisms	Harden et al. (2003)
Tritium Oxide (HTO)		Low recoveries	Crohn et al. (2005)

1.6.3 Application to Ideal Reactor Models

Tracer study results and results of treatability tests are often applied to chemical reaction engineering and reactor modelling, which have been discussed extensively in Levenspiel (1999). Their application to environmental systems has been discussed in Weber and DiGiano (1996), and Weber (2001), and their application to surface and subsurface flow wetlands, treating primarily municipal wastewater, has been discussed in Kadlec and Knight (1996) and Kadlec and Wallace (2009). Typical reactor models employed include continuous-mixed flow reactor (CMFR), which is sometimes referred to as the continuous-stirred tank (CSTR), tanks in series (TIS) and plug flow reactor (PFR). Neither the CMFR or PFR models represent flow hydraulics and reaction chemistry that occur in passive mine-water treatment systems (Wildeman et al., 2006). The CMFR model undersizes them, and PFR models over design them. The TIS model best represents the flow hydraulics of passive treatment systems (Wildeman et al., 2006; Kadlec and Wallace, 2009). Additionally, differences in reactor characteristics (including size, shape, depth and flow distribution) alters flow hydraulics, treatment performance and, consequently, influences modelling results.

Application of the TIS model in passive mine-water treatment design has not been reported. For VFWs treating other wastewaters, Schwager and Boller (1997) determined that their downward-flow plate reactors operated as five TIS. Tanner et al. (2002) found that each of five VFWs operated as upflow reactors (inflow at bottom and outflow at top) were modelled as two TIS (total of 10 TIS for the five tanks). Schwager and Boller (1997) found that their downward-flow plate reactors operated as an equivalent of five TIS. The average number of TIS determined from the Kadlec and Wallace (2009) summary of tracer studies was 10±7.2 (median of 7.8; range of 2.5-34) for 32 subsurface flow wetlands was and 4.2±2.8 (median of 3.8; range of 0.3-11) for 30 surface flow wetlands using Li or Br inert tracers.

Treatability tests are required to determine reaction rate constants. Kadlec and Wallace (2009) stated that reaction rate constants were typically variable for wastewaters containing a mixture of contaminants such as the AMD used in this study. This occurs because individual components of mixtures are removed at different rates and, therefore, individually contain different removal rate constants (Crites and Tchobanoglous, 1998; Tchobanoglous et al., 2000; Shepherd et al., 2001; Kadlec, 2003). Reaction rates also decline at longer HRTs due to the removal of some of the contaminant concentrations during the early stages of the HRT (Kadlec and Wallace, 2009). Under these circumstances, the relaxed TIS model can be employed, which is essentially the same as the TIS model except the number of TIS and reaction rates become fitting parameters to minimise error between the empirical and modelled results.

2. Variability of Stockton Coal Mine Acid Mine Drainage Chemistry and Its Feasibility for Passive Treatment

Thirteen AMD sites, consisting of seeps emanating from waste rock dumps and associated sediment ponds, were monitored at Stockton Coal Mine (Figures 1.2 and 2.1) during the initial stages of this research. The objective of this monitoring was to analyse water chemistry to characterise and quantify contaminants of concern and delineate their spatial and temporal variability across the mine site. The primary contaminants of concern included acidity, metals (primarily Fe and Al with Cu, Ni, Zn, Cd, Pb and As of lesser concern) and sulphate. Additional water chemistry parameters analysed included temperature, pH, DO, Eh, conductivity, TSS, turbidity and cations (Ca, Mg, Na and K). Metal, acidity and sulphur loading rates (the product of concentration and flow rate) were also calculated, which denote quantities impacting receiving water bodies over a period of time.

Another objective of analysing water chemistry results was to evaluate the feasibility of passive treatment systems at Stockton Coal Mine for neutralising acidity, sequestering metals and removing sulphate. These results were also compared with other MIWs from coal mines throughout New Zealand and the U.S.A., including sites where passive treatment has been implemented. One AMD seep was chosen as a candidate site for conducting more extensive monitoring and subsequent studies pertaining to the design and performance of passive treatment systems. Other factors including flow rates, seep location, site topography, available treatment area, likelihood for on-site mine disturbances that could impact water chemistry or downstream passive-treatment systems and available logistical support were also considered when choosing the candidate site. This was because passive treatment systems typically incur larger footprints than active treatment systems, and their effectiveness can be compromised by changing water chemistry resulting from upgradient land disturbances.

Geochemical modelling was also conducted to determine the saturation states of numerous minerals within the AMD seeps analysed. These results theoretically quantify the extent that minerals would continue to dissolve (or precipitate). The results provided an indication of possible minerals from which the AMD was derived and potential minerals that could precipitate.

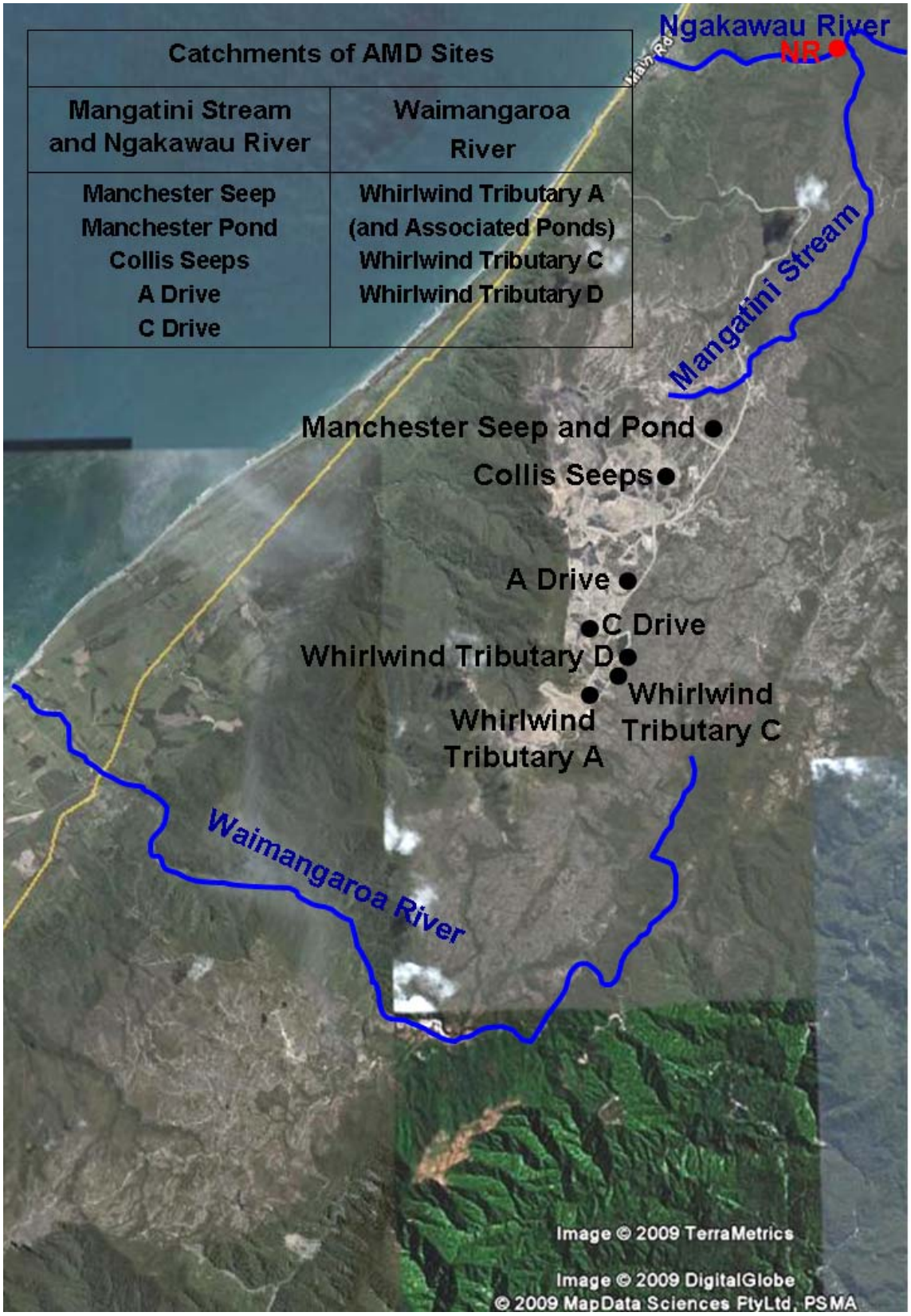

Figure 2.1. Location of AMD seeps sampled at Stockton Coal Mine and the catchments they drain into including the Waimangaroa River, Mangatini Stream and Ngakawau River (aerial photo from Google Earth (2009)). NR represents the off site monitoring location for discharge compliance.

2.1 Acid Mine Drainage Seep Site Descriptions

The AMD seeps sampled as part of this study are summarised in Table 2.1. The summaries include seep name and/or sampling location, delineated catchment, sampling regime and a brief rationale of the feasibility of employing passive treatment systems at each sampling location. The AMD sampling locations and their receiving catchments are shown in Figure 2.1.

Table 2.1: Summary of AMD seeps sampled.

Seep Name /Sampling Location	Catchment	Sampling Regime	Explanation Regarding Feasibility for Passive Treatment Systems
Whirlwind Tributary A (Seep into Pond A)	Waimangaroa River	Monthly from January-March 2006	Unfeasible due to future mining proposed in project area which could contribute to variable water chemistry and fluctuating flow.
Whirlwind Tributary A (Outlet of Pond A1)			
Whirlwind Tributary A (Outflow from Pond A2)			
Whirlwind Tributary C			Unfeasible due to the hydrogeology of the potential treatment areas, their proximity to an AMD-impacted dam and equipment access issues.
Whirlwind Tributary D			
A Drive	Mangatini Stream / Ngakawau River	Once (May 2006)	Unfeasible due to inadequate treatment area.
C Drive Seep 1		Once (May 2006)	Unfeasible due to rehabilitation activities and sedimentation at the time of sampling.
C Drive Seep 2			
Collis Seep 1		Approximately monthly from May to September 2006	Unfeasible due to extremely high concentrations of acidity, sulphate and metals and inadequate treatment area.
Collis Seep 3			
Downstream of Collis Seeps			
Manchester Seep		Monthly from May 2006-February 2007	Seep chosen to conduct subsequent research pertaining to passive treatment due to acceptable (moderate) acidity, sulphate and metal concentrations and adequate treatment area *in-situ* to conduct pilot-scale treatability tests.
Outlet of Manchester Seep Pond		Monthly	Sampling discontinued to reduce sampling costs associated with the project.

The initial sites sampled as part of this study included Whirlwind Tributaries A, C and D, which were sampled monthly from January to March 2006 and drain into the Waimangaroa River. Whirlwind Tributary A (Figures B.1-B.4 in Appendix B) was deemed an unfeasible candidate site for passive treatment due to mining activities planned in its vicinity. The complex hydrogeology associated with Whirlwind Tributaries C and D (Figures B.5-B.6), their proximity to an AMD-impacted dam and challenging equipment access deemed these seeps unsuitable for conducting passive treatment trials.

The A and C Drive Seeps were sampled once during May 2006. The A Drive Seep (Figures B.7 and B.8) was excluded as a candidate site due to minimal treatment area in the vicinity. C Drive (Figures B.9 and B.10) was excluded because the area underwent rehabilitation efforts during this study, which was not conducive to the project timeframe.

The Collis Seeps consisted of three seeps (Figures B.11-B.12). Because of minimal and intermittent flow, Collis Seep 2 was not monitored as part of this study. Monitoring of the Collis Seeps was terminated due to acidity, sulphate and metal concentrations (e.g. excessive dissolved Fe concentrations as visibly seen in Figure B.13) above those recommended in passive treatment systems, coupled with inadequate treatment area based on the calculated metal loading rates.

The acidity, sulphate and metals concentrations measured from the Manchester Seep (Figures B.14-B.15) were conducive for passive treatment. The seep water was also not expected to be influenced by present or future mining activities. Ample treatment area was available to construct pilot or full-scale treatment systems. Therefore, Manchester Seep was chosen as the most suitable research site for evaluating the performance and feasibility of passive-treatment systems to neutralise acidity, remove sulphate and immobilise metals from its AMD. Monthly chemistry and flow monitoring was conducted for ten months at this site to assess temporal water chemistry and flow variations over all seasons.

2.2 Sampling and Analytical Methods

2.2.1 Sample Collection and Methodology

Surface water and sediment samples were collected following applicable criteria denoted in the Australian and New Zealand Environment and Conservation Council (ANZECC) Water Quality Guidelines (2000). Samples were collected from surface water either directly in method-specified containers or from a decontaminated syringe and then transferred directly into method-specified containers. Sample bottles were either provided by RJ Hill Laboratories Limited, an International Accreditation New Zealand (IANZ) certified lab, or were HDPE containers from the University of Canterbury Environmental Engineering Laboratory. Sample bottles, syringes and associated tubing, digital pipette tips and components of filtering apparatuses (with exception of disposable filters) sourced at the University of Canterbury were decontaminated with an initial washing in an Alconox® solution followed by a tap water rinse, deionised water rinse, a 24-72 hour immersion in a five-percent nitric acid (HNO_3) solution followed by a tap water rinse and a final deionised water rinse. All samples were collected head-space free, with exception of those for TSS, and were chilled at 2-6^{o}C immediately upon collection until the time of analysis following appropriate criteria specified in APHA (1998) and/or APHA (2005). Water quality parameters measured using portable probes (e.g. temperature, pH, conductivity, DO and Eh) were measured directly *in-situ* with data recorded when readings stabilised. Turbidity samples were collected directly into instrument specific cuvettes and

analysed immediately upon collection. Samples collected for Fe^{2+} analysis were collected initially with a digital pipette and diluted with deionised water to the appropriate volume in instrument specific glass cylinders. Sediment samples from the Manchester Pond were collected into method specified HDPE containers provided by RJ Hill Laboratories Limited using decontaminated gloves.

2.2.2 Calibration and Operation of Portable Water Quality Instruments

Water quality parameters including temperature, pH, conductivity, DO, Eh, turbidity and Fe^{2+} were measured using pre-calibrated portable water quality instruments. Instruments were calibrated just prior to sample collection using fresh standards and validated to ensure they maintained calibration following measurements. Sample pH was measured using a YSI Model 60 pH meter field calibrated with pH 4.01 and 7.00 standards (and pH 10.00 standard when applicable) and checked with a pH 1.68 standard. Conductivity was measured with a Hach sension 156 multiparameter meter field calibrated to a 0.01 M (1413 µS/cm at 25°C) potassium chloride (KCl) solution and checked with a 0.1 M (12,890 µS/cm at 25°C) KCl solution. Specific conductance and TDS were calculated from conductivity and temperature measurements using Equations 2.1 and 2.2 (from Tchobanoglous and Schroeder (1985)), respectively.

$$\text{Specific Conductance } (25^{o}C) = \text{Conductivity} / (1+TC * (T-25)) \quad \textbf{(2.1)}$$

where:

TC represents a constant ≈ 0.0191; and
T represents temperature in °C.

$$\text{TDS (mg/L)} \approx \text{Specific Conductance (µS/cm)} * (\text{a constant between 0.55 and 0.70}) \quad \textbf{(2.2)}$$

The constant commonly used for Equation 2.2 is 0.6563, which is representative of a pure KCl solution (APHA, 1998). Salinity was also estimated from conductivity (Standard Methods 2520B, 1998). The value is comparable to that of TDS but standardised at a temperature of 15°C in a similar manner to specific conductance being a standardised value of conductivity at 25°C. Dissolved oxygen was measured utilising a YSI 550A DO instrument. Percent DO saturation was adjusted to account for temperature, salinity and barometric pressure as specified in YSI Inc. (1999). The DO meter was calibrated with oxygen-saturated water in the laboratory prior to transport to the research site and checked with oxygen-saturated water on arrival back from the field. Dissolved oxygen was recalibrated on site in the instrument's calibration chamber maintained at 100% water-saturated air. Barometric pressure was measured using a Silva Alba Windwatch equipped with a barometer. Oxidation-reduction potential was measured with a YSI pH 100 portable instrument equipped with an ORP probe and values standardised to a hydrogen electrode (Eh). Calibration was validated with

solutions of quinhydrone saturated pH 4 and pH 7 solutions. Turbidity measurements were performed using a Hach Model 2100P portable turbidimeter. Calibration was performed with either Hach StablCal® calibration standards or freshly prepared formazin standards (<0.1, 20, 100 and 800 NTU). Calibration was performed when validation exceeded five percent of a standard. Calibration validation was either determined using Hach StablCal® calibration standards or three Gelex® standards whose values were determined during instrument calibration. Ferrous iron was measured following HACH Method 8146 using 1,10 phenanthroline powder pillows and a Hach Spectrophotometer at 510 nm (Hach Company, 2003). Samples were collected with pre-calibrated digital titrators and diluted to 25 mL in instrument specific glass cuvettes.

2.2.3 Analytical Methods

Most samples collected for analytical analysis were analysed by RJ Hill Laboratories Limited following accredited procedures. Exceptions included TSS and acidity (and alkalinity), which were typically analysed at the University of Canterbury Environmental Engineering Laboratory.

Water samples were analysed for metals using inductively coupled plasma–mass spectrometry (ICP-MS). Dissolved metals were analysed by APHA Method 3125B (APHA, 1998). Total metals were analysed by APHA Method 3125B with nitric acid digestion (APHA, 1998). Metal samples were preserved with 1:1 nitric-acid to reduce pH to <2.0. Dissolved metal samples were filtered during sample collection with 0.45 μm nitrocellulose filters encapsulated in a Pall 47 mm polycarbonate in-line filter holder. All components of the Pall filters were decontaminated by washing in an Alconox solution followed by a tap water rinse, deionised water rinse, a 24-72 hour immersion in a five-percent nitric acid solution followed by a tap water rinse and a final deionised water rinse. Ferric iron was calculated as the difference between total Fe and Fe^{2+} (analysed *in-situ* via HACH Method 8146). Sediment samples for total metals were digested with nitric and hydrochloric acid and analysed via ICP-MS following method US EPA 200.2.

Total sulphur was determined using inductively coupled plasma optical emission spectrometry (ICP-OES). Total sulphur concentrations were calculated as mg/L of sulphate assuming 100% of the sulphur was present in the oxidised state based on high DO concentrations and Eh readings. Calcium, Mg, Na and K samples were collected in unpreserved HDPE containers, filtered by RJ Hill Laboratories Limited and analysed following APHA Method 3125B (APHA, 1998). Hardness was calculated using Equation 2.3 where C_{Ca} and C_{Mg} represent Ca and Mg concentrations, respectively. Total suspended solids were measured following American Public Health Association APHA Method 2540D (APHA, 1998).

$$\text{Hardness (mg/L as } CaCO_3) = 50.045(C_{Ca}/20.04 + C_{Mg}/12.153) \quad \textbf{(2.3)}$$

Acidity (pH 3.7), total acidity (pH 8.3) and alkalinity (pH 4.5) were either analysed by RJ Hill Laboratories Limited or at the University of Canterbury Environmental Engineering Laboratory. Alkalinity (pH 4.5) was analysed using a modified version of APHA Method 2320B (APHA, 2005). Acidity (pH 3.7) and total acidity (pH 8.3) were analysed using a modified version of APHA Method 2310B (APHA, 2005). Sample pH endpoints for titrations performed by RJ Hill Laboratories Limited were determined using a radiometer autotitrator and method specified indicators. Alkalinity (pH 4.5), acidity (pH 3.7) and total acidity (pH 8.3) were determined from titration curves for samples analysed at the University of Canterbury Environmental Engineering Laboratory. Titrants used were either ~0.02 N or ~0.10 N NaOH. Hot peroxide treatment was performed on all AMD samples to oxidise Fe by adding five drops of 30% hydrogen peroxide (H_2O_2) and boiling the solution in a covered Erlenmeyer flask for two to three minutes. Samples were allowed to cool to room temperature prior to titration. An EDT Instruments RE357 TX pH meter calibrated with pH 4, 7 and 10 standards was used to measure pH when determining titration curves. Calculated acidity was determined using Equation 2.4 where C_{Fe}^{2+}, C_{Fe}^{3+}, C_{Al}, C_{Cu}, C_{Ni}, C_{Zn} and C_{Mn} represent their respective metal concentrations in mg/L (modified from Watzlaf et al., 2003).

$$\text{Total Calculated Acidity (mg/L as } CaCO_3) = 50.045(2\,C_{Fe}^{2+}/55.85 + 3\,C_{Fe}^{3+}/55.85 + 3\,C_{Al}/26.98 + 2\,C_{Cu}/63.55 + 2\,C_{Ni}/58.71 + 2\,C_{Zn}/65.38 + 2\,C_{Mn}/54.94 + 1000(10^{-pH})) \quad \textbf{(2.4)}$$

These metals typically contributed over 99.6% of metal acidity present in samples. The metal acidity represents the equivalent contribution of metals to acidity (Equation 2.4 excluding the $1000(10^{-pH})$ term), whereas proton acidity represents the contribution of protons (H^+ cations) to acidity.

2.2.4 Flow Measurements

A limited number of samples were analysed from AMD sources deemed unfeasible to construct pilot-scale BGCRs. Consequently, infrastructure was not implemented at these locations to accurately measure flow. Flow was monitored monthly using the bucket and stopwatch method to ascertain flow rates emanating from the Manchester and Collis Seeps. A minimum of five replicates were taken and averaged to determine mean flow during each flow measurement sampling event. Flow was measured from the outlet culvert of Manchester Pond (Figures B.14-B.15). Flow from the Collis Seeps (Figures B.11-B.12) were either measured from the drainage ditch immediately downstream of Seep 3 or from the PVC collection pipes collating Seeps 1 and 3. When flow was measured from the PVC collection pipes the flow from Seeps 1 and 3 were combined to determine total flow.

2.3 New Zealand Water Quality Guidelines

The Australia and New Zealand Environmental and Conservation Council (ANZECC) water quality guidelines (ANZECC, 2000) present guideline "trigger values" that represent concentrations of various contaminants that may be deleterious to the biota in receiving freshwater aquatic ecosystems. The trigger values represent generic effects-based guidelines and are not legally binding compliance

levels. Separate guideline values are established at levels of protection including 80%, 90%, 95% and 99%, which signify the percentage of aquatic species expected to be unaffected. The 80% level of protection typically applies to the most disturbed ecosystems such as mine sites; however, they often do not represent site-specific ecotoxicity since most are established based on ecotoxicity tests performed on species present outside of New Zealand and, therefore, only represent a first indication of whether or not ecosystem perturbation is probable (Niyogi and Harding, 2007; O'Halloran et al., 2008). ANZECC (2000) includes algorithms for calculating hardness modified trigger values (HMTV) for Cd, Cu, Pb, Ni and Zn based on water hardness (Table 2.2), typically of the receiving water body. The ANZECC guidelines are also most applicable to the dissolved metal fraction since this proportion is considered bioavailable (ANZECC, 2000). ANZECC (2000) states that there is "insufficient data" to establish trigger values for Fe and Al at a pH<6.5. Therefore, application of ecotoxicological studies using local ecology to establish site-specific thresholds are typically preferred and deemed more appropriate. The current community agreed discharge compliance level from the Stockton Coal Mine research site is stipulated to achieve pH>4.0 and an Al concentration <1 mg/L off the mine site boundary (sample location NR at the confluence of the Mangatini Stream and Ngakawau River; Figure 2.1)) 99% of the time based on localised ecotoxicological data such as that reported in Niyogi and Harding (2007) and O'Halloran et al. (2008). To achieve the Al concentration consent condition, pH≥4.7 is typically targeted to precipitate Al. A more detailed description of international ecotoxicity and compliance thresholds for Fe and Al are discussed in Chapter 5.

Table 2.2: Hardness-dependent algorithms for calculating modified ANZECC trigger values in freshwater where HMTV represents the hardness modified trigger value, TV signifies the standardised trigger value at a hardness of 30 mg/L as $CaCO_3$ and H denotes hardness in units mg/L as $CaCO_3$.

Metal	Hardness Dependent Algorithm
Cd	$HMTV = TV(H/30)^{0.89}$
Cu	$HMTV = TV(H/30)^{0.85}$
Pb	$HMTV = TV(H/30)^{1.27}$
Ni	$HMTV = TV(H/30)^{0.85}$
Zn	$HMTV = TV(H/30)^{0.85}$

The ANZECC guidelines also list water quality guidelines for recreational purposes with the primary purpose of protecting human health. The primary objectives of these guidelines are to avoid skin irritation and accidental ingestion of up to 100 mL of water during a normal swimming session. The Ngakawau and Waimangaroa Catchments do not include any water bodies that contain commonly used swimming spots so the likelihood of accidental ingestion is minimal. The most likely human contact would be incidental contact primarily by whitebait fisherman. A summary of ANZECC ecotoxicological trigger values and water quality guidelines for recreational purposes for applicable metals and also including sulphate and pH are summarised in Table 2.3. The trigger values for a freshwater ecosystem are typically more stringent than the guideline values for recreational purposes with exception of Mn and the presence of guideline values for Fe and Al. Hardness values of 30 mg/L

as $CaCO_3$ and 90 mg/L as $CaCO_3$ were assumed to determine HMTVs for hardness-dependent metals. These are generally representative of the hardness values measured from the AMD seeps and associated sediment ponds (median values ranged from 3.07 mg/L as $CaCO_3$ (Whirlwind Tributary Pond A2) to 70.6 $CaCO_3$ (Manchester Pond)) excluding the Collis Seeps (hardness values ≥1420 mg/L as $CaCO_3$). Hardness modified trigger values increase with increasing hardness, which has implications for Stockton Coal Mine since the current treatment of AMD on site by ultrafine limestone results in elevated hardness (average of 680 mg/L as $CaCO_3$ (range of 59-1044 mg/L as $CaCO_3$) from the Mangatini sump treated decant).

Table 2.3: "Trigger values" established in ANZECC (2000) for dissolved metals at various levels of protection and hardness values for a freshwater ecosystem. Freshwater trigger values for As are listed separately for its two cationic states, whereas the As guideline value for recreational purposes considers the summation of each cationic state. Only Cu, Ni, Zn, Cd and Pb contain hardness dependent algorithms. The 80% level of protection is typically most applicable to highly-disturbed ecosystems.

Water Quality Parameter	Trigger Values for a Freshwater Aquatic Ecosystem (mg/L)				Guidelines for Recreational Purposes (mg/L)
	Level of Protection				
	80%	90%	95%	99%	
	Hardness = 30 mg/L as $CaCO_3$ (or Non-Hardness Dependent)				
Fe	ID	ID	ID	ID	0.300
Al	ID	ID	ID	ID	0.200
Cu	0.0025	0.0018	0.0014	0.0010	1.00
Ni	0.0017	0.0013	0.0011	0.0008	0.100
Zn	0.030	0.015	0.0080	0.0024	5.00
Cd	0.0008	0.0004	0.0002	0.00006	0.005
Pb	0.0094	0.0056	0.0034	0.001	0.050
As^{3+}	0.360	0.094	0.024	0.001	0.050
As^{5+}	0.140	0.042	0.014	0.0008	
Mn	3.6	2.5	1.9	1.2	0.100
Sulphate	n/d	n/d	n/d	n/d	400
pH	n/d	n/d	n/d	n/d	6.5-8.5
	Hardness = 90 mg/L as $CaCO_3$				
Cu	0.0063	0.0045	0.0035	0.0025	NA
Ni	0.0043	0.0033	0.0028	0.002	NA
Zn	0.075	0.038	0.020	0.0060	NA
Cd	0.0022	0.0011	0.0005	0.0002	NA
Pb	0.038	0.022	0.014	0.004	NA

ID, insufficient data; NA, non-applicable; n/d, not defined

2.4 Water Chemistry Results

Results from monitoring numerous AMD seeps during this study indicated spatial and temporal variability in water chemistry at Stockton Coal Mine. A summary of water chemistry at each of the sampling locations (Table 2.1) is collated in Figures 2.2-2.8 and detailed in Tables B.1-B.11 (Appendix B). The figures compare individual contaminants across sampling locations. The primary contaminants from all seep waters were typically metals, acidity and sulphate, which are common with MIWs impacted by disturbances of pyritic overburden material and coal containing sulphur (Skousen,

1996; Rose and Cravotta, 1998; Watzlaf et al., 2004). Low pH values (ranging from 2.04 (Collis Seep 1) to 3.80 (Whirlwind Tributary C)) were also prevalent in AMD seep water resulting from acidity.

2.4.1 Metals

The primary metal contaminants were consistently Fe and Al, which accounted for >95% of metal acidity (e.g. calculated from Equation 2.4) at each sampling location. Secondary metal contaminants included Cu, Ni, Zn, Cd, Mn, Pb and As. These metals were commonly measured at concentrations exceeding the 80% ANZECC trigger values for a freshwater aquatic ecosystem with exception of limited exceedances measured for Mn, Pb and As.

Dissolved metal concentration ranges from each sample location are displayed as hanging bar graphs in the following figures: Figure 2.2) Fe and Al; Figure 2.3) Cu and Ni; Figure 2.4) Mn and Zn; and Figure 2.5) Pd, Cd and As. The x-axis delineates the sample locations, while the y-axis represents metal concentrations (on a logarithmic scale). Horizontal black lines within the bar graphs represent mean metal concentrations when $n \leq 2$ and median concentrations when $n \geq 3$. Bolded continuous horizontal lines delineate ANZECC trigger values for protection of 80% species with exception of Figure 2.1, which displays the Al compliance concentration. There is currently no ANZECC trigger value or compliance target for Fe. For metals where hardness dependent algorithms are established (Cd, Cu, Pb, Ni and Zn), trigger values are shown assuming hardness values of 30 (low hardness) and 90 (moderate hardness) mg/L as $CaCO_3$. With exception of the Collis Seeps, which showed extremely high hardness values (1180-1710 mg/L as $CaCO_3$), average hardness (Tables B.1-B.11 in Appendix B) ranged from 6.99 mg/L as $CaCO_3$ (Whirlwind Pond A2) to 75.5 mg/L as $CaCO_3$ (Manchester Pond). Based on these hardness values, metal concentrations presented in Figures 2.3-2.5 were compared to HMTVs calculated assuming 30 mg/L as $CaCO_3$ and 90 mg/L as $CaCO_3$.

Metal concentrations differed quite extensively at the seeps monitored. For example, dissolved Fe concentrations measured at seep locations ranged from 0.31 mg/L (Whirlwind Tributary C) to 1430 mg/L (Collis Seep 1), which represents a difference of over three orders of magnitude. Dissolved Al ranged from 3.22 mg/L (Whirlwind Tributary C) to 627 mg/L dissolved Al (Collis Seep 1), a difference exceeding two orders of magnitude. Of the other metals analysed, Zn (Figure 2.4), Cu and Ni (Figure 2.3) were the most common to exceed 80% ANZECC trigger values. Lead (Figure 2.5) was only measured at a concentration exceeding the 80% ANZECC trigger value from one sample collected from Manchester Seep. Arsenic (Figure 2.5) was only measured at elevated concentrations from Collis Seep 1 and downstream from the Collis Seeps, whereas Cd (Figure 2.5) exceeded the 80% ANZECC trigger value from the Collis Seeps and Manchester Seep. In general, metal concentrations were greatest at the Collis Seeps followed by the Manchester Pond and Seep. The lowest metal concentrations were measured from Whirlwind Tributary Pond A2, likely due to dilution from non-AMD influenced surface water runoff. The high metal concentrations at the Collis Seeps were likely a

result of recent rehabilitation earthworks, which exposed pyrite containing overburden to atmospheric oxygen resulting in the release of proton and metal acidity.

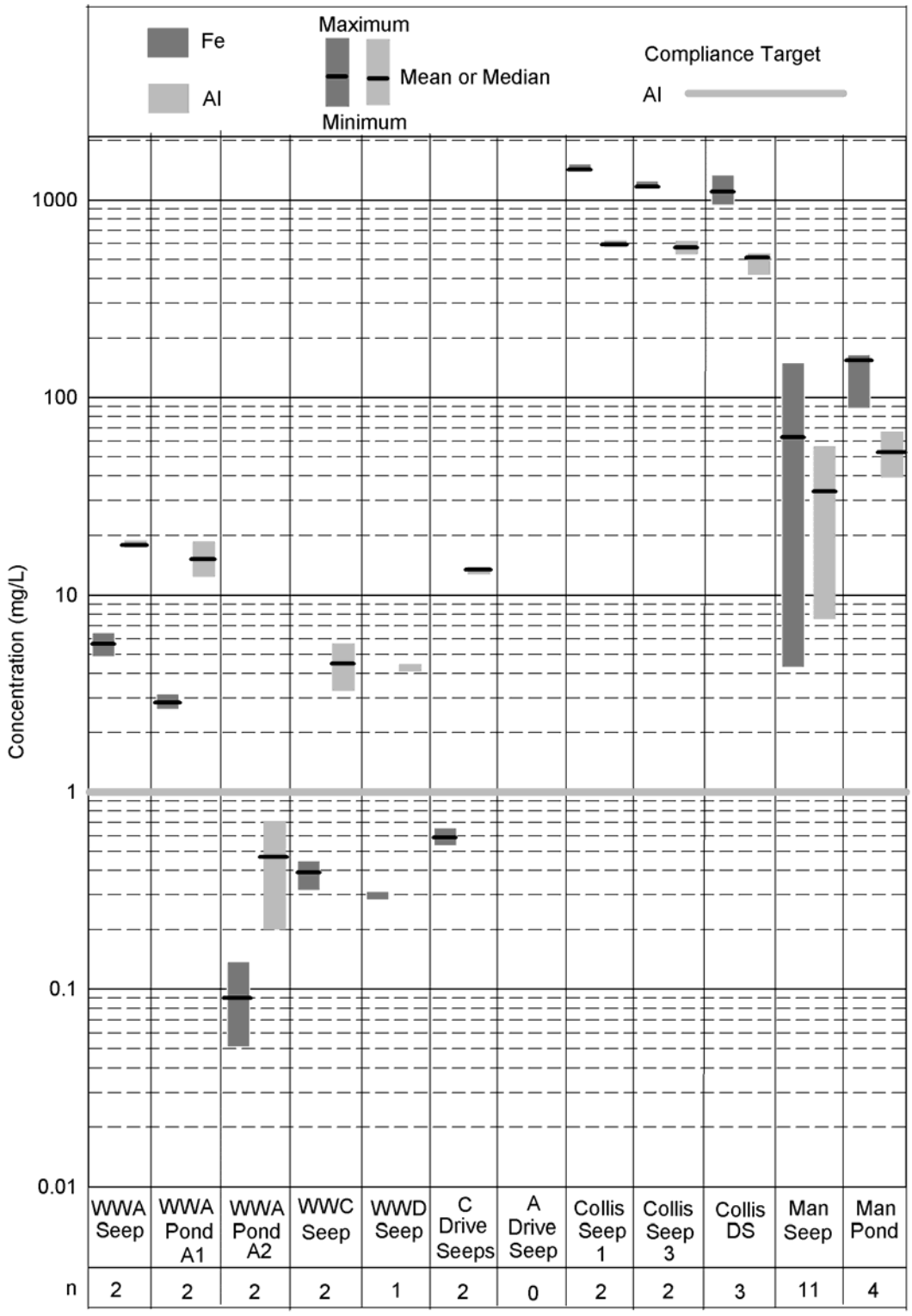

Figure 2.2. Dissolved Fe and Al concentration ranges from AMD sample locations at Stockton Coal Mine. Mean concentrations are displayed when n≤2. Median concentrations are displayed when n≥3.

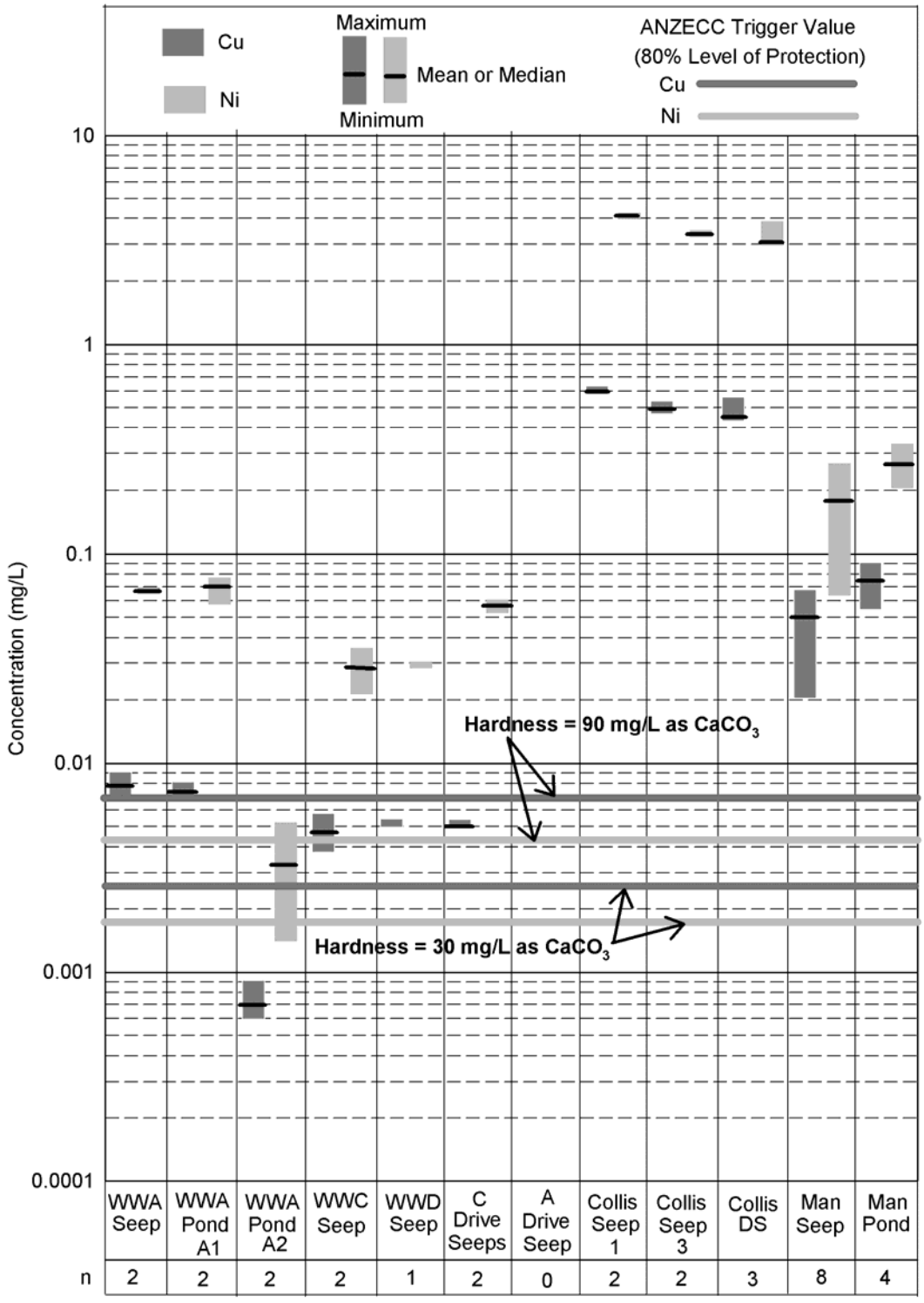

Figure 2.3. Dissolved Cu and Ni concentration ranges from AMD sample locations at Stockton Coal Mine. Mean concentrations are displayed when n≤2. Median concentrations are displayed when n≥3. The ANZECC trigger values for Cu and Ni are hardness dependent with hardness values incorporating the typical ranges measured from AMD (excluding the Collis Seeps).

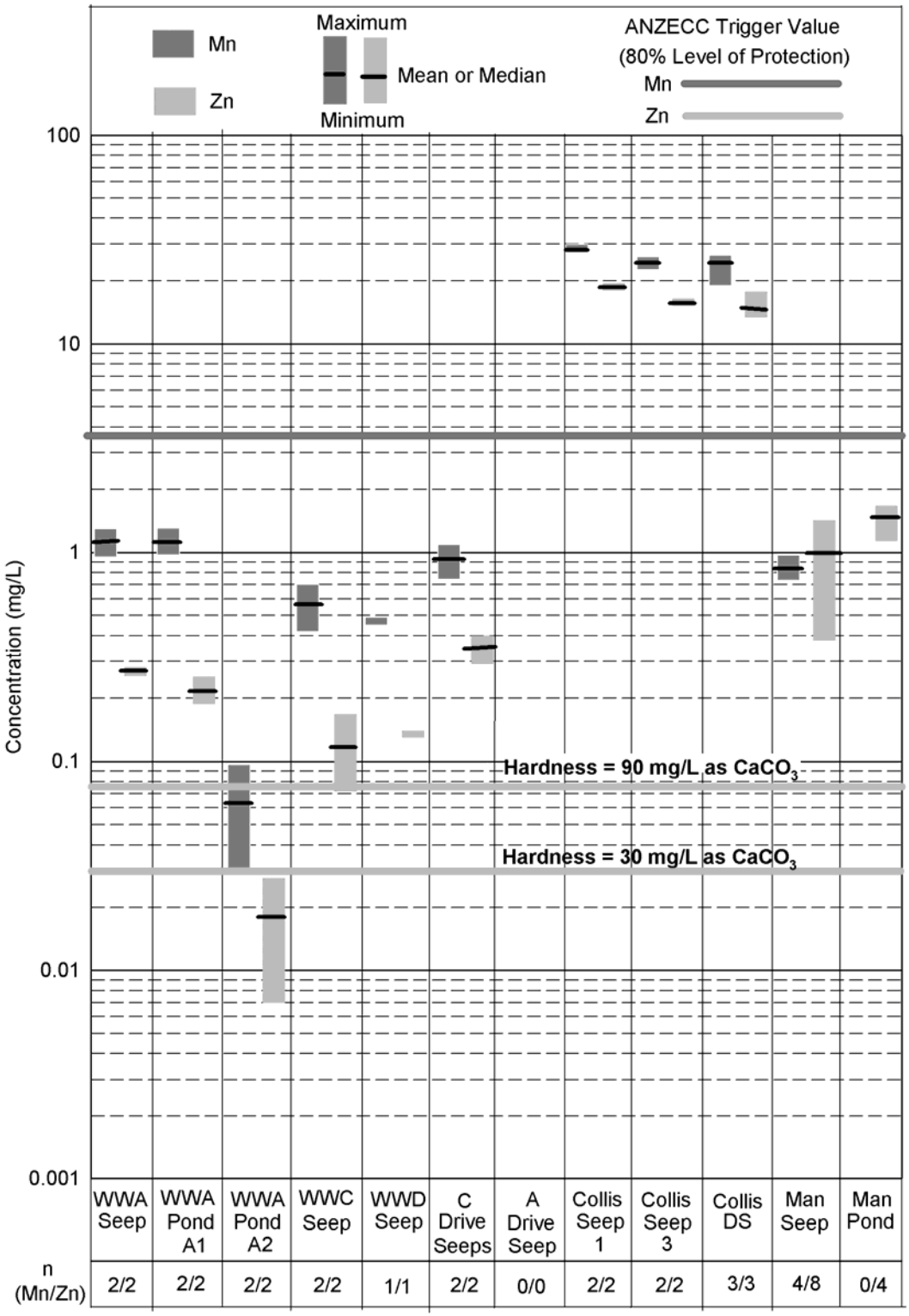

Figure 2.4. Dissolved Mn and Zn concentration ranges from AMD sample locations at Stockton Coal Mine. Mean concentrations are displayed when n≤2. Median concentrations are displayed when n≥3. The ANZECC trigger value for Zn is hardness dependent with hardness values incorporating the typical ranges measured from AMD (excluding the Collis Seeps).

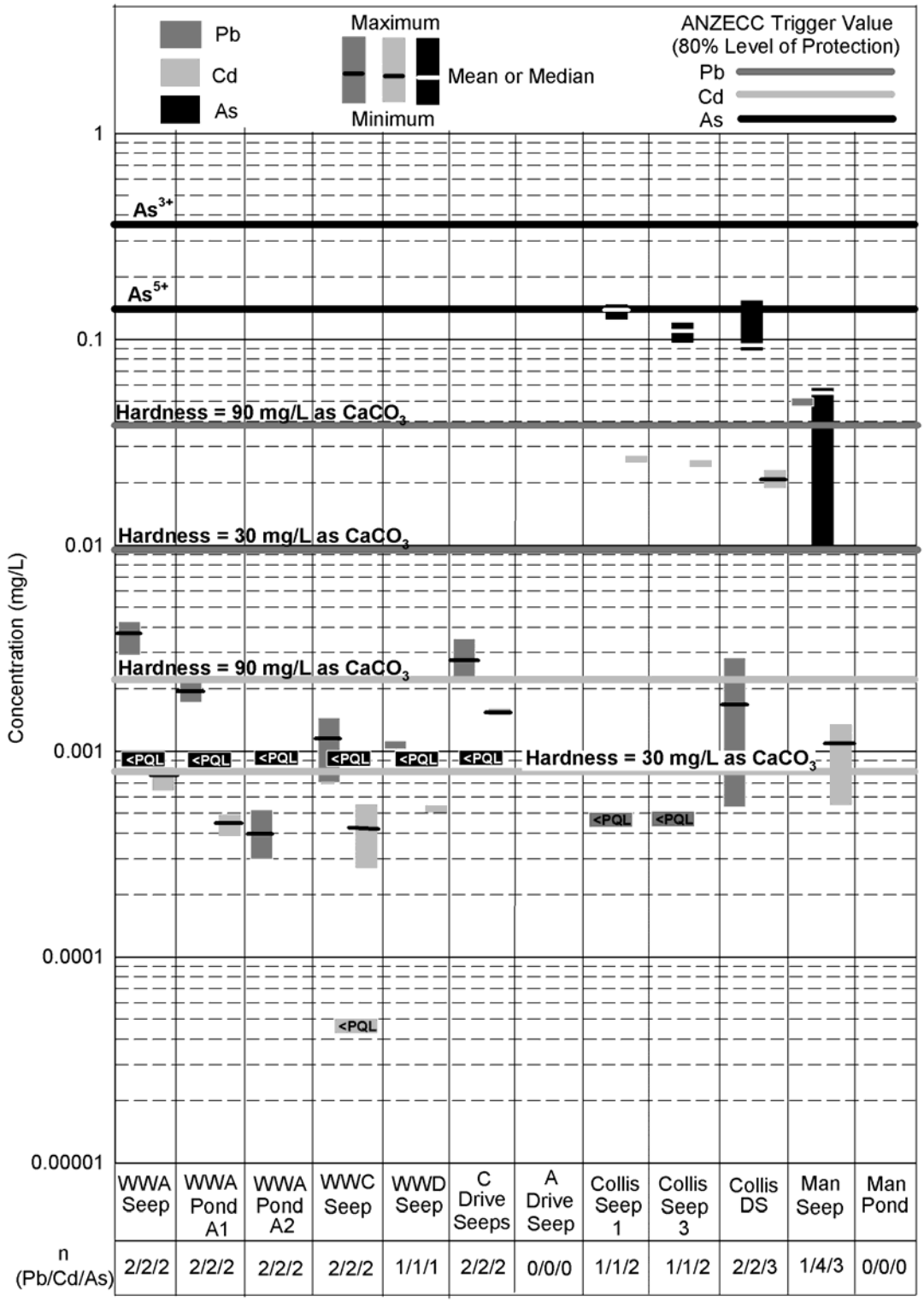

Figure 2.5. Dissolved Pb, Cd and As concentration ranges (hanging bar graphs) from AMD sample locations at Stockton Coal Mine. Mean concentrations are displayed when n≤2. Median concentrations are displayed when n≥3. The ANZECC trigger values for Cd and Pb are hardness dependent with hardness values incorporating the typical ranges measured from AMD (excluding the Collis Seeps). The PQLs were 0.001 mg/L As, 0.0005 mg/L Pb and 0.00005 mg/L Cd.

2.4.2 Acidity

Acidity represents the capacity of water to react with a strong base to a designated pH (APHA, 2005). In the analysis of AMD, acidity (pH 3.7) gives a quantitative indication of the acidity associated with Fe. Total acidity (pH 8.3) and calculated acidity (Equation 2.4) also include the influences of other metals, principally Al in this study, on mineral acidity. A summary of calculated acidity, total acidity (pH 8.3) and acidity (pH 3.7) are displayed as hanging bar graphs in Figure 2.6. Calculated acidity generally corresponded closely to total acidity (pH 8.3), during this study, with values typically within 5% of each other. This supports results presented by Cravotta III and Kirby (2004) and Hedin (2006b) who concluded that calculated and measured acidity values were comparable and could be used as a reliable QA/QC check.

Acidity values between AMD sample locations differed by approximately three orders of magnitude. Acidity values followed similar trends with Fe, Al and sulphate concentrations. Although there were no samples from A Drive that were analysed for metals, acidity (pH 3.7) and total acidity (pH 8.3) concentrations from one sampling event indicated that A Drive AMD was most similar to Whirlwind Tributary A, but possibly contained higher Al concentrations (based on higher total acidity (pH 8.3)) and lower Fe concentrations (based on lower acidity (pH 3.7)).

Metal acidity contributed substantially more to calculated (and total) acidity than proton acidity. A summary of the percent contribution of proton acidity to calculated acidity from the AMD is summarised in Table 2.4.

Table 2.4: Percent contribution of proton acidity to calculated acidity from AMD sample locations at Stockton Coal Mine.

AMD Sample Location	Percent Contribution of Proton Acidity to Calculated Acidity	
	Median	**Range**
Manchester Seep	19.3	11.6-54.8
Manchester Pond	15.7	10.5-17.5
Collis Seeps (1, 3 and Downstream Samples)	4.59	4.20-6.86
C Drive Seeps	10.1	9.78-10.4
Whirlwind Tributary A, C and D Seeps and Whirlwind Pond A1	24.2	21.9-29.0
Whirlwind Pond A2	57.6	49.7-65.4

Iron and Al were the major contributors to metal acidity (excludes proton acidity) accounting for over 95% from all samples analysed as part of this study (≥98.7% for the Collis Seeps and ≥99.0% for the Manchester Seep). Iron, Al and H^+ accounted for ≥96.6% of calculated acidity during this study (≥98.8% for the Collis Seeps and ≥99.2% for the Manchester Seep).

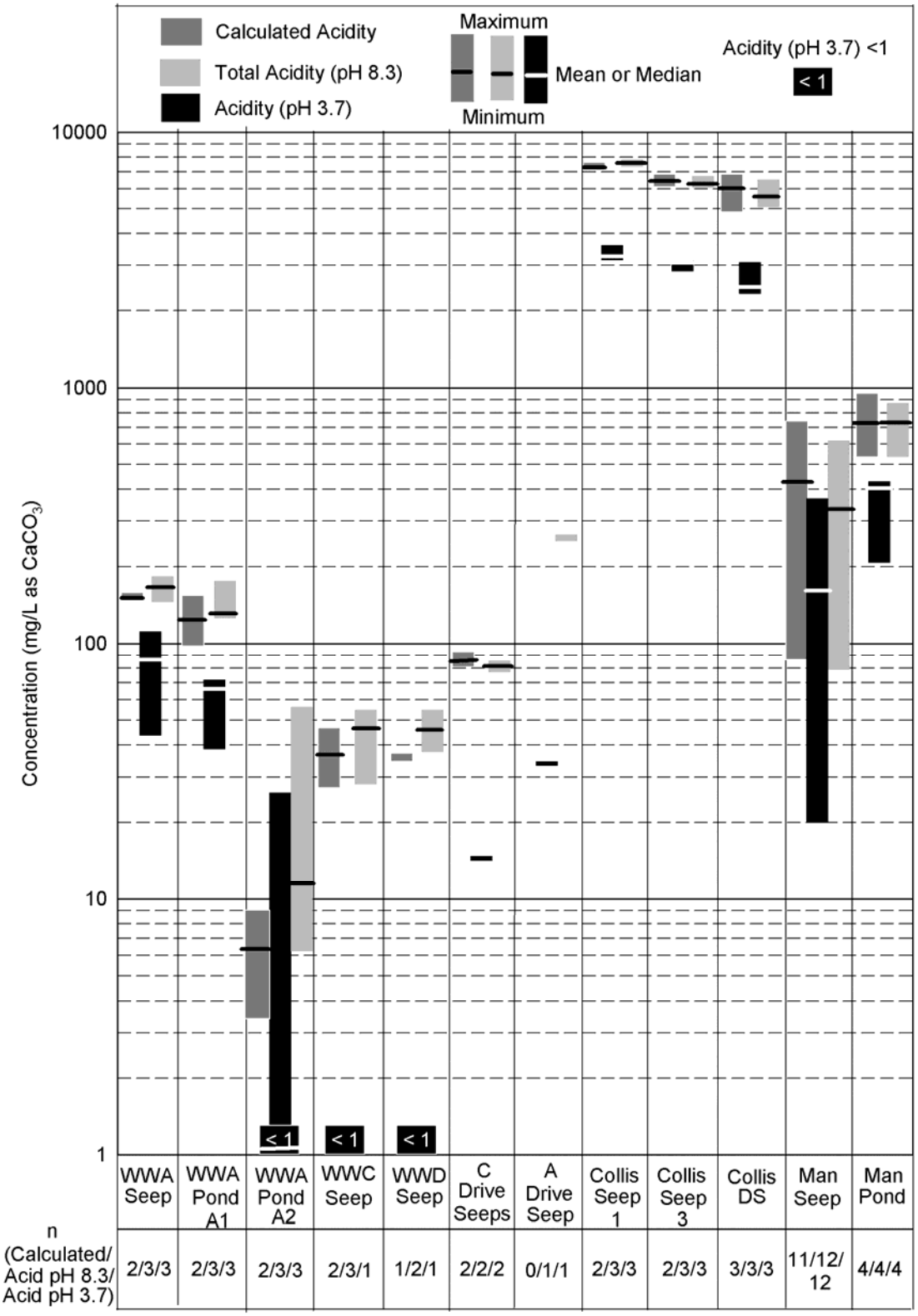

Figure 2.6. Acidity ranges from AMD sample locations at Stockton Coal Mine. Mean concentrations are displayed when n≤2. Median concentrations are displayed when n≥3.

2.4.3 Sulphate

A summary of sulphate concentration ranges are displayed as hanging bar graphs in Figure 2.7 along with specific conductance (Section 2.4.4). Sulphate concentrations essentially followed the same trends as metal concentrations with the highest concentrations measured from Collis Seeps, followed by the Manchester Seep and Pond, Whirlwind Tributary A and Pond A1, the C-Drive Seeps, Whirlwind Tributaries C and D and Whirlwind Tributary Pond A2 containing the lowest concentrations.

Sulphate concentrations spanned over three orders of magnitude (minimum of 7.0 mg/L at Whirlwind Tributary Pond A2 and maximum of 8780 mg/L at Collis Seep 1). Manchester Seep and Pond and the Collis Seeps had sulphate concentrations exceeding the guideline value for recreational purposes of 400 mg/L, but there are no ANZECC trigger values for sulphate.

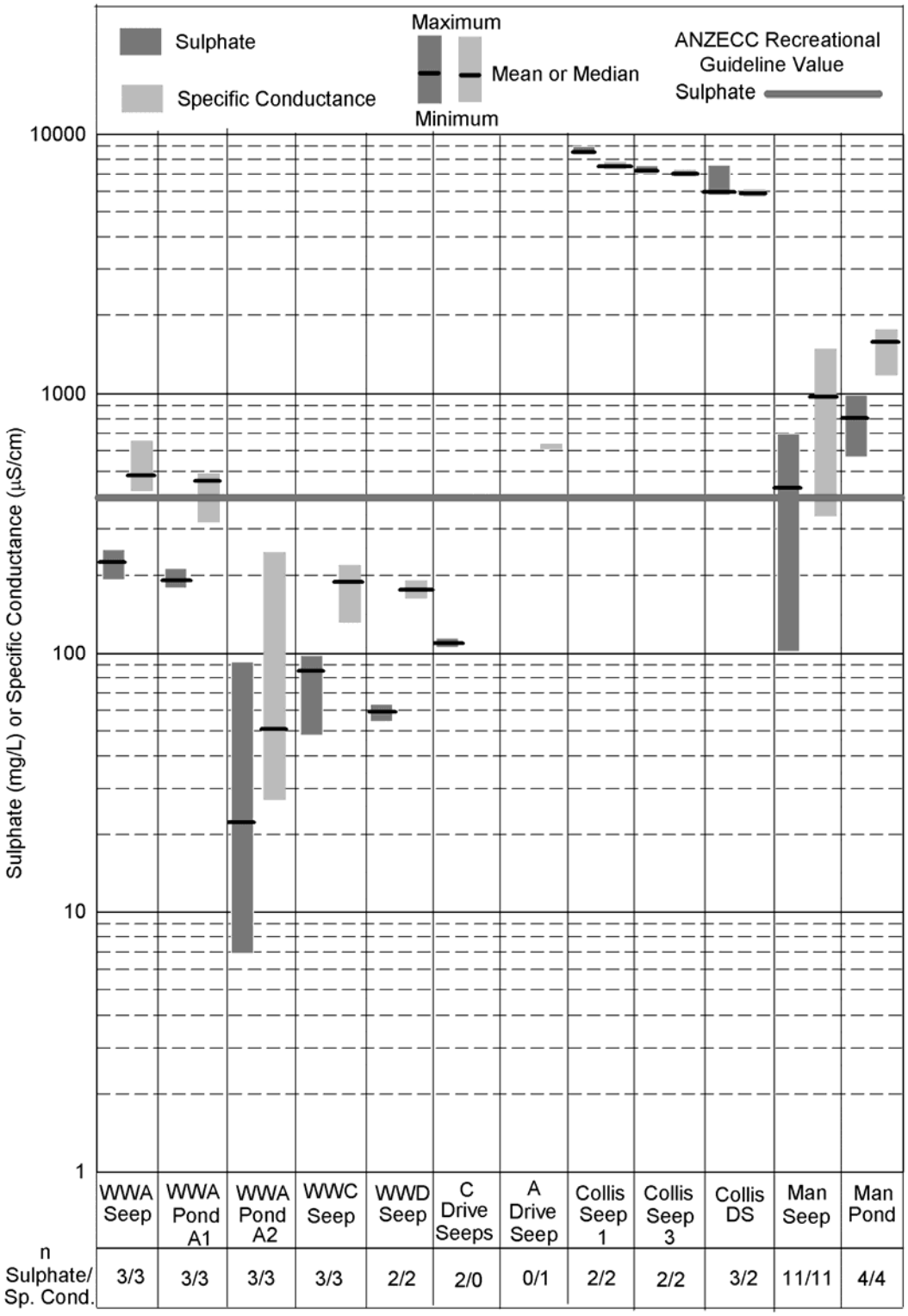

Figure 2.7. Sulphate concentration and specific conductance ranges from AMD sample locations at Stockton Coal Mine. Mean concentrations are displayed when n≤2. Median concentrations are displayed when n≥3.

2.4.4 Physical-Chemical Parameters

The physical-chemical parameters measured included temperature, pH, conductivity, Eh and DO. A summary of these results (along with key water chemistry data) for each sampling location are detailed in Tables B.1-B.11. A summary of specific conductance and pH values are additionally displayed in Figures 2.7 and 2.8, respectively. The primary importance of measuring pH pertains to its influence on the dissolution of metals and, consequently, the ecological perturbations associated with their synergistic effects (Niyogi and Hardin, 2007; O'Halloran et al., 2008). Conductivity provides an easy and inexpensive method to determine the presence of net concentrations of dissolved anions and cations in water. It is also a temperature-dependent parameter that can be measured continuously via conductivity probes equipped with data loggers; therefore, the conductivity could be used as a surrogate to determine variability in metal concentrations once clear relationships between these parameters are developed. Sample Eh and DO give an indication of whether the water is oxidised or reduced and, therefore, influences treatment options and the precipitation of metals.

Temperatures were variable and primarily dependent on sample date with respect to seasonal and ambient temperature fluctuations. The only location where sampling was conducted over each season was the Manchester Seep, which contained temperatures ranging from 7.9-12.6^{o}C. Temperatures were more stable at sampling locations where groundwater daylighted (e.g. Manchester Seep, Whirlwind Tributary A and Collis Seeps 1 and 3) since groundwater is more buffered from ambient temperatures than surface water. As a result, temperatures measured from standing surface water bodies were more variable.

The pH values (Figure 2.8) were variable spatially and temporally but followed similar trends to acidity and metal concentrations highlighting the influence of metal acidity on pH. For example, -log molar metal concentration showed good linear relationships with pH (coefficient of determinations (R^2) of 0.97 for Fe, 0.83 for Al and 0.95 for the summation of Fe and Al concentrations (Figure 2.9)). Sample pH values were as low as 2.04 (Collis Seep 1) and as high as 4.31 (Whirlwind Pond A2) but were typically <3.8 and, thus, below the minimum compliance level of 4.0. The most temporal variability was measured at the Manchester Seep (range of 2.49-3.34; median=2.81) and Whirlwind Pond A2 (range of 3.46-4.31; median=4.05). The pH variability measured from Whirlwind Pond A2 was highly influenced by surface water runoff. The greater variability in pH from Manchester Seep AMD was likely a consequence of the number of times it was sampled (n=12) compared to other AMD sites (1-5) and, therefore, may offer a better representation of temporal variability compared to other monitoring sites.

Specific conductance, like pH, also followed similar trends to acidity and metal concentrations. Median specific conductance values (Figure 2.5) were between approximately 200 and 1000 μS/cm with exception of Collis Seeps 1 and 3 (average values of 7588 and 7045 μS/cm, respectively).

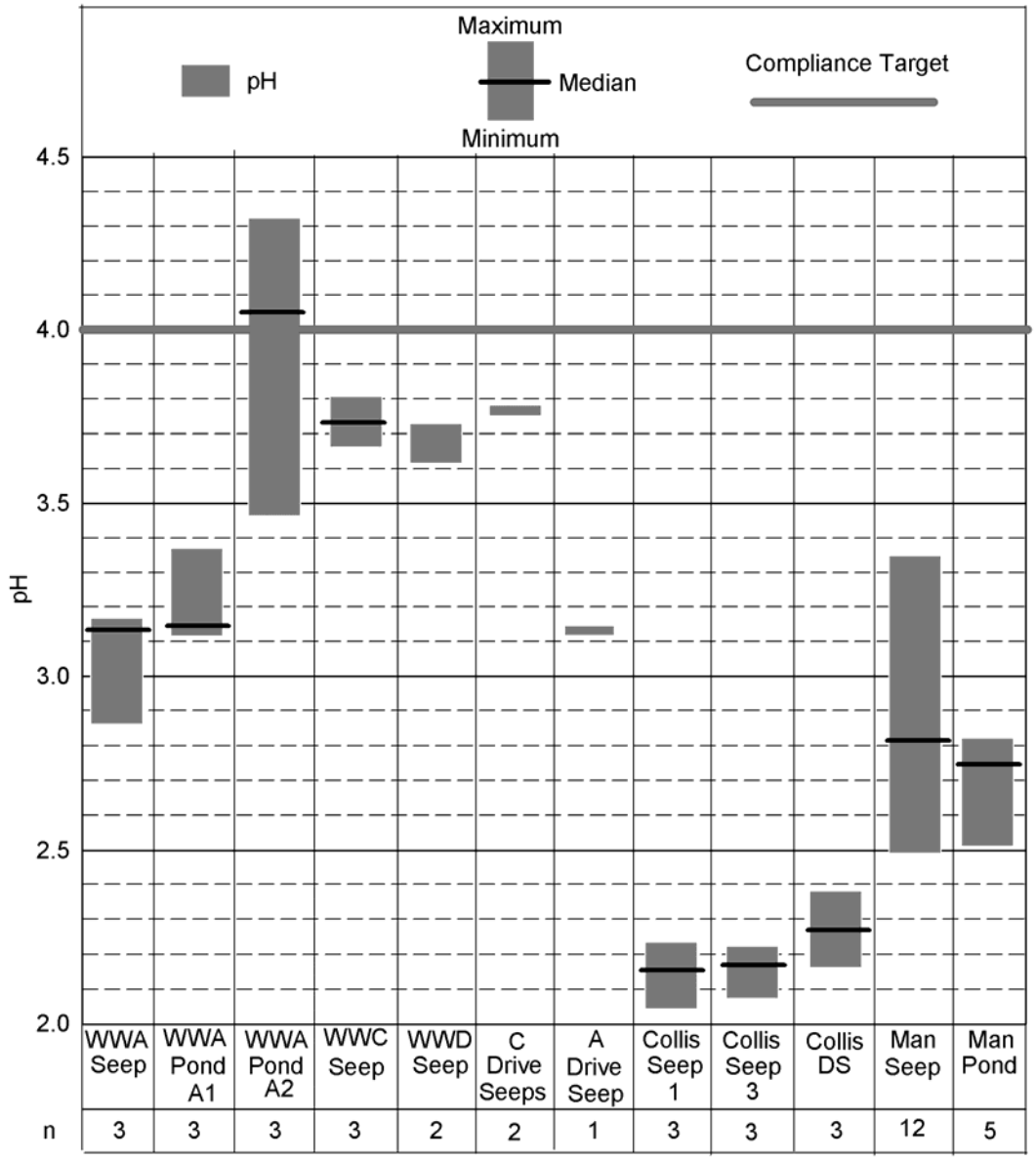

Figure 2.8. pH ranges (hanging bar graphs) from AMD sample locations at Stockton Coal Mine. Mean concentrations are displayed when n≤2. Median concentrations are displayed when n≥3.

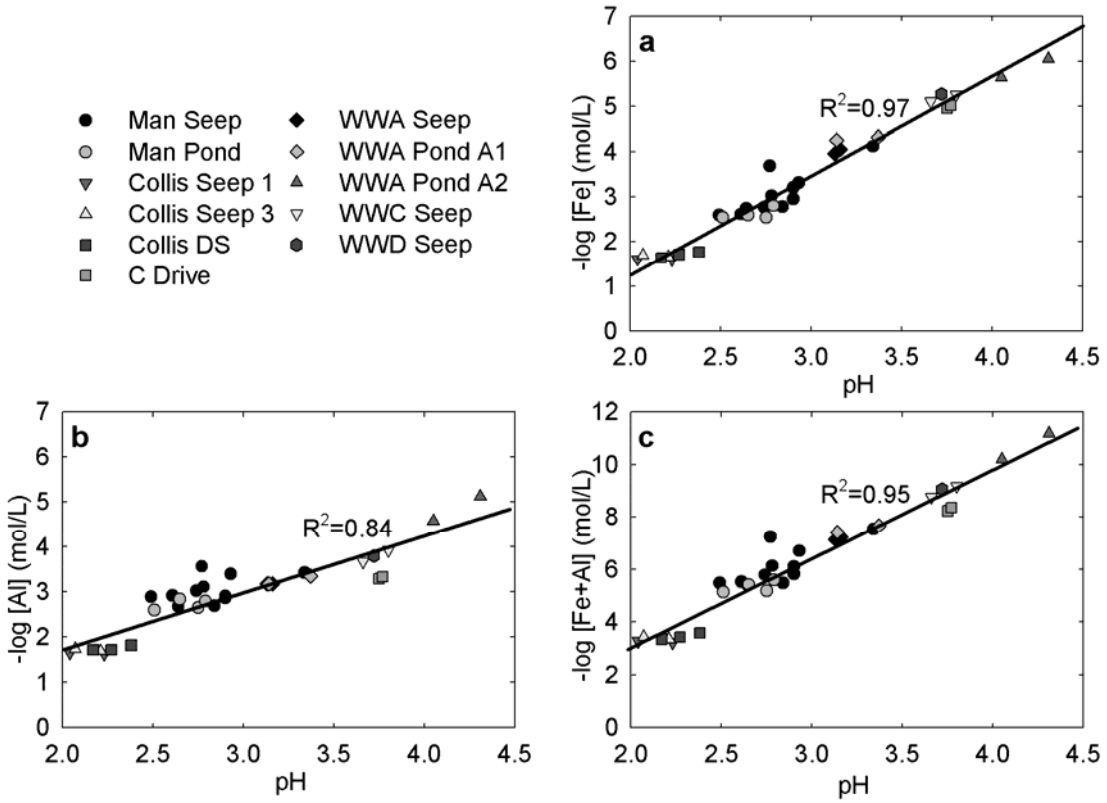

Figure 2.9. Comparisons of a) pH and –log molar Fe concentrations; b) pH and –log molar Al concentrations; and c) pH and –log of the summation of molar Fe and Al concentrations from AMD sample locations at Stockton Coal Mine. Solid lines represent the linear best fit, and R^2 values represent coefficients of determination.

Sample Eh values, DO concentrations and percent DO saturation indicated that all AMD waters were present in the oxidised state (Tables B.1-B.11). Eh values were high ranging from 620 mV (Whirlwind Pond A2) to 761 mV (A Drive Seep). Dissolved oxygen percent saturation was typically >80% with exception of the Collis Seeps. Oxygen was likely depleted from Collis Seeps (mean of 32.6% saturation from Collis Seeps 1 and 3) due to its excessive consumption during the oxidation and hydrolysis reactions associated with pyrite (and other metal and minerals) and the oxidation of sulphur from recently disturbed overburden material where the seeps daylight. Dissolved oxygen concentrations were also typically greater from the outlet of ponds than seeps, possibly due to oxygen diffusion and oxygenation from riffles and photosynthetic algae.

2.4.5 Cations

Cation equivalent concentrations can be compared with anion equivalent concentrations as a QA/QC check for laboratory accuracy and/or to determine if there are additional cations and/or anions that could be present in a water sample that were not measured. During this study, the anion and cation equivalent concentrations were typically within 6% of each other. Multivalent cations also contribute to water hardness (typically expressed as Ca and Mg equivalent concentrations standardised to $CaCO_3$)

which influence ecotoxicity of some metals as previously indicated via the hardness dependent threshold values (Table 2.1).

Cation (Na, K, Mg and Ca) concentrations typically increased with decreasing pH indicating that acidity was primarily responsible for their dissolution from parent rock and overburden. For example Whirlwind Tributary Pond A2 contained a median hardness of 3.07 mg/L as $CaCO_3$ and a median pH of 4.05, whereas Collis Seep 1 contained a median hardness of 1670 mg/L as $CaCO_3$ and a median pH of 2.15. Hardness values from each seep were generally low with median values typically <40 mg/L as $CaCO_3$ with exception of the Manchester Seep (53.8 mg/L as $CaCO_3$) and Pond (70.6 mg/L as $CaCO_3$) and the Collis Seeps (≥1420 mg/L as $CaCO_3$). Calcium and Mg mass concentrations were typically greater than those of Na and K, but not significantly. The only exception to this trend occurred for the Collis Seeps where Ca and Mg concentrations were about two orders of magnitude greater than those of Na and K.

2.4.6 Solids

Total suspended solids, and associated turbidity, can negatively impact receiving surface water and components of wastewater treatment facilities. Therefore, it is important to quantify them so they can be properly managed. The presence of TSS and turbidity in AMD were primarily influenced by sample location, erosion during precipitation events and mining activities. Generally, TSS and turbidity were lower in samples collected at locations where seeps daylight. One exception was during the 20 December 2006 sampling event at the Manchester Seep when a TSS concentration of 2960 mg/L and turbidity of 4250 NTUs was measured as a result of an upgradient site disturbance which transported fine sediment into the Manchester Seep. Just minutes prior to the influence of the site disturbance, a turbidity of 30.9 NTUs was measured. Median TSS and turbidity measured at the Manchester Seep were 18.8 mg/L and 2.45 NTUs, respectively. The higher TSS concentrations measured at the outlets of Whirlwind Ponds A1 and A2 compared with the seep location (approximately 25-50 times higher) were influenced by sediment runoff into the ponds from overland flow. The same trend was also measured at the Collis Seeps where TSS concentrations and turbidity were greater at the sampling location directly downstream of the seeps due to sediment transport along the drainage channel. Since TDS and salinity were calculated from conductivity, their concentrations followed the same trends as previously discussed for conductivity (Section 2.3.4) and were influenced by the presence of dissolved cations and anions (primarily Fe, Al and sulphate).

2.4.7 Manchester Seep Water Chemistry

Water chemistry from the Manchester Seep was studied to a greater extent and detail than other seeps since it was chosen as the candidate site for subsequent research pertaining to passive treatment. Temporal trends measured during monthly sampling for the major contaminants of concern including acidity, sulphate, metals (total and dissolved Fe and Al and dissolved Cu, Ni, Zn, Cd and As) and pH are summarised in Figure 2.10. Each of these parameters followed similar trends of increasing

concentrations with decreasing pH. Dissolved trace metals spanned concentrations ranging from three orders of magnitude with the following concentration trends in descending order: Zn>Ni>Cu>As>Cd. Iron and Al concentrations were typically about one and a half to two orders of magnitude greater than Zn. Median dissolved metal concentrations were measured at 62.9 mg/L Fe; 32.5 mg/L Al; 0.993 mg/L Zn; 0.175 mg/L Ni; 0.0514 mg/L Cu; 0.055 mg/L As; and 0.00109 mg/L Cd. The AMD pH ranged from 2.49-3.34.

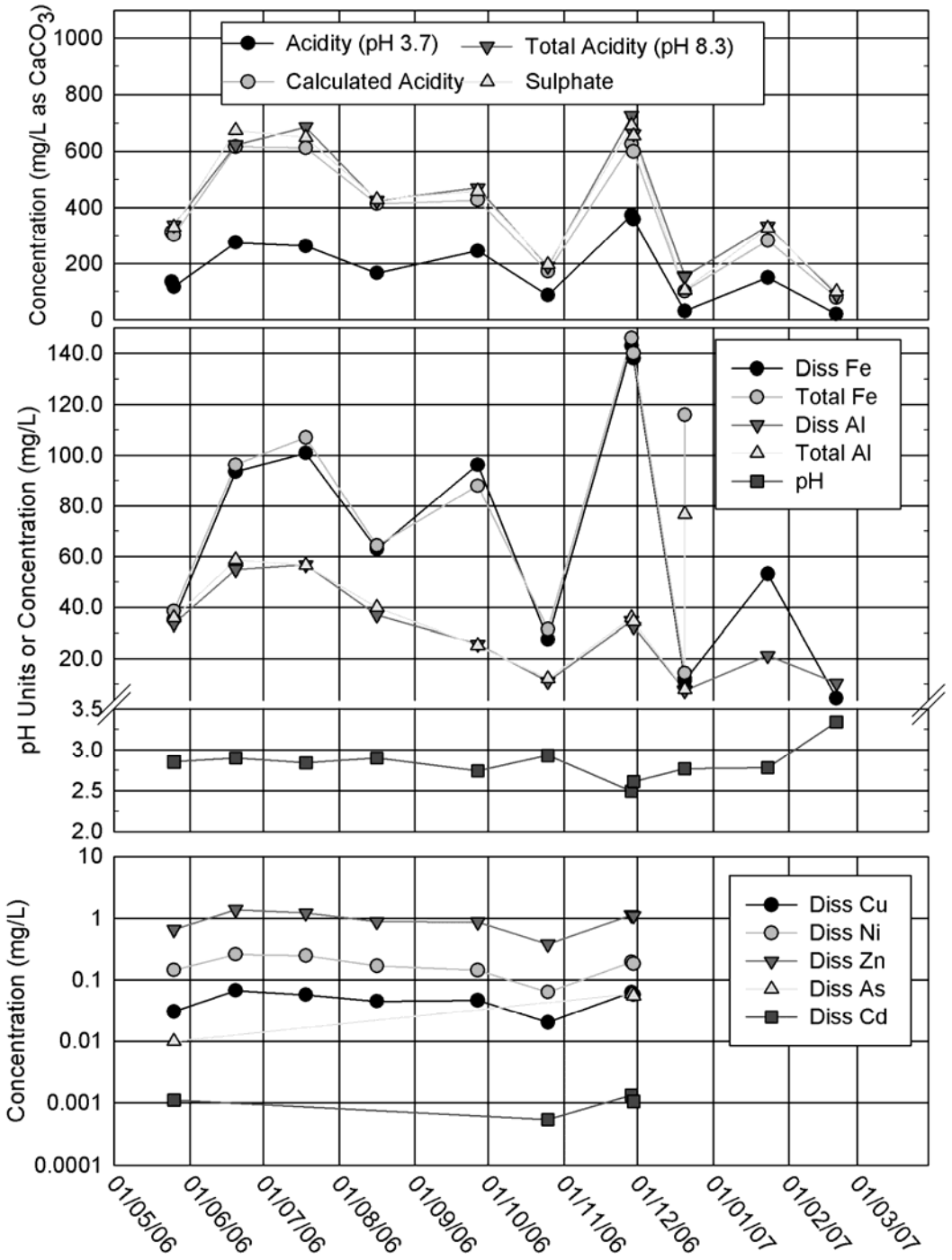

Figure 2.10. Temporal water chemistry measured from Manchester Seep during monthly monitoring.

Total acidity (pH 8.3) and calculated acidity were similar but calculated acidity was generally greater than measured total acidity (median difference of 11.0% when assuming Fe^{2+} and Fe^{3+} speciation). When assuming all Fe contributed two equivalents of acidity due to Fe^{3+} complexing with hydroxide cations (Cravotta and Kirby, 2004), the median difference between total acidity (pH 8.3) and calculated acidity was 1.23% greater total acidity (pH 8.3) as demonstrated in Figure 2.10. Iron and Al contributed to the majority of metal acidity. Hydrogen, Fe and Al cations contributed >99.2% of calculated acidity for all samples. Median percent contributions to calculated acidity were 37.1% Fe (10.0-53.8%), 35.3% Al (26.5-64.3%) and 19.3% H^+ (11.6-54.8%). Interestingly, sulphate concentrations were also similar to total and calculated acidity. The equivalent weights of $CaCO_3$ and sulphate are similar (50 g/equivalent and 48 g/equivalent, respectively). Since sulphur represented nearly 100% of the anionic equivalents in AMD samples and metals and H^+ consistently represented 90-95% of cationic equivalents, it is expected that sulphur and acidity values calculated on a mass basis would be similar (within 5-10%).

The total and dissolved Fe and Al fractions were typically similar indicating that most Fe and Al were dissolved into the aqueous state. Excluding the December 2006 site disturbance anomaly, comparison of total and dissolved Fe yielded a linear best-fit slope of 0.991 with an R^2 of 0.993. Aluminium concentrations were generally less variable than Fe concentrations. Excluding data from the December 2006 sampling event, comparison of total and dissolved Al concentrations yielded an R^2 value of 0.994 with a linear best-fit slope of 1.032. Total Fe and Al concentrations and dissolved Fe and Al concentrations correlated poorly yielding R^2 values of 0.336 and 0.480, respectively, indicating no strong relationship between Fe and Al concentrations in AMD at Manchester Seep.

2.5 Flow Rates and Loading Rates

Flow rates were variable at both the Manchester Seep and the Collis Seeps as shown in Figure 2.11. Acidity, metal and sulphur loading were calculated as the product of flow rates and concentrations and were also variable. The following figures show total mass loading rates on a temporal basis from the Manchester Seep, Manchester Pond outflow and Collis Seeps: Figure 2.12) acidity; Figure 2.13) dissolved metals; Figure 2.14) dissolved Fe; Figure 2.15) dissolved Al; and Figure 2.16) sulphur. Figures B.16 and B.17 in Appendix B show dissolved metal and sulphate loading on a molar basis. During sampling events when multiple flow measurements were taken, loading rates presented in Figures 2.12-2.16 and Figures B.16-B.17 were calculated from the average of the minimum and maximum flow rates. A basic statistical summary of all flow and loading data is presented in Table 2.5.

Table 2.5: Flow rates and loading rates emanating from Manchester Seep, the Manchester Pond and the Collis Seeps. Units are: 1) kg $CaCO_3$/day for acidity loading; 2) kg/day for mass loading; and 3) mol/day for molar loading. During sampling events when multiple flow measurements were made, all flow measurements were included in computing minimum and maximum statistics; however, the average of the minimum and maximum flow rates measured during a sampling event were used as representative values for that particular sampling event for computing average, median and standard deviation statistics representative of all sampling events.

	Mean	Median	Min	Max	Std. Dev.
Manchester Seep (n=11)					
Flow (L/s)	2.36	1.68	0.34	10.5	2.44
Acidity	86.9	81.4	2.7	231	69.9
Metal Molar	462	312	13.8	1560	385
Metal Mass	20.2	12.5	0.44	72.3	18.2
Fe Mass	14.7	7.80	0.13	57.5	15.0
Al Mass	5.27	4.42	0.31	13.9	3.26
Sulphate Molar	866	578	31.6	2890	707
Sulphur Mass	27.8	18.5	1.02	92.8	22.7
Manchester Pond (n=4)					
Flow (L/s)	1.50	1.56	0.87	2.00	0.48
Acidity	95.8	94.8	67.9	125	30.6
Metal Molar	569	556	402	763	191
Metal Mass	24.8	24.7	16.7	33.2	9.01
Fe Mass	18.1	18.1	11.2	25.1	7.45
Al Mass	6.53	6.08	5.09	8.87	1.72
Sulphate Molar	1050	1010	699	1480	392
Sulphur Mass	33.7	32.4	22.4	47.4	12.6
Collis Seeps (n=5)					
Flow (L/s)	0.33	0.33	0.17	0.53	0.14
Acidity	167	189	99.2	226	51.7
Metal Molar	1090	1230	652	1500	343
Metal Mass	46.1	52.2	27.3	63.4	14.7
Fe Mass	31.8	35.2	18.4	43.8	10.3
Al Mass	13.8	14.9	8.59	18.9	4.25
Sulphate Molar	1960	1980	1210	2840	622
Sulphur Mass	63.0	63.5	38.9	91.1	20.0

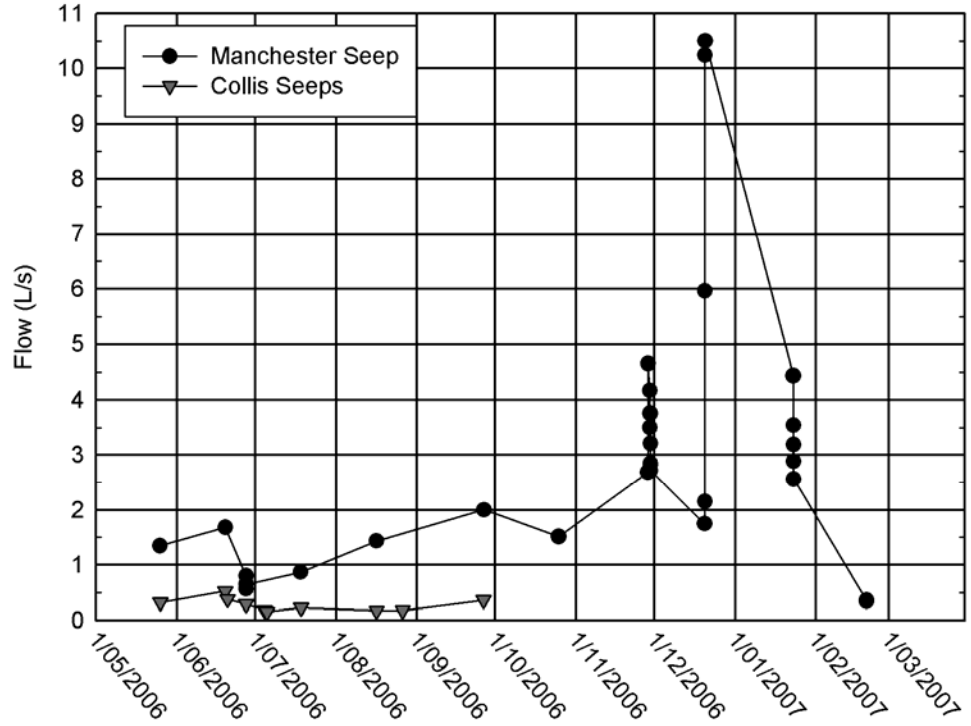

Figure 2.11. Flow rates measured from the Manchester Seep and Collis Seeps (cumulative from Seeps 1 and 3). Multiple data points showing variable flow rates at near identical times reflect multiple flow measurements on the same day (e.g. during precipitation events on 29 November 2006 and 23 January 2007 and during the suspected upgradient site disturbance on 20 December 2006).

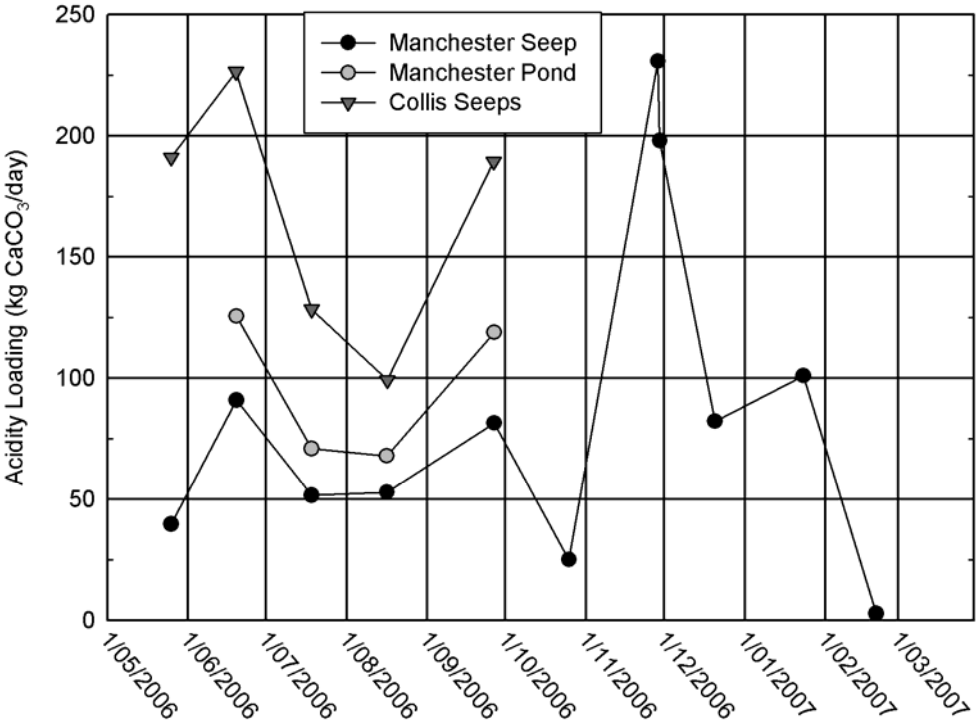

Figure 2.12. Acidity loading from the Manchester Seep, the outlet of the Manchester Pond and the Collis Seeps (cumulative from Seeps 1 and 3).

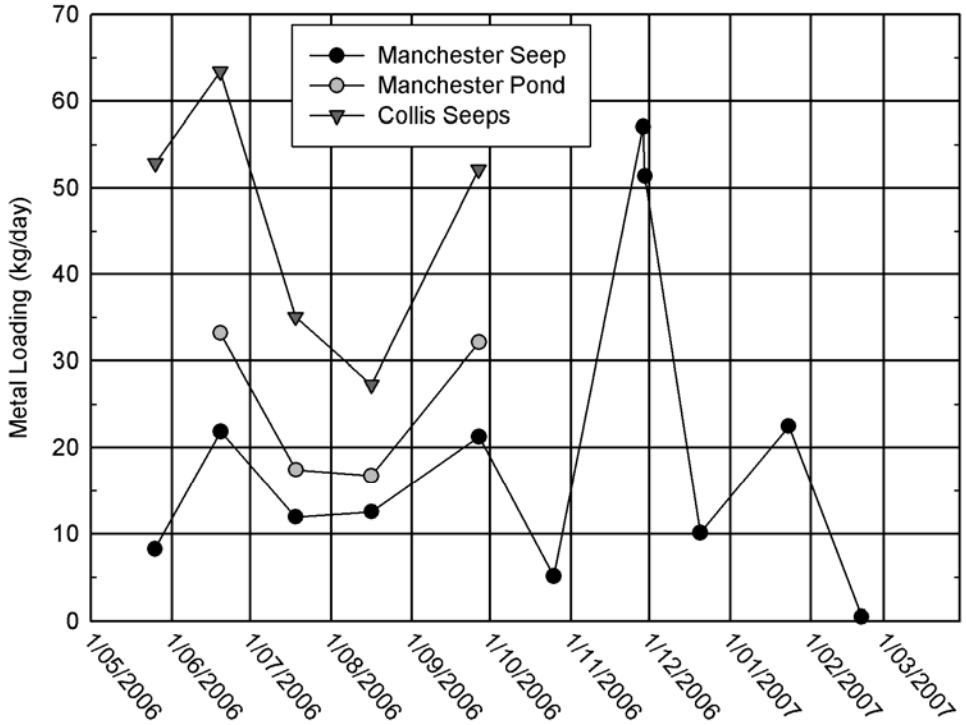

Figure 2.13. Dissolved metal loading from the Manchester Seep, the outlet of the Manchester Pond and the Collis Seeps (cumulative from Seeps 1 and 3). Loading rates include the total mass of Fe, Al, Cu, Ni, Zn, Cd, Pb, As and Mn.

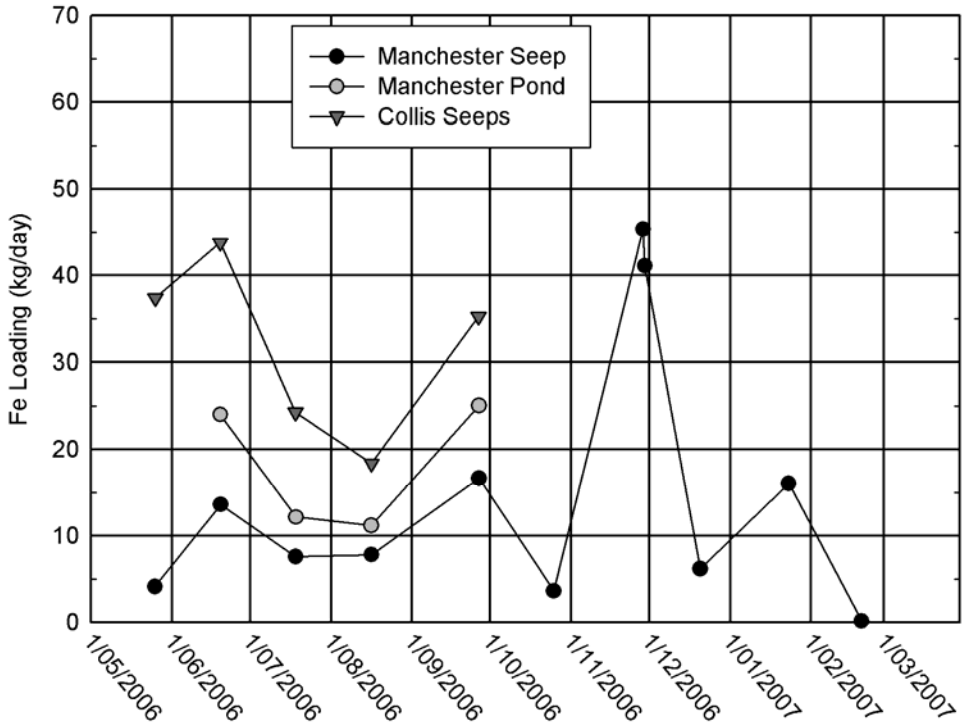

Figure 2.14. Dissolved Fe loading from the Manchester Seep, the outlet of the Manchester Pond and the Collis Seeps (cumulative from Seeps 1 and 3).

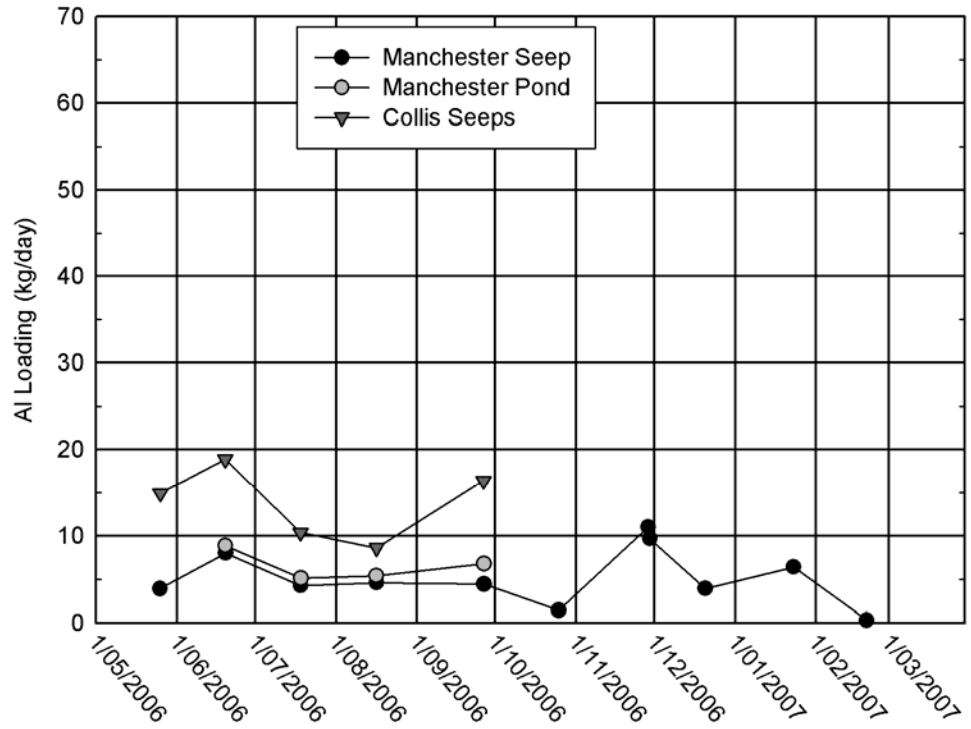

Figure 2.15. Dissolved Al loading from the Manchester Seep, the outlet of the Manchester Pond and the Collis Seeps (cumulative from Seeps 1 and 3).

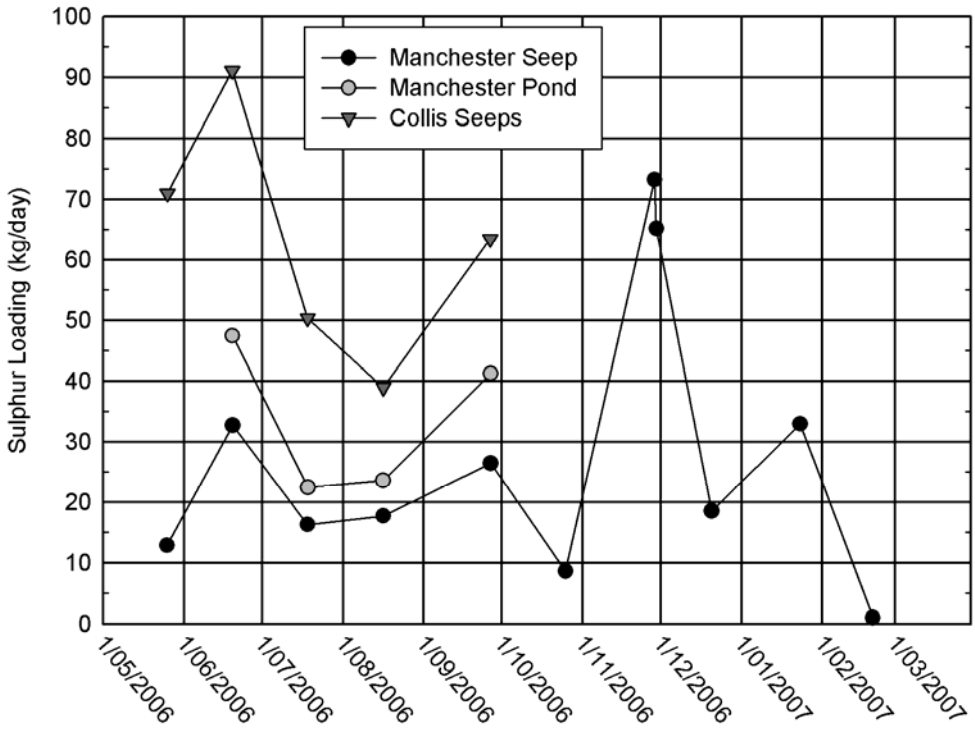

Figure 2.16. Total sulphur loading from the Manchester Seep, the outlet of the Manchester Pond and the Collis Seeps (cumulative from Seeps 1 and 3).

Metal, acidity and sulphate loading rates generally followed similar temporal trends for the Manchester Seep and Pond and the Collis Seeps (Figures 2.12-2.16). The highest metal, acidity and sulphate loading rates typically occurred when flow rates were the greatest (e.g. the 28 and 29 November 2006 sampling events). The primary exception to this trend involved the 20 December 2006 sampling event at the Manchester Seep during the suspected site disturbance, which resulted in a pulse of high flow (up to 10.5 L/s). The source of the increased flow was likely discharge from an upgradient sediment pond during maintenance activities, which contained diluted concentrations of acidity and metals. Therefore, although the flow was high, acidity and metal loading were comparable to median values. No trends were evident pertaining to flow rate and concentrations (e.g. R^2=0.074 comparing flow with the summation of Fe and Al molar concentrations for the Manchester Seep AMD).

Flow and loading rates followed similar temporal trends from the Manchester Seep and the Collis Seeps during the sampling periods from May to October 2006. Although flow from the Collis Seeps ranged from three to nine times less than flow from the Manchester Seep during this period, loading rates from the Collis Seeps were always greater than those calculated from the Manchester Seep. For example, metal loading rates (Figure 2.13) were typically two to three times greater from the Collis Seeps than the Manchester Seep (measured as high as 6.4 times). The primary reason for this phenomenon was Fe and Al concentrations about an order of magnitude greater from the Collis Seeps compared with the Manchester Seep (Figure 2.2).

Loading rates were less from the Manchester Seep compared with the outlet of the Manchester Pond. The primary contribution was dissolution of Fe and, to a lesser extent, Al from sediment in the pond. A sediment sample collected from the pond contained 45.1% Fe and 16.9% Al. The following summarises the median percent differences in concentrations (followed by ranges in parenthesis) in water samples collected from the Manchester Seep compared with the outlet pipe of the Manchester Pond (n=4): acidity) 30.0% (24.0-46.2%); dissolved Fe) 46.4% (35.5-55.2%); dissolved Al) 15.9% (10.5-41.9%); and sulphur) 31.8% (28.2-43.1%).

2.6 Inverse Geochemical Modelling

Inverse geochemical modelling was performed for representative AMD samples from each seep to determine the stability of various chemical species with respect to $CaCO_3$ saturation and to give an indication of the mineral origin of the AMD. AquaChem software interfaced with the PHREEQC aqueous modelling programme was used to compute saturation indices (SIs) for numerous minerals present in the PHREEQC geochemical database. Saturation indices were computed as shown in Equation 2.5 where pH_{act} represents the actual pH of the sample and pH_{eq} represents the pH required for the sample to be in equilibrium with a specified mineral based on theoretical solubility constants:

$$SI = pH_{act} - pH_{eq} \quad \textbf{(2.5)}$$

Therefore, negative SI values indicate that a mineral is undersaturated and will be present in the dissolved state, positive values indicate that a mineral is oversaturated and will precipitate and values between about -0.50 and +0.50 generally indicate that equilibrium conditions are present with respect to saturation. Therefore, with respect to the dissolution of minerals and the subsequent AMD formation, the lowest SI values indicate the mineral origin for dissolved cations and anions.

A summary of samples analysed during the inverse geochemical modelling are included in Table B.12. These samples are generally representative of median metal concentrations measured from each seep and their data were analysed in the inverse geochemical models. The water chemistry (including metals, cations, sulphate, temperature, conductivity, pH, Eh, dissolved oxygen and alkalinity) measured for these samples is detailed in Table B.13.

Saturation indices computed from these water chemistry parameters are summarised in Table 2.6. Because silica (Si) was not analysed as part of this study, PHREEQC did not report SIs for the primary minerals reported as the source of Al in AMD at Stockton Coal Mine and within the Brunner Coal Measures, which include microcline, muscovite and kaolinite (Black et al., 2005). Therefore, for hypothetical purposes, Si concentrations (as SiO_2) were assumed for two additional scenarios based on the molar ratios of Si and Al found in muscovite (1 mol Si:1 mol Al), kaolinite (also 1 mol Si:1 mol Al) and microcline (3 mol Si:1 mol Al). These data are summarised in Table 2.7. PHREEQC did not compute SIs for minerals comprised predominately from trace metals (e.g. Cu, Ni, Cd, Pb and As) since their concentrations were too low.

Table 2.6: Results of PHREEQC inverse geochemical modelling from AMD seeps excluding minerals containing Si.

Mineral	Chemical Nomenclature	Man Seep 1	Man Seep 2	Man Pond 1	Man Pond 2	Collis Seep	C Drive	WW Trib A	WW Pond A1	WW Pond A2	WW Trib C	WW Trib D
Iron Containing Minerals												
Pyrite	FeS_2	-139	-137	-131	-133	-124	-37.0	-138	-139	-150	-158	-159
Iron Sulphide	**FeS**	-89.4	-88.6	-85.4	-86.0	-81.2	-30.9	-88.6	-89.0	-95.0	-100	-101
Sphalerite	**(Zn, Fe)S**	-82.7	-81.8	-78.7	-79.4	-74.4	-22.6	-81.7	-82.0	-87.5	-92.2	-93.0
Mackinawite	$(Fe,Ni)_{1+x}S$ **(where x=0-0.11)**	-88.7	-87.8	-84.7	-85.2	-80.5	-30.2	-87.8	-88.3	-94.3	-99.4	-100
Goethite	**FeO(OH)**	4.69	4.22	3.76	4.31	3.38	4.98	4.35	4.48	4.64	4.67	4.97
Jarosite	$KFe^{3+}(OH)_6(SO_4)_2$	2.28	1.89	1.13	1.81	0.737	-0.144	0.261	-0.141	-3.81	-1.14	-0.958
Melanterite	$FeSO_4*7H2O$	-4.12	-4.10	-3.67	-3.73	-2.82	-6.48	-4.95	-5.21	-7.28	-6.54	-6.68
Ferric Hydroxide (amorphous)	$Fe(OH)_3$	-0.554	-1.10	-1.40	-0.816	-2.03	-0.307	-1.06	-0.903	-0.755	-0.797	-0.412
Hematite	Fe_2O_3	11.3	10.4	9.42	10.5	8.70	11.9	10.6	10.9	11.2	11.3	11.9
Aluminium Containing Minerals												
Aluminium Hydroxide (amorphous)	$Al(OH)_3$	-7.00	-7.91	-8.23	-7.55	-8.37	-4.48	-6.23	-5.74	-4.41	-4.82	-4.79
Alunite	$KAl_3(SO_4)_2(OH)_6$	-4.45	-6.21	-6.39	-5.30	-6.34	-0.211	-3.32	-2.64	-2.77	-1.53	-2.04
Gibbsite	$Al(OH)_3$	-4.15	-5.07	-5.36	-4.67	-5.56	-1.63	-3.42	-2.92	-1.59	-2.02	-1.97
Zinc Containing Minerals												
Zinc Hydroxide (amorphous)	$Zn(OH)_2$	-10.8	-11.4	-11.4	-11.0	-11.4	-9.41	-10.8	-10.5	-9.82	-9.92	-9.86
Manganese Containing Minerals												
Pyrolusite	MnO_2	--	-13.4	--	--	-14.2	-25.9	-11.9	-11.5	-10.1	-8.35	-8.55
Hausmannite	$Mn^{2+}Mn^{3+}2O_4$	--	-34.3	--	--	-34.0	-41.7	-29.9	-28.5	-26.4	-24.5	-24.9
Manganite	**MnO(OH)**	--	-10.0	--	--	-10.4	-14.9	-8.80	-8.29	-7.45	-6.73	-6.64
Pyrochroite	$Mn(OH)_2$	--	-15.1	--	--	-14.7	-12.5	-13.8	-13.3	-12.9	-12.9	-12.9
Calcium Containing Minerals												
Anhydrite	$CaSO_4$	-2.27	-2.17	-1.92	-2.06	-0.619	-2.86	-2.43	-2.66	-4.41	-2.94	-3.36
Gypsum	$CaSO_4*2H_20$	-2.02	-1.92	-1.67	-1.80	-0.366	-2.60	-2.18	-2.40	-4.15	-2.69	-3.11
Sulphur and Gases												
Sulphur	**S**	-62.7	-61.4	-58.9	-59.9	-55.6	-19.2	-62.2	-62.7	-67.9	-71.1	-71.7
Hydrogen Sulphide	$H_2S(g)$	-87.3	-85.9	-82.8	-83.9	-78.4	-28.6	-86.3	-86.9	-93.1	-97.7	-98.5
Oxygen	$O_2(g)$	-27.7	-27.6	-30.1	-30.1	-29.9	-57.8	-27.3	-27.3	-25.3	-21.8	-22.2
Hydrogen	$H_2(g)$	-30.8	-30.5	-30.0	-30.1	-28.9	-15.5	-30.2	-30.3	-31.3	-32.6	-32.9
Water	$H_2O(g)$	-1.98	-1.93	-2.04	-2.06	-1.87	-1.95	-1.86	-1.88	-1.87	-1.82	-1.88

--, data parameters not computed because Mn was not sampled.

Table 2.7: Results of PHREEQC inverse geochemical modelling from AMD seeps for minerals containing Si. Silicon concentrations were inferred.

Mineral	Chemical Nomenclature	Molar Ratio Si:Al	Man Seep 1	Man Seep 2	Man Pond 1	Man Pond 2	Collis Seep	C Drive	WW Trib A	WW Pond A1	WW Pond A2	WW Trib C	WW Trib D
Aluminium Containing Minerals													
Kaolinite	$Al_2Si_2O_5(OH)_4$	1:1	-4.77	-6.78	-6.60	-5.59	-5.32	-0.667	-4.06	-3.39	-3.19	-2.29	-2.39
		3:1	-3.82	-5.82	-5.64	-4.63	-4.36	0.288	-3.10	-2.43	-2.24	-1.33	-1.43
Microcline (K-feldspar)	$KAlSi_3O_8$	1:1	-7.62	-9.05	-8.32	-7.93	-7.20	-5.44	-7.64	-7.60	-9.67	-7.42	-7.77
		3:1	-6.19	-7.62	-6.89	-6.49	-5.77	-4.01	-6.21	-6.17	-8.24	-5.99	-6.34
Muscovite (K-mica)	$KAl_2(AlSi_3O_{10})(F,OH)_2$	1:1	-10.4	-13.7	-13.5	-11.8	-12.8	-3.19	-8.93	-7.91	-7.31	-5.92	-6.18
		3:1	-8.97	-12.2	-12.1	-10.3	-11.3	-1.76	-7.50	-6.48	-5.88	-4.48	-4.74
Chlorite	$(Fe, Mg, Al)_6(Si, Al)_4O_{10}(OH)_8$	1:1	-64.0	-68.3	-69.4	-66.5	-62.7	-51.4	-59.6	-57.4	-56.0	-54.0	-55.0
		3:1	-62.6	-66.9	-67.9	-65.0	-61.3	-50.0	-58.2	-56.0	-54.5	-52.6	-53.6
Illite	$(K,H_3O)(Al,Mg,Fe)_2(Si,Al)_4O_{10}[(OH)_2*H_2O$	1:1	-12.7	-15.4	-14.9	-13.7	-12.9	-7.5	-11.9	-11.2	-12.2	-10.0	-10.4
		3:1	-11.0	-13.7	-13.2	-12.0	-11.2	-5.8	-10.2	-9.6	-10.5	-8.4	-8.7
Chrysotile	$(Mg,Fe)_3Si_2O_5(OH)_4$	1:1	-34.3	-35.9	-35.9	-35.0	-31.7	-29.9	-32.8	-32.1	-33.0	-31.2	-31.9
		3:1	-33.4	-34.9	-35.0	-34.1	-30.8	-29.0	-31.8	-31.1	-32.1	-30.3	-30.9
Anorthite	$CaAl_2Si_2O_8$	1:1	-22.7	-25.1	-25.4	-23.9	-23.2	-16.9	-21.1	-20.3	-19.6	-18.4	-18.8
		3:1	-21.7	-24.2	-24.4	-23.0	-22.3	-16.0	-20.2	-19.3	-18.7	-17.4	-17.8
Albite	$NaAlSi_3O_8$	1:1	-9.93	-11.2	-10.3	-10.1	-8.71	-7.92	-9.92	-9.88	-11.9	-9.68	-9.98
		3:1	-8.50	-9.73	-8.88	-8.69	-7.27	-6.49	-8.49	-8.45	-10.5	-8.25	-8.55
Montmorillonite	$Ca(Al, Mg)_6(Si_4O_{10})_3(OH)_6 *nH_2O$	1:1	-8.18	-10.7	-10.1	-9.06	-7.28	-3.73	-7.69	-7.10	-8.45	-6.15	-6.45
		3:1	-6.43	-8.93	-8.30	-7.31	-5.52	-1.98	-5.94	-5.35	-6.70	-4.40	-4.70
Silicon Dioxide Minerals													
Chalcedony	SiO_2	1:1	0.901	0.823	1.19	1.01	2.04	0.442	0.532	0.372	-0.862	0.0232	-0.0791
		3:1	1.38	1.30	1.67	1.49	2.52	0.919	1.01	0.849	-0.385	0.501	0.398
Quartz	SiO_2	1:1	1.39	1.30	1.69	1.50	2.52	0.924	1.00	0.845	-0.389	0.489	0.395
		3:1	1.86	1.78	2.17	1.98	2.99	1.40	1.48	1.32	0.0880	0.967	0.872
Silicon Dioxide (amorphous)	SiO_2	1:1	-0.0004	-0.0717	0.285	0.0966	1.16	-0.455	-0.353	-0.515	-1.75	-0.857	-0.967
		3:1	0.477	0.406	0.762	0.574	1.64	0.0219	0.124	-0.0382	-1.27	-0.379	-0.490
Other Minerals													
Willemite	Zn_2SiO_4	1:1	-18.4	-19.3	-19.5	-18.8	-17.9	-15.9	-18.3	-17.9	-17.7	-16.8	-17.0
		3:1	-17.9	-18.8	-19.0	-18.4	-17.4	-15.4	-17.8	-17.4	-17.2	-16.3	-16.6
Talc	$Mg_3Si_4O_{10}(OH)_2$	1:1	-29.1	-30.7	-30.1	-29.6	-24.1	-25.6	-28.2	-27.8	-31.3	-27.6	-28.5
		3:1	-27.2	-28.8	-28.2	-27.7	-22.2	-23.7	-26.3	-25.9	-29.3	-25.7	-26.6
Sepiolite	$Mg_4Si_6O_{15}(OH)_2*6H2O$	1:1	-20.9	-22.2	-21.4	-21.1	-17.5	-18.8	-20.7	-20.4	-23.2	-20.6	-21.1
		3:1	-19.5	-20.7	-20.0	-19.7	-16.0	-17.4	-19.2	-19.0	-21.7	-19.1	-19.6

Results of the inverse geochemical modelling indicated that pyrite (FeS_2) was the most undersaturated mineral (typically SI < 130) for all samples, which supports the most common explanation for AMD generation via pyrite oxidation and subsequent Fe hydrolysis (Skousen, 1996; Rose and Cravotta, 1998; Pennsylvania Department of Environmental Protection, 1999; Ford, 2003; Watzlaf et al., 2004). Most minerals were undersaturated (as determined by their negative SI values) indicating that the acidity associated with the AMD samples was sufficiently high to generate further mineral and metal dissolution. The primary exceptions were goethite (FeO(OH); SI values >3.38), hematite (Fe_2O_3; SI values >8.70) and silicon dioxide minerals (e.g. chalcedony and quartz). The SI values for silicon dioxide minerals were greater when assuming the higher Si concentrations (3 mol Si:1 mol Al) and were typically >0.37. Whirlwind Pond A2 was an exception and contained SI values that were either undersaturated or near equilibrium (range of -0.86-0.088). The predominant Al-containing minerals associated with AMD at Stockton Coal Mine (microcline, muscovite and kaolinite) were undersaturated, but less so than pyrite by over an order of magnitude (SI values typically 1-14). The only exception pertained to kaolinite from C Drive assuming a 3 mol Si to 1 mol Al molar ratio, which was slightly oversaturated and near equilibrium conditions. C Drive contained the lowest Fe concentration (0.59 mg/L), which contributed to <2.0% of its metal acidity, of all samples analysed during this study.

2.7 Discussion

2.7.1 Water Chemistry

There was substantial spatial variability in AMD water chemistry at the Stockton Coal Mine (Figures 2.2-2.8), which is attributed to geological heterogeneity, mining management practices, the prevalence of acid producing rocks and the degree of overburden exposure to atmospheric oxygen and water. Acidity and metal concentrations varied by about three orders of magnitude between sample locations. The primary reasoning pertains to the geological heterogeneity at Stockton Coal Mine and the prevalence of acid producing rocks. Mining practices and the influence of precipitation also likely contributed to some of the variability. For instance, the Collis dump, where the Collis Seeps daylighted from, had just been recontoured for rehabilitation at the start of this research leading to a pulse of acidity associated with reinvigorating the AMD process by introducing oxygen to the system.

A summary of water chemistry from surface waters impacted by coal mining in New Zealand and the U.S.A. are summarised in Table 2.8. All references reported significant variability in water chemistry between MIWs with pH spanning five pH units and, Fe, Al and acidity concentrations differing up to four or five orders of magnitude between sites.

Table 2.8: Water chemistry from seeps and streams impacted by coal mining. Values shown are medians with ranges shown in parenthesis below median values. Calculated acidity concentrations were reported from this study and Cravotta and Kirby (2004), whereas, net acidity (calculated acidity minus alkalinity) was reported from other studies. The only exception was A Drive from this study where the total acidity (pH 8.3) value was used.

Location(s)	n	pH	Fe (mg/L)	Al (mg/L)	Calculated or Net Acidity	Reference
New Zealand						
Stockton Coal Mine	11-12	3.13 (2.15-4.05)	5.59 (0.09-1410)	17.9 (0.459-607)	205 (6.39-7340)	This Study
Brunner Coal Measures - Opencast	17	3.01 (2.60-5.85)	2.89 (0.56-43.3)	12.3 (0.021-115)	--	Pope et al. (2006)
Brunner Coal Measures - Underground	19-20	2.91 (2.41-3.79)	15.7 (0.91-134)	12.7 (0.21-216)	--	
Paparoa Coal Measures (Opencast)	3	7.2 (6.8-7.3)	0.66 (0.04-11.9)	0.004 (0.003-0.005)	--	
Paparoa Coal Measures (Underground)	1	7.0	0.27	0.204	--	
United States of America						
West Virginia	118	3.7 (2.5-7.2)	--	--	139 (-237-2389)	Skousen and Ziemkiewicz (2005)
Kentucky	1	2.8	--	--	843	
Tennessee	8	2.9 (2.3-3.2)	--	--	182 (70-781)	
Maryland	5	6.1 (2.8-6.7)	--	--	299 (-20-841)	
Ohio	5	3.6 (2.9-6.8)	--	--	173 (13-712)	
Alabama	4	5.3 (3.8-7.0)	--	--	-1 (-29-92)	
Indiana	1	2.7	--	--	515	
Pennsylvania (Anthracite)	41	5.1 (3.0-6.3)	15 (0.046-312)	0.280 (0.007-26)	51 (0-702)	Cravotta III and Kirby (2004)
Pennsylvania (Bituminous)	99	5.2 (2.7-7.3)	43 (0.16-512)	1.5 (0.008-108)	119 (1-1587)	
Pennsylvania	24-33	4.32 (3.0-6.8)	16 (0.2-208)	5.2 (0-48.0)	154 (-168-506)	Rose (2004)
	12-17	3.3 (2.5-4.3)	97 (1.0-281)	11 (0.3-70)	400 (43-1230)	Rose and Dietz (2002)

--, data parameters not measured; n, number of samples.

Only Pope et al. (2006) and this study summarised water chemistry from numerous streams impacted by coal mining in New Zealand. Pope et al. (2006) delineated water chemistry based on coal mining impacts from opencast and underground mines and whether the MIWs were located within the Brunner or Paparoa Coal Measures. There was generally a higher Al:Fe molar concentration ratio in opencast compared with underground mines. This was attributed to the greater disturbances of

overburden and sediments in open mine pits, which allow greater reaction time of AMD with Al-containing minerals (Pope et al. 2006; 2010). Newman (1988) and Pope et al. (2006; 2010) also report that sediment surrounding coal seams is often feldspar depleted and contains less Al compared with sediments stratigraphically further from the coal seams. During underground mining, most sediment disturbance occurs near the coal seam(s), whereas overburden extracted during open-pit mining includes sediment stratigraphically further from the coal seam(s). Stockton Coal Mine is an opencast coal mine so Al was the most prevalent contaminant from all seeps (on a molar basis), with exception of the Collis Seeps.

Water chemistry measured during this study from Stockton Coal Mine generally corresponded to that reported by Pope et al. (2006) for the Brunner Coal Measures; however, it was highly variable. The Collis Seeps contained lower pH and higher Fe and Al concentrations compared with any of the data reported in any of the studies reported in Table 2.8. Manchester Seep water chemistry was comparable to the worst water chemistry reported by Pope et al. (2006) from Hood's Seep. Data from Whirlwind (Tributary unspecified), A Drive and C Drive were reported in Pope et al. (2006). These results were generally comparable with those measured during this study, which could indicate that spatial variability in AMD chemistry at Stockton is more prominent than temporal variability. The most significant difference was the pH measured at C Drive which was 3.76 during this study and 3.23 reported in Pope et al. (2006), although Fe concentrations were similar and Al concentrations were 36% greater in this study. Despite chemical variability in AMD across sampling locations, metal concentration and pH relationships strongly correlated indicating that metal dissolution was a result of sulphuric acid produced during pyrite oxidation.

Water chemistry reported by Pope et al. (2006) was significantly worse from the Brunner Coal Measures than the Paparoa Coal Measures. The reasoning pertains to differences in geology and subsequent changes to geochemistry during mining processes. Pope et al. (2006) reported that the Paparoa coals were formed in a stable fluvial to lacustrine environment where carbonate-bearing minerals were preserved, whereas the Brunner coals were formed in an estuarine environment where repeated reworking of sediments resulted in unfavourable conditions for preserving carbonate-bearing minerals but favourable to the formation of pyrite; therefore, coal mining from the Brunner Coal Measures results in the generation of AMD, whereas AMD is not present in MIWs emanating from the Paparoa Coal Measures.

Water chemistry from surface waters impacted from coal mining was generally comparable between New Zealand and those reported from the U.S., both of which contained AMD and MIW that was not overly acidic. One notable difference was generally higher Al concentrations in New Zealand. These could be contributed to its greater presence in the ubiquitous mica and feldspar present within the Brunner Coal Measures (Black et al., 2005).

Although metal concentrations, as sampled, were elevated, they do not provide a true indication of the overall water quality leaving the mine site. Solid Energy has installed, and is progressing with, treatment systems for all AMD generated at Stockton Coal Mine including calcium hydroxide ($Ca(OH)_2$) and ultrafine limestone treatment of AMD. Furthermore, Solid Energy currently mitigates AMD at Stockton via minimisation technologies that include selective rock placement and the construction of engineered covers. Further treatment solutions such as this work pertaining to passive treatment systems and BGCRs are being investigated.

2.7.2 Inverse Geochemical Modelling

Results of inverse geochemical modelling were compared with those presented by Cravotta (2007) and Cravotta and Ward (2008). Cravotta (2007) reported SIs from a pH 6.2 mine water, whereas Cravotta and Ward (2008) reported SIs from a pH 3.9 mine water. Both mine waters had elevated concentrations of Fe, Al, Mn, Ni and Zn. The SI values from the pH 3.9 mine water were undersaturated and comparable to those measured from AMD evaluated as part of this study. The pH 6.2 mine water contained a positive ferric hydroxice SI, indicating that conditions were favourable for its precipitation, and an amorphous aluminium hydroxide that was near equilibrium. Both the pH 6.2 and pH 3.9 mine waters were undersaturated for Mn-containing minerals including mangatite (MnO(OH)) (median SIs of -5.6 and -8.1, respectively) and pyrolusite (MnO_2) (median SIs of -11.9 and -12, respectively).

The most common sequence of chemical reactions illustrating that AMD generation is associated with pyrite oxidation and subsequent Fe hydrolysis (Equations 1.1-1.4), which involves sulphur and Fe present in a two to one molar ratio. The sulphur to Fe molar ratios measured during this study were always greater than two with averages ranging as low as 3.36 from the monitoring site downstream of the Collis Seeps and as high as 37.2 from C Drive Seep 2. Molar ratios were highest from seeps (and samples) containing the lowest acidity values. For example, the sulphur to Fe molar ratios were >13 for all samples analysed during this study containing an acidity (pH 3.7) <20 mg/L as $CaCO_3$. The sulphur to Fe molar ratios were commonly <4 when acidity (pH 3.7) values were >150 mg/L as $CaCO_3$.

Results of inverse geochemical modelling provided an estimation of the mineralogical sources of AMD sampled. Based on these results, only pyrite would have contributed significant quantities of sulphur upon dissolution. Alunite ($KAl_3(SO_4)_2(OH)_6$) was the only Al-containing mineral modelled that contained sulphur; however, Black et al. (2005) reported that the source of Al at Stockton Coal Mine and within the Brunner Coal Measures included microcline, muscovite and kaolinite, which contain no sulphur in their mineralogical structures. The only other mineral that could have contributed notable quantities of sulphur included Ca-containing minerals including anhydrite ($CaSO_4$) and gypsum ($CaSO_4*2H_2O$); however, Ca was not measured at concentrations to offset the sulphur

contributions from minerals in addition to pyrite. There is potential that some sulphur was leached from coal seams and other organics that were contacted by the AMD. Results of the inverse geochemical modelling indicated that sulphur was extremely undersaturated (median SI of -62.2; range of -19.2 to -71.7), so its dissolution would be expected. The mineralogical dissolution involved in AMD generation is likely more complex than the chemical processes typically associated with pyrite oxidation and Fe hydrolysis alone. It is possible that following pyrite dissolution, Fe precipitates as goethite (FeO(OH)) or hematite (Fe_2O_3). Inverse geochemical modelling indicated that these minerals were oversaturated and could potentially precipitate, immobilising them, while sulphur remained dissolved in solution.

2.7.3 Potential Passive Treatment Options

Based on the water chemistry results, passive treatment options targeting neutralisation of acidity and sequestration of metals (primarily Fe and Al) would be recommended. The most feasible options of those presented in Chapter 1 include BGCRs and LLBs. Assuming adequate and feasible treatment areas were available, BGCRs would likely treat all AMD waters evaluated with potential exception of the Collis Seeps; however, they could likely be employed to improve its water chemistry, but treatment may not be completely adequate depending on treatment goals. The high Fe and Al concentrations associated with the Manchester and Collis Seep waters would potentially result in rapid plugging of LLBs with ferric hydroxide precipitate and settling and storage of aluminium hydroxide precipitate could be problematic.

2.8 Conclusions

Mine-water chemistry was variable on a spatial and temporal basis at Stockton Coal Mine (by up to three orders of magnitude for major contaminants). Despite the variability, Fe, Al, acidity and sulphate were consistently the primary contaminants of concern with Cu, Ni, Zn, Cd, Pb, As and Mn considered secondary pollutants, which typically exceeded ANZECC trigger values for protection of 80% of freshwater aquatic species. Because of the acidic conditions, nearly 100% of metals were present in the dissolved state. Metals present in the solid state were typically associated with sediment as opposed to metal precipitates.

Results of inverse geochemical modelling indicated that pyrite was consistently the most undersaturated mineral. Therefore, conditions were present for its continual oxidation and dissolution, which resulted in persistent hydrolysis and subsequent release of proton acidity. The resultant effect was undersaturation of nearly all minerals modelled resulting in the further dissolution of minerals and metals, which contributed metal acidity. Although inverse geochemical modelling provided an indication of the saturation state of numerous minerals, analytical inputs into the model must include appropriate water chemistry to determine likely mineralogical sources of dissolved ions (e.g. Si concentrations were not measured during this study, so excluding their input into the models resulted in no SIs reported for the primary Al containing minerals reported at Stockton Coal Mine).

Based on AMD chemistry alone, the majority of sites evaluated during this study were deemed suitable for treatment via passive treatment methods based on results of systems employed oversees. The only exception pertained to the Collis Seeps, which contained Fe, Al and acidity concentrations that were an order of magnitude greater than that of any other AMD water sampled as part of this study. The precipitation of an average of 45 kg of metals/day could also likely result in excessive passive treatment system clogging, and a high-frequency of system maintenance would also be likely. Available treatment area, site topography, and current and planned mining activities deemed most sites unfeasible for passive treatment during the project timeframe. Therefore, the Manchester Seep site was chosen as the candidate site for conducting mesocosm-scale treatability tests utilising BGCRs.

3. Biogeochemical Reactor Substrate Geotechnical Properties and Chemistry

Biogeochemical reactors were identified as the most appropriate passive-treatment option for treating the Manchester Seep AMD. Appropriate substrate media is required to sustain biogeochemical processes including biological sulphate reduction and alkalinity generation. A carbon source is required for microbial sulphate reduction (Equation 1.11) and surface attachment of SRB and carbon degrading bacteria. Additional alkaline materials are required to increase alkalinity production, neutralise acidity and induce subsequent metal immobilisation. Previous studies also reported better metal removal and sulphate reduction when utilising a mixture of organic products augmented with an alkaline material, as opposed to individual carbon sources alone (Pereyra et al., 2005; Zagury et al., 2006).

Clogging, primarily by sediment and/or ferric hydroxide precipitate, and the development of preferential flow paths in passive treatment systems has been reported (Younger et al., 2002; Watzlaf et al., 2004). Therefore, an objective of this study was to select substrate materials with adequate porosity and hydraulic throughput potential to achieve adequate flow throughput and minimise the potential for hydraulic-short circuiting, which would compromise treatment performance. Hydraulic conductivity tests were performed to determine the flow through each individual substrate material and through a selection of substrate mixtures containing alkalinity amendments. Substrate mixtures were selected on a volumetric basis since it was more consistent than on a weight basis where changes in moisture content would influence mixture composition. Volumetric mixing is also more pragmatic on a larger scale where earth-moving machinery of known bucket volumes would be required to transport and mix substrate compositions. Since many studies reported substrate mixture compositions on a weight basis (e.g. Waybrant et al., 1998; Wildeman et al., 2006; Buccambuso, 2007b; Blumenstein et al., 2008; Smart et al., 2008; Venot et al., 2008b), an objective was to determine various substrate weight-volume relationships so that substrate mixtures selected in this study could be converted from a volumetric basis to a weight basis for comparison. The air porosity was also used for calculating HRT during subsequent analysis of BGCR treatment performance (Chapter 4) and reactor modelling (Chapter 6).

The final objectives required analysis of substrate materials for chemical parameters. One reason was to identify and quantify deleterious substances that could potentially leach from substrates. Another was to estimate the alkalinity that could be theoretically generated from sulphate reduction based on the quantity of organic carbon present in each substrate mixture. Furthermore, calcium concentrations were used to estimate the total amount of alkalinity that could be generated as bicarbonate from the dissolution of calcium carbonate within alkaline materials.

3.1 Materials and Methods

3.1.1 Substrate Materials and Mixtures

Economically viable industrial-waste products were the primary substrate materials considered for the BGCRs. Organic substrate materials included post peel and wood shavings from untreated fence post manufacture (50-120 mm length and 5-20 mm width) and *Pinus radiata* bark (20-250 mm length and 20-100 mm width) and compost comprised of degraded forestry waste products such as bark, wood chips from the forestry industry (Figure 3.1). Alkaline materials included mussel shells, from mussel farm waste, nodulated stack dust (NSD), derived from the cement industry, and 20-70 mm diameter limestone, which was mined offsite (Figure 3.2). Rounded and sub-rounded river gravel (20-40 mm diameter) was used as bedding material and comprised the drainage layer of the BGCRs (Figure 3.2).

Figure 3.1. Organic substrate materials including: a) post peel; b) *Pinus radiata* bark; c) delignified bark compost; and d) wood shavings.

Figure 3.2. Alkaline materials and bedding material including: a) mussel shells; b) NSD; c) 20-50 mm diameter limestone; and d) 20-40 mm diameter bedding material.

Substrate mixtures were chosen to evaluate BGCR treatment performances as a function of different organic and alkalinity components (Table 3.1). The proportion of alkalinity amendments selected was based on the maximum composition of limestone recommended for VFWs and generally contained approximately 30 wt. % alkalinity amendments on an as-received basis (Wildeman et al., 2006). Mix 4 was an exception and contained a higher percentage of mussel shells (43.6 wt. %) to determine its influence on BGCR performance. Nodulated stack dust was not utilised in any of the substrate mixtures evaluated for geotechnical properties because it was too highly dissolvable, which could have contaminated the reticulated water supply used during hydraulic conductivity testing.

Substrate mixtures included a mixture of labile and long-term organic substrates based on studies, such as those conducted by Pereyra et al. (2005) and Zagury et al. (2006), which found more effective sulphate reduction and metal removal compared with VFWs incorporating individual substrate materials. Alkalinity amendments were included in the substrate mixtures as this has become standard practice for passive AMD treatment applications to increase the alkalinity generating potential (Watzlaf et al., 2004; Wildeman et al., 2006). The different alkalinity amendments incorporated in the substrate mixtures, including limestone, mussel shells and NSD, were tested to determine their influence on treatment performance.

Table 3.1: Composition (vol. %) of substrate mixtures evaluated for geotechnical properties.

	Mix 1	Mix 2	Mix 3	Mix 4	Mix 5
Alkalinity Amendments					
Limestone	12.5	0.0	0.0	0.0	5.0
Mussel Shells	0	20	20	30	12
Organic Carbon Sources					
Bark	37.5	40	30	30	30
Post Peel	25	25	35	25	38
Compost	20	15	15	15	15
Wood Shavings	5	0.0	0.0	0.0	0.0

3.1.2 Geotechnical Testing

3.1.2.1 Hydraulic Conductivity

Hydraulic conductivity represents the ease of water flow through porous media, which is influenced by fluid viscosity, pore-size distribution, grain-size distribution, void ratio, roughness or particles and degree of saturation (Das, 1998). Its importance regards verifying that adequate flow can be achieved in BGCRs at design flow rates. Hydraulic conductivity is measured experimentally by either constant-head or falling-head tests. The constant-head method was used due to the pervious nature of the substrate materials and mixtures. Hydraulic conductivity (K) using the constant-head method was calculated using Equation 3.1 where V represents the volume of water collected, L is the length of substrate material, A depicts the substrate surface area, h represents the hydraulic head and t signifies time.

$$K = VL/Aht \quad \textbf{(3.1)}$$

A schematic showing the constant-head set up used during this study and variables listed in Equation 3.1 is presented in Figure 3.3. A photo showing the experimental set-up is presented in Figure C.1 in Appendix C. Flow direction for the constant-head tests was downwards to simulate the operation of a downflow reactor (as performed for the BGCRs discussed in Chapters 4-6).

Permeameters consisted of HDPE cylindrical drums with 0.138 m^3 capacity and upper-surface area of 0.170 m^2 (average diameter of 465 mm). Bedding material was placed at the bottom of each permeameter and on top of the substrate (except for limestone) to promote uniform flow conditions during the hydraulic conductivity testing. Substrates were hand compacted and lightly shaken to facilitate settlement. Flow entering (influent) and exiting (effluent) the permeameters (Figures 3.3 and C.1) occurred through 32 mm diameter polyethylene tubing. A 25 mm diameter polyethylene tubing was used as a standpipe for measuring the hydraulic head. Substrates were carefully saturated from the bottom upwards in the permeameters to allow entrapped air to escape through the top of the permeameters.

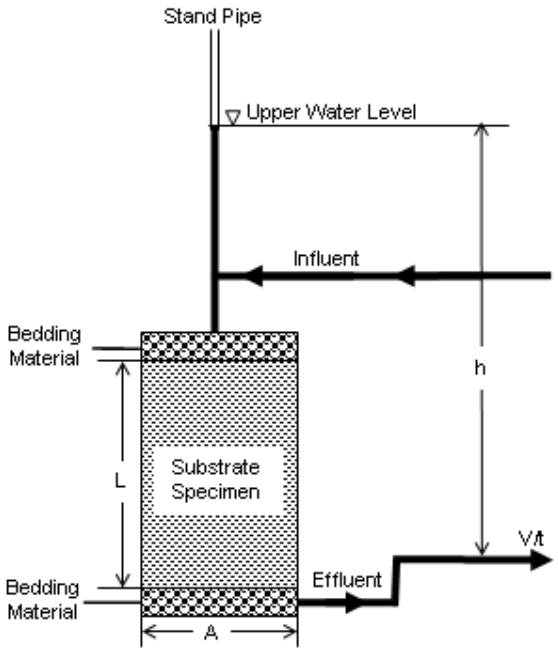

Figure 3.3. Schematic of hydraulic conductivity test apparatus.

Flow was conveyed to the permeameters via a 150 mm diameter pressurised water main. Flow rates were monitored using an Aquaflux 010K/D/6 flowmeter equipped with a Krohne IFC 010D signal converter attached to the water main. Flow calibration was confirmed using the bucket and stopwatch method (time to fill a vessel of known volume) for flow rates between 0.5 and 2.5 L/s with differences between readings averaging 2.5% (range of 1.1-3.9%). The volumetric flow rate (Q) was calculated using Equation 3.2.

$$Q = V/t \quad \textbf{(3.2)}$$

Equation 3.2 was substituted into Equation 3.1 to obtain Equation 3.3.

$$K = QL/Ah \quad \textbf{(3.3)}$$

The constant-head tests were performed in triplicate (three separate permeameters prepared) for each substrate and substrate mixture. Hydraulic conductivities were measured at three different head heights during each test. Flow rates, and the resultant change in head heights, were controlled by adjusting a ball valve in-line with the flow meter.

The water temperature was measured during each test so that hydraulic conductivities could be standardised to a temperature of 20^{o}C. Water becomes less viscous as temperature increases, which results in greater flow rates and hydraulic conductivities (Bear, 1972; Freeze and Cherry, 1972; Das, 1998). To account for this phenomenon, the flow during each run was standardised to 20^{o}C by using

Equation 3.4 (Das, 1998) where Q and μ represent flow and dynamic viscosity, respectively, at the experimental temperature and Q_{20^oC} and μ_{20^oC} represent flow and dynamic viscosity at 20°C.

$$Q_{20^oC} = Q\mu/\mu_{20^oC} \quad \textbf{(3.4)}$$

3.1.2.2 Porosity

Following each hydraulic conductivity test, the porosity of each substrate and substrate mixture were measured. Total porosity (ε) represents the fraction of substrate occupied by voids and is calculated using Equation 3.5 where V_v represents the volume of voids and V represents the total volume (volume occupied by voids and substrate).

$$\varepsilon = V_v/V \quad \textbf{(3.5)}$$

The voids within the substrate can either be occupied by air, liquid or a combination of both. The total porosity also represents the sum of the air porosity (ε_{air}) and the water holding capacity (ε_{whc}) as shown in Equation 3.6.

$$\varepsilon = \varepsilon_{air} + \varepsilon_{whc} \quad \textbf{(3.6)}$$

Air porosity, sometimes referred to as specific yield, represents the void volume occupied by free draining liquid in a saturated substrate. It represents the portion of the voids where flow occurs and is important when calculating HRT, or the time that a fluid spends in porous media. The water holding capacity, sometimes referred to as field capacity, represents the ratio of water that is retained within a substrate via sorption following free draining of a saturated substrate.

Air porosity was measured at the conclusion of each hydraulic conductivity test. The mass and temperature of the water that freely drained from the permeameters were measured. The mass of water was converted to volume using Equation 3.7 where $V_{v(air)}$ represents the volume of water drained from the voids of the substrate, $m_{w(air)}$ signifies the mass of water drained from the substrate and ρ represents the density of water at the temperature it was measured (Davis and Cornwell, 1991) when drained from the permeameter.

$$V_{v(air)} = m_{w(air)}/\rho \quad \textbf{(3.7)}$$

Air porosity was then computed by Equation 3.8.

$$\varepsilon_{air} = V_{v(air)}/V \quad \textbf{(3.8)}$$

Once the permeameters were drained and the mass of water was measured, substrate materials were dried in a convection oven at 105°C until all water evaporated and a constant mass was achieved. The total volume of water ($V_{v(tot)}$) present in the substrate materials (sum of free draining voids and sorbed portions) was calculated using Equation 3.9 where $m_{s(dry)}$ specifies the mass of dried substrate, $m_{s(sat)}$ represents the mass of saturated substrate (includes the summation of $m_{s(dry)}$ and the mass of water (m_w) present when all voids are saturated with water) and ρ represents the density of water at the temperature of water measured when saturating the permeameters.

$$V_{v(tot)} = (m_{s(sat)} - m_{s(dry)})/\rho \quad \textbf{(3.9)}$$

Total porosity was then computed using Equation 3.10.

$$\varepsilon_{tot} = V_{v(tot)}/V \quad \textbf{(3.10)}$$

The water holding capacity was finally computed using Equation 3.11:

$$\varepsilon_{whc} = \varepsilon_{tot} - \varepsilon_{air} \quad \textbf{(3.11)}$$

3.1.2.3 Bulk Density

Bulk density (ρ_s) of a substrate refers to the total mass of material (m_s), including substrate and moisture, which occupies a specified volume (V) as defined in Equation 3.12.

$$\rho_s = m_s/V \quad \textbf{(3.12)}$$

Bulk density was determined by weighing the mass of each substrate, as received from the supplier, and substrate mixture in the permeameters.

The saturated bulk density (ρ_{sat}) represents the bulk density when all voids are saturated with water and was calculated using Equation 3.13.

$$\rho_{sat} = m_{s(sat)}/V \quad \textbf{(3.13)}$$

The mass of each substrate material and mixture was measured following saturation of the substrate or substrate mixture.

The wet bulk density (ρ_{wet}) represents the bulk density after water from a saturated specimen is allowed to free drain and was computed using Equation 3.14 where $m_{s(wet)}$ represents the mass of the wet substrate.

$$\rho_{wet} = (m_{s(sat)} - m_{w(air)})/V = m_{s(wet)}/V \quad \textbf{(3.14)}$$

The dry bulk density (ρ_d) was computed using Equation 3.15.

$$\rho_d = m_{s(dry)}/V \quad \textbf{(3.15)}$$

The mass of dry substrate was determined by removing all of the substrate from the permeameters following the hydraulic conductivity tests and drying it in a convection oven at a temperature of approximately 105°C until all water evaporated and a constant mass was achieved.

3.1.2.4 Moisture Content

Moisture content (ω) represents the ratio of the mass of water (m_w) in a substrate to the mass of dry substrate ($m_{s(dry)}$) as shown in Equation 3.16.

$$\omega = m_w/m_{s(dry)} \quad \textbf{(3.16)}$$

The moisture content was determined on substrate materials as received from the suppliers (ω_s; Equation 3.16), on a wet basis following free drainage of void water when measuring air porosity (ω_{wet}; Equation 3.17) and on saturated substrates (ω_{sat}; Equation 3.18). The moisture content on a wet basis (ω_{wet}) represents the moisture content at the water holding capacity.

$$\omega_s = (m_s - m_{s(dry)})/m_{s(dry)} \quad \textbf{(3.16)}$$

$$\omega_{wet} = (m_{wet} - m_{s(dry)})/m_{s(dry)} \quad \textbf{(3.17)}$$

$$\omega_{sat} = (m_{sat} - m_{s(dry)})/m_{s(dry)} \quad \textbf{(3.18)}$$

3.1.3 Chemical Analyses

All chemical analyses were conducted by RJ Hill Laboratories Limited. Total carbon concentrations were measured by catalytic combustion separation and a thermal conductivity detector for organic substrates including bark, post peel, compost and wood shavings since organic carbon is required for microbial sulphate reduction and other biological processes in BGCRs (Stumm and Morgan, 1981). It was assumed that the carbonate concentrations in organic materials were negligible, as typical in New Zealand, and that total carbon was representative of total organic carbon (RJ Hill Laboratories Limited, 2009). Metal (Fe, Al, Cu, Ni, Zn and As) and cation (Ca, Mg, Na and K) concentrations were measured using ICP-MS following U.S. EPA method 200.2. Additionally, the Cr concentration of the compost was measured since it was stored at a timber treatment facility that potentially used

chromated copper arsenate (CCA) treatment. The pH of the compost was determined following method APHA 4500-H (APHA, 2000).

3.2 Results and Discussion

3.2.1 Geotechnical Properties

3.2.1.1 Hydraulic Conductivity

Results of geotechnical analysis for individual substrate materials and substrate mixtures are summarised in Tables 3.2 and 3.3, respectively. Hydraulic conductivity averages and ranges for each individual substrate material and the substrate mixtures are also shown in Figure 3.4. Hydraulic conductivities for individual substrates, with exception of the compost, were on the order of clean gravels. The hydraulic conductivity of the compost was comparable to fine sand or silty sand (Freeze and Cherry, 1979; Das, 1998). For the substrate mixtures, hydraulic conductivities were comparable to sandy gravel.

Hydraulic conductivities for individual substrates, excluding compost, were all on the 1E-3 m/s order of magnitude (range of 2.66E-3 for bark to 9.22E-3 m/s for bedding material, equivalent to a range of 317 to 778 m/day, respectively) as shown in Figure 3.4. The hydraulic conductivities for the substrate mixtures (Figure 3.4) were less due to the more heterogeneous material sizes and the inclusion of compost but were still typically around the 1E-3 m/s order of magnitude (range of 7.50E-4 for mix 5 to 3.46E-3 m/s for mix 2 equivalent to a range of 75.0 to 778 m/day, respectively). Hydraulic short-circuiting was suspected in the compost during two of the test runs (average hydraulic conductivity of 1.90E-4 m/s (16.4 m/day; n=6) compared with 4.67E-5 m/s (4.03 m/day; n=3) for the non-suspect test run) based on differences in hydraulic conductivities and the presence of cracking visually observed in the compost following the tests.

Although the downward flow direction was used when measuring hydraulic conductivities, it is often recommended to conduct testing using an upflow direction to reduce the risk of air entrapment within the substrate media impeding flow. Measures were taken during this study to minimise this risk such as saturating the substrate media from the bottom upwards and closing valves in a manner to prevent the ingress of air. Hypothetically, if air entrapment did occur during testing, the hydraulic conductivity values would have been biased low (Das, 1998). Despite this, the hydraulic conductivities measured for substrate mixtures indicate adequate hydraulic throughput and minimal to no risk for clogging or developing preferential flow paths.

Table 3.2: Geotechnical parameters from individual substrate materials (n=9 for flow and n=3 for porosity, bulk density and moisture content). Values represent averages ± standard deviation with ranges below in parentheses. Hydraulic conductivities reported should be multiplied by 1E-3 to give units m/s and flow (volumetric basis) should be multiplied by 1E-2 to give units L/s/m^3.

Geotechnical Parameter	Units	Bedding Material	Limestone	Mussel Shells	Post Peel	Bark	Compost
Flow							
Hydraulic Conductivity	**m/s *10^3**	7.34±1.20 (5.90-9.01)	7.31±1.26 (5.64-9.22)	4.59±0.674 (3.77-5.51)	4.81±7.29 (3.86-5.86)	3.67±0.680 (2.66-4.79)	0.142±0.103 (0.035-0.295)
Hydraulic Conductivity	**m/day**	634±104 (510-778)	629±106 (487-778)	396±58.2 (326-476)	416±63.0 (334-506)	317±58.7 (230-414)	12.3±8.86 (3.06-25.5)
Flow (Volumetric Basis)	**L/s/m^3 *10^2**	1.45±0.147 (1.23-1.69)	1.45±0.241 (1.19-1.98)	1.95±0.168 (1.73-2.17)	1.89±0.197 (1.63-2.19)	1.46±0.212 (1.14-1.85)	0.062±0.051 (0.014-0.016)
Flow (Areal Basis)	**L/s/m^2**	11.9±1.21 (10.1-13.8)	11.9±1.98 (9.74-16.2)	11.4±0.981 (10.1-12.7)	11.1±1.15 (9.53-12.8)	8.56±1.23 (6.70-10.8)	0.362±0.300 (0.081-0.943)
Porosity							
Total	**m^3/m^3**	0.396±0.008 (0.391-0.407)	0.469±0.012 (0.453-0.477)	0.718±0.023 (0.687-0.734)	0.856±0.007 (0.846-0.861)	0.739±0.014 (0.721-0.753)	0.664±0.045 (0.605-0.702)
Air		0.389±0.004 (0.385-0.393)	0.441±0.013 (0.424-0.454)	0.592±0.0545 (0.519-0.633)	0.635±0.001 (0.628-0.648)	0.495±0.020 (0.468-0.513)	0.173±0.014 (0.162-0.192)
Water Holding Capacity		0.007±0.009 (0.002-0.016)	0.028±0.005 (0.023-0.033)	0.126±0.081 (0.054-0.214)	0.220±0.009 (0.213-0.231)	0.245±0.034 (0.208-0.275)	0.491±0.068 (0.413-0.540)
Bulk Density							
As Received	**kg/m^3**	1630±23.7 (1610-1650)	1530±25.0 (1500-1550)	793±31.8 (759-823)	296±16.4 (285-315)	349±18.2 (331-367)	856±44.7 (821-906)
Dry		1510±24.3 (1500-1540)	1420±22.0 (1410-1450)	698±35.7 (657-722)	139±6.32 (133-146)	180±12.1 (168-192)	485±33.3 (460-523)
Wet		1620±15.1 (1600-1630)	1530±99.7 (1450-1640)	824±97.0 (767-936)	359±14.7 (350-376)	424±40.5 (387-467)	975±37.9 (935-1010)
Saturated		2020±19.5 (2000-2040)	1970±10.1 (1960-1980)	1420±34.8 (1390-1450)	993±13.6 (978-1004)	918±18.0 (899-935)	1150±22.8 (1130-1170)
Moisture Content							
As Received	**kg/kg**	--	--	0.137±0.021 (0.114-0.156)	1.13±0.047 (1.07-1.16)	0.949±0.202 (0.819-1.18)	0.767±0.0527 (0.733-0.828)
Wet		--	--	0.180±0.111 (0.076-0.296)	1.58±0.048 (1.53-1.63)	1.36±0.173 (1.16-1.48)	1.02±0.200 (0.789-1.14)
Saturated		0.240±0.006 (0.233-0.244)	0.294±0.014 (0.278-0.306)	1.03±0.079 (0.961-1.12)	6.15±0.235 (5.89-6.36)	4.12±0.316 (3.86-4.47)	1.38±0.190 (1.16-1.49)

--, not determined

Table 3.3: Geotechnical parameters from substrate mixtures (n=9 for flow parameters and n=3 for porosity, bulk density and moisture content measurements). Values represent averages with ranges below in parentheses. Hydraulic conductivities reported should be multiplied by 1E-3 to give units m/s and flow (volumetric basis) should be multiplied by 1E-2 to give units $L/s/m^3$.

Geotechnical Parameter	Units	Mix 1	Mix 2	Mix 3	Mix 4	Mix 5
Flow						
Hydraulic Conductivity	**m/s *10^3**	1.56±0.440 (0.925-2.26)	1.91±0.776 (1.05-3.46)	1.74±0.833 (0.871-3.29)	1.58±0.462 (1.08-2.50)	1.04±0.225 (0.750-1.47)
Hydraulic Conductivity	**m/day**	135±38.0 (79.9-196)	165±67.1 (90.9-299)	150±72.0 (75.2-284)	137±39.9 (93.7-216)	90.2±19.4 (64.8-127)
Flow (Volumetric Basis)	**$L/s/m^3$ *10^2**	0.664±0.179 (0.416-1.01)	0.760±0.277 (0.463-1.24)	0.711±0.332 (0.355-1.27)	0.652±0.169 (0.469-0.962)	0.430±0.0702 (0.329-0.551)
Flow (Areal Basis)	**$L/s/m^2$**	3.89±1.05 (2.43-5.88)	4.45±1.63 (2.71-7.25)	4.16±1.94 (2.08-7.41)	3.82±0.987 (2.74-5.63)	2.52±0.414 (1.93-3.23)
Porosity						
Total	**m^3/m^3**	0.598±0.012 (0.586-0.613)	0.701±0.021 (0.676-0.724)	0.679±0.012 (0.670-0.694)	0.686±0.019 (0.672-0.711)	0.662±0.003 (0.659-0.667)
Air		0.410±0.038 (0.359-0.435)	0.478±0.028 (0.451-0.514)	0.483±0.012 (0.472-0.499)	0.506±0.022 (0.481-0.531)	0.472±0.010 (0.459-0.481)
Water Holding Capacity		0.189±0.035 (0.160-0.228)	0.223±0.012 (0.210-0.234)	0.196±0.002 (0.195-0.198)	0.180±0.011 (0.170-0.191)	0.191±0.008 (0.186-0.200)
Bulk Density						
As Received	**kg/m^3**	499±17.4 (480-514)	416±29.0 (395-449)	409±14.4 (394-422)	450±20.7 (428-469)	494±11.3 (487-507)
Dry		453±4.63 (449-458)	303±26.0 (286-333)	315±9.39 (304-323)	358±14.0 (342-367)	394±11.9 (386-408)
Wet		641±32.3 (612-676)	526±30.6 (496-557)	510±7.94 (502-518)	538±24.2 (511-558)	585±11.5 (572-594)
Saturated		1050±17.8 (1030-1070)	1000±8.71 (993-1010)	992±21.6 (973-1020)	1040±29.2 (1020-1070)	1060±15.7 (1050-1070)
Moisture Content						
As Received	**kg/kg**	0.102±0.042 (0.061-0.145)	0.374±0.023 (0.348-0.392)	0.299±0.008 (0.293-0.308)	0.259±0.017 (0.245-0.278)	0.254±0.009 (0.244-0.261)
Wet		0.416±0.080 (0.354-0.506)	0.738±0.066 (0.675-0.806)	0.622±0.024 (0.604-0.648)	0.503±0.015 (0.494-0.520)	0.483±0.029 (0.455-0.513)
Saturated		1.32±0.016 (1.31-1.34)	2.33±0.264 (2.03-2.53)	2.15±0.041 (2.12-2.20)	1.92±0.078 (1.83-1.97)	1.68±0.041 (1.63-1.71)

One of the major mechanisms for potential system failure of VFWs treating MIWs is clogging of substrates with metal precipitates (Kepler and McCleary, 1997; Rose and Dietz, 2002; Younger et al., 2002; Rose, 2006) or hydraulic-short circuiting due to preferential flow paths forming (Rose and Dietz, 2002; Wildeman et al., 2006). Clogging of VFWs can be minimised by the use of porous media with large pore spaces, good hydraulic conductivity and the ability to flush out precipitates (Lyew and Sheppard, 1997; Tsukamoto et al., 2004). Clogging issues have typically been associated with formation of ferric and aluminium hydroxide precipitates (Rose, 2006). Sediment could also potentially clog systems if not mitigated in preceding sedimentation ponds (Gusek, 2004; Wildeman et al., 2006). Hydraulic short-circuiting has typically been associated with preferential flow paths developed in homogenous compost-based systems including scouring at the interfaces of substrate and drainage pipes (Demchak et al., 2001; Rose, 2006) and non-uniform flow distribution (Busler et al., 2002; Gusek, 2004).

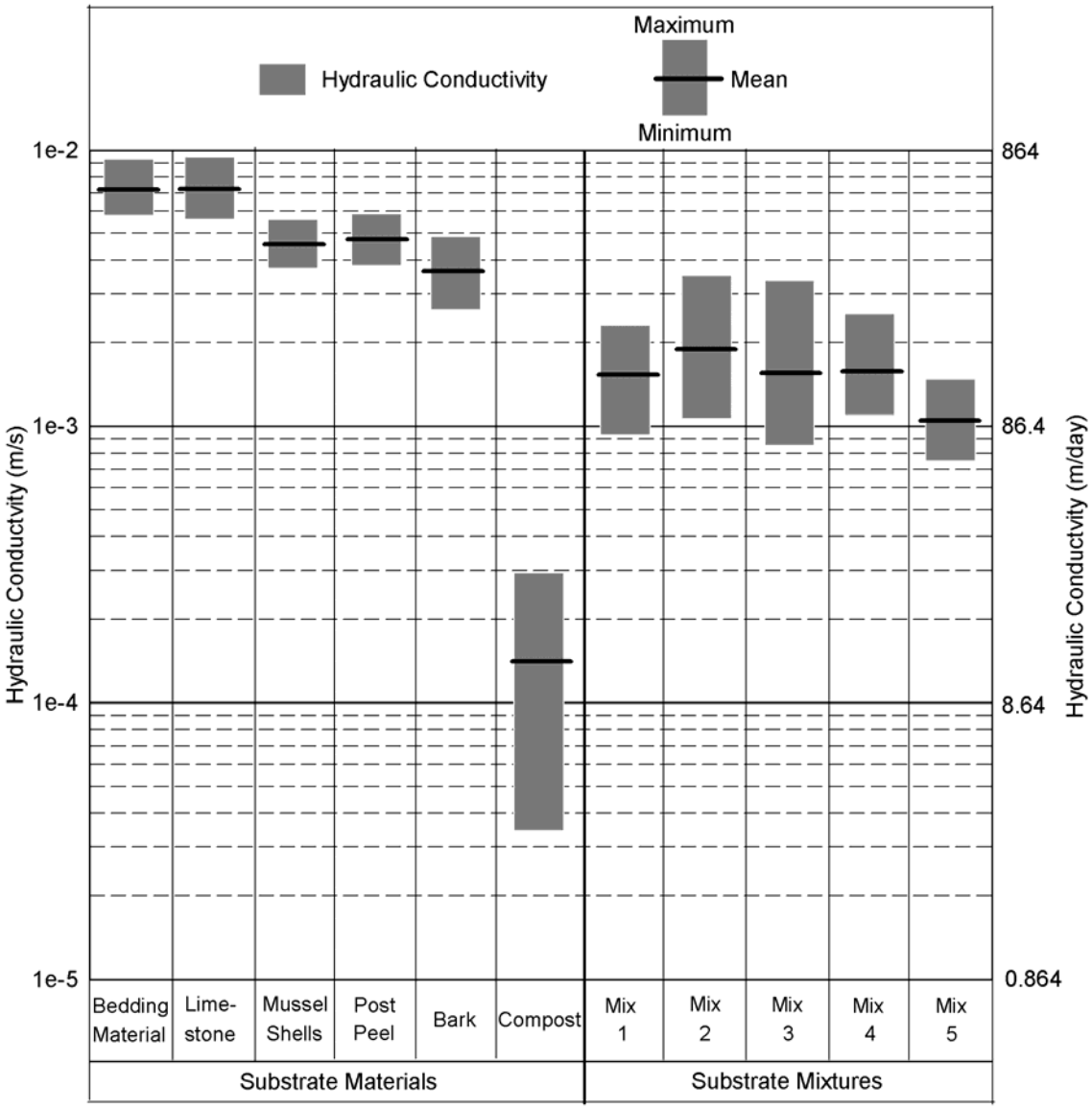

Figure 3.4. Hydraulic conductivity ranges and averages of the individual substrate materials and substrate mixtures (n=9).

Numerous VFWs have employed compost as the sole organic component including those evaluated by Rose and Dietz (2002), Skousen and Ziemkiewicz (2005) and Rose (2006). Busler et al. (2002) used iridescent dye to evaluate hydraulic short-circuiting in VFWs comprising spent-mushroom compost or a mixture of spent-mushroom compost with fine limestone. Their study concluded that plugging was occurring so alterations in the effluent drainage piping were made, which achieved more uniform flow distribution and reduced short circuiting. Hutchinson and Nairn (2005) measured hydraulic conductivities from a VFW consisting of composted horse manure mixed with limestone that was in operation for about five years. Hydraulic conductivities decreased with operational time based on increased water levels required to achieve adequate flow through the substrate. Hydraulic conductivities in the Hutchinson and Nairn (2005) study averaged approximately 2.6E-5 m/s, which

was an order of magnitude less than the average hydraulic conductivity of the compost in this study and two orders of magnitude less than the substrate mixtures reported here. Gusek (2004) reported that early VFW designs utilising solely compost (with potentially a mixture of manure) contained a low hydraulic conductivity on the order of 1E-6 m/s, which is comparable to silt and not optimal for use in BGCRs (Freeze and Cherry, 1979; Das, 1998). This value is two orders of magnitude less than the compost (comprised of de-lignified bark) used during this study and three orders of magnitude less than the substrate mixtures. Modifications to the VFW designs reported by Gusek (2002), including use of heterogeneous substrate mixtures containing bulking materials such as wood chips and crushed limestone, resulted in increased hydraulic conductivities of several orders of magnitude (values not reported) and no observed clogging. Since these adjustments, treatment performance of VFWs has been more reliable.

The substrate mixtures selected during this study are not likely to clog based on the assessment of Gusek (2002). Although changes in hydraulic conductivities (or porosity) were not measured at the conclusion of the mesocosm-scale treatability tests subsequently discussed in Chapter 4, it is estimated that <10% of the reactor pore volumes would be occupied by metal precipitates during the design life of the BGCRs. This is based on converting the mass of metals that would be removed during the design life of the system (discussed in Chapter 8) to a volumetric basis using conservative assumptions on metal densities. Reliable treatment performance should also be achieved since most failures in VFW treatment performance have been a function of inefficient hydraulics (including development of preferential flow paths and short circuiting) and contaminant overloading (Wildeman et al., 2006).

3.2.1.2 Flow

Design criteria for VFW systems for mine-water treatment applications have typically been reported on a molar substrate volumetric or acidity areal removal basis (e.g. Watzlaf et al., 2004; Wildeman et al., 2006). The maximum volumetric flow capacity per unit volume of substrate for all the substrate mixtures and compost alone used in this study as a function of hydraulic head is shown in Figure 3.5. The areal flow as a function of hydraulic head is presented in Figure 3.6. The hydraulic heads during this study ranged from 943 to 1959 mm, which generally falls within the recommended hydraulic head of 1.5-2.0 metres for systems comprised of compost as the sole substrate (PIRAMID, 2003; Watzlaf et al., 2004). The flow capacity was generally greater with increasing hydraulic head by an average of 1.94E-3 L/s/m^3 (for volumetric flow) and 1.14 L/s/m^2 (for areal flow) per 1000 mm hydraulic head for the substrate mixtures and 6.01E-4 L/s/m^3 (volumetric) and 0.352 L/s/m^2 (areal) per 1000 mm hydraulic head for the compost. When applying linear best fit lines to each test run (at the three hydraulic head heights), the hydraulic throughput potential interpolated at zero hydraulic head ranged from 1.31-4.03 L/s/m^2 and 2.23E-3-6.88E-3 L/s/m^3 (R^2=0.999) considering all substrate mixtures grouped together. Negative flow was computed for the compost (average of -0.152 L/s/m^2 and -2.59E-4 L/s/m^3; R^2=0.989) with an average hydraulic head of 585 mm required to attain flow. These

results indicated that minimal hydraulic head is required to maintain flow through all substrate mixtures. They should, therefore, be much less susceptible to clogging compared to VFWs comprising of compost without bulking materials which require significant hydraulic head to maintain flow even during the initial stages of operation (Gusek, 2004; Watzlaf, 2004; Wildeman et al., 2006).

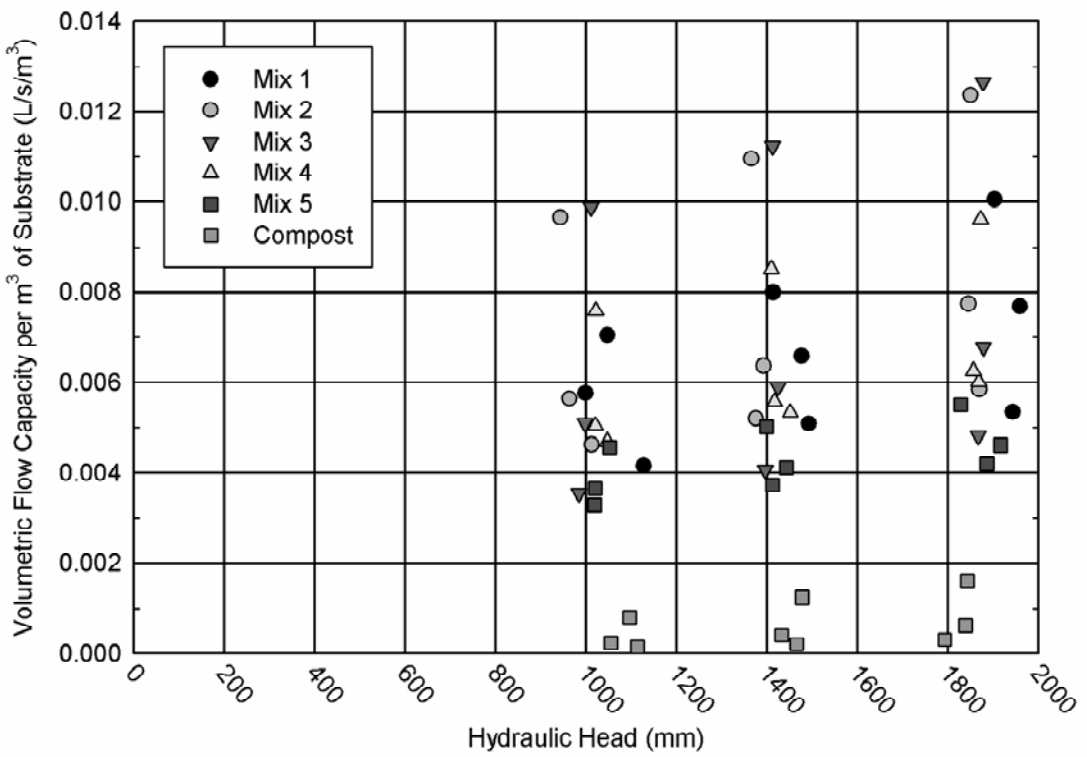

Figure 3.5. Data showing the flow capacity that would have passed through a cubic metre of the substrate mixtures and compost at the hydraulic heads tested.

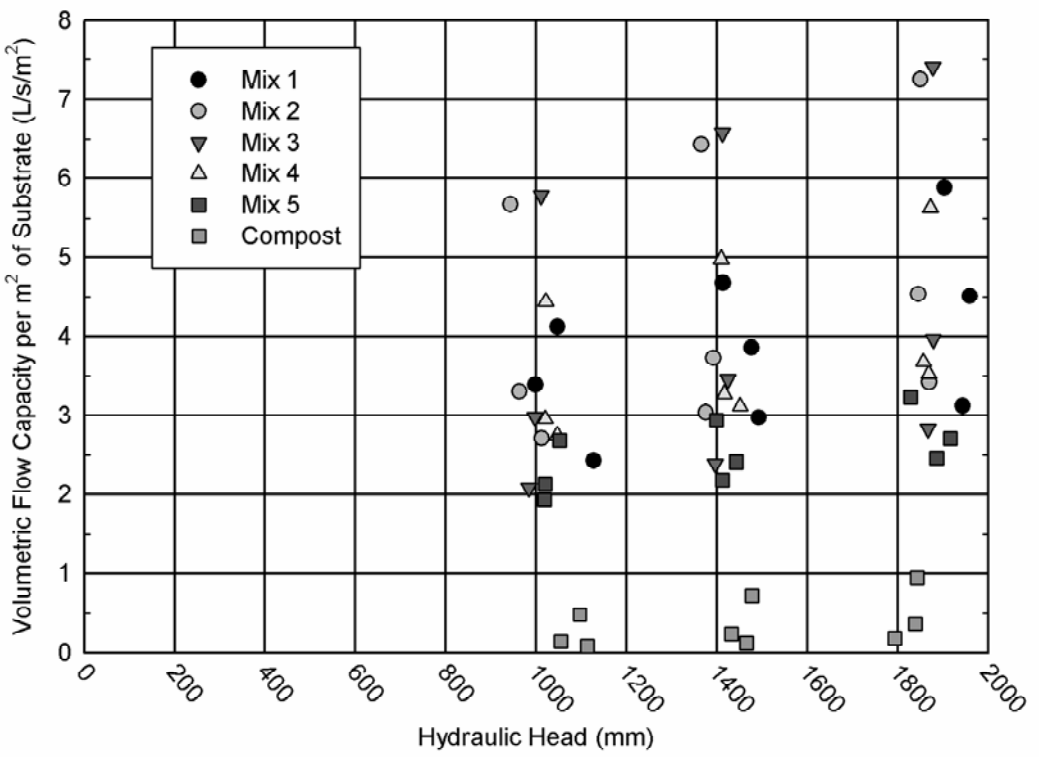

Figure 3.6. Data showing the flow capacity that would have passed through a square metre of the substrate mixtures and compost at the hydraulic heads tested.

3.2.1.3 Porosity and Water Holding Capacity

Porosity and water holding capacity were generally similar among the substrate mixtures (Table 3.3), but notably different in the individual substrate materials (Table 3.2). The porosity parameter of most relevance in this study is air porosity as this value represents the fraction of a substrate volume where liquid flows and was used for determining HRT in this study (e.g. Chapters 4 and 6). Air porosities were greatest for the post peel (average of 0.635) followed by the mussel shells (average of 0.592). Substrate mixtures (mixes 2-4) containing the highest vol. % of mussel shells (20-30%) contained the highest air porosities (0.478-0.506). The air porosity was substantially lower for the compost (average 0.173).

The compost, like the other organic substrate materials (including post peel and bark), contained higher water holding capacities than the inorganic mineralogical-based materials such as limestone, mussel shells and bedding material since water was absorbed and retained within the organic matrices. Water did not drain from the compost as easily as the more pervious post peel and bark. The water holding capacities of the bedding material and limestone were extremely low (average of 0.007 and 0.028, respectively) since these materials are free draining and the individual particles (or rocks) are, for all practical purposes, impervious (Bear, 1972; Freeze and Cherry, 1979). The mussel shells, although composed primarily of calcium carbonate like the limestone, contained a higher water

holding capacity (average of 0.126) than the bedding material and limestone. The organic material (non-decomposed mussel fragments) bound to the mussel shells likely contributed to this.

3.2.1.4 Bulk Density and Moisture Content

The primary importance of knowing bulk density and moisture content relate to the ability to convert substrate compositions between a volumetric and weight basis. From an operational perspective, it is easier, and more reproducible, to create substrate mixtures by mixing known volumes compared with weights. The bucket volumes of earthmoving and transport machinery are commonly known or can easily be determined, whereas an industrial scale is required to weigh materials. Furthermore, the moisture contents of substrate materials can be variable depending on how they were stored and the weather they were exposed to, which influences substrate mass and, consequently, substrate mixture compositions on a wt. % basis. For example, the moisture contents of substrate materials as received from the supplier or during storage can vary substantially.

Bulk density of the bedding material and limestone were substantially greater than the other substrates (Table 3.2). The bulk density of the mussel shells were less (approximately one-half) despite being comprised mostly of calcium carbonate like the limestone (mussel shells 53% average Ca concentration and limestone 39% average Ca concentration (Hutchinson and O'Sullivan (2008)). The differences were likely due to specific gravity and shape. The average specific gravity of the limestone used in this study was 2.57, whereas the average specific gravity of the mussel shells was 2.42. The mussel shells contained a concaved shape, which resulted in the presence of greater air voids (greater air porosity) compared with the subangular-shaped limestone. The bulk density of the organic materials were substantially less than the mineralogical-based materials (typically less than one-half as received from the supplier), which was likely due to greater porous voids within their solid matrices, which contributed to greater total porosities and water holding capacities (Table 3.2).

The differences in composition of the substrate mixtures on a wt. % basis are summarised in Table 3.4. Substrate mixture compositions varied depending on their moisture content. Differences in wt. % composition of alkalinity amendments in each substrate mixture (summation of limestone and mussel shells) differed by an average of 6.5 wt. % (range of 1.8-15%) comparing wt. % compositions on as-received, dry and wet basis. This could have implications if adopting design recommendations reported on a weight basis that do not specify moisture content. The substrate mixtures evaluated during this study generally contained approximately 30 wt. % alkalinity amendments on an as-received basis with exception of Mix 4, which contained 43.6 wt. % mussel shells. This concurs with Wildeman et al. (2006) who recommended incorporating no more than 30 wt. % (assumed on an as-received basis) of limestone in VFW substrate mixtures.

Table 3.4: Composition of substrate mixtures evaluated for geotechnical properties. Table values represent wt. % of the substrate materials as received from the supplier, dried and wet following free drainage from saturated specimens.

	Mix 1	Mix 2	Mix 3	Mix 4	Mix 5
As-Received Basis (wt. %)					
Limestone	26.9	0.0	0.0	0.0	14.8
Mussel Shells	0.0	31.7	32.0	43.6	18.4
Bark	29.1	27.9	21.2	19.2	20.3
Post Peel	6.7	14.8	20.9	13.6	21.7
Compost	32.1	25.7	25.9	23.6	24.8
Wood Shavings	5.1	0.0	0.0	0.0	0.0
Summation of Limestone and Mussel Shells	***26.9***	***31.7***	***32.0***	***43.6***	***33.2***
Dry Basis (wt. %)					
Limestone	41.9	0.0	0.0	0.0	21.2
Mussel Shells	0.0	34.8	36.8	47.6	20.2
Bark	22.4	31.1	24.7	21.3	22.6
Post Peel	4.4	5.8	8.5	5.3	8.5
Compost	29.0	28.3	30.0	25.9	27.5
Wood Shavings	2.3	0.0	0.0	0.0	0.0
Summation of Limestone and Mussel Shells	***41.9***	***34.8***	***36.8***	***47.6***	***41.4***
Wet Basis (wt. %)					
Limestone	31.6	0.0	0.0	0.0	15.2
Mussel Shells	0.0	27.7	28.6	39.2	16.2
Bark	24.0	31.7	24.5	22.4	23.1
Post Peel	9.3	11.5	16.7	10.9	17.1
Compost	31.4	29.1	30.1	27.5	28.4
Wood Shavings	3.6	0.0	0.0	0.0	0.0
Summation of Limestone and Mussel Shells	***31.6***	***27.7***	***28.6***	***39.2***	***31.4***

3.2.2 Substrate Chemistry

A summary of substrate chemistry and ANZECC (2000) low and high effects-based interim sediment quality guidelines stipulated for protection of freshwater aquatic organisms are presented in Table 3.5. Copper, Ni, Zn, As and Cr are the only elements measured during this study which contain sediment quality guidelines. Effects-base low indicates the concentration that deleterious effects on freshwater biota are rarely observed, whereas effects-base high represents the concentration at which deleterious effects are frequently observed. The only exceedances to these thresholds were Ni in compost, which exceeded the low and high guideline values, and As in the wood shavings, which exceeded the low guideline value. The wood shavings were excluded from further use in this study to prevent potential As leaching. Although Ni was present in the compost at an elevated concentration, it was not anticipated to leach from the VFWs since Ni was reportedly easily sequestered within these types of systems (Wildeman et al., 2006; Neculita et al., 2007). Although Fe and Al concentrations were typically one to three orders of magnitude greater than other heavy metals, they were also not expected

to leach significantly from the substrates in the BGCRs. Easily soluble mono-valent cations including Na and K were expected to leach since they are highly soluble.

Table 3.5: Substrate chemistry. All concentrations in units mg/kg on a dry weight basis with exception of pH. The recommended sediment quality guidelines provide an indication of sediment concentrations that may be deleterious to freshwater aquatic organisms (ANZECC, 2000).

Substrate Material	Total Carbon	Ca	Mg	Na	K	Fe	Al	Cu	Ni	Zn	As	Cr
Mussel Shells	--	530000*	570	8510	466	608	224	3	7	136	<2	2
Limestone	--	390000*	2210	125	326	4140	1120	<2	11	9	<2	
Compost	192000	11100	8020	1140	1400	23300	16000	23	66	61	4	57
Post Peel	44100	1240	351	<40	887	522	278	3	16	10	<2	--
Bark	350000	1150	280	59	610	324	577	<2	3	11	<2	--
Bedding Material	--	2410	4500	115	583	19900	10500	5	9	44	3	--
Wood Shavings	478000	1570	154	<40	196	52	26	28	<2	7	25	--
Recommended Sediment Quality Guidelines (ANZECC, 2000)												
Effects-Base Low	--	--	--	--	--	--	--	65	21	200	20	80
Effects-Base High	--	--	--	--	--	--	--	270	52	410	70	370

--, data parameters not measured or no sediment quality guidelines available; *average reported by Hutchinson and O'Sullivan (2008).

The potential bicarbonate alkalinity that could be generated from organic carbon decomposition during sulphate reduction (Equation 1.11) and from calcium carbonate dissolution (Equation 1.10) is presented in Table 3.6. Assumptions included: 1) all organic carbon is converted to bicarbonate during sulphate reduction based on the stoichiometry presented in Equation 1.11 and total carbon concentrations identified in Table 3.5; 2) organic content in mussel shells is negligible; 3) all Ca in the limestone and mussel shells was present as calcium carbonate; 4) any Ca in organic substrates would not contribute to alkalinity; 5) all calcium carbonate dissolved to generate bicarbonate alkalinity and 6) mass concentrations (mg/kg) were converted to a volumetric basis (kg/m^3) by multiplying by substrate dry bulk densities shown in Table 3.4.

Results indicated greater theoretical capacity for alkalinity generation from sulphate reduction (68.1-80.7% of total) compared with calcium carbonate dissolution (Table 3.6) by an average factor of 3.47 (range of 2.13-4.17). Despite this, reaction kinetics would dictate the amount and rate of alkalinity produced from each of these two reaction mechanisms, which are discussed in Chapters 4 and 5. The reaction kinetics would also be influenced by AMD chemistry in mine-water treatment applications.

The dissolution of calcium carbonate proceeds faster than and is a more reactive process than the sulphate-reduction process (Cubillas et al., 2005; Wildeman et al., 2006). This is important for metal

removal and maintaining a pH (>5.5) so that SRB can proliferate (Ross et al., 2003; Wildeman et al., 2006). Because of the faster dissolution of calcium carbonate, there is a high likelihood that alkalinity amendments will completely dissolve before the organic substrates.

Table 3.6: Potential alkalinity that could be generated (assuming 100% conversion) from the conversion of organic carbon to bicarbonate during the sulphate reduction process and the dissolution of calcium carbonate from limestone and mussel shells.

	Mix 1	Mix 2	Mix 3	Mix 4	Mix 5
Potential Alkalinity Generation (kg $CaCO_3/m^3$ substrate)					
Sulphate Reduction	584	535	543	484	564
Calcium Carbonate Dissolution	140	148	151	227	148
Total	724	683	694	712	711
Percentage of Total Potential Alkalinity Generation (%)					
Sulphate Reduction	80.7	78.3	78.3	68.1	79.3
Calcium Carbonate Dissolution	19.3	21.7	21.7	31.9	20.7

The assumptions made above are indicative and intended only so that preliminary estimates of the potential amount bicarbonate alkalinity generated can be made. The sulphate reduction process presented in Equation 1.11 is likely oversimplified assuming that carbon is decomposed into its simplest form as a carbohydrate (CH_2O). Despite this, Logan et al. (2005) demonstrated that dissolved organic carbon (DOC) present in more complex forms, such as lactate or acetate, is readily utilised by SRB as electron donors. There is potential that some of the carbon will not be utilised by SRB or subsequently converted to bicarbonate alkalinity and will, therefore, be utilised by other bacteria or leach out into the reactor effluent. Additional studies would be required to determine the amount of bicarbonate generated from the utilisation of DOC by SRB. Studies such as that by Demsi et al. (2010) have attempted to advance models of the bacterial sulphate-reduction process and organic decomposition rates in batch processes by including elements such as bacterial fate and surface-limiting processes associated with organic decomposition. Advances in such studies offer potential that the relationships between bacterial sulphate reduction and alkalinity generation can be better understood.

There is also potential that not all Ca in the limestone and mussel shells is present as calcium carbonate; however, studies such as Nelson et al. (1966) and Cubillas et al. (2005) have demonstrated high calcium carbonate purity in bivalves, typically at reagent-grade purities (>98%). An Estimate of the BGCR design life and potential acidity neutralised during the design life are presented in the Conclusions chapter (Section 8.3) based on results of the mesocosm-scale treatability tests (Chapter 4). These were estimated assuming calcium carbonate dissolution from alkalinity amendments was

the limiting design factor, and there was limited contribution to alkalinity generation from sulphate reduction. It may be plausible to add additional alkalinity amendments, such as mussel shells, and mix them in with undissolved organic substrate in the BGCR substrate mixtures during the operation of the BGCRs to extend their design life.

3.3 Conclusions

Hydraulic conductivity tests confirmed that the substrate mixtures in this study provided substantial hydraulic throughput potential for a BGCR and would be much less likely to clog or develop preferential flow paths compared with VFWs that incorporate exclusively compost. Such hydraulic inefficiencies have resulted in a decline in treatment performance of numerous VFWs, whereas those that contain bulking materials, such as the post peel and bark in BGCR substrate mixtures evaluated during this study have achieved more reliable treatment performance. The hydraulic conductivities of the substrate mixtures were an order of magnitude greater than the compost alone and two to three orders of magnitude greater than the compost used in other VFWs reported that were prone to clogging. The air porosities indicated that approximately one-half of the volumes incorporating the substrate mixtures were available for water to flow through, whereas less than 20 vol. % was available in the compost. The visual observations of cracking in the compost at the conclusion of two of the hydraulic conductivity test runs confirmed the potential for preferential flow paths to form in compost-based VFWs.

Bulk density and moisture content were used to calculate the compositions of substrate mixtures on a weight basis, which is more commonly reported in VFW literature but were originally measured on a more pragmatic volumetric basis. The wt. % composition of substrate mixtures was dependent on the moisture contents of the individual substrate materials, especially for the organic-based ones that have much higher water-holding capacities compared to mineralogical-based alkaline amendments. Therefore, more consistency in replicating substrate mixtures and applying optimal design guidelines can be achieved when using volumetric mixing ratios of known porosities.

The substrate mixtures have the theoretical capacity to generate approximately 700 kg of alkalinity as $CaCO_3/m^3$ substrate. Approximately 75% of this is attributed to organic carbon decomposition during sulphate reduction and the remainder from dissolution of calcium carbonate in limestone and/or mussel shells. This has implications to BGCR longevity but would be dependent on reaction kinetics and the amount of alkalinity generated by each mechanism during BGCR operation.

4. Acidity, Metal and Sulphate Removal from Mesocosm-Scale Biogeochemical Reactor Treatability Tests

The objective of this study was to examine the effectiveness of seven mesocosm-scale BGCRs with different reactor shapes and substrate compositions in removing metals (primarily Fe and Al), acidity and sulphate from AMD. The AMD feed rate was increased incrementally (0.05-1.44 mol total metals/m^3 substrate/day; 5.26-156 g acidity (as $CaCO_3$)/m^2/day; and 0.134-2.88 mol sulphate/m^3 substrate/day) throughout the study to investigate removal efficiency at different metal, acidity and sulphate loading rates and ascertain system treatment limits. This chapter evaluates contaminant removal with additional discussion on changes in water chemistry that occur with treatment. Metal and sulphate removal was analysed on a molar volumetric loading and a removal efficiency basis, whereas acidity removal was considered on an areal loading basis so that results could be better compared with other studies.

4.1 Materials and Methods

4.1.1 Biogeochemical Reactor Physical Characteristics

Mesocosm-scale BGCRs were established in the laboratory using two different types of containers providing for different flow configurations and substrate depth. Four reactors (S1-S4) were Stowers E4 low-density polyethylene (LDPE) trapezoidal-prism containers (Figure 4.1) with 0.337 m^3 capacity and a midpoint substrate surface area of 0.491 m^2 (upper dimensions of 900 mm X 600 mm, lower dimensions of 830 mm X 545 mm and a height of 680 mm). Three other BGCRs (P1-P3) were HDPE cylindrical drums (Figure 4.2) with 0.138 m^3 capacity and upper-surface area of 0.170 m^2 (average diameter of 465 mm).

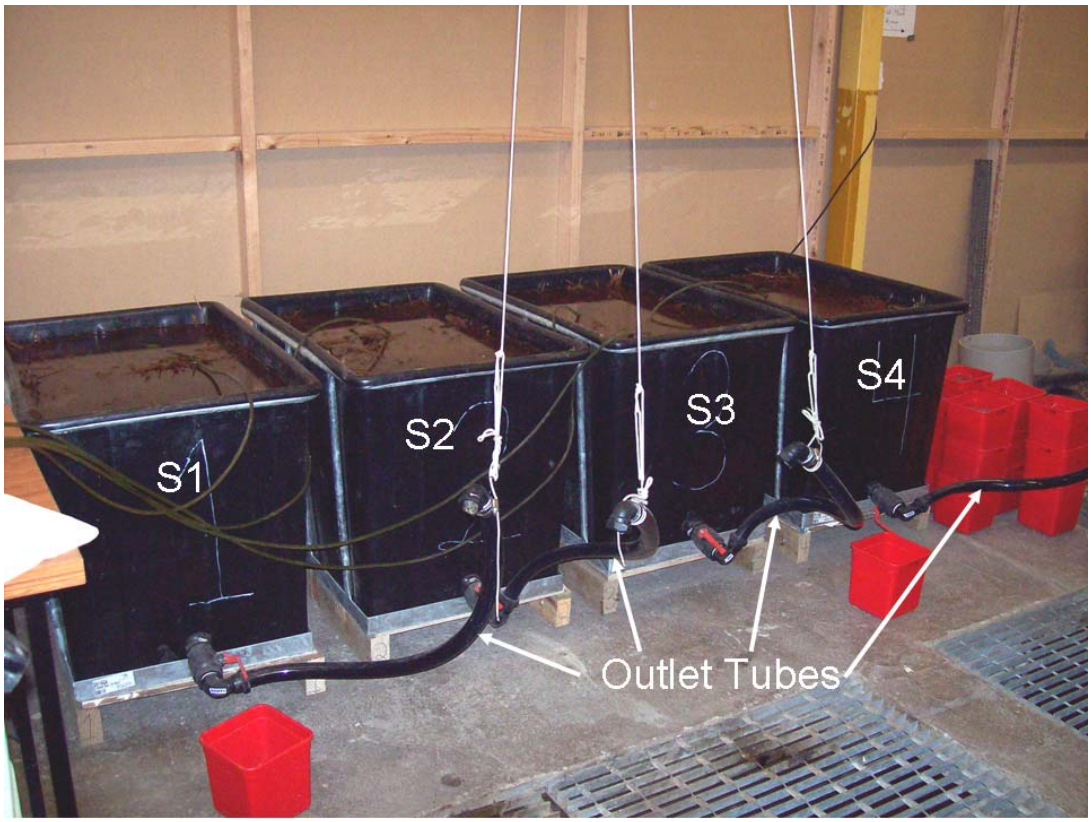

Figure 4.1. Trapezoidal-prism shaped mesocosm BGCRs (S1, S2, S3 and S4).

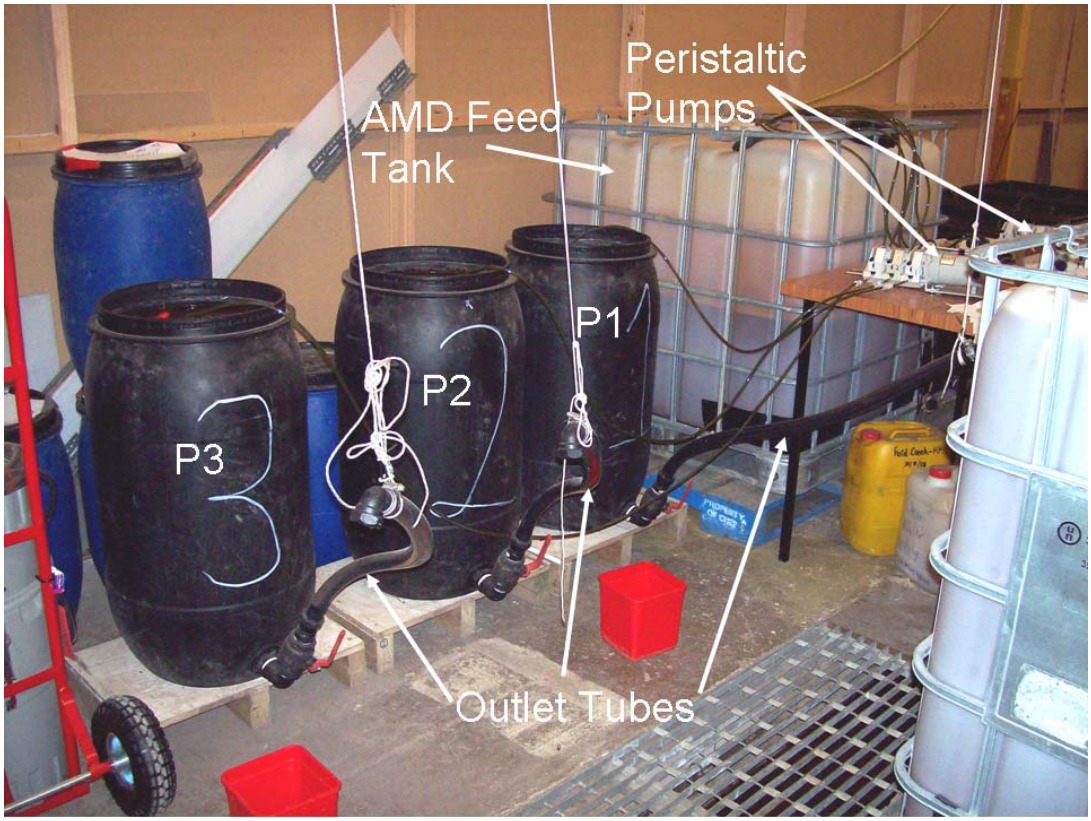

Figure 4.2. Drum-shaped mesocosm BGCRs (P1, P2 and P3) and AMD feed tank.

4.1.2 Substrate Materials

Substrate materials included predominately industrial-waste products (Figure 4.3). Alkaline materials included mussel shells, from mussel farm waste, nodulated stack dust (NSD), derived from the cement industry, and 20-70 mm diameter limestone, which was mined offsite. Organic substrate materials included post peel from untreated fence post manufacture (50-120 mm length and 5-20 mm width), *Pinus radiata* bark (20-250 mm length and 20-100 mm width) and compost comprised of degraded forestry waste products such as bark and wood chips. None of the substrate materials were intentionally used as inoculants for SRB.

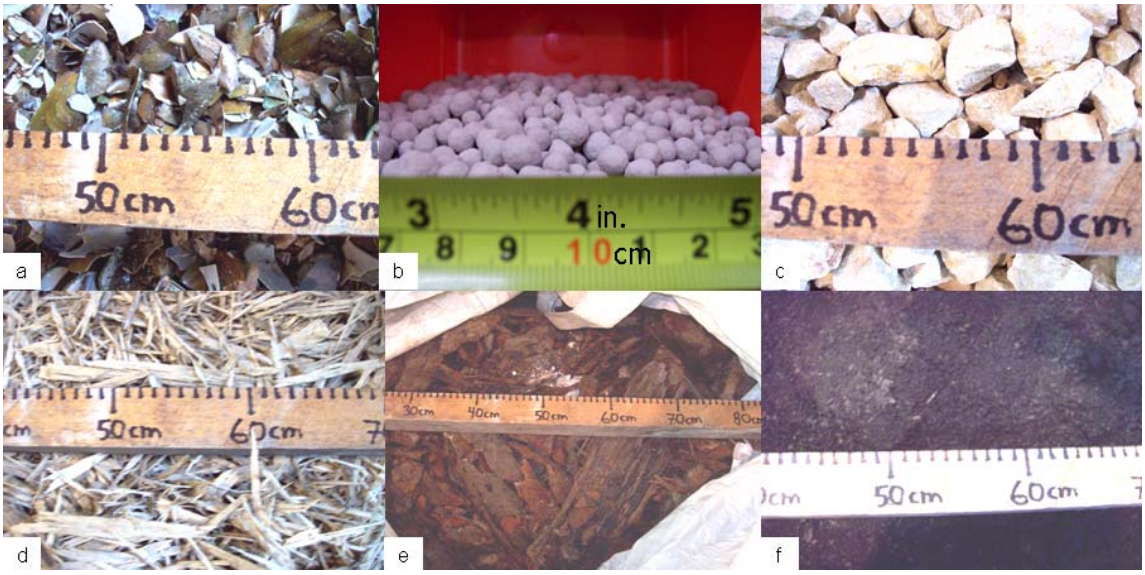

Figure 4.3. Biogeochemical reactor substrate materials including: a) mussel shells; b) NSD; c) limestone; d) post peel; e) *Pinus radiata* bark; and f) compost.

4.1.3 Substrate Mixtures

Each BGCR contained a different substrate mixture, with exception of two systems, as summarized in Table 4.1. Substrate mixtures were chosen based on their hydraulic properties (e.g. low risk of system plugging) and amounts of alkaline and organic materials. The nomenclature "S" denotes 337 L (E4) trapezoidal prism reactors, whereas "P" specifies 138 L drum reactors. S1 utilised only limestone for alkalinity generation. S2 and S3 contained equal quantities of mussel shells (20 vol. %) and compost (15 vol. %) but differing amounts of bark (30-40 vol. %) and post peel (25-35 vol. %). S4 and P2 contained identical substrate mixtures incorporating both mussel shells (12 vol. %) and limestone (5 vol. %); however, they were operated in different sized containers to determine how reactor dimensions affect removal efficacy. P1 contained the highest percentage of mussel shells (30 vol. %) of all reactors. P3 included NSD (5.0 vol %) mixed with limestone (2.5 vol. %) and mussels shells (12 vol. %). All BGCRs contained similar percentages of alkalinity amendments on a mass basis (31.7-34.6 wt. %) with exception of P1 and P3 containing more (43.6 and 46.4 wt. %, respectively).

Table 4.1: Substrate composition of each mesocosm BGCR in vol. % and wt. % (as received from the supplier).

	S1	S2	S3	S4	P1	P2	P3
	337 L Trapezoidal-Shaped BGCRs (Substrate Depth – 440 mm)				138 L Cylindrical Drum BGCRs (Substrate Depth – 562 mm)		
	Volumetric %						
Limestone	12.5	0.0	0.0	5.0	0.0	5.0	2.5
Mussel Shells	0.0	20.0	20.0	12.0	30.0	12.0	12.0
NSD	0.0	0.0	0.0	0.0	0.0	0.0	5.0
Bark	35.0	40.0	30.0	30.0	30.0	30.0	30.0
Post Peel	37.5	25.0	35.0	38.0	25.0	38.0	35.0
Compost	15.0	15.0	15.0	15.0	15.0	15.0	15.0
Total Alkalinity Amendments	**12.5**	**20.0**	**20.0**	**17.0**	**30.0**	**17.0**	**19.5**
	Weight %						
Limestone	34.6	0.0	0.0	14.8	0.0	14.8	17.2
Mussel Shells	0.0	31.7	32.0	18.4	43.6	18.4	17.9
NSD	0.0	0.0	0.0	0.0	0.0	0.0	11.3
Bark	22.1	27.9	21.2	20.3	19.2	20.3	19.7
Post Peel	20.1	14.8	20.9	21.7	13.6	21.7	19.8
Compost	23.2	25.7	25.9	24.8	23.6	24.8	24.2
Total Alkalinity Amendments	**34.6**	**31.7**	**32.0**	**33.2**	**43.6**	**33.2**	**46.4**

4.1.4 Experimental Preparation and Operation

4.1.4.1 Biogeochemical Reactor Preparation

Each BGCR contained bedding material comprised of 20-40 mm diameter rounded and sub-rounded gravel (0.241 wt. % Ca) as the drainage layer. Shade cloth was placed on top of the bedding material as a pervious barrier to prevent the overlying substrate from clogging it. Known volumes of each substrate for each BGCR were measured using 22-litre buckets and mixed uniformly on an asphalt slab with shovels prior to placement into their respective BGCR container. Substrates were hand compacted and saturated with a mixture of tap water and AMD in approximately 150-200 mm lifts. The pH of the tap water/AMD mixture was 4.5 as measured with a calibrated YSI Model 60 pH meter. The AMD was diluted to decrease the potential of deleteriously affecting benevolent microorganisms (e.g. SRB or cellulose decomposers) likely present within the organic substrate materials. Post peel was placed on top of the substrate mixtures to promote flow equalization and could potentially serve as a thermal insulation layer for reactors operating in cold climates. The reactors were allowed to sit stagnant for two days prior to initiating AMD flow into them. A summary of the thickness and volumes of each layer in the trapezoidal and drum-shaped BGCRs and the substrate surface area perpendicular to flow are presented in Table 4.2.

Table 4.2: Thickness and volumes of bedding material, substrate mixtures and post peel layer in the trapezoidal and drum-shaped BGCRs and the substrate surface area perpendicular to flow.

	Trapezoidal Shaped BGCRs	Drum Shaped BGCRs
Thickness (m)		
Bedding Material	0.090	0.0148
Substrate	0.440	0.562
Post Peel	0.050	0.050
Volume (m^3)		
Bedding Material	0.0408	0.0183
Substrate	0.216	0.0994
Post Peel	0.0262	0.00785
Surface Area (m^2)		
Substrate	0.491	0.170

4.1.4.2 Experimental Set-Up and Operation

The mesocosm-scale treatability tests were performed at the University of Canterbury to ascertain treatment effectiveness of different substrate mixtures in a relatively controlled laboratory setting. The experimental set-up is shown in Figures 4.1 and 4.2 and a schematic representation is shown in Figure 4.4. The AMD used in this study was sourced from Manchester Seep at Stockton Coal Mine near the outlet of the sedimentation pond that captures the seep water (Figure B.16 in Appendix B). Multiple batches of AMD were collected and transported to the lab in 1.0 m^3 HDPE containers throughout this study. The mine water was stored and left undisturbed in the tanks and pumped into the 1.0 m^3 HDPE feed tank when additional AMD was required. The AMD was aerated continuously in the feed tank with an open tube to simulate DO conditions measured at the research site (8.12-10.93 mg/L (73.4-94.3% saturation)). Masterflex peristaltic pumps and speed controllers equipped with Easy-Load pump heads and No. 16 Tygon® tubing connected to 5 mm inner diameter (ID) polyurethane tubing were used to control and convey undiluted AMD into each BGCR. Separate pumps were used for trapezoidal and drum reactors due to their differences in substrate volumes, and consequently, experimental design flow rates. Influent into each reactor was measured typically on a daily basis using 25 mL graduated cylinders and a stopwatch. The BGCRs were downflow systems with AMD feed at the upper surface and effluent discharge at the bottom outlet. Water elevation in each reactor was controlled by adjusting the height of the 32 mm ID PVC outlet tubing. Water level was maintained at about 50 mm above the upper post peel surface. The primary reasoning for maintaining surface water above the post peel layer was to act as a mixing zone and minimise the risk of creating short-circuiting pathways from influent velocity. No special procedures were performed to establish SRB within the BGCRs except operating them initially at very low loading rates (e.g. loading rates averaging 0.06 mol metals/m^3 substrate/day; 5.59 g $CaCO_3$/m^2/day; and 0.15 mol sulphate/m^3 substrate/day during the first week).

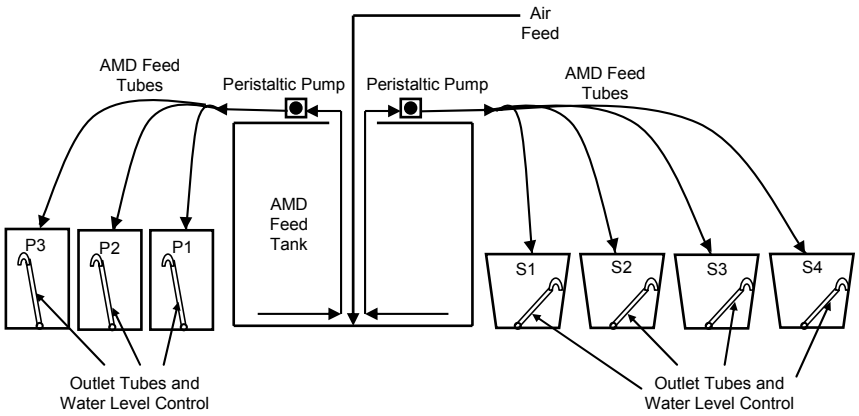

Figure 4.4. Schematic of laboratory set up for the mesocosm-scale BGCRs.

4.1.5 Experimental Design

Influent AMD flow rates were increased incrementally (0.05-1.44 mol metals/m^3 substrate/day; 5.26-156 g $CaCO_3/m^2$/day; and 0.14-2.88 mol sulphate/m^3 substrate/day) throughout the experiment to test treatment limits and efficiency of each BGCR. The only exception occurred during the week 14.4 sampling event when AMD loading was decreased temporarily due to a shortage of AMD feed. Reactors operated continuously for 16.7 weeks with exception of S1 (12.4 weeks) due to significantly less effective metal removal compared with other BGCRs and P3 (11.3 weeks) which was considered a non-pragmatic treatment option due to caustic effluent. The operation of these aforementioned systems was also terminated to reduce demand shortage of AMD.

4.1.6 Water Chemistry Sampling and Analytical Methods

Effluent samples were typically collected weekly to biweekly and prior to increasing AMD flow rate. They were collected directly into method-specified sample bottles and chilled at 2-6^{o}C until analysed by RJ Hill Laboratories Limited or at the University of Canterbury Environmental Engineering Laboratory. The AMD was also sampled from influent into the BGCRs. Samples for water quality parameters measured using portable instruments (temperature, pH, conductivity, ORP/Eh, DO and turbidity) were collected in HDPE sampling bottles. Water quality probes were then inserted into the sampling bottles, and data was recorded when readings stabilised. Water quality probes were inserted directly into the feed tank for measuring AMD. Most samples were collected head-space free in non-preserved HDPE sample bottles unless otherwise indicated below. All sampling was performed prior to increasing metal loading (and flow) rates.

Metal (Fe, Al, Cu, Ni, Zn, Mn, As, Cd, Pb and As), total sulphur, cations (Ca, Mg, K and Na), total nitrogen (TN), total kjeldahl nitrogen (TKN), total oxidised nitrogen (TON; includes summation of nitrate (NO_3^-) and nitrite (NO_2^-)), total phosphorous (TP), dissolved organic carbon (DOC), total organic carbon (TOC), faecal coliforms and five day biochemical oxygen demand (BOD) concentrations were analysed and measured by RJ Hill Laboratories Limited. Total suspended solids and acidity/alkalinity were analysed in the University of Canterbury Environmental Engineering

Laboratory. The only exceptions included acidity and alkalinity samples collected on 7 and 20 June 2007 (weeks 9.4 and 11.3, respectively), which were analysed by RJ Hill Laboratories Limited.

4.1.6.1 Metals

Metal samples were analysed using ICP-MS. Dissolved metals were analysed by APHA Method 3125B (APHA, 1998) for samples collected until week 9.5 and filtered as described in Section 2.2.3 in Chapter 2. The only exception was that most samples were filtered using disposable Waterra WAT45 groundwater filters containing 0.45 μm polyethersulphone filter media. Acid-soluble metals were analysed by APHA Method 3125B (APHA, 2005) with dilute nitric acid extraction for samples collected after week 9.5. Metal samples were preserved with 1:1 nitric-acid preserved to maintain pH<2.0.

For AMD samples, Fe^{2+} was measured at the time of sample collection following Hach Method 8146 (1,10 Phenanthroline Method) and analysed using a Hach Spectrophotometer at 510 nm (Hach Company, 2003) as previously described in Section 2.2.2. Ferric Fe was calculated as the difference between total Fe and Fe^{2+}. From BGCR effluent samples, Fe^{3+} concentrations were assumed to be zero due to low DO (<1.0 mg/L) and Eh (0-80 mV).

4.1.6.2 Sulphur

Total sulphur concentrations were measured using ICP-OES as previously described in Section 2.2.3. Total sulphur concentrations were computed as mg/L of sulphate for comparative purposes (to determine sulphate removal). It was assumed that the majority of sulphur in the AMD samples was present as sulphate due to high DO (91.7-99.1% saturation) and Eh (709-803 mV) conditions; however, sulphur was likely prevalent in BGCR effluent in reduced states such as monosulphide, hydrogen sulphide, mobile metal sulphides, and potentially mercaptans or other sulphur and organic-sulphur complexes based on low and Eh readings and olfactory observations of a hydrogen sulphide odour.

4.1.6.3 Acidity and Alkalinity

Acidity (pH 3.7) and total acidity (pH 8.3) were analysed using a modified version of APHA Method 2310B (APHA, 2005), and alkalinity (pH 4.5) was analysed using a modified version of APHA Method 2320B (APHA, 2005) as previously discussed in Section 2.2.3. Calculated acidity was explained in Section 1.3.3 and computed using Equation 1.9 (modified from Watzlaf et al., 2004); however, acidity contribution from Mn was excluded for this study. Therefore, metal acidity contributions were only computed from Fe, Al, Cu, Ni and Zn. Other metals (e.g. Cd, As and Pb) contributed minimal acidity (<0.4%) so were not included in calculated acidity. Manganese contribution was excluded since its removal in BGCRs is not expected due to the high solubility of MnS (Watzlaf et al., 2004; Wildeman et al., 2006). It typically accounted for <1% of molar loading and <0.6% of acidity loading (median concentration was 1.65 mg/L (1.40-2.61 mg/L)).

4.1.6.4 Water Quality Parameters Measured with Portable Probes including pH, Conductivity, Dissolved Oxygen and Oxidation-Reduction Potential/Eh

Water quality parameters including pH, conductivity, DO and ORP/Eh were measured at the time of sampling using portable water quality instruments as previously described in Section 2.2.2. Instruments were calibrated just prior to sample collection using fresh standards and validated to ensure they maintained calibration following measurements.

4.1.6.5 Other Cations, Anions and Nutrients

The cations Ca, Mg, K and Na were filtered by RJ Hill Laboratories Limited using 0.45 μm filters prior to analysis via ICP-MS following APHA Method 3125B (APHA, 1998) as previously described in Section 2.2.3. Total kjeldahl nitrogen was analysed following modified versions of methods APHA 4500-N_{org} B and APHA-NH_3 F (phenol/hypochlorite colorimetry) with sulphuric acid digestion with copper sulphate catalyst following a modified version of APHA 4500-N_{org} D (APHA, 1998). Samples were preserved with sulphuric acid to achieve pH<2. Total oxidised nitrogen was analysed by automated Cd reduction with a flow injection analyser following APHA 4500-NO_3^--I (Proposed in APHA, 1998). Total nitrogen was computed by summing concentrations of TKN and TON. Total P was analysed following method APHA 4500-P E (modified from manual analysis) using acid persulphate digestion, ascorbic acid colorimetry and a discrete analyser (APHA, 1998). Samples were preserved with sulphuric acid to achieve pH<2.

4.1.6.6 Organics and Biological Parameters

Dissolved organic carbon (DOC) samples were filtered using the same process as previously described for dissolved metal samples and analysed following method APHA 5310B, which included catalytic oxidation and infrared detection for determining total carbon (TC) and acidification followed by purging to measure total inorganic carbon (TIC) (APHA, 1998). Dissolved organic carbon represented the difference between TC and TIC, which both excluded filtered carbon fractions >0.45 μm in diameter. For samples collected after week 9.5, TOC was measured instead of DOC (e.g.. samples were not filtered after week 9.5). Faecal coliform was analysed following method APHA 9222B utilising membrane filtration count on mFC agar at 44.5^oC for 24 hours (APHA, 1998). Samples were collected non-headspace free in sterile polycarobonate containers and submitted for analysis immediately upon collection. Biochemical oxygen demand was analysed following method APHA 5210B (APHA, 1998). No seeding was implemented as part of the BOD analysis.

4.1.6.7 Total Suspended Solids and Turbidity

Total suspended solids represent the fraction of solids obtained on a 1.2 um Whatman® GF/C glass-fibre filter and were measured following APHA Method 2540D (APHA, 1998) using vacuum filtration as previously described in Section 2.2.3. Turbidity measurements were performed using a Hach Model 2100P portable turbidimeter at the time of sample collection following the methodology previously described in Section 2.2.2.

4.2 Results

Data analysis of the BGCR treatability tests focused primarily on metal and acidity loading and removal with an emphasis on Fe and Al removal efficiencies since they contributed the majority of metal loading (>98.0% on a molar basis). Metal removal was considered on a molar volumetric basis (mol/m^3 of substrate/day) and calculated acidity removal was determined on an areal acidity loading basis (g $CaCO_3$/m^2 of upper reactor surface area/day) so results could be compared more readily with other studies. Molar metal loadings were computed considering all metals analysed (Fe, Al, Cu, Ni, Zn, Cd, Pb and As) with exception of Mn. Acidity loadings were computed from Fe, Al, Cu, Ni, Zn and H^+ concentrations. Sulphate reduction and removal was also considered on a molar volumetric basis. Effluent Fe and Al concentrations were also compared as a function of the theoretical (or nominal) HRT, which assumes all flow passes uniformly through the BGCRS. All removal efficiencies were calculated using the following equation where X represents loading rates (mol/m^3/day or g acidity/m^2/day) or concentrations (mg/L):

$$\text{percent removal efficiency} = 100(X_{in}-X_{out})/X_{in} \quad \textbf{(4.1)}$$

Manganese sulphide (MnS) was not expected to form under reduced conditions due to its high solubility rate compared with other metal sulphides (Gusek, 2002; Watzlaf et al., 2004; Wildeman et al., 2006). Maximum Mn removal in this study was 36.2%; however, there was an average net export of 20.8% Mn over the duration of the experiment indicative of Mn release from substrate materials. A similar trend was also reported by Blumenstein et al. (2008) where a net export of Mn was measured due to leaching from substrate. Because Mn removal is not expected under reduced conditions present in VFWs and contributed <1% of metal loading and <0.6% of acidity loading in this study, Mn results were not considered in metal or acidity loading computations (median concentration was 1.65 mg/L (1.40-2.61 mg/L).

4.2.1 AMD Chemistry

Influent AMD chemistry varied amongst batches reflecting the stochastic nature of the Manchester Seep AMD. Eleven batches were sampled throughout this study. A summary of AMD sulphate and metal concentrations is presented in Table 4.3. Excluding Mn, average percent contribution to molar metal loading was 41.6% Fe, 57.4% Al and 0.987% other metals (Cu, Ni, Zn, Pb and Cd). Manganese contribution averaged 0.941%. The AMD pH, acidities and alkalinity are summarised in Table 4.4. Total acidity (pH 8.3) and calculated acidity values were comparable (generally within 4%). Additional water quality parameters including conductivity, specific conductance, TDS, salinity, Eh, DO, turbidity, TSS, DOC (or TOC) and additional cation (Ca, Mg, K, Na,) concentrations are summarised in Tables 4.5 and 4.6.

Table 4.3: AMD influent sulphate and metal concentrations (mg/L) (n=11 (n=8 for Mn)). For statistical calculations, results measured at concentrations below laboratory practical quantitation limits (PQLs), which is applicable only to As, were halved.

	SO_4^{2-}	Fe	Al	Cu	Ni	Zn	Pb	Cd	As	Mn
Mean	655	71.0	47.9	0.201	0.228	1.28	0.0155	0.00180	0.002	1.81
Median	608	65.8	46.5	0.199	0.210	1.27	0.0138	0.00169	0.001	1.65
Min	493	49.7	33.5	0.108	0.198	1.07	0.0085	0.00145	<0.001	1.40
Max	1007	113	72.4	0.287	0.309	1.61	0.0284	0.00245	0.004	2.60
St. dev.	160	19.2	11.2	0.0621	0.040	0.178	0.0068	0.00032	0.001	0.443

Table 4.4: AMD influent pH, measured acidities and alkalinity and calculated acidity (mg/L as $CaCO_3$; n=11).

	pH	Acidity (pH 3.7)	Total Acidity (pH 8.3)	Calculated Acidity	Alkalinity (pH 4.5)
Mean	2.56	247	569	593	-376
Median	2.61	234	512	580	-349
Min	2.45	189	450	421	-539
Max	2.73	315	844	869	-287
St. dev.	NA	45.0	117	126	74.9

NA, non-applicable.

Table 4.5: Chemical-physical parameters based on results from each individual batch of AMD influent used during the mesocosm-scale treatability tests (n=11).

	Temperature (^oC)	Conductivity (µS/cm)	Specific Conductance (µS/cm)	Eh (mV)	DO (mg/L)	DO (% saturation)
Mean	14.7	1204	1502	751	9.69	96.0
Median	15.5	1164	1469	740	9.65	97.2
Min	12.1	1029	1239	709	9.22	91.2
Max	16.8	1555	1909	8003	10.53	99.8
St. dev.	1.85	143.7	186.5	35.8	0.344	3.17

Table 4.6: Solids, DOC (or TOC) and cations (Ca, Mg, Na and K) concentrations from each individual batch of AMD influent used during the mesocosm-scale treatability tests (n=11 except n=4 for TSS). Total dissolved solids and salinity were computed from conductivity values.

	Solids				Organics	Cations			
	Turbidity (NTUs)	TSS (mg/L)	TDS (mg/L)	Salinity (ppt)	DOC (or TOC) (mg/L)	Ca (mg/L)	Mg (mg/L)	Na (mg/L)	K (mg/L)
Mean	1.91	27.9	988.1	0.77	3.20	18.9	11.0	5.05	1.98
Median	1.11	27.6	969.0	0.78	1.70	19.2	10.6	5.04	2.08
Min	0.37	2.72	825.5	0.65	1.00	13.9	8.09	4.35	1.61
Max	8.48	53.5	1252	1.00	15.4	25.8	15.9	5.86	2.20
St. dev.	2.40	21.7	120.5	0.098	4.61	3.39	2.33	0.4731	0.209

Despite the variability in AMD chemistry, data from individual batches showed relatively constant molar ratios of sulphate to total metals (average 2.19), sulphate to Fe (average 5.26) and sulphate to Al

(average 3.82). Graphical representations of these relationships on a molar volumetric loading basis are shown in Figure 4.5 which indicates a strong correlation between molar ratios of sulphate to total metals (R^2=0.998), sulphate to Fe (R^2=0.995) and sulphate to Al (R^2=0.994). This reflects consistent stoichiometry and mineralogy from which AMD was generated and also the excessive sulphur to metal ratios for these contaminants to be removed solely as metal sulphides.

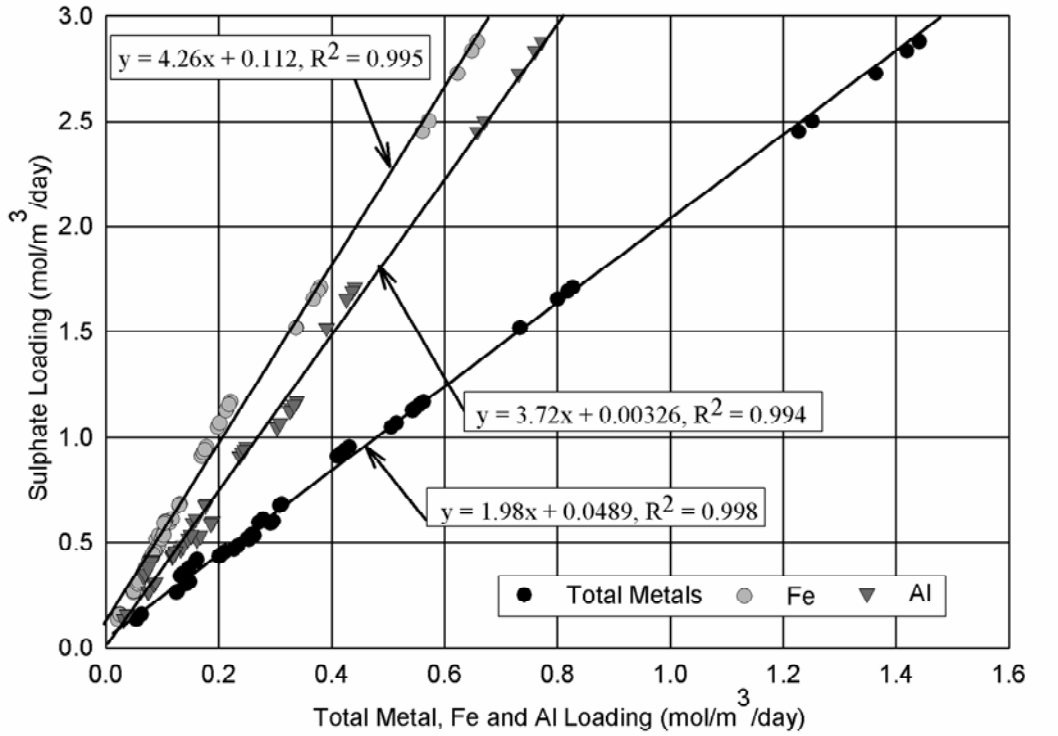

Figure 4.5. Relationship of molar metal (total), Fe and Al loadings versus molar sulphate loading. Solid lines represent linear best-fit models.

4.2.2 Acidity, Metal and Sulphate Loading, Removal and Water Chemistry

4.2.2.1 Acidity Areal, Metal Molar Volumetric and Sulphate Molar Volumetric Loading

Area plots showing calculated acidity loaded and retained within each BGCR are presented in Figure 4.6 (on a log scale). Black-shaded areas represent acidity neutralised, or retained. Areas shaded grey display effluent acidity discharged. Therefore, plots showing less grey shading (e.g. P3) indicate better acidity neutralisation. Conversely, plots displaying more grey shading (e.g. S1) indicate less effective acidity removal. Area plots were also developed illustrating total metals (Figure 4.7 on a probability scale), Fe (Figure 4.8 on a logarithmic scale), Al (Figure 4.9 on a logarithmic scale) and sulphate (Figure 4.10 on a probability scale) retained and discharged from the seven BGCRs. These plots are interpreted the same as previously discussed for acidity retained and discharged in Figure 4.6. There was a net export of sulphate from P3 throughout its operation as demonstrated in Figure 4.10 by

the lack of black shading. The amount of sulphate exported in excess of the influent loading is represented as the area above the faint white line that intersects the grey shading.

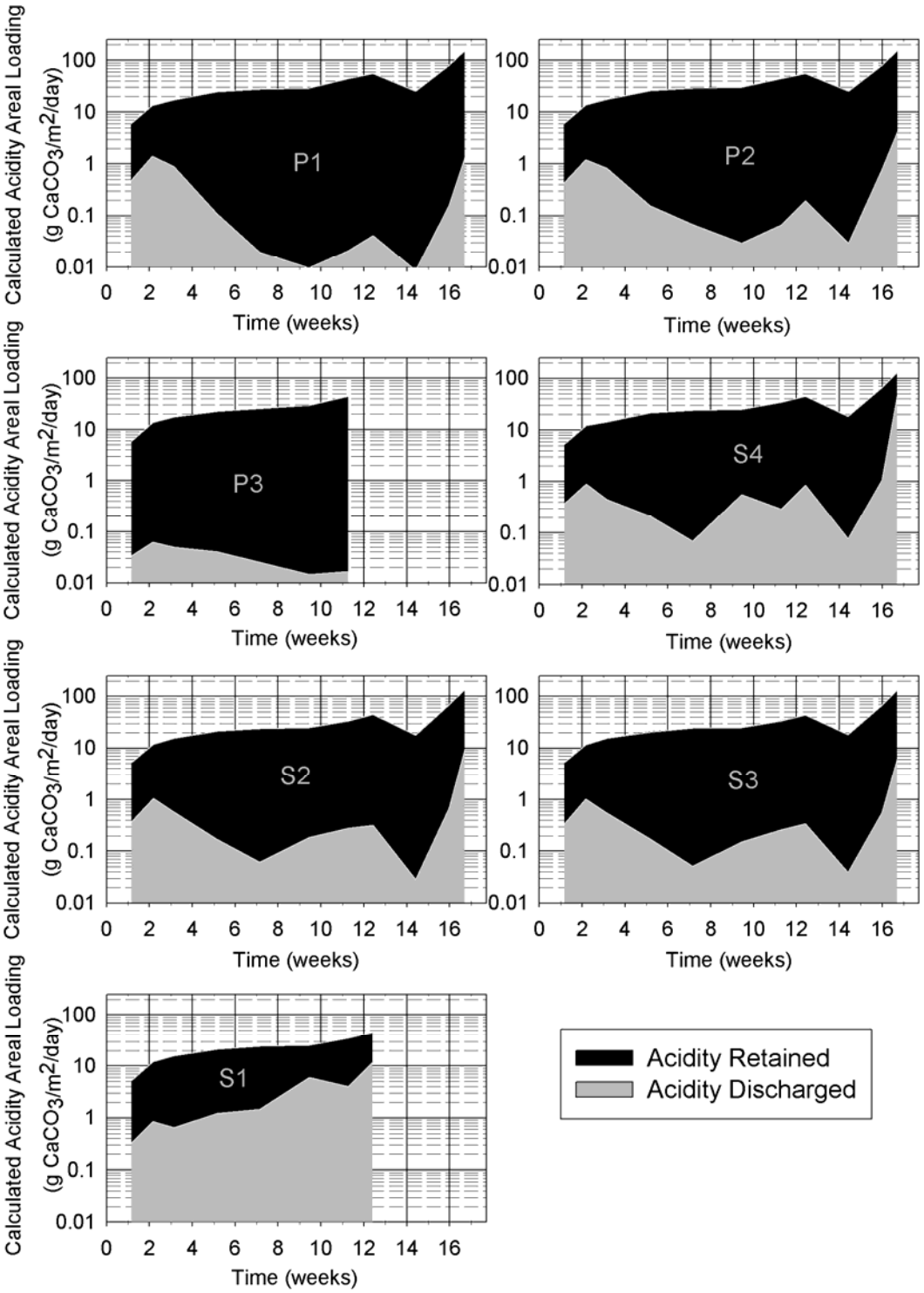

Figure 4.6. Area plots showing calculated acidity retained and discharged from each BGCR on an areal basis and a logarithmic scale.

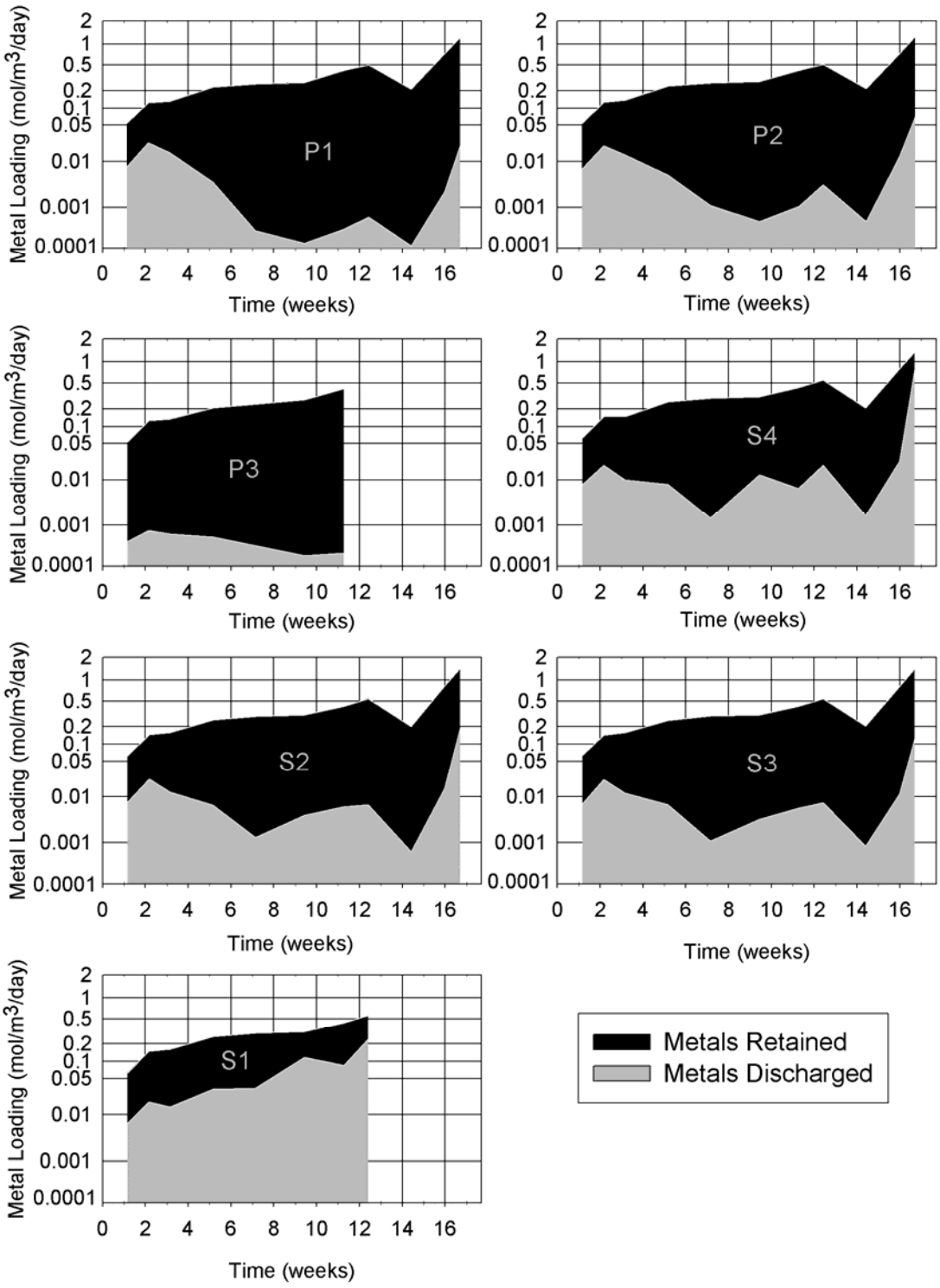

Figure 4.7. Area plots illustrating metals retained and discharged from each BGCR on a molar volumetric loading basis and a probability scale.

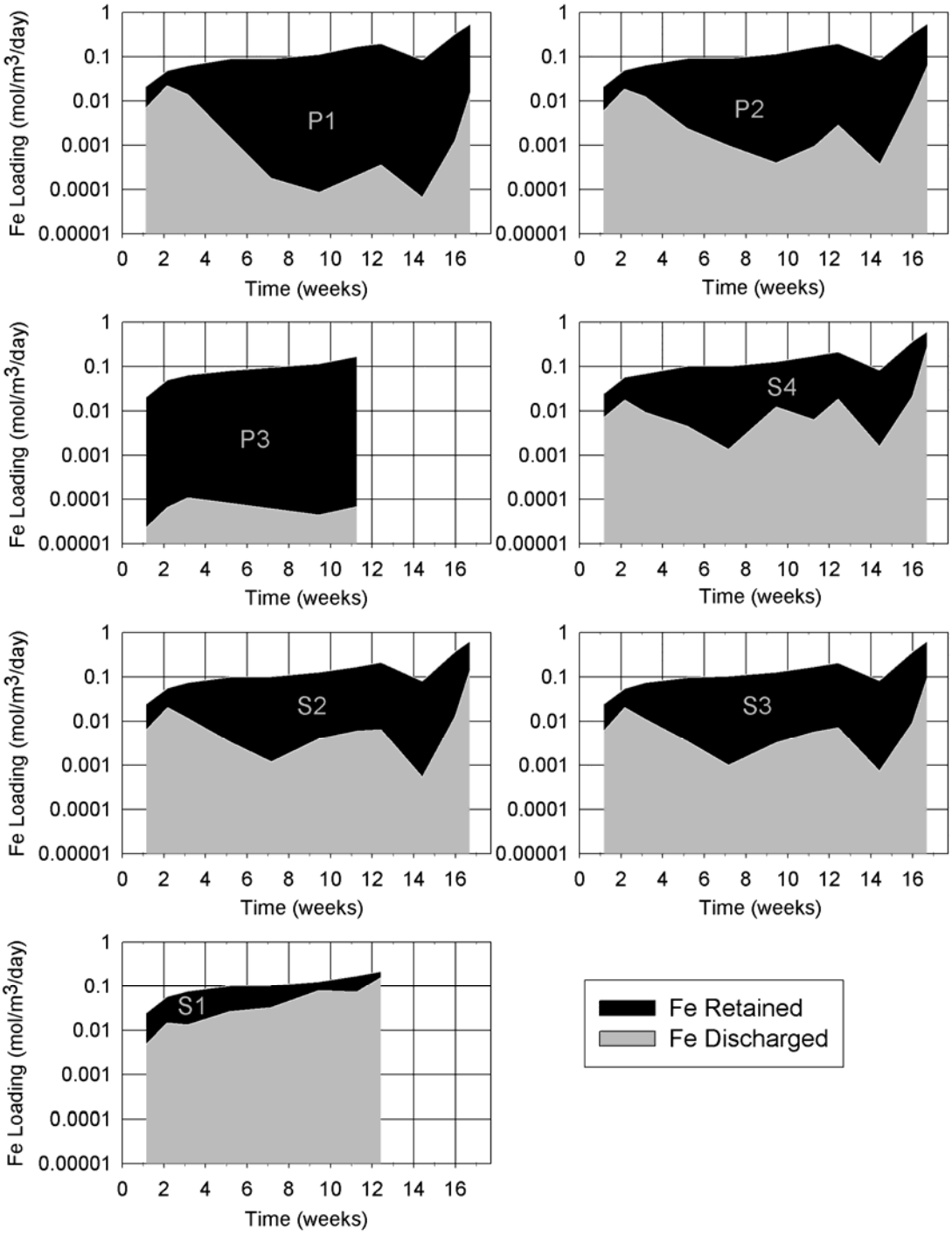

Figure 4.8. Area plots illustrating Fe retained and discharged from each BGCR on a molar volumetric loading basis and a logarithmic scale.

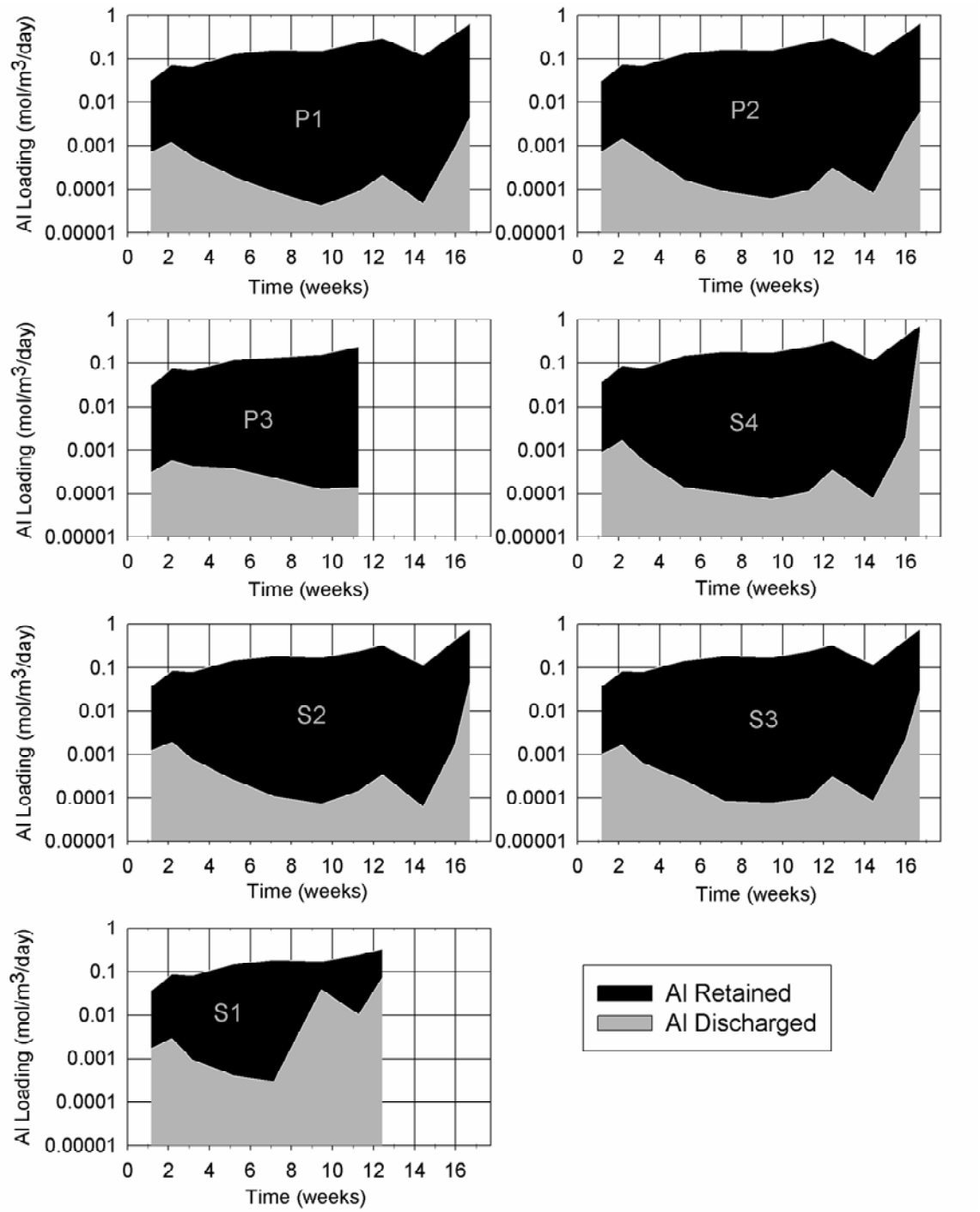

Figure 4.9. Area plots illustrating Al retained and discharged from each BGCR on a molar volumetric loading basis and a logarithmic scale.

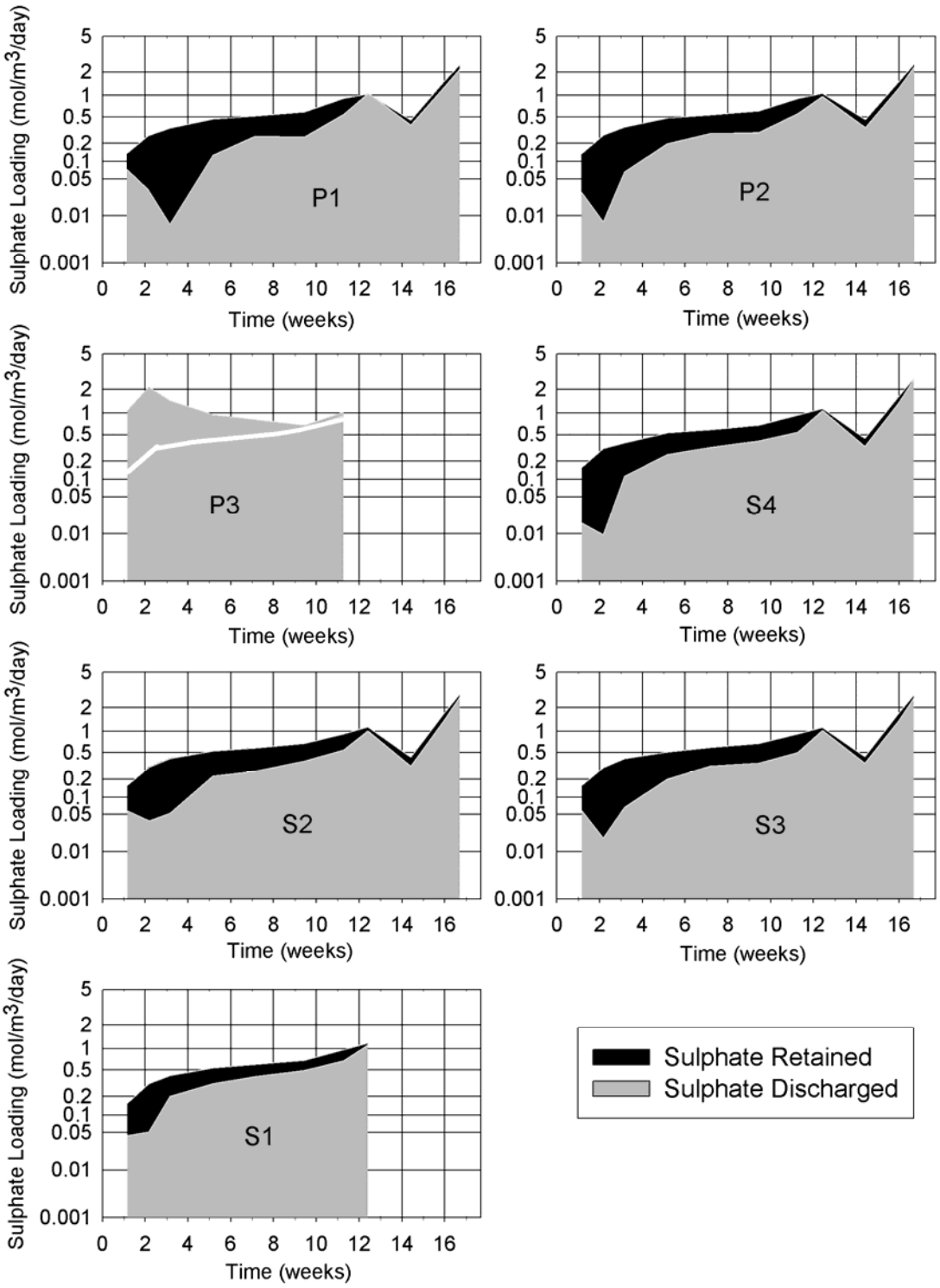

Figure 4.10. Area plots illustrating sulphate retained and discharged from each BGCR on a molar volumetric loading basis and a probability scale.

Contaminant loading and removal were also compared as a function of each other for acidity (Figure 4.11), total metals (Figure 4.12), Fe (Figure 4.13), Al (Figure 4.14) and sulphate (Figure 4.15). The dashed lines represent equal loading and removal. Data points where loading and removal are most similar indicate the best contaminant sequestration (e.g. metal and acidity removal from P1). Conversely, data deviating the most from the dashed line indicates less effective contaminant removal and, consequently, system stress or overloading (e.g. S1 and S4).

The BGCRs were still achieving stable operating conditions during the initial operating period (first three to four sampling events (weeks 1.1-5.2)) and was accompanied with an initial net export, or first flush of dissolved Ca, Mg, Na, K (Section 4.2.3) and, consequently, high conductivities (Section 4.2.4). Elevated concentrations of easily soluble cations hindered metal precipitation and also contributed to excess effluent alkalinity. Alkalinity was measured at 879-2283 mg/L as $CaCO_3$ during the first three (weeks 1.1-3.2) sampling events for BGCRs containing mussel shells or a mixture of mussel shells and limestone (P1, P2, S2, S3 and S4). Effluent alkalinity ranged from 458 to 880 mg/L as $CaCO_3$ during this same period for S1 (limestone only) and from 725 to 1642 mg/L as $CaCO_3$ for P3 (mussel shells, limestone and NSD). During week 5.2, alkalinities ranged from 538 to 753 mg/L as $CaCO_3$ for BGCRs containing mussel shells or a mixture of mussel shells and limestone, 268 mg/L as $CaCO_3$ for P1 and 287 mg/L as $CaCO_3$ for P3. Effluent alkalinities decreased steadily thereafter due to higher loading rates, which contributed to less alkalinity generation via sulphate reduction and calcium carbonate dissolution. The additional alkalinity was also attributed to higher concentrations of Mg, K and Na during the first flush. A more detailed analysis of effluent alkalinities and their relationship with effluent Fe and Al concentrations is presented in Chapter 5 with results summarised in Figures 5.1 and 5.4.

The performance of BGCRs were near stabilisation within the fourth (week 5.2) sampling event of operation (average loading rates of 22.5 g $CaCO_3/m^2/day$; 0.242 mol total metals/m^3/day; 0.0969 mol Fe/m^3/day; 0.0969 mol Fe/m^3/day; 0.141 mol Al/m^3/day; and 0.499 mol sulphate/m^3/day). Average removal efficiencies prior to this time were 94.4% acidity, 88.0% total metals, 77.6% Fe and 98.2% Al compared with 98.6% acidity, 96.5% metals, 94.0% Fe and 99.8% Al during the week 5.2 sampling event. On the contrary and excluding results from P3, maximum sulphate removal efficiencies were achieved prior to the first 5.2 weeks of system operation (79.8%) compared with week 5.2 (57.5%). It is also plausible that some metal removal occurred due to the establishment of a diverse consortium of microorganisms with time.

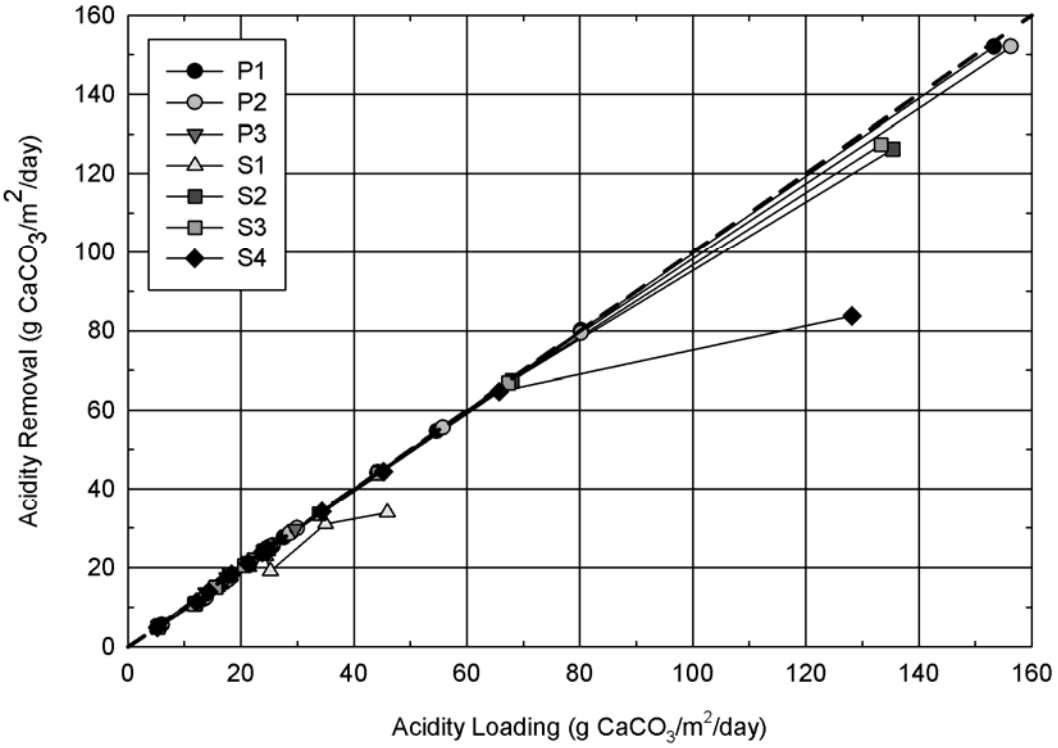

Figure 4.11. Acidity areal loading rates versus acidity areal removal rates for each BGCR. The dashed line represents equal loading and removal.

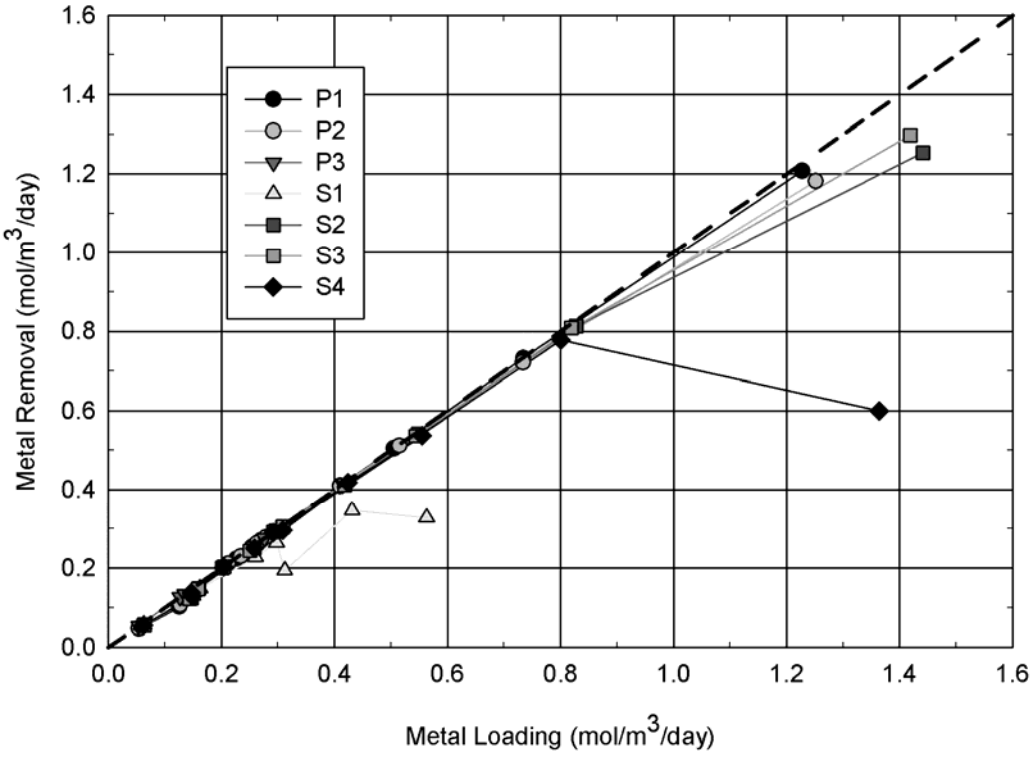

Figure 4.12. Comparison of total metal loading and removal rates considering all BGCRs on a molar volumetric basis. The dashed line represents equal loading and removal.

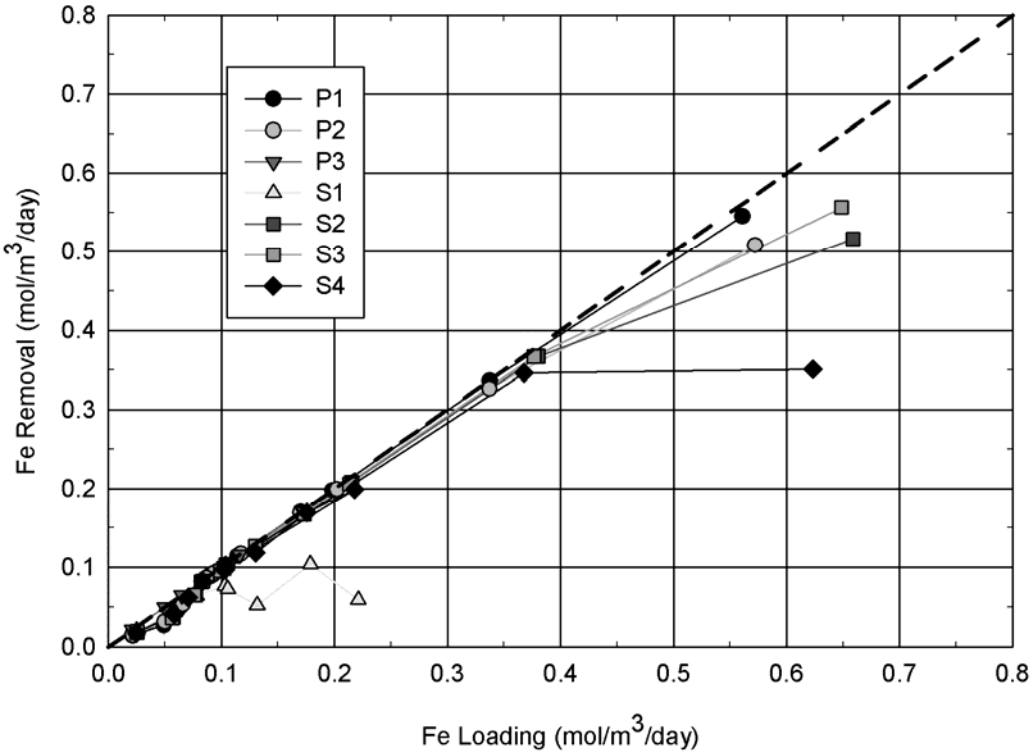

Figure 4.13. Comparison of Fe loading and removal rates considering all BGCRs on a molar volumetric basis. The dashed line represents equal loading and removal.

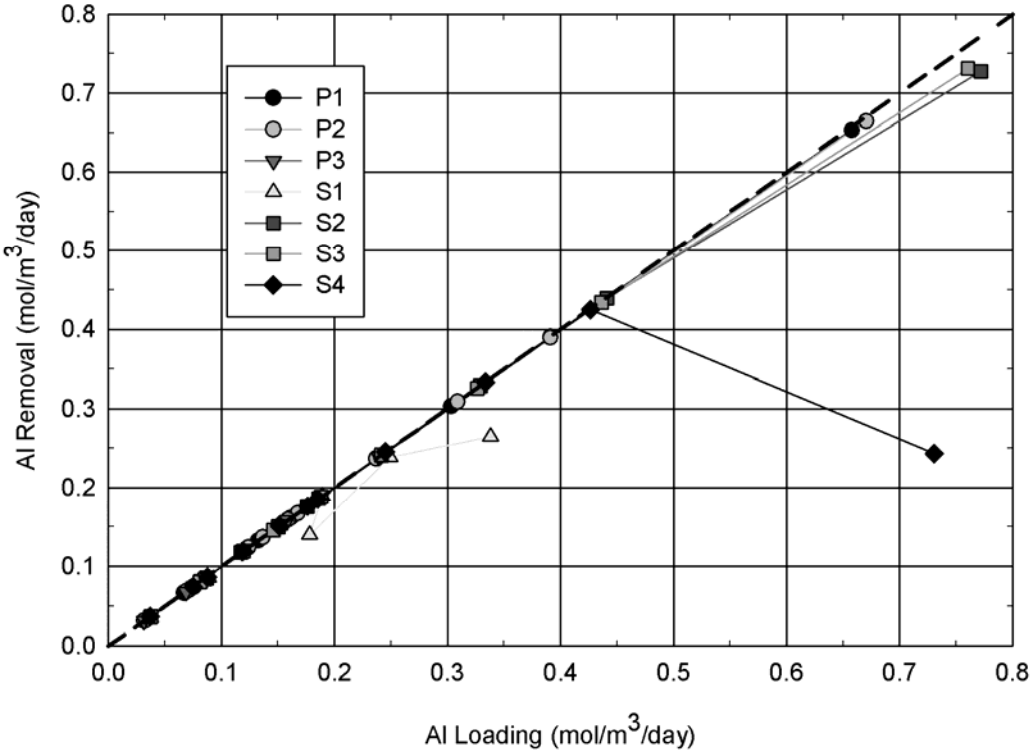

Figure 4.14. Comparison of Al loading and removal rates considering all BGCRs on a molar volumetric basis. The dashed line represents equal loading and removal.

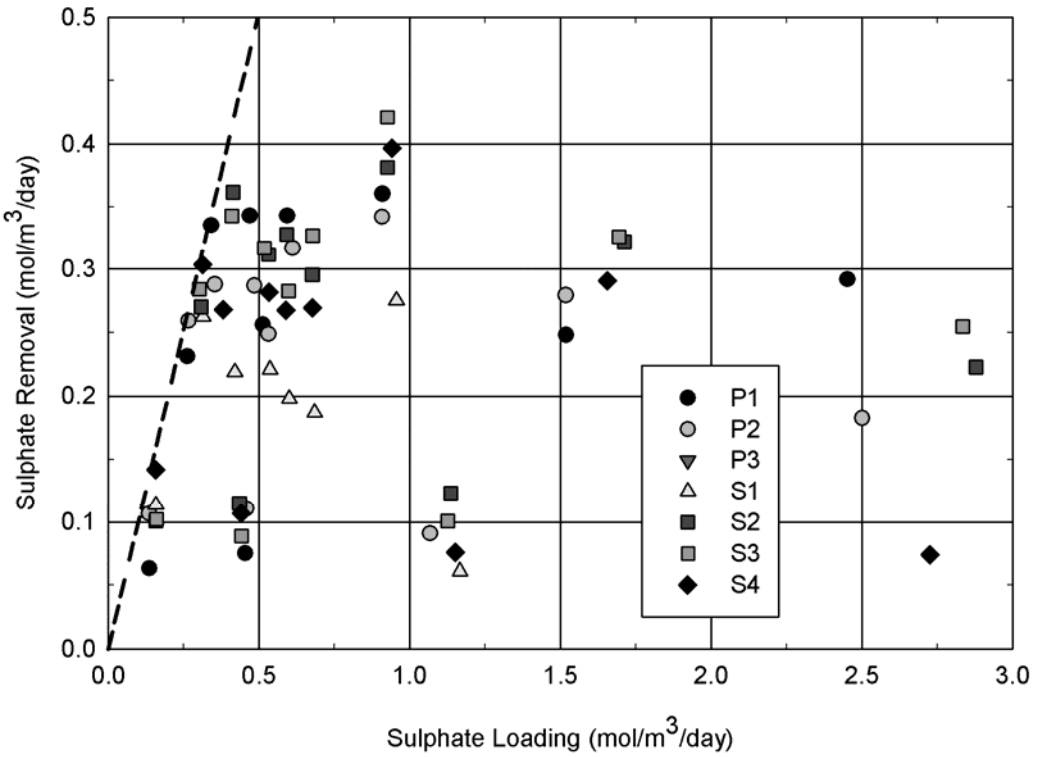

Figure 4.15. Comparison of sulphate loading and removal rates from each BGCR on a molar volumetric basis. The dashed line represents equal loading and removal. The scale of the sulphate removal rate axis (y-axis) contains a minimum of 0.0 mol/m^3/day, so data points indicative of sulphur export from BGCR P3 are not shown.

Loading rates were temporarily reduced prior to week 14.4 (third to last) sampling event due to a shortage of AMD. Loading rates were increased again once additional AMD was obtained. Maximum loading tested for drum-shaped reactors (P1 and P2) averaged 155 g $CaCO_3$/m^2/day, 1.24 mol total metals/m^3/day, 0.567 mol Fe/m^3/day, 0.664 mol Al/m^3/day and 2.48 mol sulphate/m^3/day. For trapezoidal-shaped reactors (S2, S3 and S4) maximum loading tested averaged 132 g $CaCO_3$/m^2/day, 1.41 mol total metals/m^3/day, 0.644 mol Fe/m^3/day, 0.754 mol Al/m^3/day and 2.81 mol sulphate/m^3/day for trapezoidal-shaped reactors (S2, S3 and S4). A significant decline in metal removal was measured in all BGCRs at these loading rates, especially the trapezoidal-shaped reactors, signifying that system treatment limitations were exceeded.

Operation of BGCRs P3 and S1 were terminated early (week 11.3 for P3 and week 12.4 for S1) to conserve AMD. P3 effluent was caustic (pH 9.23-10.56) resulting from rapid dissolution of calcium oxide within the NSD utilised in the substrate mixture. There was also a substantial net export of sulphur (average 316%; range of 11.7-723%) from the NSD, deeming the system unfeasible as a passive treatment option; however, it showed the best acidity and metal removal of all BGCRs (Figures 4.6-4.9) compared with the other BGCRs due to the quicker dissolution of calcium oxide in the NSD and higher pH compared with calcium carbonate in the limestone and mussel shells. This

was especially evident with Fe removal (Figure 4.8). More than 99.9% of metals were removed, including Fe, at the highest metal and acidity loading rates tested in P3 (0.414 mol/m^3/day and 44.6 g $CaCO_3$/m^2/day). P3 also did not show as drastically less efficient acidity and metal removal during the first few weeks of operation compared with other systems. S1 provided significantly less acidity and metal removal compared with other reactors.

Acidity and metal removal were best in P1, which contained the highest percentage of mussel shells at 30 vol. %. Acidity and metal removal were also better in drum-shaped reactors than trapezoidal-shaped reactors based on comparison of BGCRs P2 and S4, which contained identical substrate mixtures. Acidity and metal removal were better in reactors containing just mussel shells (P1, S2 and S3) as an alkalinity amendment compared with those that included a mixture of mussel shells and limestone (P2 and S4). Aluminium removal was better than Fe removal with Fe discharged at rates (and concentrations) about an order of magnitude greater than that of Al. Better acidity and metal removal were measured when using a higher percentage of post peel than bark in the substrate mixture.

Acidity (Figure 4.11), metal (Figure 4.12), Fe (Figure 4.13) and Al (Figure 4.14) removals were consistently good for all BGCRs containing mussel shells (P1, S2 and S3) or a mixture of mussel shells and limestone (P2 and S4) for loading rates up to at least those established during the second to last (week 16.0) sampling event (average of 67.1 g $CaCO_3$/m^2/day, 0.816 mol metals/m^3/day, 0.375 mol Fe/m^3/day and 0.434 mol Al/m^3/day for trapezoidal-shaped reactors and 80.2 g $CaCO_3$/m^2/day, 0.734 mol metals/m^3/day, 0.337 mol Fe/m^3/day and 0.391 mol Al/m^3/day for drum-shaped reactors). There was a subtle deviation of data points below the dashed line signifying 100% Fe removal efficiency in Figure 4.13, potentially indicating that the maximum, or near maximum, Fe loading rate (average of 0.36 mol Fe/m^3/day)) was achieved during week 16.0. Acidity, metal, Fe and Al removal efficiencies during the final two sampling events (weeks 16.0 and 16.7) are summarised in Table 4.7. Contaminant overloading occurred during the week 16.7 sampling (132 g $CaCO_3$/m^2/day, 1.41 mol total metals/m^3/day, 0.644 mol Fe/m^3/day and 0.754 mol Al/m^3/day for trapezoidal-shaped reactors and 155 g $CaCO_3$/m^2/day, 1.24 mol metals/m^3/day, 0.567 mol Fe/m^3/day and 0.664 mol Al/m^3/day for drum-shaped reactors). This was especially notable for the trapezoidal-shaped BGCRs, as evident by the decline in acidity and metal removal efficiencies shown in Table 4.7.

Sulphur removal (Figures 4.10 and 4.15) was less effective than acidity and metal removal. It was most effective at loading rates of approximately 0.3 mol/m^3/day (average 93.6% for all BGCRs), which were achieved during the third sampling event (week 3.2). Sulphate removal efficiency declined at higher loading rates. Sulphate removal was greatest and averaged 0.380 mol/m^3/day (41.2%) at average loading rates of 0.922 mol/m^3/day (0.416 mol total metals/m^3/day) during week 11.3 (excluding S1). Sulphate removal efficiency declined to an average of 10.8% (maximum 19.2%)

during subsequent sampling events when higher loading rates were present. Even during week 14.4, when average sulphate loading rates were decreased to 0.446 mol/m^3/day, sulphate removal only averaged 22.3% (16.6-26.5%).

Table 4.7: A comparison of the percent removal efficiency of acidity, total metals, Fe and Al during the final two (weeks 16.0 and 16.7) sampling events.

	Acidity (%)	Total Metals (%)	Fe (%)	Al (%)
BGCR	**Week 16.0 - Second to Last Sampling Event (Second Highest Loading Rates)**			
P1	99.8	99.7	99.6	99.8
P2	99.0	98.3	96.9	99.5
S2	99.0	98.2	96.6	99.6
S3	99.2	98.6	97.5	99.5
S4	98.4	97.1	94.2	99.6
BGCR	**Week 16.7 - Final Sampling Event (Highest Loading Rates)**			
P1	99.1	98.4	97.2	99.3
P2	97.3	94.4	88.8	99.1
S2	93.2	87.0	78.4	94.3
S3	95.5	91.4	85.8	96.1
S4	65.3	44.0	56.3	33.3
BGCR	**Decrease in Removal Efficiencies from Week 16.0 to Week 16.7**			
P1	0.7	1.3	2.4	0.5
P2	1.7	3.9	8.1	0.4
S2	5.8	11.2	18.2	5.3
S3	3.7	6.2	11.7	3.4
S4	33.1	53.1	37.9	66.3

4.2.2.2 Influent and Effluent Metal and Sulphate Chemistry

Iron and Al contributed to the majority of metal (98.0-99.0%) and acidity (median 79.2% (66.8-81.3%)) loading to each system. Iron and Al loading correlated generally well (R^2 = 0.984) with Al loading exceeding Fe loading an average of 1.40 times throughout this study. Influent and effluent Fe and Al concentrations and removal efficiency for each BGCR are displayed in Figure 4.16. A comparison of Fe and Al percent removal efficiencies from each BGCR are shown in Figure 4.17 where data points below the dashed lines indicate a greater percentage of Fe removal, and data points above the dashed lines represent a greater percentage of Al removal.

Removal efficiency was generally stable for Fe and Al (with exception of S1); however, treatment effectiveness was better for Al except at the highest loading rate tested for S4 (1.36 mol total metals/m^3/day and 2.73 mol sulphate/m^3/day) and for P3. A decrease in Fe removal efficiency was more notable, especially during the final sampling event, for most BGCRs (at metal loading>0.8 mol/m^3/day) and throughout the operation of S1. Excluding S1, Al removal was always >99% following the first flush (third sampling event; week 5.2 onwards) and prior to the highest loading rates tested. Iron removal during the same period was less effective and more variable and typically

ranged between 94% and 99%, which further demonstrates the more effective removal efficiency of Al compared with Fe.

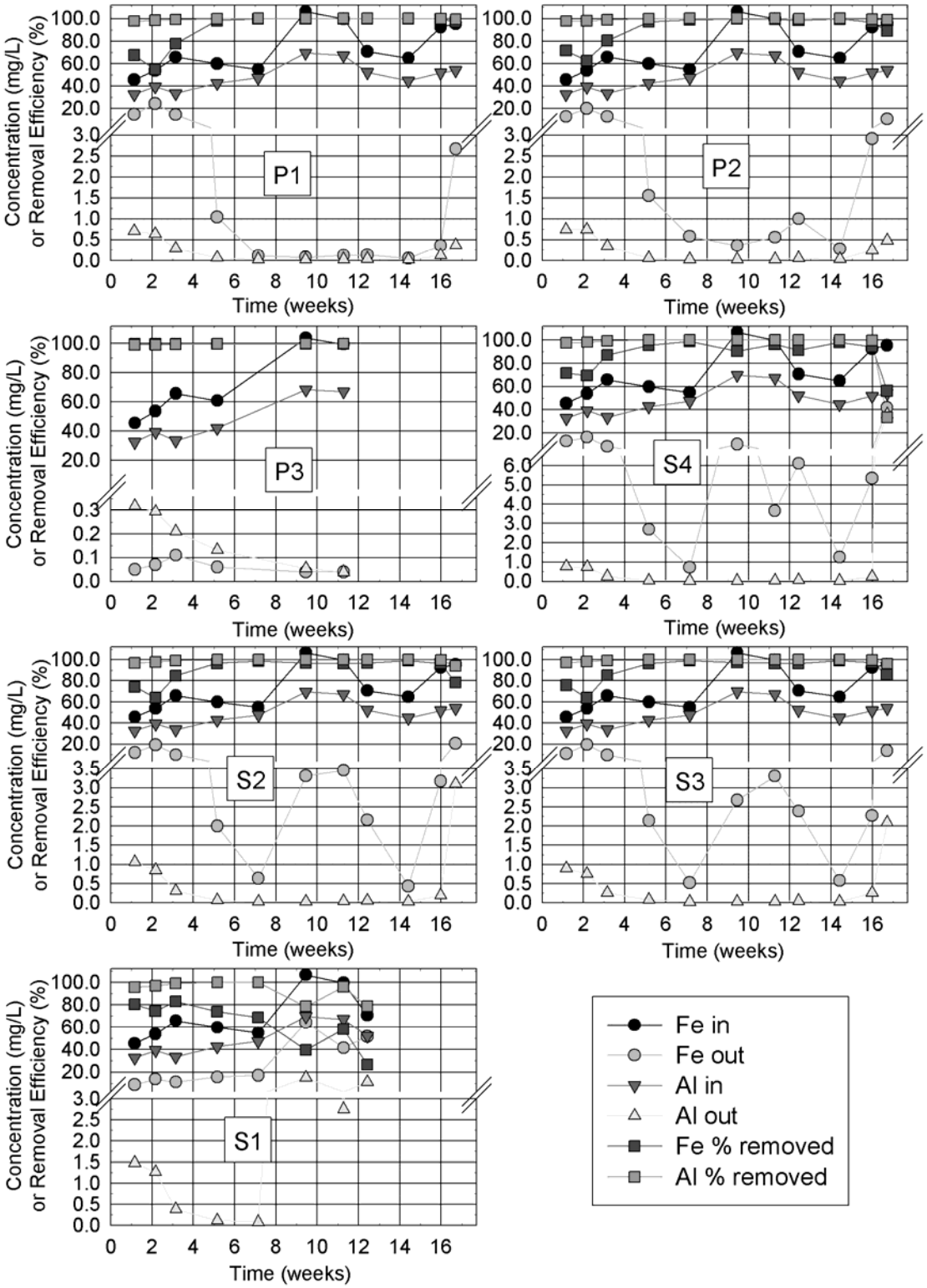

Figure 4.16. Influent and effluent Fe and Al concentrations during the mesocosm-scale treatability tests. Removal efficiencies were computed from concentration reductions.

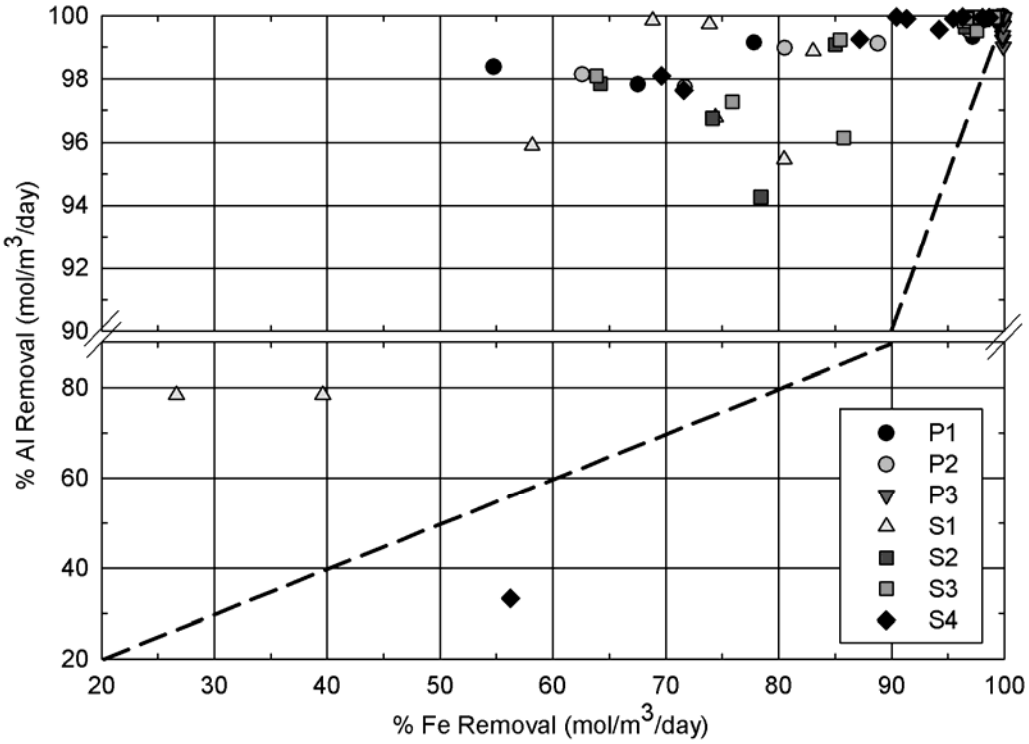

Figure 4.17. Relationship of Fe and Al percent removal efficiencies from each BGCR. Data points below the dashed lines indicate a greater percentage of Fe removal, whereas data points above the dashed lines represent a greater percentage of Al removal.

A summary of influent and effluent metal and sulphate concentrations from each reactor during stable operating conditions (weeks 5.2-16.0; metal loading rates 0.23-0.83 mol/m^3/day; and acidity loading rates 21-80 g $CaCO_3$/m^2/day) are summarised in Table D.1 in Appendix D. Data excludes the first three (weeks 1.1-3.2) sampling events due to effects from the first flush and the final (week 16.7) sampling events due to system overloading. Effluent data from P3 and S1 includes samples collected from week 5.2 until BGCR operation ceased (during week 11.3 for P3 and week 12.4 for S1).

Influent and effluent dissolved Fe and Al concentrations during stable operating conditions are shown in Figure 4.18. The x-axis illustrates influent AMD and effluent from each BGCR. The y-axis shows Fe (dark grey bars) and Al (light grey bars) concentration ranges (on a logarithmic scale). Horizontal black lines represent median Fe and Al concentrations. Dissolved metal influent (AMD) and effluent concentrations and calculated removal efficiencies from BGCRs P1, S2 and S3 (20-30% mussel shells as sole alkalinity amendments to substrate) during metal loading rates of 0.23 to 0.83 mol/m^3 substrate/day and acidity loading rates of 25 to 80 g as $CaCO_3$/m^2/day are shown in Table 4.8. These represent the results of BGCRs containing mussel shells solely as an alkalinity amendment and represent recommended operational ranges for metal removal. Metal removal was most effective for Al, Cu, Ni, Zn, Cd and Pb, but a substantial amount of Fe (96.5-99.8 %) was also removed. There was typically a net export of As, likely as a result of leaching from substrate materials. Effluent As

concentrations were greatest from BGCRs containing mussel shells (P1, S2 and S3) during the first three (weeks 1.1-3.2) sampling events, averaging 0.026 mg/L (range of 0.013-0.042 mg/L), while the lowest As concentrations were from S1 averaging 0.010 mg/L (range of 0.006-0.018 mg/L). For sampling events thereafter, effluent As concentrations were 0.002-0.003 mg/L.

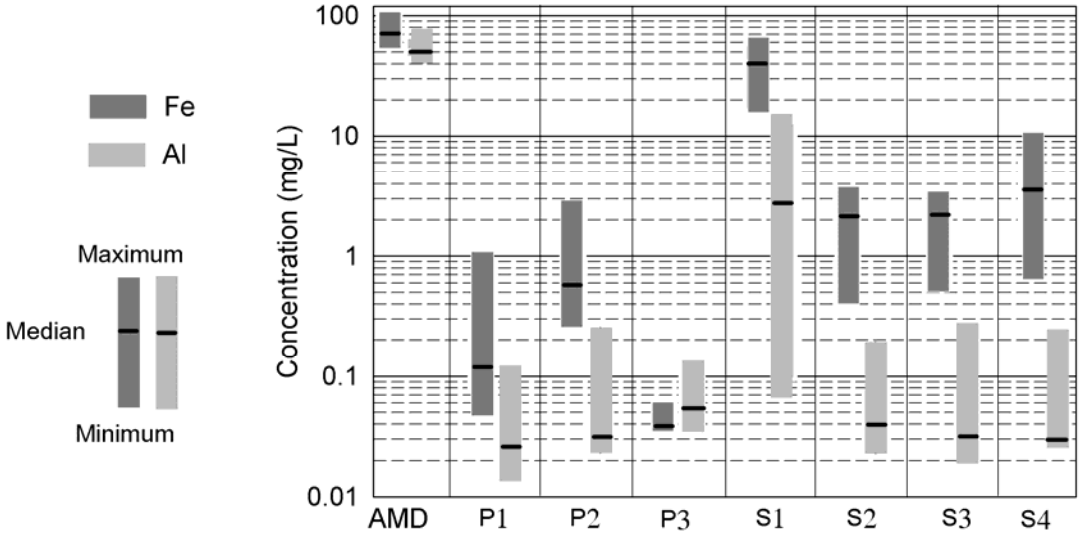

Figure 4.18. Influent (AMD) and effluent (P1, P2, P3, S1, S2, S3 and S4) dissolved Fe and Al concentrations from mesocosm-scale BGCR experiments during metal loading rates from 0.23 to 0.83 mol/m^3 substrate/day and acidity loading rates from 25-80 g (as $CaCO_3$)/m^2/day. Data represents samples collected between weeks 5.2-16.0 during stable operating conditions. Effluent data from P3 and S1 includes samples collected from week 5.2 until BGCR operation ceased (during week 11.3 for P3 (0.41 mol metals/m^3/day and 45 g $CaCO_3$/m^2/day) and Week 12.4 for S1 (0.56 mol metals/m^3/day and 46 g $CaCO_3$/m^2/day)).

Table 4.8: Dissolved metal influent (AMD) and summarised effluent concentrations and removal efficiencies from BGCRs containing 20-30 vol.% mussel shells (P1, S2 and S3) during metal loading rates from 0.23-0.83 mol/m^3 substrate/day and acidity loading rates from 25-80 g $CaCO_3$/m^2/day. Median concentrations were computed assuming sample concentrations detected below laboratory PQLs were equal to one-half the PQL values.

	AMD Conc. (mg/L)	**Effluent Conc. (mg/L)**			***Removal Efficiency (%)***
	Median	**Median**	**Min**	**Max**	***Range***
Fe	70.7	1.04	0.05	3.46	96.5-99.8
Al	51.8	0.031	0.0170	0.277	99.5-99.9
Cu	0.199	0.00025	<0.0005	<0.001	>99.7->99.9
Ni	0.210	0.001	<0.0005	0.0020	99.3->99.7
Zn	1.23	0.002	<0.001	0.005	99.7->99.9
Cd	0.00169	0.000025	<0.00005	<0.00005	>98.3-98.9
Pb	0.0150	0.00005	<0.0001	0.0001	99.5->99.7

A summary of influent and stoichiometric equivalent effluent sulphate concentrations and removal efficiencies from each BGCR are shown in Figure 4.19. Sulphate removal was not as effective as Fe, Al and most other metals. Sulphate removal was less effective as loading rates increased. This was likely due to decreasing organic matter decomposition, which resulted in lower DOC concentrations (Figure D.11 in Appendix D). This trend differed from those observed for metals where steady removal efficiencies were achieved until distinct loading rates were reached. Aluminium removal was greater than sulphate removal throughout the experiments; however, sulphate removal was better than Fe removal on several occasions during the first three sampling events (weeks 1.1-3.2) when sulphate removal averaged 0.30 mol/m^3/day (excluding P3).

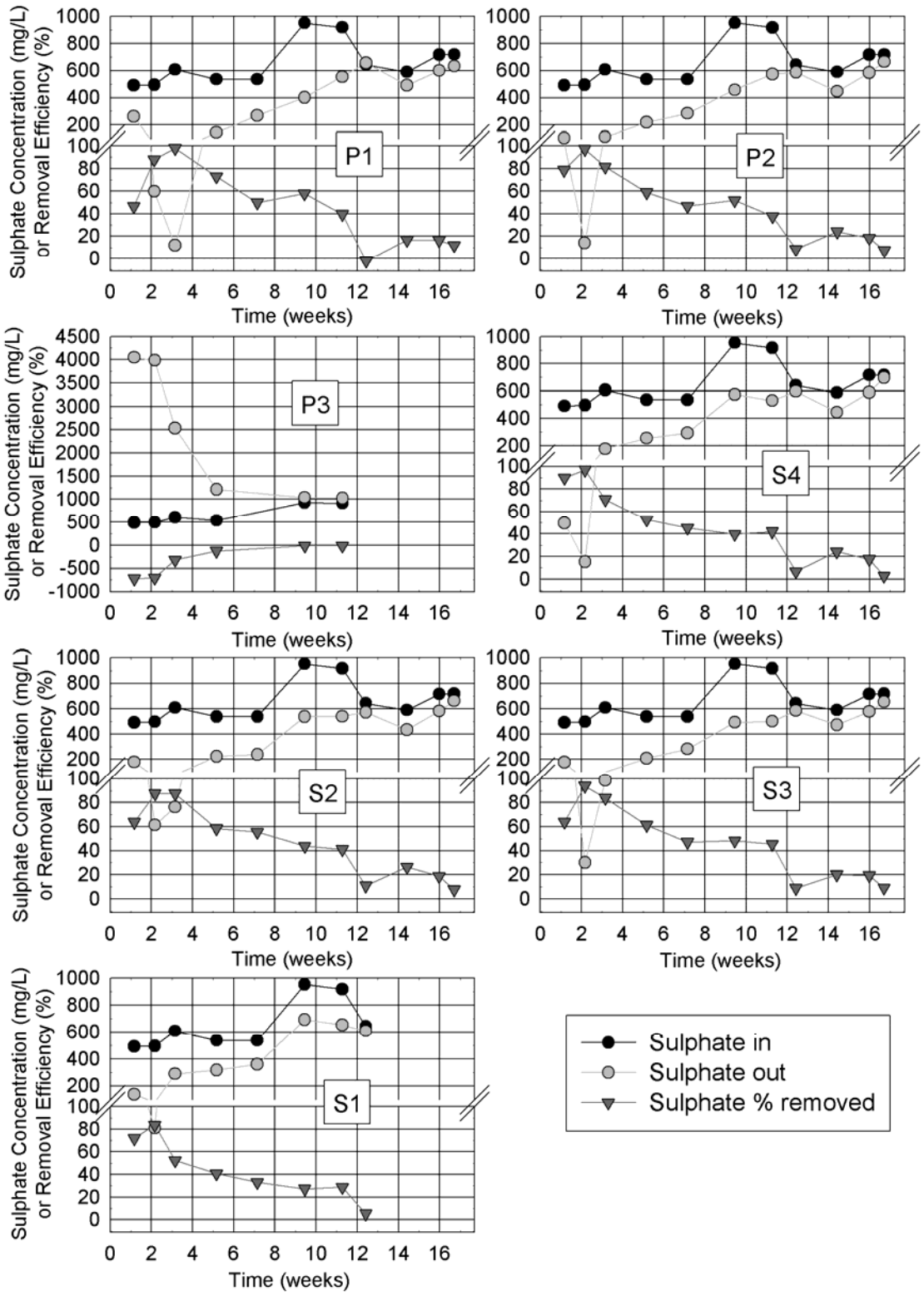

Figure 4.19. Influent and effluent sulphate concentrations and removal efficiencies from each BGCR. The y-axis scale is different for BGCR P3 due to the extensive export of sulphur from the NSD within its substrate mixture.

4.2.2.3 Removal Effectiveness of Fe, Al and Sulphate Based on Hydraulic Residence Time

BGCR effluent Fe (Figure 4.20), Al (Figure 4.21) and sulphate (Figure 4.22) concentrations were investigated as a function of the theoretical HRT of AMD within the BGCRs (τ_{BGCR}). This was calculated by summing the HRTs of the various components of the BGCRs (Equation 4.2) including the surface water overlying the post peel (τ_{sw}), the post peel flow equalisation layer (τ_{pp}), the substrate mixture (τ_{sub}) and the bedding material (τ_{bm}).

$$\tau_{BGCR} = \tau_{sw} + \tau_{pp} + \tau_{sub} + \tau_{bm} \quad \textbf{(4.2)}$$

The HRTs of the BGCR components were calculated as shown in Equations 4.3-4.6 where ε represents air porosity, V indicates reactor volume occupied by each component and Q represents the average volumetric flow rate of influent AMD.

$$\tau_{sub} = \varepsilon_{sub} V_{sub} / Q \quad \textbf{(4.3)}$$

$$\tau_{sw} = \varepsilon_{sw} V_{sw} / Q \quad \textbf{(4.4)}$$

$$\tau_{pp} = \varepsilon_{pp} V_{pp} / Q \quad \textbf{(4.5)}$$

$$\tau_{bm} = \varepsilon_{bm} V_{bm} / Q \quad \textbf{(4.6)}$$

Results from the first three sampling events (weeks 1.1-3.2) were excluded for Fe and Al in Figures 4.20-4.21 due to the influence of the first flush on their removal; however, these data were included for sulphate (Figure 4.22) since its removal was greatest during these sampling events. Sulphate concentrations from P3 were excluded because of the net export of sulphur. Generally, greater Fe, Al and sulphate removal was achieved with increasing HRT; however, this trend was not consistent, especially at a theoretical HRT in the BGCRs >6.7 days for Fe and Al. This was due primarily to variable influent concentrations, which influenced loading rates. Based on this assessment, operating the BGCR performance on a loading basis provided an effective means of achieving consistent effluent concentrations despite variable influent Fe (49.7-113 mg/L), Al (33.5-72.4 mg/L) and sulphate (493-1007 mg/L) concentration ranges.

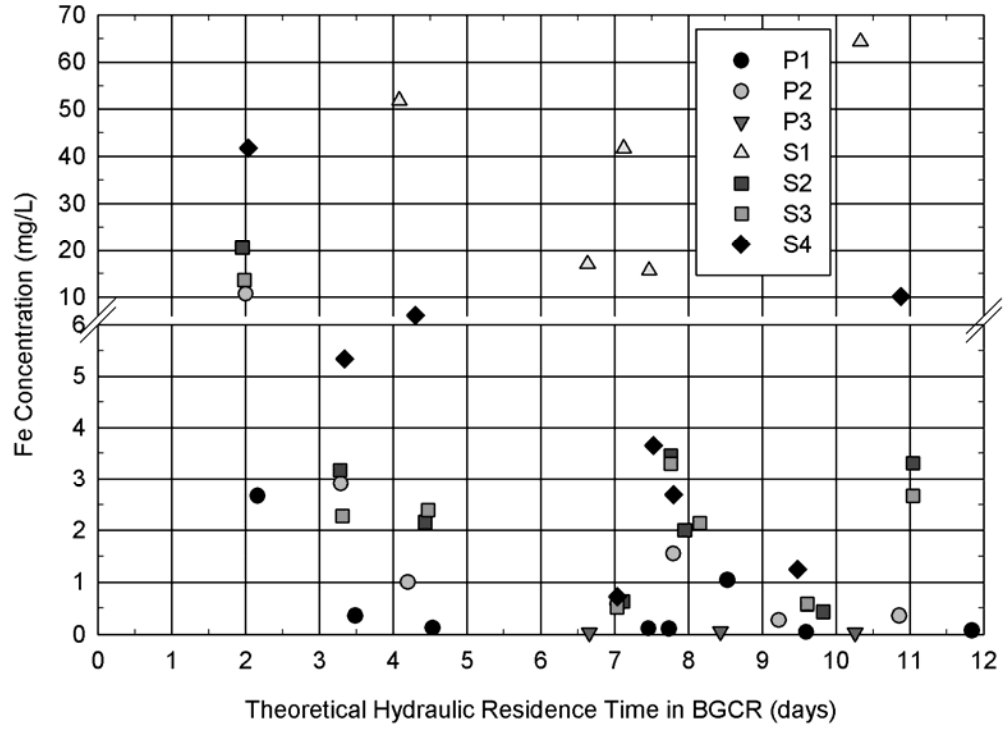

Figure 4.20. Relationships between theoretical HRT in all components of the BGCRs and effluent Fe concentrations for each BGCR (excluding results from the first flush during the first three (weeks 1.1-3.2) sampling events).

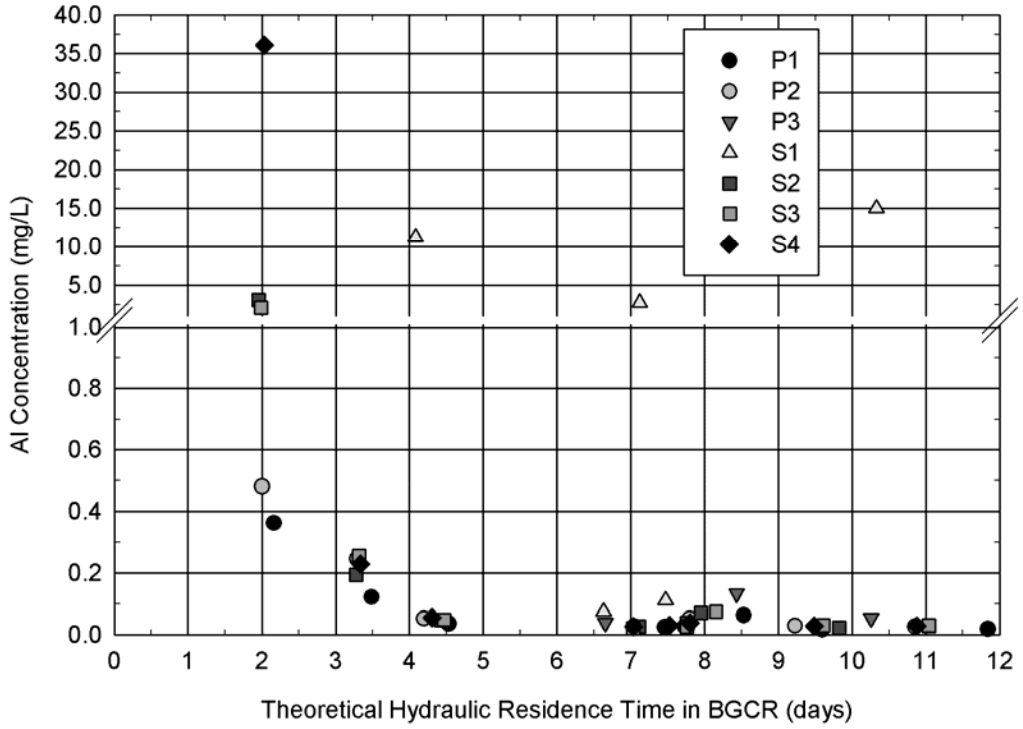

Figure 4.21. Relationships between theoretical HRT in all components of the BGCRs and effluent Al concentrations for each BGCR (excluding results from the first flush during the first three (weeks 1.1-3.2) sampling events).

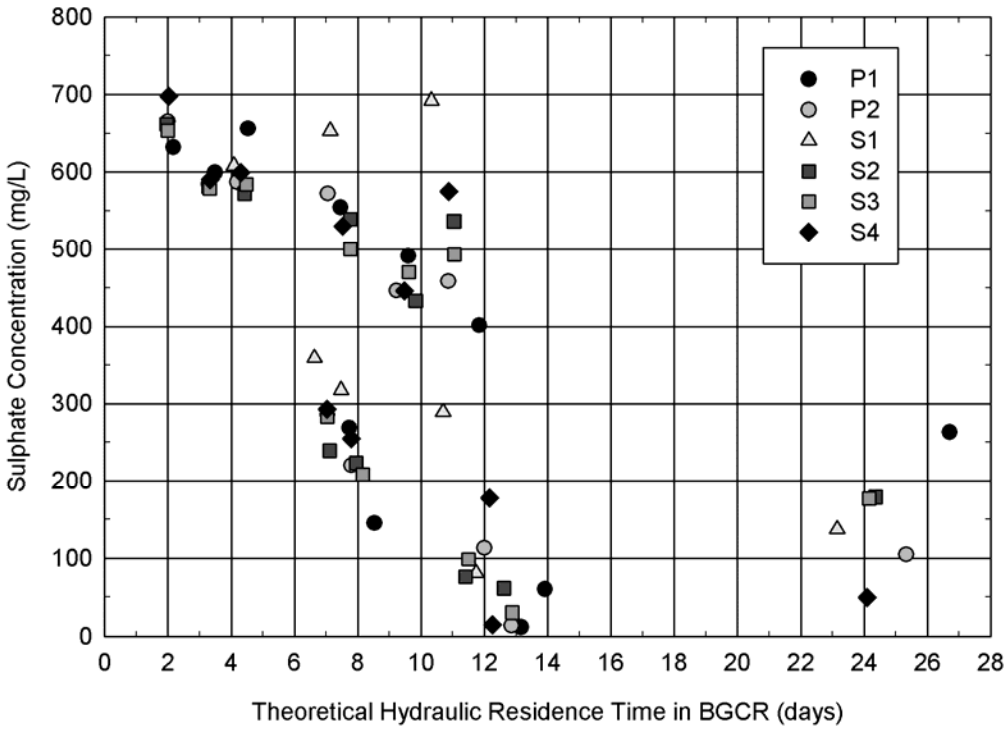

Figure 4.22. Relationships between theoretical HRT in all components of the BGCRs and effluent sulphate concentrations for each BGCR (excluding results from BGCR P3 due to the extensive export of sulphur from the NSD within its substrate mixture).

Although the majority of treatment occurs within the substrate media, it is more pragmatic to consider the HRT within all components of the BGCRs, especially from an operational standpoint or when comparing theoretical HRT with those measured during tracer analysis (as discussed in Chapter 6). The theoretical HRT ranged from 61.7-63.7% of the total theoretical HRT in trapezoidal-shaped reactors and 68.7-71.8% in the drum-shaped reactors.

The residence-time distribution (RTD), which represents the cumulative number of effluent pore-water volumes, of effluent Fe (Figure 4.23), Al (Figure 4.24) and sulphate (Figure 4.25) concentrations (excluding P3) were also plotted. Biogeochemical reactor pore-water volume ($V_{w(BGCR)}$) was computed using Equation 4.7.

$$V_{w(BGCR)} = \varepsilon_{sw}V_{sw} + \varepsilon_{pp}V_{pp} + \varepsilon_{sub}V_{sub} + \varepsilon_{bm}V_{bm} \quad \textbf{(4.7)}$$

The theoretical RTD (θ_{BGCR}) was computed using Equation 4.8 where t represents time.

$$\theta_{BGCR} = t/\tau_{BGCR} \quad \textbf{(4.8)}$$

A complete pore-water volume cycle was achieved shortly after the second (week 2.2) sampling event. Excluding the first three (weeks 1.1-3.2) and final two (weeks 16.0 and 16.7) sampling events, the number of pore-water volumes between sampling events ranged from 1.36 to 2.30 with an average of 1.72. The number of pore-water volumes averaged 3.29 and 2.50, respectively, for the final two sampling events. The RTD represented a total of 16.6-17.8 pore-water volumes for BGCRs operated throughout the duration of this study. The first flush was especially evident during the first three pore-water volumes.

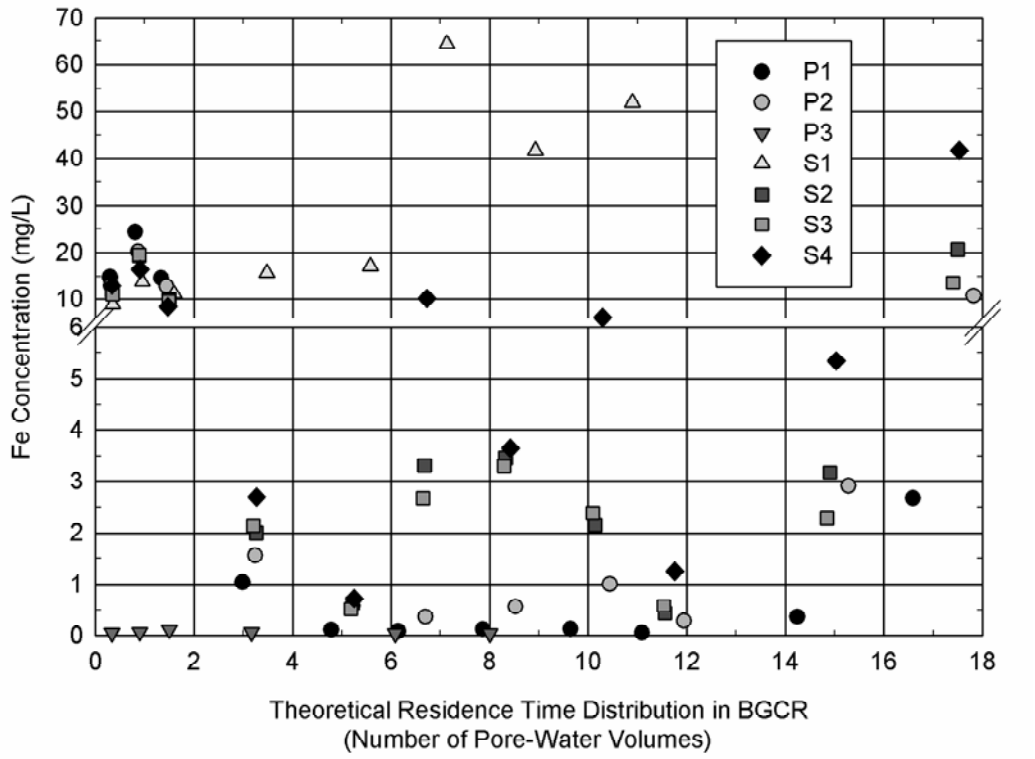

Figure 4.23. Summary of Fe concentrations from BGCR effluent on a theoretical RTD basis considering all components of the BGCRs.

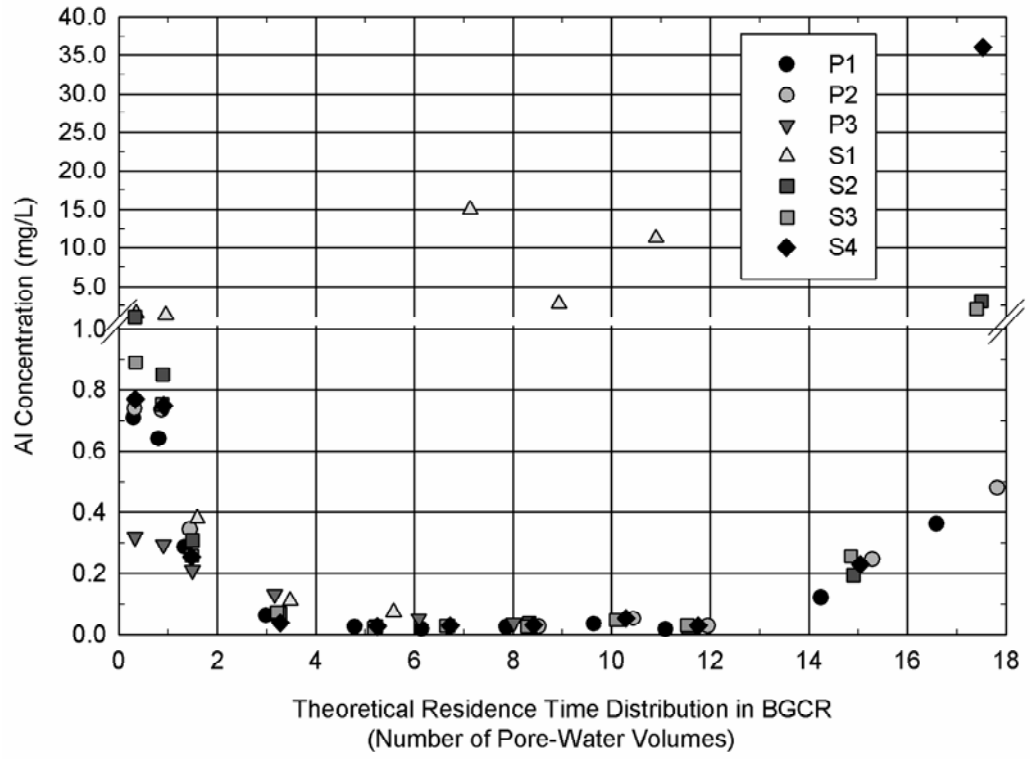

Figure 4.24. Summary of Al concentrations from BGCR effluent on a theoretical RTD basis considering all components of the BGCRs.

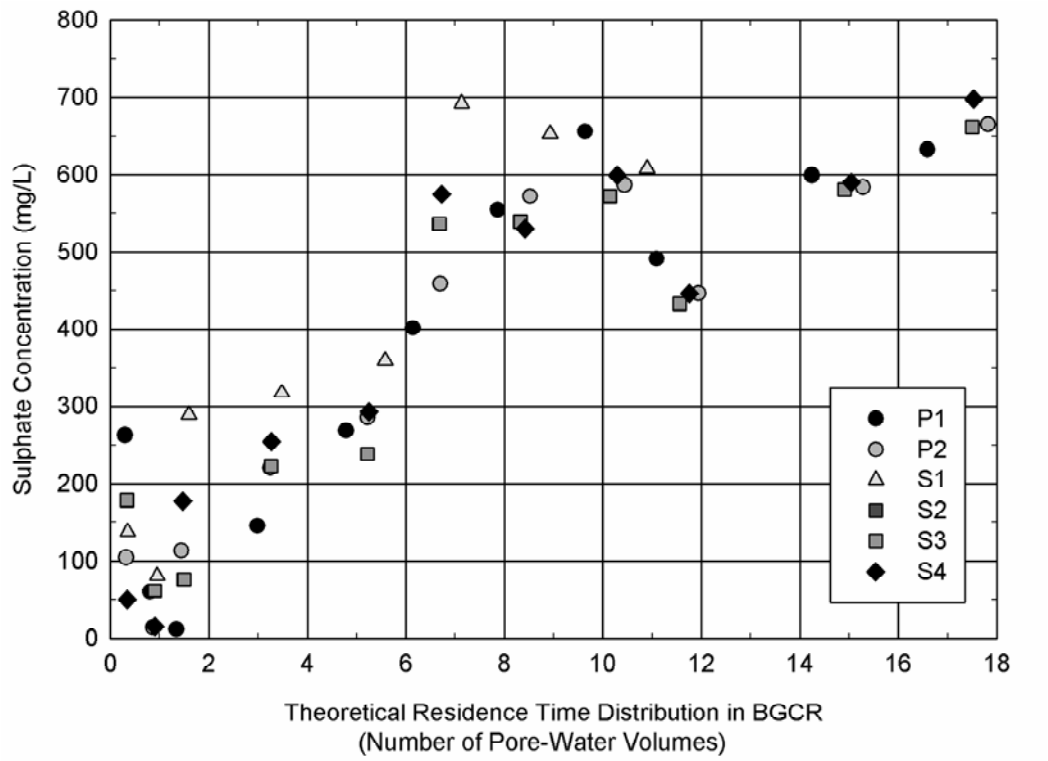

Figure 4.25. Summary of sulphate concentrations from BGCR effluent on a theoretical RTD basis considering all components of the BGCRs (excluding results from BGCR P3 due to the extensive export of sulphur from the NSD within its substrate mixture).

4.2.3 Additional Water Chemistry Parameters

Additional water chemistry parameters monitored included cations (Na, K, Mg and Ca), chemical and physical parameters (temperature, specific conductance, DO and Eh), solids (turbidity, TSS, TDS and salinity), organics (DOC/TOC), nutrients (TN, TKN, TON and TP) and biological parameters (faecal coliforms and BOD). Their results are discussed in Appendix D. Generally, cation, organic, nutrient and biological parameter concentrations were present in the effluent at higher concentrations during the first flush and declined thereafter. Dissolved oxygen and Eh were generally lower with increasing HRT and mussel shell composition in substrates. Alkalinity and pH, and their association with effluent Fe and Al concentrations, will be discussed in greater detail in Chapter 5.

4.3 Discussion

4.3.1 Effect of Substrate Mixture on Treatment Performance

Biogeochemical reactors containing the most mussel shells in their substrate composition displayed the best acidity (Figures 4.6 and 4.11), total metal (Figures 4.7 and 4.12), Fe (Figures 4.8, 4.13 and 4.16), Al (Figures 4.9, 4.14 and 4.16) and sulphate (Figures 4.10, 4.15 and 4.19) removal of all feasible systems (P1>P2>S2 and S3>S4>S1). S1 showed poor system performance compared with other systems and removed about two-thirds of total metals at a metal loading rate of approximately 0.3 mol metals/m^3 substrate/day (25 g $CaCO_3/m^2$/day). Limestone used in S1 was likely too large (20-70 mm diameter) to achieve optimal calcite dissolution due to less surface area compared with a smaller diameter material. Gusek and Wildeman (2002) used crushed limestone in VFWs that adequately removed Al (to concentrations <0.1 mg/L) from AMD. Thomas and Romanek (2002a) reported similar results in effluent from VFWs using a volumetric mixture of 75% compost and 25% fine-grained limestone (nominal grain size of 1.23 mm diameter). Although metal and acidity removal was greatest in P3, effluent was unfeasible due to rapid dissolution of calcium oxide present in the NSD, which resulted in caustic effluent (pH 9.23-10.56) and a net export of sulphur (Figure 4.10; Table D.1) and K (Figure D.2; Table D.2). The greater metal and acidity removal from P3 compared with other reactors was due to the greater effluent pH. This was especially important for the chemical precipitation of Fe in its reduced form as ferrous hydroxide, which only occurs when pH≥8.5 (Wildeman et al., 2006).

Treatment performance of S3 and S2 were similar throughout most of this study; however, S3, containing 10 vol. % greater post peel material and 10 vol. % less bark, outperformed S2 at the maximum metal (1.44 and 1.42 mol/m^3/day, respectively) and acidity (135 and 133 g as $CaCO_3/m^2$/day, respectively) loadings tested. *Pinus radiata* bark was larger, flatter and more heterogeneous than post peel thus potentially leading to greater horizontal hydraulic conductivity and hydraulic short circuiting in S2 compared with S3. Post peel also contained a higher surface area so may have provided more sorption sites than bark. It is possible that different dissolved organics leached from bark compared to post peel, which may have influenced BGCR performance. A detailed

analysis of flow hydraulics within these two reactors, such as tracer studies, would have been required to determine if short circuiting was the reasoning for better treatment performance in S3 at the highest loading rates tested. Studies such as Hemsi et al. (2010) offer promise that mechanisms and reaction rates of organic decomposition in passive AMD treatment systems, such as the BGCRs analysed in this study, and how they influence treatment performance may someday be better understood.

The better performance of BGCRs containing only mussel shells as an alkalinity amendment compared with those containing limestone may be attributed to faster acid dissolution kinetics for mussel shells compared with limestone. Possible contributing factors include grain size, shape, calcium carbonate percentage, unique mineralogy (mixture of calcite and aragonite), reactive surface area and consequent structural change during the dissolution process. Effluent Ca concentrations were greater in BGCRs containing mussel shells compared with those containing limestone (or a mixture of mussel shells and limestone). Reactors S2 and S3 (20% mussel shells) contained an average effluent Ca concentration 39% greater than S1 (12.5% limestone). Hutchinson and O'Sullivan (2008) measured mean Ca composition of 39% (range of 30-46%) for limestone and 53% (range of 44-63%) for the prismatic (middle and thickest) layer of mussel shells used in this study by scanning electron microscopy (SEM) and electron dispersive spectrophotometry (EDS). The calcium carbonate in limestone is presumed to consist entirely of calcite. Mussel shells (*Mytilis* sp.) examined by Cubillas et al. (2005) consisted of 90% calcite and 10% aragonite. Cubillas et al. (2005) found similar BET surface-area normalised dissolution rates for calcite and aragonite; however, geometric surface-area normalized dissolutions rates were 30% greater for aragonite. BET surface areas increased 80% for mussel shells following dissolution experiments and only 30% for calcite, indicating unique characteristics and mineralogical changes associated with mussel shell dissolution (Cubillas et al., 2005).

In addition to alkalinity and pH augmentation benefits, labile carbon attached to the mussel shells and the nitrogen within proteins comprising the periostracium (outer) mussel shell layer may have benefited the consortium of microorganisms, which develop as systems reach stable treatment conditions (within 5.2 weeks in this study). Organic carbon sources (compost, *Pinus radiata* bark and post peel) seemed to provide adequate carbon, and potentially nitrogen, and interfaces to sustain microorganisms and associated biofilms and solid interfaces to support their growth.

4.3.2 Effect of Reactor Shapes and Dimensions on Treatment Performance

Acidity, metal and sulphate removal were consistently greater in P2 than S4 (Figures 4.6-4.16 and 4.19; Table D.1) indicating that reactor shape, and consequently, substrate depth (562 mm for P2 (drum) and 440 mm for S4 (trapezoidal)) influenced treatment performance. For example, the Fe effluent concentration from P2 was 2.91 mg/L, and the Fe effluent concentration from S4 was 5.34 mg/L at total metal loading rates of 0.734 and 0.800 mol/m^3/day, respectively. Aluminium effluent

concentrations were comparable at about 0.24 mg/L at these metal loading rates. At the highest total metal loading tested (1.25 mol/m^3/day for P2 and 1.37 mol/m^3/day for S4), P2 yielded 94.4% total metal removal with effluent concentrations of 10.7 mg Fe/L and 0.481 mg Al/L. Total metal removal for S4 was 44.0% with effluent concentrations of 41.8 mg Fe/L and Al 36.1 mg Al/L. Sulphate removal efficiency was also greater in P2 (average 43.2%; range of 7.3-97.2%) than S4 (average 39.8%; range of 2.7-96.9%) throughout system operation.

It was suspected that there was less short circuiting in the drum reactors because of lower cross-sectional area and greater substrate depth compared with the trapezoidal prism reactors. The greater substrate depth in P2, which was 27.7% greater compared with S4, also likely contributed to better treatment performance. A comparison of flow hydraulics within the drum and trapezoidal-shaped reactors and their application to reactor modelling is explored in Chapter 6.

4.3.3 Acidity and Metal Removal and Recommended Design Criteria

The design criteria recommended for acidity, metal and sulphate removal is based on the maximum loading rates at which there was not a significant decline in treatment performance (e.g. >≈98% metal removal and >≈99% acidity removal). This threshold was established during the second to last (week 16.0; $14.2 \leq \theta_{BGCR} \leq 15.3$) sampling event for acidity and metal removal from BGCRs containing mussel shells or a mixture of mussel shells and limestone (P2, S2, S3 and S4) as shown in Figures 4.11 and 4.12 where data points begin deviating from the 100% removal efficiency dashed line. Good treatment performance was achieved throughout for P1, but a decline in treatment performance was measured during the final sampling event (week 16.7). The decline in treatment performances occurred when increases in effluent DO (Figures D.7 and D.8) and Eh (Figure D.9) and declines in effluent pH and alkalinity (Figure 5.1) were measured.

Pilot and industrial-scale VFWs constructed *in-situ* have typically been trapezoidal-prism shaped basins (e.g. Gusek and Wildeman, 2002; Rose and Dietz, 2002; Ziemkiewicz et al., 2003; Rose, 2004; Skousen and Ziemkiewicz, 2005; Gusek et al., 2008; Reisman et al., 2008); therefore, it was most appropriate to assume the shape and treatment performance of trapezoidal-container reactors (S1-S4) for establishing design criteria rather than the cylindrical drums (P1-P3). It was also appropriate to assume that alkalinity amendments in the substrate compositions of future BGCR systems would consist of mussel shells and no limestone or NSD. Therefore, the most appropriate design criteria established based on results of this study were based on the results of BGCRs S2 and S3 (20 vol. % mussel shells) during the second to last (week 16.0) sampling event. This includes 66 g acidity (as $CaCO_3$)/m^2/day and 0.8 mol total metals/m^3 substrate/day. Acidity and total metal removals averaged 99.1% and 98.4%, respectively. Better acidity and metal removal could potentially be obtained if the quantity of mussel shells in the substrate mixture was increased to 30 vol. %. Design criteria based on the treatment performance of P1 (30 vol. % mussel shells) in this study would be approximately 150 g

acidity (as $CaCO_3$)/m^2/day and 1.2 mol total metals/m^3 substrate/day based on treatment performance during the final (week 16.7) sampling event. Acidity and total metal removals were 99.1% and 98.4%, respectively, the same as the average removals measured for S2 and S3 during the second to last (week 16.0) sampling event.

It should also be noted that BGCRs have a limited design life and treatment performance is dependent on a number of factors. Eventually, the reactive substrate media will be used up so treatment performance will eventually decline. The initial decline in treatment performance will likely occur due to the decomposition of the mussel shells. In a field application, such factors as variable AMD chemistry will influence treatment longevity. BGCRs should be designed to treat the greatest metal loading measured during monthly monitoring (such as that discussed in Chapter 2). Therefore, the BGCRs will nearly always be operating well below design criteria. Pilot-scale studies are recommended prior to designing and operating a full-scale system so that any short comings detected during field operation, such as less effective treatment performance, but not observed during laboratory treatability tests can be addressed (Gusek, 2002; Gusek, 2004; Wildeman et al., 2006). Pilot-scale studies and scaling-up challenges of BGCRs are discussed in detail in Chapter 7. Estimates pertaining to the design life and sizing of a full-scale BGCR treating Manchester Seep AMD *in-situ* are discussed in Chapter 8 (Section 8.3).

A summary of design criteria and results of empirical studies evaluating the performance of VFWs and results of this study are summarised in Tables 4.9 (acidity removal) and 4.10 (metal removal). Overall, acidity and metal removal from the BGCRs containing mussel shells exceeded recommended design criteria used for similar VFWs employed in mine-water treatment incorporating limestone as the primary alkalinity amendment. Acidity design criteria was about two times greater in this study (66 g as $CaCO_3$/m^2/day) compared with design criteria recommended by Watzlaf et al. (2004) (25-30 g as $CaCO_3$/m^2/day) and Rose (2004) (35 g as $CaCO_3$/m^2/day). Wildeman et al. (2006) recommended design criterion of 0.3 mol total metal removal/m^3 substrate/day for VFWs containing a mixture of organic materials and crushed limestone, which was approximately three times less than results of this study for S2 and S3 (>0.8 mol total metals/m^3 substrate/day). The acidity design criteria recommended by Watzlaf et al. (2004) and the metal design criteria recommended by Wildeman et al. (2006) were comparable to those determined during this study for BGCR S1, which also incorporated limestone as an alkalinity amendment.

It may be plausible to design BGCRs to remove the majority of Al and rely on a subsequent aerobic treatment stage to remove Fe and residual Al in BGCR effluent. Sufficient effluent alkalinity and an adequate HRT in a subsequent pond and/or aerobic wetland would be essential for this to be feasibly implemented. Loading rates during the final (week 16.7) sampling event (average 132 g $CaCO_3$/m^2/day and 1.41 mol metals/m^3/day for trapezoidal-shaped reactors and 155 g $CaCO_3$/m^2/day

and 1.24 mol metals/m^3/day for drum-shaped reactors) are likely near the maximum loading threshold to confidently achieve this; however, this would not be plausible for S4. Effluent alkalinity from S4 was 5.15 mg/L as $CaCO_3$, which is only sufficient to oxidise and precipitate 2.86 mg/L of Fe as a hydroxide based on stoichiometry discussed and empirically validated by Hedin (2008a). Average Al loading during the final (week 16.7) sampling event was 0.718 mol/m^3/day.

Table 4.9: Design criteria established and empirical evaluations of acidity removal from VFWs treating AMD.

Study	Description	Recommended Design Criteria and Empirical Study Findings/Removal Rates (g as $CaCO_3$/m^2/day)
Rose and Dietz (2002)	Results from evaluation of 12 full-scale VFWs	Removal rates between 25 and 50.
Thomas and Romanek (2002a)	Laboratory-based column studies of VFWs incorporating 75 vol.% compost and 25 vol. % limestone	Average acidity removal was 87.8; average acidity feed rate was 57.8
Ziemkiewicz et al. (2003)	Results from a comprehensive evaluation of RAPS	Average acidity removal of 62.3
Rose (2004)	Re-evaluation of earlier study (Rose and Dietz, 2002)	Proposed a non-Mn acidity design criterion of about 35
		Twice the acidity removal was observe in systems incorporating fine limestone
Watzlaf et al (2004)	Evaluation of treatment performance of numerous full-scale VFWs	Design criteria of 25-30 recommended
Skousen and Ziemkiewicz (2005)	Results from evaluation of 16 full-scale VFWs	>200 for two systems
		Five between 39 and 87
		Eight between 2 and 17
		One that did not remove acidity
This study	S1 (trapezoidal shaped; 12.5 vol.% limestone)	Design criterion established at 24
	S2 and S3 (trapezoidal shaped; 20 vol. % mussel shells)	Design criterion established at 66
	S4 (trapezoidal shaped; 12 vol. % mussel shells and 5 vol. % limestone)	Design criterion established at 66
	P1 (drum shaped; 30 vol. % mussel shells)	Design criterion established at 153
	P2 (drum shaped; 12 vol. % mussel shells and 5 vol. % limestone)	Design criterion established at 80

Table 4.10: Design criteria established and empirical evaluations of metal removal from VFWs treating AMD.

Study	Description	Recommended Design Criteria and Empirical Study Findings/Removal Rates (mol/m^3/day)
Wildeman et al. (2006)	Based on empirical data of full-scale systems	Recommended a design criterion of 0.3
This study	S1 (trapezoidal shaped; 12.5 vol.% limestone)	Design criterion established at 0.3
	S2 and S3 (trapezoidal shaped; 20 vol. % mussel shells)	Design criterion established at 0.8
	S4 (trapezoidal shaped; 12 vol. % mussel shells and 5 vol. % limestone)	Design criterion established at 0.8
	P1 (drum shaped; 30 vol. % mussel shells)	Design criterion established at 1.2
	P2 (drum shaped; 12 vol. % mussel shells and 5 vol. % limestone)	Design criterion established at 0.8

Iron and Al removal efficiencies reported from other VFW studies were variable and dependent on a number of factors (e.g. mine water chemistry, metal loading rates, system designs, environmental conditions, etc.). Rose and Dietz (2002) reported Fe removal efficiencies ranging from 14.3% to 96.8% (mean 65.2%; n=15 systems; Fe influent concentrations ranging from 16.0 to 208 mg/L (mean 69.6 mg/L) and Al removal efficiencies ranging from 25.0% to 100% (mean 59.0%; n=10 systems; Al influent concentrations ranging from 11.1 to 48.0 mg/L (mean 22.8 mg/L)) from full-scale VFWs. Gusek and Wildeman (2002) used crushed limestone in VFWs that achieved consistent Al concentrations <0.1 mg/L. Gusek et al. (2008) and Wildeman et al. (2006) demonstrated successful metal removal (average 96.1%) by a pilot-scale VFW treating AMD laden with Fe, Al, Cu, Zn, Cd, Co, Pb and Mn. Trumm et al. (2006; 2010) reported Fe and Al removal of 99% and 96%, respectively, from a small-scale VFW. Results of this study demonstrated substantial total metal removal (mean 99.0%) in VFWs incorporating mussel shells (P1, P2, S2, S3 and S4). Metal removal from BGCRs in this study (Figures 4.18 and 4.20) incorporating mussel shells (P1, P2, S2, S3 and S4) ranged from 94.2%-99.9% Fe and 99.5%-100% Al at loading rates up to approximately 0.8 mol total metals/m^3/day. Effluent Fe concentrations were <1 mg/L at average total metal loading rates of 0.286 mol/m^3/day and ranged from 2.28 to 5.34 mg/L for trapezoidal-shaped BGCRs S2, S3 and S4 up to loading rates of 0.827 mol total metals/m^3/day. All systems incorporating mussel shells showed a significant decline in Fe removal at the highest metal and acidity loading rates tested with effluent concentrations 3.7-7.8 times greater than at the second highest metal and acidity loading rates. Effluent Al concentrations increased about an order of magnitude for all reactors at the second highest metal and acidity loading rates compared with lower loading rates (e.g. average of 0.036 mg/L increased to 0.210 mg/L). Aluminium concentrations increased an additional order of magnitude at the highest metal loading rates evaluated for S2 and S3 (3.10 and 2.09 mg/L, respectively) and an

additional two orders of magnitude for S4 (36.1 mg/L). Effluent Al concentrations for P1 and P2 were about two to three times greater at the highest metal and acidity loading rates (0.363 and 0.481 mg/L, respectively) compared with the second highest metal loading rates (0.122 and 0.246 mg/L, respectively).

The BGCRs operated during this study typically removed over 99% of Cu, Ni, Zn, Cd and Pb with effluent concentrations typically below laboratory PQLs. Effluent Cd concentrations remained below PQLs throughout this study for all BGCRs. Effluent Pb concentrations remained below practical quantitation limits (PQLs) except for the final sampling event (week 16.7) for S4 (0.0015 mg/L). Copper and Ni concentrations were below PQLs throughout the experiments for P1 and P2, but detectable at the highest metal loading rates tested for S2 (0.0015 mg/L Cu and 0.009 mg/L Ni), S3 (0.0007 mg/L Cu and 0.007 mg/L Ni) and S4 (0.0325 mg/L Cu and 0.084 mg/L Ni). Effluent Zn concentrations were relatively consistent throughout the experiments (median of 0.002 mg/L; range of <0.001-0.005 mg/L; Table 4.5) except at the highest loading rates tested for S2, S3 and S4 where Zn concentrations increased about an order of magnitude for S2 (0.04 mg/L) and S3 (0.025 mg/L) and about two orders of magnitude for S4 (0.628 mg/L). Reisman et al. (2008) reported successful treatment of Cu, Cd, Pb and Zn from a VFW with concentrations reduced by >96% on average but showed less success reducing Fe (average 1%) and Mn (average 12%) concentrations because of leaching from substrates. Figueroa et al. (2007) utilised a VFW as the second stage of a passive-treatment system and measured a reduction of Zn concentrations from a range of 45-55 mg/L to <0.1 mg/L. Trumm et al. (2006; 2010) reported 95% Ni and 99% Zn removal from a small-scale VFW.

4.3.4 Sulphate Removal and Recommended Design Criteria

It was more difficult to establish a distinct design criterion for sulphate removal since it was more sporadic than that of acidity and metals. A summary of sulphate removal rates from AMD measured during this and other studies using VFWs is shown in Table 4.11. Generally, results from all studies evaluated, including this study, indicated a typical sulphate removal rate of about 0.3 mol/m^3/day, which supports the design criterion recommended by Gusek (2002).

Sulphate concentrations were reduced during this study from the AMD during treatment with exception of P3 (Figure 4.17). Influent sulphate concentrations averaged 657 mg/L (491-1007 mg/L). Equivalent effluent concentrations ranged from 145 to 656 mg/L sulphate. Sulphur was likely prevalent in BGCR effluent in reduced states such as monosulphide, hydrogen sulphide, mobile metal sulphides, and potentially mercaptans or other sulphur and organic-sulphur complexes based on low DO and Eh readings and olfactory observations of a hydrogen sulphide odour. Hydrogen sulphide can be toxic to SRB. Effluent concentrations were well below those where toxic effects of hydrogen sulphide have been reported on SRB ranging from 477-617 mg/L hydrogen sulphide, which are

equivalent to 1346-1742 mg/L sulphate (Okabe et al., 1992; Reis et al., 1992; Al-Ani, 1994; Kolmert et al., 1997; Neculita et al., 2007).

Table 4.11: Design criteria established and empirical evaluations of sulphate removal from VFWs treating AMD. Removal rates measured for BGCRs during this study excluded results from the first (week 1.1) sampling event because flow had not completed a pore-water volume (n=7 for S1; n=20 for S2 and S3 combined; n=10 for P1, P2 and S4). Design criteria established for sulphate removal was based on removal rates observed during empirical studies and not necessarily loading rates where the majority of or consistent sulphate removal efficiency was achieved.

Study	Description	Recommended Design Criteria and Empirical Study Findings/Removal Rates ($mol/m^3/day$)
Dvorak et al. (1992)	Based on empirical results from pilot-scale systems containing mushroom compost and limestone	Removal rates of 0.214-0.333 (17-20% removal)
Gusek (2002)	Based on empirical data of full-scale systems containing a mixture of organic materials and crushed limestone	Design criterion established at 0.3
Thomas and Romanek (2002a)	Laboratory-based column studies of VFWs incorporating 75 vol.% compost and 25 vol. % limestone	0.25 to 0.35 (about 20% removal)
Gibert et al. (2004)	Based on results of laboratory column experiments containing sheep manure and limestone.	0.44 (18% removal) and 0.17 (27% removal)
This study	S1 (trapezoidal shaped; 12.5 vol.% limestone)	Median 0.21 (range of 0.061-0.27)
	S2 and S3 (trapezoidal shaped; 20 vol. % mussel shells)	Median 0.30 (range of 0.089-0.42)
	S4 (trapezoidal shaped; 12 vol. % mussel shells and 5 vol. % limestone)	Median 0.27 (range of 0.074-0.40)
	P1 (trapezoidal shaped; 30 vol. % mussel shells)	Median 0.27 (range of -0.023-0.36)
	P2 (trapezoidal shaped; 12 vol. % mussel shells and 5 vol. % limestone)	Median 0.27 (range of 0.091-0.34)

The highest effluent concentrations were measured at the highest loading rates, while the lowest effluent concentrations were typically measured at lowest loading rates. P3 exhibited a net export of sulphur throughout the experiments with an effluent sulphate concentration initially 4044 mg/L but reduced to 1025 mg/L after 11 weeks of operation. Dvorak et al. (1992), Thomas and Romanek (2002a) and Gibert et al. (2004) reported about 20% sulphate removal efficiency during their studies. Results of this study showed a considerable range (Figure 4.19), which were typically dependent on loading rates (Figure 4.15) and could have also been influenced by sorption to substrate materials

during the earlier stages of the study (Fumoto and Sverdrup, 2001). As loading rates increased, sulphate removal efficiency decreased (Figures 4.10, 4.15 and 4.19). This was likely affected by the decline in DOC throughout reactor operation as shown in Figure D.11. Sulphate removal rates ranged from 0.0610 to 0.421 mol/m^3/day throughout the experiments with removal efficiencies 2.71-98.0% (excluding P3 and the fourth to last (week 12.4) sampling event from P1 where a 2.21% net export of sulphur was measured). Sulphate removal efficiency from S1 (12.5 vol.% limestone) was on average 16.0% less than from P1, P2, S2, S3 and S4 considering sampling events up to week 12.4 when operation of S1 was terminated.

The following design criteria for a combination of total metal and sulphate removal are recommended for similar BGCR systems incorporating mussel shells (or a mixture of mussel shells and limestone) as alkalinity amendments in the substrate mixtures: 1) 0.3 mol sulphate loading/m^3/day for sulphate removal (mean of 94.1% (87.6-98.0%)); 2) 0.4 mol metals/m^3/day for metal (mean of 99.0% (98.5-99.9%)) and partial sulphate removal (mean of 0.38 mol/m^3/day (0.34-0.42 mol/m^3/day); mean of 46.0% (39.6-57.8%)); and 3) 0.8 mol metals/m^3/day for metal (mean of 98.4% (98.2-98.6%)) and minimal sulphate removal (mean of 0.29 mol/m^3/day (0.25-0.33 mol/m^3/day); mean of 16.6% (11.9-19.2%)). Longer duration studies, such as pilot-scale treatability tests conducted *in-situ*, are recommended to fine-tune design criteria for sulphate removal due to the decline in DOC measured throughout this study.

4.3.5 Fate of Metals and Sulphate in Biogeochemical Reactors

There are numerous mechanisms for precipitation and sequestration of metals and sulphur in VFWs. An amorphous iron hydroxide coating was observed on the upper post peel surface, and a distinct blackened sulphide zone was observed near the bottom of the VFWs, similar to that described by Thomas and Romanek (2002b). Scanning electron microscopy and EDS confirmed Fe was present as amorphous iron(oxy)hydroxides at the upper post peel surface, while Al seemed to be precipitated as aluminium oxyhydroxysulphates in deeper substrate zones (Hutchinson and O'Sullivan, 2008). Metal removal likely occurred via precipitation due to increased pH in the BGCRs as well as sorption onto substrates.

Excluding P3, sulphate removal efficiency was 87.6-98.0% during this study for reactors containing mussel shells and no limestone when sulphate loading was 0.302-0.342 mol/m^3/day. If sulphur was only removed as metal sulphides, a maximum sulphur removal of 19.7-30.3% was possible, which would yield effluent sulphate concentrations between 376-722 mg/L. Clearly, other mechanisms for sulphur removal occurred. At metal loading rates of 0.308-0.418 mol/m^3/day and sulphate loading rates of 0.676-0.926 mol/m^3/day, there was 98.5-99.9% metal removal and 39.6-48.3% sulphur removal, corresponding to sulphate reductions from 918-950 mg/L to 493-554 mg/L. This suggests that sulphur was probably also removed through hydrogen sulphide degassing. Gaseous bubbles were

observed rising to the reactor surface in periodic pulses. A distinct hydrogen sulphide odour was also observed. Gypsum ($CaSO_4*2H_20$) formation may have also occurred and contributed to some sulphur removal (Thomas and Romanek, 2002b).

4.3.6 Treatment Performance Based on a Hydraulic Residence Time Basis

There are advantages and disadvantages to evaluating treatment performance based on HRT. The major advantage is simplicity and convenience from an operational perspective; however, it only considers flow rates, whereas looking at treatment performance from a loading perspective considers both flow rate and contaminant concentrations. Developing design criteria solely on HRT does not take into account MIW variability (Younger et al., 2002; Pope et al., 2006; Wildeman et al., 2006). For example, the maximum Fe (113 mg/L) and Al (72.4 mg/L) concentrations from AMD batches used during this study were over two times greater than minimum concentrations (49.7 mg/L Fe and 33.5 mg/L Al) with standard deviations of 19.2 mg/L Fe and 11.2 mg/L Al (Table 4.3). Additionally, Neculita et al. (2007) state that the variability of hydraulics associated with different substrate media may result in HRTs specific to each reactor.

It is recommended to design passive-treatment systems for treating AMD and other MIWs based on the worst water chemistry measured on a loading perspective (Wildeman et al., 2006). This ensures that treatment objectives are met and prevents contaminant overloading that could hinder or damage the treatment system, especially microbiological treatment processes. A summary of applicable theoretical HRT in substrate and all components of the BGCRs considering a potential range of the most concentrated water chemistry anticipated from Manchester Seep AMD is presented in Table 4.12. The design criteria for maximum metal and acidity loading (for BGCRs S2, S3 and S4) was established during the second to last (week 16.0) sampling event when the theoretical HRT was 3.31 days in the BGCR. This represented the fourth worst water chemistry measured during this study based on the summation of molar Fe and Al concentrations. This would have never been detected if this study just analysed treatment performance based on HRT. Considering the summation of molar Fe and Al concentrations, there was a concentration range of 56.6-126% of that measured during the week 16.0 sampling event. Based on the treatment design criteria established during the week 16.0 sampling event, the design HRT would range from 1.87 to 4.17 days in the BGCR. Based on monthly monitoring of water chemistry at the Manchester Seep (Chapter 2), the worst water chemistry measured from the seep water and from the outlet pipe of the subsequent flow-equalisation pond were 110% and 151%, respectively, of that measured during the week 16.0 sampling event. This would yield design theoretical HRT values of 3.64 and 5.00 days in the BGCR, respectively.

Table 4.12: Theoretical HRTs required based on average acidity and metal loading rates measured during the second to last (week 16.0) sampling event during the mesocosm-scale treatability tests, considering the most Fe and Al laden AMD measured during the treatability tests (week 9.4) and from the Manchester Seep and outlet of the Manchester Pond during monthly monitoring. These represent appropriate design HRTs.

Scenario	HRT in Substrate (τ_{sub}) (days)	HRT in BGCRs (τ_{BGCR}) (days)	Fe (mg/L)	Al (mg/L)	Summation of Fe and Al Molar Concentration Ratio Compared with Week 16.0
Week 16.0 – Treatability Tests	2.11	3.31	92.5	51.8	1.00
Week 9.4 – Treatability Tests	2.66	4.17	106	69.5	1.26
Manchester Seep (180706)	2.32	3.64	101	57.0	1.10
Manchester Pond Outlet Pipe (180706)	3.19	5.00	162	67.9	1.51

There is limited literature that reports HRTs for VFW systems treating AMD. A comparison of the treatment performance, with respect to acidity, Fe, Al and sulphate removal, and associated HRTs from the Rose and Dietz (2002) study and this study is presented in Table 4.13. Rose and Dietz (2002) only presented acidity loading rates and did not include metal or sulphate loading rates; therefore, only acidity loading and discharge rates are presented. Data from this study includes those measured during sampling events representative of maximum recommended design metal and acidity loading rates including the following: P1) 1.2 mol total metals/m^3/day and 150 g $CaCO_3$/m^2/day (week 16.7); P2) 0.8 mol total metals/m^3/day and 80 g $CaCO_3$/m^2/day (week 16.0); S1) 0.3 mol total metals/m^3/day and 25 g $CaCO_3$/m^2/day (week 7.1); and S2/S3 and S4) 0.8 mol total metals/m^3/day and 66 g $CaCO_3$/m^2/day (week 16.0). Sulphate loading rates included the following: P1) 2.45 mol/m^3/day (week 16.7); P2) 1.52 mol/m^3/day (week 16.0); S1) 0.60 mol/m^3/day (week 7.1); and S2/S3 and S4) average of 1.69 mol/m^3/day (week 16.0); range of 1.66-1.71 mol/m^3/day. Results from S2 and S3 (S2/S3) were averaged since their treatment performances were similar. Rose and Dietz (2002) reported HRTs ranging from 1.5 to 26 days (average of 8.0 days) from five full-scale VFWs containing influent Fe (average 87.6 mg/L; range of 68.0-122 mg/L; n=5), Al (average 19.3 mg/L; range of 0.1-42.0 mg/L; n=4) and sulphate (average 910 mg/L; range of 775-1153 mg/L; n=5) concentrations comparable with those of the AMD used in this study (average 78.4 mg/L Fe, 53.6 mg/L Al and 698 mg/L sulphate; range of 54.8-106 mg/L Fe, 42.6-69.5 mg/L Al and 536-950 mg/L sulphate.

Results presented in Table 4.13 show that HRT was not a good indication of how well a VFW removed acidity, Fe, Al or sulphate. For example the best treatment performance from systems evaluated by Rose and Dietz (2002) were from the Harb-Walk and PMAC systems which contained

HRTs of 1.7 and 26.0 days, respectively. In this study, substrate composition and reactor shape influenced treatment performance and, consequently, appropriate design criteria including recommended HRTs. Of the BGCRs evaluated as part of this study, design HRTs ranged from 2.16 (P1) to 6.63 (S1) days.

Table 4.13: A comparison of acidity, Fe, Al and sulphate removal from VFWs with respect to HRTs from the Rose and Dietz (2002) study and this study.

	Rose and Dietz (2002)					**This Study**				
	Pot Ridge Test	Pot Ridge C6	Oven Run B1	Harb-Walk	PMAC	P1	P2	S1	S2/S3	S4
Acidity Loading ($g/m^2/day$)	32.6	111	74.3	30.3	5.06	153	80.2	24.1	67.7	65.8
Acidity Discharged ($g/m^2/day$)	2.80	62.2	37.3	0.591	0.0723	1.31	0.787	1.47	0.619	1.06
% Acidity Removal	91.4	44.1	49.8	98.0	98.6	99.1	99.0	93.9	99.1	98.4
Fe In (mg/L)	72.0	84.0	68.0	92.0	122.0	95.5	92.5	54.9	95.5	92.5
Fe out (mg/L)	28.1	35.0	45.5	21.0	15.5	2.67	2.91	17.1	2.72	5.34
% Fe Removal	61.0	58.3	33.1	77.2	87.3	97.2	96.9	68.8	97.1	94.2
Al In (mg/L)	19.0	16.0	42.0	0.1	NA	54.1	51.8	47.4	51.8	51.8
Al out (mg/L)	1.6	12.0	28.1	0.1	NA	0.363	0.246	0.075	0.225	0.230
% Al Removal	91.5	25.0	33.1	0.0	NA	99.3	99.5	99.8	99.6	99.6
Sulphate In (mg/L)	811	921	775	891	1153	717	716	536	716	716
Sulphate out (mg/L)	898	875	831	875	1107	632	584	359	580	590
% Sulphate Removal	-10.7	5.0	-7.2	1.8	4.0	11.9	18.4	33.0	19.0	17.6
HRT (days)	7.8	1.5	3.0	1.7	26.0	2.16	4.30	6.63	4.50	4.46

NA, non-applicable or value not measured.

4.3.7 First Flush Effects

Although not documented extensively in the literature, there is an initial export of easily soluble constituents from VFWs during system start up (Blumenstein et al., 2008). This causes a lag in initial treatment performance and the potential of releasing elevated concentrations of constituents (e.g. metals not removed and highly soluble, labile and/or easily mobilised cations, anions, sediments, organics and bacteria) until system stabilisation occurs.

Blumenstein et al. (2008) reported what they referred to as a "flushing maturation condition" (referred to as first flush in this study) for four bench-scale VFWs (comprised of various organics, including manure, and limestone) treating a MIW with elevated concentrations of Se, Tl, Zn and nitrate. Less effective metal and nitrate removal was measured during the first one to two pore-water volumes in their study compared with operation between the second and third (and final) pore-water volumes. During this study, the period of less effective metal removal was >1.59 pore-water volumes (first three sampling events (weeks 1.1-3.2)) and presumed to be somewhere between two and three pore-water volumes.

Blumenstein et al. (2008) reported that the "flushing maturation" condition occurred due to an initial first flush of labile organics and TSS. Based on the results they reported, there also appears to be a first flush effect with Ca, conductivity and BOD, which was also observed during this study. A comparison of Ca, specific conductance and BOD from the Blumenstein et al. (2008) study and this study during and post first flush is presented in Table 4.14. Specific conductance values from the Blumenstein et al. (2008) study were computed using Equation 2.1 based on the temperature and conductivity values they presented. Because Blumenstein et al. (2008) only reported results from three pore-water volumes, only results from data measured during the fourth (week 5.2) sampling event is presented for post first flush sampling results in this study ($3.21 \leq \theta_{BGCR} \leq 3.48$), so that data comparisons between the two studies are more representative. Since there were only a limited number of BOD samples collected during this study, first flush results presented in Table 4.14 are based only on samples collected during the first (week 1.1) sampling event ($\theta_{BGCR}=0.34$).

Table 4.14: A comparison of effluent Ca, specific conductance and BOD values measured during the first flush and following the first flush from Blumenstein et al. (2008) and this study (excluding P3). Exceptions to the number of BOD observations recorded are presented in parenthesis below their concentrations. The % reductions represent decreases from the first flush to the post first flush.

VFW or BGCR ID	Ca (mg/L)	Ca (mg/L)	% Red. in Ca	Sp. Cond (µS/cm)	Sp. Cond (µS/cm)	% Red. in Sp. Cond	BOD (mg/L)	BOD (mg/L)	% Red. in BOD
	First Flush	Post First Flush		First Flush	Post First Flush		First Flush	Post First Flush	
Blumenstein et al. (2008)									
n	7	4	NA	8	4	NA	2	1	NA
Influent	381	409	-7.3	6410	3890	39.3	3 (n=1)	NA (n=0)	NA
BCR Eff 1	1739	636	63.4	12,700	5170	59.3	11,400	1933	83.0
BCR Eff 2	1360	404	70.3	15,400	6660	56.8	13,000	2567	80.3
BCR Eff 3	1736	647	62.7	13,500	6130	54.6	12,714	2400	81.1
BCR Eff 4	1668	678	59.4	12,400	6360	48.7	11,743	2800	76.2
Average	**1626**	**591**	**64.0**	**13500**	**6080**	**54.9**	**12214**	**2425**	**80.2**
Standard Deviation	**180.2**	**126**	**4.578573**	**1349**	**644.3**	**4.527324**	**764.2**	**366.7**	**2.87**
This Study									
n	3	1	NA	3	1	NA	1	1	NA
Influent	15.7 (13.1-19.2)	18.6	-18.5	1344 (1178-1552)	1378	-2.5	NA	NA	NA
P1	594 (412-729)	248	58.2	5403 (3583-6588)	1642	69.6	NA	NA	NA
P2	443 (324-552)	252	43.1	3484 (2445-4178)	1372	60.6	NA	NA	NA
S1	307 (235-356)	186	39.4	2045 (1483-2335)	1134	44.5	1070	81.5	92.4
S2	540 (366-650)	256	52.6	4262 (2650-5072)	1532	64.1	2150	116	94.6
S3	497 (336-602)	256	48.5	4063 (2645-4781)	1473	63.8	NA	97.5	NA
S4	403 (287-495)	239	40.7	3197 (2183-3704)	1388	56.6	1270	NA	NA
Average	**464**	**240**	**47.1**	**3742**	**1424**	**59.9**	**1497**	**98.3**	**93.5**
Standard Deviation	**103**	**27.0**	**7.37**	**1129**	**173.0**	**8.67**	**574.6**	**17.3**	**1.56**

ID, identification; Red., reduction; Cond, conductivity; Sp. Cond, specific conductance; n, number of observations; NA, non-applicable.

Results from this study and the Blumenstein et al. (2008) study indicated a clear distinction between Ca and BOD concentrations and specific conductance values in effluent from the first two pore-water volumes (first flush) and the third pore-water volume (post first flush). Percent reductions in Ca concentrations were more prominent in the Blumenstein et al. (2008) study (average 64.0%), compared with this study (average 47.1%), likely because of higher concentrations present in the influent water and potentially greater quantities of easily mobilised and/or dissolved calcium carbonate sediment from the crushed limestone they used compared with the limestone and mussel shells used in this study. The reduction in effluent specific conductance was more notable in this study for BGCRs containing mussel shells (average 62.9%) compared with the Blumenstein et al. (2008) study (average 54.9%) and BGCR S1 in this study (44.5%) due to the dissolution of Na from the mussel shells. There was a greater reduction between first flush and post first flush effluent BOD concentrations (average of 80.2% in the Blumenstein et al. (2008) study and 93.5% in this study) compared with Ca and specific conductance. The primary reason for this was the initial export of labile organics associated predominately with bark compost and residual meat from mussel shells in this study and manure in the Blumenstein et al. (2008) study, whereas Ca was plentiful and continually dissolved when contacted with AMD. The effluent BOD concentrations, both the first flush and post first flush, were about an order of magnitude greater in the Blumenstein et al. (2008) study compared with this one likely due to the presence of manure in their substrate.

In this study, there was a first flush phenomenon associated with numerous water chemistry constituents aside from those previously mentioned in Table 4.14. A summary of the percent reduction from the average effluent values measured during the first flush period and the subsequent post first flush sampling event (unless otherwise indicated) for each BGCR (excluding P3) are summarised in Table 4.15. The first flush period considers average results from the first three sampling events ($\theta_{BGCR} \leq 1.59$). The post first flush sampling event considers the fourth (week 5.2) sampling event (average $\theta_{BGCR}=3.24$), unless otherwise indicated, for each BGCR. No TSS samples were collected during the fourth (week 5.2) sampling event, so the fifth (week 7.2) sampling event (average $\theta_{BGCR}=5.21$) was used for calculation purposes. The BOD, faecal coliforms, TN, TKN, TON and TP sample results from the first flush were analysed during the first (week 1.1) sampling event (average $\theta_{BGCR}=0.34$), whereas the post first flush sample results are representative of the sixth (week 9.5) sampling event (average $\theta_{BGCR}=6.82$). Concentrations of these parameters may have still been gradually decreasing, but subsequent samples were not collected to confirm this. The average percent reduction and standard deviation considers results from all BGCRs (excluding P3).

Table 4.15: A summary of the percent reduction of water chemistry parameters from the average effluent values measured during the first flush period and the subsequent post first flush sampling event from the BGCRs (excluding P3).

Water Chemistry Parameter	P1	P2	S1	S2	S3	S4	Average	Standard Deviation
	Percent Reduction from First Flush and Post First Flush							
Metals								
Fe	94.2	89.9	NFF	85.4	84.0	78.7	**86.4**	**5.90**
Al	88.5	91.4	89.2	90.3	88.3	93.4	**90.2**	**1.96**
Cations								
Na	93.0	90.0	83.2	90.2	88.3	88.5	**88.9**	**3.25**
K	88.0	85.6	77.6	85.2	84.0	83.2	**83.9**	**3.51**
Mg	81.5	76.2	62.8	76.1	74.8	73.7	**74.2**	**6.19**
Ca	58.2	43.1	39.4	52.6	48.5	40.7	**47.1**	**7.37**
Specific Conductance and Solids								
Specific Conductance	69.6	60.6	44.5	64.1	63.8	56.6	**59.9**	**8.67**
TSS	95.8	96.8	87.0	92.8	94.8	95.1	**93.7**	**3.55**
Turbidity	81.2	84.2	78.3	78.3	82.6	59.1	**77.3**	**9.21**
TDS	69.6	60.9	44.5	64.0	63.7	56.5	**59.9**	**8.66**
Salinity	72.7	61.8	41.9	63.6	68.2	58.8	**61.2**	**10.6**
Organics and Biological Parameters								
DOC/TOC	92.1	96.7	93.4	92.5	95.6	93.5	**94.0**	**1.81**
BOD	NA	NA	99.1	99.2	NA	NA	**99.2**	**0.071**
Faecal Coliforms	NA	NA	>99.8	99.9	NA	NA	**99.9**	**NA**
Anions								
TN	NA	NA	77.3	90.5	NA	NA	**83.9**	**9.33**
TKN	NA	NA	84.1	90.9	NA	NA	**87.5**	**4.81**
TON	NA	NA	NFF	72.4	NA	NA	**72.4**	**NA**
TP	NA	NA	91.3	80.2	73.5	NA	**81.7**	**8.99**

NA, non-applicable, NFF, no first flush observed.

A time lag was observed in the consistent removal of Fe (Figures 4.8, 4.16 and 4.23) and Al (Figures 4.9, 4.16 and 4.24) which corresponded with the RTD associated with the first flush. As concentrations of cations (Na, K, Mg, Ca), specific conductance (including TDS and salinity) and solids (TSS and turbidity) were reduced, so were effluent concentrations of Fe and Al. The percent reduction of Fe (average 86.4%) and Al (average 90.2%) concentrations from the average effluent values measured during the first flush period ($\theta_{BGCR} \leq 1.59$) and the subsequent post first flush sampling event (fourth (week 5.2; average $\theta_{BGCR} = 3.24$) were similar to those of Na (average 88.9%) and K (average 83.9%).

The percent differences between the first flush and post first flush water chemistry concentrations/values were typically >80% (Table 4.15). They were also typically greater in drum-shaped BGCRs (P2>S4) and BGCRs containing the highest percentage of mussel shells in their substrate mixture (P1>P2; S2 and S3>S4). Theoretically, the pore-water volume within the substrate layer accounted for an average of 71.0% of the pore and surface water present in all components (surface water, post peel, substrate and bedding material) of P1 and P2 and 63.1% of S1-S4, which

computes to a difference of 7.9%. The majority of easily dissolvable and highly mobile constituents were likely affiliated with substrate material so there was a greater percent reduction of these in drum-shaped reactors compared with trapezoidal-shaped reactors.

The parameters that experienced average percent differences >80% consisted of monovalent cations (Na and K), biological parameters (BOD and faecal coliforms), DOC/TOC and most anions (TN, TKN and TP). Parameters where percent differences were <80% included divalent cations (Mg and Ca), specific conductance and parameters computed from conductivity (TDS and salinity), turbidity and TON. Generally, there was a greater percent reduction in the easily soluble species since the majority of these constituents became dissolved relatively instantaneously and were therefore easily flushed from the BGCRs. Sediment and solids were likely transported via advection as a result of interstitial pore-water velocities dislodging fine particles. Since specific conductance, TDS and salinity consist of ionic contributions from mono and divalent species, its percent reduction was less than that of Na and K but greater than Ca.

The primary source of Na was mussel shells, which contained concentrations nearly two orders of magnitude greater than that of limestone. Potassium was primarily derived from wood products (compost>post peel>bark). Much of the initial export of Ca was likely associated with its dissolution from fine sediment, and its associated high surface area, derived from mussel shells and limestone. The source of TSS and turbidity was likely compost and fine fragments from bark, mussel shells and limestone. The major sources of DOC/TOC were the more labile carbon fractions of residual meat on mussel shells and the wood products, especially the compost. The DOC/TOC concentrations showed a gradual decrease throughout this study, which was influenced by first flush and HRT. The majority of nitrogen (TN, TKN, TON) and microbes (BOD and faecal coliforms) were likely derived from residual labile organics attached to the mussel shells and the proteins within the shell matrices as evident by greater concentrations measured in effluent from BGCRs containing mussel shells (S2 and S4) compared with S1, which contained no mussel shells. The primary secondary source was labile organics associated with the compost. The lesser reduction of TON comparing first flush and post first flush data was attributed to the nitrogen present in the reduced state throughout. Although the final samples for nitrogen, phosphorous and BOD were collected during the sixth sampling event (week 9.4; θ_{BGCR}=6.14-7.13), these concentrations were likely still declining as the study progressed, potentially at a similar rate to DOC/TOC concentrations.

Based on the similarities of RTD of the first flush associated with this study and the Blumenstein (2008) study, the time frame before easily soluble and transported constituents will reach quasi-equilibrium concentrations and metal removal will reach steady removal efficiencies is achieved after approximately two to three pore-water volumes. The RTD of an inert sodium bromide tracer "instantaneously spiked" into BGCRs P2 and S4, which contained the same substrate mixtures but

different reactor shapes, will be investigated further in Chapter 6. This will provide an estimate of the number of pore-water volumes required to completely flush each BGCR.

4.4 Conclusions

Biogeochemical reactors offer a promising technology for treating AMD containing high concentrations of sulphate, Fe, Al and other trace metals. Mixtures of economically viable industrial waste products were successfully used as reactive substrates in these systems. Biogeochemical reactors using predominately mussel shells as an alkalinity generating source performed better than systems using limestone exclusively or a mixture of limestone and mussel shells. Possible contributing factors include grain size, shape, reactive surface area, unique mineralogy (aragonite and calcite) or mineralogical dynamics and consequent structural change when dissolved. Additionally, labile carbon attached to the mussel shells and nitrogen within the mussel shell matrix may potentially benefit the consortium of microorganisms which develop as systems reach stable treatment conditions (after five weeks in this study or about three pore-water volumes of AMD were fed into the reactors). Forestry waste products including *Pinus radiata* bark, post peel and composted wood provide sustainable short and long-term carbon sources for microorganisms. Nodulated stack dust dissolved too quickly resulting in caustic effluent and an initial export of extremely high concentrations of sulphur and K; therefore, its use in passive mine-water treatment is unfeasible.

Hydraulics influence BGCR performance. Cylindrical drum reactors (562 mm substrate depth) outperformed trapezoidal prism reactors (400 mm substrate depth) in terms of contaminant removal. System hydraulics and substrate depth were likely the prominent reasons; therefore, for field applications, maximizing BGCR substrate depth and minimizing surface area footprint should be considered to potentially reduce discrepancies between actual HRT and theoretical HRT.

Operation of BGCRs should be contingent on treatment goals (e.g. compliance targets and ecotoxicity criteria). From our results, the following design criteria are recommended for similar systems based on results of trapezoidal-shaped BGCRs incorporating 20 vol. % mussel shells as an alkalinity amendment: 1) 0.3 mol sulphate loading/m^3/day for sulphate removal (mean of 94.1% (87.6-98.0%)); 2) 0.4 mol metals/m^3/day for metal (mean of 99.0% (98.5-99.9%)) and partial sulphate removal (mean of 46.0% (39.6-57.8%)); and 3) 0.8 mol metals/m^3/day for metal (mean of 98.4% (98.2-98.6%) and minimal sulphate removal (mean of 16.6% (11.9-19.2%)). On an acidity areal loading basis, a design criterion of 65 g/m^2/day is recommended. Design HRTs would be 3.64 days based on the highest metal loading rates measured from the Manchester Seep and 5.00 days based on the highest metal loading rates measured from the Manchester Pond outflow (18 July 2006). Pilot-scale studies should be conducted to confirm that this treatment performance can be attained in a field application. There is potential to remove an average of 85.2 kg acidity (as $CaCO_3$), 14.4 kg Fe and 5.16 kg Al on a daily

basis from the Manchester Seep assuming 98% removal efficiency. This equates to 31.1 tonnes acidity (as $CaCO_3$), 5.26 tonnes Fe and 1.88 tonnes Al per annum.

It should be noted that an initial first flush of easily dissolvable and transported water chemistry parameters including Na, K, Ca, Mg, TN, TKN, TP, TSS, DOC/TOC, BOD and faecal coliforms will occur during the initial stages of system start up (approximately the first three pore-water volumes in this study for most parameters). Metal removal was not reliable and consistent until the first flush was completed. Reactor hydraulics, substrate chemistry and mine-water chemistry likely influence the duration of the "first flush."

While this study has demonstrated successful treatment of AMD with BGCRs at a mesocosm scale using waste products as the substrate media, there are further considerations required in up-scaling to operational-sized systems. Ideally, a BGCR would comprise part of an overall treatment train (discussed in Chapter 7) which would be preceded with a sedimentation pond to capture diffuse sediment inputs upstream. Further downstream, aerobic wetlands, rock filters or ponds should be incorporated to increase DO from BGCR effluent and reduce faecal coliforms, BOD, nitrogen and residual metal concentrations. Overall, water quality discharging from a passive treatment technology should aim to achieve compliance and not cause deleterious impacts to biodiversity and ecological health of the receiving water body.

Future research would help reveal numerous characteristics of BGCRs and their performance that were not evaluated as part of this study. More detailed analysis of organics (both in substrates and leached) would help to understand the differing performance of carbon sources. A better understanding of sulphur chemical transformations and a sulphur mass balance are needed to better understand the relationship between sulphate and metal removal. Additionally, a better understanding of the metal and sulphur precipitation processes within the substrate media would help elucidate the biogeochemical transformations that occur within the BGCRs and give a better understanding of system longevity. This study demonstrated that different alkalinity amendments influence treatment performance; therefore, it would be beneficial to conduct detailed acid dissolution tests to determine how dissolution kinetics can affect design and operation. Finally, a better understanding of BGCR hydraulics and their influence on treatment performance is needed.

5. Use of pH and Alkalinity as Surrogate Measurements for Assessing Iron and Aluminium Concentrations in Biogeochemical Reactor Effluent

5.1 Purpose and Scope

Passive treatment systems such as VFWs are typically utilised to treat AMD emanating from decommissioned or abandoned mine sites (Wildeman et al., 2006). Therefore, their application is often in remote locations that are not easily accessible for frequent inspection and monitoring. This Thesis chapter includes: 1) evaluation of the relationships of effluent pH and alkalinity with effluent Fe and Al concentrations from the mesocosm-scale BGCRs (previously discussed in Chapter 4); and 2) data analysis approaches (statistical, graphical best-fit modelling and contour plotting using kriging interpolation and two-component regression analysis) that best, and most pragmatically, exemplify these relationships. The primary objective of these analyses were to investigate the feasibility of using pH and alkalinity as surrogate indicators of effluent metal concentrations, therefore, reducing costs associated with sampling and analysis of metals. There is also potential to employ remote monitoring techniques to continuously monitor pH with offsite data acquisition capabilities as a potential cost-effective method to monitor BGCR performance.

5.2 Ecotoxicity and Compliance Targets

The primary purpose of remediating most (AMD) impacted streams in New Zealand is to re-establish biodiversity and ecological health to the receiving ecosystem, although recreation and aesthetics and use as a potential source for drinking or industrial use water also represent potential remediation goals (ANZECC, 2000). Ecotoxicity guidelines and/or compliance targets in discharges represent thresholds to achieve a healthy in-stream ecosystem. These vary amongst different ecosystems and aquatic species and should influence AMD (and wastewater) treatment and compliance targets.

In New Zealand, the ANZECC (2000) water quality guidelines present “trigger values” that represent concentrations of various contaminants that may be deleterious to the biota in receiving freshwater aquatic ecosystems. These were discussed in Section 2.3, and trigger values for metals found in Stockton Coal Mine AMD were presented in Table 2.3. ANZECC (2000) states that there are “insufficient data” to establish trigger values for Fe and Al (pH<6.5). Application of local biological effects ecotoxicological studies to establish site-specific thresholds are typically preferred and deemed more scientifically valid. Current community agreed discharge levels at the Stockton Coal Mine site is <1 mg/L Al and pH>4.0 99% of the time at the mine site boundary (at monitoring site NR at the confluence of the Mangatini Stream and Ngakawau River; Figure 2.1) based on localised ecotoxicological data such as that reported in Niyogi and Harding (2007), Harding (pers. comm., 2008) and O’Halloran et al. (2008).

A summary of Fe and Al concentrations and associated 'trigger' values, 'guidelines' or 'recommended' water quality criteria based on various ecotoxicological studies, regulatory documents and compliance targets are given in Table 5.1. These values do not necessarily indicate ecotoxicity in every ecosystem or consider synergistic toxicity effects from multiple metal species and acidity but are listed for comparative and discussion purposes only since they often represent default treatment targets. Additionally, the recommended effluent Fe concentration range (3-5 mg/L) from VFWs where stable treatment performance is maintained is presented. This also represents the concentration ranges where subsequent aerobic treatment could be employed to remove residual Fe (Gusek, 2002; Ziemkiewicz et al., 2003; Watzlaf, 2004; Skousen, 2006; Wildeman et al., 2006; Hedin, 2008a; 2008b; Gusek, 2009a; 2009b). If pH and alkalinities that consistently achieve Fe and Al concentrations below applicable values presented in Table 5.1 can be confirmed, then there is potential application of employing them as cost-effective surrogates.

Internationally applied ecotoxicity thresholds listed in Table 5.1 show Fe concentrations ranging from 0.300 mg/L (in the Canadian Water Quality Guidelines for the Protection of Aquatic Life (Canadian Council of Ministers of the Environment, 2007)) up to 3.0 mg/L (30 day average) and 6.0 mg/L (one day maximum) in the U.S. Coal Mining Discharge Effluent Limits Applicable to New Coal Mines Generating Acid or Ferruginous Mine Water (U.S. Code of Federal Regulations, 2008). U.S. EPA National Recommended Water Criteria (U.S. EPA, 2006) and UK Environmental Quality Standards for List 2 Dangerous Substances (UK Environmental Agency, 2008) list maximum Fe concentrations of 1.0 mg/L. The Canadian Water Quality Guidelines for the Protection of Aquatic Life (Canadian Council of Ministers of the Environment, 2007) was the only legislation stipulating an Al threshold for discharge to receiving water bodies containing a pH<6.5, which was 0.005 mg/L. This is below the 1 mg/L threshold (99% of the time) set at Stockton Coal Mine and the 1-2 mg/L threshold measured by Harding (pers. comm., 2008) on localised endemic macroinvertebrate species in New Zealand, which may be a function of site specific conditions and sensitivity of the receiving environment.

O'Halloran et al. (2008) reported results of 96-hour ecotoxicity tests of a New Zealand mayfly (*Deleatidium* spp.), a benthic macroinvertibrate, exposed to AMD. Results showed that species sourced from naturally acidic streams (pH≈5.7-6.5) were more tolerant to AMD and its associated low pH (3.5-4.0) than species sourced from neutral streams (pH≈7.0-7.4). Species sourced from naturally acidic streams showed no statistically significant mortality occurring at pH≥3.8 (2.29 mg/L Fe and 1.22 mg/L Al).

Table 5.1: Ecotoxicity data, compliance targets and water quality guideline values reported for Fe and Al for freshwater ecosystems. Concentrations represent the dissolved metal fraction (<0.45 μm diameter particle size) unless otherwise noted.

	Fe (mg/L)	Al (mg/L) pH>6.5	Al (mg/L) pH<6.5
Site Specific / Regional Ecotoxicity Studies			
Current Compliance at Confluence of the Mangatini and Ngakawau Rivers	n/d	n/d	1
Harding, pers. comm. (2008)	1-2	n/d	1-2
Recommended VFW Effluent Concentrations if Proceeded by Subsequent Aerobic Polishing Stage Assuming Final Discharge Goal is <1 mg/L Fe			
	3-5	NA	NA
ANZECC Trigger Values for Freshwater (ANZECC, 2000)			
99% Level of Protection	ID	0.027	ID
95% Level of Protection	ID	0.055	ID
90% Level of Protection	ID	0.080	ID
80% Level of Protection	ID	0.150	ID
U.S. Coal Mining Discharge Effluent Limits – Applicable to New Coal Mines Generating Acid or Ferruginous Mine Water (U.S. Code of Federal Regulations, 2008b)			
One Day Maximum	6.0 (T)	n/d	n/d
30 Day Average	3.0 (T)	n/d	n/d
U.S. EPA National Recommended Water Criteria (U.S. Environmental Protection Agency, 2006)			
CMC	n/d	0.750 (TR)	n/d
CCC	1.000	0.087 (TR)	n/d
NOAA Screening Quick Reference Table (Buchman, 2008)			
Acute (CMC)	n/d	0.750 (TR)	n/d
Chronic (CCC)	1.000	0.087 (TR)	n/d
Canadian Water Quality Guidelines for the Protection of Aquatic Life (Canadian Council of Ministers of the Environment, 2007)			
	0.300	0.100	0.005
Environmental Quality Standards for List 2 Dangerous Substances (UK Environmental Agency, 2008)			
	1.000	n/d	n/d

n/d, not defined; NA, non-applicable; ID, insufficient data; AS, acid soluble; TR, total recoverable; T, total; CMC, criteria maximum concentration (highest level of one hour average exposure not to be exceeded more than once every three years); CCC, criteria continuous concentration (highest level of four day average exposure not to be exceeded more than once every three years)

Neculita et al. (2007) reported an update of mining legislation in the U.S.A. and Canada with respect to mine water discharges. Canadian metal mines that discharge >50 m^3/day of flow are required to abide by regulated prescribed limits on discharge of deleterious substances, verify effluent is not acutely lethal to rainbow trout or *Daphnia magna* and conduct a series of four freshwater sub-lethal

tests two to four times per year to determine the potential of effluent to affect fish, invertebrates, algae and plants (Environment Canada, 2002). In U.S. legislation, all industrial point-source discharges are required to be registered and operate under a "National Pollutant Discharge and Eliminations System (NPDES)" permit as authorised by the Clean Water Act of 1977 (U.S. Code of Federal Regulations, 2008a). Furthermore, the U.S. Environmental Protection Agency (EPA) (2002) established whole effluent toxicity (WET) tests as a means of standardising acute (24 hour) and short-term chronic (96 hours) toxicity to freshwater, marine and estuarine organisms. There are no standardised ecotoxicological or water quality guidelines uniformly applied throughout the European Union; however, initiatives such as the Environmental Regulation of Mine Waters in the European Union (ERMITE) and various legislation imposed by the European Commission have been implemented to reduce environmental impacts from the resource extraction industries in Europe (ERMITE Consortium, 2004). Key European legislation includes: 1) Directive 2000/60/EC (establishing a framework for community action in the field of water policy), for protecting water resources pertaining to both quality and quantity for safe public use (European Commission, 2000); and 2) Directive 2006/21/EC (the management of waste from the extractive industries), which requires all resource extraction industries to operate under a permit that prevents or minimizes impacts to the environment (European Commission, 2006). In New Zealand, mining companies are required to minimise deleterious impacts to the environment and abide by resource consent conditions stipulated by local regional and district councils based on public consultation and interpretation of the Resource Management Act (Ministry for the Environment, 1991). Regional plans set minimum standards for the discharge of pollutants to water. Consent conditions are often imposed to avoid and mitigate adverse environmental effects including discharge conditions, monitoring requirements and rehabilitation works.

5.3 Materials and Methods

Experimental materials and methods applicable to the mesocosm-scale treatability tests were discussed in detail in Section 4.1. Results presented in this chapter focus primarily on those from BGCRs incorporating mussel shells or a mixture of limestone and mussel shells (P1, P2, S2, S3 and S4) as substrate alkalinity amendments. These reactors were considered most feasible for metal removal and acidity neutralisation (as discussed in Sections 4.3.1 and 4.3.3) and represent a range of treatment performance that could be expected if the systems were scaled up to pilot or full-scale systems. P3 contained NSD, which dissolved too quickly resulting in caustic effluent (pH>9.23), whereas, S1 contained only limestone (and no mussel shells) as an alkalinity amendment, so treatment performance was much less effective compared with the other BGCRs. For these reasons, P3 and S1 were excluded from data analysis regarding the use of pH and alkalinity as surrogate parameters for estimating effluent Fe and Al concentrations; however, their results are presented in the initial data figures for comparative purposes.

5.3.1 Data Analysis

A primary objective was to ascertain a relationship of BGCR effluent pH and alkalinity data with effluent Fe and Al concentrations. Because of differences in reactor characteristics (drum-shaped versus trapezoidal-prism shaped) including size, shape, substrate depth and hydraulics, which subsequently influenced treatment performance (Chapter 4), data from each reactor type were analysed separately.

Data during the first flush, the first four sampling events (samples collected between weeks 1.1-5.2), were not included in this analysis since the BGCRs were still stabilising which affected pH, alkalinity generation and Fe and Al removal. Data analyses were conducted for scenarios including the middle three (weeks 7.1-11.3) and final four (weeks 12.4-16.7) sampling events separately. A summary of operational parameters during the data analyses scenarios is presented as Table 5.2. Metal loading rates were at or below the design threshold for complete metal and partial sulphate removal (0.4 mol metals/m^3/day) during the middle three sampling events (Scenarios 1 and 2). Metal loading rates exceeded this during the final four sampling events (Scenarios 3 and 4) when good metal removal and minimal sulphate removal was achieved (excluding the final sampling event when metal overloading occurred).

Table 5.2: Characteristics and operational parameters associated with the data scenarios evaluated in this study. The first four sampling events (weeks 1.1-5.2) were excluded from analysis in all scenarios due to the influence of the first flush. The middle three sampling events represent samples collected from weeks 7.1-11.3, and the final four sampling events represent samples collected from weeks 12.4-16.7.

Scenario	BGCRs	Sampling Events	Sulphate Loading (mol/m^3/day)	Metal Loading (mol/m^3/day)	Metal Loading (g/m^3/day)	Acidity Loading (g as $CaCO_3$/m^2/day)
1	P1 and P2	Middle 3	0.513-0.910	0.254-0.410	9.53-16.1	25.6-44.2
2	S2, S3 and S4	Middle 3	0.589-0.941	0.292-0.425	11.0-16.7	23.9-34.4
3	P1 and P2	Final 4	0.454-2.50	0.210-1.25	8.21-50.6	25.0-156
4	S2, S3 and S4	Final 4	0.435-2.88	0.210-1.44	7.86-58.3	18.0-135

Effluent Fe and Al concentrations were initially plotted versus pH and alkalinity separately so that the relationships could be observed. The negative log of Fe and Al molar concentrations were also plotted versus pH to determine if this established a better relationship since pH is a logarithmic function. Linear best-fit modelling was also considered; however, since the data spread was such that a linear or curved line could not fit the data, it was not deemed effective. Analysis of Variance (ANOVA) statistics were also applied but the results were not a useful predictive tool for using pH and/or alkalinity as surrogate parameters. The ANOVA statistics indicated that there is a consistent relationship of decreasing Fe and Al effluent concentrations with increasing pH and alkalinity but did not give a clear indication of how well best-fit modelling could be used as a predictive tool.

Two-component regression analysis was then performed using both pH and alkalinity as predictor variables for estimating Fe and Al effluent concentrations. This showed better relationships than using pH or alkalinity as a sole predictor variable. The best relationships were typically achieved when applying the negative log of the molar concentrations, although there were exceptions. The relationships considering negative log molar concentrations with pH and log alkalinity were also considered, although these results were less comparable with exception of predicting Fe concentrations for the middle three sampling events considering the trapezoidal-shaped BGCRs (average absolute percent difference of 27.8% versus 33.3%). The best relationships for each scenario will be presented and discussed in Section 5.4.3.

Three-dimensional concentration contour plots were developed using Sigma Plot® 10 software (Systat Software, Inc., 2006), which show Fe and Al concentration contours at various pH and alkalinity values. Contours were generated from predicted values computed from the two-component regression analysis and by non-linear kriging interpolation of empirical data.

5.4 Results

5.4.1 pH and Alkalinity

Biogeochemical reactors were successful at neutralising AMD resulting in an increase in effluent alkalinity and pH. A time-series representation of influent and effluent pH and alkalinity are presented in Figure 5.1 (for all BGCRs). Systems were stabilising during the first three to five weeks of operation (first three to four sampling events) due to the effects of the first flush. Effluent pH (Figure 5.1b) remained fairly stable (pH 6.54-6.89) by the fourth sampling event (week five), which was a significant increase from influent AMD feed pH of 2.45-2.73 (Figure 5.1b); however, the lingering effects of the first flush during the fourth (week 5.2) sampling event was evident with alkalinities ranging from 538 to 753 mg/L (Figure 5.1d) as $CaCO_3$ and slightly less effective treatment performance compared with subsequent sampling events (Section 4.2). Treatment efficiency of the BGCRs became compromised once the systems were overloaded during the final sampling period at the highest metal and acidity loading rates tested (1.23-1.44 mol/m^3 substrate/day; 49.6-58.3 g/m^3 substrate/day; 128-156 g as $CaCO_3$/m^2/day). Effluent pH (Figure 5.1b) declined to between 6.24 and 6.58 and alkalinities (5.1d) reached their lowest values (5.15-141 mg/L as $CaCO_3$ for trapezoidal-shaped BGCRs and 195-312 mg/L as $CaCO_3$ for drum-shaped BGCRs).

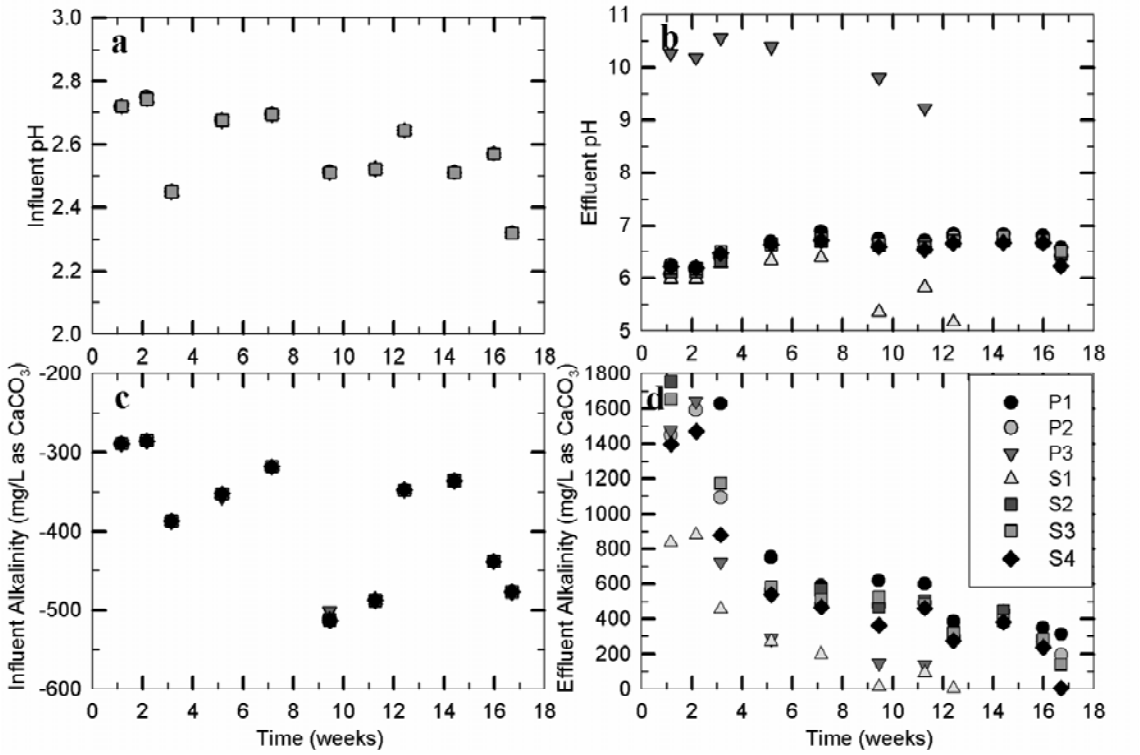

Figure 5.1. Influent (AMD) and effluent pH and alkalinity from BGCR mesocosm-scale treatability tests. First-flush conditions were prevalent during the first four sampling periods (up to week 5.2) resulting in depressed pH values and elevated alkalinities.

There was a distinct difference in alkalinity when comparing data from the middle three (weeks 7.12-11.3) and final four (weeks 12.4-16.7) sampling events as shown in Figure 5.2 considering only BGCRs containing mussel shells (or a mixture with limestone). Greater bicarbonate generation occurred during the middle three sampling events from sulphate reduction compared with the final four sampling events. Assuming all sulphate was removed by the bacterial sulphate reduction mechanism associated with organic decomposition (Equation 1.11), which would generate one mole of bicarbonate alkalinity for every mole of organic carbon decomposed, sulphate reduction contributed to an average of 39.6% (range of 30.7-52.0%) of alkalinity during the middle three sampling events and 11.9% (range of -2.01-20.7%) during the final four sampling events for the drum-shaped reactors and 40.2% (range of 31.9-46.4%) during the middle three sampling events and 14.1% (range of 4.21-20.8%) for the final four sampling events for the trapezoidal-shaped BGCRs. Data points from the final four sampling events are shaded in Figure 5.2, whereas those from the middle three sampling events are not. The correlation coefficient (R^2) was 0.402 for the middle three sampling events and 0.776 for the final four sampling events, although analysis from the final four sampling events was heavily biased by the isolated data point containing the lowest pH and alkalinity. The differences between influent and effluent pH and alkalinity are shown in Figure E.1 in Appendix E, which demonstrate the general trend of greater alkalinity change with greater pH change. Influent pH and

alkalinity varied amongst batches (as can be seen in Figure 5.2) so changes in alkalinity and/or pH did not necessarily give a good indication of effluent Fe or Al concentrations.

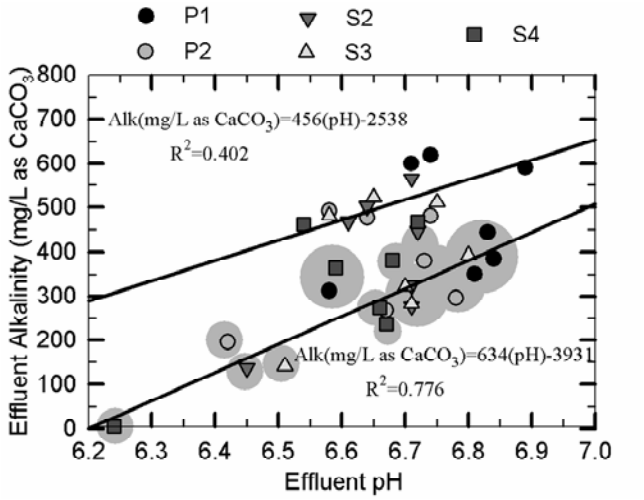

Figure 5.2. Comparison of effluent pH versus alkalinity from BGCRs containing mussel shells (P1, S2 and S3) or a mixture of mussel shells and limestone (P2 and S4). Results from the first four sampling events (up to week 5.2) were excluded since the BGCRs were operating under first-flush conditions. The data highlighted grey represents the final four sampling events. The non-highlighted cells represent the middle four sampling events. Data used for establishing best-fit lines were separated from the middle three and final four sampling events.

The effluent pH and alkalinities of BGCRs containing mussel shells (or a mixture with limestone) are compared with the theoretical HRT in BGCRs in Figures 5.3 and 5.4, respectively. Results from the first four sampling events were excluded. Effluent pH and alkalinity showed a positive trend with HRT though this is masked to an extent by the variation of influent water chemistry between test conditions. Nonetheless, the pH values were relatively stable at HRT≥3.31 days. Alkalinities were more variable at HRT≥7.03 days and otherwise showed a steady decline as HRT decreased. The influent and effluent RTDs within the BGCRs versus pH and alkalinity are shown in Figures 5.5 and 5.6, respectively, which demonstrate the effects of the first flush on these parameters and their decline with time as influent loading rates increased.

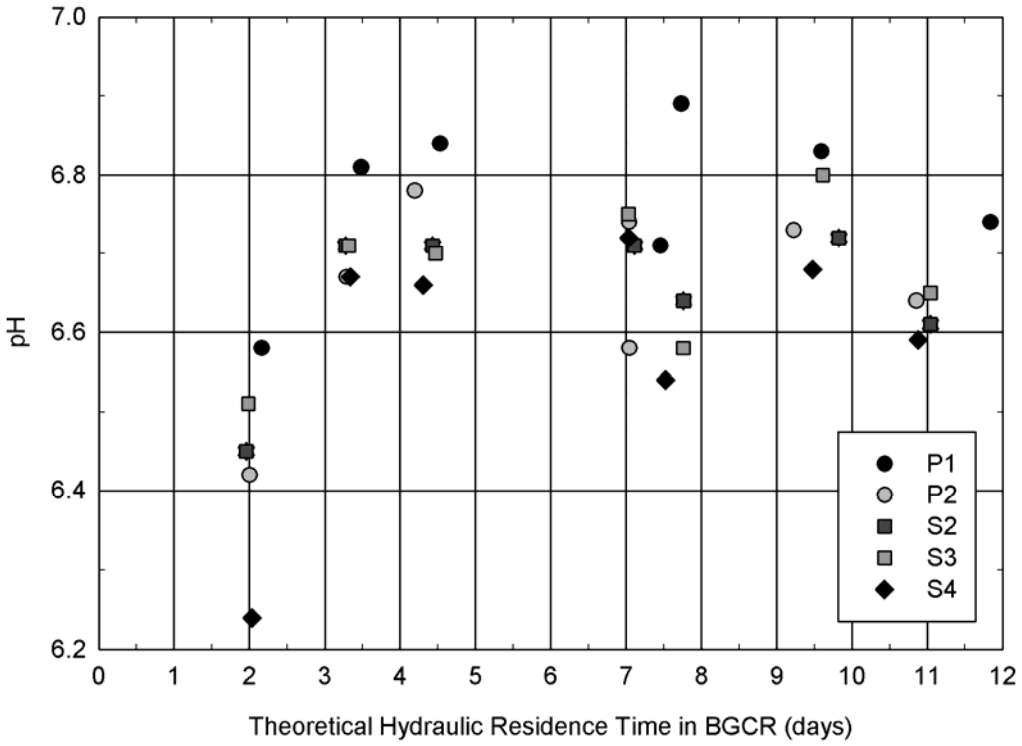

Figure 5.3. Theoretical HRT in BGCRs versus effluent pH for BGCRs containing mussel shells (or a mixture with limestone). Results from the first four sampling events are excluded.

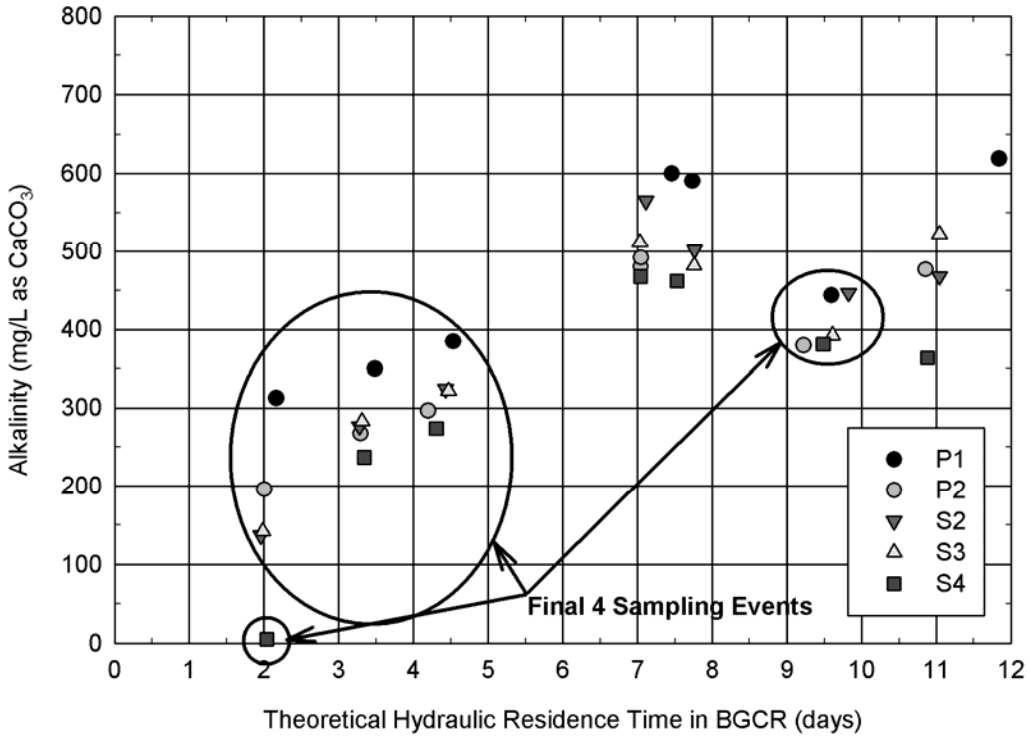

Figure 5.4. Theoretical HRT in BGCRs versus effluent alkalinity for BGCRs containing mussel shells (or a mixture with limestone). Results from the first four sampling events are excluded.

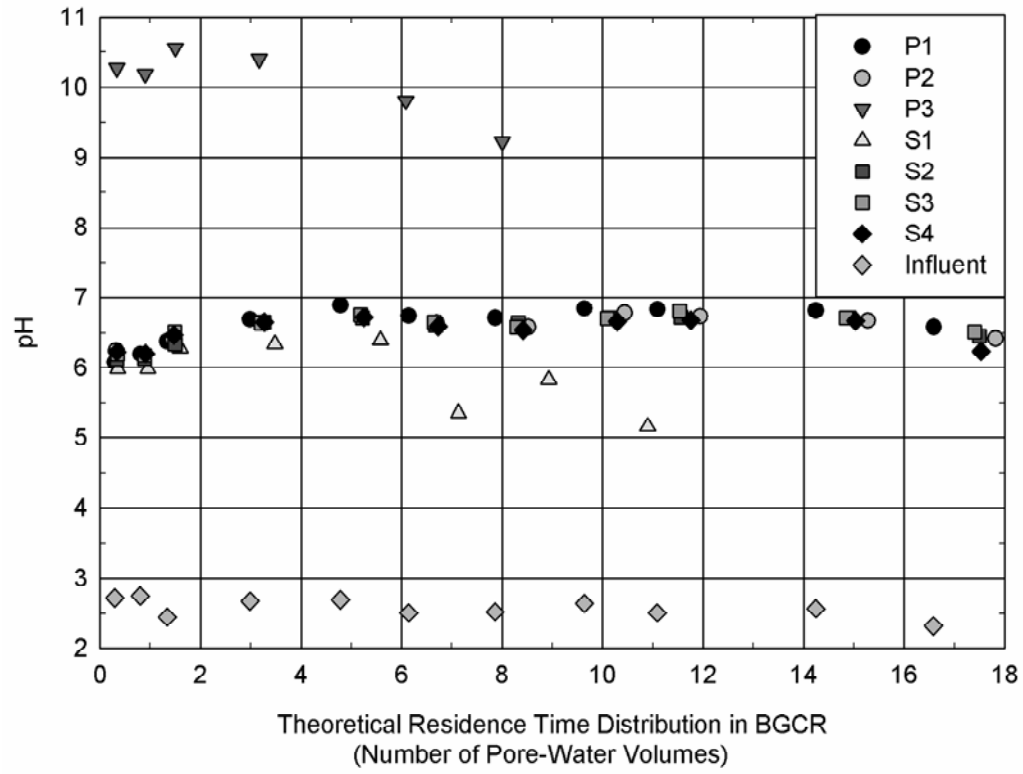

Figure 5.5. Influent and effluent RTDs within the BGCRs containing mussel shells (or a mixture with limestone) versus pH. The first three RTDs demonstrated first flush conditions.

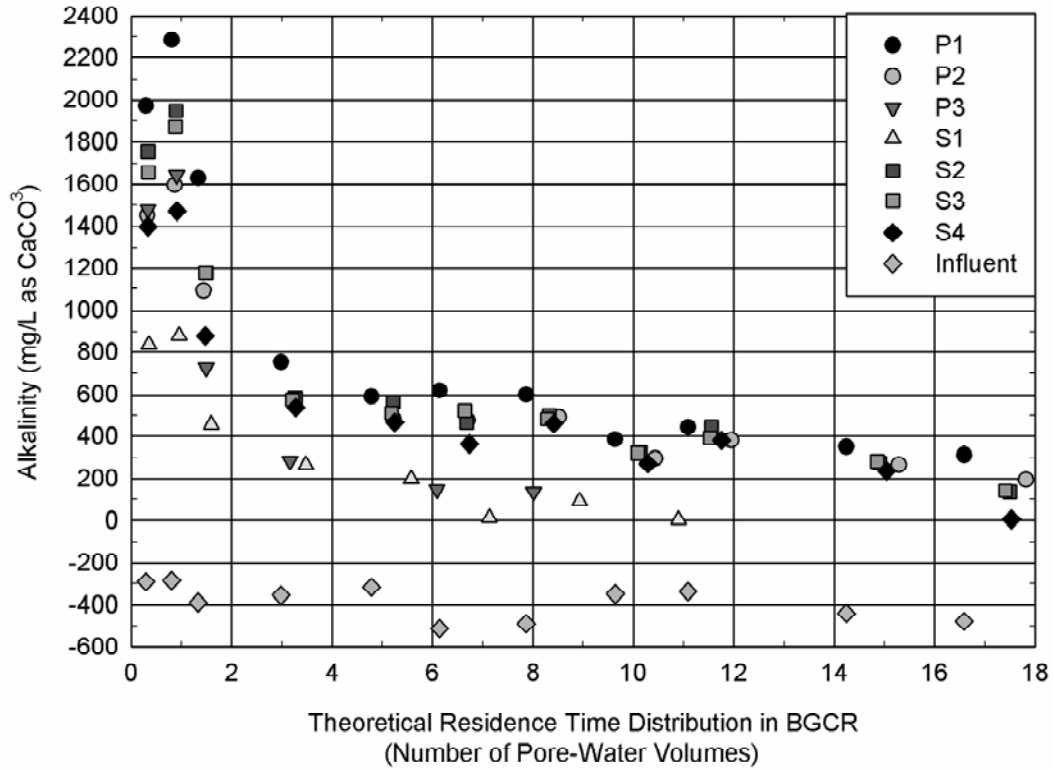

Figure 5.6. Influent and effluent RTDs within the BGCRs containing mussel shells (or a mixture with limestone) versus alkalinity. The first three RTDs demonstrated first flush conditions.

5.4.2 Effluent Fe and Al Concentrations versus pH and Alkalinity

Uni-dimensional comparisons of effluent Fe and Al concentrations with effluent pH and alkalinity were conducted to determine the effectiveness of pH and alkalinity to predict effluent Fe and Al concentrations. These comparisons were made separately for drum and trapezoidal-shaped BGCRs and also for the middle three and final four sampling events (Scenarios 1-4 in Table 5.2). The relationships of pH with Fe and Al concentrations are shown in Figures 5.7-5.10, whereas the relationships of alkalinity with Fe and Al concentrations are shown in Figures 5.11-5.14. The most appropriate water quality guidelines were also integrated into the analyses including the 1 mg/L Al compliance target (99% of the time) for Stockton Coal Mine. Additionally, the recommended effluent Fe concentration range (3-5 mg/L) from VFWs where stable treatment performance is maintained, which also represents concentrations where subsequent aerobic treatment could be employed to remove residual Fe, is presented. Key relationships observed between pH and effluent Fe and Al concentrations in Figures 5.7-5.14 are summarised in Tables E.1 (Fe) and E.2 (Al), and those observed between alkalinity and Fe and Al concentrations are summarised in Tables E.3 (Fe) and E.4 (Al).

The negative log of Fe and Al molar concentrations were also compared with pH to determine if this established a better relationship for each scenario since pH represents a molar logarithmic function (Figures E.2-E.5). Generally, the relationships were only slightly better than considering mass Fe and Al concentrations and only for half of the scenarios (based on R^2 values).

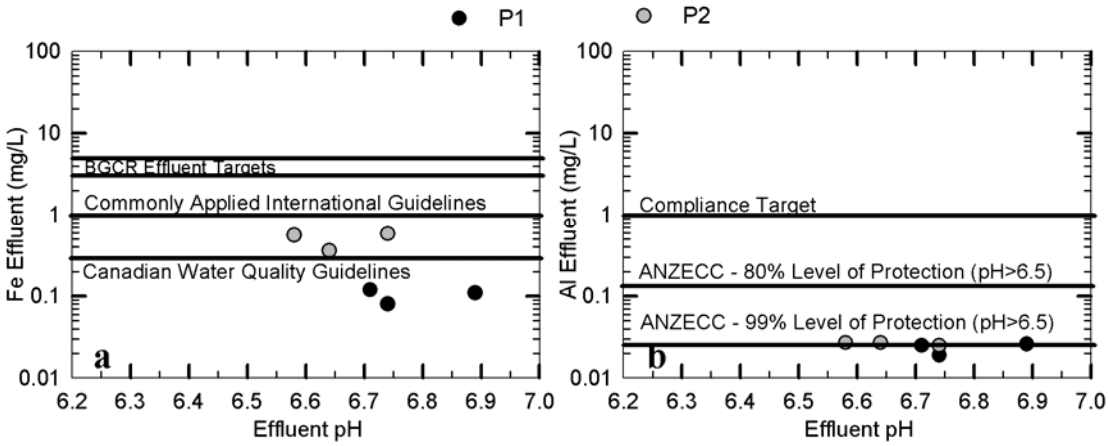

Figure 5.7. Effluent a) Fe and b) Al concentrations versus pH for drum-shaped BGCRs containing mussel shells (P1) or a mixture of mussel shells and limestone (P2) during the middle three sampling events (Scenario 1).

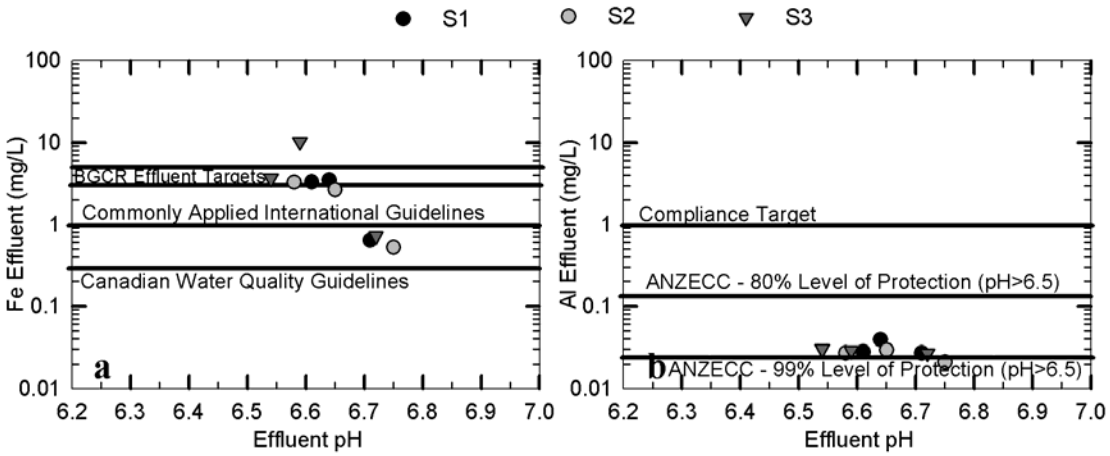

Figure 5.8. Effluent a) Fe and b) Al concentrations versus pH for trapezoidal-shaped BGCRs containing mussel shells (S2 and S3) or a mixture of mussel shells and limestone (S4) during the middle three sampling events (Scenario 2).

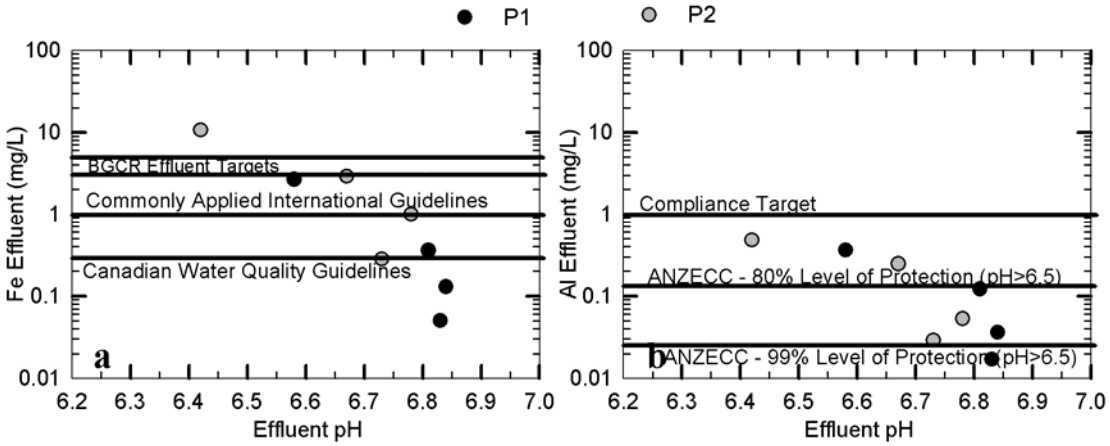

Figure 5.9. Effluent a) Fe and b) Al concentrations versus pH for drum-shaped BGCRs containing mussel shells (P1) or a mixture of mussel shells and limestone (P2) during the final four sampling events (Scenario 3).

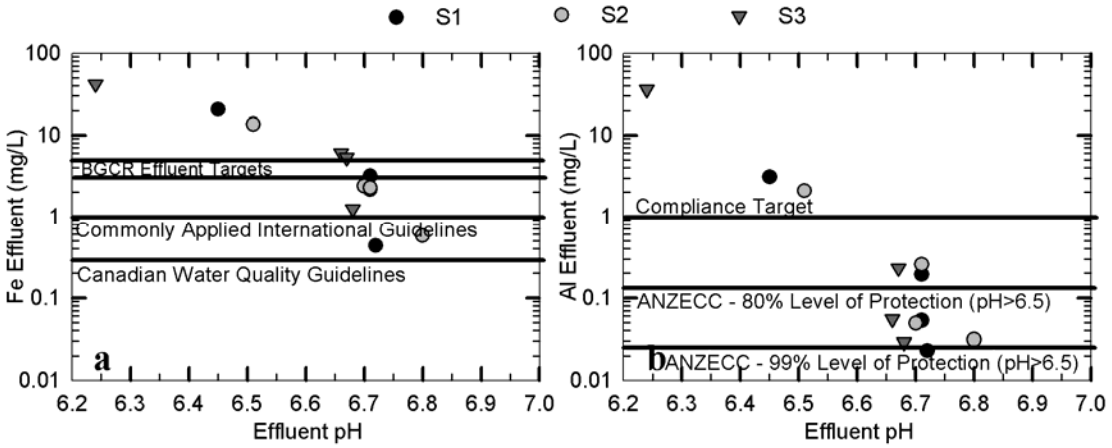

Figure 5.10. Effluent a) Fe and b) Al concentrations versus pH for trapezoidal-shaped BGCRs containing mussel shells (S2 and S3) or a mixture of mussel shells and limestone (S4) during the final four sampling events (Scenario 4).

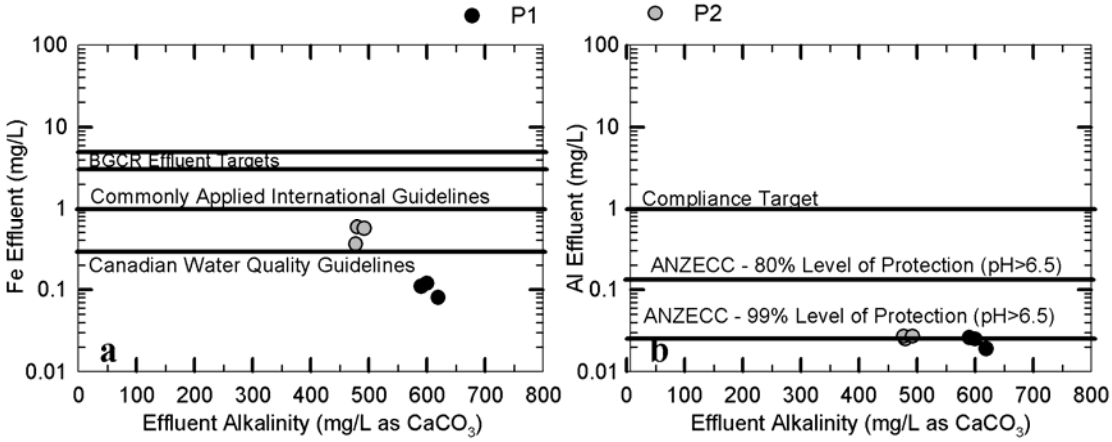

Figure 5.11. Effluent a) Fe and b) Al concentrations versus alkalinity for drum-shaped BGCRs containing mussel shells (P1) or a mixture of mussel shells and limestone (P2) during the middle three sampling events (Scenario 1).

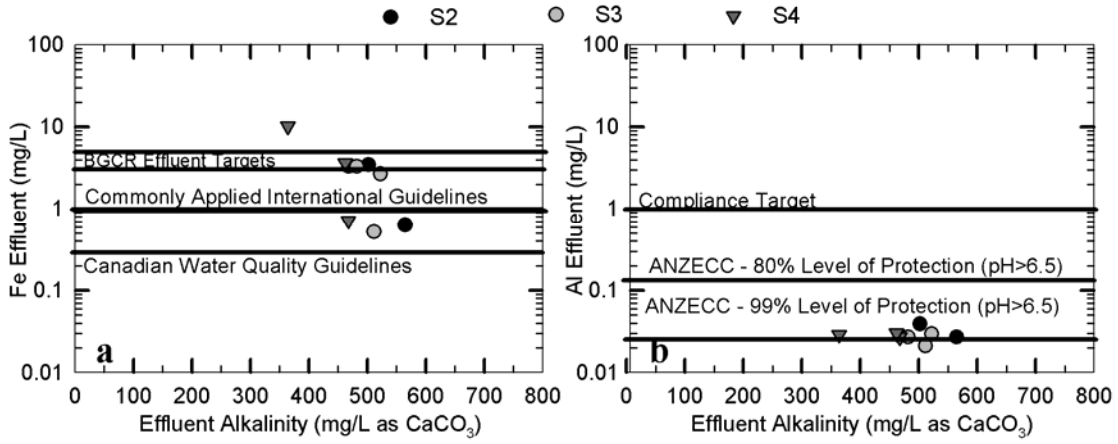

Figure 5.12. Effluent a) Fe and b) Al concentrations versus alkalinity for trapezoidal-shaped BGCRs containing mussel shells (S2 and S3) or a mixture of mussel shells and limestone (S4) during the middle three sampling events (Scenario 2).

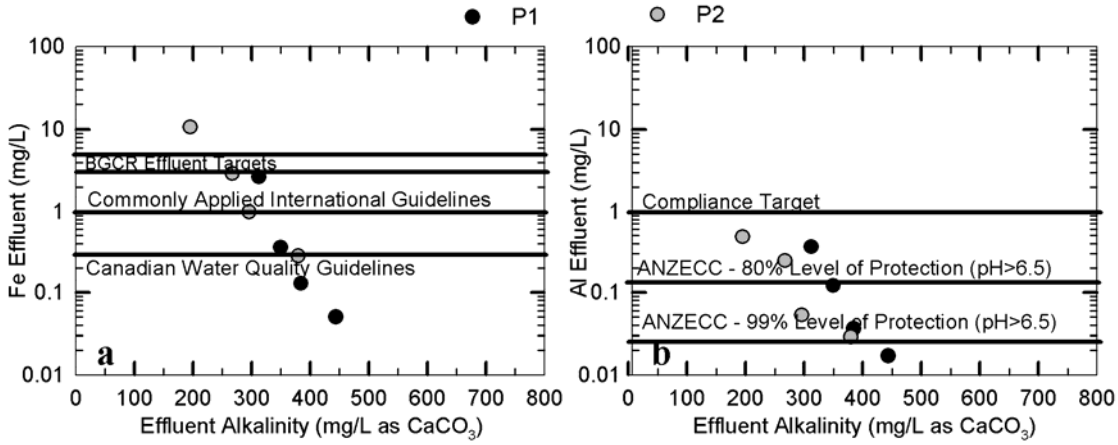

Figure 5.13. Effluent a) Fe and b) Al concentrations versus alkalinity for drum-shaped BGCRs containing mussel shells (P1) or a mixture of mussel shells and limestone (P2) during the final four sampling events (Scenario 3).

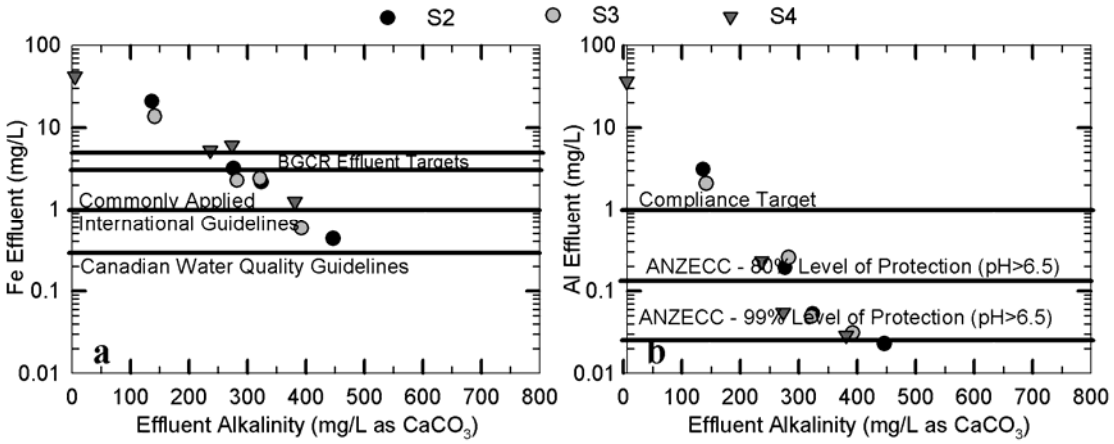

Figure 5.14. Effluent a) Fe and b) Al concentrations versus alkalinity for trapezoidal-shaped BGCRs containing mussel shells (S2 and S3) or a mixture of mussel shells and limestone (S4) during the final four sampling events (Scenario 4).

5.4.3 Kriging Interpolation and Two-Component Regression Analysis of Effluent Fe and Al Concentrations with pH and Alkalinity

Contour plots were developed to determine if multiple (two-component) linear regression analysis was adequate for predicting effluent Fe and Al concentrations from effluent pH and alkalinity or if the curvature associated with non-linear regression, such as kriging interpolation used in this analysis, was required. The slopes of contour lines are dependent on the influence of pH (x-axis) and alkalinity (y-axis). Although Fe and Al concentration contours were generally developed to encompass the complete range of pH and alkalinity values measured, caution should be taken when interpreting them since contours were sometimes generated in regions where no empirical data exists. Comparisons were also made between the actual Fe and Al concentrations measured in effluent with those predicted using two-component interpolation as shown in to validate model predictions.

5.4.3.1 Drum-Shaped BGCRs (P1-P2) during the Middle Three Sampling Events

Contour plots comparing effluent Fe and Al concentrations predicted using kriging interpolation and two-component regression analysis from the drum-shaped BGCRs (P1 and P2) during the middle three sampling events (Scenario 1; Table 5.2) are shown in Figure 5.15. Iron concentration contours were similar for both methods and were influenced almost exclusively by alkalinity as demonstrated by the horizontal contours. All Fe concentrations predicted were less than the commonly applied international guideline of 1.0 mg/L. Kriging interpolation predicted that effluent Fe concentrations should be less than the stringent Canadian water quality guideline value of 0.300 mg/L when alkalinities are greater than approximately 550 mg/L as $CaCO_3$ (Figure 5.15a). Results from the two-component regression analysis (Figure 5.15b) showed the 0.3 mg/L contour at a less conservative alkalinity of 530 mg/L as $CaCO_3$, which was comparable to the 0.5 mg/L Fe contour generated by the kriging method from pH≥6.8. Both statistical methods gave a false indication that one data point exceeded the ANZECC Al guideline value of 0.027 mg/L for 99% level of protection (pH>6.5).

Kriging interpolation also showed that Al concentrations from P1 were close to 0.027 mg/L (Figure 5.15c), whereas results from two-component regression analysis (Figure 5.15d) showed Al concentrations from P1 at approximately 0.023 mg/L. A comparison of the actual measured Fe and Al concentrations with the predicted concentrations using two-component regression analysis are shown in Figure 5.16, which shows that the predicted data was similar to measured data.

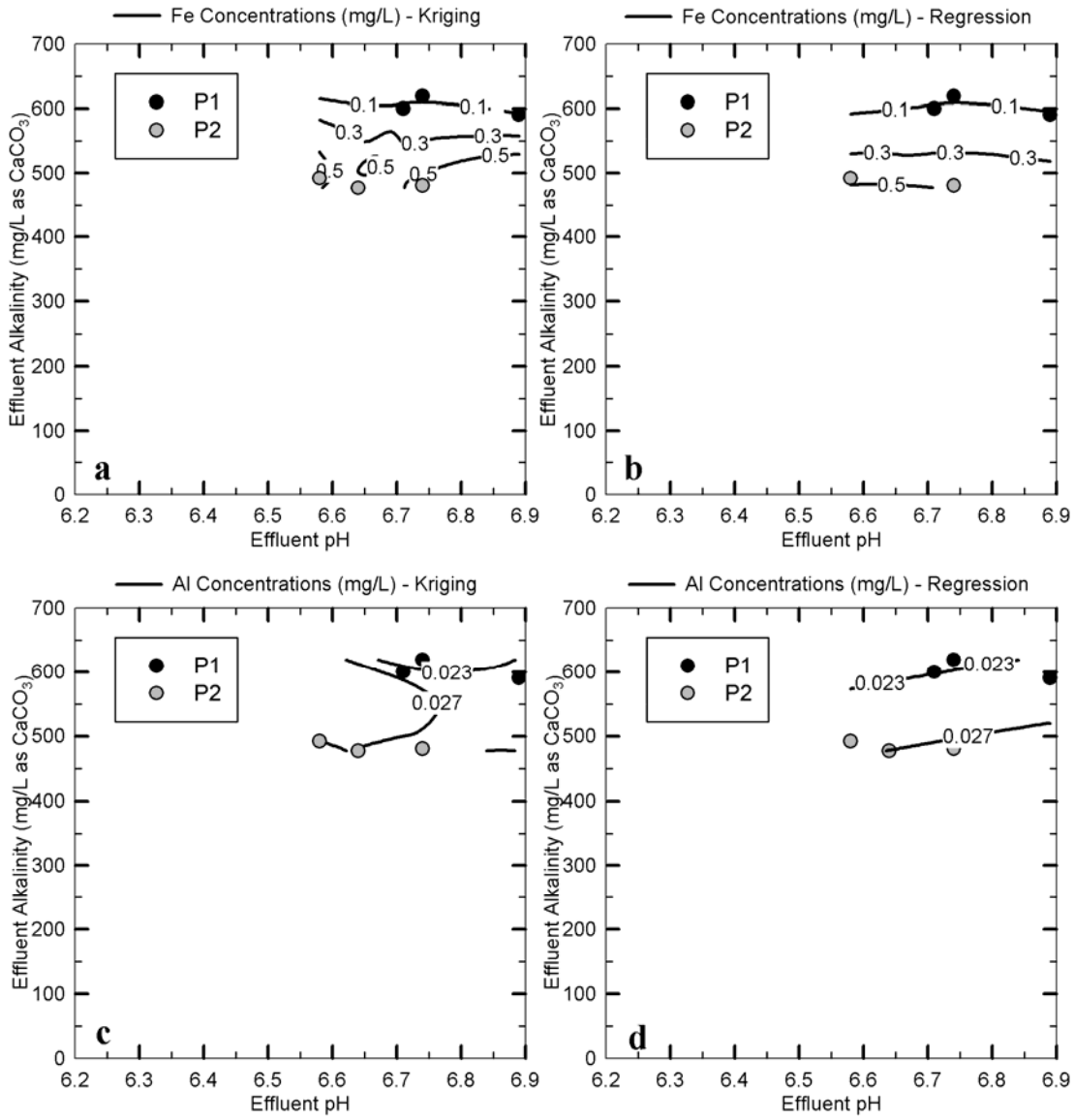

Figure 5.15. Effluent Fe and Al concentration predictions based on pH and alkalinity using kriging interpolation (a and c) and two-component regression analysis (b and d). The concentrations were predicted using the two-component regression analyses of the negative log molar concentrations. Data is representative of the middle three sampling events for drum-shaped BGCRs (Scenario 1) containing mussel shells (P1) or a mixture of mussel shells and limestone (P2). Data points shown represent effluent pH and alkalinities measured from BGCR effluent. The concentration contour of 0.3 mg/L Fe represents the stringent Canadian water quality guideline value. The 0.027 mg/L Al concentration contour represents the most stringent ANZECC guideline value (99% level of protection for pH>6.5).

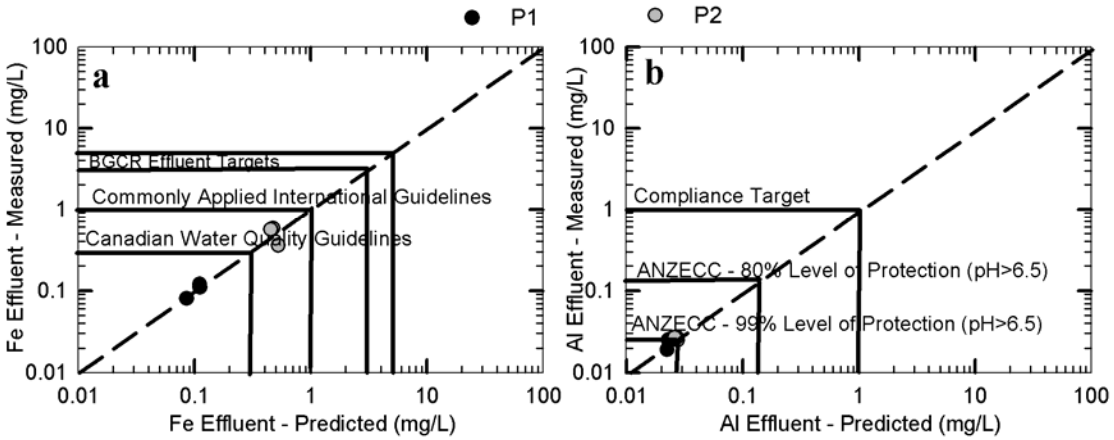

Figure 5.16. A comparison of measured a) Fe and b) Al effluent concentrations and those predicted using two-component regression analysis from effluent pH and alkalinity for drum-shaped BGCRs containing mussel shells (P1) or a mixture of mussel shells and limestone (P2) during the middle three sampling events (Scenario 1). The two-component regression analysis was conducted using the negative log Fe and Al molar concentrations and converted to mass concentrations.

5.4.3.2 Trapezoidal-Shaped BGCRs (S2-S4) during the Middle Three Sampling Events

Results of kriging interpolation and two-component regression analysis of Fe and Al concentrations from the trapezoidal-shaped BGCRs (S2-S4) during the middle three sampling events (Scenario 2; Table 5.2) are presented in Figure 5.17. Kriging interpolation predicted Fe concentrations <1 mg/L when pH≥6.71 regardless of the alkalinity range (468-565 mg/L as $CaCO_3$). All concentrations that exceeded 3 mg/L Fe were accurately predicted by the kriging contour (Figure 5.17a), whereas two-component regression (Figure 5.17b) falsely predicted two of these samples at concentrations <3 mg/L Fe. Two-component regression analysis showed an Fe concentration of approximately 7 mg/L when the data result was 10.2 mg/L (Figure 5.17a).

Kriging interpolation contours were convoluted for predicted effluent Al concentrations due to the presence of a narrow concentration range (0.021-0.039 mg/L). The maximum Al effluent concentration of 0.039 mg/L contained a similar pH and alkalinity as an Al concentration measured as low as 0.028 mg/L (Figure 5.17c). Therefore it was not a useful predictive tool. There were four samples that contained ≤0.027 mg/L Al, the most stringent ANZECC guideline value (ANZECC 99% level of protection guideline value for pH>6.5). Results from the two-component regression analysis (Figure 5.17d) only predicted two samples ≤0.027 mg/L Al and was, therefore, a conservative predictive tool. The Al concentration contours presented in Figure 5.17d contained positive slopes, which literally interpreted indicates that Al concentrations increase with increasing alkalinity. This is counterintuitive to the expected trend, and that observed from two-component regression analysis for all other scenarios. A comparison of the measured Fe and Al concentrations with those predicted using two-component regression analysis are shown in Figure 5.18, which shows that six of nine data

points contained measured Fe concentrations that were greater than those predicted and five of eight for Al indicating and overall trend in under estimating concentrations for most samples.

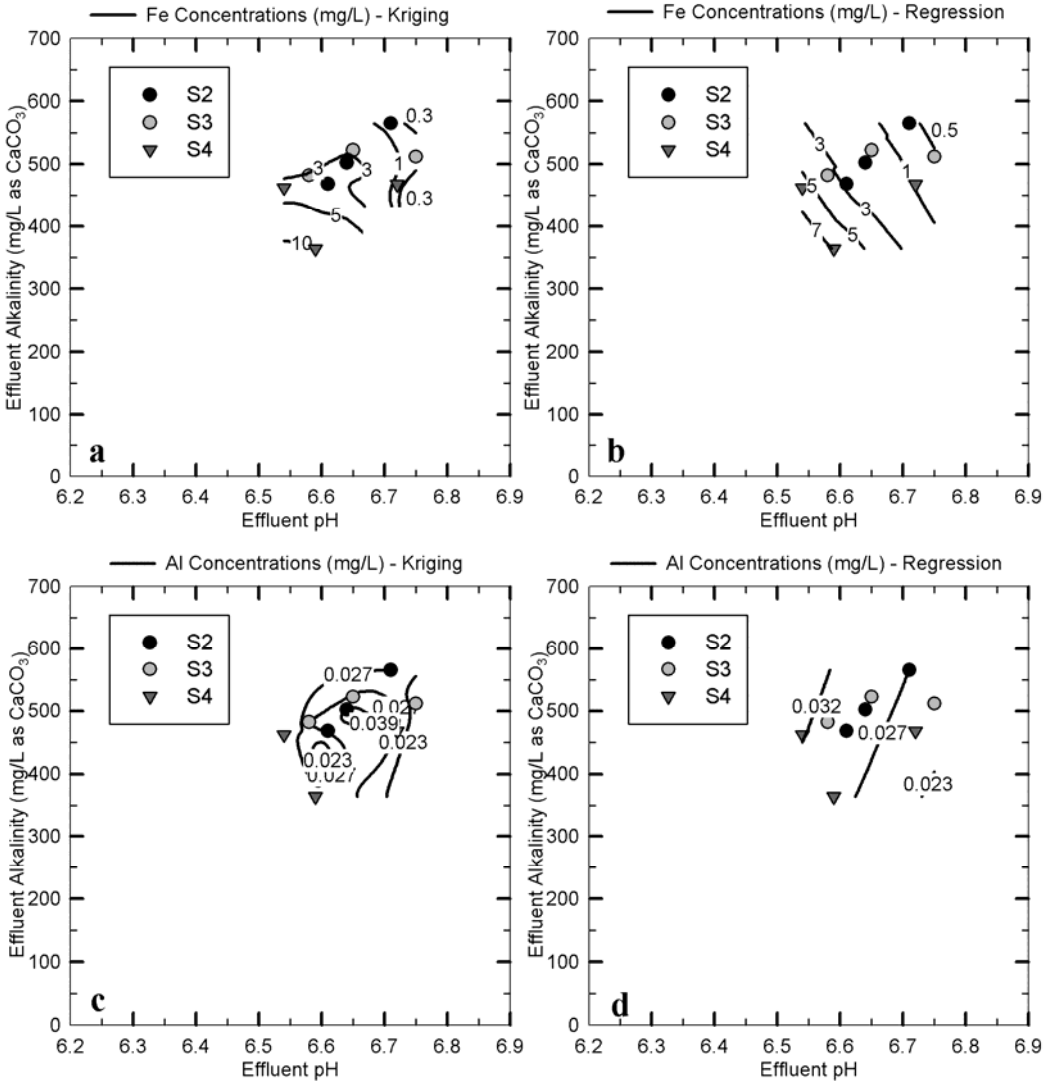

Figure 5.17. Effluent Fe and Al concentration predictions based on pH and alkalinity using kriging interpolation (a and c) and two-component regression analysis (b and d). Aluminium concentrations were predicted using the two-component regression analyses of the negative log molar concentrations with pH and alkalinity, whereas Fe concentrations were predicted using the two-component regression analyses of the negative log molar concentrations with pH and log alkalinity. Data is representative of the middle three sampling events for trapezoidal-shaped BGCRs (Scenario 2) containing mussel shells (S2 and S3) or a mixture of mussel shells and limestone (S4). Data points shown represent effluent pH and alkalinities measured from BGCR effluent. The concentration contour of 0.3 mg/L Fe represents the stringent Canadian water quality guideline value, the 1 mg/L Fe contour represents commonly applied international guideline values and the 3 mg/L Fe contour represents the lower BGCR effluent target (e.g. BGCR operation is still stable yet concentrations can be further reduced via a subsequent aerobic treatment stage). The 0.027 mg/L Al concentration contour represents the most stringent ANZECC guideline value (99% level of protection for pH>6.5).

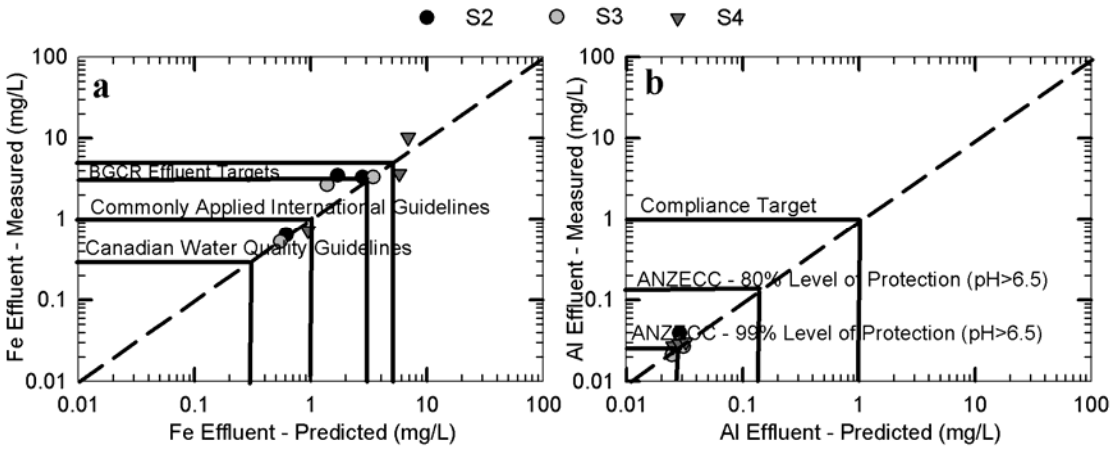

Figure 5.18. A comparison of measured a) Fe and b) Al effluent concentrations and those predicted using two-component regression analysis from effluent pH and alkalinity for trapezoidal-shaped BGCRs containing mussel shells (S2-S3) or a mixture of mussel shells and limestone (S4) during the middle three sampling events (Scenario 2). Aluminium concentrations were predicted using the two-component regression analyses of the negative log molar concentrations with pH and alkalinity, whereas Fe concentrations were predicted using the two-component regression analyses of the negative log molar concentrations with pH and log alkalinity.

5.4.3.3 Drum-Shaped BGCRs (P1-P2) during the Final Four Sampling Events

Results of kriging interpolation and two-component regression analysis of Fe and Al concentrations from the drum-shaped BGCRs (P1-P2) during the final four sampling events (Scenario 3; Table 5.2) are presented in Figure 5.19. Iron concentration contours generated using both kriging interpolation (Figure 5.19a) and multiple-regression analysis (Figure 5.19b) showed consistent angles and curvature; therefore, predictions clearly defined whether sample concentrations were within the various guideline values and compliance targets at different pH and alkalinity ranges. The two most notable discrepancies using two-component regression analysis were associated with samples containing the greatest Fe concentrations and representative of the highest metal loading rates tested. These included over predicting the most concentrated sample from P2 by 7.1 mg/L (17.8 mg/L Fe predicted and 10.7 mg/L measured) and under predicting the most concentrated sample from P1 by 1.27 mg/L (1.40 mg/L Fe predicted and 2.67 mg/L measured). For both predictive modelling methods, Fe concentration contours were more horizontal indicating that alkalinity was more influential than pH in predicting Fe concentrations.

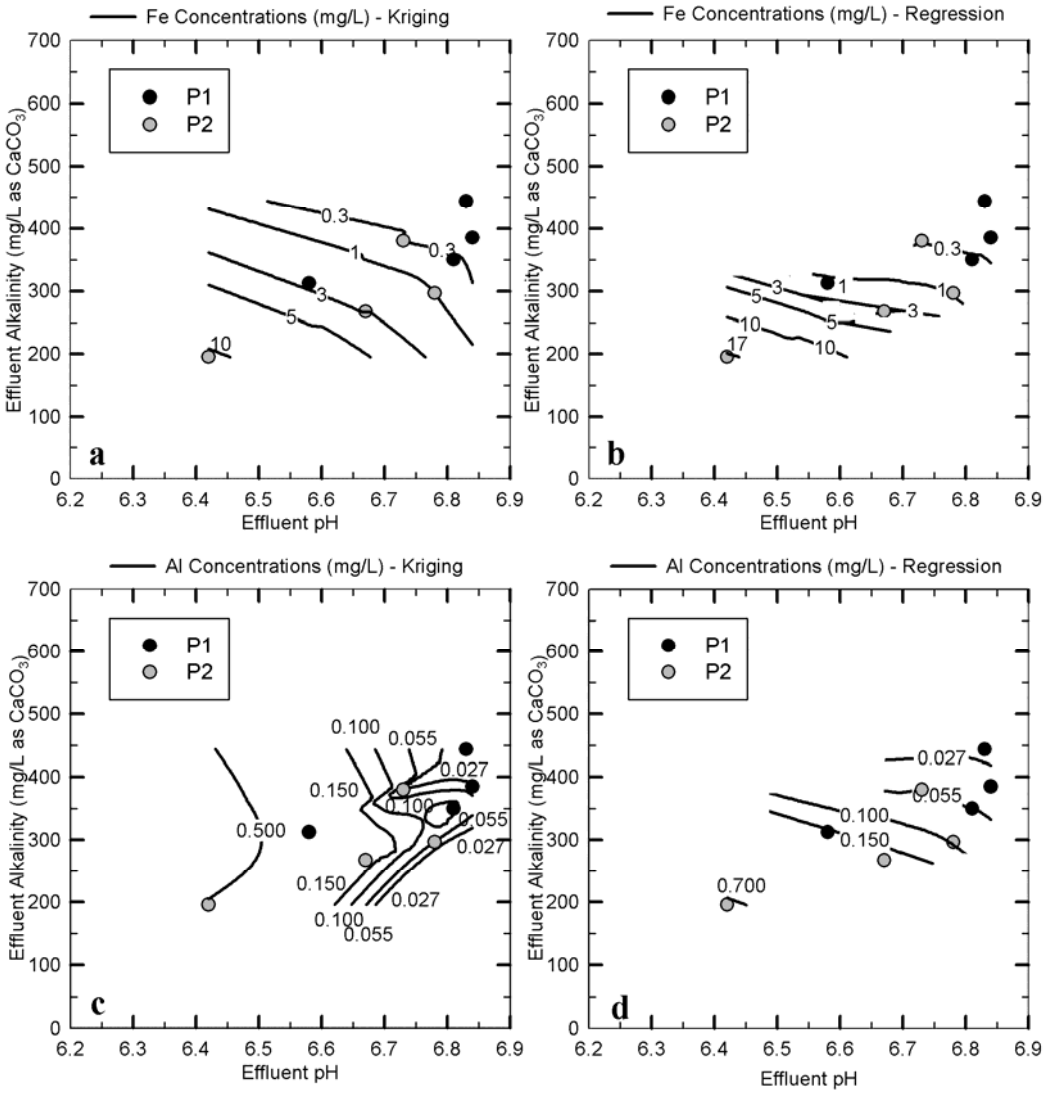

Figure 5.19. Effluent Fe and Al concentration predictions based on pH and alkalinity using kriging interpolation (a and c) and two-component regression analysis (b and d). The concentrations were predicted using the two-component regression analyses of the negative log molar concentrations. Data is representative of the final four sampling events for drum-shaped BGCRs (Scenario 3) containing mussel shells (P1) or a mixture of mussel shells and limestone (P2). Data points shown represent effluent pH and alkalinities measured from BGCR effluent. The concentration contour of 0.3 mg/L Fe represents the stringent Canadian water quality guideline value, the 1 mg/L Fe contour represents commonly applied international guideline values and the 3 mg/L Fe contour represents the lower BGCR effluent target (e.g. BGCR operation is still stable yet concentrations can be further reduced via a subsequent aerobic treatment stage). The 0.027 mg/L, 0.055 mg/L and 0.150 mg/L Al concentration contours represent ANZECC guideline values for 99%, 90% and 80% levels of protection, respectively, for pH>6.5. All Al concentrations were less than the 1 mg/L compliance target (99% of the time) at Stockton Coal Mine.

The most applicable trend with kriging interpolation of Al concentrations (Figure 5.19c) pertained to the 0.150 mg/L contour, which is the ANZECC guideline for 80% level of protection (pH>6.5). Concentrations <0.150 mg/L Al were convoluted, but there was a clear trend that Al<0.150 mg/L would be achieved at about pH≥6.64. Alkalinity showed less influence based on the vertical nature of the contour. Results from the two-component regression analysis would have detected all Al concentrations ≥0.150 mg/L and were biased more towards alkalinity than pH based on the horizontal contours (Figure 5.19d). Two-component regression analysis over predicted the highest Al concentration by 40%. A comparison of the actual measured Fe and Al concentrations with the predicted concentrations using two-component regression analysis are shown in Figure 5.20. Results indicated that there were no Fe (Figure 5.20a) or Al (Figure 5.20b) concentrations predicted via either method that gave a false indication whether or not a data point did or did not exceed a specified ANZECC guideline value or compliance or treatment target. There were greater discrepancies between measured and predicted Al concentrations than Fe.

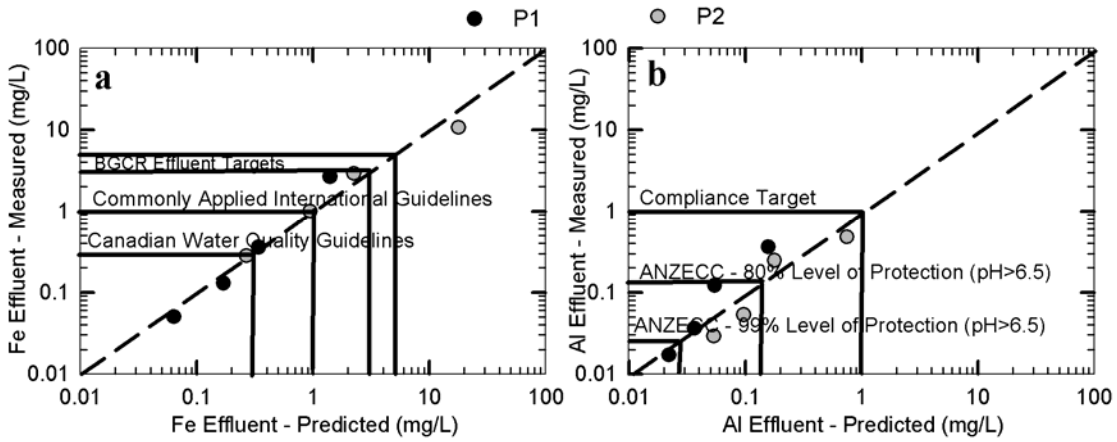

Figure 5.20. A comparison of measured a) Fe and b) Al effluent concentrations and those predicted using two-component regression analysis from effluent pH and alkalinity for drum-shaped BGCRs containing mussel shells (P1) or a mixture of mussel shells and limestone (P2) during the final four sampling events (Scenario 3). The two-component regression analysis was conducted using the negative log Fe and Al molar concentrations and converted to mass concentrations.

5.4.3.4 Trapezoidal-Shaped BGCRs (S2-S4) during the Final Four Sampling Events

Results of kriging interpolation and two-component regression analysis of Fe and Al concentrations from the trapezoidal-shaped BGCRs (S2-S4) during the final four sampling events (Scenario 4; Table 5.2) are presented in Figure 5.21. Iron concentrations were generally predicted at accurate and comparable concentrations with empirical data using both kriging interpolation and two-component regression analysis. The two exceptions involved prediction of the two highest concentrations using the two-component regression analysis. Excluding these two highest Fe concentrations, which under predicted one at a concentration by 5.9 mg/L (measured at 20.6 mg/L and predicted at 14.7 mg/L) and

over predicted the other by 17.5 mg/L (measured at 41.8 mg/L and predicted at 59.2 mg/L), the average absolute difference and absolute percent difference were 0.6 mg/L and 21.7%, respectively. Kriging interpolation was effective for accurately presenting and predicting Fe concentrations <1 mg/L and <3 mg/L (Figure 5.21a). Results from two-component regression analysis (Figure 5.21b) predicted one sample Fe concentration greater than 3 mg/L (BGCR effluent treatment target) when the actual concentration was <3 mg/L. This is demonstrated in Figure 5.22, which shows comparison of the actual measured Fe (Figure 5.22a) and Al (Figure 5.22b) concentrations with the predicted concentrations using two-component regression analysis.

There were two Al concentrations measured at concentrations exceeding 0.15 mg/L (ANZECC guideline for 80% level of protection guideline value (pH>6.5)) but were predicted at lower concentrations with two-component regression analysis (Figure 5.21d), falsely implying that there was no exceedance if the guideline value was applicable. Both kriging interpolation and two-component regression analysis (Figure 5.21d) provided a general indication that Al concentrations were ≤0.15 mg/L (or at least similar) throughout a pH range of 6.66-6.80 and an alkalinity range of 237-447 mg/L as $CaCO_3$. Results from both methods also correctly identified conditions where Al concentrations exceeded 1 mg/L but the two-component regression analysis predicted a sample concentration <3 mg/L (at 2.61 mg/L) when it was measured at a concentration of 3.10 mg/L.

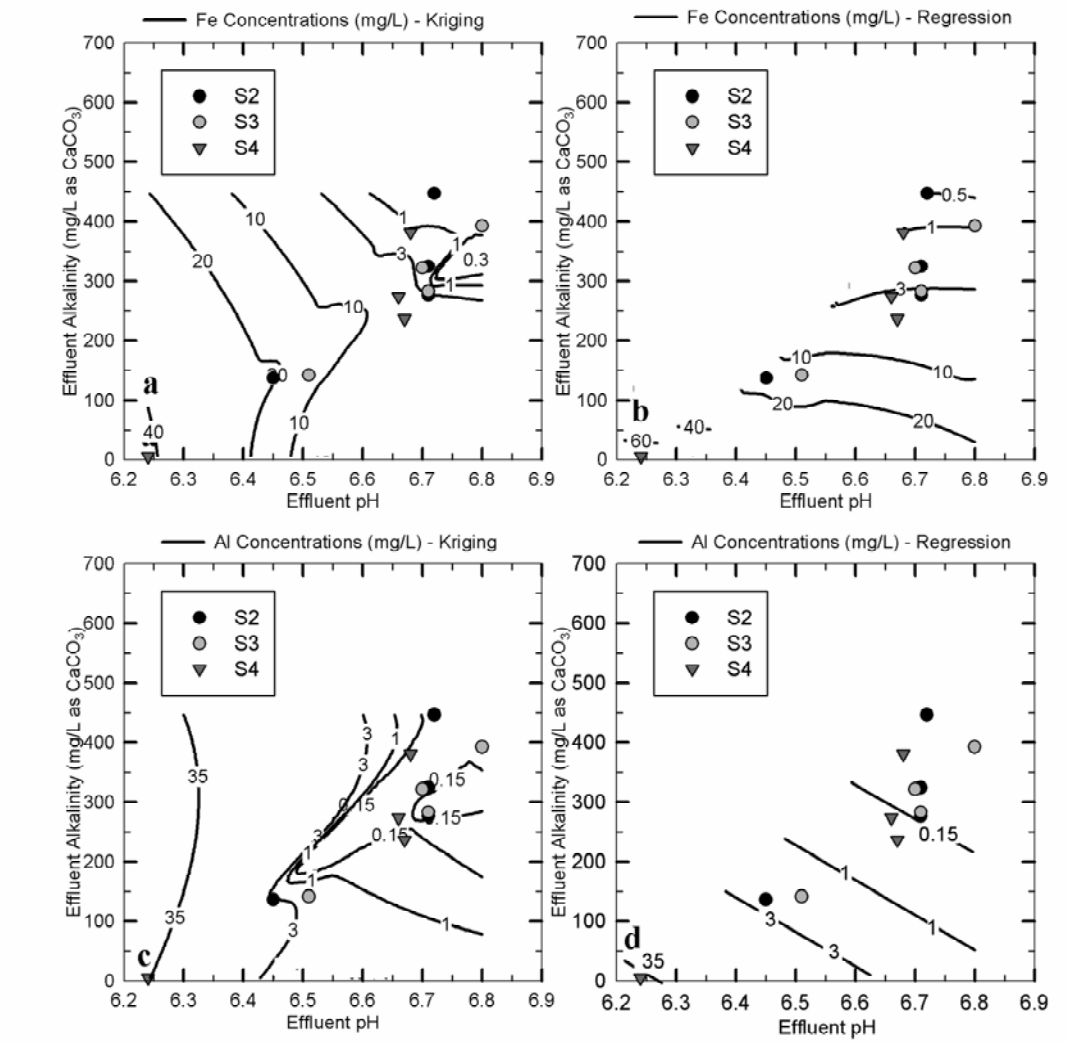

Figure 5.21. Effluent Fe and Al concentration predictions based on pH and alkalinity using kriging interpolation (a and c) and two-component regression analysis (b and d). The concentrations were predicted using the two-component regression analyses of the negative log molar concentrations. Data is representative of the final four sampling events for trapezoidal-shaped BGCRs (Scenario 4) containing mussel shells (S2 and S3) or a mixture of mussel shells and limestone (S4). Data points shown represent effluent pH and alkalinities measured from BGCR effluent. The concentration contour of 0.3 mg/L Fe represents the stringent Canadian water quality guideline value, the 1 mg/L Fe contour represents commonly applied international guideline values and the 3 mg/L Fe contour represents the lower BGCR effluent target (e.g. BGCR operation is still stable yet concentrations can be further reduced via a subsequent aerobic treatment stage). The 0.150 mg/L Al concentration contour represents the ANZECC guideline value for a 80% level of protection (pH>6.5), and the 1 mg/L Al concentration contour represents the current compliance target (99% of the time) at Stockton Coal Mine.

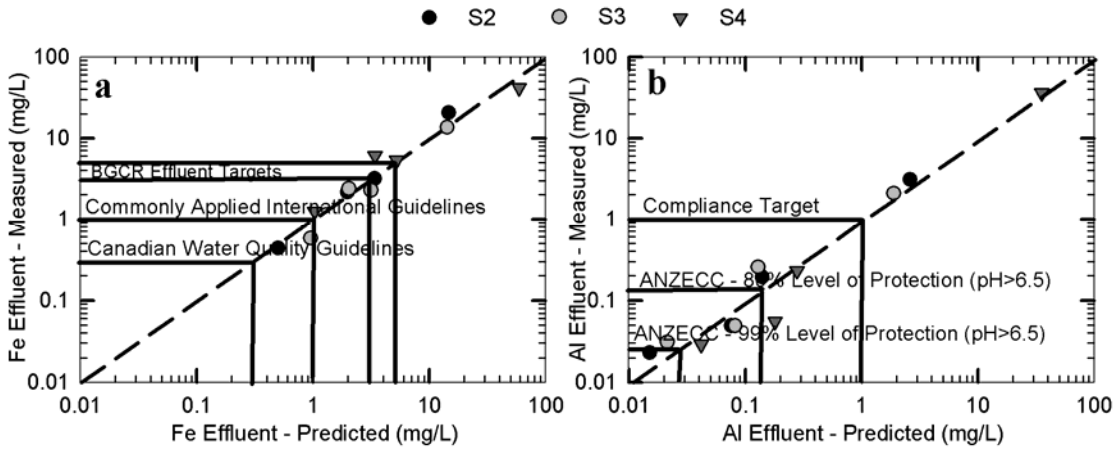

Figure 5.22. A comparison of measured a) Fe and b) Al effluent concentrations and those predicted using two-component regression analysis from effluent pH and alkalinity for trapezoidal-shaped BGCRs containing mussel shells (S2-S3) or a mixture of mussel shells and limestone (S4) during the final four sampling events (Scenario 4). Aluminium and Fe concentrations were predicted using the two-component regression analyses of the negative log molar concentrations with pH and alkalinity.

5.5 Discussion and Conclusions

Alkalinity and pH were useful surrogates for predicting effluent Fe and Al concentrations based on results from the mesocosm-scale treatability tests. Concentration contours generated from kriging interpolation provided a more accurate prediction of Fe and Al concentrations than two-component regression analysis; however, there were only a limited number of occasions when two-component regression analysis falsely predicted a data concentration above or below a potential compliance target or guideline value. Since kriging interpolation can be easily employed with contouring software (such as Sigma Plot® used in this study, Surfer, Origin®, etc.), it is recommended over two-component regression analysis. It is easier to discern both pH and alkalinities that achieve target concentrations using three-dimensional concentration contours created from two-component regression modelling compared with uni-variate plots; however, any discrepancies between empirical and modelled concentrations need to be considered. Care should be taken when interpreting contours generated in regions where there is no empirical data. For example, Figure E.6 (Scenario 2; Table 5.2) shows the same results as Figure 5.17 except questionable contours generated in regions that lacked empirical data were not removed (as shown in circled areas in Figure E.6a). By excluding contours outside of the vicinity of empirical data, a more reliable and defensible predictive tool is generated. The contouring patterns also need to be considered with caution as they are generated from limited data and represent an attempt to interpolate data in areas where data does not always exist. For example, there was a general pattern in this study of lower Fe and Al concentrations with increased pH and alkalinities. If contours contradict this trend, they need to be considered with caution, especially in regions where no empirical data exists. Containing additional data outside of the limited range measured during this study would enhance the robustness of the predictive tool.

There have been consistent trends of lower measured Fe and Al effluent concentrations with higher effluent pH and alkalinities noted from other studies including Rose and Dietz (2002), Rose (2004), Thomas and Romanek (2002a) and Gibert et al. (2004). These studies presented statistical summaries of their data, but no efforts have been reported on application of pH and/or alkalinity as surrogates or other predictive approaches. In this study, it is likely most pragmatic to consider results from the trapezoidal-shaped BGCRs S2, S3 and S4 since they represent the reactor shape and substrate composition of BGCRs likely to be upscaled to pilot or full-scale systems constructed from earth embankments. Operational parameters should also be considered since results of this study demonstrated a distinct trend in the contribution of alkalinity generated from sulphate reduction, as opposed to calcium carbonate dissolution and subsequent bicarbonate generation, during the middle three (40.0%) and final four (13.2%) sampling events.

Equilibrium speciation and inverse geochemical modelling using Visual MINTEQ software showed that effluent Fe and Al were typically present in the dissolved state. Although pH and alkalinity do influence whether Fe and/or Al will precipitate, they showed minimal influence within the ranges measured and anticipated in the effluent. The redox state of the effluent and the magnitude of Fe and Al concentrations were the primary contributors. Typically, >99% of Al was modelled as a dissolved organic acid complex. With exception of the highest loading events measured for the trapezoidal shaped BGCRs (and ≥2.09 mg/L Al), amorphous aluminium hydroxide contained negative saturation indices (SI; see Section 2.6 for explanation) indicating that it was undersaturated containing a preference for the dissolved state. This preference was most significant under the reduced conditions (-3.87--1.84) prevalent in BGCR effluent but was also evident during oxidised conditions (-3.07--0.742). The SIs for amorphous aluminium hydroxide from trapezoidal shaped BGCRs at the highest metal loading rates with ≥2.09 mg/L Al concentrations, pH≤6.45 and alkalinity ≤141 mg/L as $CaCO_3$ were always ≥1.18 indicating a preference for its precipitation. Iron was typically present (>99%) as the iron hydrogen sulphide cation ($FeHS^+$), the common precursor for iron sulphide formation under reduced conditions. The iron sulphide mineral was undersaturated or at equilibrium with the reduced conditions prevalent in BGCR effluent (SIs ranging from -2.03-0.103) except for S4 at the highest metal loading rate when the Fe concentration was 41.8 mg/L, pH was 6.24 and alkalinity was 5.15 mg/L as $CaCO_3$. If oxidised conditions were achieved, such as in a subsequent oxidation treatment stage (Sections 7.2 and 7.3.5), there would be a strong preference for Fe to precipitate as a hydroxide based on positive SIs (ranging from 1.40-5.19) modelled for ferrihydrite ($Fe_2O_3*0.5H_2O$) when effluent contained ≥0.58 mg/L Fe and pH≥6.80.

Kriging interpolation of Fe and Al concentrations from pH and alkalinity data was a useful tool for predicting effluent concentrations and, hence, exceedances of applicable guideline values and/or compliance targets. This was most applicable when empirical data contained concentrations that spanned across the various water quality guidelines or applicable treatment targets. This was

especially useful when applied to some of the lesser stringent treatment targets such as the 1 mg/L Al compliance target (99% of the time) at Stockton Coal Mine (e.g. 1 mg/L Al) and the recommended 3-5 mg/L effluent BGCR Fe concentration (so that a subsequent aerobic treatment stage can reduce concentrations to <1 mg/L). For more stringent compliance targets, there were some ambiguities, primarily with respect to Al concentrations. There was a relatively narrow Al concentration range measured of 0.017-0.055 mg/L throughout relatively broad pH (6.54-6.89) and alkalinity (274-590 mg/L as $CaCO_3$) ranges. The Fe concentration range during these conditions was much broader at 0.05-10.2 mg/L. The measured Al concentrations were both greater than and less than the 0.027 mg/L ANZECC trigger value for 99% level of protection (pH>6.5), so kriging interpolation would not be an effective means of discerning the likelihood of an exceedance based solely on pH and alkalinity data. The only scenario where there was a distinct trend of Al concentrations ≤0.027 mg/L pertained exclusively to BGCR P1 during the middle three sampling events. There was a distinct indication of when Al concentrations were expected to exceed the 0.115 mg/L ANZECC trigger value for 80% level of protection (pH>6.5) during the final four sampling events for all BGCRs and 1 and 3 mg/L considering only trapezoidal-shaped BGCRs. Contours generated in pH and alkalinity regions where no empirical data exists should be interpreted with caution and possibly disregarded. Fewer ambiguities were noted for Fe concentrations compared with Al concentrations. Iron concentrations ≤0.300 mg/L were discernible for all scenarios with exception of the final four sampling events for trapezoidal-shaped BGCRs. All effluent Fe concentrations exceeded 0.300 mg/L during this scenario. The 1 and 3 mg/L Fe target values were discernible for all scenarios with exception of the middle three sampling events for BGCRs P1-P2 due to the lack of empirical data within those concentration ranges.

The concept of utilising continuous pH monitoring offers a potential technology for offsite monitoring of BGCR performance. Telecommunication systems have been employed in remote locations for water quality data acquisition including telemetry radio signals (Lasorso et al., 2009; Meyer and Huey, 2006) and, in more remote areas, satellite telecommunications (Reisman et al., 2008; Reisman et al., 2009). There is also potential to employ an alarm system that alerts an operator when a specified water quality threshold is exceeded (Lung, 2009; Cochrane et al., 2010).

Although application of this concept by utilising continuous pH monitoring seems like a potentially attractive option conceptually in passive AMD treatment, it could be problematic in remote locations. Reisman et al. (2008) utilised remote monitoring, data acquisition and sampling equipment to measure water chemistry from VFW effluent. Initially, unanticipated expenditures accrued due to significant trouble shooting efforts undertaken to solve problems associated with equipment malfunction and issues with data acquisition via Stratolink™ satelline transmitters (Reisman et al., 2008); however, these problems were later rectified when the Stratolink™ satelline transmitters were replaced with satellite phones for data transmission (Reisman et al., 2009). Regardless, site visits and maintenance would still be required, especially with regards to pH probe calibration and removal of biofilm that

would likely accrue on the pH probe and impact its accuracy. Therefore, it may be more pragmatic to undertake a monitoring program that requires site visits by qualified personnel including onsite measurements of pH, using a calibrated portable meter, and alkalinity, via digital titration. Sampling costs could be reduced if pH and field alkalinity are deemed sufficient parameters to validate adequate treatment performance. If these parameter values were outside of an appropriate range, metal samples could then be collected and analysed for their concentrations quantitatively. If VFWs are employed at decommissioned locations on an active mine site, there is potential that personnel on site could measure pH and alkalinity on a more regular basis than a decommissioned mine and more quickly assess if treatment performance could potentially be compromised.

Although results of this study showed that effluent Fe and Al concentrations could be predicted quite accurately with pH and alkalinity, metal concentrations should still be monitored periodically to refine the kriging contours and validate the consistency or any potential declines in treatment performance with time. This should be performed in conjunction with the monitoring of influent Fe and Al concentrations to assess any changes in mine-water chemistry, which could be influencing metal and acidity loading rates and, consequently, treatment performance.

6. Tracer Testing to Determine the Hydraulic Characteristics of Mesocosm-Scale Biogeochemical Reactors and Their Application to Reactor Modelling

6.1 Introduction

Differences in flow hydraulics and efficiencies due to different reactor shapes were hypothesised to influence differences in treatment performance between BGCRs P2 and S4, which were discussed extensively in Chapter 4. Other studies have reported that flow hydraulics in VFWs impact treatment performance in mine-water treatment and have also stated conceptual design recommendations to achieve efficient flow hydraulics whilst minimising undesirable flow characteristics such as short circuiting, scouring and stagnant zones (Busler et al., 2002; Younger et al., 2002; PIRIMID, 2003; Gusek, 2004; Wildeman et al., 2006; Panuvatvanich et al., 2009). Despite this, detailed analysis of the hydraulic characteristics within these systems and their influence on treatment performance has largely been ignored. Additionally, studies utilising VFWs in passive mine water treatment have not reported on modelling how differences in reactor shape influence flow hydraulics and treatment performance. This has important implications since most bench-scale treatability tests have utilised cylindrical columns or drums similar to P2 (e.g. Thomas and Romanek, 2002a; Figueroa et al., 2007; Smart et al., 2008, Venot et al., 2008a; Venot et al., 2008b; Blumenstein et al., 2008; Robinson-Lora and Brennan, 2009), while pilot and full-scale VFWs have typically consisted of trapezoidal-prism shaped basins similar in shape to S4 (e.g. Gusek and Wildeman, 2002; Rose and Dietz, 2002; Ziemkiewicz et al., 2003; Rose, 2004; Skousen and Ziemkiewicz, 2005; Gusek et al., 2008; Reisman et al., 2008). Therefore, direct upscaling from bench to field scale is not always appropriate.

Understanding the flow hydraulics of VFWs is important to determine if non-ideal flow characteristics are occurring that may be reducing treatment performance. The objective of this study was to investigate the flow hydraulics of two mesocsosm-scale BGCRs (P2 and S4), which contained identical substrate mixtures but different reactor shapes, via tracer study analysis. These results were analysed and applied to reactor modelling techniques to determine if there was a consistent relationship between flow hydraulics and underlying reaction rate kinetics. The application of reactor modelling to upscaling designs from the laboratory scale to larger pilot or full-scale systems were investigated with respect to reactor shape and flow hydraulics.

6.2 Materials and Methods

6.2.1 Equipment and Operation

The tracer studies were conducted for BGCRs P2 and S4 since they were the only two reactors analysed during the mesocosm-scale treatability tests that contained the same substrate mixture (12 vol. % mussel shells, 5 vol. % limestone, 30 vol. % bark, 38 vol. % post peel and 15 vol. % compost), yet contained different reactor shapes and sizes. This allowed for the flow hydraulics of two

differently shaped reactors to be compared and modelled. Details regarding reactor characteristics, preparation, substrate materials, equipment and materials used and experimental operation were previously discussed in detail throughout Section 4.1. The only exception to the reactor characteristics was that the depth of surface water over the upper post peel layer was maintained at 70 mm during this study instead of 50 mm.

6.2.2 Experimental Design and Sampling

Tracer studies were conducted for BGCRs P2 and S4 following completion of the mesocosm-scale treatability tests discussed throughout Chapter 4. The AMD feed was maintained with peristaltic pumps at volumetric flow rates equivalent to metal loading rates of approximately 0.52 mol/m^3/day, which was representative of operating conditions below the recommended design loading rate of 0.8 mol/m^3/day concluded from results of the mesocosm-scale treatability tests for metal removal (Chapter 4); however, it is likely representative of common metal loading during a field application when loading rates would be variable. Panuvatvanich et al. (2009) confirmed that flow rate had minimal impact on hydraulic behaviour in their study, which analysed vegetated VFWs. An instantaneous spike of sodium bromide (NaBr) prepared in a 100 mL solution was introduced at the inlet feed of each reactor. Sodium bromide was chosen since it represents a cost-effective inert tracer that would not sorb to the organic substrates. Additionally, Br was only present at low background concentrations in the AMD (0.14 mg/L).

Effluent sampling was conducted at the time of tracer spiking and subsequently at six to 12 hour intervals. Sampling was conducted more frequently (e.g. every six hours) during the initial 2.0 RTD and less frequently thereafter as the majority of tracer mass was already recovered in the effluent. Approximately 50 mL of effluent was collected into method-specified unpreserved HDPE sampling containers and analysed by RJ Hill Laboratories Limited. Samples were initially filtered through 0.45 μm membrane filters and preserved with nitric acid following method APHA 3030B prior to Br analysis by method APHA 3125B using ICP-MS (APHA, 2005). The tracer studies were conducted for 10.8 days (θ_{BGCR}=3.2 for P2 and θ_{BGCR}=3.3 for S4). Barometric pressure was also measured at the time of Br sampling, using a Silva Alba Windwatch equipped with a barometer, since barometric pressure influences gas transfer and flow in porous media.

6.3 Analysis and Calculations

The tracer test results were analysed using methodology and modelling commonly applied in chemical reaction engineering and chemical reactor design. Chemical reaction engineering and reactor modelling have been discussed extensively in Levenspiel (1999). Their application to environmental systems has been discussed in Weber and DiGiano (1996), and Weber (2001), and their application to surface and subsurface flow wetlands has been discussed in Kadlec and Wallace (2009).

The initial analysis involved examining the tracer response curves to determine the flow characteristics of BGCRs P2 and S4 and compare these with ideal and non-ideal flow patterns. The mean tracer HRT time was then determined. The distribution of the tracer response curves were then normalised by a methodology termed detention time distribution (DTD). The DTD functions determined from tracer study results were compared with ideal reactor models including the completely mixed flow reactor (CMFR), which is sometimes referred to as a continuously stirred tank reactor (CSTR), and the plug flow reactor (PFR). In an ideal CMFR, perfect mixing occurs so the reactant is instantly diluted upon entering the reactor; therefore, the concentration is uniform throughout the reactor. In a PFR, no internal mixing occurs; therefore, the reactants enter at a high concentration and decrease exponentially throughout the reactor as the products are formed. This essentially represents the perfect reactor which can be achieved in theory but not in practice.

Kadlec and Wallace (2009) state that most environmental systems, including surface and subsurface flow wetlands, behave somewhere between an ideal CMFR and PFR. This is a result of a process referred to as dispersion, which represents spreading of a contaminant (or a tracer) as flow proceeds through a reactor. There are two models that are commonly employed to represent reactors that deviate from plug flow due to dispersion. The tanks in series (TIS) model is often applied to assess treatment system performance in such reactors. The TIS model represents the modelled number of equally sized CMFRs operated in series where an infinite number of TIS represents plug flow conditions and one TIS represents a CMFR with perfect mixing. It does not represent the physical configuration of a treatment system but employs the number of TIS to represent the amount of dispersion. The other model commonly employed is the plug flow with dispersion model. The plug flow with dispersion model is roughly equivalent to the TIS model except the dispersion is quantified by a parameter referred to as the dispersion coefficient (D) containing units area/time (Levenspiel, 1999).

In this study, the DTD functions derived from tracer testing were initially applied to theoretical curves derived using the TIS model. The tracer response variance, dispersion coefficients and flow distribution efficiencies were then calculated. Reaction rate constants for the BGCRs were computed using the TIS and relaxed TIS models and results of the tracer studies and treatability tests for Fe, Al and acidity removal (as presented in Chapter 4). These were assessed to determine their implications for predicting and assessing BGCR performance and scaling-up BGCRs to larger pilot or full-scale treatment systems.

6.3.1 Benchmark Bromide Concentration

The amount of tracer added was based primarily on the expected dilution, the laboratory PQLs and AMD background concentrations. It is typical to estimate the amount of tracer to be added based on the benchmark concentration, which represents the amount of tracer added per nominal wetland

volume (Kadlec and Wallace, 2009). This was calculated using Equation 6.1 where m_{Br} represents the mass of Br and $V_{w(BGCR)}$ represents the pore-water volume with the BGCR.

$$C_{BM(Br)} = m_{Br}/V_{w(BGCR)} \quad \textbf{(6.1)}$$

6.3.2 Tracer Mass Recovery

It is important to perform a mass balance to verify complete tracer recovery at the conclusion of tracer testing (Kadlec and Wallace, 2009). The mass of tracer recovered ($m_{Br(o)}$) was computed using the following equation where Q is the volumetric flowrate, $C_{Br}(t)$ represents the Br concentration at time t, Δt signifies the time between sampling events and n represents the number of observations (or samples collected).

$$m_{Br(o)} = \sum_{i=1}^{n} QC_{Br}(t)\Delta t \quad \textbf{(6.2)}$$

6.3.3 Mean Tracer Hydraulic Residence Time and Volumetric Efficiency

There are two different methods for computing HRT within the BGCRs. The first methodology is referred to as theoretical (or nominal) HRT (τ_{BGCR}), which was discussed in Section 4.2.2.3 and represents the expected hydraulic residence time assuming all flow passes uniformly through all surface water and void spaces. This was calculated using Equations 4.2-4.6. The mean tracer HRT (τ) represents the time when half of the tracer input has exited the reactor and is presumed to represent the actual mean HRT and was calculated using the following equation where t represents time since the tracer spike, Q_{avg} represents average volumetric flow rate and C_{Br} signifies the non-background Br concentration (e.g. background concentration of 0.14 mg/L subtracted from the measured Br concentration).

$$\tau = \sum_{i=1}^{n} [(tQ_{avg}C_{Br}(t)\Delta t)/m_{Br(o)}] \quad \textbf{(6.3)}$$

The volumetric efficiency (e_V) is defined in Equation 6.4 as the ratio of the mean tracer HRT and the theoretical HRT.

$$e_V = \tau/\tau_{BGCR} \quad \textbf{(6.4)}$$

It reflects how much of the theoretical water volume within a system was involved in the flow.

6.3.4 Detention Time Distribution and Tanks in Series Modelling

The DTD represents the fraction of incoming water that stays within the treatment systems for a length of time between t and Δt (Kadlec and Wallace, 2009). The DTD for the tracer studies were calculated using Equation 6.5 where f(t) represents the DTD function at time t in units 1/days.

$$DTD = f(t)\Delta t \quad \textbf{(6.5)}$$

The DTD function is related to the exit tracer concentration by Equation 6.6.

$$f(t) = QC_{Br}(t)/m_{Br(o)} \quad \textbf{(6.6)}$$

The DTD function represents the fraction of incoming water that stays within the reactor for a particular length of time (or throughout the RTD). This is sometimes referred to as the E curve, or exit age distribution. Plotting time versus the DTD function yields an area under the curve of one, which allows for a uniform comparison of reactors of different shape and size (such as P2 and S4 in this study).

The DTD function can also be employed to the tanks in series (TIS) model. The DTD function for the TIS model ($f(t)_{TIS}$) can be represented as either a two or three-component DTD function as shown in Equations 6.7 and 6.8, respectively, where N represents the number of TIS, $\Gamma(N)$ represents the gamma function and t_d denotes the time delay.

$$f(t)_{TIS} = N^N t^{N-1}/\tau^N \Gamma(N) \exp(-Nt/\tau) \quad \textbf{(6.7)}$$

$$f(t)_{TIS} \begin{cases} = N^N (t-t_d)^{N-1}/\tau^N \Gamma(N) \exp(-N(t-t_d)/\tau) & [t > t_d] \\ = 0 & [t < t_d] \end{cases} \quad \textbf{(6.8)}$$

The gamma function is defined in Equation 6.9.

$$\Gamma(N) = \int_0^\infty \exp(-t) t^{N-1} dt \quad \textbf{(6.9)}$$

The gamma function can be simplified if N represents a positive integer to the factorial shown in Equation 6.10.

$$\Gamma(N) = (N-1)! \quad \textbf{(6.10)}$$

Mean tracer detention time (τ) and the number of TIS (N) are the only variables that alter the characteristics (height and width) of the two-component TIS model (Equation 6.7). Since the computation of the mean tracer detention time is dependent on results from the tracer study, the number of TIS is the only variable that can be altered to best fit the empirical tracer study results. The three-component TIS model (Equation 6.8) adds (or subtracts) a time-delay component (t) which shifts the DTD function of the TIS model along the time or RTD axis (x-axis). The time delay term allows a model correction so that the breakthrough delay of tracer is accounted for. Kadlec and Wallace (2009)

state that it is most important to best fit the peak of the tracer response curve since the majority of tracer is detected in this region. Without such an adjustment, the best-fit of the DTD function can overemphasise the tail, or final gradual exponential decline of the empirical tracer DTD curve. This reflects only the final residual and typically a minority of the tracer mass. For this reason, Kadlec et al. (1993), Kadlec and Knight (1996) and Marsili-Libelli and Checchi (2005) recommend the inclusion of a time delay (t_d) in TIS modelling.

The goal of TIS modelling is to determine the theoretical number of TIS that creates a DTD distribution ($f(t)_{TIS}$) that minimises the sum of squared errors (SSQE) with the DTD function developed from empirical tracer study analysis ($f(t)$). The SSQE errors was determined using Equation 6.11.

$$SSQE = \sum_{i=1}^{n} (f(t)-f(t)_{TIS})^2 \quad \textbf{(6.11)}$$

6.3.5 Tracer Response Variance, Dispersion Coefficient and Flow Distribution Efficiencies

Simple parameters can be calculated from results of tracer studies and TIS modelling to provide a quick indication of flow hydraulics. The dimensionless variance (σ_θ^2) and variance (σ^2) essentially provide a measure of the dispersive flow processes and the distribution of mixing and flow velocities through passage (Kadlec and Wallace, 2009). They represent the spread of a tracer response curve from the mean of the distribution or the variation in residence times around the mean tracer HRT (Weber, 2001; Kadlec and Wallace, 2009). Therefore, smaller values would be indicative of more distinct steep tracer response curves (less dispersion) whereas larger values would demonstrate a wider lateral spread in the tracer response curve (greater dispersion). Dimensionless variance can be calculated from TIS modelling as the inverse of the number of TIS and using Equation 6.12 where t_p denotes the tracer peak time (time of the greatest tracer concentration).

$$\sigma_\theta^2 = 1/N = (\tau-t_p)/\tau \quad \textbf{(6.12)}$$

The variance is related to the dimensionless variance as shown in Equation 6.13 and also represents the square of the standard deviation.

$$\sigma^2 = \sigma_\theta^2\tau^2 \quad \textbf{(6.13)}$$

The dispersion coefficient (D) represents the spreading of the tracer as it proceeds through the reactor, or the deviation from plug-flow conditions; therefore, the greater the dispersion coefficient, the greater the dispersion. For an open system, such as the BGCRs used in this study, it can be solved by trial and

error or the goal seek/solver functions in Microsoft Excel from Equation 6.14 where L represents length and Q denotes volumetric flow rate.

$$\sigma_\theta^2 = 2DL/Q + 8(DL/Q)^2 \quad (6.14)$$

Equation 6.14 represents a modified version of the equation originally derived from Levenspiel and Smith (1957). The plug flow dispersion model is physically represented as a pipe or tube where the length is much greater that pipe or tube diameter. The BGCRs used in this study do not physically represent this so the length was assumed to be equivalent to the length from the reactor inlet to outlet.

The concepts of the DTD and hydraulic efficiencies were developed by Persson et al. (1999). The DTD efficiency (e_{DTD}) represents the amount of internal mixing within a reactor and can be calculated as shown in Equation 6.15.

$$e_{DTD} = 1 - \sigma_\theta^2 \quad \textbf{(6.15)}$$

The DTD efficiency approximates a reactors prospective performance based on a single TIS (e_{DTD}=0) or plug flow characteristics (e_{DTD}=1). The hydraulic efficiency (λ) represents the product of the volumetric (Equation 6.4) and DTD (Equation 6.15) efficiencies or the ratio of the tracer peak time (t_p) and the theoretical HRT as defined in Equation 6.16.

$$\lambda = e_V e_{DTD} = t_p/\tau_{BGCR} \quad \textbf{(6.16)}$$

Essentially, the hydraulic efficiency considers the combined influence of the ineffective volume within a reactor and internal mixing.

6.3.6 Reaction Rate Kinetics

6.3.6.1 Tanks in Series Modelling

Results from TIS modelling and the treatability tests (discussed in Chapter 4) were used to calculate reaction rate constants (k) for Fe, Al and acidity removal since these were the predominant contaminants present in the Manchester Seep AMD (Chapters 2 and 4). The reaction rate constants were computed using the TIS model as shown in Equation 6.17. The TIS model assumes first-order kinetics, where C_{in} and C_{out} represent the influent and effluent concentrations, respectively, measured during the BGCR mesocosm treatability tests (Chapter 4) at their respective HRTs. N was determined from the analysis discussed in Section 6.3.4 such that SSQE were minimised between the theoretical TIS model and the empirical DTD curve of each reactor.

$$k = N/\tau_{BGCR}[(C_{in}/C_{out})^{1/N} - 1] \quad \textbf{(6.17)}$$

There was potential to substitute the theoretical HRT (τ_{BGCR}) with the actual mean HRT (τ) in Equation 6.17 by multiplying the theoretical HRTs calculated during the treatability tests by the volumetric efficiencies (Equation 6.4) determined during the tracer studies; however, this was not performed during this study. The effect would be insignificant for the purposes of this analysis. The influence of the volumetric efficiency is thus absorbed into the rate constants (Kadlec and Wallace, 2009).

6.3.6.2 Relaxed Tanks in Series Concentration Modelling

For wastewaters containing a mixture of contaminants such as AMD, the relaxed TIS concentration model can be employed (Kadlec, 2003). The relaxed TIS concentration model is very similar to the TIS model described in Equation 6.17. It is typically denoted as shown in Equation 6.18 where P represents the apparent number of TIS.

$$C_{out}/C_{in} = 1/(1+k\tau_{BGCR}/P)^{P} \quad \textbf{(6.18)}$$

With the typical TIS model, the number of TIS (N) is determined from the DTD function, as explained in Section 6.3.4., and this value is used to calculate the reaction rate constant as shown in Equation 6.17. In the relaxed TIS model, the number of TIS is assumed to be and unknown; hence, it is referred to as the apparent number of TIS (P). When applying the relaxed TIS model, the apparent number of TIS and the reaction rate constant become fitting parameters to minimise the SSQE of the C_{out}/C_{in} ratio, which is known empirically from results of treatability testing (Kadlec, 2003). The apparent number of TIS should be less than the number of TIS determined from the DTD function derived from an inert tracer study, which occurs as a result of the rate constants decreasing with increased travel time (Kadlec and Wallace, 2009).

6.4 Results and Discussion

6.4.1 Benchmark Bromine Concentrations

The benchmark Br concentrations ($C_{BM(Br)}$) were 4.6 mg/L for S4 and 5.0 mg/L for P2. Keller and Bays (2001) recommended that the benchmark tracer concentration should be at least 10 to 20 times the background concentration to allow adequate detection. The benchmark Br concentrations during this study ranged from 32-36 times the background Br concentration of 0.14 mg/L. Additionally, Kadlec and Wallace (2009) suggested that the target peak effluent tracer concentration should be at least 20-50 times the background concentration. For this study, the peak effluent concentrations ranged from 25-30 times the Br background concentration.

6.4.2 Bromine Tracer Response Curves and Conceptual Flow Characteristics

Tracer response curves were developed from the Br concentrations measured in the effluent of BGCRs P2 and S4. A time-series representation of these curves is shown in Figure 6.1 along with a summary

of atmospheric barometric pressure throughout this study. The NaBr tracer was introduced at time 0.0 days, and the testing lasted 10.2 days when background Br concentrations were nearly achieved in the effluent. The background Br concentration of 0.14 mg/L was subtracted from the analysed concentrations. The RTD (Equation 4.8) of Br concentrations is shown in Figure 6.2.

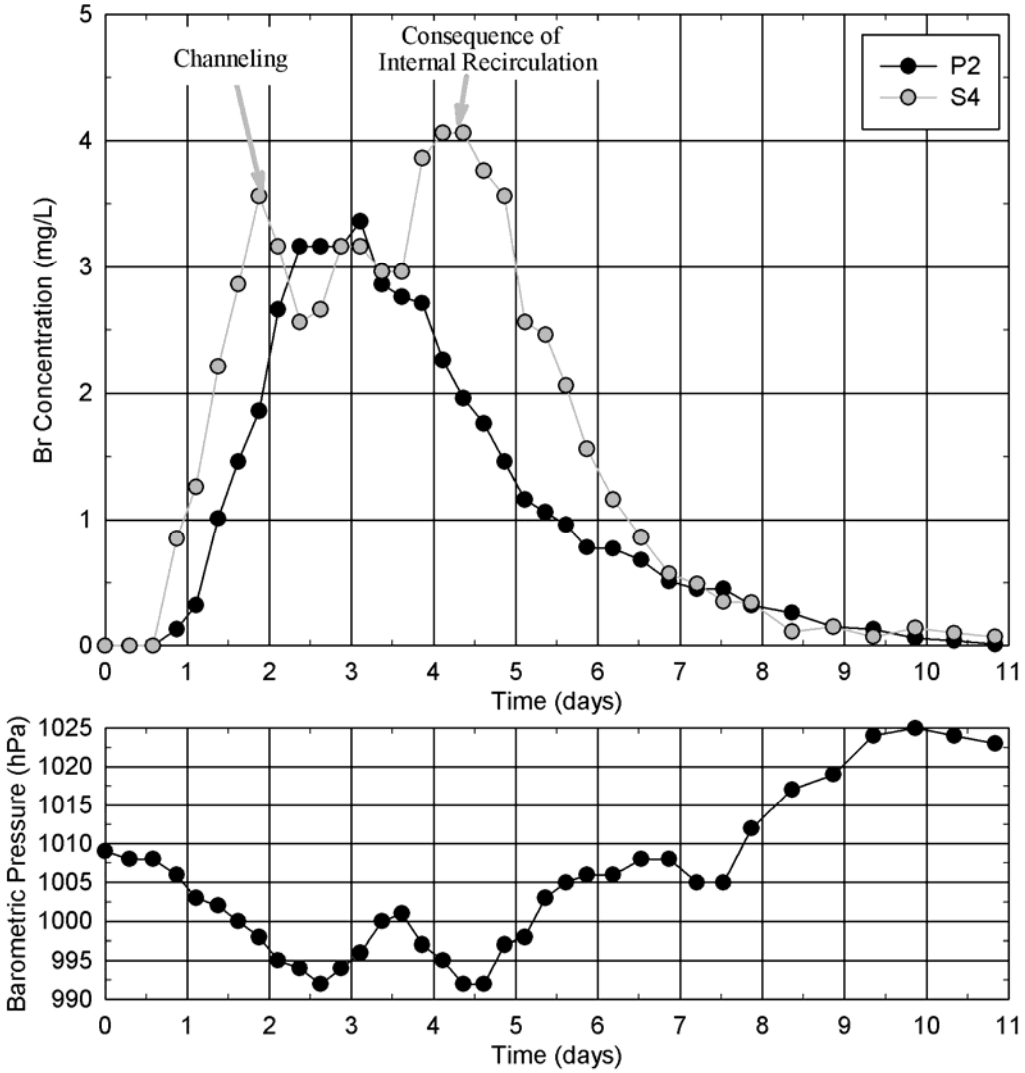

Figure 6.1. Bromine concentration tracer-response curves from effluent samples collected from BGCRs P2 and S4 and a summary of the atmospheric barometric pressure throughout the study. The background Br concentration of 0.14 mg/L was subtracted from the values shown.

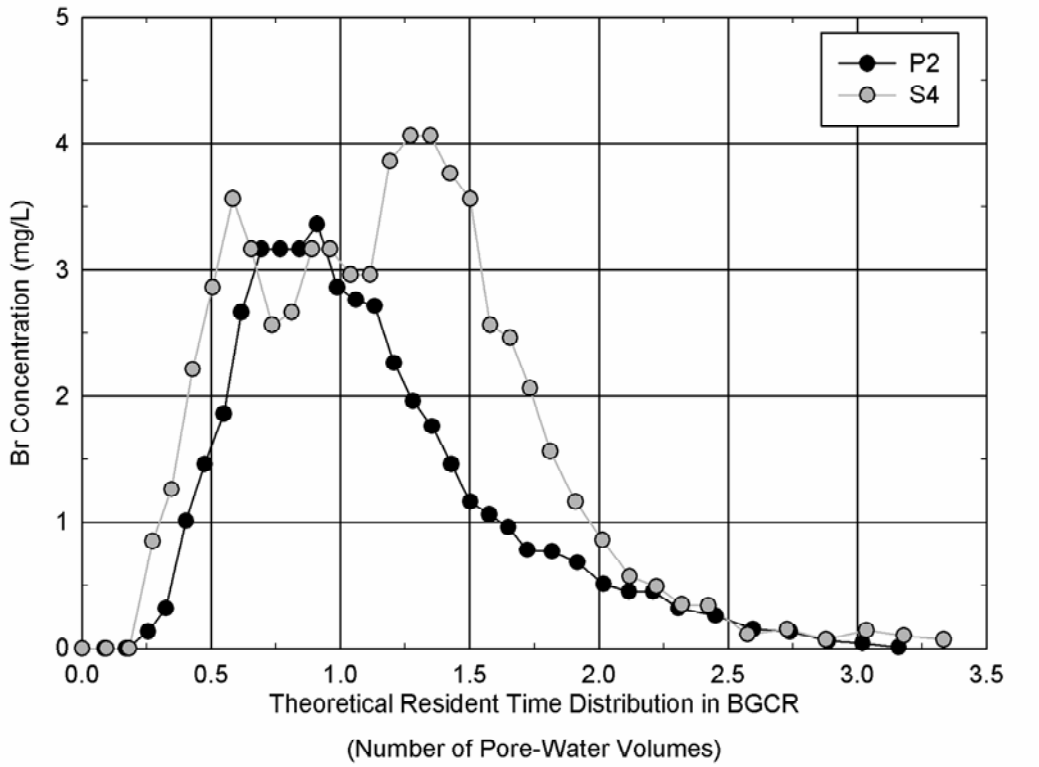

Figure 6.2. Bromine concentration tracer-response curves showing the RTD for BGCRs P2 and S4.

Results from the cylindrical-drum reactor (P2) generally showed the expected trend for a reactor operating somewhere between the ideal conditions of a CMFR and a PFR indicative of the skewed bell-shaped curve (Weber, 2001; Kadlec and Wallace, 2009). The tracer response curve for P2 rose relatively steeply until it peaked at θ_{BGCR}=0.91 (3.1 days) and then gradually decreased throughout the remaining duration of the study (Figures 6.1 and 6.2). The timing of this peak was likely influenced by the position of the reactor's drainage, which was located near the upper surface of the bedding material (Figure 6.3); therefore, flow within the bedding material could have been relatively stagnant.

The multiple peaks present in the trapezoidal-shaped reactor (S4) curve indicated that channelling was likely occurring in the reactor. Tracer peaks occurred at a RTD of 0.58 (1.9 days), 0.92 (3.0 days) and 1.31 (4.0 days) as shown in Figures 6.1 and 6.2. These peaks could have occurred from a number of processes within the reactor. These include short circuiting, the bedding material being located below the outlet of the reactor and internal recirculation due to rising hydrogen sulphide and carbon dioxide gas bubbles.

Internal recirculation could result in countercurrent two-phase flow. Although not quantified during this study, the release of what was inferred as hydrogen sulphide and carbon dioxide gas bubbles were visually observed at the upper water surface of the BGCRs on occasion throughout the tracer studies and treatability tests. A hydrogen sulphide odour was also observed. Levenspiel (1999) reported that rising bubbles can cause countercurrent two-phase flow in reactors resulting in internal recirculation

and sometimes arbitrary flow characteristics. Such arbitrary flow conditions can result in multiple tracer peaks and sometimes even the occurrence of late peaks (e.g. after θ_{BGCR}=1.0).

Hydrogen sulphide and carbon dioxide collecting within piping networks and stagnant areas of VFWs, sometimes impeding flow in these areas, have been previously reported by Gusek (2004) and Wildeman et al. (2006). The barometric pressure was generally dropping during the first half of this study (Figure 6.1), which would have provided conditions conducive to gas transfer and countercurrent two-phase flow. Decreases in barometric pressure have been reported to influence gas flow and release in porous media systems (Neeper and Stauffer, 2005). The same phenomenon has also been reported with landfills where methane and hydrogen sulphide emissions have negatively correlated with atmospheric pressure (Czepiel et al., 2003; Lee et al., 2006).

Conceptual models demonstrating scaled reactor dimensions and suspected flow patterns within BGCRs P2 and S4 are presented in Figure 6.3. Flow velocities would have been more uniform in the downward vertical direction in P2 compared to S4 due to reactor shape. In P2, the flow was required to travel a much shorter horizontal length (0.38 m) relative to vertical length (0.66 m), which gives a horizontal to vertical travel length ratio of 0.58. In S4, the horizontal length of travel was 0.90 m, and the vertical length of travel was 0.57 m giving a horizontal to vertical travel length ratio of 1.58. Based on these reactor characteristics coupled with the slow laminar inlet feed rates (16.0 mL/min for P2 and 34.3 mL/min for S4), eddies, countercurrent two-phase flow and stagnant zones likely contributed to the non-uniform flow characteristics present in S4. In P2, countercurrent two-phase flow could have contributed to shorter, wider and more skewed bell-shaped curves than if this recirculation did not occur. Because the prominent flow direction in P2 was vertical, whereas the prominent flow direction in S4 was horizontal, stagnant zones were less likely in P2 compared with S4. As a result, the tracer response curve for P2 was indicative of a gamma distribution, but the tracer response curve for S4 contained an arbitrary late peak.

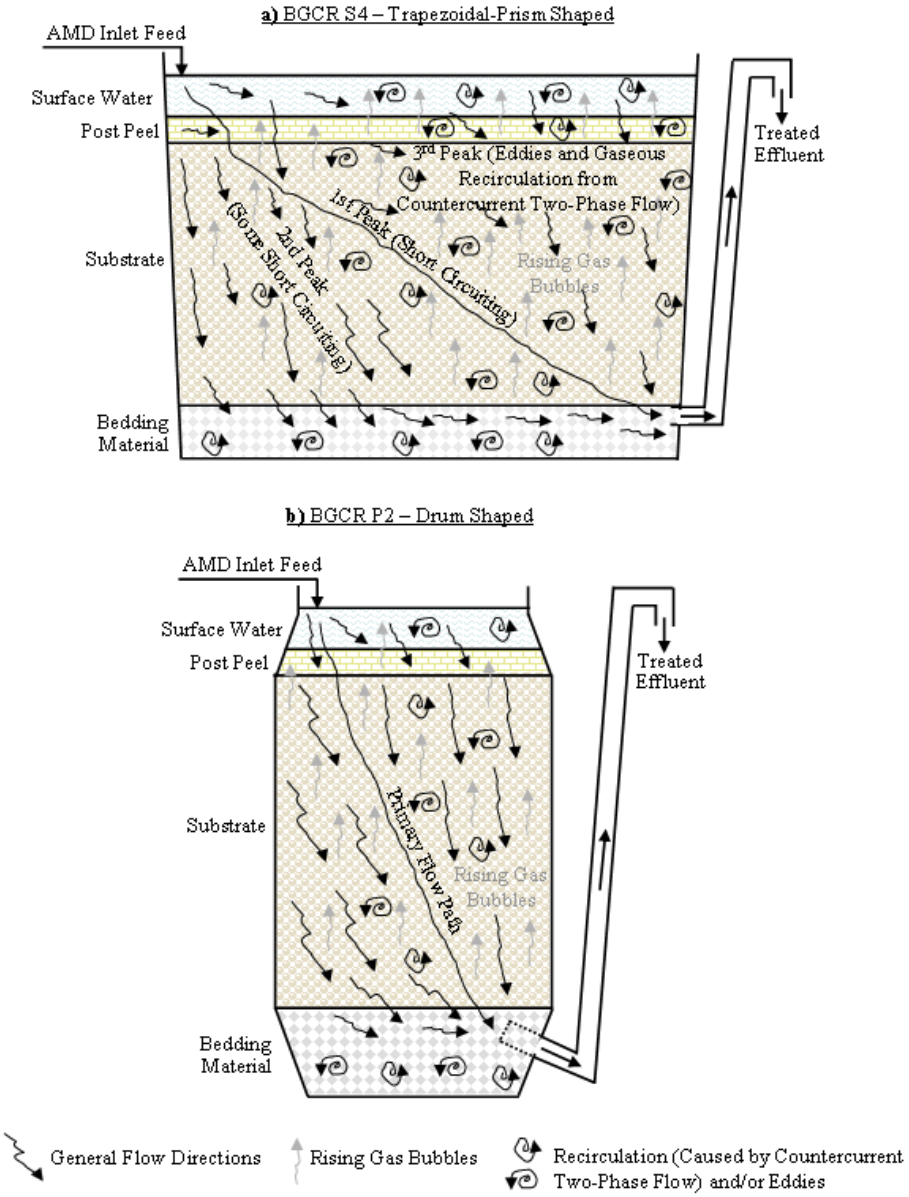

Figure 6.3. A conceptual model demonstrating scaled reactor dimensions and suspected flow patterns within a) BGCR S4; and b) BGCR P2.

6.4.3 Tracer Mass Recovery

The percentage of tracer recovered was 74.5% for P2 and 103% for S4. This indicates that tracer recovery was very good for S4, but approximately one-quarter of the tracer in P2 was retained. Theoretically, the maximum percent recovery possible was 100%. The Br measured in S4 above the theoretical maximum was likely attributed to experimental error. In P2, Br molecules potentially remained stagnant within portions of the bedding material reflecting its low recovery.

The Br solution used to spike the reactors was potentially more dense (1.003 mg/L for P2 and 1.007 mg/L for S4) than tap water (estimated at 1.000 mg/L) and or AMD; therefore, some density

stratification could have occurred allowing the heavier Br solution to settle at the bottom of the reactor where it became relatively immobilised once reaching the stagnant flow area. The methodology for computing the density for sodium bromide solutions is presented by Equations F.1 and F.2 in Appendix F. Schmid et al. (2004a; 2004b) indicated that density stratification can significantly distort tracer response curves and the DTD. Kadlec and Wallace (2009) recommended that the density of a tracer solution should be significantly less than 1% heavier than the inlet feed water, which is typically the density difference required to maintain stratification in lakes. The tracer solutions used in this study were 0.3% greater than tap water for P2 and 0.7% for S4.

There have been minimal studies reporting results of tracer studies for vertical flow type reactors, especially with application to mine-water treatment. The most comparable type of passive treatment system to the VFWs implemented in mine-water treatement relate to subsurface flow wetlands since they are natural treatment systems that involve flow through porous media; however, flow within subsurface flow wetlands is predominately horizontal, whereas flow in VFWs is typically both horizontal and vertical. Kadlec and Wallace (2009) summarised tracer study results from 32 subsurface flow wetlands that employed inert tracers including Br, Li or Cl. The median percent tracer recovery was 93.5%±20.3% (range of 45-160%), which is comparable to the this study.

6.4.4 Mean Hydraulic Residence Time and Volumetric Efficiency

A summary of the theoretical and mean tracer HRT and the volumetric efficiency for P2 and S4 are summarised in Table 6.1. The mean tracer HRTs for P2 and S4 occurred later than theoretically expected. As a result, the volumetric efficiencies were greater than 1.00 indicating the presence of non-uniform flow conditions including eddies and internal recirculation. Kadlec and Wallace (2009) indicated that the tracer HRT is typically less than the theoretical HRT (or e_v is typically <1.00) because not all of the components of a system are involved in the flow path. Although this is typical, 40.6% of the subsurface flow wetlands they summarised also contained mean HRT that were greater than the theoretical HRT. Of these results (n=13), the average volumetric efficiency was 1.15±0.134 (range of 1.01-1.38), which is similar to results of this study.

Table 6.1: Summary of the theoretical and mean tracer HRT for BGCRs P2 and S4.

	Theoretical HRT (days)	Mean Tracer HRT (days)	Volumetric Efficiency
P2	3.42	3.82	1.12
S4	3.25	3.86	1.19

6.4.5 Detention Time Distribution and Tanks in Series Model

A summary of the number of TIS that minimised the SSQE for the two (Equation 6.7) and three-component (Equation 6.8) TIS models, the SSQE and the time-delay component (from the three-component model) are summarised in Table 6.2. The DTD functions derived using the two-component TIS model from the tracer studies for P2 and S4 are shown in Figures 6.4 and 6.5,

respectively, and are compared with the gamma distribution developed employing the number of TIS which best fit the empirical data (via minimisation of SSQE). The DTD functions derived using the three-component TIS model for P2 and S4 are shown in Figures 6.6 and 6.7, respectively, and are also compared with the gamma distribution developed employing the number of TIS which best fit the empirical data (via minimisation of SSQE). To demonstrate how the number of TIS influenced the gamma distributions in the TIS model, the gamma distributions developed assuming 1, 3, 5, 7, 10 and an infinite number (PFR model) of TIS are compared with the DTD functions of P2 and S4 for the three component TIS model in Figures F.1 and F.2, respectively, in Appendix F.

Table 6.2: The number of TIS that minimised the SSQE for the two and three-component TIS models, the SSQE and the time-delay component (from the three-component model).

BGCR	Number of TIS	Minimised SSQE (1/day)	Time Delay (days)
Two-Component TIS Model			
P2	5.2	0.0120	NA
S4	4.1	0.0437	NA
Three-Component TIS Model			
P2	6.3	0.00764	-0.21
S4	3.7	0.0400	0.22

NA, non-applicable.

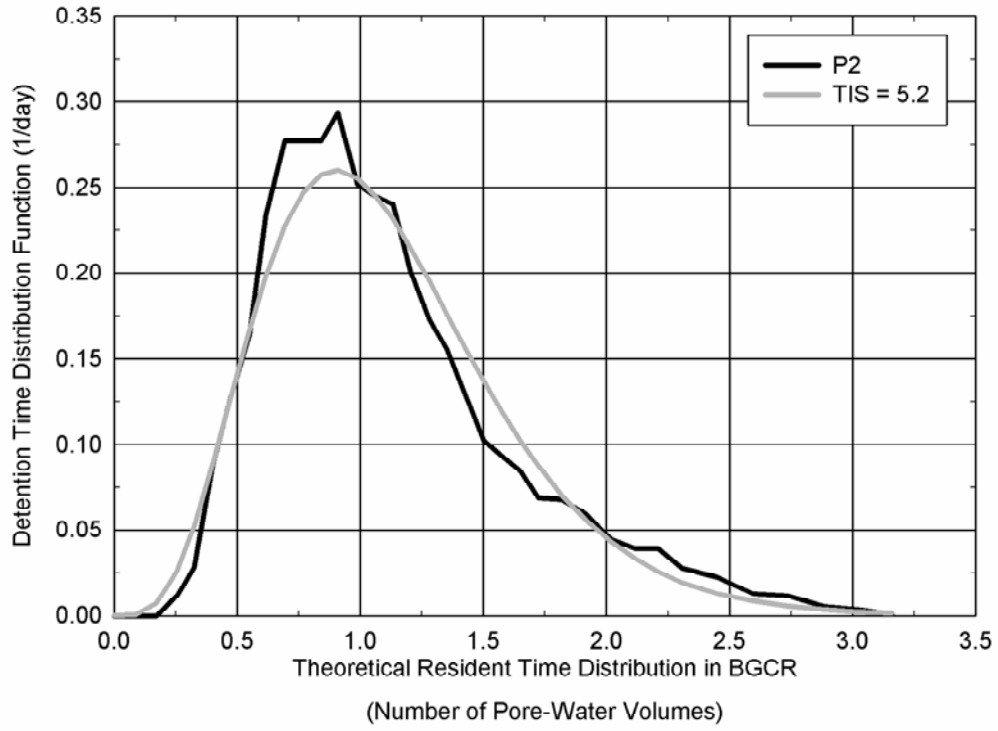

Figure 6.4. The DTD function derived from the tracer study analysis of BGCR P2 and the gamma distribution developed employing 5.2 TIS for the two-component model, which best fit the empirical data (via minimisation of SSQE).

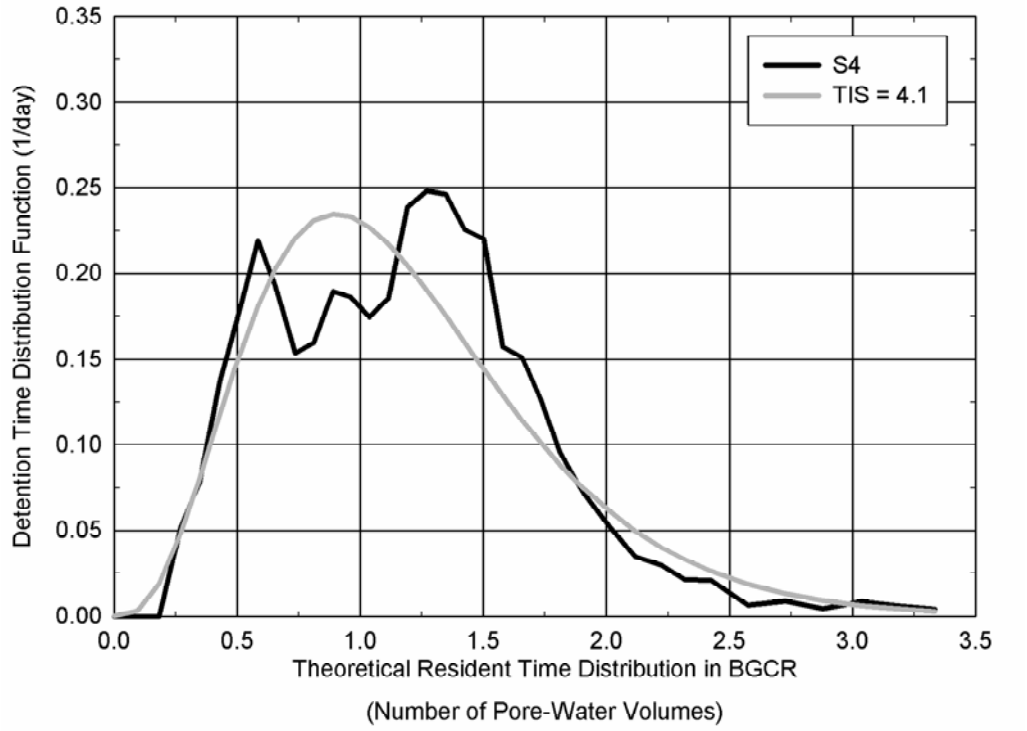

Figure 6.5. The DTD function derived from the tracer study analysis of BGCR S4 and the gamma distribution developed employing 4.1 TIS for the two-component model, which best fit the empirical data (via minimisation of SSQE).

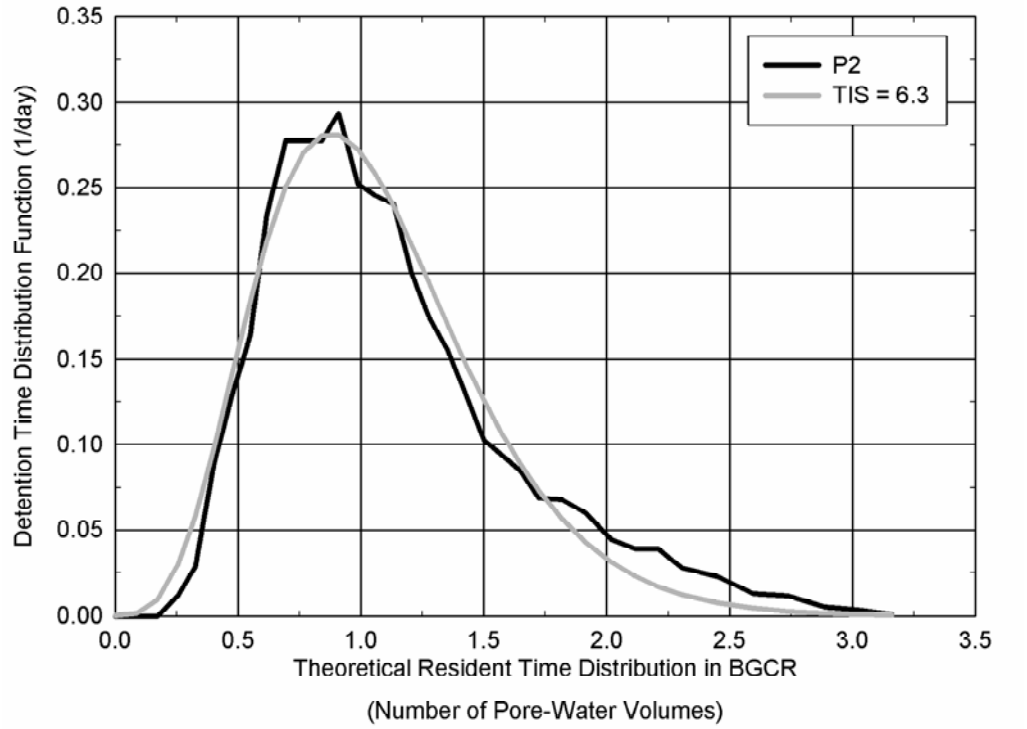

Figure 6.6. The DTD function derived from the tracer study analysis of BGCR P2 and the gamma distribution developed employing 6.3 TIS for the three-component model, which best fit the empirical data (via minimisation of SSQE).

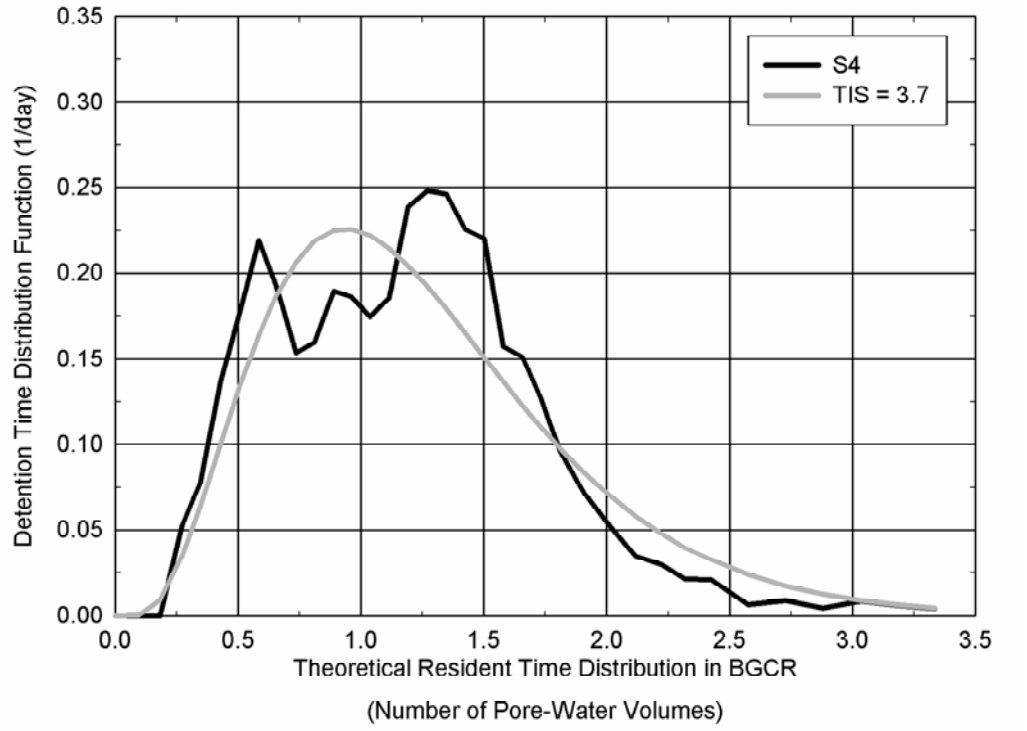

Figure 6.7. The DTD function derived from the tracer study analysis of BGCR S4 and the gamma distribution developed employing 3.7 TIS for the three-component model, which best fit the empirical data (via minimisation of SSQE).

The three-component TIS model fit P2 (Figure 6.6) quite well and better matched the tracer peak and contained a lower SSQE compared with the two-component model (Figure 6.4); however, the TIS model for S4 (Figures 6.5 and 6.7) did not fit the shape of the S4 DTD function and its multiple peaks. Consequently, its SSQE was over five times greater than those calculated for P2. The TIS model for S4 essentially provided an interpolation of the average of the three peaks observed. If only matching the gamma distribution peaks with the observed tracer peaks was applied, the number of TIS were 3.4 for the first peak, 2.0 for the second and 4.7 for the third.

Overall, Kadlec and Wallace (2009) state that most wetland type treatment systems, which are commonly trapezoidal-prism shaped, operate between 3 and 8 TIS. The average number of TIS determined from the Kadlec and Wallace (2009) summary of tracer studies performed for 32 subsurface flow wetlands was 10±7.2 (median of 7.8; range of 2.5-34).

Schwager and Boller (1997) found that tracer studies performed on their downward-flow plate reactors treating sceptic discharge yielded a gamma function response equivalent to five TIS. The flow pattern of these systems would have been comparable to that of BGCR P2, which yielded 5.2 (two-component) and 6.3 (three-component) TIS.

Tanner et al. (2002) performed tracer studies on five upflow VFWs (opposite to the downflow operation of the BGCRs in this study) operated in series treating either high-strength dairy effluent wastewater or pretreated dairy effluent. Their tracer-response curves generally demonstrated a gamma distribution with each tank modelled as two TIS (total of 10 TIS for the five tanks). The shape of the tanks were trapezoidal and comparable to S4. Although ammonia (NH_3) and methane (CH_4) gasses were released from their reactors, the presence of multiple tracer-response or late peaks were not observed like they were for S4. This was likely a result of the upflow operation in which the two-phase gaseous and liquid flow would have occurred in the same direction, whereas in this study, the release of hydrogen sulphide and carbon dioxide gases in the downflow reactors likely resulted in countercurrent two-phase flow. This may suggest that VFWs for treating AMD should be operated as upflow systems to achieve more ideal flow characteristics. Vertical-flow wetlands in mine-water treatment have largely been operated as downflow systems so that an adequate hydraulic head could be maintained to achieve adequate flow through compost predominated substrate (PIRAMID, 2003; Watzlaf et al., 2004); however, the presence of a more permeable substrate mixture such as that used in this study may better facilitate the use of upflow BGCRs as a more pragmatic option.

6.4.5.1 Relevance of Additional Reactor Models

Additional reactor models were considered to determine if their application would better represent the DTD functions of BGCRs P2 and S4 and if they were practical. Kadlec and Wallace (2009) discussed a number of techniques that have been employed for modelling DTD functions of treatment wetlands and other environmental treatment systems. The most commonly applied is the PFR with diffusion model, which can also be applied to DTD function curves; however, the model is physically more applicable to tubular reactors and there is generally no advantage of applying it over the TIS model in systems operating under laminar flow conditions. Additionally, Panuvatvanich et al. (2009) found that the TIS model correlated better with results from tracer studies conducted on VFWs compared with the PFR with diffusion model. Other models such as the parallel paths and finite and infinite stages models can better fit the breakthrough delay and long tails of DTD functions; however, they are of limited use for computing pollutant removal and still maintain the shape of a skewed bell-shaped response like the TIS model (Kadlec and Wallace, 2009). Based on this assessment, the TIS model for P2 is adequate to describe its flow characteristics.

It is plausible to suggest that the TIS model should not be employed for S4 and that another model should be used. For example, Levenspiel (1992) suggested that models can be fit to match variances and to minimise error; however, if the shape is wrong, the model should either not be used or treated with extreme caution. Kadlec and Wallace (2009) even suggest that if DTD functions do not fit the shape of a gamma distribution, then the treatment system configuration requires alteration, not the model. Because there was no uniformity in the tracer peaks for S4 and the largest peak occurred after θ_{BGCR}=1.0, application of models that employ consistent recirculation, exponential decay, multiple

passes through a reactor or combinations of PFR and TIS models incorporating recycle loops are of little practical value. It is likely that the release and rising of gas bubbles within the reactor was arbitrary, as visually observed, and the rates and magnitude of such occurrence would be inconsistent throughout operation. Additional studies would be required to determine the extent barometric pressure influenced the flow hydraulics of the BGCRs. It is possible that during high and steady atmospheric pressure conditions, there is less release of rising gas bubbles and, therefore less internal recirculation. If this hypothesis were correct, it would be expected that there would be less spread in the tracer response curves and TIS modelling would yield a greater number of TIS. It is also possible that the tracer response curve for S4 would better resemble the gamma distribution due to less transport of Br to dead zones within the reactor.

6.4.5.2 Tracer Response Variance, Dispersion Coefficient and Flow DistributionEfficiencies

A summary of the tracer response variances, dispersion coefficients and flow distribution efficiency parameters for BGCRs P2 and S4 are summarised in Table 6.3. The variance of S4 was 1.7 times that of P2, which is a reflection of greater mixing and the late tracer spike observed in S4 (Figures 6.6 and 6.7). The dispersion coefficient was also greater for S4 compared with P2, by 2.24 times, reflecting the greater amount of tracer spreading and deviation from plug flow conditions that occurred in the trapezoidal-shaped reactor. Because TIS modelling yielded a greater number of TIS for P2 than S4, the DTD efficiency was greater for P2 than S4. Although the volumetric efficiency was greater for S4 than P2, the overall hydraulic efficiency was greater for P2 than S4 and likely contributed to the better treatment performance measured from P2 (Chapter 4).

Table 6.3: Summary of the theoretical and mean tracer HRT and flow distribution efficiency parameters and variances for BGCRs P2 and S4.

	BGCR	
Parameter	**P2**	**S4**
Dimensionless Variance – σ_θ^2	0.16	0.27
Variance – σ^2 (day^2)	2.31	4.02
Dispersion Coefficient – D (m^2/s)	4.08E-8	9.12E-8
Volumetric Efficiency – e_v	1.12	1.19
DTD Efficiency – e_{DTD}	0.84	0.73
Hydraulic Efficiency – λ	0.94	0.87

6.4.6 Reaction Rate Kinetics

6.4.6.1 Tanks in Series Modelling

A comparison of the ratio of the effluent and influent Fe, Al and acidity concentrations with the reaction rate constants for BGCRs P2 and S4 are shown in Figure 6.8. The initial four sampling events were not included in this analysis due to the influence of the first flush on treatment performance. The reaction rate constants typically increased with decreasing HRT, as shown in Figure

6.9, and an increasing ratio of the effluent and influent concentrations (Figure 6.8). These trends were especially notable for Al and acidity, but there was a decline in reaction rate constants when system overloading occurred at the lowest HRT (2.0 days) for S4. There was less of a distinct trend for Fe in BGCR S4; however, for P2, there was a decline in the reaction rate constant at the lowest HRTs (2.0 days) indicating system overloading. Similar trends were also observed for BGCRs P1, S2 and S3 (BGCR composition summarised in Table 4.1) if assuming that flow hydraulics were consistent amongst reactor shapes (e.g. 6.3 TIS for drum-shaped reactors and 3.7 TIS for trapezoidal-shaped reactors); however, the reaction rate constants were greater for these BGCRs due to the presence of a higher percentage of mussel shells and better treatment performance. A summary of the reaction rate constants calculated from empirical Fe, Al and acidity data for BGCRs P1, P2, S2, S3 and S4 are presented in Table F.1 in Appendix F.

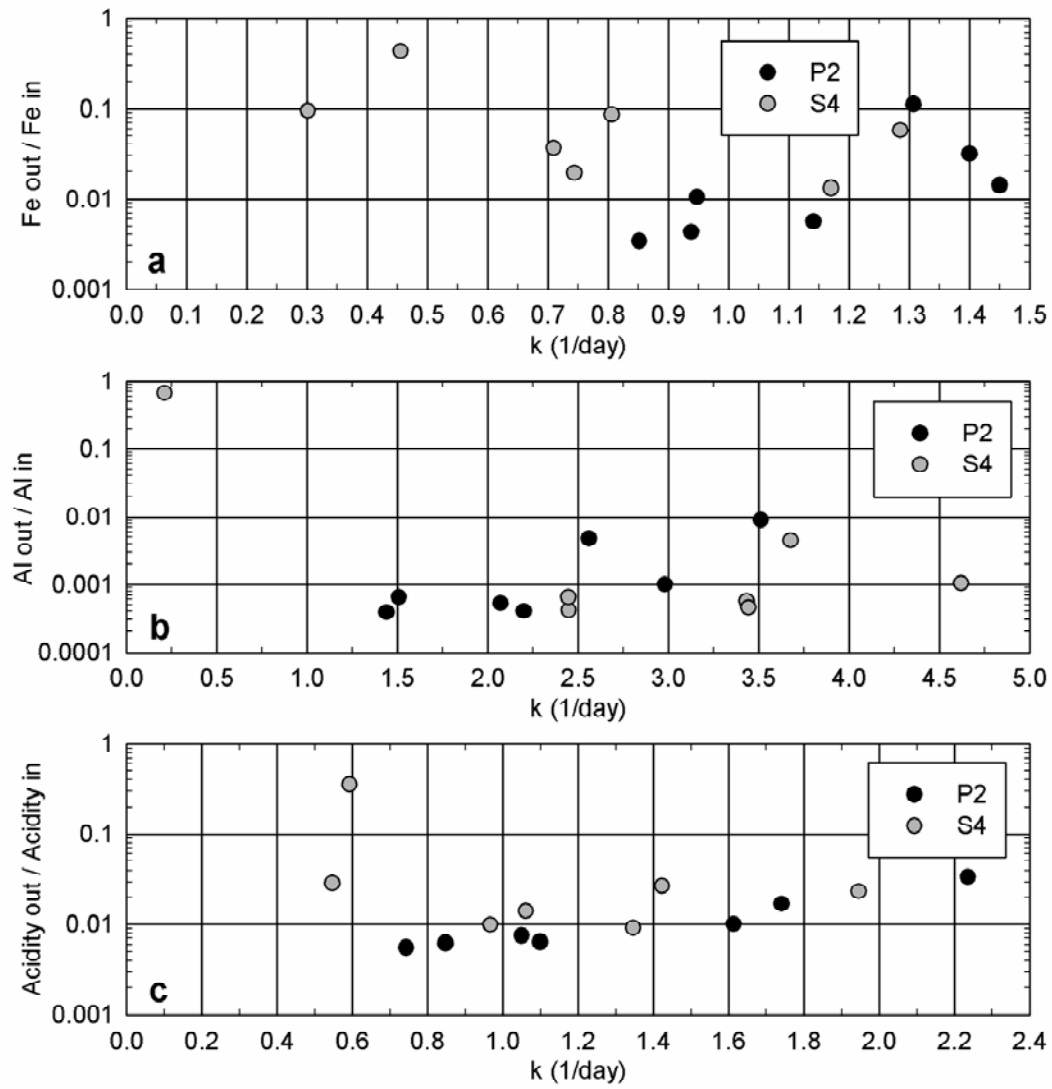

Figure 6.8. A comparison of the ratio of the effluent and influent a) Fe; b) Al; and c) acidity concentrations with the reaction rate constants for BGCRs P2 and S4. Reaction rate constants were calculated using the first-order TIS model assuming 6.3 TIS for P2 and 3.7 TIS for S4.

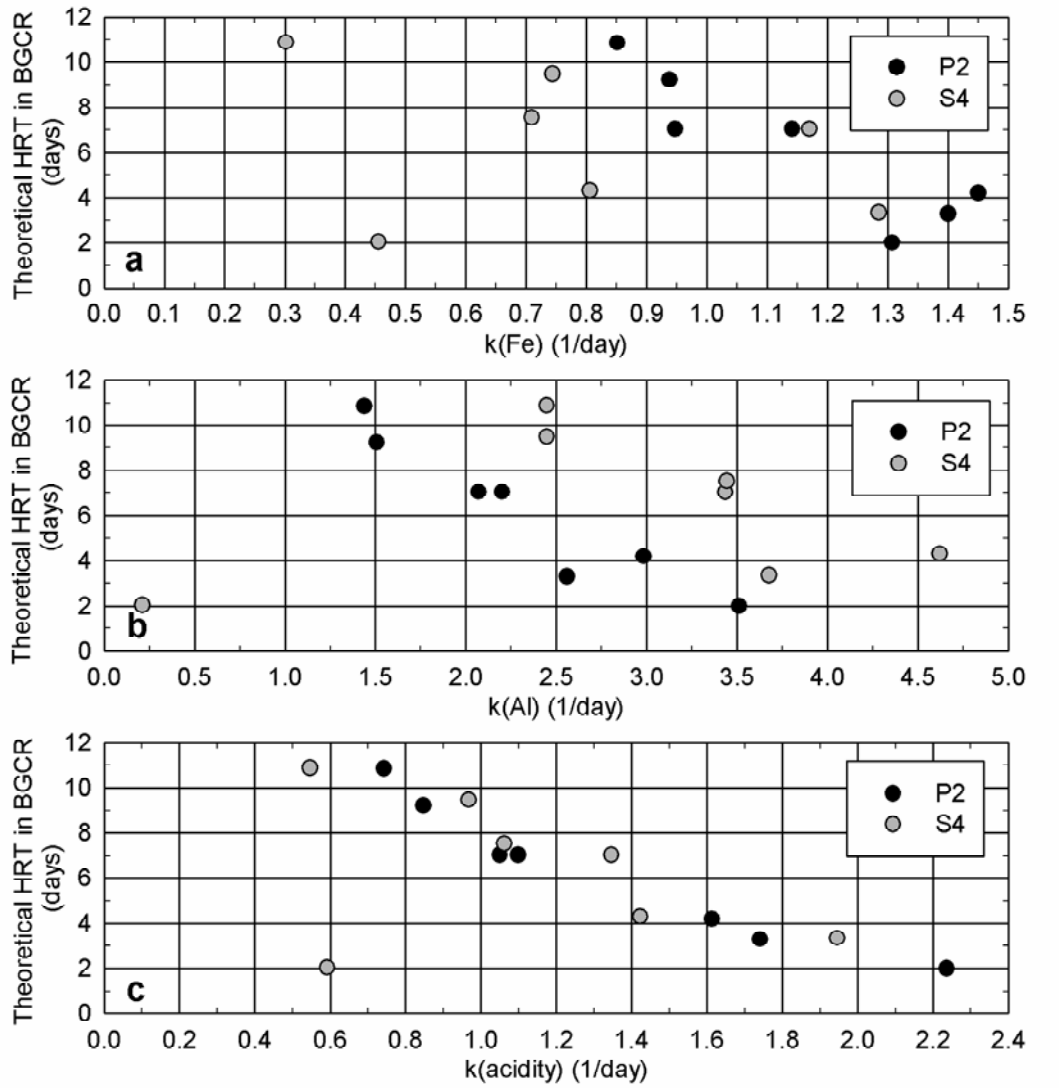

Figure 6.9. A comparison of the ratio of the theoretical HRT in BGCRs P2 and S4 with the reaction rate constants calculated for a) Fe; b) Al; and c) acidity. Reaction rate constants were calculated using the first-order TIS model assuming 6.3 TIS for P2 and 3.7 TIS for S4.

Kadlec and Wallace (2009) stated that reaction rate constants were typically variable for wastewaters containing a mixture of contaminants, which was found for the AMD in this study. This occurs because individual components of mixtures are removed at different rates and, therefore, individually contain different removal rate constants (Crites and Tchobanoglous, 1998; Tchobanoglous et al., 2000; Shepherd et al., 2001; Kadlec, 2003). In this study, Fe removal was less efficient compared with other metals and, consequently, influenced acidity removal (Chapter 4). Reaction rates decline at longer HRTs due to the reduction of some of the contaminant concentrations during the early stages of the HRT (Kadlec and Wallace, 2009).

The range of reaction rate constants calculated suggests that the reaction rate kinetics for P2 and S4 do not follow the first-order TIS model despite results of the tracer study analysis indicating that the flow

conditions in P2 closely resembled the gamma distribution of 6.3 TIS. An alternative reaction order could be considered; however, it is difficult to determine the best reaction order to use when applying the TIS model and computation of reaction rate constants for reaction orders other than one in the TIS model is an exhaustive iterative process that is typically not pragmatic (Weber, 2001). Results of modelling the reaction order or verifying first-order kinetics considering a single CMFR proved inconclusive as a consistent reaction order was not obtained. This was likely attributed to complexities of metal removal mechanisms within the reactors. These include such factors as not all metal removal occurring in the aqueous phase, a likely array of complex biogeochemical reactions occurring at the interface of solid substrate media and increased reaction rates and metal removal in microenvironments where alkaline conditions are most prevalent (e.g. near mussel shells). Under such circumstances, consideration of the relaxed TIS concentration model is recommended (Kadlec, 2003; Kadlec and Wallace, 2009).

6.4.6.2 Relaxed Tanks in Series Concentration Model

A summary of the apparent number of TIS and the reaction rate constants that minimised the SSQE for Fe, Al and acidity removal in BGCRs P1, P2, S2, S3 and S4 are presented in Table 6.4. Data from when the BGCRs were operating under overloaded contaminant conditions were excluded from this analysis (theoretical HRT=2.0 days for Fe, Al and acidity removal from BGCRs S2-S4 and (theoretical HRT=2.0-2.2 days for Fe removal from BGCRs P1 and P2) since they do not represent realistic operating conditions and their inclusion resulted in substantial increases in the SSQE. A comparison of the theoretical HRT with the C_{out}/C_{in} ratios determined from empirical data and the relaxed TIS model for Fe, Al and acidity are presented for these BGCRs in Figures 6.10-6.14.

The number of TIS modelled using the relaxed TIS were quite variable between the reactors as were the reaction rate constants. The relaxed TIS model is essentially an attempt to mathematically relate results of empirical treatability tests by adjusting two fitting parameters: the apparent number of TIS and the reaction rate constants. The apparent number of TIS has no real physical meaning. For example, it does not represent dispersion like the number of TIS derived using the standard TIS model (Equations 6.7 and 6.8) from an empirically derived DTD function. Essentially, the apparent number of TIS is typically reduced from the actual number of TIS derived from a DTD function at the expense of modelling a greater reaction rate constant than actually empirically occurs. Therefore, the relaxed TIS model should be applied and interpreted with caution as the fitting parameters do not physically represent what they are conceptually defined as.

For the drum-shaped BGCRs (P1-P2; Figures 6.10 and 6.11, respectively), the relaxed TIS model typically accurately or under predicted Fe, Al and acidity treatment performance when the theoretical HRT was ≤4.3 days, which represents appropriate operating conditions to achieve metal and acidity removal. For a theoretical HRT ≥7.0 days, the model typically accurately or over predicted treatment

performance. Overall, the relaxed TIS model generally gave a fairly useful prediction of the removal ratio from the drum-shaped BGCRs (Figures 6.10-6.11). The apparent number of TIS was always less than 6.3 (average of 2.1; range of 0.9-2.7), the number of TIS predicted from the tracer studies, as expected.

Table 6.4: A summary of the apparent number of TIS and the reaction rate constants that minimised the SSQE in the relaxed TIS model for Fe, Al and acidity removal in BGCRs P1, P2, S2, S3 and S4. Data from when the BGCRs were operating under overloaded contaminant conditions were excluded from this analysis (theoretical HRT=2.0 days for Fe, Al and acidity removal from BGCRs S2-S4 and (theoretical HRT=2.0-2.2 days for Fe removal from BGCRs P1 and P2) since they do not represent realistic operating conditions and their inclusion resulted in substantial increases in the SSQE.

BGCR	n	Apparent Number of TIS	Reaction Rate Constant (1/day)	Minimised SSQE	Average SSQE per Observation
Fe					
P1	6	1.3	38.3	3.7E-6	6.2E-7
P2		2.3	2.5	4.2E-5	7.0E-6
S2		0.5	129	6.2E-4	1.0E-4
S3		0.4	830	5.4E-4	8.9E-5
S4		0.3	932	5.7E-3	9.5E-4
Al					
P1	7	2.7	6.7	3.8E-7	5.4e-8
P2		2.1	8.8	3.2E-6	4.5E-7
S2	6	3.4	4.4	7.6E-7	1.3E-7
S3		15.5	1.9	9.6E-7	1.6E-7
S4		13.9	2.0	1.1E-6	1.8e-7
Acidity					
P1	7	0.9	49.3	5.2E-6	7.4E-7
P2		1.4	7.2	1.7E-5	2.4E-6
S2	6	0.4	3897	4.3E-5	7.1E-6
S3		0.4	4532	3.4E-5	5.7E-6
S4		0.4	1336	3.4E-4	5.7E-5

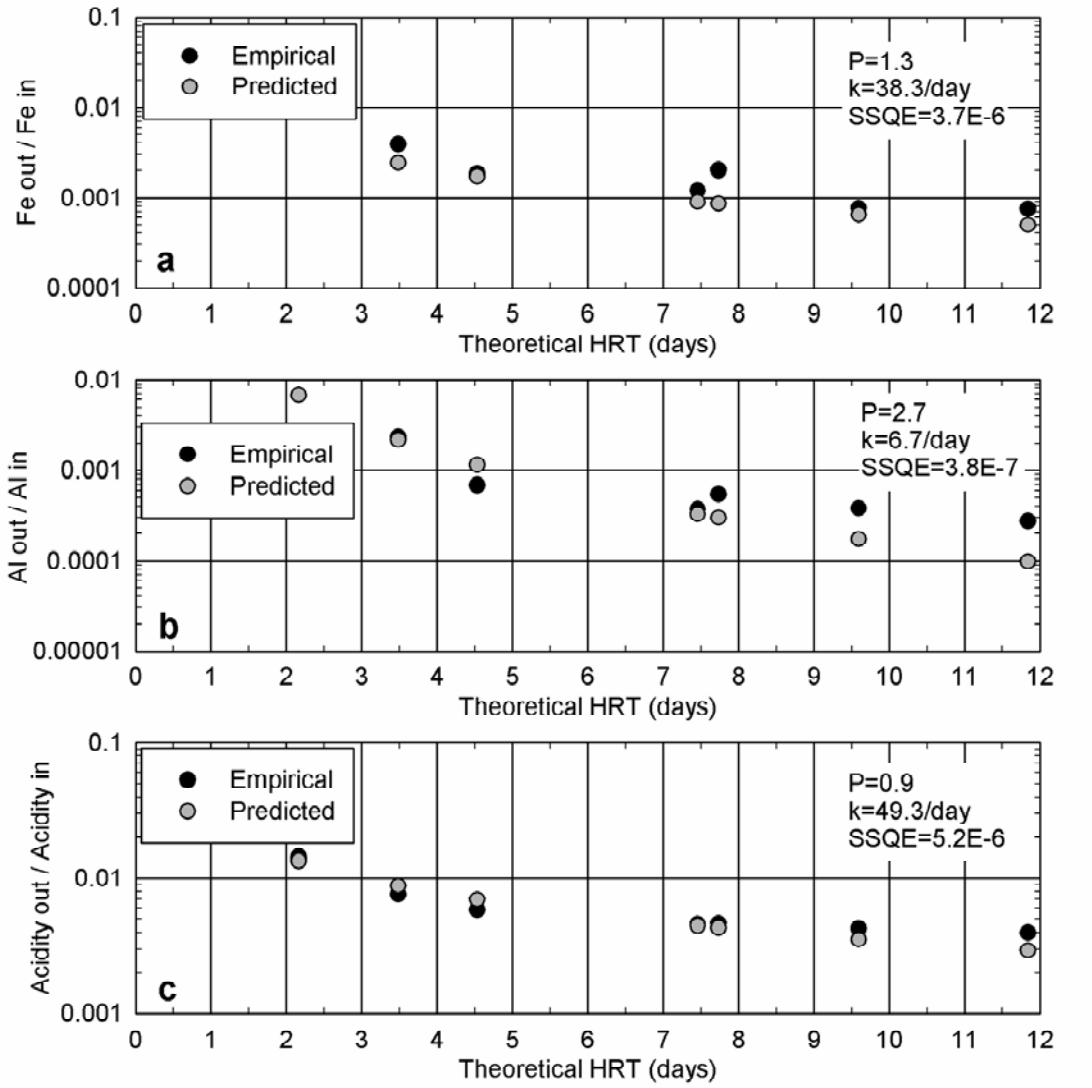

Figure 6.10. A comparison of the theoretical HRT with the C_{out}/C_{in} ratios determined from empirical data and the predicted values computed by minimising the SSQE from the relaxed TIS model for a) Fe; b) Al; and c) acidity for BGCR P1. The data point from the highest Fe loading rate was excluded from this analysis (theoretical HRT in BGCR=2.2 days) because it does not represent realistic operating conditions due to overloading. The apparent number of TIS (P) and the reaction rate constants (k) that resulted in the minimum SSQE are shown on the graphs.

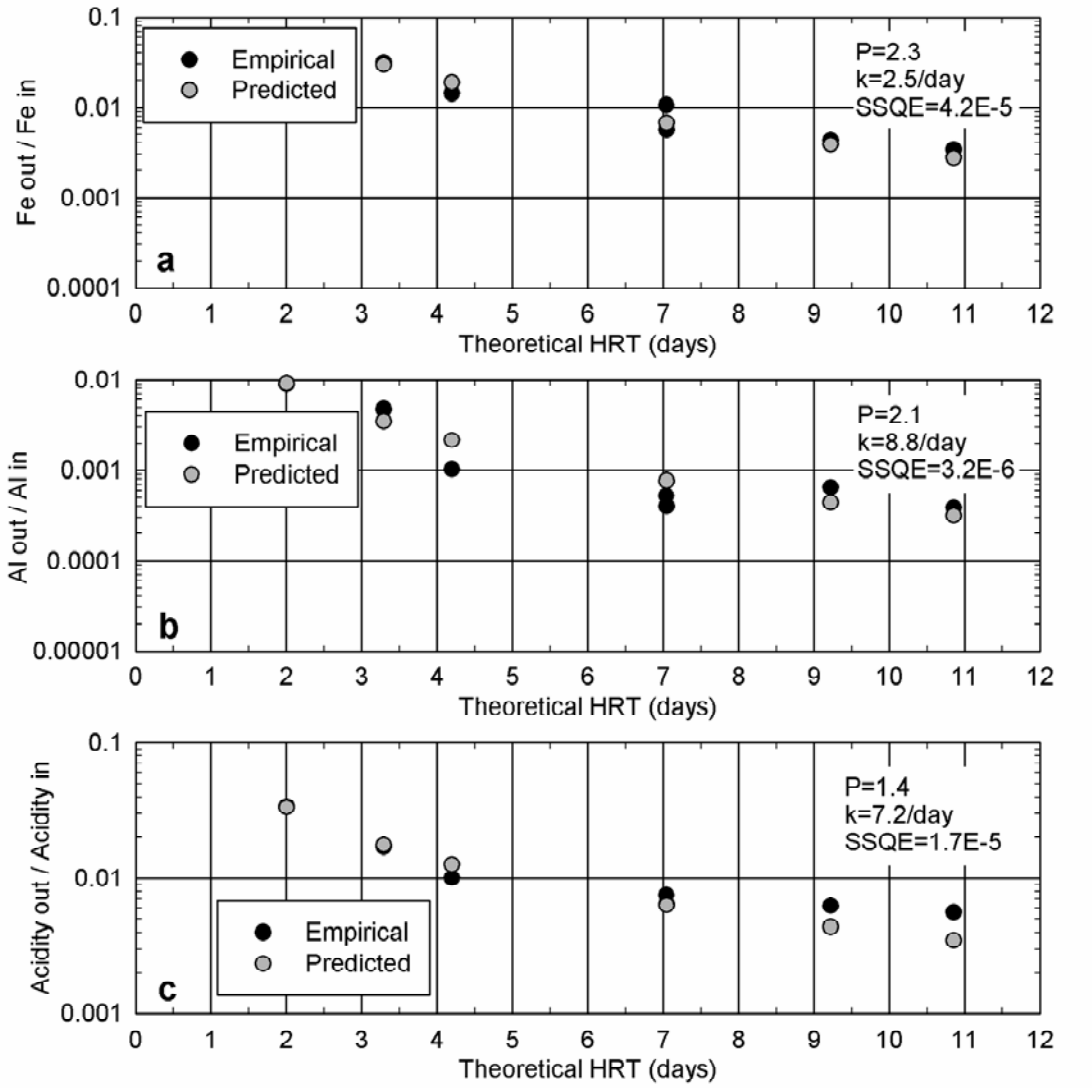

Figure 6.11. A comparison of the theoretical HRT with the C_{out}/C_{in} ratios determined from empirical data and the predicted values computed by minimising the SSQE from the relaxed TIS model for a) Fe; b) Al; and c) acidity for BGCR P2. The data point from the highest Fe loading rate was excluded from this analysis (theoretical HRT in BGCR==2.2 days) because it does not represent realistic operating conditions due to overloading. The apparent number of TIS (P) and the reaction rate constants (k) that resulted in the minimum SSQE are shown on the graphs.

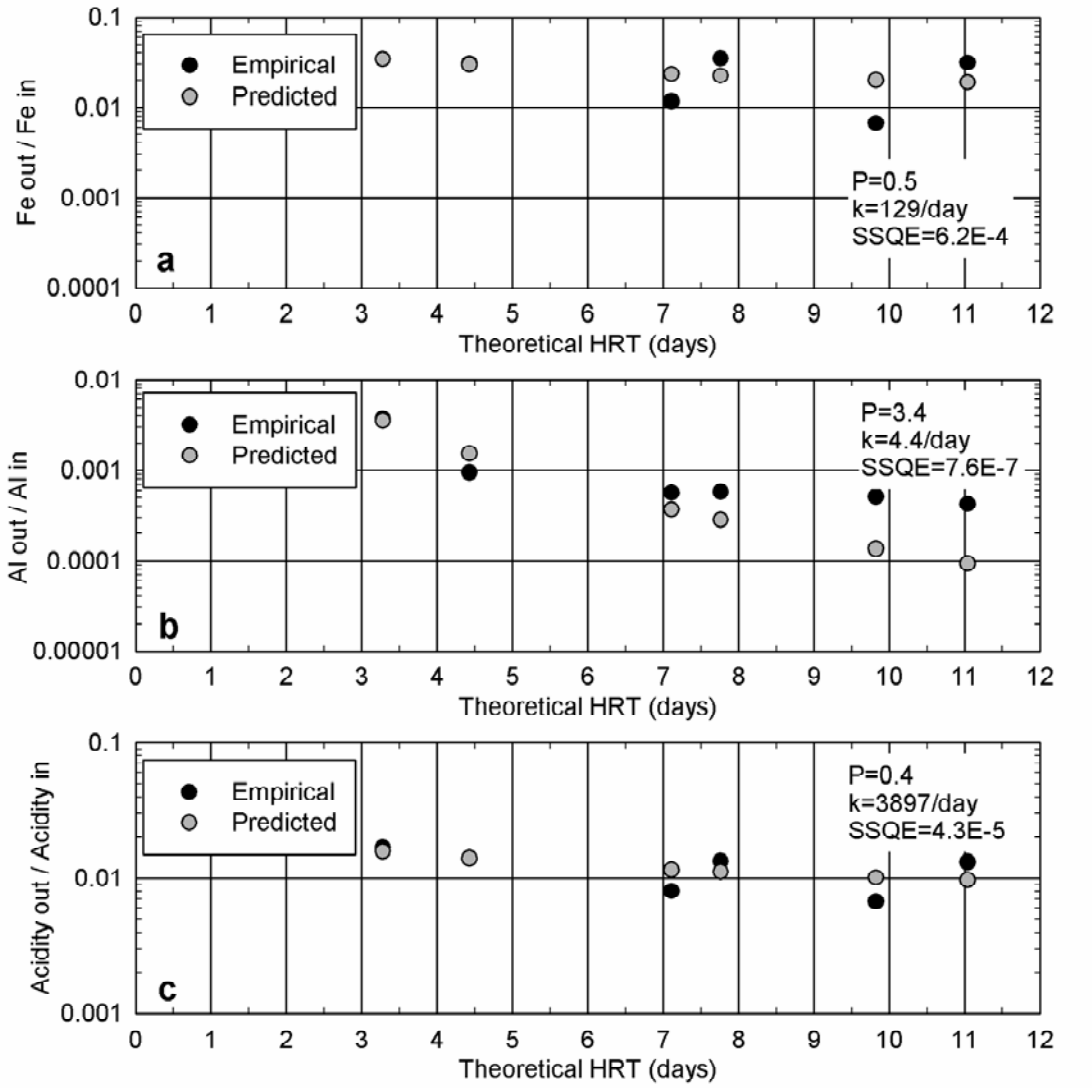

Figure 6.12. A comparison of the theoretical HRT with the C_{out}/C_{in} ratios determined from empirical data and the predicted values computed by minimising the SSQE from the relaxed TIS model for a) Fe; b) Al; and c) acidity for BGCR S2. Data from when the BGCRs were operating under overloaded contaminant conditions were excluded from this analysis (theoretical HRT in BGCR=2.2 days for Fe, Al and acidity removal) since they do not represent realistic operating conditions. The apparent number of TIS (P) and the reaction rate constants (k) that resulted in the minimum SSQE are shown on the graphs.

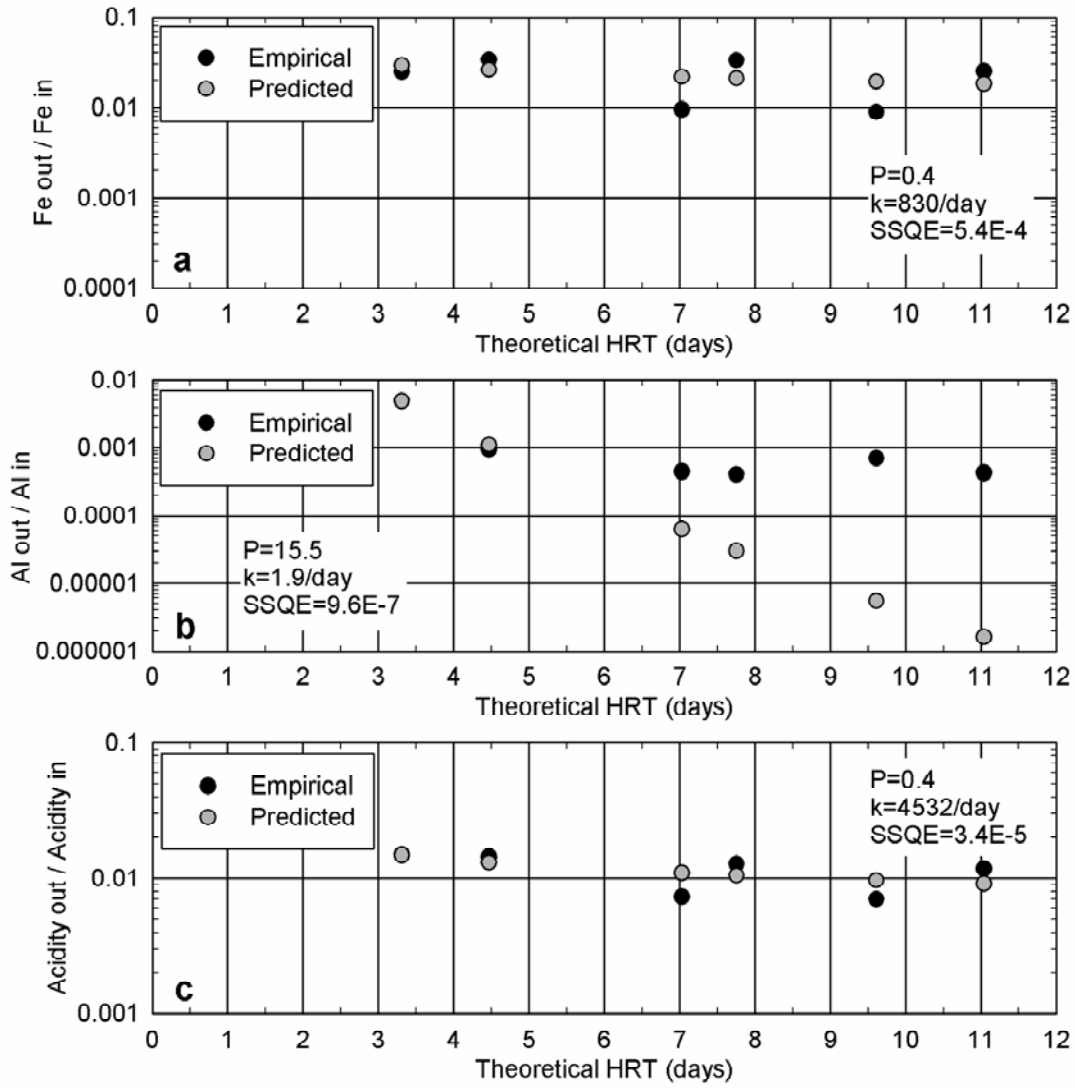

Figure 6.13. A comparison of the theoretical HRT with the C_{out}/C_{in} ratios determined from empirical data and the predicted values computed by minimising the SSQE from the relaxed TIS model for a) Fe; b) Al; and c) acidity for BGCR S3. Data from when the BGCRs were operating under overloaded contaminant conditions were excluded from this analysis (theoretical HRT in BGCR=2.2 days for Fe, Al and acidity removal) since they do not represent realistic operating conditions. The apparent number of TIS (P) and the reaction rate constants (k) that resulted in the minimum SSQE are shown on the graphs.

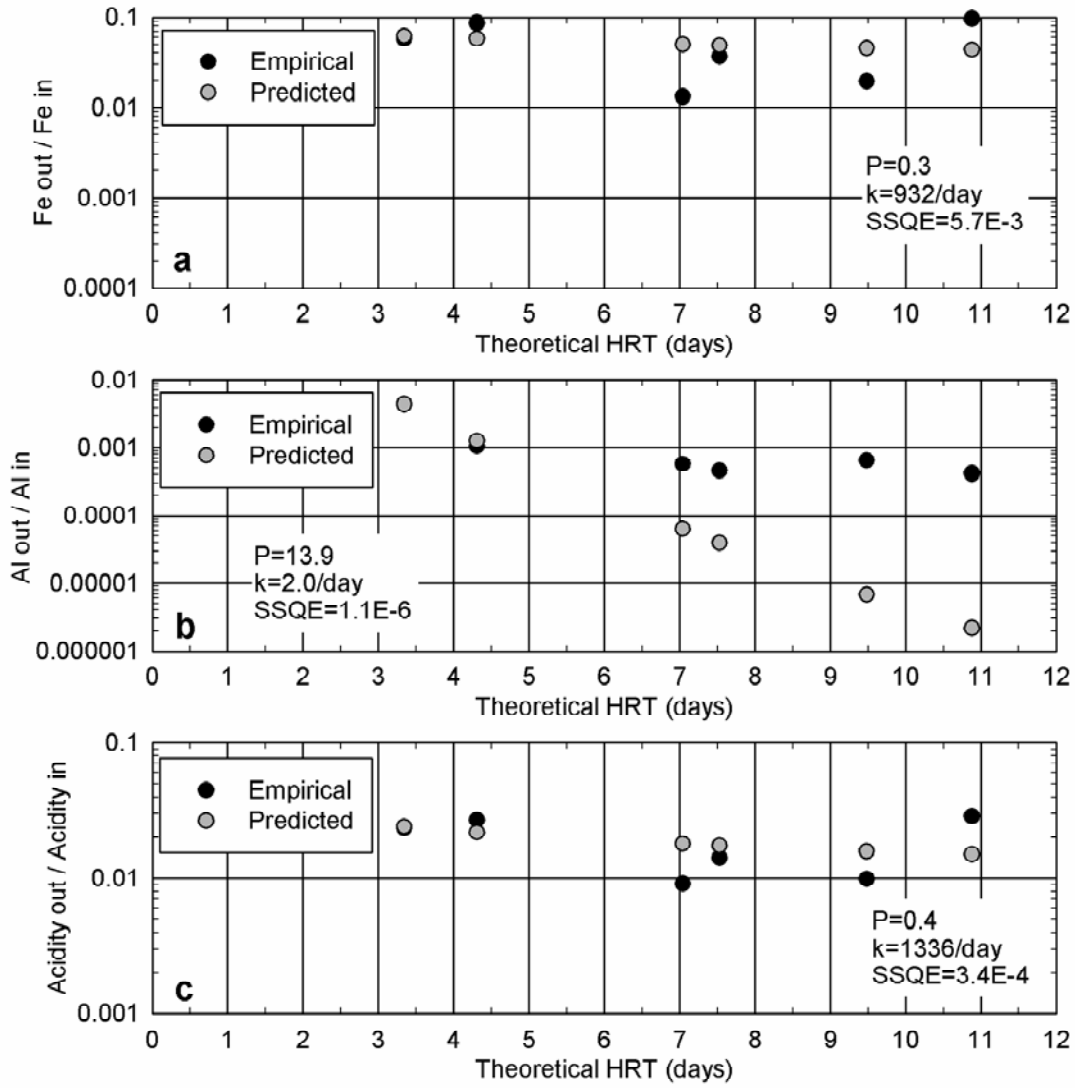

Figure 6.14. A comparison of the theoretical HRT with the C_{out}/C_{in} ratios determined from empirical data and the predicted values computed by minimising the SSQE from the relaxed TIS model for a) Fe; b) Al; and c) acidity for BGCR S4. Data from when the BGCRs were operating under overloaded contaminant conditions were excluded from this analysis (theoretical HRT in BGCR=2.2 days for Fe, Al and acidity removal) since they do not represent realistic operating conditions. The apparent number of TIS (P) and the reaction rate constants (k) that resulted in the minimum SSQE are shown on the graphs.

The relaxed TIS model did not fit the empirical data from the trapezoidal-shaped BGCRs (S2-S4; Figures 6.12-6.14, respectively) as accurately as for the drum-shaped BGCRs (P1-P2; Figures 6.10-6.11) and does not represent a useful method for BGCR design or modelling reactor performance. This is evident by a greater average SSQE per observation (Table 6.4) compared with the drum-shaped BGCRs and the data fits in Figures 6.10-6.14. This was largely attributed to the inconsistent trend of decreasing effluent to influent concentration ratios for a theoretical HRT ≥7.0 days. The apparent number of TIS averaged 0.4 (range of 0.3-0.5) for Fe and acidity. For Al, the relaxed TIS model

overly biased predicted values and minimisation of the SSQE for a theoretical HRT ≤4.5 days and fit the empirical data under these conditions quite well; however, there was a substantial difference between predicted and empirical values at greater theoretical HRTs. There generally was not a substantial difference in the Al effluent to influent concentration ratios when the theoretical HRT was ≥7.0 days (average of 5.1E-4; range of 4.0E-4 to 6.9E-4). The apparent number of TIS for S3 (Figure 6.13) and S4 (Figure 6.14) that yielded the least amount of SSQE were 15.5 and 13.9, respectively, which was substantially greater than the 3.7 TIS calculated from the tracer study. Theoretically, this should not be possible (Kadlec and Wallace, 2009). The relaxed TIS model over predicted Al removal for a theoretical HRT ≥7.0 days with Al effluent to influent concentration ratios one to over two orders of magnitude less than those empirically measured. For S2, the apparent number of TIS that minimised the SSQE was a more realistic 3.4, and the relaxed TIS model better fit empirical data when the theoretical HRT was ≥7.0 days than for S3 and S4. This likely occurred because the effluent to influent Al concentration ratio demonstrated a better decreasing trend with increasing HRT from S2 than S3 and S4.

6.5 Conclusions

Inert tracer study analysis provided useful information regarding flow hydraulics within VFW treatment systems for AMD treatment. Results indicated that the flow hydraulics of cylindrical-shaped reactors commonly employed in bench and mesocosm-scale treatability tests differ quite substantially from those of trapezoidal prism-shaped reactors commonly employed for pilot and full-scale treatment systems. More uniform flow occurred in cylindrical-shaped reactors, which resulted in a tracer-response curve that fit a gamma distribution characteristic of ideal flow characteristics. For the trapezoidal-shaped reactor, the tracer response curve did not fit the gamma distribution pattern indicating non-ideal flow conditions. There were characteristics indicative of short-circuiting, channelised flow paths, eddies and internal recirculation. There was also a greater amount of dispersion measured from the trapezoidal prism-shaped reactor compared with the drum-shaped reactor indicative of greater tracer spreading and deviation from plug-flow conditions.

Further research is required to analyse the influence of barometric pressure changes and gaseous two-phase flow on flow hydraulics and treatment performance of VFWs in mine-water treatment. Results of the tracer study analyses could have potentially differed if the testing was performed under rising barometric pressure conditions instead of declining. Less dispersion and internal mixing would have likely occurred as a result of less countercurrent flow caused by rising hydrogen sulphide and carbon dioxide gas bubbles. It is suspected that the mean tracer HRT would be less than during declining barometric pressure conditions. The spread, or variance, of the DTD curves would likely be less, and the magnitude of the peaks of the curves would also likely be greater resulting in a gamma distribution indicative of a greater number of TIS. There is also the possibility that the DTD curve for trapezoidal-shaped reactors would better emulate a gamma distribution and ideal flow conditions due to less

internal recirculation. Regardless, continuous operation of BGCRs would be subjected to variable atmospheric pressure changes, so a range of flow hydraulic characteristics could be expected.

It may be worthwhile to investigate how operating VFWs as upflow instead of downflow reactors would influence flow hydraulics and treatment performance. In downflow reactors, release of hydrogen sulphide and carbon dioxide creates countercurrent two-phase flow, which results in non-ideal flow patterns including mixing and internal recirculation. In upflow reactors, gaseous release would occur in the direction of flow so ideal flow characteristics would more likely maintained.

Overall, it is worthwhile to perform inert tracer study analysis to understand and improve flow hydraulics and, consequently, increase treatment performance. Application of first-order TIS modelling from the results of tracer study analysis did not yield a consistent reaction rate constant for the BGCRs in this study at the operating conditions tested. It is, therefore, not recommended as a methodology for upscaling the size of VFWs treating AMD, even if results of tracer studies match the TIS gamma distribution. Application of the relaxed TIS model showed promise as a modelling technique for predicting the treatment performance of drum-shaped reactors; however, numerous anomalies were affiliated with the model application for trapezoidal-shaped reactors. Because most pilot and full-scaled VFWs have been and will continue to be comprised of trapezoidal-prism basins excavated into the ground, the rate-removal methods employed in Chapter 4 (e.g. mol metals/m^3 substrate/day) should be used to determine treatment performance and develop design criteria. If cylindrical tanks or vessels are employed as VFWs, the relaxed TIS model may be applicable.

7. Advancing Scaling Challenges Associated with Passive Acid Mine Drainage Treatment Systems

7.1 Purpose and Scope

A phased scaling-up approach is recommended prior to the design, construction and operation of a full-scale staged passive AMD treatment system (Gusek, 2002; Gusek, 2004; Wildeman et al., 2006); however, details regarding this scaling effort are not well demonstrated in the literature. Gusek (2004) recognised challenges regarding the scale up of bench and pilot-scale VFWs to large-scale systems. He suggested that the following issues should be considered: vandalism, seasonal temperature variations, temporal variations in metal loading rates due to variable water chemistry and flow, stormwater influence, minimisation of short-circuits, variability and local availability of substrate materials including organic substrates and gas lock-up. Despite these recommendations, a detailed model of scaling up from the laboratory to the pilot-scale has not been reported. Results from pilot-scale treatability tests treating a portion of MIW *in-situ* provide essential information relevant to full-scale design to treat all of the MIW that may not be possible to assess in laboratory studies. This includes information on compromised treatment performance during cold operating conditions or less efficient flow characteristics and potential hindrances such as excess sediment loading or metal precipitation in piping networks and treatment components (Gusek, 2004; Wildeman et al., 2006; Spangler et al., 2008).

The objective of this applied research chapter relates to bridging the gap between smaller-scale laboratory studies such as the mesocosm-scale BGCRs previously discussed in this thesis (Chapters 4-6) through the development of a physical and experimental model detailing methods for designing, testing and validating the performance of pilot-scale systems. Different design stages comprise the model, which was applied to the Manchester Seep AMD as a prototype since the majority of this research was focused on the passive treatment of this water chemistry. Issues relating to sedimentation, mine site topography, weather (precipitation and temperature), available infrastructure and treatment area and discharge compliance goals were considered since these will determine the effectiveness of any successful model implementation. Although these physical model designs were not implemented, they provide valuable knowledge and a template for other researchers and practitioners to advance scaling efforts in AMD treatment.

7.2 Multiple-Staged Conceptual Treatment Model

The pilot-scale model was designed using water chemistry and flow data from the Manchester Seep (Chapter 2), geotechnical and chemical data from BGCR substrates (Chapter 3), BGCR mesocosm-scale treatability tests (Chapter 4) and flow hydraulics from the tracer study (Chapter 6). This integrated information is required to design effective passive treatment systems such as BGCRs or

similar VFW technologies. The treatment components of the pilot-scale model are shown in Figure 7.1.

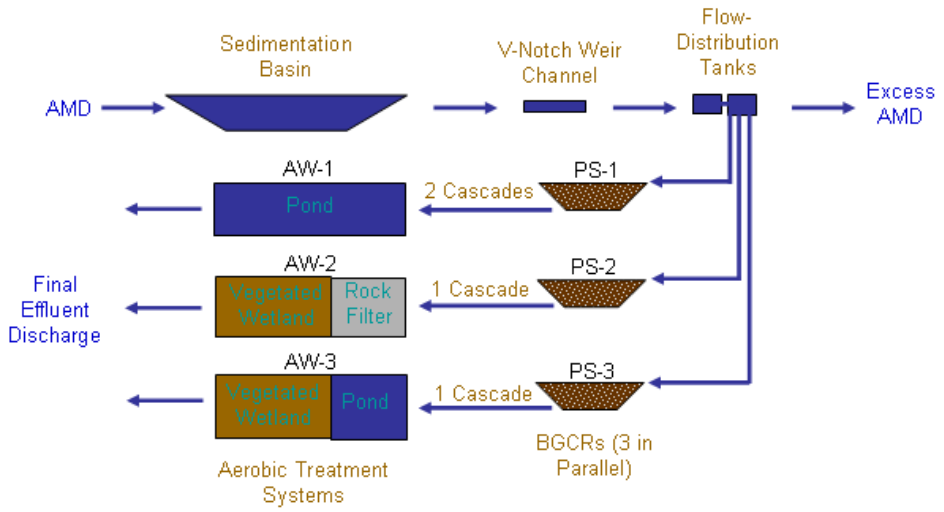

Figure 7.1. Treatment components of the pilot-scale model.

A multiple staged passive treatment approach was employed in the pilot-scale model for treating a portion of the AMD emanating from the Manchester Seeps. Multiple treatment stages comprising an initial sedimentation basin followed by VFWs and aerobic treatment ponds and wetlands are typically utilised in full-scale passive treatment systems (Gusek, 2002; Ziemkiewicz et al., 2003; Watzlaf et al., 2004; Skousen, 2006; Wildeman et al., 2006; Gusek, 2009a; 2009b; Nairn et al., 2009). The initial treatment stage in the proposed model consists of a sedimentation basin designed to capture all Manchester Seep AMD, equalise flow and settle and capture sediment that could otherwise clog subsequent treatment stages. It was considered more practical to use readily available land area in the vicinity of the Manchester Pond as opposed to developing infrastructure to segregate a portion of the Manchester Seep flow. Acid mine drainage discharging from the sedimentation basin is then piped into a v-notch weir channel for flow monitoring. A portion of the flow is piped to flow distribution tanks with excess conveyed untreated into the Mangatini Stream (Figures 1.2 and 2.1) where it is subsequently treated downgradient via the Mangatini fine limestone dosing plant. A portion of the AMD is then conveyed from the flow distribution tanks at controlled flow rates into three BGCRs (PS-1, PS-2 and PS-3) operated in parallel and designed to remove metals, neutralise acidity and reduce sulphate concentrations. These BGCRs, which were analysed on a smaller mesocosm-scale in Chapter 4, represent the primary treatment stage where most contaminant removal occurs. Each BGCR in the pilot-scale prototype model contains different design specifications to assess differences in treatment performance based on substrate composition and substrate depth. Treated effluent from each BGCR is then cascaded into different aerobic treatment stages (AW-1, AW-2 and AW-3) for "final polishing" prior to discharge. The cascades are designed to increase DO. Each aerobic treatment system contains

a different design to evaluate and compare the effectiveness of open ponds, vegetated wetlands and rock filters for final Fe and other residual metal removal.

7.3 Pilot-Scale Treatment System Designs

7.3.1 Sedimentation Basin

Studies report that sediment in MIWs can clog piping and treatment cells, so sedimentation basins are recommended as the first stage of any passive mine-water treatment system (Gusek, 2002; Watzlaf et al., 2004; Wildeman et al., 2006). This is applicable to the Manchester Seep were TSS concentrations (average=298±883 mg/L; median=18.8 mg/L; range=0.51 to 2960 mg/L) were relatively high at times (Chapter 2). Factors such as sedimentation basin size and shape, water temperature and density, particulate size, shape and density, turbulence created by wind and potential bioturbation (although unlikely in AMD) influence particle settling rates and, therefore, sediment removal (e.g. Thibodeaux, 1996; Das, 1998; Building Industry Authority, 2001; Tchobanoglous et al., 2003). The sedimentation basin (Figure G.1 in Appendix G) was designed to capture all surface flow from the Manchester Seep. The flow velocity would be reduced due to the increase in the cross section area perpendicular to the flow at the basin inlet. A velocity barrier could be incorporated to further reduce flow velocity if required. A more detailed description of the design is presented in Appendix G.

Since the Manchester Seep flow is known to be variable like most AMD seeps, a comparison of the particle size that would settle out of suspension at varying flow rates for the sedimentation basin is presented in Figure 7.2. The calculations were based on Stoke's Law assuming a water temperature of 4^{o}C (worst-case scenario) and particle-effective specific gravity and typical sedimentation settling efficiency (Christchurch City Council Waterways, Wetlands and Drainage Guide, 2003). Particle sizes ≥2.73 μm should be removed at the lowest flow rate measured (0.34 L/s; HRT=13.1 days), ≥10.6 μm during the highest flow rate (10.5 L/s; HRT=11.7 hours) and ≥5.79 μm at the average flow rate (2.36 L/s; HRT=2.05 days). Younger et al. (2002) recommended designing for the removal of 4 μm shale particles as robust enough for most mining applications, which is comparable to this design.

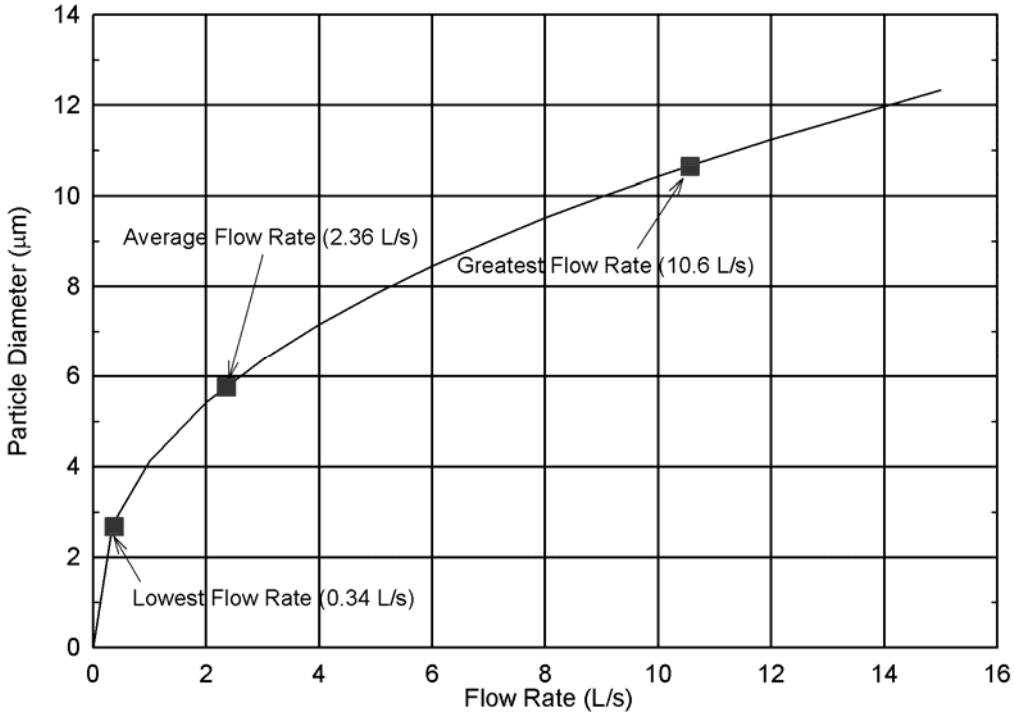

Figure 7.2. A comparison of the particle size that will settle out of suspension at varying flow rates for the designed sedimentation basin.

7.3.2 Flow Monitoring

It is recommended to pipe outflow from the sedimentation basin into a v-notch weir plume so flow can be easily and accurately measured either manually or via deployment of continuous monitoring. Accurate flow rate measurement is important for computing contaminant loading rates (as previously discussed in Chapters 2 and 4) and for hydraulic sizing of a full-scale treatment system and associated overflow diversion structures. The recommended design dimensions of the v-notch weir and associated channel are shown in Figure G.2. A detailed description of recommended construction materials and design are presented in Appendix G. Based on criteria from the International Organisation for Standardization (ISO) 1438 (2008), the v-notch weir channel length should be 6.1 m so that there in no flow turbulence at the weir; however, as a means of reducing material requirements and costs, it is recommended that the channel length is reduced to a length of 2.26 m but contain a plywood barrier near the inlet to reduce flow velocity and turbulence. The weir should be constructed to comply with the limitations recommended by Ackers (1978), Herschy (1999) and the International Organisation for Standardization (ISO) 1438 (2008) including: 1) h= 0.05 to 0.38 m where h represents the hydraulic head above the bottom of the v-notch weir corresponding to flow rates ranging from 0.38 to 60.6 L/s; 2) $P \geq 0.45$ m where P represents the distance from the bottom of the v-notch weir to the bottom of the channel; 3) $B > 1.0$ m where B represents channel width; 4) $h/P \leq 0.4$; and 5) $h/B \leq 0.2$ (see Figure G.2).

The v-notch should be constructed at an angle of 28° 4' and dimensions 190 mm width at top and 380 mm depth. This corresponds to flow rates ranging from 0.38-60.6 L/s as calculated from Equation 7.1.

$$Q\ (L/s) = 347h^{5/2} \quad \textbf{(7.1)}$$

Based on the dimensions shown in Figure G.2, the maximum recommended h/P ratio of 0.4 is achieved at h= 0.300 m, which corresponds to a flow rate of 33.6 L/s. The maximum recommended h/B ratio of 0.2 is achieved at h= 0.240 m, which corresponds to a flow rate of 19.2 L/s, which is nearly twice the maximum measured from the Manchester Seep AMD (10.5 L/s). A comparison of the discharge flow rate versus the v-notch weir head height for a 28° 4' weir is presented in Figure 7.3.

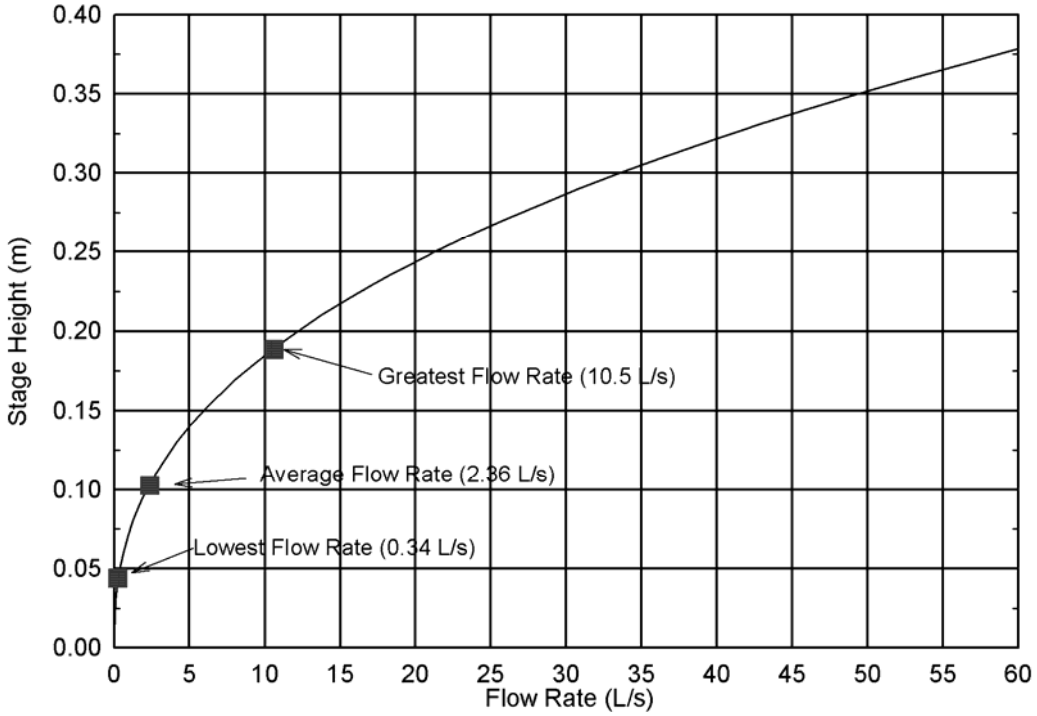

Figure 7.3. Discharge flow rate versus the v-notch weir stage height for a 28° 4' weir.

7.3.3 Flow Distribution

AMD cascading over the v-notch weir should be captured in a box structure and gravity fed through a 50 mm diameter LDPE pipe to the flow distribution tanks, which will allow approximately 2.0 L/s flow depending on final gradients. Excess flow from the box structure should be conveyed into the Mangatini Stream where it would be subsequently treated by the Mangatini fine limestone dosing plant.

A schematic of the recommended flow-distribution system and associated piping is shown in Figure G.3 and described in more depth in Appendix G. Two header tanks are recommended, which are designed to maintain a constant hydraulic head so that consistent flow can be obtained from the outlet

pipes that convey AMD to the subsequent treatment stage consisting of three BGCRs operated in parallel. Flow rates would be controlled by adjusting a clamp that restricts flow in the tubing to emulate a pinch valve. It is anticipated that periodic flushing of the tubing may be required to prevent potential clogging with ferric hydroxide.

7.3.4 Biogeochemical Reactors

The BGCRs represent the primary treatment stage where acidity is neutralised and metals (and some sulphate) are removed (Gusek, 2002; Gusek, 2004; Wildeman et al., 2006). Three BGCRs operated in parallel were designed for the pilot-scale model incorporating different substrate depths (1.0 and 2.0 m) and compost percentages (15 vol.% and 30 vol.%) to test their influence on treatment performance. A summary of the design criteria and substrate composition for each BGCR are shown in Table 7.1. Schematics showing the design dimensions of the pilot-scale BGCRs include: Figure G.4) PS-1; Figure G.5) PS-2a; Figure G.6) PS-2b (alternative flow design incorporating baffles); and Figure G.7) PS-3. An example basin arrangement is illustrated in Figure G.8. A more detailed description regarding system designs are described in Appendix G. The purpose of the bedding material is to achieve good drainage and to encapsulate drainage piping (Figures G.9-G.11) placed at the basin bottom and connected to the outlet control structure (Gusek, 2002; Gusek, 2004; Wildeman et al., 2006). The substrate mixture overlies the bedding material. A post peel layer is recommended to equalise flow and protect the underlying substrate. Its purpose is to provide flow equalisation and minimise short-circuit pathways and other perturbations to the underlying substrate that could potentially result from high intensity precipitation or clogging due to Fe precipitation. Post peel also provides thermal insulation, which should improve treatment efficiency during periods of colder ambient temperatures. The post peel flow equalisation layer is designed to hold 190 mm of rainwater, or roughly the maximum amount of precipitation expected at Stockton Coal Mine in a 24 hour period. The operational water level should be approximately at the top of the post peel or slightly above it (e.g. <0.1 m). A greater freeboard depth is recommended for PS-3 (1.0 m compared with 0.5 m for PS-1 and PS-2) since it contains a higher percentage of compost in its substrate and, therefore, may require a greater hydraulic head due to reduced hydraulic throughput capacity (based on results of hydraulic conductivity tests discussed in Chapter 3 and reported for compost-dominant substrate mixtures in Gusek (2002), Gusek (2004) and Hutchinson and Nairn (2005)).

A greater composition of compost is recommended in one of the BGCRs to determine if the addition of this more labile carbon source, compared with post peel and bark, results in better treatment performance since numerous studies have stated the importance of a labile carbon source in passive sulphate-reducing treatment systems (e.g. Waybrant et al., 1998; Cocos et al., 2002; Gibert et al., 2004; Kaksonen et al., 2004; Gibert et al., 2005a; Hemsi et al., 2005; Zagury et al., 2006). Each BGCR should contain 30 vol.% mussel shells since the best treatment performance was obtained with the BGCRs containing the highest percentage of mussel shells (Chapter 4).

Table 7.1: Proposed design criteria of the three pilot-scale BGCRs. Design metal removal assumes the worst water chemistry measured from Manchester Seeps (sample Manchester-180706B1). Additionally, a 2% safety factor was added to design volume.

	BGCR		
	PS-1	**PS-2a and 2b**	**PS-3**
Design Metal Loading and Flow			
Design Metal Removal (mol Fe and Al/m^3/day)	0.75 (+2% safety factor incorporated into BGCR sizing)		
Flow Rate (L/s)	0.1	0.2	0.1
Material and Freeboard Depths (m)			
Bedding Material	0.2	0.2	0.2
Substrate	1.0	2.0	1.0
Post Peel (Flow-Equalisation Layer)	0.3	0.3	0.3
Freeboard	0.5	0.5	1.0
Substrate Composition (vol.%)			
Mussel Shells	30	30	30
Bark	20	20	15
Post Peel	35	35	25
Compost	15	15	30

The design for PS-2b (Figure G.6) includes utilising a liner to provide a barrier between the post peel and upper substrate layer and another liner that divides the substrate layer at its centre. The liners would act as baffles to reduce the potential of short circuiting within the substrate and thus achieve better metal and acidity removal. Gusek (2004) and Wildeman et al. (2006) reported that gas lock up could be a potential issue in VFWs treating AMD so mitigation measures should be considered to prevent it; However, the BGCRs in this study were more pervious than those discussed in Gusek (2004) containing hydraulic conductivity values three orders of magnitude greater (10^{-3} m/s versus 10^{-6} m/s) so gas lock up would be less likely. The baffles should be sloped at least 2^{o} so that gas bubbles (primarily hydrogen sulphide and carbon dioxide) can rise and be exhumed from the reactor. The outlet pipe should be situated at the top of bedding material beneath the lower baffle to allow gas bubbles to escape the system.

Each BGCR was designed to remove 0.75 moles of Fe and Al/m^3 substrate/day, plus a two percent safety factor, based on the worst water chemistry analysed from Manchester Seeps (sample Manchester-180706B1 discussed in Chapter 2 containing a calculated acidity of 690 mg/L as $CaCO_3$, 106 mg/L total Fe and 36.0 mg/L total Al). The two-percent safety factor accounts for removal of additional metals such as Cu, Ni, Zn, Cd and Pb which contributed ≤2% metal loading. A slightly more conservative design criterion was used than that concluded from results of the mesocosm-scale treatability tests (at 0.8 mol metals/m^3 substrate/day; Chapter 4) to account for potential decreases in treatment performance due to colder temperatures (Gusek, 2004; Wildeman et al., 2006) or water chemistry variability. Based on this design criterion, the theoretical HRT in the prototype field BGCRs would be 4.62 days. Design HRTs determined from the highest loading rates measured

during seep monitoring (Chapter 2) and results of the mesocosm treatability tests employing a design criterion of 0.8 mol metals/m^3/day (Chapter 4) were 3.64 days for the Manchester Seep and 5.00 days for the Manchester Pond outflow (Table 4.14).

The design flow rates for PS-1 and PS-3 (1.0 m substrate depth) are 0.10 L/s, and the design flow rate for PS-2 is 0.20 L/s (2.0 m substrate depth); however, because these are pilot-scale systems that are not designed to treat all Manchester Seep AMD, flow rates into the BGCRs can be reduced or increased as needed to determine the best operational metal loading rates. Gusek (2004), Wildeman et al. (2006), Hedin (2008a; 2008b) and Panuvatvanich et al. (2009) recommend distributing flow over as large of an area as possible to achieve more uniform flow and, hence, more effective treatment performance. This could be accomplished by conveying the AMD into a pipe arrangement containing one inlet tee and four outlet tees that can be adjusted to achieve uniform flow.

7.3.5 Aerobic Treatment Systems

Aerobic treatment systems are commonly employed for oxygenating VFW effluent and removing residual BOD, DOC, nutrients and metals (Wildeman et al., 2006). Therefore, treated effluent from each BGCR should be conveyed into passive aerobic treatment systems for "final polishing" prior to final discharge. The aerobic treatment systems were designed to improve the water quality of BGCR effluent, which is depressed in DO and may contain Fe concentrations or other metals that require further removal (e.g. exceed effluent treatment targets such as those discussed in Chapter 5). Additionally, an aerobic treatment system can remove any excess DOC, BOD or nutrients, albeit these were present in low concentrations in BGCR effluent during the mesocosm-scale treatability tests.

Effluent from the BGCRs should be cascaded into the aerobic treatment systems to provide aeration. Effluent from the BGCR mesocosm-scale treatability tests contained depressed dissolved oxygen concentrations. For example, the average DO concentration from BGCR P1 (Chapter 4), which contained 30% mussel shells, was 0.89 mg/L (range of 0.53-1.49 mg/L). Low DO concentrations, typically less than about 5 or 6 mg/L depending on species, can cause asphyxiation for aquatic life (ANZECC, 2000). Furthermore, the majority of Fe (typically around 95%) in BGCR effluent from the mesocosm-scale studies was in the reduced state as Fe^{2+}. Oxygen is required to oxidise Fe^{2+} to Fe^{3+} and precipitate Fe as ferric hydroxide or other Fe oxyhydroxides (Equation 1.12).

The discharge from each BGCR is designed to be treated via different aerobic treatment systems (AW-1, AW-2 and AW-3 as shown in Figures 7.1 and G.8) to compare the treatment effectiveness of an open (Fe floc) basin (AW-1), vegetated wetland (AW-2) or a combination of the two (AW-3). Designs for AW-1, AW-2 and AW-3 are illustrated in Figures G.13, G.14 and G.15, respectively. A summary of the design criterion and components for each aerobic treatment system are shown in Table 7.2. A more detailed description regarding these designs are described in Appendix G.

Table 7.2: Proposed design criteria of the three pilot-scale aerobic treatment systems.

	Aerobic Treatment System		
	AW-1	**AW-2**	**AW-3**
Aerobic Treatment Cells			
Cell Components	Open Basin	Rock Filter Followed by Vegetated Wetland	Open Basin Followed by Vegetated Wetland
Number of Cascades	2	1	1
Design Removal Rates and Flow			
Design Fe removal	5 mg/L at a rate of 10 $g/m^2/day$		
Flow Rate (L/s)	0.1	0.2	0.1

The aerobic treatment systems are designed as a series of sub-stages to promote the required chemical transformations to achieve treatment goals. The first component of the aerobic treatment systems involves cascading to provide aeration and increase oxygen transfer into BGCR effluent. Subsequent components would provide detention time and target primarily Fe, residual metal and, to a lesser extent, Mn and sulphur removal (due to gas escapement of hydrogen sulphide gas).

The effectiveness of increasing DO concentrations via cascading can be computed as the oxygen transfer coefficient as illustrated by Gulliver et al. (1990) in Equation 7.2 where E represents the oxygen transfer coefficient and C_d, C_u and C_s represent downstream (following cascading), upstream (effluent) and saturated DO concentrations, respectively.

$$E = (C_d - C_u)/(C_s - C_u) \quad \textbf{(7.2)}$$

Baylar and Bagatur (2000) reported that maximum aeration was achieved when the drop height (Figure G.16) was 0.9 m, which is the maximum height where the free-flowing nappe typically does not break apart reducing its penetration depth into the pool. Avery and Novak (1978) found that oxygen transfer efficiency was at its maximum when the tailwater depth (the maximum depth that air bubbles will penetrate (Figure G.16)) was 0.6 times the drop height (e.g. a tailwater depth of 0.54 m for a drop height of 0.9 m). The cascading designs in this pilot-scale model utilised these research findings. If assuming a temperature of 10^{o}C, an oxygen transfer coefficient of 0.41 (from Baylar and Bagatur (2000) for a flow rate of 1 L/s and employing a semi-circular weir) and a BGCR effluent DO concentration of 1 mg/L, a single cascade can increase DO to 5.22 mg/L (AW-2 and AW-3). Implementation of a second cascade could further increase the DO concentration to 7.71 mg/L (AW-2).

Based on effluent concentrations from the mesocosm-scale treatability tests, Fe removal is primarily targeted subsequent to the aeration component of the aerobic treatment systems. An open basin (AW-1) represents the simplest aerobic treatment option from both a construction and operational perspective and treatment occurs primarily via the precipitation and settling of ferric hydroxide precipitates. Vegetated wetlands (AW-2) can additionally sequester Fe by 1) precipitation as sulfides

and oxyhydroxides; 2) binding to soils, sediments, particulates and organics; and 3) plant and algae uptake (Kadlec and Knight, 1996; Kadlec and Wallace, 2009). A rock filter (AW-2) should be considered to evaluate whether algae will grow on it and, if so, assess the increase in DO concentrations and effects on Fe (and Mn) removal. The theory behind implementing an open pond followed by vegetated wetland arrangement (AW-3) is to accumulate the majority of Fe precipitate in the open pond, which can be easily be removed and maintained, and achieve residual treatment through the vegetated wetland as discussed by Hedin (2008a; 2008b).

Design criteria for sizing ponds and aerobic wetlands for Fe removal ranges from an areal loading rate of 10-20 $g/m^2/day$ (Hedin et al., 1994a; Younger et al., 2002; PIRAMID, 2003; Watzlaf et al., 2004). For this study, a design criterion of 10 $g/m^2/day$ was employed and accounts for the areas of the open ponds and vegetated wetlands only. Therefore, no treatment is considered in the areas partitioned to receive the BGCR effluent cascades or the rock filter. The aerobic treatment systems are sized to remove 5 mg/L of Fe. Iron effluent concentrations from the mesocosm-scale treatability tests of BGCRs containing exclusively mussel shells as alkalinity amendments averaged 1.62 mg/L and ranged from 0.05 to 3.79 mg/L during stable operating conditions. The conservative sizing of the aerobic treatment systems accounts for potential less effective treatment from the BGCRs due to colder operating conditions (Wildeman et al., 2006) or less efficient system hydraulics. There is potential that Fe removal would occur within the partitioned areas that receive the cascades and the rock filter. If Fe is removed from these sections at the design criterion of 10 $g/m^2/day$, then there is potential to remove 5.6 mg/L Fe from AW-1 (Figure G.13), 7.4 mg/L Fe from AW-2 (Figure G.14) and 5.8 mg/L Fe from AW-3 (Figure G.15).

7.4 System Operation, Flow Monitoring and Water Chemistry Sampling

Performance monitoring of the pilot-scale treatment systems would be required to determine the effectiveness of the different treatment stages/components. Such issues as site accessibility, available financial resources and equipment availability and robustness can influence the amount of sampling feasible. For example, it would be ideal to conduct continuous monitoring of flow and basic chemical and physical water quality parameters such as temperature, conductivity, pH, turbidity and dissolved oxygen; however, the cost to achieve this may be prohibitively expensive. Sampling frequency must also balance cost and what is required to attain sufficient information regarding treatment effectiveness.

The experimental model recommended for this study, including treatment component sampling locations and recommended analytes to sample for at each location, is summarised in Table 7.3. The purpose for selecting the sampling analytes are summarised in Table 7.4. Chemical and physical water quality parameters most relevant to the various treatment stages are recommended and should be analysed using the same methodology as employed in Chapters 2 and 4.

Table 7.3: Recommended analytes to sample for from the different components of the proposed pilot-scale treatment study. A limited number of parameters are recommended to sample during the first flush from the BGCRs. Sampling for first flush constituents shall cease once their concentrations stabilise.

Sampling Location	Sampling Analytes
Sample Throughout Study	
All (see Sampling Locations Below)	Temperature, pH, Conductivity, Eh, Turbidity, DO and Total Sulphur
AMD Seep	Acid Soluble Metals (Fe, Al, Cu, Ni, Zn, Cd, As, Pb, Mn), Acidity (pH 3.7), Total Acidity (pH 8.3), Cations (Ca, Mg, K and Na) and TSS
Sedimentation Basin Outlet	Same as AMD Seep plus TOC
Effluent from BGCRs PS-1, PS-2 and PS-3	Acid Soluble Metals (Fe, Al, Cu, Ni, Zn, Cd, As, Pb, Mn), Alkalinity (pH 4.5), Cations (Ca, Mg, K and Na), TSS and TOC
Just Downstream of Cascades from AW-1, AW-2 and AW-3 and the Rock Filter in AW-2	Acid Soluble Metals (Fe, As and Mn)
Effluent from AW-1, AW-2, the Iron Floc Basin from AW-3 and the Vegetated Wetland from AW-3	Acid Soluble Metals (Fe, Al, Zn, As, Mn), Alkalinity (pH 4.5), Cations (Ca, Mg, K and Na), TSS and TOC
Sample During First Flush Only (Cease Sampling when Concentrations Stabilise)	
Effluent from BGCRs PS-1, PS-2 and PS-3	Faecal Coliforms, TN, TP, BOD
Effluent from AW-1, AW-2, the Iron Floc Basin from AW-3 and the Vegetated Wetland from AW-3	Faecal Coliforms, TN, TKN, TON (including Nitrate and Nitrite),TP, BOD

Primary sampling locations include the Manchester Seeps, effluent from the sedimentation basin (which is assumed to be equivalent to BGCR influent), effluent from each of the BGCRs and effluent from the aerobic treatment systems. Additionally, sampling for select water chemistry parameters should also be conducted at locations within the various sub-stages of the aerobic treatment systems including the cascades (for all aerobic treatment systems), the outlet of the rock filter in AW-2 and the outlet of the open pond in AW-3.

The sampling frequency proposed is monthly. This would allow for comparisons in treatment results due to seasonal fluctuation and variable loading rates, which are expected based on the variability of water chemistry measured during temporal sampling presented and discussed in Chapter 2. The only exception is that sampling should also be performed at two, four and six weeks of system operation to monitor the first-flush from the BGCRs. Stable water quality parameters would indicate that the first flush has passed. All effluent from the BGCRs should be conveyed into AW-1 until the first flush is completed to minimise risk of harming vegetation.

Table 7.4: Reasoning for analysing for the various sampling analytes.

Sampling Analytes	Purpose for Sampling
Temperature, pH, Conductivity, Eh, Turbidity and DO	Measure changes in basic physical and chemical water quality parameters between treatment stages with portable probes.
Acid Soluble Metals Fe, Al, Cu, Ni, Zn, Cd, As, Pb, Mn	Primary metal contaminants in AMD that require treatment in BGCRs.
Acid Soluble Metals Fe, Al, Zn, As, Mn	Primary metals likely to be detected above laboratory PQLs from BGCR effluent. Concentrations should be reduced within the aerobic treatment systems.
Acid Soluble Metals Fe, As, Mn	Iron and Mn are removed via oxidation, settling and precipitation so concentrations should be reduced as a result of oxidation from the cascades. Arsenic sorbs to Fe and Mn precipitates.
Cations (Ca, Mg, K and Na)	Measure Ca dissolution (primarily from mussel shells) and required for conducting cation-anion balance.
Total S	Measure S (and sulphate) reduction in the BGCRs and S loss through primarily hydrogen sulphide escapement from the cascades and within the aerobic treatment systems.
Faecal Coliforms, TN, TKN, TON (including Nitrate and Nitrite), TP, BOD	Contaminants associated with the first flush from the BGCRs. Sampling should be conducted during first flush conditions until concentrations stabilise. Nitrogen from BGCR effluent can be assumed to be in the form of TKN since it will be in the reduced.
TOC	Labile organic carbon is a required substrate for SRB in the BGCRs. Concentrations in BGCR and aerobic treatment system effluent are expected to decrease with time (due to first flush).
Acidity (pH 3.7) and Total Acidity (pH 8.3)	Primary contaminant and necessary to determine the amount of alkalinity required to neutralise AMD and precipitate metals.
Alkalinity (pH 4.5)	Determine the amount of acidity neutralised by the BGCRs and discharged from the aerobic treatment systems.
TSS	Determine the amount of solids removed by the sedimentation basin, exported from the BGCRs (especially during the first flush) and removed by the aerobic treatment systems.

The initial flow rate into the BGCRs should be set at one-quarter of their design flows so that three pore-water volumes of flow will pass through the substrate in 32 days (an approximate one-month period). This equates to flow rates of 0.025 L/s for PS-1 and PS-3 and 0.050 L/s for PS-2. After six weeks of system operation, the flow rates should be incrementally increased at monthly intervals until the design flow is obtained. For example, influent flow rates into the BGCRs during the following month of operation should be one-half of design flow, increased to three-quarters of the design flow the following month and design flow could be attained during the following and subsequent months of system operation. Results should be monitored throughout the study to verify stable treatment performance. If metal and acidity overloading is suspected, flow should be decreased to that a new design flow and metal loading rates can be established. The longevity of the pilot-scale experiment should cover at least one year to account for seasonal variability.

It is suspected that results of numerous pilot-scale studies reported in the literature assume consistent metal and acidity loading; however, temporal variability of AMD and other MIWs is common (Rose and Dietz, 2002; Cravotta III and Kirby, 2004; Rose, 2004; Skousen and Ziemkiewicz, 2005; Pope et al., 2006) and occurs in Manchester Seep AMD (Chapter 2). Because temporal variability in AMD

chemistry is expected, sampling of the influent AMD should be conducted 0.9-1.4 theoretical HRTs (4.16-5.82 days at design flow rate) prior to sampling BGCR effluent. Maximum tracer concentrations were measured at these HRTs in the reactors used during the mesocosm-scale treatability tests (Chapter 6). Tracer studies such as the one employed and discussed in Chapter 6 could be conducted to validate or refine this assumption. Essentially, calculation of removal rates would be more accurate if staggering the time of sample collection such that effluent samples are representative of the treatment at the influent sample conditions.

The HRTs of the aerobic treatment systems were theoretically computed for AW-1, AW-2 and AW-3 at 12.0 hours, 2.44 hours and 7.66 hours, respectively. This assumes a vegetation porosity of 0.95 (Kadlec and Knight, 1996; Kadlec and Wallace, 2009) and rock filter porosity of 0.35. The aerobic treatment systems were designed on an areal loading basis so the differences in HRT amongst the systems are dependent on their depths (Figures G.13-G.15). Tracer studies would need to be conducted to determine the actual HRT of the aerobic treatment systems. Kadlec and Wallace (2009) report volumetric efficiencies (percentage of actual HRT compared with the theoretical HRT) of surface-flow wetland treatment systems averaging 82±8% (median = 79%; range of 20-256%; n=28); therefore, it is suspected that the actual HRTs within the aerobic treatment systems would be less than theoretically calculated. Ideally, it would be appropriate to collect effluent samples from the aerobic treatment systems at time periods equivalent to the actual HRTs following collection of their influent from BGCR effluent.

Flow monitoring of BGCR influent and effluent should be conducted whenever water samples are collected so that loading rates into the BGCRs and aerobic treatment systems can be calculated. It would be recommended for staff at Stockton Coal Mine to take manual measurements of flow from the v-notch weir channel on a daily basis and to especially target extreme flow events (high and low) to better ascertain its variability unless continuous monitoring is employed. This information should be considered when designing flow and overflow structures for scaling the passive treatment scheme from the pilot-scale prototype to full scale.

7.5 Summary and Discussion

The physical and experimental model discussed and applied to the prototype design provides a robust methodology for determining the effectiveness of passively treating AMD *in-situ* using a staged treatment approach. Monitoring water chemistry and flow from each stage of the pilot-scale study would provide the information necessary to determine the effectiveness of the design criteria used to size each system component. If necessary, design criteria could be adjusted based on the results of the site-specific trial.

7.5.1 Sedimentation Basin

The effectiveness of TSS removal from the sedimentation basin would determine the validity of using particle settling rates derived from Stoke's Law for sediment removal by measuring the reduction in TSS with flow rates. The v-notch would allow for easy and accurate measurement of Manchester Seep flow rates and allow for additional flow data to be collated. The additional AMD water chemistry data, in conjunction with flow monitoring, will allow refinement of the metal and acidity loading rates measured during previously conducted AMD monitoring reported in Chapter 2. This information can be used to increase of decrease the design flow rate proposed in this study if warranted. The maximum flow measured would have implications for sizing a full-scale treatment system to handle the hydraulics associated with the greatest flow event(s) and for designing overflow bypass structures.

7.5.2 Biogeochemical Reactors

Operating BGCRs under the *in-situ* climatic conditions treating variable loading rates would allow for design criterion to be refined if necessary (e.g. decrease in treatment performance during colder operating conditions as determined by Gusek (2004) and Wildeman et al. (2006)). Comparing results of the three BGCRs would allow the best substrate mixture and depth to be selected. It would be important to validate that effluent metal concentrations are comparable to those measured during the mesocosm-treatability test discussed in detail in Chapter 4, which also has implications in determining the design influent concentrations for subsequent aerobic treatment systems. Conducting tracer studies such as the one discussed in Chapter 6 would provide useful information on flow hydraulics, how they might have influenced treatment performance and how they compare with those conducted on the BGCRs used in the mesocosm-scale treatability tests. Increasing metal loading rates and design criterion to values greater than those measured during bench or mesocosm-scale treatability tests conducted in a controlled laboratory environment should typically be avoided because system overloading is more likely to occur and can be catastrophic decimating SRB and potentially causing precipitated metals to redissolve (Gusek, 2004). Treatment performance is often not as effective once an overloading event occurs (Gusek and Wildeman, 2002; Gusek, 2004; Wildeman et al., 2006).

There is potential that there will be differences in the treatment performance from each BGCR employed in the pilot-scale study. Therefore, the influent into each of the aerobic treatment systems could differ making it more challenging to make direct comparisons of the overall treatment performance of each system; however, trends should emerge that give an indication of the effectiveness of each aerobic treatment system design and the various sub-stages employed within each of them. This is especially true with comparing the increase in DO based on utilisation of one or two cascades and how it influences Fe and sulphur removal within the cascades. Aluminium concentrations measured from the effluent of the BGCRs and aerobic treatment systems should be compared with the current resource consent conditions (<1 mg/L Al 99% of the time at the confluence

of the Mangatini Stream and Ngakawau River; monitoring site NR in Figure 2.1)). Although there is no compliance target at Stockton Coal Mine for Fe, it may be prudent to compare these concentrations with regional ecotoxicity data (established at 1-2 mg/L by Harding pers. comm. (2008)). Additionally, effluent metal concentrations can be compared with the ANZECC guidelines and various international water quality guidelines (e.g. those listed in Table 5.1), especially if there are prospects to employ similar systems at locations containing more stringent treatment requirements and/or ecotoxicity.

7.5.3 Aerobic Treatment Systems

Iron removal and increasing DO are the two primary goals of the aerobic treatment systems. Although the aerobic treatment stage may not be necessary to achieve the community agreed treatment target of <1 mg/L Al at the mine site boundary of Stockton Coal Mine (monitoring site NR at the confluence of the Mangatini and Ngakawau Rivers; Figure 2.1), their inclusion was recommended to advance the understanding of residual treatment of the effluent from BGCRs incorporating mussel shells. Design criteria for Fe removal in mine-water treatment applications has been established at 10-20 g/m^2/day for sizing ponds and aerobic wetlands (Hedin et al., 1994a; Younger et al., 2002; PIRAMID, 2003; Watzlaf et al., 2004); however, differences in Fe removal is expected based on such parameters as influent Fe concentrations. Hedin (2008a; 2008b) reports the successful implementation of a series of ponds followed by two aerobic wetlands to treat a circumneutral (average pH=6.2) Fe laden MIW. After one year of operation and monitoring, the average Fe removal rate in the pond array was 26 g/m^2/day and contained an average influent Fe concentration of 74.4 mg/L. The average Fe removal rate in aerobic wetlands was 4.0 g/m^2/day and contained an average influent Fe concentration of 12.1 mg/L. The Hedin (2008a; 2008b) studies showed that Fe removal rates decreased as Fe concentrations and alkalinity declined. If an Fe removal rate of only 4.0 g/m^2/day were achieved in the pilot-scale design proposed in this study, which was based on applying a 10 g/m^2/day design removal rate and a 5 mg/L Fe reduction, the Fe concentration would be reduced 2 mg/L. At this removal rate, Fe concentrations would be <1 mg/L 81% of the time and <3 mg/L 100% of the time based on effluent concentrations from the mesocosm-scale treatability tests (for BGCRs containing mussel shells exclusively as alkalinity amendments) during metal loading rates <0.83 mol/m^3 substrate/day.

Residual Al removal is also important if stricter treatment goals or compliance targets are required. This could also be true for other metals including Cu, Ni, Zn, Cd, Pb and As, albeit they were consistently below or near laboratory PQLs throughout the mesocosm treatment studies and were always below the most stringent ANZECC guidelines (99% level of protection) for metal loading rates <0.83 mol/m^3 substrate/day.

Manganese removal is important if discharge concentrations must comply with ANZECC guideline values for protection of 90% of species or greater (guideline values of 3.6 mg/L for 80% level of protection, 2.5 mg/L for 90% level of protection, 1.9 mg/L for 95% level of protection and 1.2 mg/L

for 99% level of protection). Results from the mesocosm treatability tests (metal loading rates <0.83 mol/m^3 substrate/day) showed an average effluent Mn concentration of 1.91 mg/L (range of 1.11-2.69 mg/L). Design criteria commonly recommended for Mn removal of MIWs using aerobic wetlands is 0.5-1.0 g/m^2/day (Hedin et al., 1994a; Younger et al., 2002; Watzlaf et al., 2004). Based on these removal rates, Mn removal from the aerobic treatment systems should range between 0.25 and 0.50 mg/L. If additional Mn removal is required, a subsequent treatment stage comprised of a LLB would be recommended. Rose et al. (2003) reported typical Mn removal rates of 2-3 g/m^2/day in LLBs with removal rates of 8-17 g/m^2/day reported in some systems. Regardless, if Mn removal is targeted, influent should contain pH>6 and influent Fe and Al concentrations less than about 2 mg/L since Fe oxidation out competes Mn oxidation (Rose et al., 2003; Bamforth et al., 2006).

7.6 Conclusions

The prototype staged pilot-scale treatment system developed for treating Manchester Seep AMD provides useful physical and experimental models that can be applied to bridging the gap of upscaling bench and mesocosm-scale treatability tests conducted in the laboratory to larger pilot-scale studies conducted *in-situ*. Site specific characteristics including land availability, topography, AMD chemistry, flow rates, climatic conditions and treatment requirements impact on the most effective means of designing and conducting a pilot-scale study. Additionally, pilot-scale treatment systems should be more robust and refined than smaller-scale laboratory studies, and system components, including influent and effluent control structures, should emulate those of a full-scale design as much as possible. They should incorporate design components, design criteria and analysis methods that were most effectively employed in the laboratory. They must also contain flexibility to alter influent flow rates in the case of unforeseen treatment performance or AMD variability that deviates from the metal loading rates measured during previous monitoring efforts. Design criteria obtained from reported literature should be considered but applied with caution. Although a standardised design approach for pilot and full-scale passive treatment systems is likely unachievable, reporting systems, models and methods employed during the scaling-up process from the laboratory to field setting and associated treatment results can only advance our understanding.

8. Conclusions and Recommendations

This research represents a comprehensive assessment of passive treatment of AMD in New Zealand and the first in New Zealand to employ predominantly industrial waste products as reactive treatment media. It was also the first internationally to report the use of mussel shells as an alternative to traditional mined limestone for alkalinity generation and acidity neutralisation in organic-based VFWs operating under sulphate-reducing conditions. This has potential application internationally, especially in coastal regions where mussel farming and processing occurs.

This thesis reports research applied to a specific AMD application - AMD from the Manchester Seep at the Stockton Coal Mine. The research employed was progressive with each investigation evolving from previous outcomes. This approach is sensible when considering treatment of any MIW using passive treatment because of variability in MIW chemistry, flow, site topography, substrate materials, available resources and climate.

8.1 Acid Mine Drainage Monitoring

It is important to adequately quantify seasonal mine-water chemistry and loading rates prior to the design and implementation stages of passive treatment. From the 13 AMD sites monitored, mine-water chemistry was highly variable on a spatial and temporal basis (by up to three orders of magnitude for major contaminants) even though all sampling was performed at Stockton Coal Mine. Despite the variability, Fe, Al, acidity and sulphate were consistently the primary contaminants of concern with Cu, Ni, Zn, Cd, Pb, As and Mn considered secondary since they comprised typically <2% of metal loads. Contaminant loading rates need to be known so that the required treatment area can be reliably determined. Available treatment area, site topography, current and planned mining activities or other site disturbances that may alter contaminant loading need to be identified for successful passive treatment.

8.2 Biogeochemical Reactor Performance and Design Criteria

Once a comprehensive assessment of seasonal mine-water chemistry and contaminant loading has been conducted, it is important to choose a passive-treatment option that will most effectively and efficiently treat the MIW. Limestone leaching beds could be employed to treat the most benign AMD (e.g. where maximum Fe and Al concentrations were <10-20 mg/L); however, the focus of this study was on more concentrated AMD so BGCRs were researched in detail.

Substrate materials in BGCRs must provide adequate labile organic carbon for microbial activity and alkalinity generation potential yet contain adequate hydraulic throughput. To decrease capital costs, it is recommended to employ waste products that are cost-effective or free such as the post peel, *Pinus radiata* bark, bark compost and mussel shells employed in this study. Hydraulic conductivity tests confirmed that the substrate mixtures employed in this study provided substantial hydraulic throughput

potential (3-4 L/s/m^2 or 0.6-0.7E-2 L/s/m^3) and would be less likely to clog or form short-circuiting flow paths compared with VFWs that incorporate exclusively compost as a reactive media. The hydraulic conductivities of the substrate mixtures (on the order of 1E-3 m/s) were an order of magnitude greater than the compost used in this study and two to three orders of magnitude greater than compost used in other VFWs reported that were prone to clogging and hydraulic-short circuiting.

Results of mesocosm-scale treatability tests demonstrated that the BGCRs utilising substrate mixtures comprised of economically viable industrial waste products could consistently remove >98% Fe, >99% Al and Cu, Ni, Zn, Cd and Pb concentrations to levels below laboratory PQLs. Sulphate removal was less effective, typically ranging from 12-98%, and dependent on loading rates and DOC. Biogeochemical reactors using mussel shells as an alkalinity amendment performed better than systems using limestone or a mixture of limestone and mussel shells. Reactor shape and associated flow hydraulics influenced BGCR treatment performance. Cylindrical-drum reactors outperformed trapezoidal-prism reactors in terms of contaminant removal. System hydraulics were likely the prominent reason; therefore, for field applications, maximizing BGCR substrate depth and minimizing surface area footprint should be considered to minimise discrepancies between actual HRT and theoretical HRT. An initial first flush of readily dissolvable and mobile parameters including Na, K, Ca, Mg, TN, TKN, TP, TSS, DOC/TOC, BOD and faecal coliforms occurred during the initial stages of system startup. Therefore, managing this first-flush must be addressed. Furthermore, metal removal was not as effective until the first flush was completed after approximately three pore-water volumes.

Most VFWs employed in mine-water treatment consist of trapezoidal-prism basins excavated into the ground. Therefore, it was considered prudent to establish conservative design criteria from this research based on the less effective treatment performance achieved from the trapezoidal-prism reactors compared with cylindrical-drum reactors. The following design criteria are therefore recommended for BGCRs incorporating 20-30 vol. % mussel shells (as an alkalinity amendment) and are contingent on treatment goals (e.g. compliance targets and ecotoxicity criteria): 1) 0.3 mol sulphate loading/m^3/day for sulphate removal (mean of 94%); 2) 0.4 mol metals/m^3/day for metal (mean of 99%) and partial sulphate removal (mean of 46.0% (39.6-57.8%)); and 3) 0.8 mol metals/m^3/day for metal (mean of 98.4% (98.2-98.6%) and minimal sulphate removal (mean of 16.6% (11.9-19.2%)). The sulphate removal rate of 0.3 mol sulphate/m^3/day is comparable to other studies, whereas the metal removal rate of 0.4-0.8 mol metals/m^3/day in this study exceeded typically applied design criteria (for systems incorporating limestone instead of mussel shells) of 0.3 mol metals/m^3/day. On an acidity areal loading basis, a design criterion of 65 g acidity as $CaCO_3$/m^2/day is recommended, which is approximately twice the typically recommended design criteria (for systems incorporating limestone instead of mussel shells) of 25-35 g as $CaCO_3$/m^2/day. The greater metal and acidity design criteria developed from this research were likely a function of faster dissolution of mussel shells,

compared with limestone, and substrate mixtures that achieved more uniform flow. Generally, good metal removal was achieved with effluent pH≥6.65 indicating that pH, and to a lesser extent alkalinity, could be used as a surrogate parameter for determining effective BGCR operational performance.

Application of first-order TIS modelling employing the results of tracer study analysis and mesocosm-scale treatability tests did not yield consistent Fe, Al or acidity reaction rate constants. This was a result of the different species within the AMD being removed at different rates and by different biogeochemical processes. Therefore, TIS modelling is not recommended as a methodology for upscaling VFWs treating AMD, even if results of tracer studies match the TIS gamma distribution. The relaxed TIS model successfully modelled treatment performance of Fe, Al and acidity for cylindrical-shaped reactors but was unsuccessful for trapezoidal-shaped reactors. Because most pilot and full-scaled VFWs have been and will continue to be comprised of trapezoidal-prism basins excavated into the ground, rate-removal methods previously recommended (e.g. mol metals/m^3 substrate/day or g acidity as $CaCO_3$/m^2/day) are better applied to BGCR design, evaluation and operation. If cylindrical vessels are utilised as VFWs, employing the relaxed TIS model may be applicable at the larger field-scale system.

8.3 Implications of a Full-Scale Biogeochemical Reactor

Assuming the primary treatment goal of AMD is metal and acidity removal, design HRTs for a BGCR would be 3.6 days based on the highest metal loading rates measured from the Manchester Seep and 5.0 days based on the highest metal loading rates measured from the Manchester Pond outflow. There is potential to remove an average of 85 kg acidity (as $CaCO_3$), 14.5 kg Fe, 5.26 kg Al and 20.0 kg of total metals on a daily basis from the Manchester Seep and 118 kg acidity (as $CaCO_3$), 17.8 kg Fe, 6.52 kg Al and 24.6 kg of total metals on a daily basis from the Manchester Pond assuming removal efficiencies measured during the mesocosm treatability tests. This equates to 31.1 tonnes acidity (as $CaCO_3$), 5.29 tonnes Fe, 1.92 tonnes Al and 7.30 tonnes of total metals per annum from the Manchester Seep and 43.2 tonnes acidity (as $CaCO_3$), 6.49 tonnes Fe, 2.38 tonnes Al and 8.97 tonnes of total metals per annum from the Manchester Pond.

The most suitable BGCR substrate mixture in this study comprised 30 vol.% mussel shells, 30 vol.% bark, 25 vol.% post peel and 15 vol.% compost. Assuming the worst water chemistry measured from the Manchester Pond, a total substrate volume of 2080 m^3 would be required. For a trapezoidal prism-shaped basin, this would require a total surface area of 2700 m^2 (37.5 m X 72.0 m) assuming 1.0 m substrate depth, 0.2 m depth of bedding material and drainage pipe, 0.5 m freeboard/post peel flow equalisation layer, a length to width ratio of 2:1 (at the upper substrate surface) and 3:1 [horizontal:vertical] basin side slopes. If a substrate depth of 2.0 m is employed (otherwise using the previously mentioned assumptions), a total surface area of 1730 m^2 (30.2 m X 57.4 m) would be required.

Each cubic metre of substrate would neutralise 332 kg of acidity assuming that 19.7% of bicarbonate is generated from sulphate reduction (based on the average determined from BGCRs S2-S4 during the mesocosm-scale treatability tests at the design metal loading rate of 0.8 mol/m^3/day) and the balance is generated from calcium carbonate dissolution from mussel shells. This would result in a total of ≈691 tonnes of acidity neutralised. Based on an average flow rate for the Manchester Seep of 2.29 L/sec and a mean influent acidity of 700 mg/L $CaCO_3$, the anticipated design life of a full-scale BGCR would be approximately 17 years. The design life is based on calcium carbonate dissolution from the mussel shells being the limited factor. Furthermore, there is minimal potential for system clogging from metal precipitates. <10% of the void spaces would be occupied by metal precipitates at the end of the design life.

Capital costs to construct this full-scale BGCR, including material and installation costs associated with the plumbing layer, base course and substrate would be ≈$167,000. Based on cost comparisons conducted by Solid Energy New Zealand Limited, it is estimated that the BGCRs are more cost-effective by over $125/tonne of acidity compared with traditional mechanical lime-dosing ($197/tonne of acidity for BGCRs versus $324/tonne for lime dosing); however, the use of BGCRs is limited to treating AMD exclusively from distinct seeps with flows likely <50 L/sec (or less), so active lime-dosing treatment will still be required to treat the majority of AMD at Stockton Coal Mine. Although there is a margin of error in the construction costs and the performance of the system, a $125/tonne difference indicates these engineered passive treatment systems have merit, and Solid Energy is investigating these options further. There is a potential cost savings of $50,000 over 10 years for treating the Manchester Seep AMD with a BGCR. Numerous seeps exist at Stockton which may also benefit from this technology. Furthermore, Solid Energy New Zealand Limited has successfully incorporated mussel shells into passive treatment systems (e.g. in flow equalisation ponds and "mussel shell leaching beds") at Stockton Coal Mine to generate alkalinity and reduce lime requirements from their lime-dosing plant based on results of this study.

8.4 Further Research Opportunities and Recommendations

Future research would help reveal numerous characteristics of BGCRs and their performance that were not evaluated as part of this study. More detailed analysis of organics and their dissolution kinetics could help advance our understanding on their dissolution from substrate materials and the longevity of this labile organic carbon and their influence on sulphate reduction. A better understanding of the fate of metal and sulphur contaminants within BGCR substrate media and their precipitation processes would help elucidate the biogeochemical transformations that occur and offer a better understanding of system performance and longevity. This study demonstrated that different alkalinity amendments (e.g. mussel shells and limestone) influence treatment performance. Therefore, it would be beneficial to quantify their respective dissolution rates so dissolution kinetics can be mathematically related to treatment performance.

Further research in flow hydraulics within BGCRs would also be beneficial. Inert tracer study analysis showed that the flow hydraulics of the cylindrical-shaped reactors, which are commonly employed in bench and mesocosm-scale treatability tests, differed quite substantially from those of trapezoidal prism-shaped reactors, which are commonly employed in pilot-scale studies and full-scale treatment applications. More uniform flow occurred in the cylindrical-shaped reactors, whereas, non-ideal flow conditions were prevalent in the trapezoidal-shaped reactor indicative of short-circuiting, channelised flow paths, eddies and internal recirculation. Therefore, modelling hydraulic throughput (and its influence on treatment performance) in mesocosm-scale cylindrical-shaped reactors is not valid for direct application to field-scale systems given inherent differences from reactor shape.

Gaseous two-phase flow, which caused internal recirculation and mixing, was suspected in the reactors due to the generation of hydrogen sulphide from sulphate reduction and carbon dioxide from the dissolution of calcium carbonate. The release of these gases was sporadic, based on visual observations of gas bubbles throughout the study and was also suspected to be influenced to some degree by barometric pressure; however, this was not quantified. Measuring gaseous discharge from the BGCRs with respect to barometric pressure changes could help reveal the influence of gaseous formation and release on flow hydraulics. Additionally, repeating the inert tracer studies under different atmospheric pressure trends (e.g. rising versus lowering versus steady conditions) would help discern its influence. When practical, it is possibly better to operate reactors as upflow systems, as opposed to downflow systems, when gasses are produced during biogeochemical transformations to reduce mixing caused by countercurrent two-phase flow.

While this study has demonstrated successful passive treatment of AMD with BGCRs at a mesocosm scale using waste products in the substrate media, there are further considerations required in upscaling to operational-sized systems. Ideally, a BGCR would comprise part of an overall treatment train which would be preceded with a sedimentation pond to capture sediment runoff. The effluent from BGCRS should be "polished" via aerobic wetlands, rock filters or settling ponds to increase DO from BGCR effluent, remove residual metals (e.g. Fe and/or Mn) and reduce faecal coliforms, BOD, nitrogen and other nutrient concentrations, as required, prior to discharge into a receiving water body. It is also recommended to perform pilot-scale studies *in-situ* prior to investing in a full-scale passive treatment system to minimise risk associated with the design and operation of a full-scale system. Passive treatment designs such as the pilot-scale prototype system detailed in this research offer a favourable and cost-effective means of mitigating AMD compared with traditional lime dosing techniques that are inherently resource (e.g. chemical, energy and personnel) intensive. Overall, utilising the waste substrates employed (especially mussel shells) as functional resources offer a more sustainable approach than placing them in a landfill and aligns with recent national policy and legislation (e.g. 2008 Waste Minimisation Bill) that actively promotes reducing waste streams.

9. Peer-Reviewed Research Publications and Conference Presentations

9.1 Peer Reviewed Research Publications

McCauley, C.A., A.D. O'Sullivan, P.A. Weber and D.A. Trumm. 2010. Variability of Stockton Mine and its Treatment Potential with Biogeochemical Reactors. New Zealand Journal of Geology and Geophysics (Special Edition on Acid Mine Drainage in New Zealand). Vol. 53(2-3). pp. 211-226.

McCauley, C.A., A.D. O'Sullivan, M.W. Milke, P.A. Weber and D.A. Trumm. 2009. Sulfate and Metal Removal in Bioreactors Treating Acid Mine Drainage Dominated with Iron and Aluminum. Water Research, Vol. 43(2009). pp. 961-970.

McCauley, C.A., A.D. O'Sullivan, P.A. Weber and D.A. Trumm. 2008. Development of Passive Treatment Systems for Treating Acid Mine Drainage at Stockton Mine. *In*: Proceedings of the 2008 Meeting of the New Zealand Branch of the Australasian Institute of Mining and Metallurgy. Wellington, New Zealand. 31 August 31-3 September 2008. pp. 329-338.

McCauley, C.A., P.A. Weber, D.A. Trumm and A.D. O'Sullivan. 2008. Performance of Mesocosm-Scale Sulfate Reducing Bioreactors for Treating Acid Mine Drainage in New Zealand. *In*: Proceedings of the 2008 Meeting of the American Society of Mining and Reclamation. Richmond, Virginia. 14-19 June 2008. pp. 662-698.

McCauley, C.A., A.D. O'Sullivan, P.A. Weber and P. Lindsay. 2006. Mitigating AMD Impacts in New Zealand Using Engineered Wetlands. *In*: Proceedings of the 7th International Conference on Acid Rock Drainage (ICARD). St. Louis, Missouri. 25-30 March 2006. pp. 1170-1176.

9.2 Conference Oral Presentations

McCauley, C.A., A.D. O'Sullivan, P.A. Weber and D.A. Trumm. 2008. Development of Passive Treatment Systems for Treating Acid Mine Drainage at Stockton Mine. Presented at the 2008 Meeting of the New Zealand Branch of the Australasian Institute of Mining and Metallurgy. Wellington, New Zealand. 31 August-3 September 2008.

McCauley, C.A., P.A. Weber, D.A. Trumm and A.D. O'Sullivan. 2008. Results of Laboratory-Scale Bioreactors for Treating AMD in New Zealand. Presented at the 2008 Meeting of the American Society of Mining and Reclamation. Richmond, Virginia. 14-19 June 2008.

9.3 Conference Poster Presentations

McCauley, C.A., A.D. O'Sullivan, P.A. Weber and D.A. Trumm, A.K. Brough.and M.W. Milke. 2008. Research Initiatives for Developing Passive Treatment Technologies for Ameliorating Acid Mine Drainage in New Zealand. Presented at the Annual Meeting of the New Zealand Branch of the Australasian Institute of Mining and Metallurgy. Wellington, New Zealand, 31 August-3 September 2008.

McCauley, C.A., A.D. O'Sullivan, P.A. Weber and D.A. Trumm, A.K. Brough.and M.W. Milke. 2008. Research Initiatives for Developing Passive Treatment Technologies for Ameliorating Acid Mine Drainage in New Zealand. Presented at the 2008 Meeting of the American Society of Mining and Reclamation. Richmond, Virginia. 14-19 June 2008.

McCauley, C.A., A.D. O'Sullivan, P.A. Weber and P. Lindsay. 2006. Mitigating AMD Impacts in New Zealand Using Engineered Wetlands. Presented at the 7th International Conference on Acid Rock Drainage (ICARD), St. Louis, Missouri. 25-30 March 2006.

9.4 Conference Abstracts

McCauley, C.A., A.D. O'Sullivan, P.A. Weber and D.A. Trumm, A.K. Brough.and M.W. Milke. 2008. Research Initiatives for Developing Passive Treatment Technologies for Ameliorating Acid Mine Drainage in New Zealand. *In*: Proceedings of the 2008 Meeting of the American Society of Mining and Reclamation. Richmond, Virginia. 14-19 June 2008. pp. 699.

Appendix A: Literature Review

Active Treatment Overview

Lime Dosing, Sludge Characteristics and Sludge Management

The most common active processes used for AMD treatment involve lime-dosing (Aube et al., 2006). Lime is relatively accessible and the most cost-effective alkalinity generating material at most mine sites. Lime is typically applied as calcium oxide (CaO) or as a slurry of hydrated calcium hydroxide ($Ca(OH)_2$) (Aube et al., 2006). Alternative sources used for alkaline dosing include a 35% sodium hydroxide (NaOH) solution, 10% sodium hypochlorite (NaOCl) solution, sodium bicarbonate (Na_2CO_3; soda ash), magnesium oxide (MgO; magnesia), magnesium hydroxide (MgOH), potassium permanganate ($KMNO_4$), chlorination (Cl^-), ozonation and ammonia gas (Younger et al., 2002; Tchobanoglous et al., 2003; Aube et al., 2006; Trumm, 2008; 2010). Characteristics of these chemicals including maximum pH attainable, neutralisation efficiency, relative cost and use are summarised in Waters et al. (2003) and Trumm (2008; 2010).

Lime dosing processes typically involve lime addition to an aerated mix tank followed by a reactor tank receiving MIW to raise pH high enough to precipitate metals as hydroxides (Younger et al., 2002; Aube et al., 2006). If Fe and Al are the primary metals of concern, pH is typically raised to about 8.0 depending on treatment goals and other trace metals present. The pH is typically raised to about 9.0 for MIWs containing a wide variety of heavy metals, but may need to be raised to as high as 11.0 for Ni or Cd removal via hydrolysis (Aube et al., 2006). Although lime dosing is effective at removing metals, only up to 10% of sulphate is typically removed (Younger et al., 2002).

Lime feed rates and hydraulic residence time (HRT) in reactors can be adjusted rather easily in a lime dosing plant. Therefore, effluent quality can be relatively easily controlled compared to passive treatment systems. A synthetic polymer is often added to the effluent stream of the lime reactor as a flocculent to promote more efficient precipitation of metals and unreacted lime. Sedimentation and settling of the solids is typically achieved via clarifiers or lamellar plate thickeners to create sludge and reduce effluent turbidity prior to discharge (Younger et al., 2002).

Sludge density of conventional lime-treatment systems is typically low, resulting in high disposal costs and scaling in the reactor. It is more common for active lime treatment systems to incorporate a sludge recycle loop to increase lime efficiency and create a more dense sludge. There are a number of possible arrangements of where to feed recycle sludge. Some possibilities include a lime/sludge mix tank or mixing the sludge directly with AMD in a reactor and conveying effluent from that reactor to a second reactor dosed with lime. Precipitation of metals on existing particle surfaces occurs, which increases particle sizes, densification and particle settling rates. Aeration is typically performed in a

reactor as opposed to a mix tank when designed to create a high-density sludge. The main problem of incorporating sludge recycle is difficultly with pumping due to its high viscosity. Another disadvantage of lime-dosing plants using sludge recycle is higher capital costs incurred.

Sludge formation and its management is standard practice with any process treatment system. Sludge characteristics are affected by raw water chemistry, neutralisation and flocculent reagents and process design. Sludge formed from lime-treatment processes is typically not saleable since it consists of a mixture of metal oxy-hydroxides, carbonates, sulphates, gypsum, calcite, etc. Therefore, it must be managed and disposed of in a stable and controlled environment that ensures it will not leach and negatively impact water quality.

It is typically advantageous from an operations and management perspective to create a high-density sludge instead of a low-density sludge. A low-density sludge consists of a fluffy and amorphous mass containing 1-10% solids (Aube et al., 2006). A high-density sludge contains discrete particles consisting of 15-30% solids (Aube et al., 2006). Less dewatering and storage space is required for a high-density sludge making it is easier and more cost effective to store and transport (Younger et al., 2002).

Sludge characteristics are influenced by AMD chemical signature. Iron and Cu tend to densify well, whereas Al, Zn, Mn and Ni do not (Aube et al., 2006). Total metal concentrations less than 100 mg/L make it difficult to create sludge with at least 15% solids. Sludges produced from waters containing 200 mg/L or more Fe and Cu typically contain more than 20% solids from a high-density sludge process.

Sludge mineralogy is typically an amorphous mass consisting of various metals in oxy-hydroxyl, sulphate and carbonate form, calcite and gypsum as individual crystals and in the amorphous phase, quartz, silicates and sulphides in detrital origin and unreacted lime. Zinc, Cd and Ni are typically the most mobile metals. In general, stable sludge characteristics include high crystallinity and often contain high concentrations of carbonate. Aged sludges are typically more stable (e.g. less likely to leach metals) than “new” sludges produced in process treatment applications because of increased crystallinity.

Most treatment sludges must be mitigated within the context of appropriate waste management regulations; therefore, sludge characteristics influence disposal method. Sludge can become unstable if contacted with moderate levels of acidity so sludge must be disposed of in a manner to ensure long-term stability. Common disposal methods include pond disposal, disposal in mine workings or backfill, stabilisation with additives (such as alkaline industrial waste products), reprocessing (such as smelting), disposal at a landfill, reuse (such as in brick materials, cement manufacturing or agricultural

applications) and reclamation (Aube et al., 2006). The appropriate disposal method depends on sludge characteristics, site-specific considerations, cost, feasibility and long term stability. In general, it is often most cost effective to dispose of sludge on site to minimise additional handling and transport costs.

Other Active Treatment Processes

More problematic contaminants associated with some mine waters require more advanced, and typically more costly, treatment methods. Such contaminants include Na and other dissolved solids and metals such as As and Mo. Common alternative active treatment technologies include membrane filtration and biological sulphate reduction.

Membrane filtration can be subdivided into four separate classes including microfiltration (0.1 to 3.0 μm suspended solids, turbidity, cysts and bacteria), ultrafiltration (0.01 to 0.1 μm suspended solids, colloids, turbidity, cysts, bacteria and viruses), nanofiltration (0.001 to 0.01 μm dissolved solids, hardness, taste, odour, colour and TOC) and reverse osmosis (0.0001 to 0.001 μm dissolved solids such as Na, aqueous salts, pesticides, TOC and other solutes) (Younger et al., 2002; Aube et al., 2006). Feed water requirements for membrane filtration treatment systems include low turbidity (less than 1 nephelometric turbidity units (NTUs) although 0.3 NTUs is commonly recommended) and no oil or grease; therefore, pre-treatment is likely required making these treatment processes more complex and costly.

Sulphate reduction is an effective active-treatment process (and is commonly employed via passive-treatment processes as well) for acidity, metal and sulphate removal. The process is a cost-effective alternative when sulphate, metal and cation concentrations are extremely high (e.g. sulphate greater than 42,000 mg/L, Al greater than 2500 mg/L, Mg greater than 5500 mg/L and other metal concentrations greater than 150 mg/L). Sulphate is reduced to hydrogen sulphide, which is catalysed biologically by SRB (Younger at al., 2002). Metals are subsequently precipitated as metal sulphides. Sulphate is consumed by reacting with metals to form precipitates through the production of hydrogen sulphide gas and elemental sulphur (S^{2-}). Copper can be recovered during the process, which can sometimes subsidise treatment costs. Significantly lower sludge volumes and more dense sludge are produced compared with lime treatment. The process can generate effluent water with removal capabilities of over 90% for sulphate, almost 100% for Al, Cu, Fe, Mn and Zn and over 70% for Ca and Mg.

Arsenic and Mo require specific treatment which typically involves co-precipitation with Fe^{3+}. Arsenic is typically removed as ferric arsenate ($FeAsO_4*xFe(OH)_3$), which is quite stable. An Fe to As ratio of at least three to one is required for efficient removal and long-term stability. Removal rates are considerably improved when arsenic is in the oxidised form as arsenate (As^{5+}) compared with the

reduced form as arsenite (As^{3+}). Therefore, oxidation can improve treatment efficiency and effectiveness. Co-precipitation/adsorption with Fe^{3+} is a consistently cost-effective method for removal of molybdenum as well; however, a polishing pond and sand filter are required to remove excess Fe.

Additional active treatment processes are also available for treating MIWs. These include sorption and ion exchange, solvent, electrochemical and biochemical extraction methods and the barium sulphide process (Younger et al., 2002). Because these processes are quite elaborate and typically not economically feasible, they will not be discussed any further.

Substrate Materials and Alkalinity Amendments used in Sulphate-Reduction Research and Vertical Flow Wetlands

Table A.1: Substrate materials and alkalinity amendments used in sulphate-reduction research and VFWs employed in mine-water treatment including associated references.

Alkalinity Amendments	Reference(s)
Calcite	Gibert et al., 2005a
Crab Shells (Chitin) and Commercially Available Chitin Mixtures of Various Purities	Newcombe and Brennan (2008); Robinson-Lora and Brennan (2008); Venot (2008a; 2008b), Newcombe and Brennan (2009)
Limestone	Waybrant et al. (1998); Gusek and Wildeman (2002); Rose and Dietz (2002); Thomas and Romanek (2002a; 2002b); Ziemkiewicz et al. (2003); Watzlaf et al. (2004); Skousen and Ziemkiewicz (2005); Rose (2006); Buccambuso et al. (2007b); Pahler et al. (2007); Blumenstein et al. (2008); Gusek (2008); Reisman et al. (2008); Smart et al. (2008); Venot (2008a; 2008b)
Mussel Shells	This study; MacKenzie (2010)
Compost	**Reference(s)**
Compost	Gibert et al. (2002)
Conifer Compost	Zagury et al. (2006)
Leaf Compost	Cocos et al. (2002); Zagury et al. (2006)
Spent Mushroom Compost	Hedin et al. (1994a); Chang et al. (2000); Gusek and Wildeman (2002); Rose and Dietz (2002); Ziemkiewicz et al. (2003); Watzlaf et al. (2004); Skousen and Ziemkiewicz (2005); Rose (2006); Newcombe et al. (2008); Robinson-Lora and Brennan (2008)

Table A.1 cont: Substrate materials and alkalinity amendments used in sulphate-reduction research and VFWs employed in mine-water treatment including associated references.

Manure	**Reference(s)**
Animal Manure	Blumenstein et al. (2008)
Cow Manure	Gusek and Wildeman (2002); Logan et al. (2005); Buccambuso et al. (2007b); Pahler et al. (2007); Gusek (2008); Smart et al. (2008); Venot (2008a; 2008b)
Dairy Manure	Reisman et al. (2008)
Horse Manure	Venot (2008a; 2008b)
Manure	Ruiz et al. (2008)
Poultry Manure	Cocos et al. (2002); Gibert et al. (2002); Zagury et al. (2006)
Sheep Manure	Waybrant et al. (1998); Gibert et al. (2002)
Organic Mixtures (Including and Excluding Alkalinity Amendments)	**Reference(s)**
Organic Substrates	Cocos et al. (2002); Logan et al. (2005); Zagury et al. (2006); Figueroa et al. (2007); Ruiz et al. (2008)
Organic Substrates and Limestone	Waybrant et al. (1998); Gusek and Wildeman (2002); Rose and Dietz (2002); Thomas and Romanek (2002a; 2002b); Ziemkiewicz et al. (2003); Watzlaf et al. (2004); Skousen and Ziemkiewicz (2005); Rose (2006); Buccambuso et al. (2007b); Pahler et al. (2007); Blumenstein et al. (2008); Gusek (2008); Reisman et al. (2008); Smart et al. (2008); Venot (2008a; 2008b)
Municipal Compost and Calcite	(Gibert et al., 2005a)
Other Sources	**Reference(s)**
Ash	Perez-Lopez et al. (2007); Gusek (2008)
Magnetite Sand (Fe_3O_4)	Blumenstein et al. (2008)
Organic-Rich Soil	Chang et al. (2000)
Pyrolox (MnO_2)	Blumenstein et al. (2008)
Zero-Valent Fe	Pahler et al. (2007); Blumenstein et al. (2008)

Table A.1 cont: Substrate materials and alkalinity amendments used in sulphate-reduction research and VFWs employed in mine-water treatment including associated references.

Plant Derived (Excluding Wood Products)	**Reference(s)**
Alfalfa	Logan et al. (2005)
Corn Stover	Buccambuso et al. (2007b); Figueroa et al. (2007); Ruiz et al. (2008)
Hay	Gusek and Wildeman (2002); Buccambuso et al. (2007b); Pahler et al. (2007); Blumenstein et al. (2008); Gusek (2008); Reisman et al. (2008); Smart et al. (2008)
Leaf Mulch	Waybrant et al. (1998)
Oak Leaf	Gibert et al. (2002)
Rice Hulls	Gusek (2008)
Sphagnum Peat Moss	Zagury et al. (2006)
Walnuts	Logan et al. (2005)
Walnut Shells	Figueroa et al. (2007); Ruiz et al. (2008)
Sludges	**Reference(s)**
Anaerobic Digester Fluid	Chang et al. (2000)
Sewage	Waybrant et al. (1998)
Wastepaper Recycling Plant	Chang et al. (2000)
Wood Products	**Reference(s)**
Cellulose	Waybrant et al. (1998)
Conifer Sawdust	Zagury et al. (2006)
Decayed Wood	Smart et al. (2008)
Sawdust	Waybrant et al. (1998); Thompson et al. (2000); Gusek and Wildeman (2002); Pahler et al. (2007)
Spent Oak Chips	Chang et al. (2000)
Wood Chips / Waste	Waybrant et al. (1998); Chang et al. (2000); Cocos et al. (2002); Gusek and Wildeman (2002); Zagury et al. (2006); Pahler et al. (2007); Blumenstein et al. (2008); Gusek (2008); Reisman et al. (2008); Smart et al. (2008)
Simple Liquid Organics and Oils	**Reference(s)**
Ethanol (C_2H_5OH)	Kaksonen et al. (2004); Zagury et al. (2006); Buccambuso et al. (2007b); Venot (2008a; 2008b)
Sodium Lactate ($C_3H_5O_3Na$)	Elliot et al. (1998); Ingvorsen et al. (2003); Ross et al. (2003); Kaksonen et al. (2004); Robinson-Lora and Brennan (2008)
Sodium Acetate (CH_3COONa)	Webb et al. (1998); Ingvorsen et al. (2003)
Propionic Acid (CH_3CH_2COOH)	Webb et al. (1998)
Glycerol ($C_3H_5(OH)_3$)	Webb et al. (1998)
Sodium Glucose ($C_6H_{12}O_6Na$)	Ingvorsen et al. (2003)
Sucrose ($C_{12}H_{22}O_{11}$)	Lloyd et al. (2004)
Molasses	Annachhatre and Suktrakoolvait (2003)
Soybean Oil	Ross et al. (2003)

Open Limestone Channels Performance Examples

Cravotta and Trahan (1999) evaluated three OLCs receiving AMD from an abandoned coal mine. Iron and Al effluent concentrations were reduced to <5% of influent AMD, which ranged from 0.6-4.0 mg/L, and pH increased from 3.5 to 6.2. Manganese, Pb, Cu, Co, Ni and Zn concentrations were also reduced due to sorption and coprecipitation with hydroxides in these systems at pH>5. Miller et al. (2006) found Zn and Ni removal as high as 97 and 87%, respectively, in a laboratory-scale OLC receiving a synthetic mine water. Removal effectiveness was a function of Fe^{3+} concentrations with Zn removal reaching a saturation point at a Fe:Zn concentration ratio of 50:1 and Ni removal reaching a saturation point at a Fe:Ni concentration ratio of 45:1. Their study also concluded that Zn and Ni removals were greater than would be suggested by "ideal" equilibrium chemistry due to co-precipitation and sorption onto primarily ferric hydroxide surfaces.

Skousen and Ziemkiewicz (2005) evaluated the performance of ten OLCs. Removal efficiencies ranged from 0-121.1 g acidity/day/US ton of limestone, with most systems removing 15-20 g acidity/day/US ton of limestone. Crovotta et al. (2004) evaluated the alkalinity generation of two OLCs. Influent into one of the OLCs contained pH values ranging between 4.3 and 5.3. Effluent pH was typically between 6 and 7 and alkalinity between 20 and 190 mg/L as $CaCO_3$. The second OLC influent typically contained a pH of about 3.5. Effluent pH was typically between 6 and 7 during the first two years of operation but declined to values between 4 and 5 after four years of operation. Effluent alkalinity during the first year of operation was 60-140 mg/L as $CaCO_3$ but declined after five years of operation to a range of 0-25 mg/L as $CaCO_3$. Alkalinity generation decreased with time as limestone was consumed.

Slag Leaching Beds and Surface Catalysed Oxidation of Ferrous Iron Reactor Performance Examples

Simmons et al. (2002) used dams constructed of slag to remediate AMD leaching from mine spoils that contained a pH between 3.7 and 3.9, an average acidity (presumed to be calculated) of 26 mg/L and average Fe, Al and Mn concentrations of 0.6 mg/L, 3.6 mg/L and 3.3 mg/L, respectively. Initial effluent was caustic with a pH of 11.6. Within four months, the effluent stabilised at a pH of 9.0 and an alkalinity of 30 mg/L as $CaCO_3$. Excess alkalinity intersected and neutralised AMD seeps further downstream, which caused metals to precipitate within the stream.

Iron concentrations were reduced from 5 mg/L to <0.5 mg/L in unsaturated SCOOFIs (Jarvis and Younger, 2001). Saturated flow SCOOFI reactors are only suitable for waters containing sufficient DO and Fe concentrations <50 mg/L. Unsaturated flow SCOOFI reactors do not require influent water to contain DO since O_2 is readily available in pore spaces, so DO is generated within the reactor (PIRAMID, 2003).

Bowden et al. (2006) investigated the use of "basic oxygen steel slag" in removing Fe (2-5 mg/L) in circumneutral mine water. Results of saturated flow pilot-scale tests indicated mean Fe removal of 80% regardless of slag particle size (20-100 mm) and, consequently, media surface area. Iron removal rates were approximately 16 $g/m^3/day$. A decrease in hydraulic conductivity was noted in reactors containing slag of the 20 mm particle size.

Sapford et al. (2006; 2007) developed a pilot-scale and low footprint vertical flow reactor that utilised SCOOFI mechanisms (e.g. sorption and precipitation of Fe flocs). The reactor utilised a commercially available bespoke steel panelled tank where ferric hydroxide was allowed to accumulate on top of a gravel bed in a configuration that could be easily maintained. The technology was proven appropriate for treating circumneutral mine waters with average total Fe concentrations of 7.2 mg/L to concentrations <1 mg/L with an areal requirement of 66 m^2 to treat 1 L/s. Assuming all Fe was removed, areal removal rates were 9.4 g $Fe/m^2/day$ (not reported by the authors) or 8.1 g $Fe/m^2/day$ if effluent Fe concentrations were 1.0 mg/L. This corresponds to three times the removal efficiency measured at the same project site for passive treatment utilising lagoons and an aerobic wetland.

Limestone Dissolution Models in Anoxic Limestone Drains and Performance Examples

Crovatta (2002) proposed a method for evaluating sizing and longevity of ALDs utilising first-order decay equations. Mukhopadhyay et al. (2007) found that limestone dissolution was better modelled using pseudo-first order kinetics based on laboratory experiments conducted over a four-month time frame. Cubitainer® (Hedwin Corporation (2007)) experiments described by Watzlaf and Hedin (1993) can be used to determine the expected alkalinity generated by an ALD using a specific mine water and limestone. Crovatta (2003) and Crovatta et al. (2004) describe rate models developed using cubitainers® including limestone armoured with thin coatings of ferric and aluminium hydroxide

Hedin et al. (1994b), Faulkner and Skousen (1995), Ziemkiewicz et al. (2003) and Skousen and Ziemkiewicz (2005) describe performance of full-scale operational ALDs. All systems raised the pH of MIWs and alkalinity was typically increased by 150-300 mg/L as $CaCO_3$, with a maximum increase of 469 mg/L in 21 systems assessed. Iron and Al concentrations decreased between the influent and effluent indicating precipitation of hydroxides within the systems. In the 11 systems described by Faulkner and Skousen (1995), calculated acidity was reduced by 50-80% from MIWs containing acidity of 170-2200 mg/L as $CaCO_3$. Labar et al. (2008) reported alkalinity generation of 400-500 mg/L as $CaCO_3$ in discharge from a vertical ALD (VALD) constructed in an abandoned mine air shaft. Although the HRT was 2.5 to 3.5 times the typically recommended 15 hours, ionic strength was the principle determining factor (at 80%) contributing to alkalinity generation in their study. The increased alkalinity generated in their study compared with others was attributed to greater ionic strengths due to elevated concentrations of sulphate (median 7842 mg/L) and Na (median 1893 mg/L)

compared with most mine waters (e.g. Watzlaf et al. (2004) reported maximum concentrations of 1100 mg/L sulphate and 712 mg/L Na in their assessment).

Appendix B: Variability of Stockton Coal Mine Acid Mine Drainage Chemistry and Its Feasibility for Passive Treatment

Table B.1: Results of water chemistry measured from the Whirlwind Tributary A Seep from January to March 2006 (n=2 or 3).

	Mean	Median	Min	Max
Physical-Chemical Parameters				
Temp (^oC)	11.4	11.3	10.8	12.0
pH	--	3.13	2.86	3.16
Eh (mV)	716	712	677	760
Conductivity (µS/cm)	380	352	307	481
Specific Conductance (25^oC) (µS/cm)	514	483	408	651
DO (mg/L)	8.65	8.33	8.12	9.49
DO (% sat)	79.7	77.5	74.5	87.1
Acidity and Alkalinity (mg/L as $CaCO_3$)				
Calc Acidity	151	--	148	153
Acidity (pH 3.7)	80	85	43	111
Total Acidity (pH 8.3)	165	165	145	186
Alkalinity (pH 4.5)	--	--	--	--
Total Metals (mg/L)				
Fe	7.42	--	5.77	9.07
Fraction Fe^{3+}	0.54	--	0.45	0.64
Al	16.5	--	15.7	17.3
Cu	0.0075	--	0.0072	0.0077
Ni	0.0641	--	0.0634	0.0647
Zn	0.245	--	0.240	0.249
Cd	0.00067	--	0.00062	0.00071
Pb	0.0041	--	0.0035	0.0047
As	<0.001	--	<0.001	<0.001
Mn	0.983	--	0.925	1.04
Dissolved Metals (mg/L)				
Fe	5.59	--	4.91	6.26
Al	17.9	--	17.9	17.9
Cu	0.0079	--	0.0068	0.0090
Ni	0.0663	--	0.0631	0.0695
Zn	0.267	--	0.256	0.278
Cd	0.00075	--	0.00064	0.00085
Pb	0.0037	--	0.0031	0.0042
As	<0.001	--	<0.001	<0.001
Mn	1.11	--	0.940	1.27
Solids				
Turbidity (NTUs)	5.82	--	3.52	8.12
TSS (mg/L)	--	--	<3	5.00
TDS (mg/L)	302	317	271	319
Salinity (ppt)	0.3	0.3	0.2	0.3
Cations and Anions (mg/L)				
Na	3.73	3.56	3.27	4.35
K	2.26	2.17	1.97	2.63
Mg	5.42	5.44	4.25	6.57
Ca	5.94	5.82	3.19	8.80
Hardness (mg/L as $CaCO_3$)	37.1	36.9	25.5	49.0
SO_4^{2-}	222	227	190	249

--, data parameters not measured or non-applicable.

Table B.2: Results of water chemistry measured from the outlet of Pond A1 from the Whirlwind Tributary A Seep from January-March 2006 (n=2 or 3).

	Mean	Median	Min	Max
Physical-Chemical Parameters				
Temp (^oC)	13.5	11.6	11.5	17.4
pH	--	3.14	3.11	3.37
Eh (mV)	712	724	664	747
Conductivity (µS/cm)	335	345	235	426
Specific Conductance (25^oC) (µS/cm)	426	464	317	498
DO (mg/L)	9.15	9.32	8.39	9.75
DO (% sat)	89.2	89.8	85.4	92.5
Acidity and Alkalinity (mg/L as $CaCO_3$)				
Calc Acidity	123	--	98	148
Acidity (pH 3.7)	60	65	39	77
Total Acidity (pH 8.3)	144	131	125	175
Alkalinity (pH 4.5)	0.62	--	0.42	0.82
Total Metals (mg/L)				
Fe	5.60	--	3.99	7.21
Fraction Fe^{3+}	0.62	--	0.42	0.82
Al	16.5	--	12.5	20.4
Cu	0.0083	--	0.0070	0.0095
Ni	0.0681	--	0.0555	0.0807
Zn	0.210	--	0.167	0.253
Cd	0.00046	--	0.00045	0.00047
Pb	0.0057	--	0.0046	0.0067
As	<0.001	--	<0.001	<0.001
Mn	1.057	--	0.984	1.13
Dissolved Metals (mg/L)				
Fe	2.89	--	2.66	3.11
Al	15.3	--	12.2	18.3
Cu	0.0073	--	0.0066	0.0079
Ni	0.0685	--	0.0588	0.0782
Zn	0.216	--	0.185	0.247
Cd	0.00044	--	0.00039	0.00049
Pb	0.0019	--	0.0017	0.0021
As	<0.001	--	<0.001	<0.001
Mn	1.12	--	0.972	1.26
Solids				
Turbidity (NTUs)	143	38.6	1.71	390
TSS (mg/L)	91.0	--	27.0	155
TDS (mg/L)	254	242	217	304
Salinity (ppt)	0.2	0.2	0.2	0.2
Cations and Anions (mg/L)				
Na	3.06	3.08	2.74	3.35
K	1.42	1.48	1.17	1.62
Mg	6.14	6.22	5.09	7.11
Ca	4.53	4.64	3.94	5.00
Hardness (mg/L as $CaCO_3$)	36.6	35.5	32.5	41.8
SO_4^{2-}	190	190	178	203

--, data parameters not measured or non-applicable.

Table B.3: Results of water chemistry measured from the outlet of Pond A2 from the Whirlwind Tributary A Seep from January to March 2006 (n=1 to 3).

	Mean	Median	Min	Max
Physical-Chemical Parameters				
Temp (^oC)	13.8	12.2	11.7	17.6
pH	--	4.05	3.46	4.31
Eh (mV)	644	654	620	657
Conductivity (µS/cm)	89.3	38.3	20.7	209
Specific Conductance (25^oC) (µS/cm)	107	51.3	27.4	243
DO (mg/L)	9.19	9.50	8.38	9.69
DO (% sat)	88.7	88.5	88.4	89.2
Acidity and Alkalinity (mg/L as $CaCO_3$)				
Calc Acidity	6.39	6.39	3.81	8.97
Acidity (pH 3.7)	--	<1	<1	29
Total Acidity (pH 8.3)	24	11	6	55
Alkalinity (pH 4.5)	<1	--	--	--
Total Metals (mg/L)				
Fe	7.29	--	2.72	11.9
Fraction Fe^{3+}	0.72	--	0.47	0.97
Al	5.46	--	3.27	7.65
Cu	0.0051	--	0.0024	0.0079
Ni	0.0054	--	0.0052	0.0057
Zn	0.020	--	0.019	0.022
Cd	--	--	<0.00005	0.00006
Pb	0.0295	--	0.0066	0.0524
As	0.007	--	0.003	0.010
Mn	0.104	--	0.103	0.105
Dissolved Metals (mg/L)				
Fe	0.09	--	0.05	0.13
Al	0.459	--	0.200	0.718
Cu	0.0007	--	0.0006	0.0009
Ni	0.0033	--	0.0014	0.0052
Zn	0.018	--	0.007	0.029
Cd	--	--	<0.00005	0.00005
Pb	0.0004	--	0.0003	0.0005
As	<0.001	--	<0.001	<0.001
Mn	0.0621	--	0.0309	0.0934
Solids				
Turbidity (NTUs)	--	137	8.64	>1000
TSS (mg/L)	160	--	81	240
TDS (mg/L)	56.2	33.7	17.6	117
Salinity (ppt)	0.1	0.1	0.0	0.1
Cations and Anions (mg/L)				
Na	1.70	1.13	0.95	3.02
K	0.63	0.63	0.35	0.90
Mg	1.21	0.49	0.20	2.95
Ca	0.80	0.42	0.16	1.82
Hardness (mg/L as $CaCO_3$)	6.99	3.07	1.22	16.7
SO_4^{2-}	40.2	22.5	7.0	91.1

--, data parameters not measured or non-applicable.

Table B.4: Results of water chemistry measured from the Whirlwind Tributary C Seep from January to March 2006 (n=1 to 3).

	Mean	Median	Min	Max
Physical-Chemical Parameters				
Temp (^oC)	13.0	13.6	10.1	15.3
pH	--	3.73	3.66	3.80
Eh (mV)	680	663	657	720
Conductivity (µS/cm)	141	152	94.5	176
Specific Conductance (25^oC) (µS/cm)	180	194	132	215
DO (mg/L)	9.00	9.24	8.15	9.60
DO (% sat)	85.5	82.5	81.5	92.5
Acidity and Alkalinity (mg/L as $CaCO_3$)				
Calc Acidity	36.6	--	27.3	45.9
Acidity (pH 3.7)	<1	--	--	--
Total Acidity (pH 8.3)	43	46	28	55
Alkalinity (pH 4.5)	<1	--	--	--
Total Metals (mg/L)				
Fe	2.26	--	0.53	3.98
Fraction Fe^{3+}	0.49	--	--	--
Al	5.51	--	5.15	5.86
Cu	0.0058	--	0.0053	0.0063
Ni	0.0295	--	0.0239	0.0350
Zn	0.109	--	0.076	0.141
Cd	0.00040	--	0.00028	0.00052
Pb	0.0036	--	0.0015	0.0057
As	<0.001	--	<0.001	<0.001
Mn	0.528	--	0.451	0.605
Dissolved Metals (mg/L)				
Fe	0.38	--	0.31	0.44
Al	4.52	--	3.22	5.82
Cu	0.0047	--	0.0038	0.0055
Ni	0.0291	--	0.0213	0.0369
Zn	0.118	--	0.071	0.165
Cd	0.00041	--	0.00027	0.00054
Pb	0.0011	--	0.0007	0.0014
As	<0.001	--	<0.001	<0.001
Mn	0.555	--	0.418	0.691
Solids				
Turbidity (NTUs)	59.2	12.2	7.41	158
TSS (mg/L)	62.5	--	4.00	121
TDS (mg/L)	102	91.3	86.3	127
Salinity (ppt)	0.1	0.1	0.1	0.1
Cations and Anions (mg/L)				
Na	3.03	2.75	2.45	3.90
K	1.47	1.62	1.17	1.63
Mg	2.76	2.88	2.13	3.27
Ca	3.87	4.32	2.80	4.48
Hardness (mg/L as $CaCO_3$)	21.0	22.6	15.8	24.7
SO_4^{2-}	76.6	85.0	48.1	96.8

--, data parameters not measured or non-applicable.

Table B.5: Results of water chemistry measured from the Whirlwind Tributary D Seep from January to March 2006 (n=1 or 3).

	Mean	Median	Min	Max
Physical-Chemical Parameters				
Temp (^oC)	12.8	--	11.3	14.2
pH	--	--	3.61	3.72
Eh (mV)	710	--	702	717
Conductivity (µS/cm)	136	--	121	151
Specific Conductance (25^oC) (µS/cm)	177	--	164	190
DO (mg/L)	8.69	--	8.32	9.05
DO (% sat)	81.8	--	81.1	82.5
Acidity and Alkalinity (mg/L as $CaCO_3$)				
Calc Acidity	35.4	--	--	--
Acidity (pH 3.7)	<1	--	--	--
Total Acidity (pH 8.3)	46	--	37	55
Alkalinity (pH 4.5)	--	--	--	--
Total Metals (mg/L)				
Fe	0.72	--	--	--
Fraction Fe^{3+}	--	--	--	--
Al	4.33	--	--	--
Cu	0.0057	--	--	--
Ni	0.0313	--	--	--
Zn	0.136	--	--	--
Cd	0.00049	--	--	--
Pb	0.0016	--	--	--
As	<0.001	--	--	--
Mn	0.460	--	--	--
Dissolved Metals (mg/L)				
Fe	0.30	--	--	--
Al	4.30	--	--	--
Cu	0.0051	--	--	--
Ni	0.0295	--	--	--
Zn	0.133	--	--	--
Cd	0.00051	--	--	--
Pb	0.0011	--	--	--
As	<0.001	--	--	--
Mn	0.470	--	--	--
Solids				
Turbidity (NTUs)	11.1	--	0.38	21.9
TSS (mg/L)	15.0	--	--	--
TDS (mg/L)	99.4	--	91.5	107
Salinity (ppt)	0.1	--	0.1	0.1
Cations and Anions (mg/L)				
Na	2.96	--	2.38	3.53
K	1.14	--	1.08	1.19
Mg	2.00	--	1.94	2.05
Ca	2.57	--	2.55	2.59
Hardness (mg/L as $CaCO_3$)	14.6	--	14.5	14.8
SO_4^{2-}	58.2	--	53.9	62.5

--, data parameters not measured or non-applicable.

Table B.6: Results of water chemistry measured from the A Drive Seep on 24 May 2006 and C Drive Seeps 1 and 2 on 25 May 2006 (n=1).

	A Drive	C Drive	
		Seep 1	Seep 2
Physical-Chemical Parameters			
Temp (^oC)	8.9	--	--
pH	3.13	3.75	3.77
Eh (mV)	761	--	--
Conductivity (μS/cm)	432	--	--
Specific Conductance (25^oC) (μS/cm)	624	--	--
DO (mg/L)	9.67	--	--
DO (% sat)	83.7	--	--
Acidity and Alkalinity (mg/L as $CaCO_3$)			
Calc Acidity	--	91.0	81.8
Acidity (pH 3.7)	33.0	14.2	15.5
Total Acidity (pH 8.3)	258	84.1	76.9
Alkalinity (pH 4.5)	-162	-45.1	-44.5
Total Metals (mg/L)			
Fe	--	0.81	0.74
Fraction Fe^{3+}	--	--	--
Al	--	14.2	13.3
Cu	--	0.0048	0.0052
Ni	--	0.0591	0.0526
Zn	--	0.370	0.265
Cd	--	0.00153	0.00143
Pb	--	0.0034	0.0021
As	--	<0.001	<0.001
Mn	--	1.08	0.774
Dissolved Metals (mg/L)			
Fe	--	0.63	0.54
Al	--	14.0	12.6
Cu	--	0.0053	0.0059
Ni	--	0.0605	0.0524
Zn	--	0.403	0.288
Cd	--	0.00153	0.00155
Pb	--	0.0034	0.0022
As	--	<0.001	<0.001
Mn	--	1.07	0.747
Solids			
Turbidity (NTUs)	1.90	--	--
TSS (mg/L)	--	1.21	8.81
TDS (mg/L)	409	--	--
Salinity (ppt)	0.3	--	--
Cations and Anions (mg/L)			
Na	--	3.72	3.54
K	--	4.24	1.99
Mg	--	4.70	4.71
Ca	--	5.66	5.51
Hardness (mg/L as $CaCO_3$)	--	33.5	33.2
SO_4^{2-}	--	109	104

--, data parameters not measured or non-applicable.

Table B.7: Results of water chemistry measured from Collis Seep 1 from May to August 2006 (n=1 to 3).

	Mean	Median	Min	Max
Physical-Chemical Parameters				
Temp (^{o}C)	9.4	--	8.4	10.3
pH	--	2.15	2.04	2.23
Eh (mV)	671	--	664	678
Conductivity (µS/cm)	5325	--	4990	5660
Specific Conductance (25^{o}C) (µS/cm)	7588	--	7307	7870
DO (mg/L)	4.29	--	4.27	4.31
DO (% sat)	38.4	--	37.3	39.5
Acidity and Alkalinity (mg/L as $CaCO_3$)				
Calc Acidity	7341	--	7261	7421
Acidity (pH 3.7)	3286	3163	3134	3561
Total Acidity (pH 8.3)	7643	7725	7352	7851
Alkalinity (pH 4.5)	-5615	-5581	-5785	-5478
Total Metals (mg/L)				
Fe	1520	--	1490	1550
Fraction Fe^{3+}	0.77	--	0.77	0.77
Al	658	--	610	705
Cu	0.619	--	--	--
Ni	4.60	--	--	--
Zn	21.1	--	--	--
Cd	0.0265	--	--	--
Pb	<0.0005	--	--	--
As	0.131	--	--	--
Mn	31.60	--	--	--
Dissolved Metals (mg/L)				
Fe	1410	--	1390	1430
Al	607	--	586	627
Cu	0.591	--	0.588	0.594
Ni	4.10	--	3.99	4.21
Zn	18.4	--	18.0	18.8
Cd	0.0253	--	--	--
Pb	<0.0005	--	--	--
As	0.138	--	0.126	0.150
Mn	28.6	--	27.8	29.3
Solids				
Turbidity (NTUs)	0.68	--	0.61	0.74
TSS (mg/L)	13.8	--	7.03	20.6
TDS (mg/L)	4970	--	4780	5160
Salinity (ppt)	4.2	--	4.0	4.4
Cations and Anions (mg/L)				
Na	3.40	--	--	--
K	0.80	--	--	--
Mg	249	--	235	263
Ca	258	--	251	264
Hardness (mg/L as $CaCO_3$)	1670	--	1630	1710
SO_4^{2-}	8675	--	8570	8780

--, data parameters not measured or non-applicable.

Table B.8: Results of water chemistry measured from Collis Seep 3 from May to August 2006 (n=1 to 3).

	Mean	Median	Min	Max
Physical-Chemical Parameters				
Temp (^{o}C)	12.7	--	11.9	13.4
pH	--	2.17	2.07	2.21
Eh (mV)	698	--	692	704
Conductivity (µS/cm)	5380	--	5320	5440
Specific Conductance (25^{o}C) (µS/cm)	7045	--	6834	7255
DO (mg/L)	2.79	--	2.71	2.87
DO (% sat)	26.7	--	25.5	27.9
Acidity and Alkalinity (mg/L as $CaCO_3$)				
Calc Acidity	6466	--	6206	6727
Acidity (pH 3.7)	3022	3071	2873	3122
Total Acidity (pH 8.3)	6329	6193	6036	6757
Alkalinity (pH 4.5)	-4898	-4856	-5140	-4699
Total Metals (mg/L)				
Fe	1300	--	1290	1310
Fraction Fe^{3+}	0.89	--	0.88	0.91
Al	525	--	492	558
Cu	0.512	--	--	--
Ni	3.51	--	--	--
Zn	16.9	--	--	--
Cd	0.0245	--	--	--
Pb	<0.0005	--	--	--
As	0.101	--	--	--
Mn	26.5	--	--	--
Dissolved Metals (mg/L)				
Fe	1200	--	1140	1260
Al	574	--	523	626
Cu	0.501	--	0.473	0.528
Ni	3.33	--	3.24	3.42
Zn	15.5	--	15.2	15.8
Cd	0.0241	--	--	--
Pb	<0.0005	--	--	--
As	0.108	--	0.097	0.118
Mn	23.9	--	22.7	25.0
Solids				
Turbidity (NTUs)	0.66	--	0.55	0.76
TSS (mg/L)	6.70	--	6.08	7.32
TDS (mg/L)	4620	--	4490	4750
Salinity (ppt)	3.9	--	3.8	4.0
Cations and Anions (mg/L)				
Na	2.90	--	--	--
K	0.30	--	--	--
Mg	223	--	206	240
Ca	210	--	206	214
Hardness (mg/L as $CaCO_3$)	1420	--	1360	1480
SO_4^{2-}	7295	--	7130	7460

--, data parameters not measured or non-applicable.

Table B.9: Results of water chemistry measured from the channel directly downstream from the Collis Seeps from May to September 2006 (n=1 to 3).

	Mean	Median	Min	Max
Physical-Chemical Parameters				
Temp (^oC)	11.6	--	11.0	12.1
pH	--	2.27	2.17	2.38
Eh (mV)	706	--	--	--
Conductivity (µS/cm)	4445	--	4280	4610
Specific Conductance (25^oC) (µS/cm)	5980	--	5842	6117
DO (mg/L)	3.99	--	1.83	6.15
DO (% sat)	37.0	--	17.3	56.7
Acidity and Alkalinity (mg/L as $CaCO_3$)				
Calc Acidity	5951	6042	4965	6846
Acidity (pH 3.7)	2592	2408	2315	3052
Total Acidity (pH 8.3)	5666	5517	5009	6472
Alkalinity (pH 4.5)	-3992	-4058	-4918	-3001
Total Metals (mg/L)				
Fe	1110	1010	930	1390
Fraction Fe^{3+}	0.83	--	0.80	0.85
Al	484	461	433	558
Cu	0.490	--	0.449	0.531
Ni	3.44	--	3.10	3.77
Zn	16.0	--	14.1	17.9
Cd	0.0209	--	0.0179	0.0239
Pb	0.0244	--	< 0.0005	0.0241
As	0.120	--	0.091	0.149
Mn	23.2	--	20.4	25.9
Dissolved Metals (mg/L)				
Fe	1130	1110	956	1310
Al	483	515	412	522
Cu	0.478	0.444	0.441	0.549
Ni	3.31	3.11	2.94	3.89
Zn	15.3	14.7	13.3	17.8
Cd	0.0210	--	0.0188	0.0232
Pb	0.0017	--	0.0005	0.0028
As	0.111	0.092	0.088	0.154
Mn	23.1	24.2	19.4	25.8
Solids				
Turbidity (NTUs)	9.43	--	--	--
TSS (mg/L)	149	11.2	9.29	425
TDS (mg/L)	3655	--	3300	4010
Salinity (ppt)	3.1	--	2.8	3.3
Cations and Anions (mg/L)				
Na	3.60	--	2.80	4.40
K	0.95	--	0.50	1.40
Mg	212	221	180	234
Ca	194	185	174	223
Hardness (mg/L as $CaCO_3$)	1360	1430	1180	1470
SO_4^{2-}	6470	5990	5960	7460

--, data parameters not measured or non-applicable.

Table B.10: Results of water chemistry measured from Manchester Seep water chemistry from May to February 2007.

	n	Mean	Median	Min	Max	Std. Dev.
Physical-Chemical Parameters						
Temp (^{o}C)	11	9.8	9.6	7.9	12.6	1.5
pH	12	--	2.81	2.49	3.34	0.21
Eh (mV)	9	715	709	691	744	19.2
Conductivity (µS/cm)	11	689	673	256	1033	267
Specific Conductance (25^{o}C) (µS/cm)	11	979	968	335	1500	390
DO (mg/L)	11	9.47	9.59	8.12	10.93	0.72
DO (% sat)	11	84.0	82.1	73.4	94.3	6.96
Acidity and Alkalinity (mg/L as $CaCO_3$)						
Calc Acidity	11	419	426	87.6	728	226
Acidity (pH 3.7)	12	185	158	20.1	373	118
Total Acidity (pH 8.3)	12	378	363	78.5	626	203
Alkalinity (pH 4.5)	12	-272	-264	-467	-46.1	150
Total Metals (mg/L)						
Fe	10	84.2	92.2	14.3	146	45.7
Fraction Fe^{3+}	9	0.82	0.82	0.72	0.92	0.071
Al	10	38.3	36.0	7.85	76.7	21.2
Cu	3	0.0509	0.0585	0.0302	0.0640	0.0181
Ni	3	0.222	0.257	0.148	0.261	0.0641
Zn	3	1.08	1.23	0.609	1.39	0.412
Cd	1	0.00106	--	--	--	--
Pb	1	0.0056	--	--	--	--
As	1	0.011	--	--	--	--
Mn	1	0.877	--	--	--	--
Dissolved Metals (mg/L)						
Fe	11	69.7	62.9	4.31	143	48.2
Al	11	29.5	32.5	7.43	56.7	16.7
Cu	8	0.0480	0.0514	0.0201	0.0669	0.0162
Ni	8	0.176	0.175	0.0629	0.261	0.0641
Zn	8	0.957	0.993	0.380	1.39	0.327
Cd	4	0.00101	0.00109	0.00054	0.00134	0.000338
Pb	1	0.0049	--	--	--	--
As	3	0.041	0.055	0.010	0.059	0.027
Mn	4	0.819	0.801	0.727	0.947	0.0956
Solids						
Turbidity (NTUs)	9	479	2.45	0.43	4250	141
TSS (mg/L)	11	298	18.8	0.51	2960	883
TDS (mg/L)	11	649	636	220	989	265
Salinity (ppt)	11	0.5	0.5	0.2	0.8	0.2
Cations and Anions (mg/L)						
Na	11	4.46	3.86	3.41	6.58	1.16
K	8	2.13	2.18	1.74	2.48	0.22
Mg	11	5.94	6.50	3.16	8.67	1.63
Ca	11	9.73	10.5	5.84	14.2	2.65
Hardness (mg/L as $CaCO_3$)	11	48.8	53.8	27.6	71.2	13.2
SO_4^{2-}	11	420	428	101	692	227

--, data parameters not measured or non-applicable.

Table B.11: Results of water chemistry measured from the outlet pipe of the Manchester Pond from June to February 2007.

	n	Mean	Median	Min	Max	Std. Dev.
Physical-Chemical Parameters						
Temp (^{o}C)	4	5.1	5.4	4.7	13.0	4.0
pH	5	--	2.75	2.51	2.82	0.13
Eh (mV)	3	690	690	677	704	13.5
Conductivity (μS/cm)	4	942	1049	729	1147	183
Specific Conductance (25^{o}C) (μS/cm)	4	1518	1557	1180	1748	245
DO (mg/L)	4	11.4	10.8	9.64	12.6	1.30
DO (% sat)	4	90.1	90.9	82.3	98.6	6.75
Acidity and Alkalinity (mg/L as $CaCO_3$)						
Calc Acidity	4	778	748	541	944	184
Acidity (pH 3.7)	4	348	398	210	427	100
Total Acidity (pH 8.3)	4	740	746	531	867	153
Alkalinity (pH 4.5)	4	-471	-517	-555	-356	89.7
Total Metals (mg/L)						
Fe	4	146	156	92.1	178	38.2
Fraction Fe^{3+}	4	0.77	0.82	0.68	0.84	0.075
Al	4	60.8	56.7	42.0	69.0	13.5
Cu	2	0.0880	--	0.0863	0.0896	--
Ni	2	0.336	--	0.334	0.337	--
Zn	2	1.79	--	1.75	1.83	--
Dissolved Metals (mg/L)						
Fe	4	139	154	90.0	165	34.8
Al	4	57.4	52.2	39.2	67.9	13.8
Cu	4	0.0746	0.0754	0.0542	0.0875	0.0149
Ni	4	0.286	0.263	0.208	0.333	0.0664
Zn	4	1.50	1.44	1.13	1.71	0.295
Solids						
Turbidity (NTUs)	3	3.12	3.81	1.14	4.41	1.74
TSS (mg/L)	4	3.16	3.73	2.02	21.4	9.18
TDS (mg/L)	4	996	1023	774	1146	160
Salinity (ppt)	4	0.8	0.8	0.6	0.9	0.1
Cations and Anions (mg/L)						
Na	4	8.70	8.74	5.97	10.4	2.00
K	2	2.37	--	2.28	2.46	--
Mg	4	8.91	8.49	7.36	10.1	1.29
Ca	4	15.5	14.6	13.1	17.5	1.90
Hardness (mg/L as $CaCO_3$)	4	75.5	70.6	64.5	85.3	9.86
SO_4^{2-}	4	814	806	569	977	183

--, data parameters not measured or non-applicable.

Table B.12: Description of samples used for inverse geochemical modelling. Abbreviated Sample IDs are used to distinguish samples in Tables B.13 and 2.6-2.7.

Seep	Sample ID	Abbreviated Sample ID	Description
Manchester Seep	Manchester-160806B	Man Seep 1	Median Fe concentration
	Manchester-291106B	Man Seep 2	Median Al concentration
Manchester Pond	Manchester-180706A	Man Pond 1	Most representative of median water chemistry
	Manchester-160806A	Man Pond 2	
Collis Seep 3	CollisSeep3-160806	Collis Seep	Generally, representative water chemistry considering all Collis Seeps
C Drive	CDriveSeep-250506	C Drive	Seep sampled only once. Includes averages of Seeps 1 and 2, which were nearly identical
Whirlwind Tributary A	WW-Aseep-080206	WW Trib A	Most representative of median water chemistry
Whirlwind Tributary Pond A1	WW-A1out-080206	WW Pond A1	
Whirlwind Tributary Pond A2	WW-A2out-080206	WW Pond A2	
Whirlwind Tributary C	WW-Cseep-090206	WW Trib C	
Whirlwind Tributary D	WW-Dseep-080306	WW Trib D	

Table B.13: Water chemistry summary for representative samples used for performing inverse geochemical modelling.

	Man Seep 1	Man Seep 2	Man Pond 1	Man Pond 2	Collis Seep	C Drive	WW Trib A	WW Pond A1	WW Pond A2	WW Trib C	WW Trib D
	Physical-Chemical Water Quality Parameters										
Temp (^{o}C)	7.9	9.6	5.7	5	11.9	8.9	12	11.5	11.7	13.6	11.3
pH	2.90	2.61	2.51	2.79	2.21	3.76	3.13	3.37	4.05	3.66	3.72
Eh (mV)	696	709	690	677	692	--	677	664	654	720	717
Cond (µS/cm)	652	975	1027	729	5440	--	300	235	38.3	152	121
DO (mg/L)	9.59	9.20	10.24	11.35	2.71	--	8.33	9.32	9.69	9.60	9.05
	Dissolved Metals (mg/L)										
Fe^{2+}	15.2	14.4	30.3	28.9	153	0.15	3.2	1.53	0.07	0.14	0.15
Fe^{3+}	47.6	123.5	131.7	61.1	1102	0.44	3.09	1.13	0.06	0.3	0.44
Al	37.0	32.5	67.9	43.4	558	13.3	17.9	12.2	0.718	5.82	4.30
Cu	0.0448	0.0572	0.0820	0.0542	0.528	0.0056	0.0090	0.0066	0.0009	0.0055	0.0051
Ni	0.168	0.182	0.314	0.211	3.42	0.0565	0.0695	0.0588	0.0052	0.0369	0.0295
Zn	0.886	1.10	1.65	1.13	15.8	0.346	0.278	0.185	0.029	0.165	0.133
Cd	--	0.00106	--	--	--	0.00154	0.00085	0.00049	0.00005	0.00054	0.00051
Pb	--	--	--	--	--	0.0028	0.0042	0.0021	0.0005	0.0014	0.0011
As	--	0.055	--	--	0.118	--	--	--	--	--	--
Mn	--	0.727	--	--	25	1.07	1.27	1.27	0.093	0.691	0.47
	Cations and Anions (mg/L)										
Na	3.85	5.89	9.72	5.97	2.9	3.63	4.35	2.74	1.13	2.75	2.38
K	2.18	2.23	2.46	2.37	0.30	3.12	2.63	1.62	0.63	1.63	1.19
Mg	5.85	6.79	10.1	7.36	240	4.71	6.57	5.09	0.49	2.88	1.94
Ca	10.3	11.1	17.5	14.0	214	5.59	8.80	4.64	0.42	4.32	2.59
Sulphate	428	656	896	569	7460	107	227	227	22.5	96.8	53.9
	Additional Parameters										
Alkalinity (mg/L as $CaCO_3$)	-283	-432	-555	-356	-5140	-44.8	--	--	--	--	--
TSS (mg/L)	4.2	157	2	3.3	6.1	5	5	27	81	4	15

--, data parameters not measured.

Figure B.1. Sample locations of Whirlwind Tributary A Seep, Pond A1 and Pond A2 (aerial photo from Google Earth (2009)).

Figure B.2. Sample location of Whirlwind Tributary A Seep.

Figure B.3. Whirlwind Tributary A Seep, Pond A1 and Pond A2. Samples from Pond A1 were collected from the upgradient side of the dam that divides Ponds A1 and A2.

Figure B.4. Sample location from ponded water just downgradient from the outlet of Whirlwind Pond A2.

Figure B.5. Sample locations where AMD from Whirlwind Tributaries C and D daylights (aerial photo from Google Earth (2009)).

Figure B.6. Locations where Whirlwind Tributaries C and D daylight and were sampled.

Figure B.7. Sample location where A Drive Seep daylights (aerial photo from Google Earth (2009)).

Figure B.8. The A Drive Seep and collection pond.

Figure B.9. Locations of C Drive Seeps 1 and 2 and associated collection ponds (aerial photo from Google Earth (2009)).

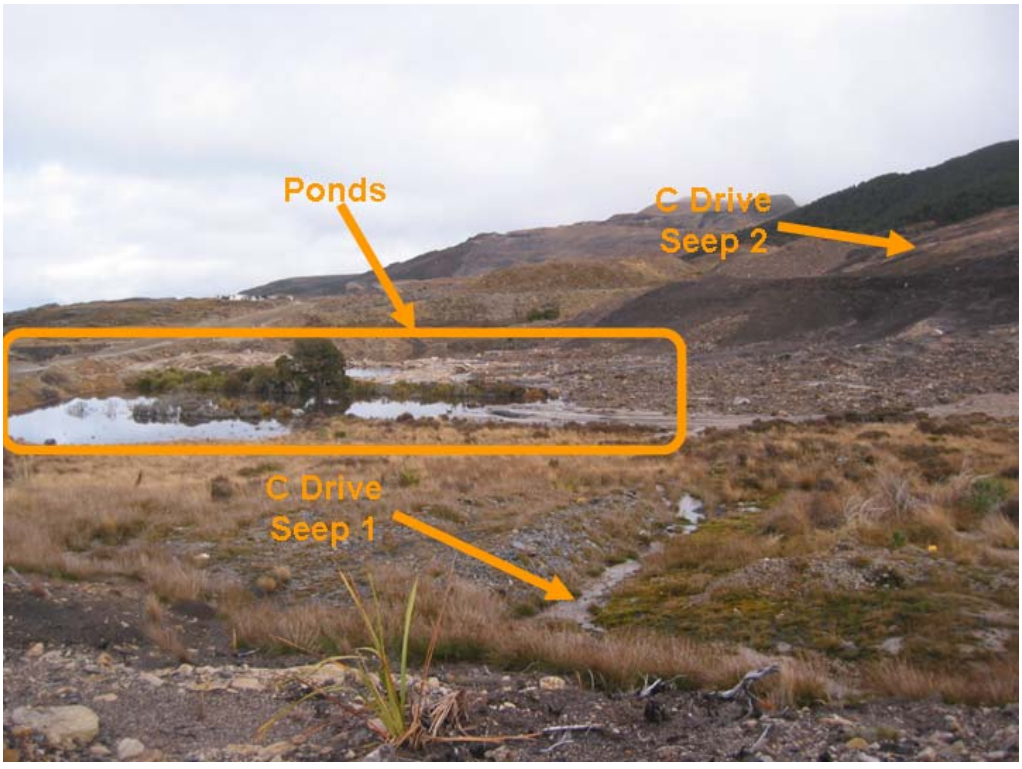

Figure B.10. Ponds that collect AMD from C Drive Seeps 1 and 2.

Figure B.11. Locations of Collis Seeps 1 and 3 and the drainage channel that conveys the AMD (aerial photo from Google Earth (2009)).

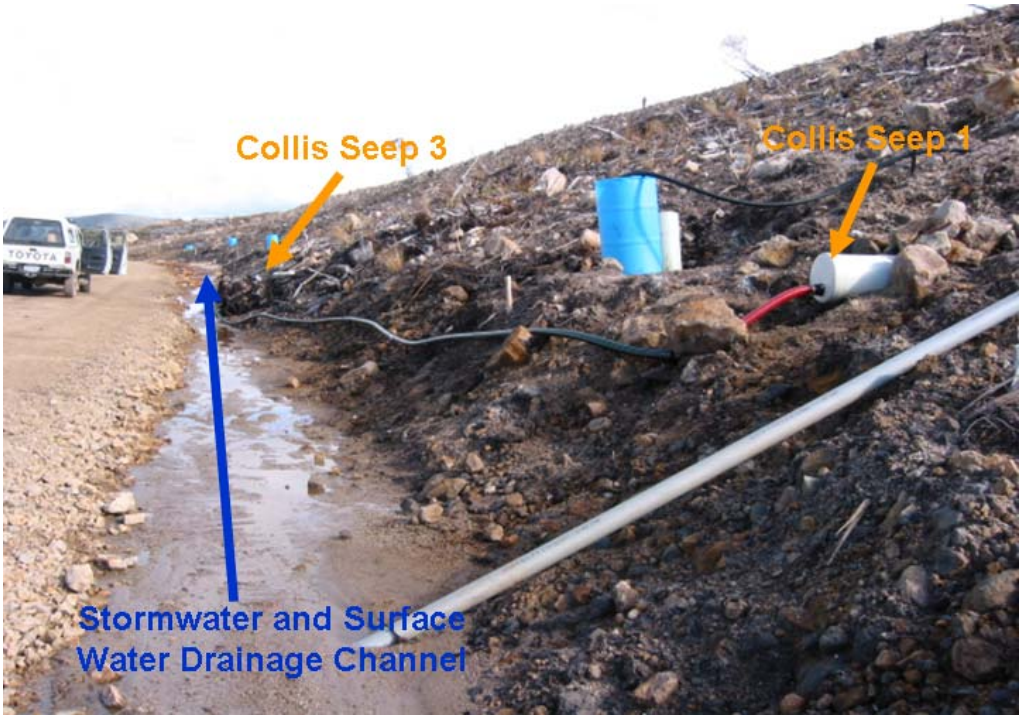

Figure B.12. Collis Seeps 1 and 3, and their associated drainage channel, following collection of the AMD in pipes to measure cumulative flow and chemistry.

Figure B.13. Dissolved Fe present in concentrations exceeding 1000 mg/L just downgradient of Collis Seeps 1 and 3.

Figure B.14. Locations of Manchester Seep and Manchester Pond. Samples were collected at the seep location and from the outlet culvert (aerial photo from Google Earth (2009)).

Figure B.15. Manchester Seep and Manchester Pond.

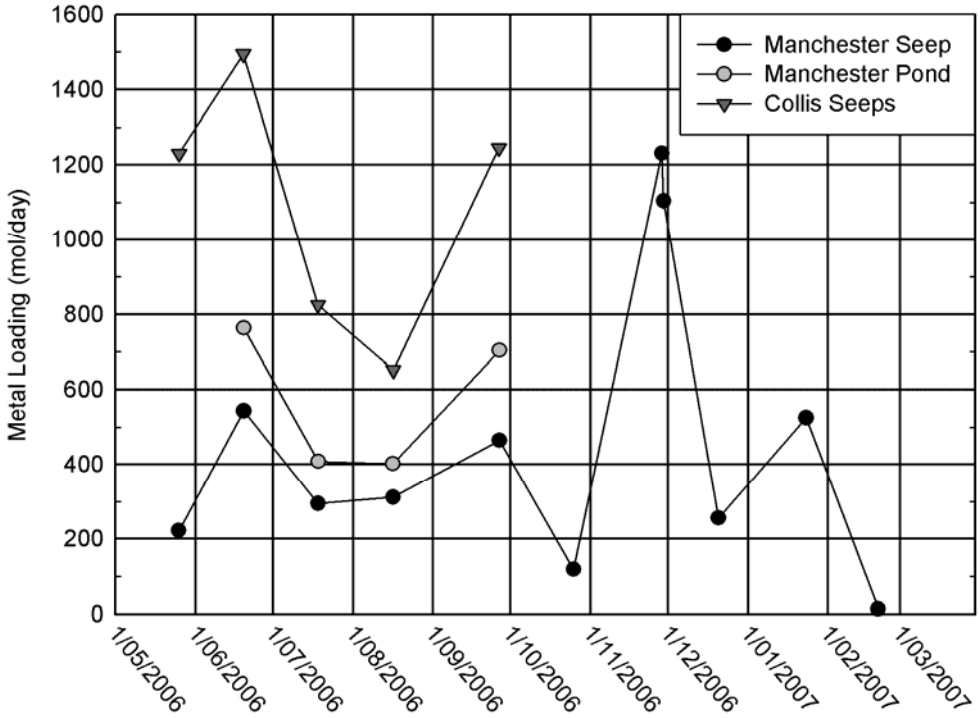

Figure B.16. Molar dissolved metal loading from Manchester Seep, the outlet of the Manchester Pond and the Collis Seeps (cumulative from Seeps 1 and 3). Loading rates include the total moles of Fe, Al, Cu, Ni, Zn, Cd, Pb, As and Mn.

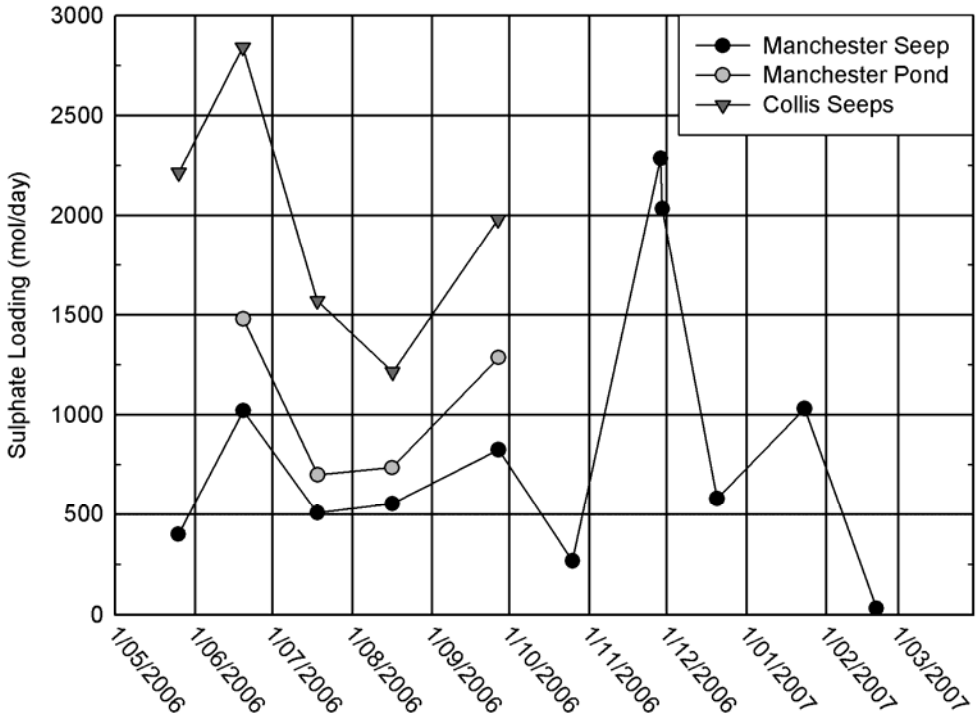

Figure B.17. Molar sulphate loading from Manchester Seep, the outlet of the Manchester Pond and the Collis Seeps (cumulative from Seeps 1 and 3).

Appendix C: Biogeochemical Reactor Substrate Geotechnical Properties and Chemistry

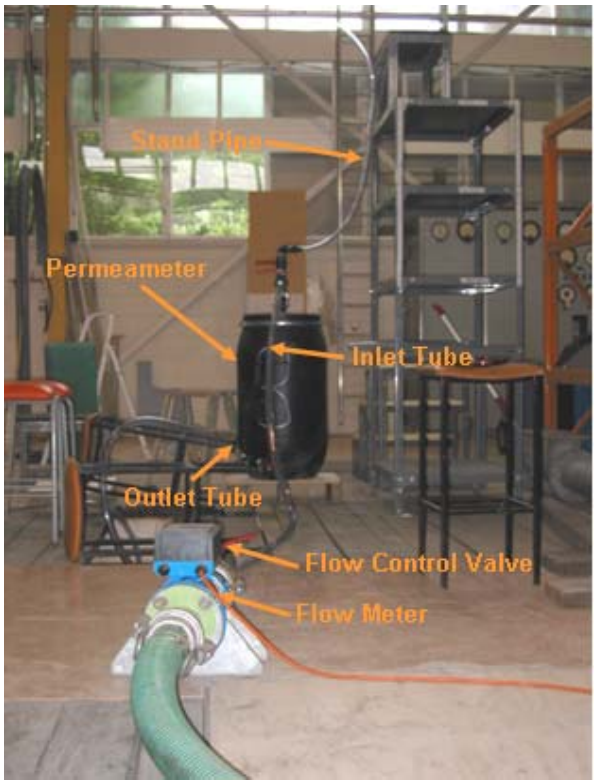

Figure C.1. Experimental setup for the hydraulic conductivity tests.

Appendix D: Acidity, Metal and Sulphate Removal from Mesocosm-Scale Biogeochemical Reactor Treatability Tests

Table D.1: Biogeochemical reactor influent and effluent metal and sulphate concentrations in units mg/L. Data represents samples collected between weeks 5.2-16.0 during stable operating conditions (metal loading rates 0.23-0.83 mol/m^3/day and acidity loading rates 21-80 g $CaCO_3$/m^2/day). Effluent data from P3 and S1 includes samples collected from week 5.2 until BGCR operation ceased (during week 11.3 for P3 (0.41 mol metals/m^3/day and 45 g $CaCO_3$/m^2/day) and Week 12.4 for S1 (0.56 mol metals/m^3/day and 46 g $CaCO_3$/m^2/day)). Sample concentrations below laboratory PQLs were halved, when necessary, for statistical calculations.

	Mean	Median	Min	Max	Std. Dev.
	AMD Influent (n=7)				
Fe	78.4	70.7	54.8	106	20.7
Al	53.6	51.8	42.6	69.5	10.7
Cu	0.209	0.199	0.146	0.272	0.048
Ni	0.230	0.210	0.187	0.296	0.043
Zn	1.27	1.23	1.03	1.55	0.197
Cd	0.00186	0.00169	0.00155	0.00235	0.00031
Pb	0.0152	0.0150	0.0090	0.0284	0.0071
As	0.001	0.001	<0.001	0.003	0.0009
Mn	1.82	1.62	1.40	2.60	0.475
Sulphate	698	642	536	950	173
	P1 (n=7)				
Fe	0.27	0.12	0.05	1.04	0.35
Al	0.044	0.026	0.017	0.122	0.038
Cu	<0.0005	<0.0005	<0.0005	<0.0005	
Ni	0.0008	0.0005	<0.0005	0.0020	0.0006
Zn	0.002	0.002	<0.002	0.003	0.0008
Cd	<0.00005	<0.00005	<0.00005	<0.00005	
Pb	<0.0001	<0.0001	<0.0001	<0.0001	
As	0.003	0.003	0.0005	0.008	0.003
Mn	1.54	1.66	1.11	2.08	0.355
Sulphate	445	491	145	656	185
	P2 (n=7)				
Fe	1.03	0.58	0.28	2.91	0.93
Al	0.066	0.029	0.025	0.246	0.080
Cu	<0.0005	<0.0005	<0.0005	<0.0005	
Ni	0.0009	0.0005	<0.0005	0.0020	0.0006
Zn	0.001	0.001	<0.001	0.003	0.0009
Cd	<0.00005	<0.00005	<0.00005	<0.00005	
Pb	<0.0001	<0.0001	<0.0001	<0.0001	
As	0.003	0.003	0.0005	0.007	0.003
Mn	1.97	2.10	1.47	2.67	0.422
Sulphate	451	458	220	587	148

Table D.1 continued:

	Mean	Median	Min	Max	Std. Dev.
	P3 (n=3)				
Fe	0.05	0.04	0.04	0.06	0.01
Al	0.075	0.054	0.039	0.133	0.051
Cu		<0.0005	<0.0005	<0.001	
Ni	0.0058	0.0070	<0.001	0.010	0.0049
Zn	0.005	0.003	0.002	0.010	0.004
Cd	0.00008	<0.00005	<0.00005	0.00020	0.00010
Pb	0.00007	<0.0001	<0.0001	<0.0002	
As	0.005	0.004	0.003	0.007	0.002
Mn	0.073	0.052	0.24	1.42	0.062
Sulphate	1093	1043	1025	1213	104
	S1 (n=5)				
Fe	38.1	41.7	15.7	64.3	21.4
Al	5.84	2.75	0.075	15.0	6.87
Cu	0.0012	<0.0005	<0.0005	0.0020	0.0012
Ni	0.036	0.0038	0.0013	0.125	0.053
Zn	0.021	0.004	0.002	0.071	0.030
Cd	<0.00005	<0.00005	<0.00005	<0.00005	
Pb	<0.0001	<0.0001	<0.0001	<0.0001	
As	0.002	<0.001	<0.001	0.002	
Mn	2.92	2.83	2.56	3.46	0.428
Sulphate	506	506	318	692	194
	S2 (n=7)				
Fe	2.17	2.16	0.44	3.46	1.25
Al	0.062	0.039	0.023	0.194	0.061
Cu		<0.0005	<0.0005	<0.0010	
Ni	0.0010	0.0005	<0.00050	0.0020	0.0008
Zn	0.002	0.002	0.00075 (or <0.001)	0.004	0.001
Cd	<0.00005	<0.00005	<0.00005	<0.00005	
Pb	<0.0001	<0.0001	<0.0001	<0.0001	
As	0.003	0.002	<0.001	0.006	0.002
Mn	2.11	2.31	1.56	2.69	0.463
Sulphate	446	536	223	581	155
	S3 (n=7)				
Fe	1.98	2.28	0.52	3.30	1.05
Al	0.070	0.031	0.021	0.256	0.084
Cu	0.0003	<0.0005	<0.0005	<0.0010	
Ni	0.0010	0.0005	<0.0005	0.0020	0.0008
Zn	0.001	0.001	<0.001	0.003	0.0007
Cd	<0.00005	<0.00005	<0.00005	<0.00005	
Pb	0.00005	<0.0001	0.00005	<0.0001	
As	0.003	0.002	0.0005	0.005	0.002
Mn	2.07	2.23	1.48	2.67	0.464
Sulphate	445	493	208	584	145

Table D.1 continued:

	Mean	Median	Min	Max	Std. Dev.
	S4 (n=7)				
Fe	4.28	3.65	0.72	10.2	3.27
Al	0.063	0.031	0.027	0.230	0.074
Cu	0.0003	<0.0005	<0.0005	<0.0010	
Ni	0.0007	0.0005	<0.0005	0.0014	0.0004
Zn	0.002	0.001	<0.001	0.003	0.0009
Cd	<0.00005	<0.00005	<0.00005	<0.00005	
Pb	<0.0001	<0.0001	<0.0001	<0.0001	
As	0.003	0.002	0.001	0.005	0.002
Mn	2.36	2.50	1.78	3.07	0.510
Sulphate	470	530	255	599	144

Additional Water Chemistry Results from Mesocosm-Scale Biogeochemical Reactor Treatability Tests

Cations (Including Ca, Mg, K and Na)

Influent and effluent cation concentrations were plotted versus theoretical RTD in BGCRs as shown in Figures D.1 (Na), D.2 (K), D.3 (Mg) and D.4 (Ca). A summary of these concentrations are presented in Table D.2. Effluent from BGCRs containing mussel shells or a mixture of limestone and mussel shells (P1, P2, S2, S3 and S4) generally contained similar cation concentrations and trends, so data from these reactors were combined in Table D.2. P3 (mussel shell, limestone and NSD) and S1 (only limestone as an alkalinity amendment) showed unique effluent characteristics so their cation concentrations are presented separately. The first flush was evident with BGCR effluent concentrations generally stabilised within the first three sampling events (weeks 1.1-3.2; $\theta_{BGCR} \leq 1.59$) so these results were presented separately from post first flush concentrations (post third sampling event during weeks 5.2-12.4 ($\theta_{BGCR} \geq 3.48$)) in Table D.2.

Effluent cation concentrations were greater than influent concentrations throughout this study due to the dissolution of substrates. The primary sources of cations were: Ca) mussel shells and limestone; Mg) compost and limestone; K) compost and post peel; and Na) mussel shells and compost. There was a greater export of each cation from BGCRs containing the highest percentage of mussel shells during the first flush, with exception of Na and K from P3 due to the quick dissolution of NSD. Thereafter, effluent cation concentrations from P1, P2, S2, S3 and S4 were generally comparable (within 25% of each other) with exception of the final sampling event (week 16.7; $\theta_{BGCR} \geq 16.6$) for Ca where there was a 39.1% difference between concentrations measured from P1 (345 mg/L) and S4 (210 mg/L).

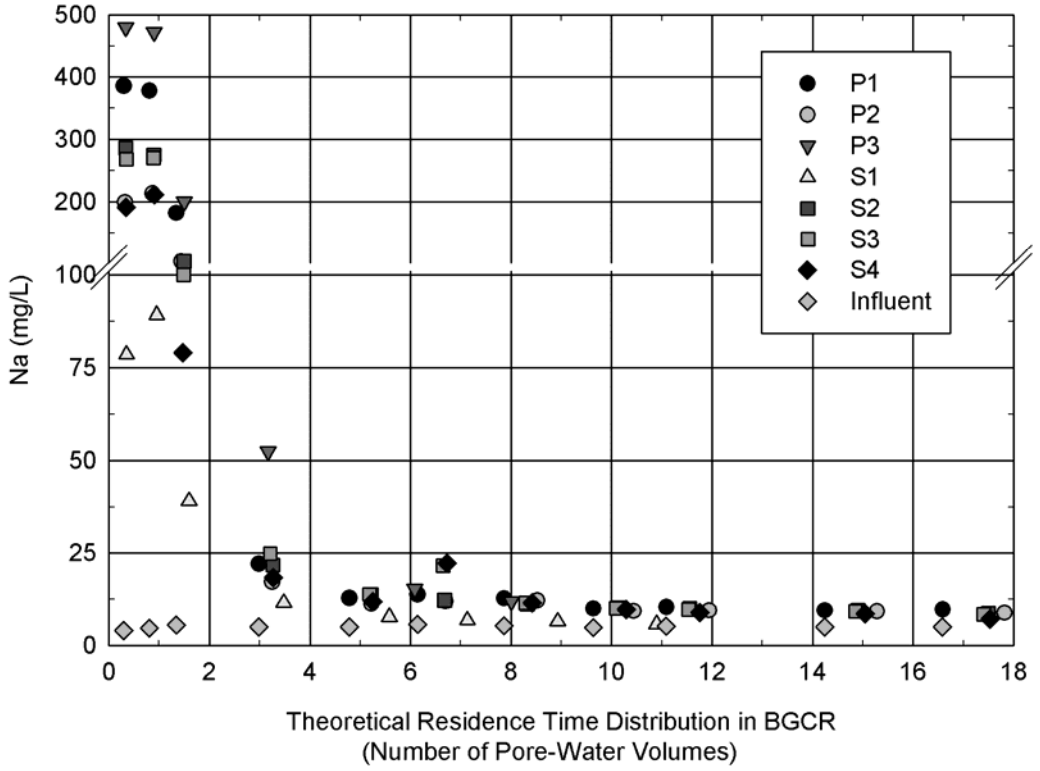

Figure D.1. Summary of influent AMD and effluent BGCR Na concentrations on a theoretical RTD basis considering all components of the BGCRs.

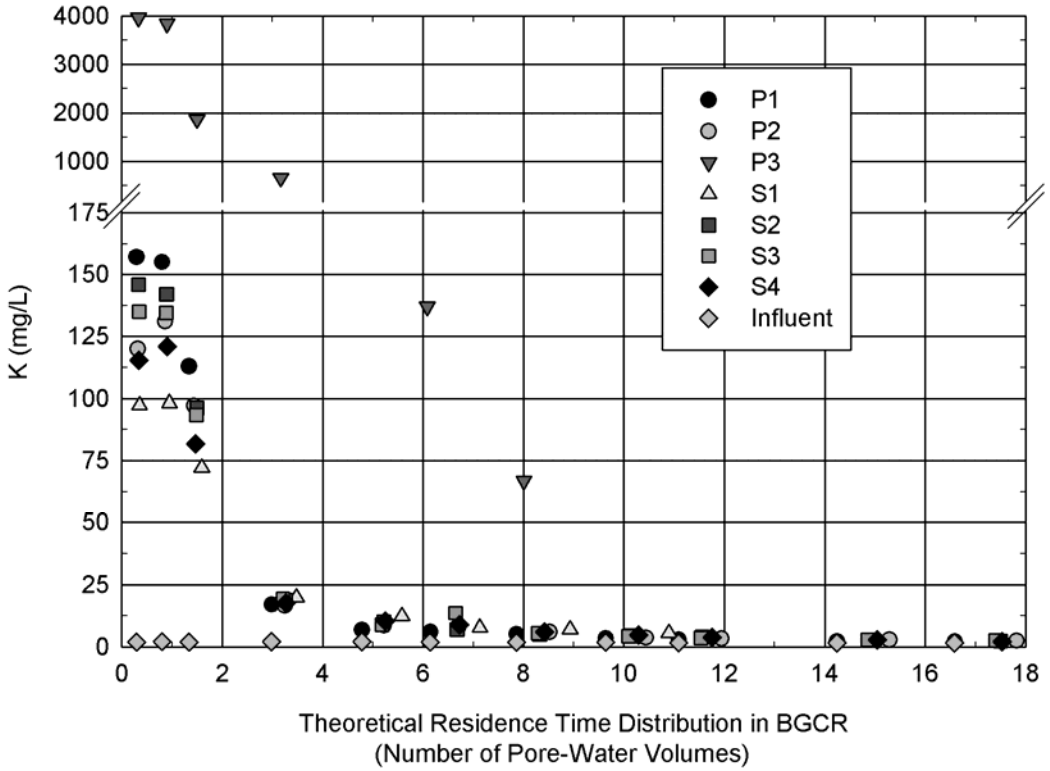

Figure D.2. Summary of influent AMD and effluent BGCR K concentrations on a theoretical RTD basis considering all components of the BGCRs.

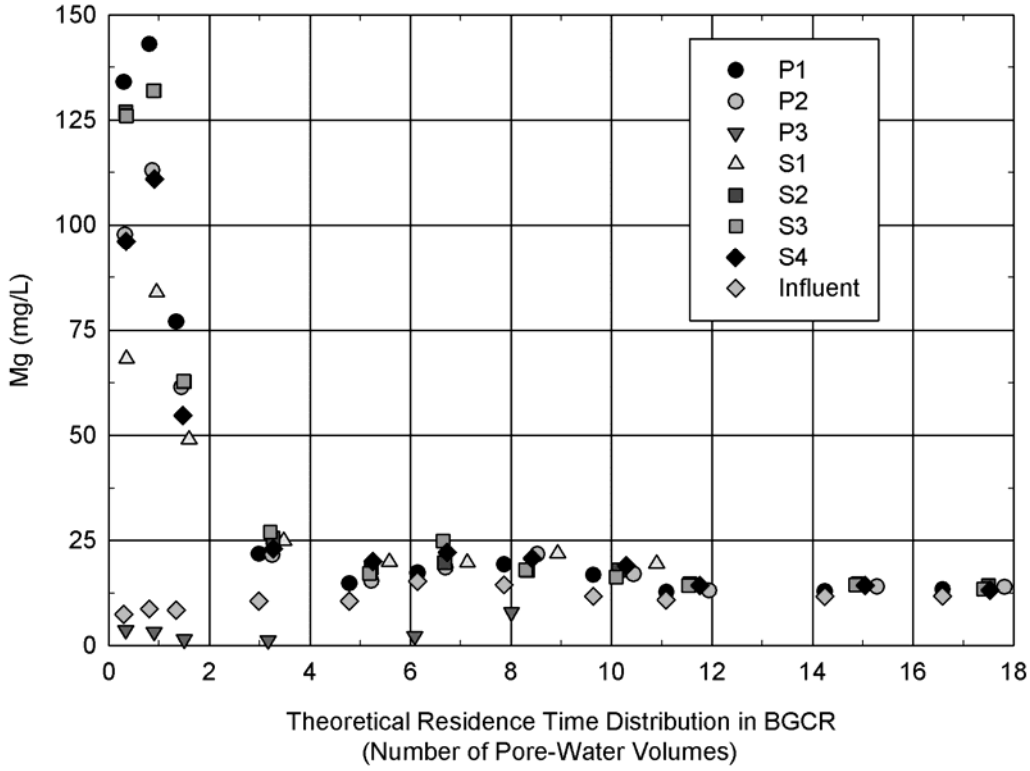

Figure D.3. Summary of influent AMD and effluent BGCR Mg concentrations on a theoretical RTD basis considering all components of the BGCRs.

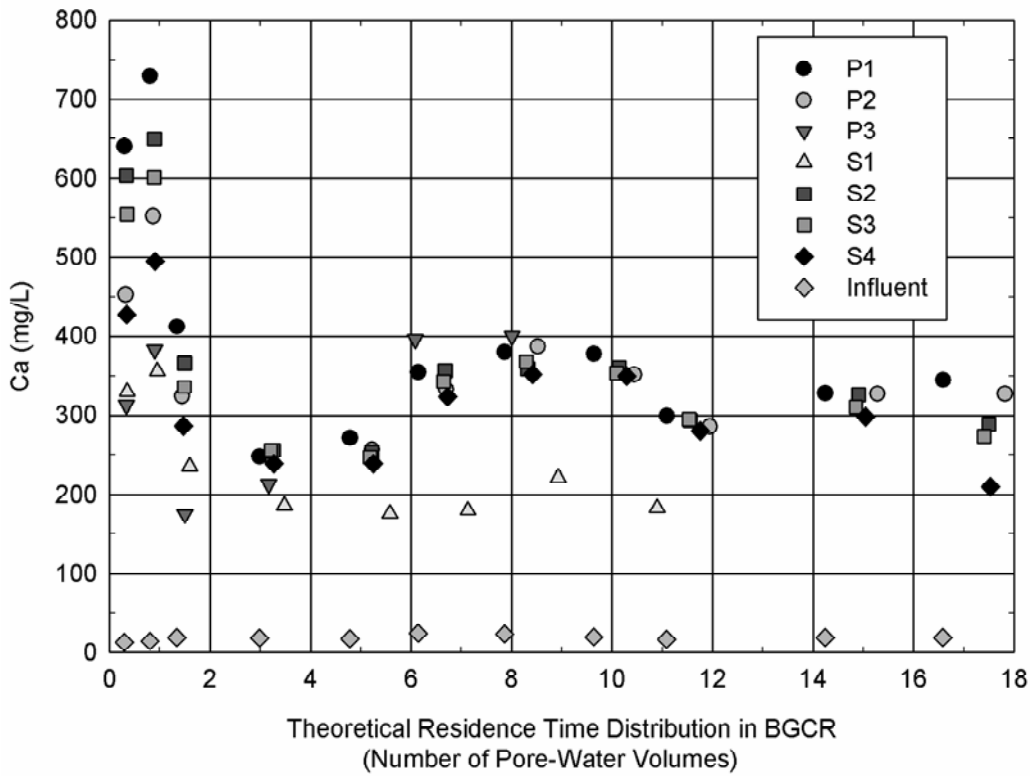

Figure D.4. Summary of influent AMD and effluent BGCR Ca concentrations on a theoretical RTD basis considering all components of the BGCRs.

Table D.2: Sodium, K, Mg and Ca concentrations from: 1) influent AMD; 2) effluent from BGCRs containing mussel shells or a mixture of mussel shells and limestone (P1, P2, S2, S3 and S4); 3) BGCR S1 (limestone); and 4) BGCR P3 (NSD, limestone and mussel shells). Values represent average concentrations with concentration ranges in parentheses below.

Sampling Events	AMD	P1, P2, S2, S3 and S4	S1	P3
	Na (mg/L)			
First Three	4.77 (4.0-5.6)	216 (79-386)	69.0 (39.2-89.2)	384 (200-480)
Post Third	5.18 (4.89-5.74)	12.4 (7.25-24.8)	7.72 (5.84-11.6)	26.6 (11.9-52.5)
	K (mg/L)			
First Three	2.16 (2.08-2.29)	123 (81.8-157)	89.2 (72.2-98.2)	3223 (1870-3960)
Post Third	1.95 (1.73-2.17)	6.80 (2.13-19.3)	10.6 (5.71-20.0)	289 (66.9-664)
	Mg (mg/L)			
First Three	8.20 (7.50-8.67)	102 (54.8-143)	67.1 (49.1-84.0)	2.82 (1.50-3.70)
Post Third	12.1 (10.6-15.3)	17.5 (12.7-27.0)	21.2 (19.5-25.0)	3.82 (1.26-7.96)
	Ca (mg/L)			
First Three	15.7 (13.1-19.2)	495 (287-729)	307 (235-356)	290 (175-383)
Post Third	20.0 (17.1-24.8)	309 (210-387)	189 (176-221)	336 (213-400)

There was significant Ca (Figure D.4) export compared to other cations due to the dissolution of calcium carbonate, which comprised the majority of mineralogy from mussel shells (average Ca concentration of 53 wt. % (range of 44-63 wt. %) (Hutchinson and O'Sullivan (2008)) and limestone (average Ca concentration of 39% (range of 30-46%) (Hutchinson and O'Sullivan (2008)). With exception of P3, Ca concentrations were consistently greatest in drum-shaped BGCRs and those containing the highest percentage of mussels shells.

Chemical and Physical Water Quality Parameters

Influent and effluent chemical and physical water quality parameters were also plotted versus theoretical RTD as shown in Figures D.5 (temperature), D.6 (specific conductance), D.7 (DO concentration), D.8 (DO % saturation) and D.9 (Eh). A summary of influent and effluent specific conductance, DO and Eh values are presented in Table D.3. Data shown was distinguished between the following sampling events: 1) the first three (weeks 1.1-3.2; $\theta_{BGCR} \leq 1.59$) due to the influence of the first flush (n=3 for AMD, S1 and P3 and n=15 considering BGCRs P1, P2, S2, S3 and S4); 2) the "middle" sampling events, which included data collected from weeks 5.2-14.4 ($2.99 \leq \theta_{BGCR} \leq 12.0$) for AMD (n=6) and BGCRs P1, P2, S2, S3 and S4 (n=30), weeks 5.2-11.3 ($3.16 \leq \theta_{BGCR} \leq 8.01$) for P3 (n=3) and weeks 5.2-12.4 ($3.48 \leq \theta_{BGCR} \leq 10.9$) for S1 (n=5); and 3) the final two sampling events

(weeks 16.0-16.7; $14.2 \leq \theta_{BGCR} \leq 17.8$), which included samples from influent AMD (n=2) and BGCR P1, P2, S2, S3 and S4 effluent (n=10).

The first flush was most notable for specific conductance due to the release of highly soluble cations from the substrate. During the final two sampling events (weeks 16.0-16.7; $14.2 \leq \theta_{BGCR} \leq 17.8$) when loading rates were greatest and HRT was lowest, DO and Eh were greater compared with earlier sampling events indicating less reducing conditions. Specific conductance was less due to less calcium carbonate dissolution. A detailed analysis of the relationships of effluent pH with effluent Fe and Al concentrations is presented in Chapter 5. Generally, treatment performance was best with effluent pH≥6.7.

Effluent temperatures (Figure D.5) ranged from 13.0-17.2^{o}C (average =15.2^{o}C), which were greater than those measured from Manchester Seep AMD (average=9.8^{o}C; range of 7.9-12.6^{o}C) and the outlet of the Manchester Pond (average=9.5^{o}C; range of 4.6-19.4^{o}C). Effluent specific conductance values (Figure D.6) were greatest for P3 due to the quick dissolution of NSD followed by systems containing the highest percentage of mussel shells (P1>S2 and S3>P2 and S4>S1). The specific conductance of AMD influent was on average 5.23% less than BGCR effluent for BGCRs containing mussel shells or a mixture of mussel shells and limestone (P1, P2, S2, S3 and S4) when excluding the first three (weeks 1.1-3.2; $\theta_{BGCR} \leq 1.49$) sampling events. Effluent DO concentrations (Figure D.7) and percent saturation (Figure D.8) were lowest for P3 followed by BGCRs containing the highest percentage of mussel shells (P1<S2 and S3<P2 and S4) with S1 consistently containing the highest DO values. Effluent BGCR DO values represent a substantial reduction compared to AMD influent (average reduction of 90.2%; range of 82.4-95.5% considering P1, P2, S2, S3 and S4). Trends for effluent Eh values (Figure D.9) were similar to those observed for DO; however, Eh values showed a more notable increase during the final two sampling events (weeks 16.0-16.7; $14.2 \leq \theta_{BGCR} \leq 18.2$), when treatment performance limitations were reached or exceeded. Effluent Eh values were substantially less than those measured for AMD influent (average reduction of 721 mV; range of 615-790 mV considering P1, P2, S2, S3 and S4).

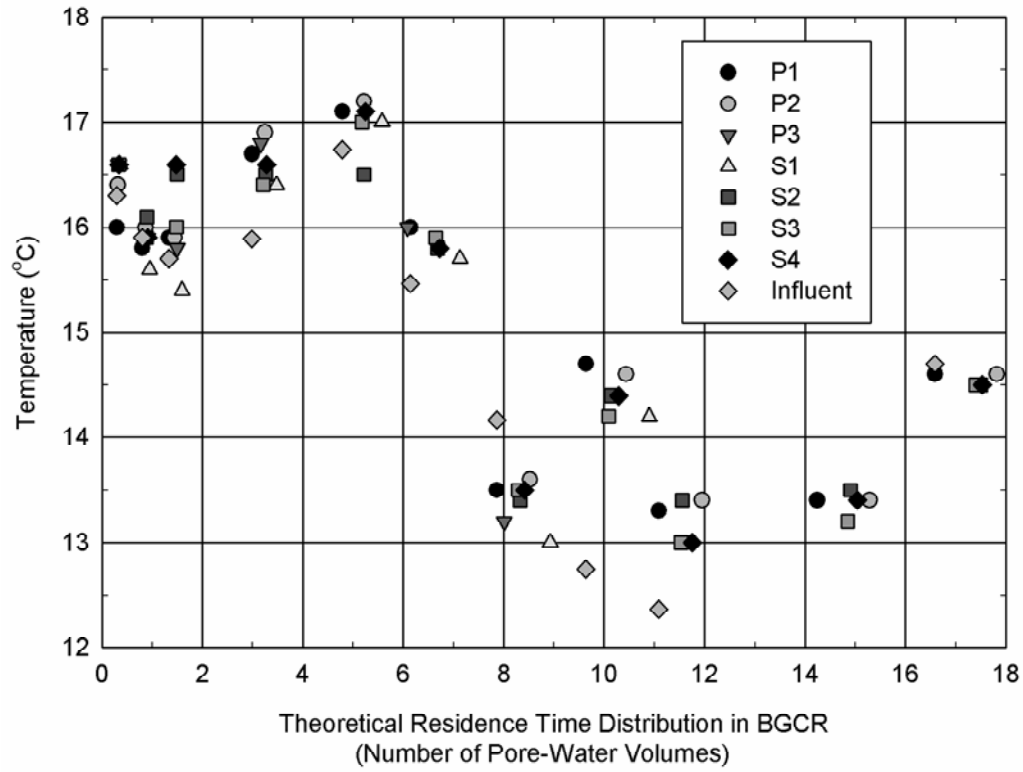

Figure D.5. Summary of influent AMD and effluent BGCR temperatures on a theoretical RTD basis considering all components of the BGCRs.

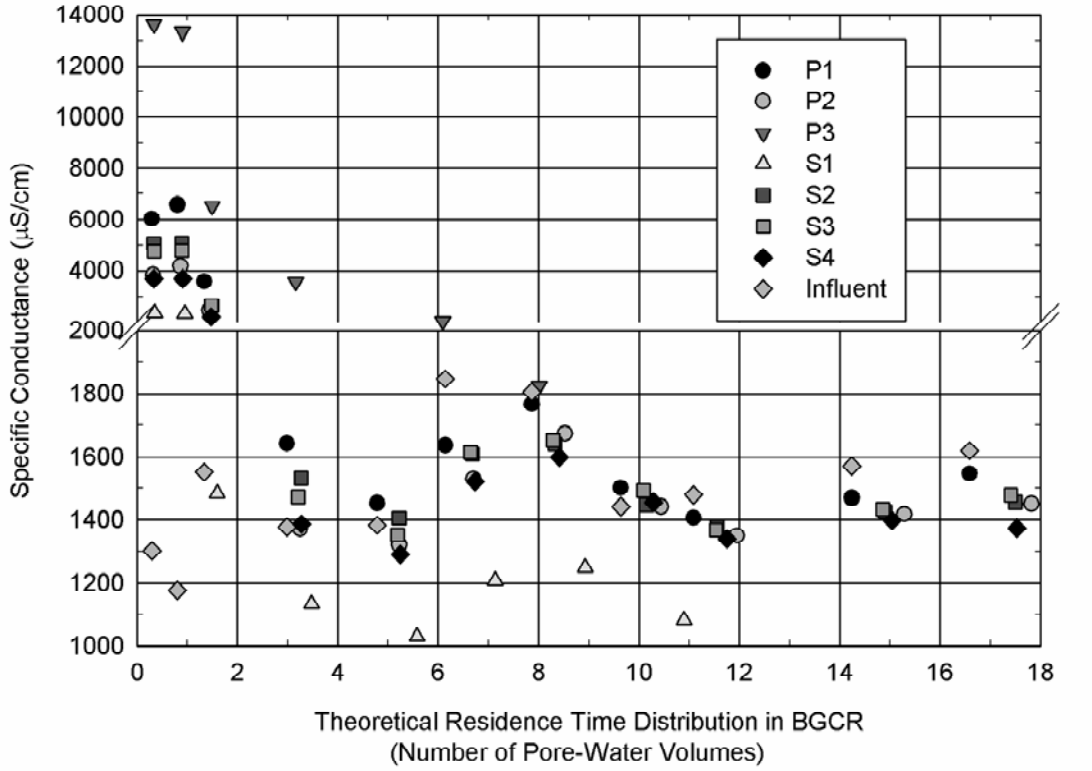

Figure D.6. Summary of influent AMD and effluent BGCR specific conductance values on a theoretical RTD basis considering all components of the BGCRs.

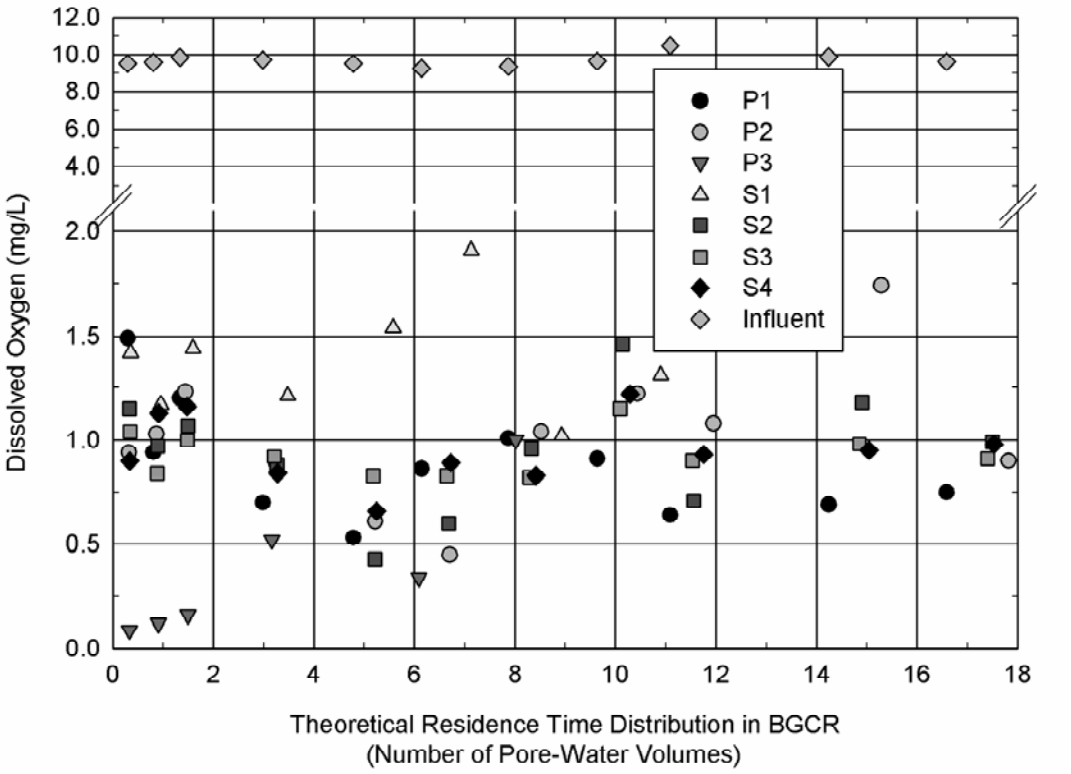

Figure D.7. Summary of influent AMD and effluent BGCR DO concentrations on a theoretical RTD basis considering all components of the BGCRs.

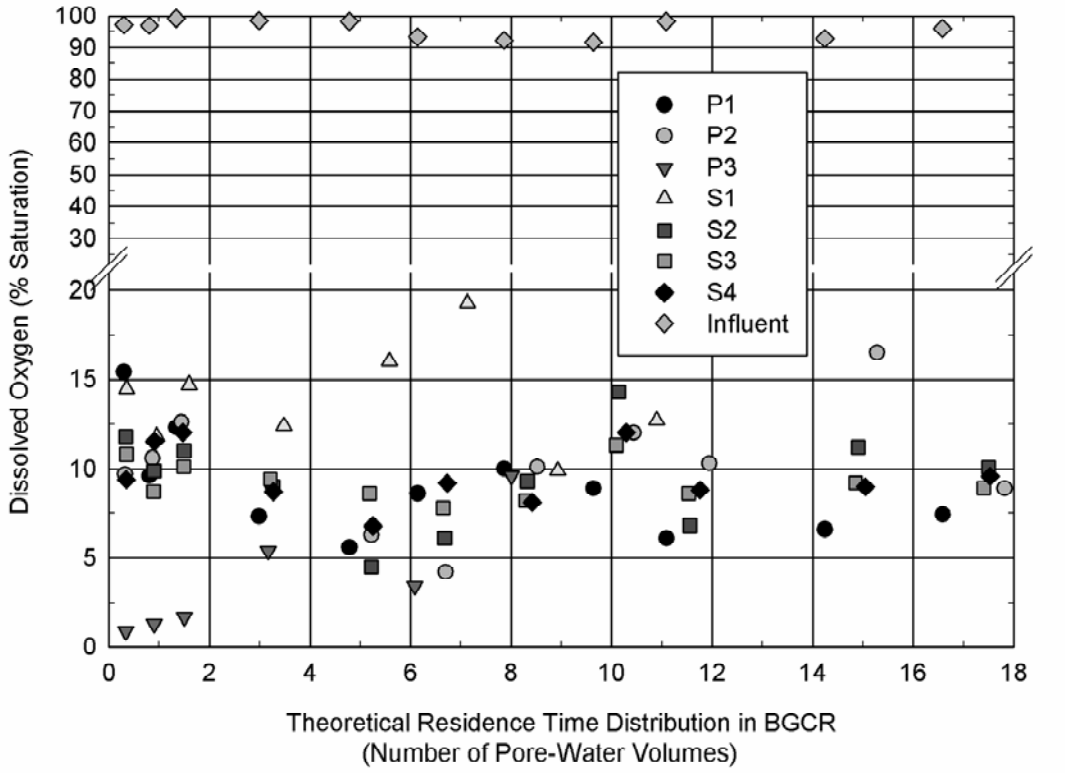

Figure D.8. Summary of influent AMD and effluent BGCR DO percent saturation on a theoretical RTD basis considering all components of the BGCRs.

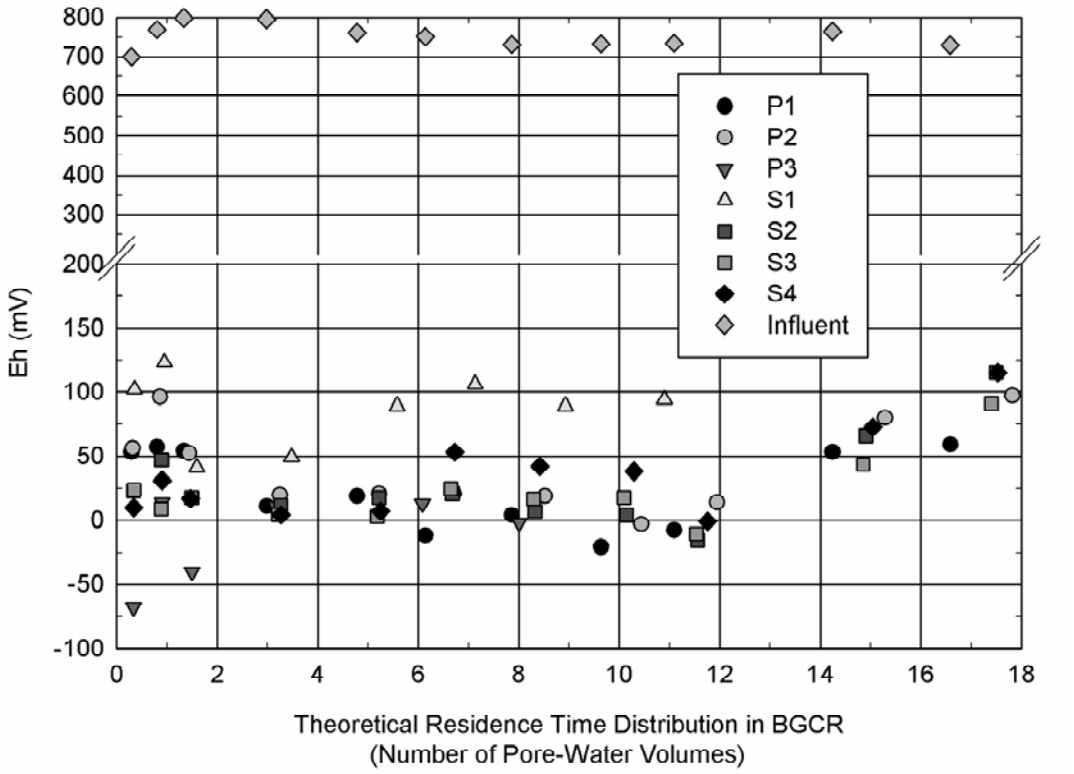

Figure D.9. Summary of influent AMD and effluent BGCR Eh values on a theoretical RTD basis considering all components of the BGCRs.

Table D.3: Comparison of specific conductance, DO (concentrations and percent saturation) and Eh data from: 1) influent AMD; 2) effluent from BGCRs containing mussel shells or a mixture of mussel shells and limestone (P1, P2, S2, S3 and S4); 3) BGCR S1 (limestone); and 4) BGCR P3 (NSD, limestone and mussel shells). Values represent average concentrations with concentration ranges in parentheses below.

Sampling Events	AMD	P1, P2, S2, S3 and S4	S1	P3
	Specific Conductance (μS/cm)			
First Three	1344 (1178-1552)	4082 (2183-6588)	2045 (1483-2335)	11,164 (6539-13,614)
Middle	1556 (1378-1848)	1519 (1290-2445)	1141 (1029-1249)	2472 (1825-3569)
Final Two	1595 (1571-1620)	1446 (1375-1547)	NA	NA
	Dissolved Oxygen (mg/L)			
First Three	9.65 (9.51-9.85)	1.06 (0.90-1.16)	1.34 (1.17-1.44)	0.12 (0.09-1.16)
Middle	9.66 (9.24-10.48)	0.86 (0.43-1.46)	1.40 (1.02-1.91)	0.62 (0.34-1.00)
Final Two	9.75 (9.62-9.87)	1.01 (0.69-1.74)	NA	NA
	Dissolved Oxygen (% Saturation)			
First Three	97.8 (97.0-99.1)	11.0 (8.7-15.4)	13.7 (11.8-14.7)	1.3 (0.9-1.7)
Middle	95.4 (91.7-98.5)	8.5 (4.2-14.3)	14.1 (9.9-19.3)	6.1 (3.4-9.6)
Final Two	94.4 (92.6-96.0)	9.7 (6.6-16.5)	NA	NA
	Eh (mV)			
First Three	756 (700-798)	38 (9-96)	89 (41-123)	-31 (-68-14)
Middle	751 (732-795)	11 (-21-53)	85 (49-106)	7 (-2-13)
Final Two	747 (730-764)	79 (43-115)	NA	NA

NA, non-applicable.

Solids (Including Turbidity, Total Suspended Solids, Total Dissolved Solids and Salinity)

To determine the presence of solids, turbidity was measured during each sampling event, and its RTD is shown in Figure D.10. Total suspended solids were also measured during the first three (weeks 1.1-3.2; $\theta_{BGCR} \leq 1.59$) and fifth (week 7.1; $4.78 \leq \theta_{BGCR} \leq 5.57$) sampling events. Total dissolved solids and salinity values were directly proportional with conductivity and, therefore, follow similar trends. AMD influent and BGCR effluent turbidity, TSS, TDS and salinity values are summarised in Table D.4, which indicated that the majority of solids from AMD influent and BGCR effluent were present in the dissolved state. Data shown is representative of appropriate sampling events depending on sample results and trends, which include: 1) the first three (weeks 1.1-3.2; $\theta_{BGCR} \leq 1.59$) when BGCR system equilibrium was being achieved (n=3 for AMD, S1 and P3 and n=15 considering BGCRs P1, P2, S2, S3 and S4); and 2) either: a) the "middle" sampling events including data collected from

weeks 5.2-16.0 ($2.99 \leq \theta_{BGCR} \leq 15.3$) for AMD (n=7) and BGCRs P1, P2, S2, S3 and S4 (n=35), weeks 5.2-11.3 ($3.16 \leq \theta_{BGCR} \leq 8.01$) for P3 (n=3) and weeks 5.2-12.4; $3.48 \leq \theta_{BGCR} \leq 10.9$ for S1 (n=5); and b) the "final" (week 16.7; $\theta_{BGCR} \geq 16.6$) sampling event (for AMD (n=1) and P1, P2, S2, S3 and S4 (n=5)); or c) the fifth (week 7.1; $4.78 \leq \theta_{BGCR} \leq 5.57$) sampling event; or d) all sampling events ("post third") subsequent to the third (week 3.2; $\theta_{BGCR} \geq 2.99$) sampling event including data collected from weeks 5.2-16.7 for AMD (n=8) and BGCRs P1, P2, S2, S3 and S4 (n=40), weeks 5.2-11.3 for P3 (n=3) and weeks 5.2-12.4 (n=5) for S1.

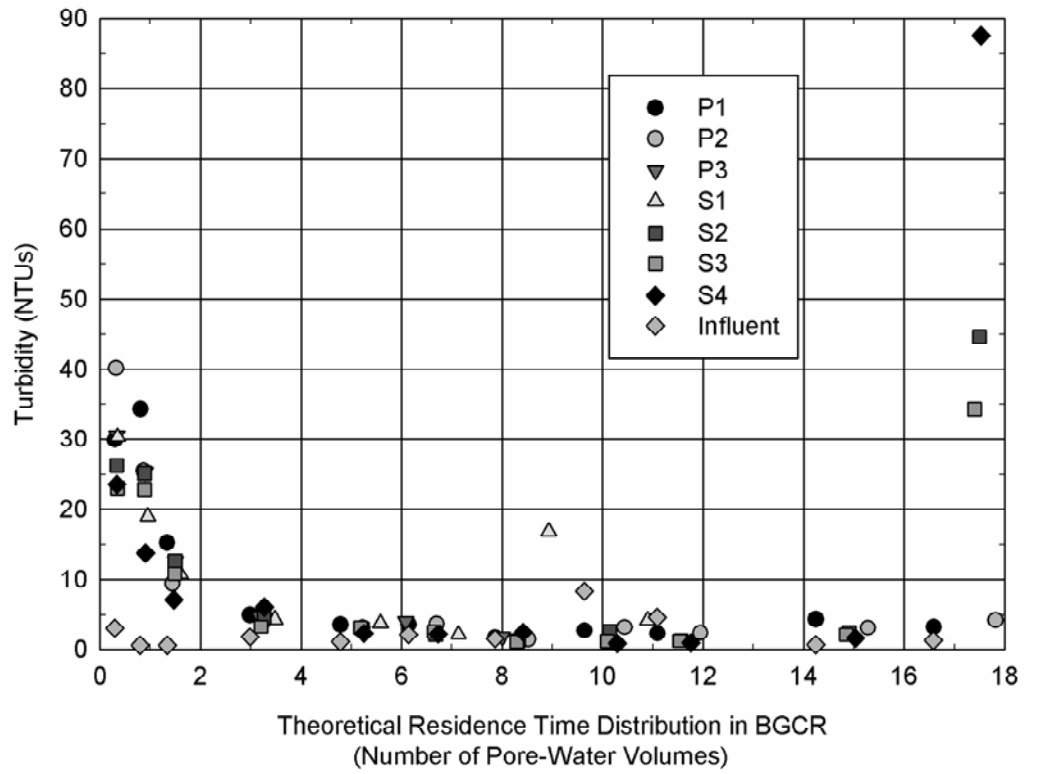

Figure D.10. Summary of influent AMD and effluent BGCR turbidity values on a theoretical RTD basis considering all components of the BGCRs.

Turbidity and TSS followed similar trends regarding a first flush effect as previously described for cations and conductivity. Most of these solids were likely derived from fine particles associated with the compost and sediment adhered to the mussel shells. Effluent turbidity measurements were similar regardless of reactor composition or dimensions with exception of the final (week 16.7; $\theta_{BGCR} \geq 16.6$) sampling event where the greatest values were measured from the trapezoidal-shaped reactors (average 55.5 NTUs; range of 34.3-87.6 NTUs). The increase was possibly a consequence of iron sulphide dissolution (due to an increase in Eh) and subsequent interstitial velocities dislodging the precipitates from substrate, bedding material and/or the outlet pipe. A similar phenomenon was also measured from S1 during its second to final (week 11.3; $\theta_{BGCR}=10.9$) sampling event, which yielded an effluent value of 16.8 NTUs.

Table D.4: Comparison of turbidity, TSS, TDS and salinity for: 1) influent AMD; 2) effluent from BGCRs containing mussel shells or a mixture of mussel shells and limestone (P1, P2, S2, S3 and S4); 3) BGCR S1 (limestone); and 4) BGCR P3 (NSD, limestone and mussel shells). Values represent average concentrations with concentration ranges in parentheses below.

Sampling Events	AMD	P1, P2, S2, S3 and S4		S1	P3
	Turbidity (NTUs)				
First Three	1.45 (0.63-3.08)	21.3 (7.2-40.2)		20.1 (10.8-30.4)	22.9 (12.7-30.6)
Middle	2.90 (0.67-8.34)	2.67 (0.91-6.08)		3.64 (2.15-4.36) Excluding Week 11.3 (Second to final Sampling event for S1)	3.56 (1.85-4.74)
				16.8 (Week 11.3)	
Final	1.31	P1 and P2	3.75 (3.25-4.25)	NA	NA
		S2, S3 and S4	55.5 (34.3-87.6)		
	Total Suspended Solids (mg/L)				
First Three	25.1 (4.39-35.4)	142 (82.2-206)		121 (94.7-159.4)	368 (116-534)
Fifth	23.9	6.93 (4.91-9.91)		15.8	NA
	Total Dissolved Solids (mg/L)				
First Three	890 (771-1019)	2678 (1433-4310)		1339 (966-1530)	7327 (4290-8940)
Post Third	1031 (902-1212)	969 (849-1156)		748 (674-820)	1622 (1198-2340)
	Salinity (ppt)				
First Three	0.7 (0.6-0.8)	2.2 (1.1-3.6)		1.0 (0.7-1.2)	6.4 (3.6-7.9)
Post Third	0.8 (0.7-1.0)	0.7 (0.6-0.9)		0.6 (0.5-0.6)	1.3 (0.9-1.9)

NA, non-applicable.

Organics, Nutrients, and Biological Parameters

The RTD of DOC/TOC concentrations from AMD and BGCR effluent are shown in Figure D.11. Based on the general consistency of turbidity following the first three (weeks 1.1-3.2) sampling events ($\theta_{BGCR} \leq 1.59$), as shown in Figure D.10, it can be assumed that TOC concentrations are representative of DOC concentrations during this period. The DOC/TOC concentrations decreased with time. The initial first flush was evident during the first three sampling events (weeks 1.1-3.2; $\theta_{BGCR} \leq 1.59$), followed by a period of gradually decreasing concentrations during the "middle four" sampling events (weeks 5.2-11.3; $2.99 \leq \theta_{BGCR} \leq 8.52$) and finally reaching quasi-stable concentrations during the final four sampling events (weeks 12.4-16.7; $\theta_{BGCR} \geq 9.64$). The distinct trend of DOC concentrations during

these three periods likely influenced sulphate reduction (Section 4.3.4) and its contribution to alkalinity (Chapter 5), which relies on labile organic carbon as part of its process. A summary of DOC/TOC concentrations during these three periods are summarised in Table D.5. The highest concentrations were measured from P3 followed by BGCRs containing the highest percentage of mussel shells (P1>S2 and S3>P2 and S4) with S1 containing the lowest. Each BGCR contained an initial efflux of compost that was easily dislodged due to interstitial flow velocities. The NSD in P3 contained combustion by-product, an easily soluble carbon source. Mussel shells still contained remnants of labile mussel meat attached to them that eventually detached and decomposed. S1 only contained limestone as an alkalinity amendment, which was abiotic, and therefore did not contain the additional organic matter that was present with mussel shells and NSD. Considering only the final four sampling events, effluent TOC concentrations during the third to final (week 14.4; $11.1 \leq \theta_{BGCR} \leq 12.0$) sampling event were greatest (average of 19.6 mg/L; range of 17.2-24.1) compared to other sampling events (average of 5.9 mg/L; range of 3.8-9.0) by an average of 2.3 times due to lower influent loading rates, and subsequently greater HRTs for organic substrate dissolution to occur (theoretical HRT was 2.94 times greater on average).

Table D.5: Comparison of DOC/TOC data from: 1) influent AMD; 2) effluent from BGCRs containing mussel shells or a mixture of mussel shells and limestone (P1, P2, S2, S3 and S4); 3) BGCR S1 (limestone); and 4) BGCR P3 (NSD, limestone and mussel shells). Values represent average concentrations with concentration ranges below in parentheses. Dissolved organic carbon concentrations were measured during the first three and middle four sampling events, whereas TOC was measured during the final four sampling events.

Sampling Events	**AMD**	**P1, P2, S2, S3 and S4**	**S1**	**P3**
	DOC or TOC (mg/L)			
First Three	10.6 (1.1-19.0)	931 (341-1500)	621 (304-814)	1345 (705-1810)
Middle	2.18 (1.90-2.56)	47.6 (8.7-97.8)	35.7 (6.20-79.2)	103 (47.8-176)
Final Four	1.43 (1.21-2.70)	9.26 (3.80-24.1)	7.35 (week 12.4)	NA

NA, non-applicable.

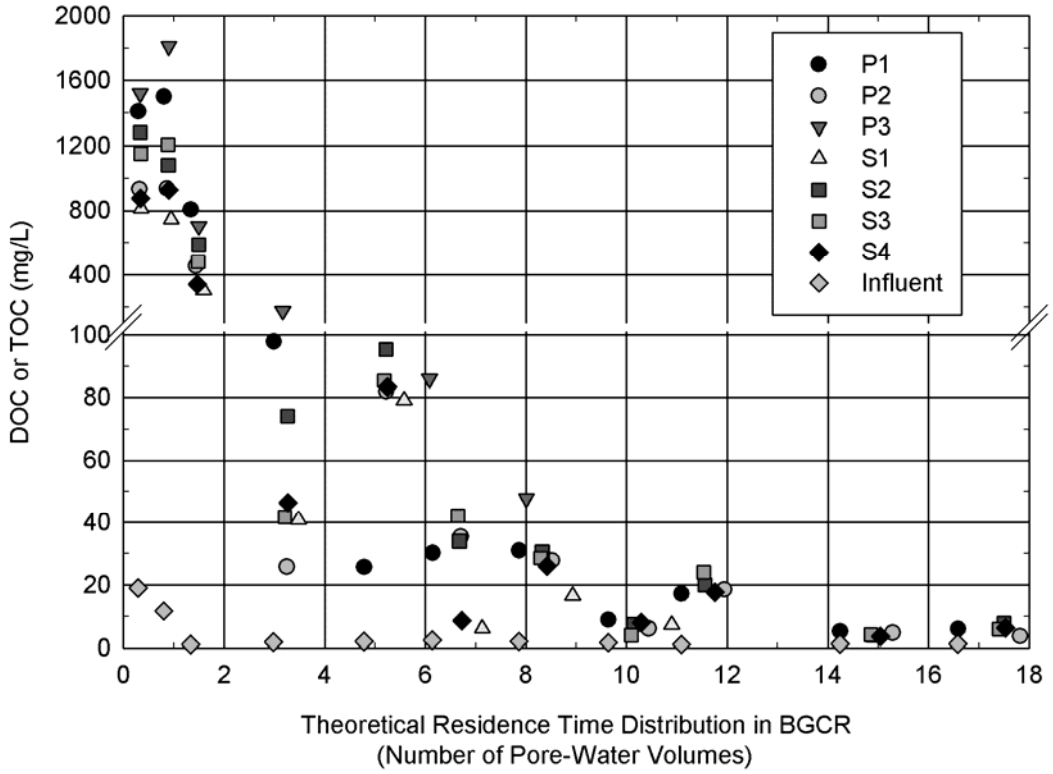

Figure D.11. Summary of influent AMD and effluent BGCR DOC (first six (up to week 9.5) sampling events) or TOC (last five (weeks 11.3-16.7) sampling events) values on a theoretical RTD basis considering all components of the BGCRs.

Nutrients and biological parameters including TN, TKN, TON, TP, faecal coliforms and BOD were only measured from the effluent of a few BGCRs during select sampling events (Table D.6). They also exhibited the first flush phenomenon with concentrations decreasing with time and presumed stabilised by the sixth sampling event (week 9.4; θ_{BGCR}=6.64-7.13). The first flush effect was most notable in systems containing the most mussel shells (S2 and S3 in this case) compared with S1, which only contained limestone as an alkalinity amendment, as previously discussed for cations, conductivity, solids and DOC/TOC. The organic carbon fraction of mussel shells likely contributed to TN, faecal coliforms and BOD. Additionally, nitrogen was present within the mineralogical mussel shell structure (New Zealand Seafood Industry Training Organisation (SITO), 2006). Nitrogen in BGCR effluent was in the reduced state as evident by the low TON concentrations, which contributed <13.5% of TN during the sixth sampling event. Total phosphorous concentrations were considerably less than TN (greater than one order of magnitude). Faecal coliform and BOD concentrations were extremely high initially, but declined to relatively low levels by the sixth sampling event (week 9.4; θ_{BGCR}=6.14-7.13). Therefore, it may be necessary to treat effluent for high faecal coliforms and BOD concentrations, depending on compliance, until concentrations stabilise to acceptable discharge levels.

Table D.6: Total nitrogen, TKN, TON, TP, faecal coliforms and BOD concentrations from effluent of BGCRs S1, S2, S3 and S4 during the following sampling events: 1) the first (week 1.1; $\theta_{BGCR} \leq 0.35$); 2) the fourth (week 5.2; $\theta_{BGCR} = 3.21\text{-}3.48$); and 3) the sixth (week 9.4; $\theta_{BGCR} = 6.14\text{-}7.13$).

Sampling Event	S1	S2	S3	S4
	TN (mg/L)			
First	4.4	77.2	NA	50.1
Fourth	1.0	22.5	15.2	NA
Sixth	1.3	7.3	11.2	NA
	TKN (mg/L)			
First	4.3	77	NA	50
Fourth	0.7	22	14	NA
Sixth	1.0	7	11	NA
	TON mg/L)			
First	0.054	0.413	NA	0.042
Fourth	0.269	0.427	1.26	NA
Sixth	0.175	0.114	0.155	NA
	Faecal Coliforms (cfu/100mL)			
First	6000	23,000	NA	80,000
Fourth	45	700	10	NA
Sixth	<10	15	<10	NA
	BOD (mg/L)			
First	1070	2150	NA	1270
Fourth	81.5	116	97.5	NA
Sixth	9.90	18.2	29.7	NA
	TP (mg/L)			
First	1.20	2.94	2.33	NA
Fourth	0.520	1.93	1.66	NA
Sixth	0.105	0.581	0.618	NA

NA, non-applicable.

Appendix E: Use of pH and Alkalinity as Surrogate Measurements for Assessing Iron and Aluminium Concentrations in Biogeochemical Reactor Effluent

Table E.1: Key observations associated with relationships of effluent Fe concentrations versus pH with respect to the most applicable water quality guidelines or results of ecotoxicity studies. Four scenarios were considered analysing drum and trapezoidal-shaped reactors separately during the middle three and final four sampling events.

BGCRs	Sampling Events	Figure	Key Observations
Fe Concentrations and pH			
P1-P2	Middle 3	5.7a	**1)** Effluent Fe concentrations remained relatively stable for each BGCR (average of 0.103 for P1 and 0.500 for P2) regardless of effluent pH (range of 6.71-6.89 for P1 and 6.58-6.74 for P2). **2)** All Fe concentrations were less than the commonly applied guideline value of 1.0 mg/L. **3)** Effluent from P1 was always below the most stringent guideline value of 0.300 mg/L from the Canadian Water Quality Guidelines for the Protection of Aquatic Life, whereas P2 effluent was always greater.
S2-S4	Middle 3	5.8a	**1)** Effluent Fe concentrations were always <1.0 mg/L when pH was ≥6.71; however, Fe concentrations were typically just greater than 3.0 mg/L during lower pH values (range of 6.54-6.65). **2)** Therefore, Fe removal would need to be incorporated in the design and performance monitoring of a subsequent aerobic oxidation treatment stage to meet this target.
P1-P2	Final 4	5.9a	**1)** Effluent Fe concentrations were <1.0 mg/L when pH≥6.73 and <3.0 mg/L when pH≥6.58. **2)** It is feasible to remove excess Fe from the effluent of the worst water chemistry (pH=6.42; 10.7 mg/L Fe) from BGCR P2 with a subsequent oxidation treatment stage.
S2-S4	Final 4	5.10a	**1)** Effluent Fe concentrations were <1 mg/L for the two effluent samples containing the highest pH (pH=6.72 and 6.80). **2)** Effluent Fe concentrations ranged from 2.16 to 3.17 mg/L when pH ranged from 6.70 to 6.71. **3)** Effluent Fe concentrations were 5.34 and 6.11 mg/L for effluent samples containing pH 6.66 and 6.67 (both data points from BGCR S4). Therefore, Fe removal would need to be incorporated in the design and performance monitoring of a subsequent aerobic oxidation treatment stage to meet this target. **4)** Effluent Fe concentrations were >10 mg/L when pH≤6.51 and system treatment capacity exceeded.

Table E.2: Key observations associated with relationships of effluent Al concentrations versus pH with respect to the most applicable water quality guidelines or results of ecotoxicity studies. Four scenarios were considered analysing drum and trapezoidal-shaped reactors separately during the middle three and final four sampling events.

BGCRs	Sampling Events	Figure	Key Observations
Al Concentrations and pH			
P1-P2	Middle 3	5.7b	**1)** Effluent Al concentrations remained relatively stable (average of 0.025 mg/L; range of 0.019-0.027 mg/L) regardless of reactor or pH (range of 6.58-6.89 mg/L as $CaCO_3$). **2)** Effluent Al concentrations were less than all ecotoxicity and guideline values shown in Table 5.1 with exception of the most stringent (0.005 mg/L (for waters containing pH<6.5) from the Canadian Water Quality Guidelines for the Protection of Aquatic Life) (Canadian Council of Ministers of the Environment, 2007).
S2-S4	Middle 3	5.8b	**1)** Effluent Al concentrations were relatively stable (average of 0.029 mg/L; range of 0.021-0.039 mg/L). **2)** Effluent Al concentrations were less than all ecotoxicity and guideline values shown in Table 5.1 with exception of the ANZECC trigger value for 99% level of protection for pH>6.5 (0.027 mg/L) and the most stringent guideline value of 0.005 mg/L (for waters containing pH<6.5) from the Canadian Water Quality Guidelines for the Protection of Aquatic Life. **3)** All effluent with pH≥6.71 contained Al concentrations ≤0.027 mg/L.
P1-P2	Final 4	5.9b	**1)** All effluent Al concentrations were less than the potential compliance target of 1.0 mg/L (minimum pH=6.42). **2)** Effluent Al concentrations were <0.15 mg/L (ANZECC trigger value for 80% level of protection for pH>6.5) when pH≥6.73.
S2-S4	Final 4	5.10b	**1)** Aluminium concentrations ranged from 0.023-0.256 mg/L within a pH range of 6.66-6.80. One-third of the samples exceeded the ANZECC trigger value of 0.150 mg/L for 80% level of protection for pH>6.5. **2)** When pH ranged from 6.45-6.51, Al concentrations exceeded the compliance target of 1 mg/L.

Table E.3: Key observations associated with relationships of effluent Fe concentrations versus alkalinity. Four scenarios were considered analysing drum and trapezoidal-shaped reactors separately during the middle three and final four sampling events.

BGCRs	Sampling Events	Figure	Key Observations
Fe Concentrations and Alkalinity			
P1-P2	Middle 3	5.11a	**1)** Effluent Fe concentrations remained relatively stable for each BGCR (average of 0.103 for P1 and 0.500 for P2) regardless of effluent alkalinity (range of 590-619 mg/L as $CaCO_3$ for P1 and 477-562 mg/L as $CaCO_3$ for P2).
S2-S4	Middle 3	5.12a	**1)** Effluent Fe concentrations were measured at concentrations <1.0 mg/L when alkalinity ranged from 512-565 mg/L as $CaCO_3$. **2)** Iron concentrations were near of just greater than the potential future compliance target of 3.0 mg/L within an alkalinity range of 468-523 mg/L as $CaCO_3$.
P1-P2	Final 4	5.13a	**1)** Effluent Fe concentrations showed a relatively linear relationship with alkalinity on a logarithmic scale. **2)** Effluent Fe concentrations were <0.300 mg/L (the stringent Canadian guideline value) when alkalinity >380 mg/L as $CaCO_3$. **3)** Effluent Fe concentrations were between 1 and 3 mg/L within an alkalinity range of 262-312 mg/L as $CaCO_3$.
S2-S4	Final 4	5.14a	**1)** Effluent Fe concentrations were <1 mg/L for the two effluent samples containing the highest alkalinities (392 and 447 mg/L as $CaCO_3$). **2)** Effluent Fe concentrations ranged from 2.16-3.17 mg/L when alkalinities ranged from 276-381. **3)** Effluent Fe concentrations were 5.34-6.11 mg/L for effluent samples containing alkalinities of 237 and 274 mg/L as $CaCO_3$. These were achieved from BGCR S4. **4)** Effluent Fe concentrations were >10 mg/L when alkalinity≤141 mg/L as $CaCO_3$ and system treatment capacity exceeded.

Table E.4: Key observations associated with relationships of effluent Al concentrations versus alkalinity. Four scenarios were considered analysing drum and trapezoidal-shaped reactors separately and the middle three and final four sampling events.

BGCRs	Sampling Events	Figure	Key Observations
Al Concentrations and Alkalinity			
P1-P2	Middle 3	5.11b	**1)** Effluent Al concentrations remained relatively stable (average of 0.025 mg/L; range of 0.019-0.027 mg/L) regardless of reactor or alkalinity (range of 477-690 mg/L as $CaCO_3$).
S2-S4	Middle 3	5.12b	**1)** Effluent Al concentrations were relatively stable averaging 0.029 mg/L (range of 0.021-0.039 mg/L) from an alkalinity range of 364-565 mg/L as $CaCO_3$. **2)** Effluent Al concentrations were ≤0.027 mg/L (ANZECC guideline value for 99% level of protection (pH>6.5)) throughout an alkalinity range of 468-565 mg/L as $CaCO_3$. The alkalinity range was 364-523 mg/L as $CaCO_3$ for effluent concentrations >0.027 mg/L.
P1-P2	Final 4	5.13b	**1)** Effluent Al concentrations showed a relatively linear relationship with alkalinity on a logarithmic scale considering each reactor separately. **2)** Effluent Al concentrations were <0.15 mg/L (ANZECC trigger value for 80% level of protection for pH>6.5) when alkalinity was ≥350 mg/L as $CaCO_3$.
S2-S4	Final 4	5.14b	**1)** Effluent Al concentrations were generally similar during each sampling event, with exception of the final sampling event, regardless of BGCR. **2)** Effluent Al concentrations ranged from 0.023-0.031 within an alkalinity range of 381-447 mg/L as $CaCO_3$, which were near the ANZECC trigger value for 99% level of protection (pH>6.5) of 0.027 mg/L. **3)** Effluent Al concentrations ranged from 0.049-0.055 mg/L within an alkalinity range of 274-324 mg/L as $CaCO_3$, which were less than the ANZECC trigger value for 80% level of protection (pH>6.5) of 0.150 mg/L. **4)** Effluent Al concentrations ranged from 0.194-0.256 mg/L within an alkalinity range of 237-283 mg/L as $CaCO_3$. **5)** Effluent Al concentrations exceeded the compliance target of 1 mg/L within an alkalinity range of 137-141 mg/L as $CaCO_3$ when Al concentrations were 2.09 and 3.10 mg/L. **6)** Effluent Al concentration was 36.1 mg/L with an alkalinity of 5.15 mg/L as $CaCO_3$, and system treatment capacity was exceeded.

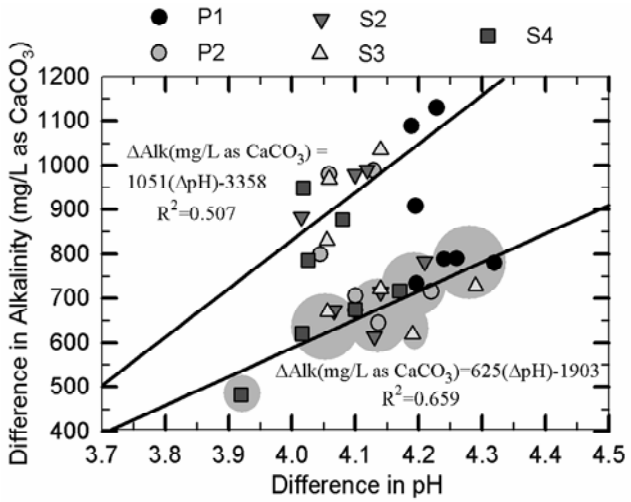

Figure E.1. Comparison of the differences between influent and effluent pH versus the differences between influent and effluent alkalinity from BGCRs containing mussel shells (P1, S2 and S3) or a mixture of mussel shells and limestone (P2 and S4). Results from the first four sampling events (up to week 5.2) were excluded since the BGCRs were operating under first-flush conditions. The data highlighted grey represents the final four sampling events. The non-highlighted cells represent the middle four sampling events. Data used for establishing best-fit lines were separated from the middle three and final four sampling events.

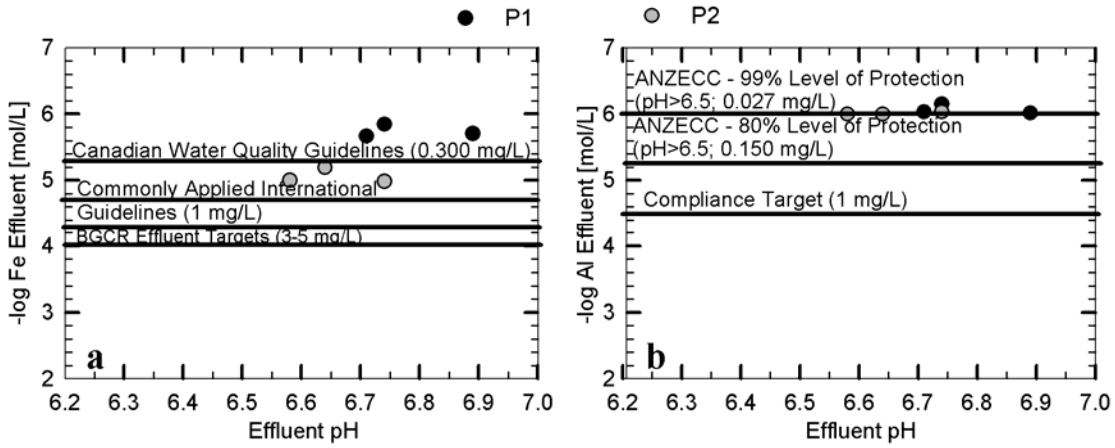

Figure E.2. Negative log of the effluent molar a) Fe and b) Al concentrations versus pH for drum-shaped BGCRs containing mussel shells (P1) or a mixture of mussel shells and limestone (P2) during the middle three sampling events (Scenario 1).

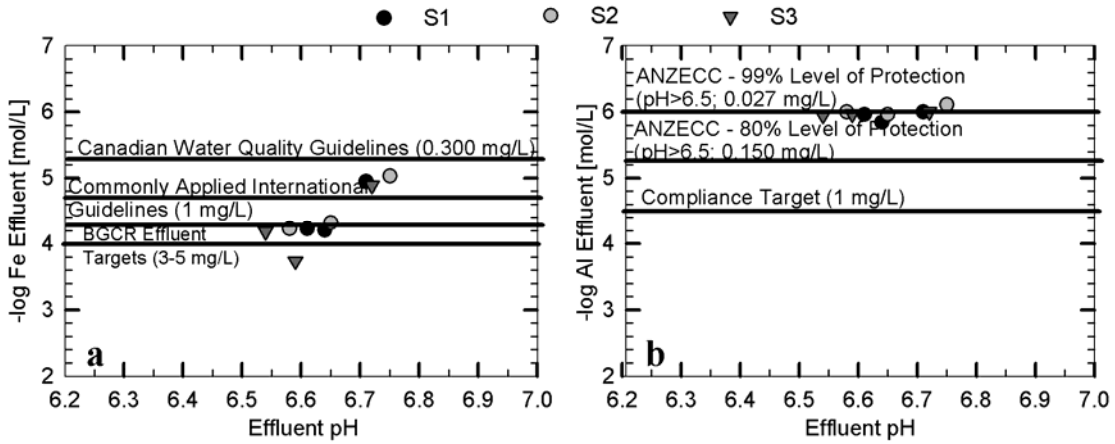

Figure E.3. Negative log of the effluent molar a) Fe and b) Al concentrations versus pH for trapezoidal-shaped BGCRs containing mussel shells (S2 and S3) or a mixture of mussel shells and limestone (S4) during the middle three sampling events (Scenario 2).

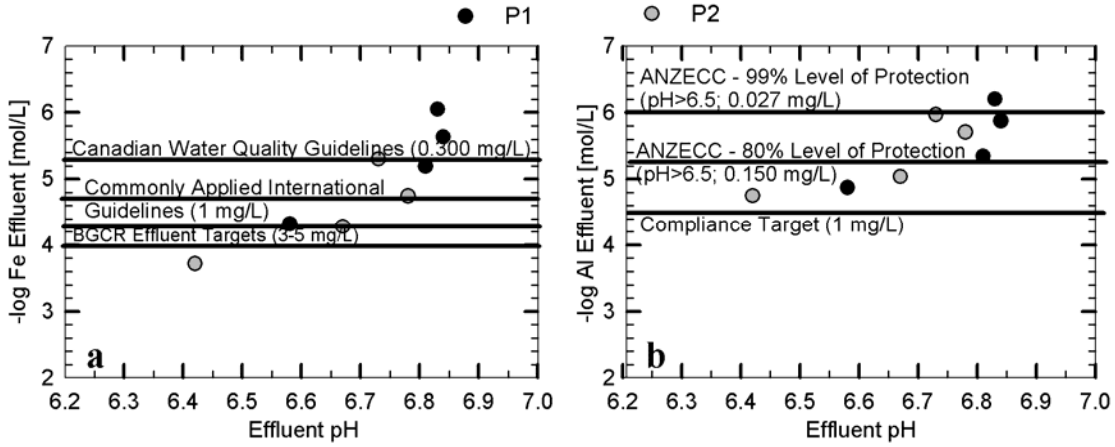

Figure E.4. Negative log of the effluent molar a) Fe and b) Al concentrations versus pH for drum-shaped BGCRs containing mussel shells (P1) or a mixture of mussel shells and limestone (P2) during the final four sampling events (Scenario 3).

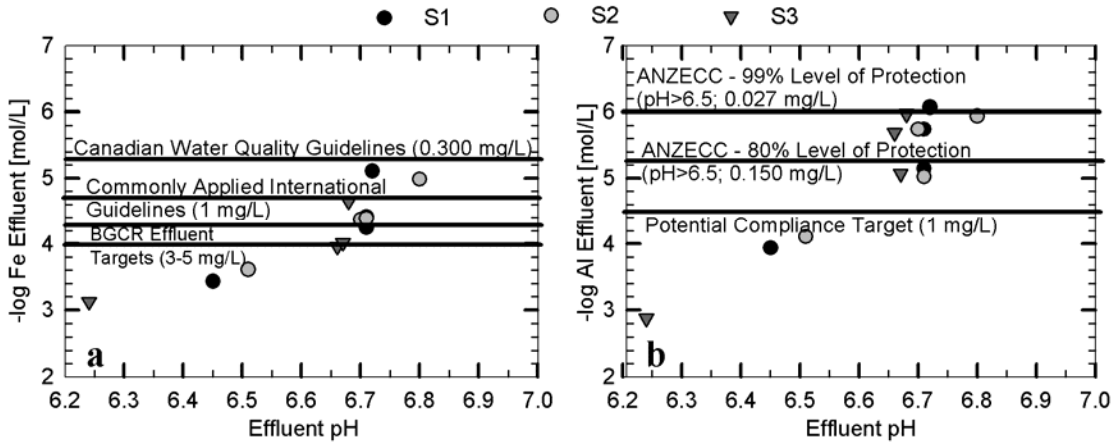

Figure E.5. Negative log of the effluent molar a) Fe and b) Al concentrations versus pH for trapezoidal-shaped BGCRs containing mussel shells (S2 and S3) or a mixture of mussel shells and limestone (S4) during the final four sampling events (Scenario 4).

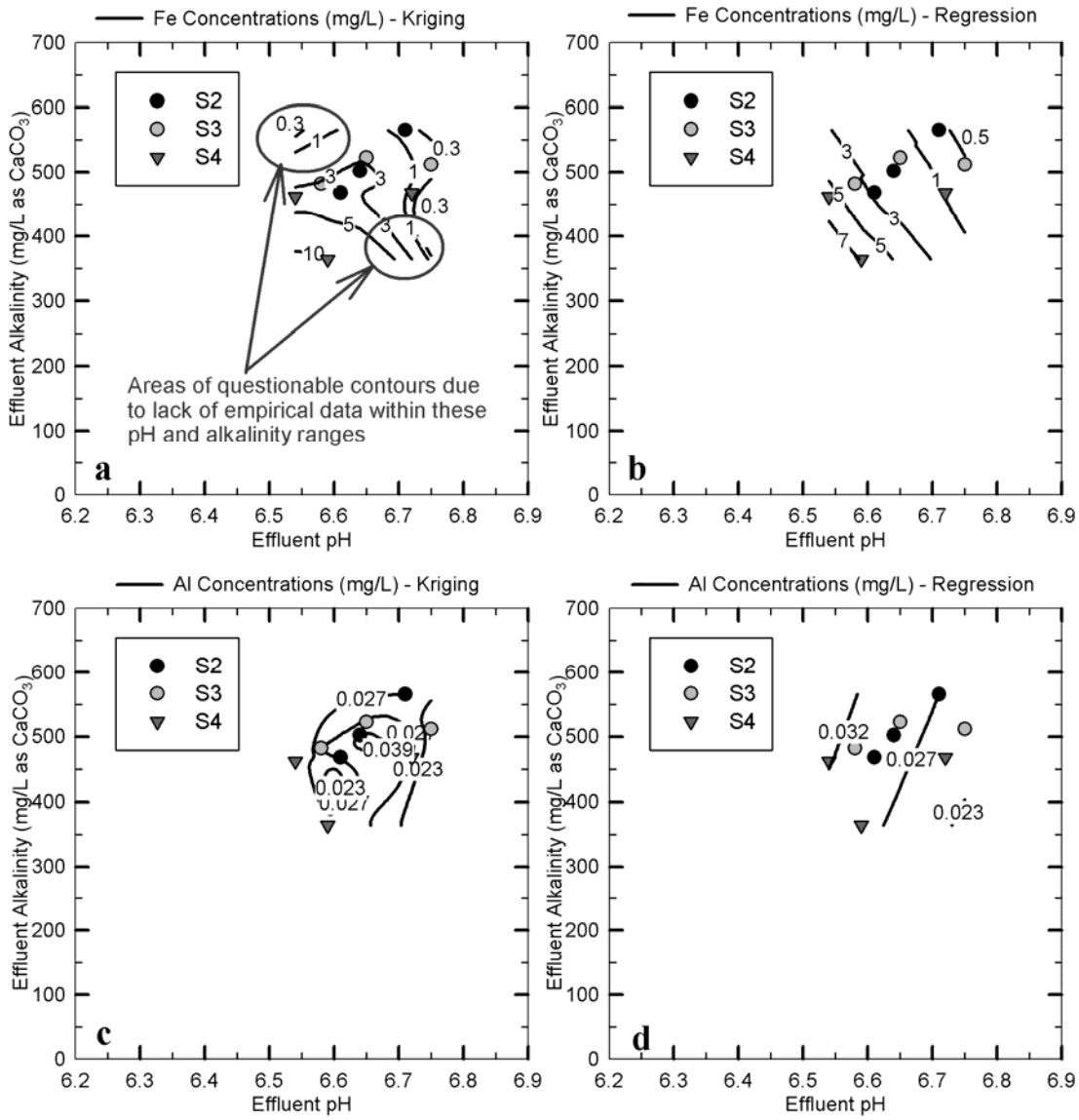

Figure E.6. Effluent Fe and Al concentration predictions based on pH and alkalinity using kriging interpolation (a and c) and two-component regression analysis (b and d). Aluminium concentrations were predicted using the two-component regression analyses of the negative log molar concentrations with pH and alkalinity, whereas Fe concentrations were predicted using the two-component regression analyses of the negative log molar concentrations with pH and log alkalinity. Data is representative of the middle three sampling events for trapezoidal-shaped BGCRs (Scenario 2) containing mussel shells (S2 and S3) or a mixture of mussel shells and limestone (S4). Data points shown represent effluent pH and alkalinities measured from BGCR effluent. Iron concentration contours were developed by SigmaPlot® in Figure E.5a in areas where there was no empirical data to validate their accuracy.

Appendix F: Tracer Testing to Determine the Hydraulic Characteristics of Mesocosm-Scale Biogeochemical Reactors and Their Application to Reactor Modelling

Calculating the Density of a Sodium Bromide Solution

The density of a sodium bromide solution was calculated using Equation F.1 (from Kadlec and Wallace, 2009) where ρ_{NaBr} is the density of the sodium bromide solution in units mg/L and $C_{NaBr(dose)}$ represents the concentration of the tracer dose solution in units mg/L.

$$\rho_{NaBr} = 1.0000 + (7.2869E\text{-}7)C_{NaBr(dose)} \quad \textbf{(F.1)}$$

$C_{NaBr(dose)}$ was calculated using Equation F.2 where m_{NaBr} represents the mass of sodium bromide in units mg and V denotes the volume of water in units L comprising the solution.

$$C_{NaBr(dose)} = m_{NaBr} / V \quad \textbf{(F.2)}$$

Table F.1: A summary of the reaction rate constants calculated for Fe, Al and acidity for BGCRs P1, P2, S2, S3 and S4 calculated based on the ratios of effluent and influent concentrations at their theoretical HRTs in the BGCRs.

Theoretical HRT in BGCR (days)	Fe Out / Fe In Ratio	k(Fe) (1/day)	Al Out / Al In Ratio	k(Al) (1/day)	Acidity Out / Acidity In Ratio	k(Acidity) (1/day)
P1						
2.16	2.80E-02	2.23	6.72E-03	3.53	1.43E-02	2.80
3.49	3.89E-03	2.55	2.36E-03	2.91	7.59E-03	2.11
4.53	1.84E-03	2.39	6.89E-04	3.02	5.82E-03	1.76
7.46	1.20E-03	1.61	3.72E-04	2.11	4.56E-03	1.14
7.73	2.01E-03	1.37	5.48E-04	1.87	4.62E-03	1.10
9.60	7.72E-04	1.39	3.80E-04	1.63	4.27E-03	0.90
11.8	7.53E-04	1.13	2.73E-04	1.42	3.96E-03	0.75
P2						
2.00	1.12E-01	1.31	8.90E-03	3.51	3.40E-02	2.24
3.29	3.15E-02	1.40	4.75E-03	2.56	1.70E-02	1.74
4.20	1.41E-02	1.45	1.02E-03	2.98	1.01E-02	1.61
7.04	1.06E-02	0.95	5.27E-04	2.07	7.52E-03	1.05
7.05	5.62E-03	1.14	4.02E-04	2.20	6.41E-03	1.10
9.23	4.32E-03	0.94	6.49E-04	1.51	6.20E-03	0.85
10.9	3.38E-03	0.85	3.88E-04	1.44	5.58E-03	0.74
S2						
1.95	2.16E-01	0.97	5.74E-02	2.21	7.52E-02	1.92
3.28	3.43E-02	1.68	3.75E-03	3.98	1.68E-02	2.27
4.43	3.06E-02	1.31	9.39E-04	4.66	1.41E-02	1.81
7.11	1.16E-02	1.22	5.69E-04	3.40	8.03E-03	1.40
7.76	3.47E-02	0.71	5.81E-04	3.09	1.34E-02	1.05
9.82	6.71E-03	1.08	5.15E-04	2.54	6.71E-03	1.08
11.0	3.11E-02	0.52	4.24E-04	2.40	1.32E-02	0.74
S3						
1.98	1.42E-01	1.29	3.87E-02	2.63	5.24E-02	2.27
3.31	2.46E-02	1.92	4.93E-03	3.58	1.49E-02	2.36
4.47	3.38E-02	1.24	9.39E-04	4.62	1.44E-02	1.78
7.03	9.48E-03	1.33	4.43E-04	3.72	7.29E-03	1.46
7.76	3.31E-02	0.72	4.02E-04	3.47	1.28E-02	1.07
9.61	8.95E-03	0.99	6.94E-04	2.36	6.99E-03	1.09
11.0	2.50E-02	0.57	4.24E-04	2.40	1.18E-02	0.78
S4						
2.04	4.37E-01	0.46	6.67E-01	0.21	3.52E-01	0.59
3.35	5.77E-02	1.28	4.44E-03	3.68	2.34E-02	1.94
4.31	8.65E-02	0.81	1.05E-03	4.62	2.69E-02	1.42
7.04	1.31E-02	1.17	5.69E-04	3.43	9.11E-03	1.35
7.53	3.67E-02	0.71	4.54E-04	3.44	1.42E-02	1.06
9.48	1.93E-02	0.74	6.49E-04	2.45	9.92E-03	0.97
10.9	9.56E-02	0.30	4.16E-04	2.45	2.88E-02	0.55

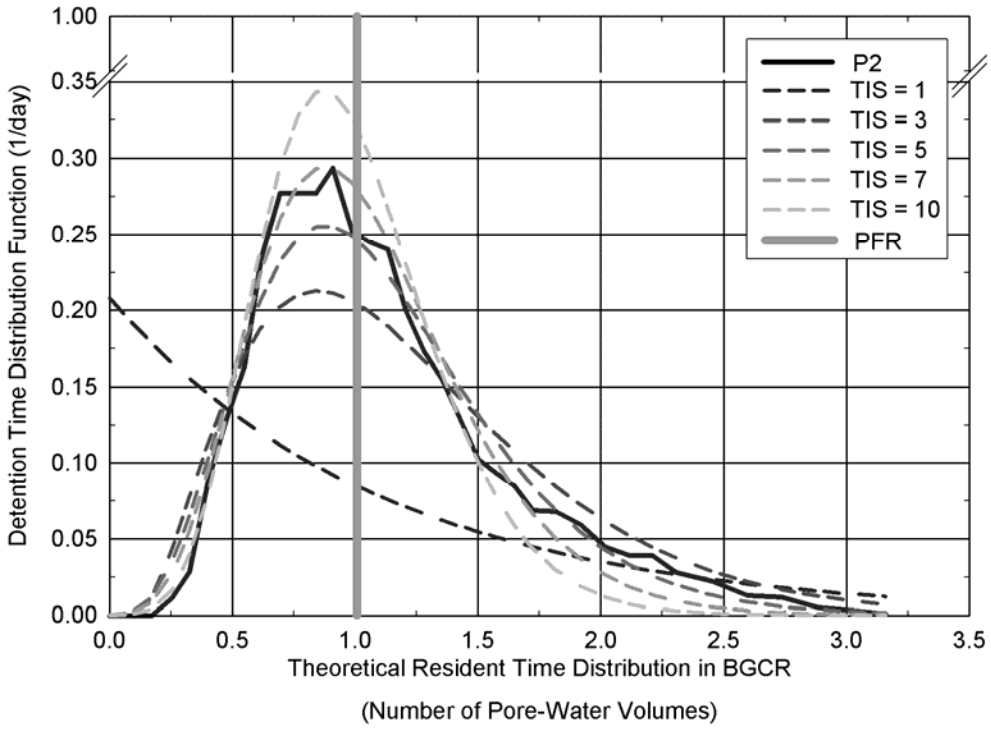

Figure F.1. The DTD functions derived from the tracer study analysis of BGCR P2 and the gamma distributions developed employing 1, 3, 5, 7, 10 and an infinite number (PFR model) of TIS. For the PFR model (or an infinite number of TIS), an instantaneous pulse would be observed at θ_{BGCR}=1.

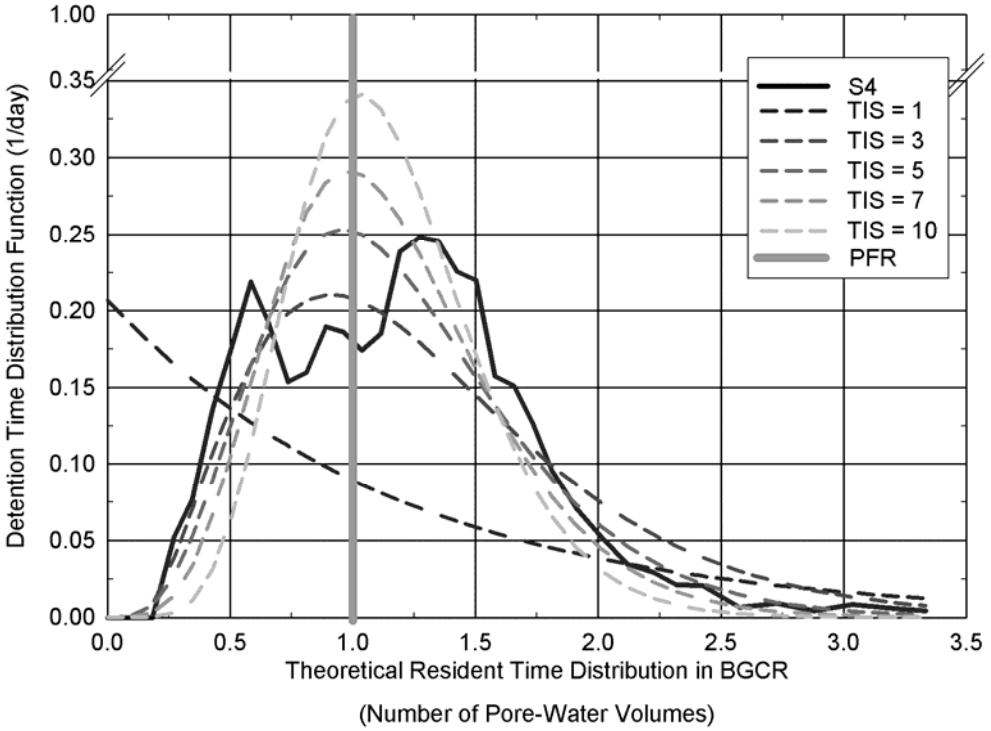

Figure F.2. The DTD functions derived from the tracer study analysis of BGCR S4 and the gamma distributions developed employing 1, 3, 5, 7, 10 and an infinite number (PFR model) of TIS. For the PFR model (or an infinite number of TIS), an instantaneous pulse would be observed at θ_{BGCR}=1.

Appendix G: Advancing Scaling Challenges Associated with Passive Acid Mine Drainage Treatment Systems

Sedimentation Basin Construction and Design Details

The sedimentation basin design (Figure G.1) is trapezoidal-prism shaped containing 3.0 m wide berms constructed (for equipment and maintenance access) at a side slope of 1:1 (vertical:horizontal). The size maximises the readily available land space (approximately 38 m X 24 m) near the seep where the flow equalisation pond exists and results in an upper water surface area of 377 m^2 (29 m X 13 m). Sediment basin depth typically ranges from one to three metres depending on such factors as groundwater depth and depth to bedrock (Younger et al., 2002; PIRAMID, 2003; Wildeman et al., 2006). The recommended basin water depth is 1.5 m with 0.5 m freeboard. The sedimentation basin should not be lined with an impermeable membrane since sediment will need to be removed periodically by an excavator that could easily damage the liner. Furthermore, the underlying bedrock coupled with the compacted berms and fine sediment that settles will result in a relatively impermeable basin. The flow capacity of the 150 mm diameter PVC outlet pipe was designed at 35 L/s assuming a 1 in 15 gradient.

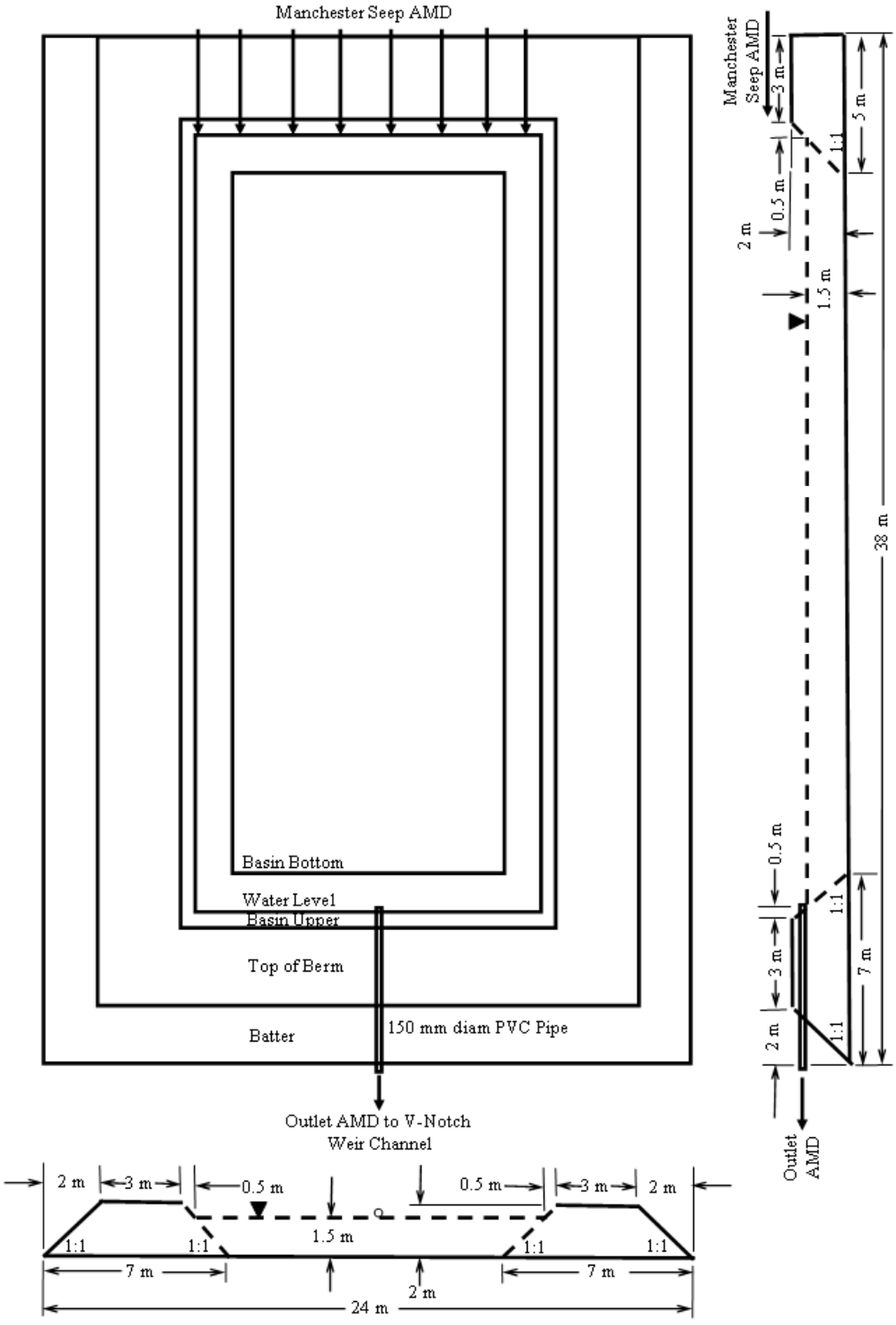

Figure G.1. Sedimentation basin design and dimensions.

V-Notch Weir Channel Construction Material and Design Details

The v-notch weir channel (Figure G.2) should be constructed from 17 mm thick H3 treated plywood sheets containing exterior reinforcement with H3 treated 4X2s and 2X2s and assembled with bolts and screws. The plywood should be made water proof by applying multiple coats of marine grade epoxy paint and water tight by sealing all joints with Sikaflex® Tank Sealant.

The recommended design dimensions of the v-notch weir channel, the v-notch weir and the flow barrier are shown in Figure G.2. As an example, the flow barrier should contain five 54 mm diameter holes and twenty-eight 33 mm diameter holes and allowed 60 mm freeboard. The v-notch should be constructed from 6 mm thick acrylic at an angle of 28^{o} 4' and dimensions 190 mm width at top and 380 mm depth. These dimensions result in one-quarter of the flow of a 90^{o} weir. The downgradient side of the weir should be chamfered at $\geq 60^{o}$ to achieve a smooth flowing nappe and critical flow. The ISO flow equation (ISO, 2008) to calculate the volumetric flow rate (Q) through a v-notch weir is shown by Equation G.1 where C_d represents the coefficient of discharge and g represents gravitational acceleration.

$$Q\ (L/s) = 8000/15((2g)C_d\tan(\theta/2)h^{5/2})^{1/2} \quad \textbf{(G.1)}$$

This is typically simplified in field applications, and in the case of a 28^{o}4' v-notch, a constant C_d value of 0.587 is assumed (ISO, 2008) and Equation G.1 simplifies to Equation 7.1.

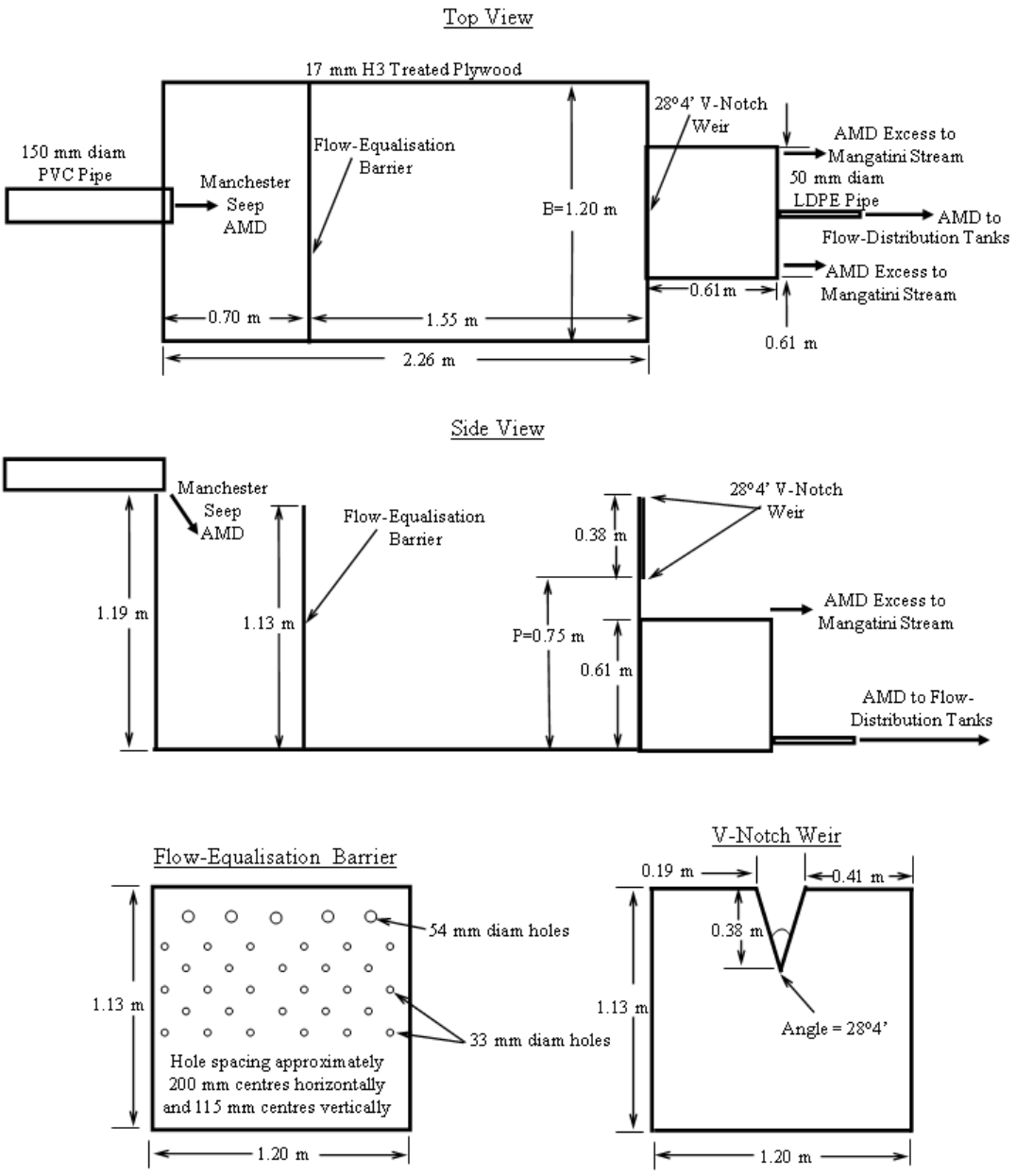

Figure G.2. Design dimensions of the v-notch weir channel, the v-notch weir and the flow barrier.

Flow Distribution Design Details

The recommended flow distribution system is comprised of two 1000 L HDPE tanks and associated piping (Figure G.3). The maximum inlet flow rate into the flow-distribution tanks would be dependent on the gradient and piping distance from the v-notch weir outlet to the inlet of the fist header tank. The 50 mm pipe has a flow capacity of approximately 2.0 L/s (calculated from Manning's Equation) assuming gravity feed at a 1 in 16.7 gradient, the approximate gradient measured at the Manchester Pond to the primary treatment area. The Manchester AMD would enter the first header tank, which should be connected with the second header tank via tank fittings and a short section of 50 mm PVC pipe. Three 32 mm diameter tank fittings, ball valves and PVC flexible tubing should be positioned near the bottom of the second tank to convey flow to the subsequent treatment

stage consisting of three BGCRs operated in parallel. Excess flow would diverted through 50 mm PVC pipes positioned near the top of the header tanks and conveyed via open channel and culverts to the Mangatini Stream for subsequent treatment downgradient. The water level would be maintained at a relatively constant level with the PVC overflow pipes and, therefore, consistent flow should be obtained into the BGCRs.

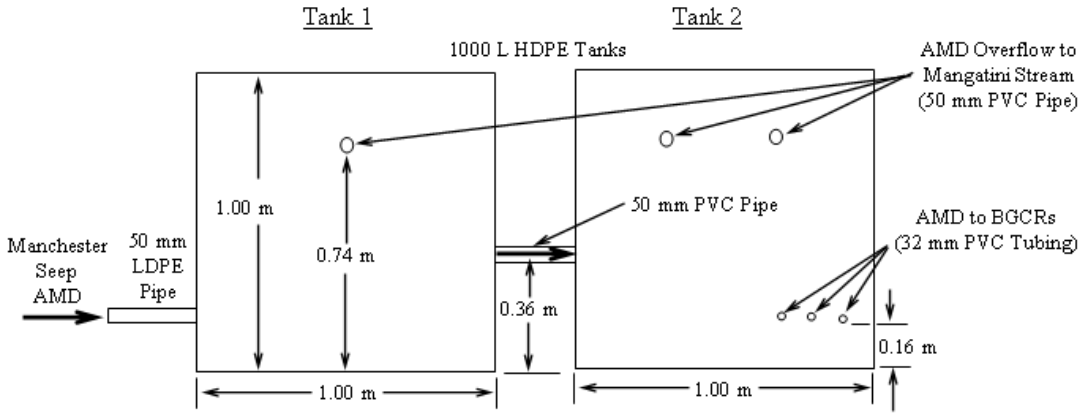

Figure G.3. The flow-distribution system for the designed BGCRs.

Biogeochemical Reactor Construction and Design Details

Schematics showing the design dimensions of the pilot-scale BGCRs include: Figure G.4) PS-1; Figure G.5) PS-2a; Figure G.6) PS-2b (alternative flow design incorporating baffles); and Figure G.7) PS-3. Two different flow configurations were considered for PS-2. PS-2a contains the standard drainage design (discussed below) whereas PS-2b incorporates two baffles using 1 mm LDPE liners. The basins should be constructed from stable earthen materials and contain the shape of trapezoidal prisms containing a length to width ratio at the upper substrate surface of two, side walls sloped at 1:1 (vertical:horizontal) and assume a 5.0 m berm width to allow maintenance equipment access. To accommodate the extra substrate depths and side slopes, PS-2a and PS-2b were designed to receive twice the flow of the other reactors and, consequently, contain twice the reactor substrate. An example basin arrangement is illustrated in Figure G.8 such that the basin PS-2 can share berms with PS-1 and PS-3. An access ramp is recommended at a 1:3 (vertical:horizontal) slope to allow equipment access to the berms for construction and maintenance operations. The locations of the aerobic treatment systems (AW-1, AW-2 and AW-3) that receive effluent from the BGCRs are also shown in Figure G.8 and include an approximate 1.0 m distance from the edge of the BGCR berms to allow room for the outlet control structures. Bedding, substrate and post peel flow-equalisation material volumes required and liner dimensions for each BGCR are summarised in Table G.1. Volume requirements for substrate assume an additional 25% for PS-1 and PS-2a and 2b (as determined during the geotechnical studies reported in Chapter 2) and 35% for PS-3 to account for volume losses that occur as result of mixing and settlement.

The BGCRs would require lining (Wildeman et al., 2006), so a 1 mm thick LDPE liner (or comparable impermeable liner) is recommended. The liner dimensions that would be required for each BGCR are shown in Table G.1, which assume 0.6 m extra material on each side so the liner can be keyed into the top of the berm. Each BGCR, with exception of PS-2b, is designed to contain 0.2 m depth of bedding material at its base comprised of free draining gravel such as 20-40 mm diameter gravel or other economically viable, non-acid generating course and non-degrading material. The drainage piping should consist of 50 mm PVC (9 bar pressure capacity) with slots created at approximate 150 mm spacing with an angle grinder and connected with appropriate fittings (e.g. PVC elbows, tees and crosses). The recommended array for PS-1 and PS-3 is shown in Figure G.9, and the recommended arrays for PS-2a and PS-2b are shown in Figures G.10 and G.11, respectively. The drainage arrays comprise the majority of the area of the basin bottom to achieve more uniform flow within the BGCRs. Outflow from the BGCRs should be conveyed from the drainage pipe via a 50 mm PVC effluent pipe. The effluent pipe should be connected to the drainage pipe via a tank fitting installed into the liner near the outlet. It is recommended to utilise a 100 mm PVC pipe situated at the outlet juncture to act as a protective barrier for the 50 mm effluent pipe. Water level within the BGCRs would be controlled via an outlet control structure such as that shown in Figure G.12. The outlet control structure should consist of a 50 mm PVC pipe reduced to a 40 mm PVC pipe (with a pipe reducer fitting), which can be moved vertically to control the water level. Piping and 90^{o} elbows should be attached to the outlet control structure to control the location and elevation (drop height) where BGCR effluent flows into the subsequent aerobic treatment stages. Overlying the bedding material is either 1.0 m (PS-1 and PS-3) or 2.0 m (PS-2) of the substrate mixture. It is recommended to include a 0.3 m thick layer of post peel overlying the substrate mixture, although this would not be essential. BGCRs PS-1 and PS-2 should contain 0.5 m of freeboard, and PS-3 should contain 1.0 m of freeboard.

For PS-2b (Figure G.6), the outlet pipe should be situated at the top of bedding material beneath the lower baffle to allow gas bubbles to escape the system. The bedding material should also be placed exclusively near the outlet, as opposed to the reactor bottom, to maximise flow through the substrate. If preferred, the outlet pipe could be situated at the basin bottom; however, vent piping would be recommended to allow gas escapement. The vent piping could be placed through the liner using a tank fitting to seal the pipe and liner interface. PS-2b was designed to contain the same material requirements as PS-2a with exception of drainage piping and the extra liners used as baffles.

Table G.1: Bedding, substrate and post peel flow-equalisation material volumes and liner dimensions required for each BGCR. Volume requirements for substrate assume an additional 25% for PS-1 and PS-2a and 2b and 35% for PS-3 to account for volume losses that occur as result of mixing and settlement. Extra settlement will occur in PS-3 due to the higher percentage of compost. Liner dimensions assume 0.6 m extra material on each side so the liner can be keyed into the top of the berm.

BGCR	PS-1	PS-2a	PS-2b	PS-3	Total
Substrate Quantities (m^3)					
Total Substrate	57.6	115		67.2	240
Mussel Shells	17.3	34.6		18.7	70.6
Post Peel (in Substrate)	20.2	40.3		15.6	76.1
Bark	11.5	23.0		9.33	43.8
Compost	8.64	17.3		18.7	44.6
Other Material Quantities (m^3)					
Bedding Material	5.93	3.42		5.93	15.3
Post Peel (Flow Equalisation Layer)	19.9	25.3		19.9	65.1
Post Peel (Total)	40.1	65.6		35.5	141
Liner Dimensions (m) and Area (m^2)					
Basin Bottom	15.5X10.0 (155 m^2)	17.8X11.5 (205 m^2)		16.9X11.4 (193 m^2)	553 m^2 (837 m^2 with Baffles)
Top Baffle	NA	NA	11.0X14.0 (154 m^2)	NA	NA
Lower Baffle	NA	NA	10.0X13.0 (130 m^2)	NA	NA

NA, non applicable

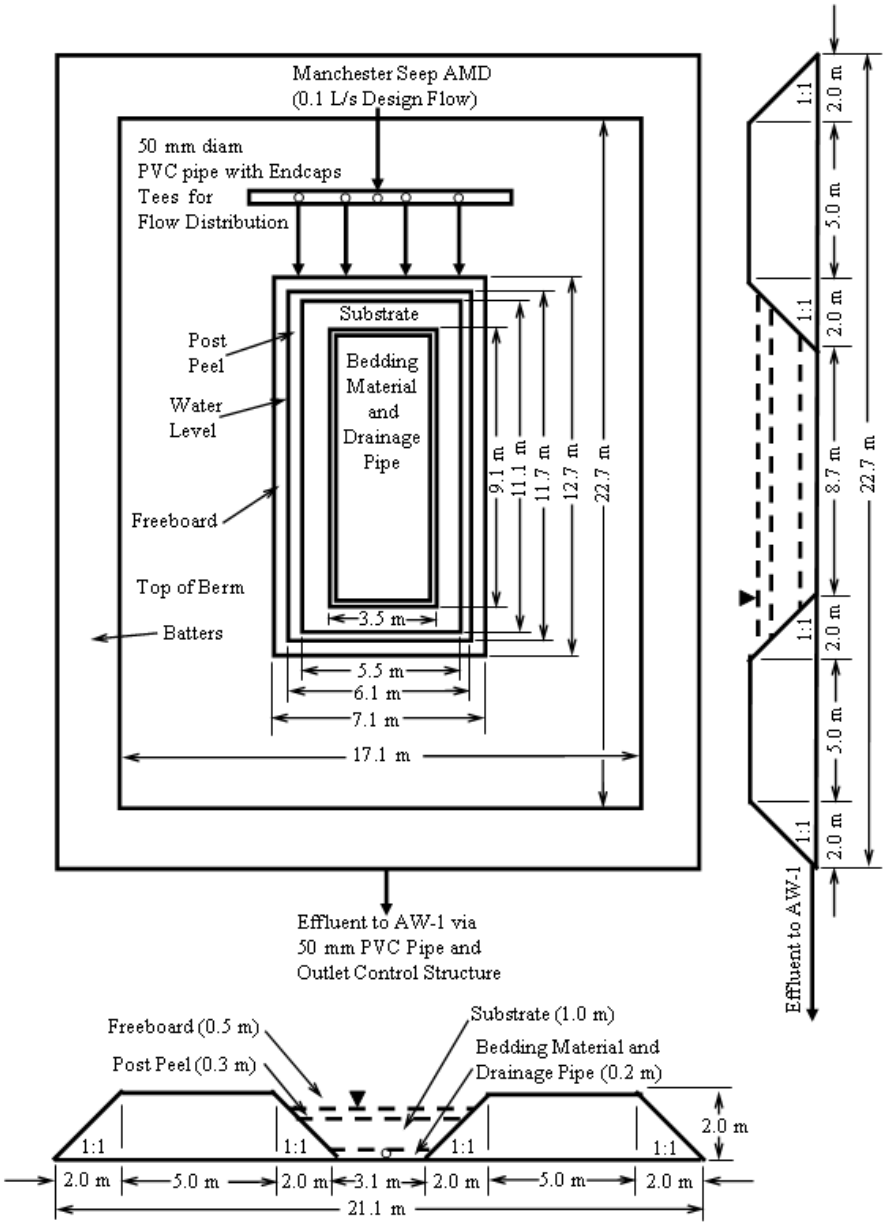

Figure G.4. Design dimensions of the pilot-scale BGCR PS-1.

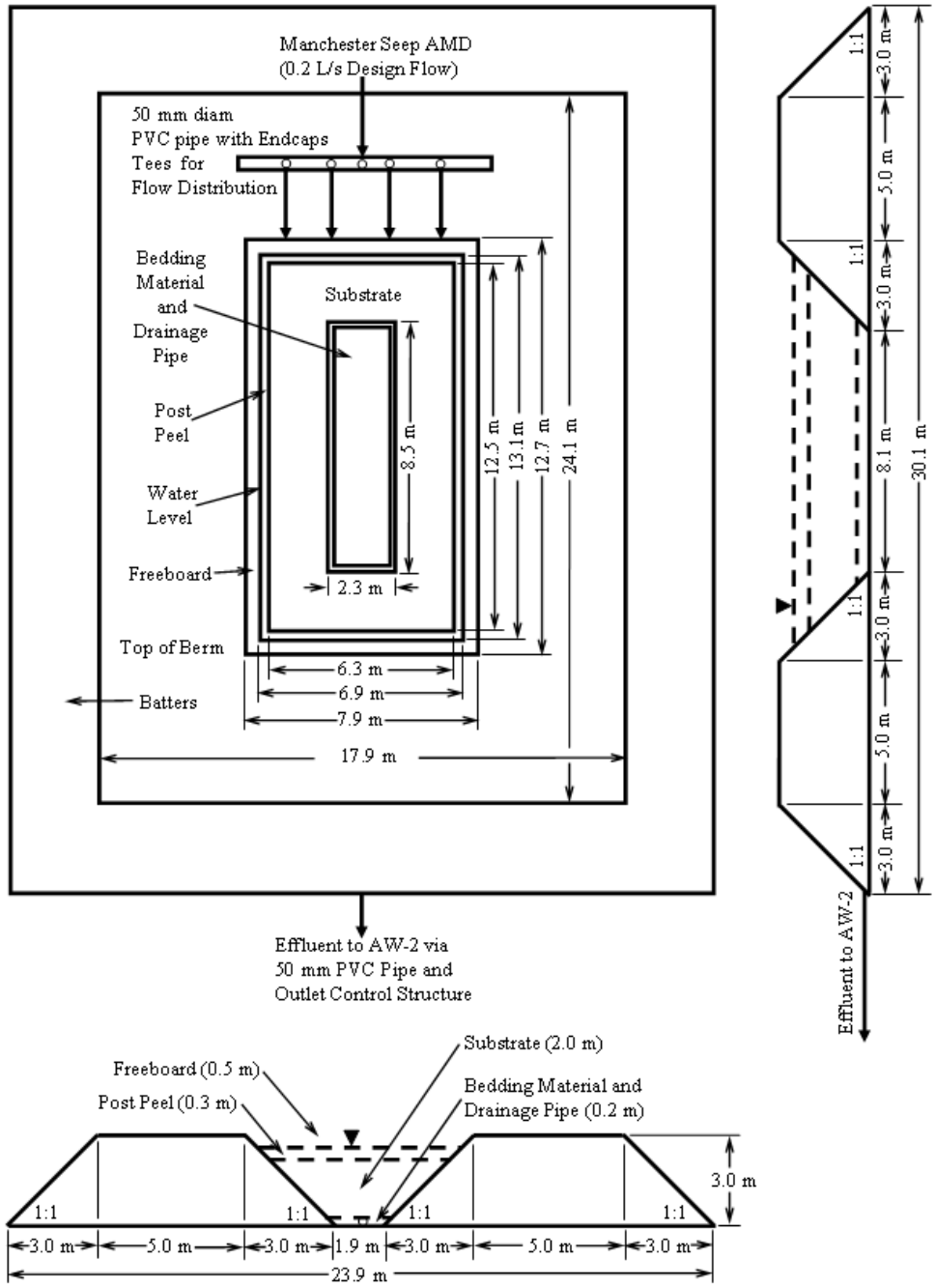

Figure G.5. Design dimensions of the pilot-scale BGCR PS-2.

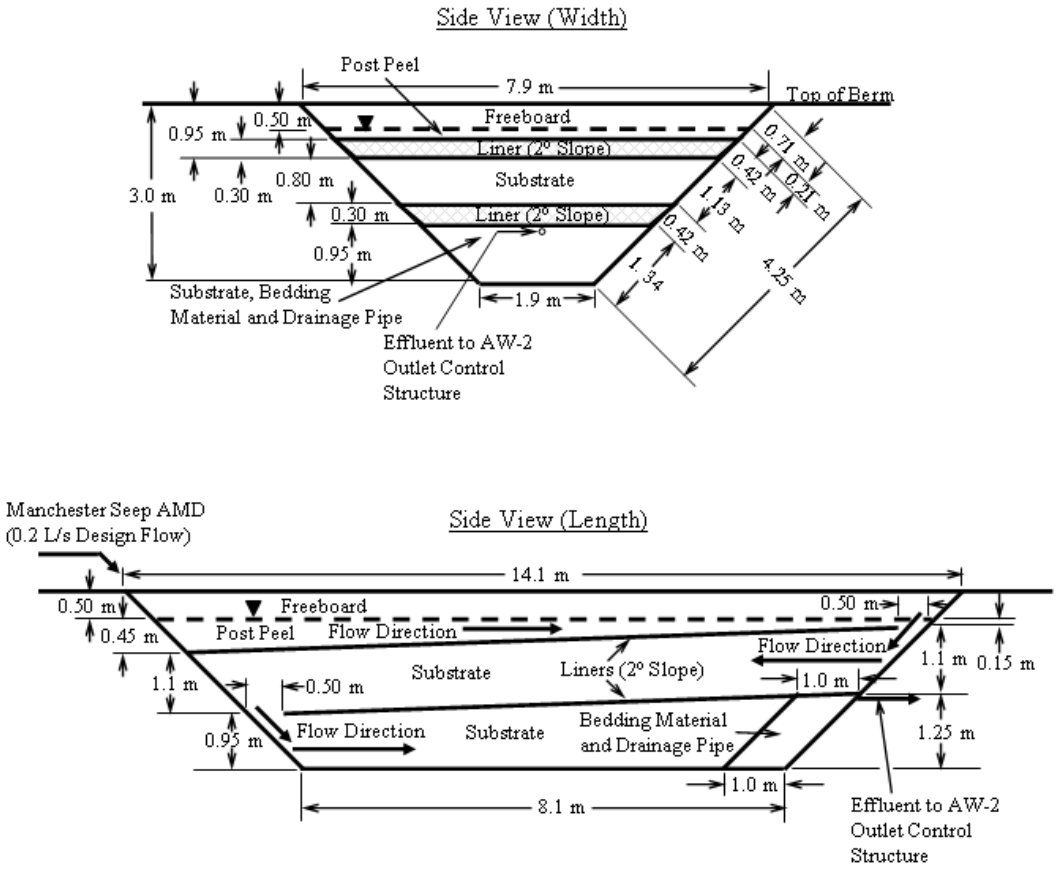

Figure G.6. Design dimensions for the alternative flow design of the pilot-scale BGCR PS-2 where two liners would be placed at a 2^{o} slope and are used as baffles to minimise hydraulic short circuiting.

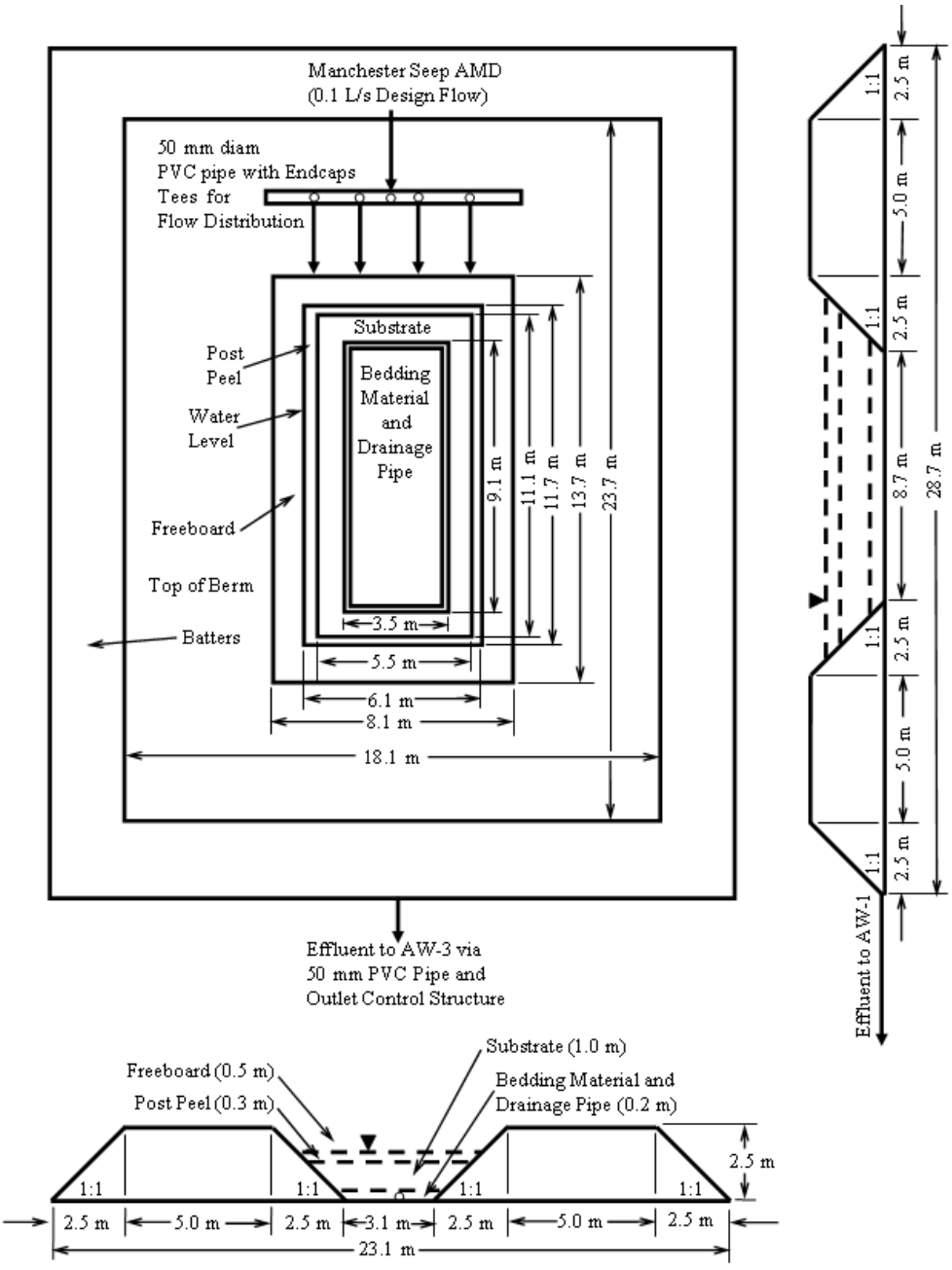

Figure G.7. Design dimensions of the pilot-scale BGCR PS-3.

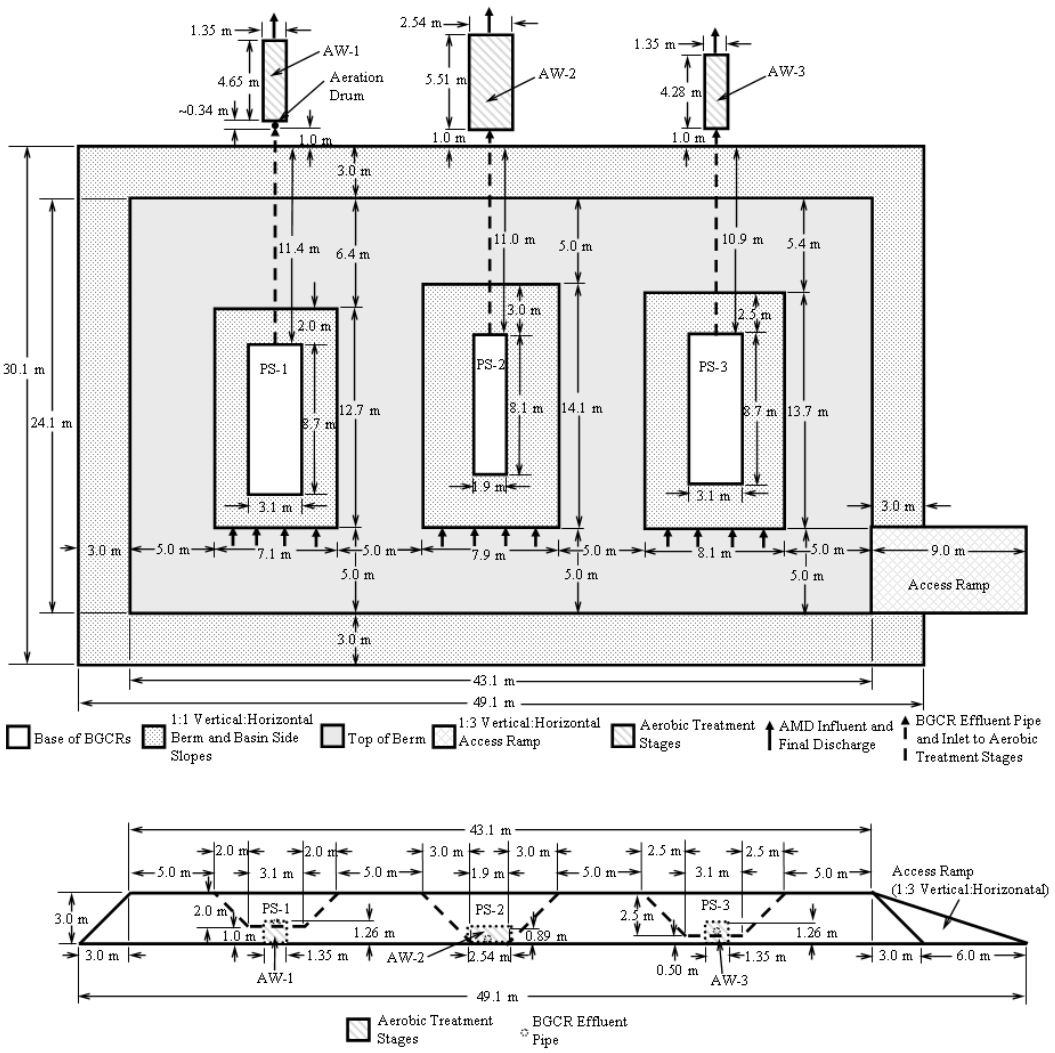

Figure G.8. The design of the layout of the BGCR basins and aerobic treatment systems.

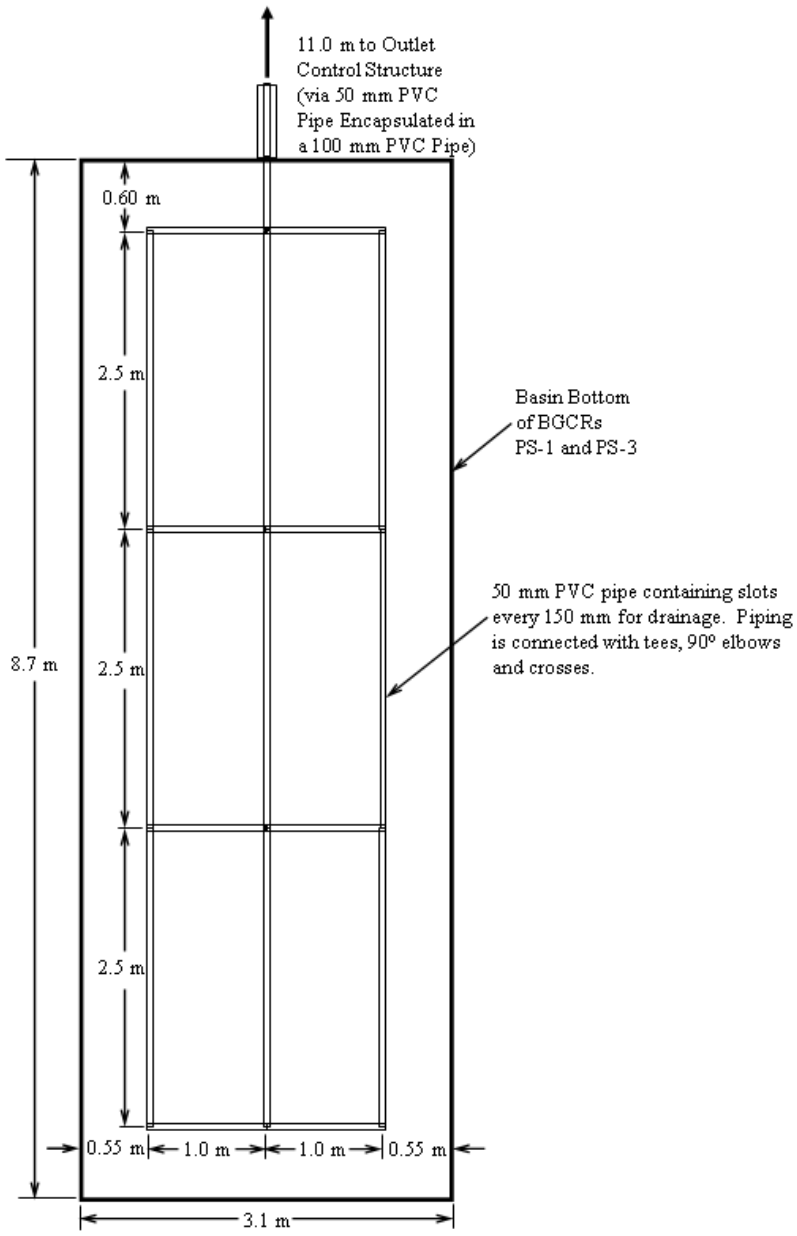

Figure G.9. The drainage piping array for BGCRs PS-1 and PS-3.

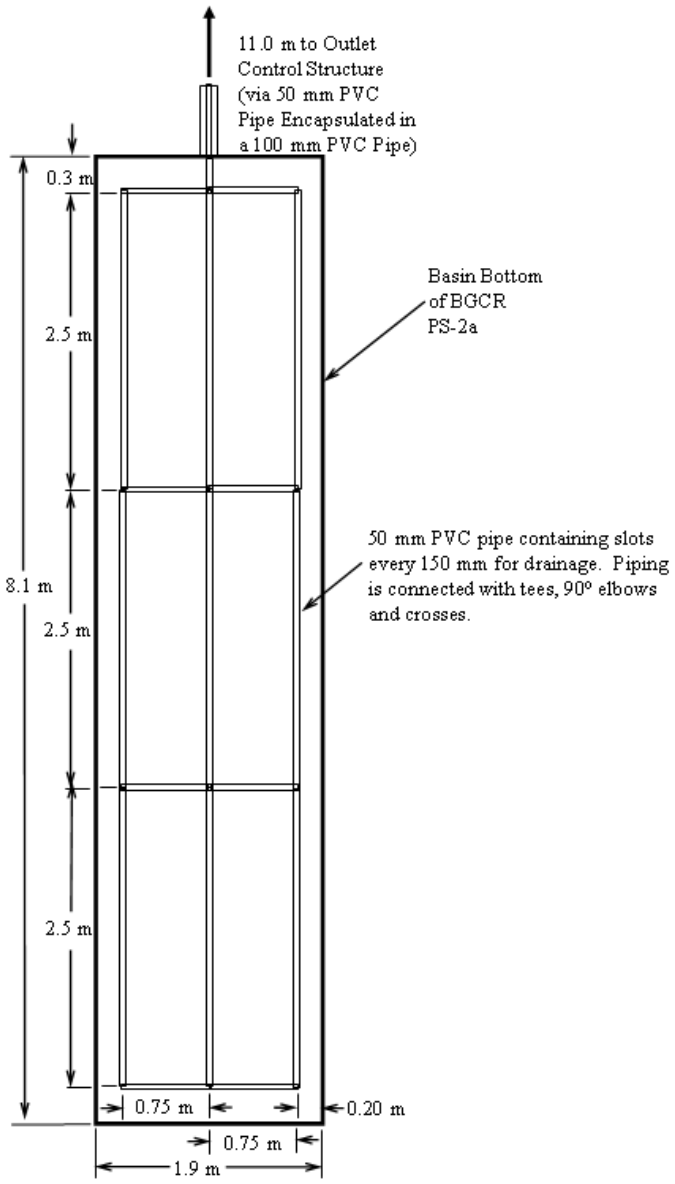

Figure G.10. The drainage piping array for BGCR PS-2a.

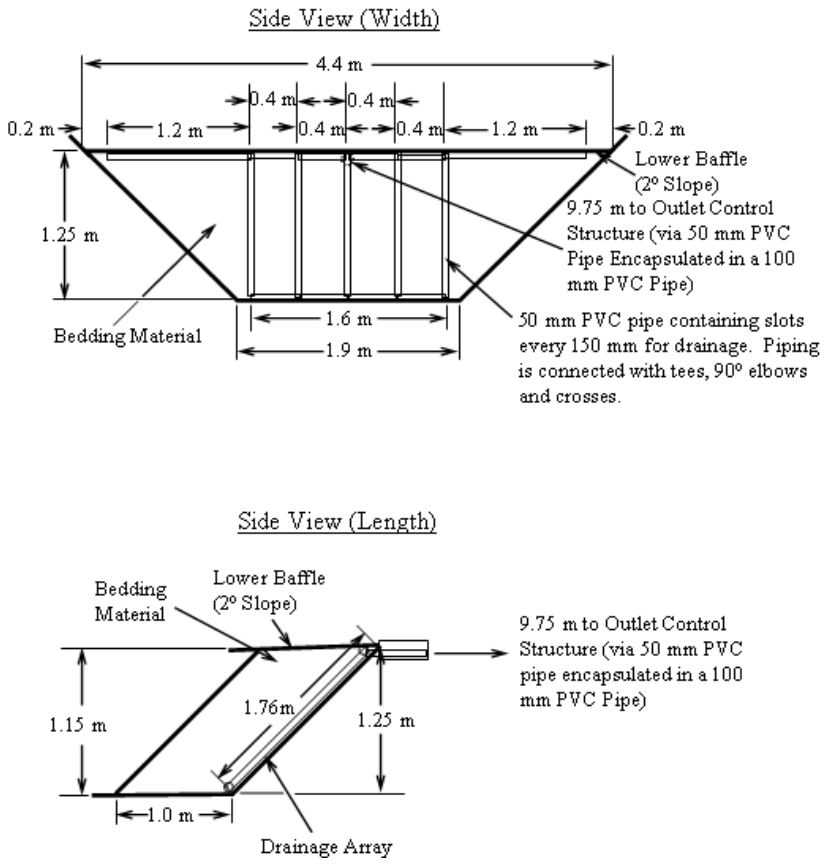

Figure G.11. The drainage piping array for BGCR PS-2b.

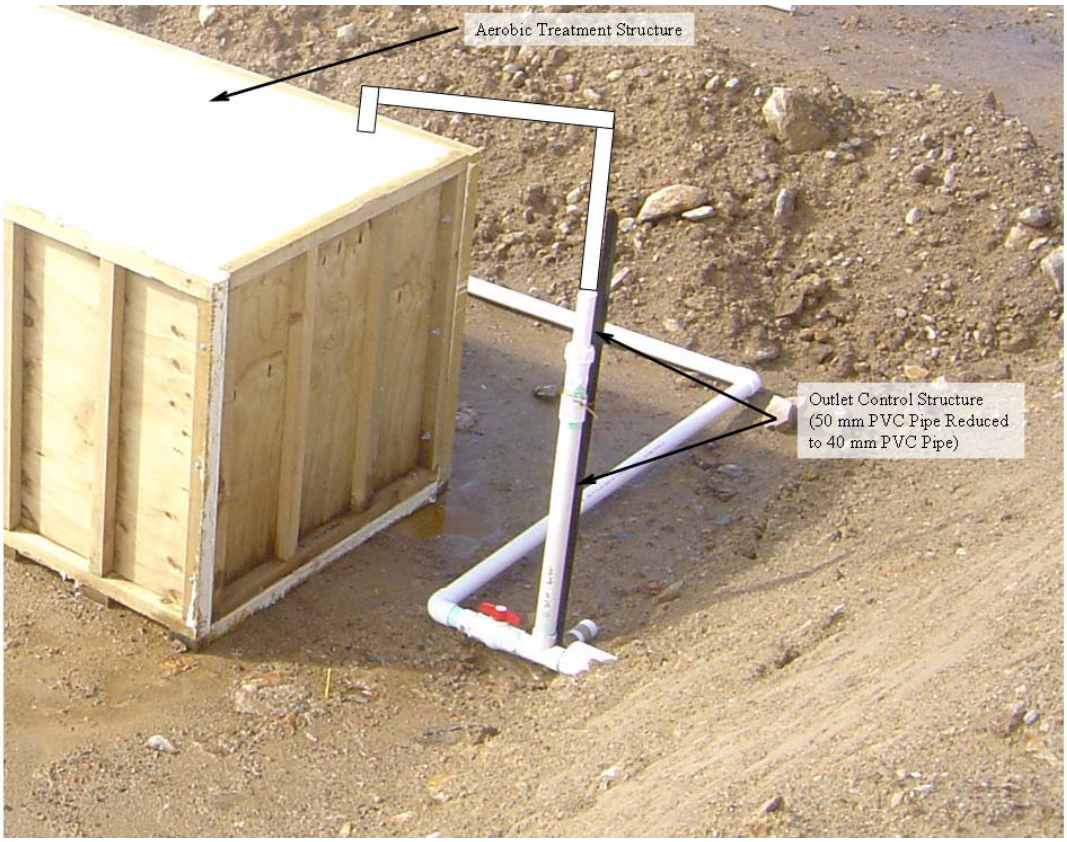

Figure G.12. Outlet control structure to maintain the required water level within the BGCRs.

Aerobic Treatment System Construction and Design Details

Because of the abundance of bedrock in the primary treatment area, it is recommended to construct and water proof the aerobic treatment systems (Figures G.13-G.15) and water proof using the same materials (plywood sheets containing exterior reinforcement with 4X2s and 2X2s) and methods recommended for the v-notch weir channel; therefore, the design widths are the same as commercially available plywood (1.2 m for AW-1 and AW-3 and 2.4 m for AW-3) and should be constructed and waterproofed in a manner consistent with that previously discussed for the v-notch weir channel. Outflow from each of the aerobic treatment systems should occur via a rectangular weir the width of the treatment systems so that more uniform flow is achieved.

The drop height from the outlet control structure (Figure G.16) can be achieved via an arrangement of 40 mm PVC pipe and 90^{o} elbows (Figure G.12). Baylar and Bagatur (2000) reported that the drop height plays a more important role in oxygen transfer efficiency than tailwater depth because a larger drop height results in nappe oscillations that entrain more air and achieve greater bubble penetration depths and longer contact time in the downstream collection pool (Baylar and Bagatur, 2000).

A single cascade is recommended in the design of AW-2 and AW-3, whereas two cascades are recommended in AW-1. The first cascade into AW-1 can drop into a polyethylene drum. Because of elevation constraints (maximum elevation difference from the water level of BGCR PS-1 to the

ground surface of 2.5 m), the recommended drop height is only 0.6 m instead of the ideal drop height of 0.9 m. The subsequent cascade from the polyethylene drum used in AW-1 and the cascades into AW-2 and AW-3 should contain drop heights of 0.9 m and tailwater depths of 0.54 m. These cascades can occur into a partitioned portion (referred to as cascade trenches) at the entrance of the aerobic treatment system structures as shown in Figures G.13-G.15.

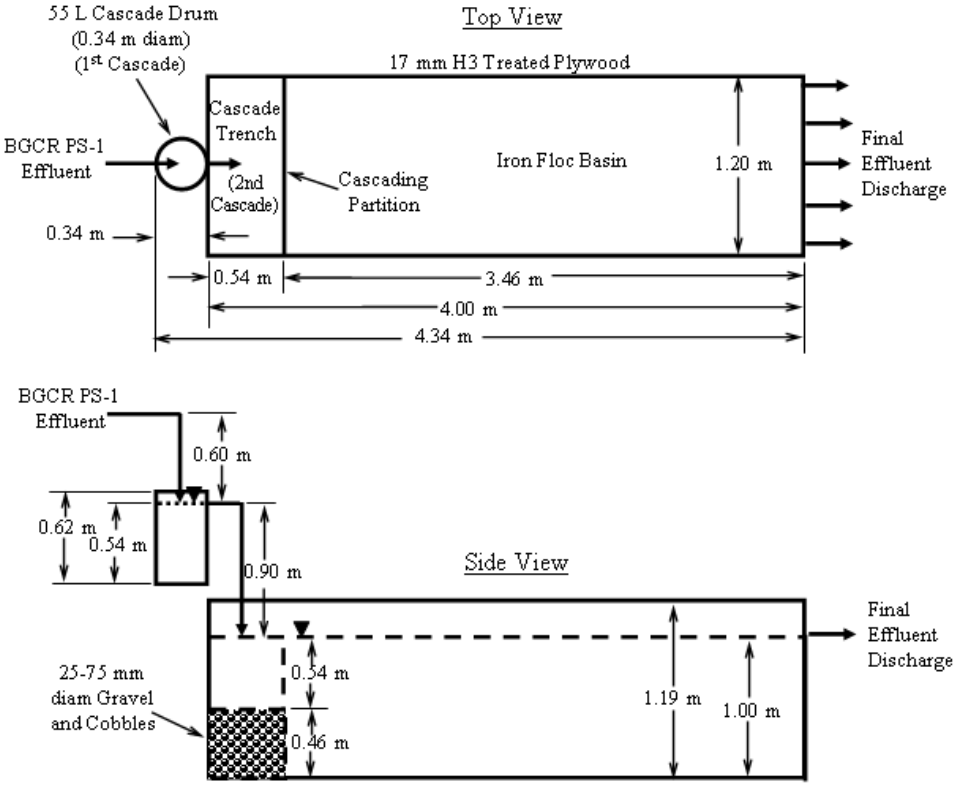

Figure G.13. Design dimensions of aerobic treatment system AW-1.

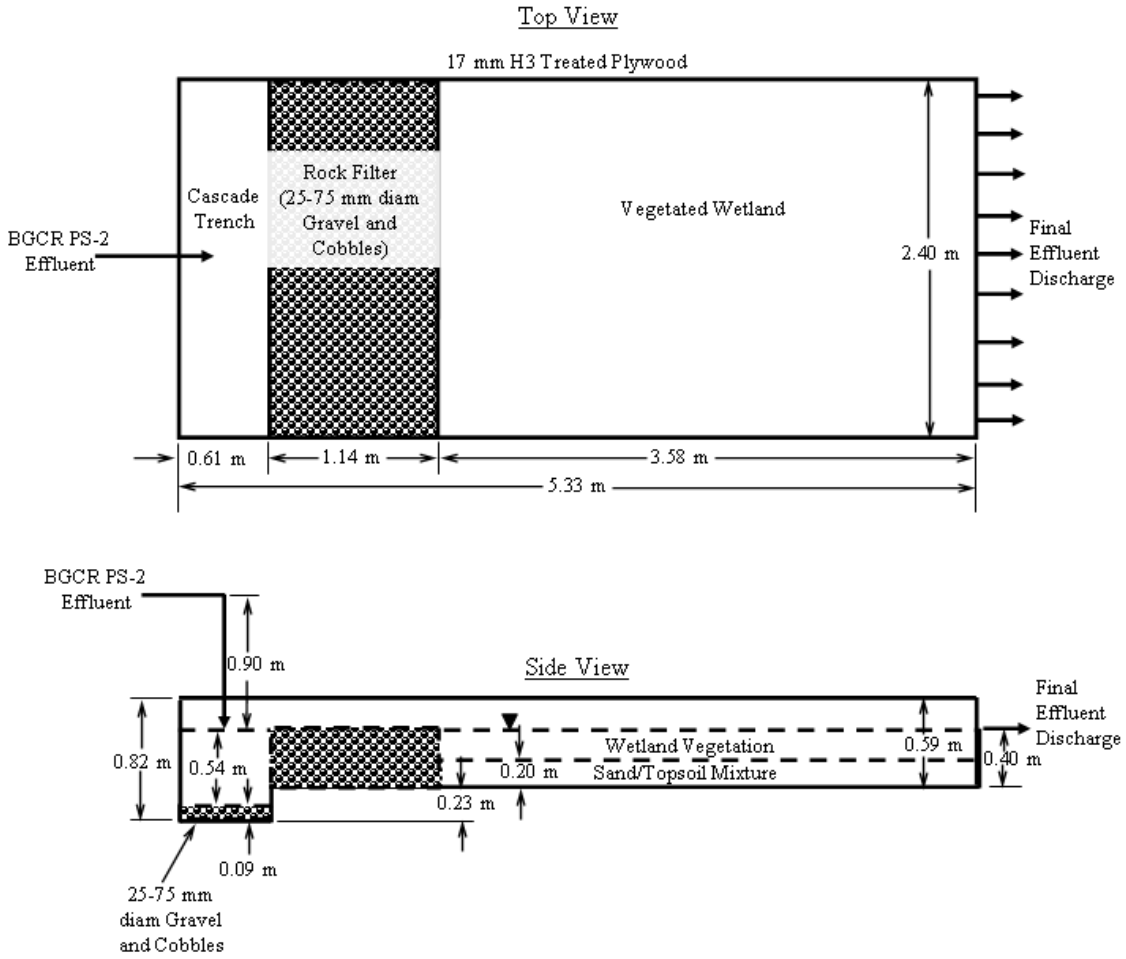

Figure G.14. Design dimensions of aerobic treatment system AW-2.

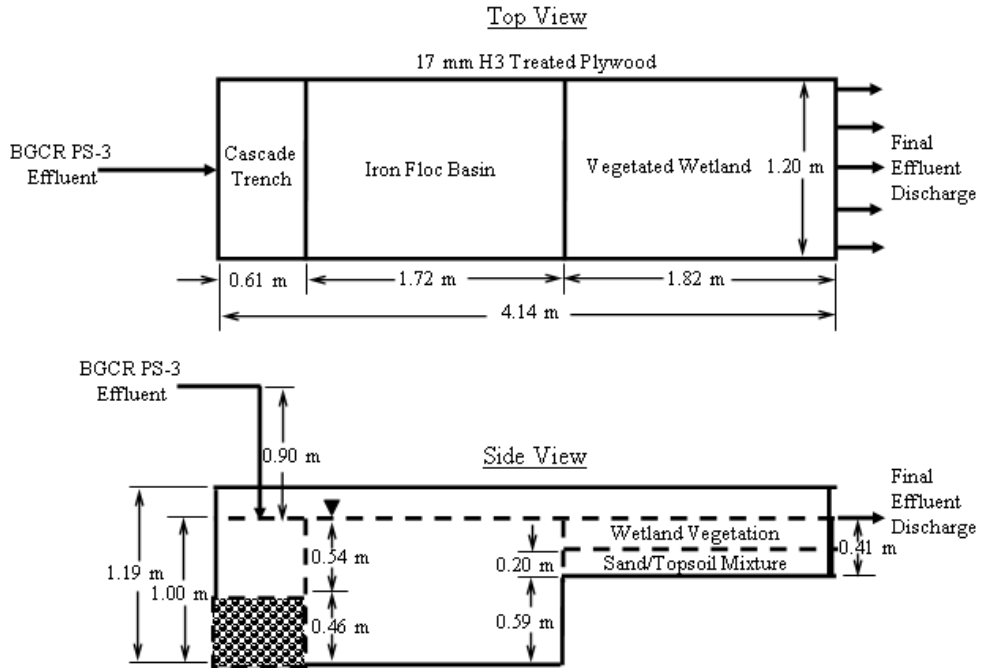

Figure G.15. Design dimensions of aerobic treatment system AW-3.

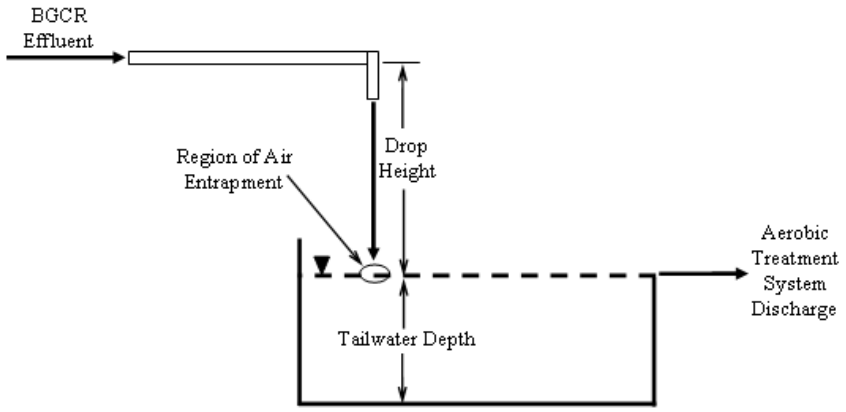

Figure G.16. Components associated with cascading to achieve aeration and oxygen transfer into water.

It is recommended to convey effluent from BGCRs PS-1, PS-2 and PS-3 into AW-1 during first-flush conditions to reduce the potential of causing perturbation to wetland vegetation transplants. The first flush is anticipated to occur during the initial three hydraulic RTDs (cumulative pore-water volumes) of the BGCRs based on results of the treatability tests and tracer studies discussed in Chapters 4 and 6, respectively. The water level in the vegetated wetlands should be increased incrementally and initially just cover the topsoil to allow wetland vegetation to establish. Inclusion of three different wetland plant species (*Schoenoplectus tabernaemont*, *Isolepus sp.* and *Juncus bulbosus*) in the vegetated wetlands are recommended, with comparisons of how transplants collected from the wild acclimate compared with those propagated in a nursery.

References

Ackers , P. 1978. Weirs and flumes for flow measurement. 327 pp. John Wiley, Chichester.

Al-Ani, W.A.G. 1994. Effect of COD/SO_4^{2-} ratio on the sulfate reduction in anaerobic digestion. M.A.Sc. Thesis. Department of Chemical Engineering and Applied Chemistry. University of Toronto.

Alloway, B.J. 1990. Soil processes and the behavior of metals. pp. 7-28. *In*: Alloway, B.J. (Ed.), Heavy metals in soils. Blackie and Son Ltd.

American Public Health Association (APHA). 1998. Standard methods for the examination of water and wastewater. 20th edition. Washington, D.C. American Public Health Association.

American Public Health Association (APHA). 2005. Standard methods for the examination of water and wastewater. 21st edition. Washington, D.C. American Public Health Association.

Annachhatre, A.P. and S. Suktrakoolvait. 2003. Biological sulphate reduction using molasses as a carbon source. Water Environment Research. Vol. 73. pp. 118-126.

Anthony, M.K. 1999. Ecology of streams contaminated by acid mine drainage near Reefton, South Island. M.Sc. Thesis. University of Canterbury. Christchurch, New Zealand.

Aube, B., H.G. Bayer, J. Zinck and others. 2006. Active treatment of mine influenced waters. *In*: Course Material for the ARD Treatment Short Course presented at the 7th International Conference on Acid Rock Drainage (ICARD). St. Louis, Missouri. 25-30 March 2006.

Australian and New Zealand Environment and Conservation Council (ANZECC) and Agricultural and Resource Management Council of Australia and New Zealand. 2000. Australian and New Zealand Environment and Conservation Council (ANZECC) water quality guidelines.

Avery, S. and P. Novak. Oxygen transfer at hydraulic structures. 1978. Journal of Hydraulic Engineering (ASCE). Vol. 104. pp. 1521-1540.

Bamforth, S.M., D.A.C. Manning, I. Singleton, P.L. Younger and K.L. Johnson. 2005. Utilisation of waste products for manganese removal from mine waters. pp. 419-425. *In*: Proceedings of the 9th International Mine Water Conference. Oviedo, Spain. 5-7 September 2005.

Bamforth, S.M., D.A.C. Manning, I. Singleton, P.L. Younger and K.L. Johnson. 2006. Manganese removal from mine waters – investigating the occurrence and importance of manganese carbonates. Applied Geochemistry. Vol. 21. pp. 1274-1287.

Baylar, A. and T. Bagatur. 2000. Aeration performance of weirs. Water SA. Vol. 26. pp. 521-526.

Bear, J. 1972. Dynamics of fluids in porous media. Dover Publications.

Bechard, G., H. Yamazaki, W.D. Gould and P. Bedard. 1994. Use of cellulosic substrates for the microbial treatment of acid mine drainage. Journal of Environmental Quality. Vol. 23. pp. 111-116.

Benjamin, M.M. 2002. Water chemistry. 668 pp. McGraw-Hill, New York

Black, A., D.A. Trumm, and P. Lindsay. 2005. Impacts of coal mining on water quality and metal mobilization: case studies from West Coast and Otago. pp. 247-260. *In*: Moore, T.A., A. Black,

J.A. Centeno, J.S. Harding, J.S. and D.A. Trumm (Eds.). Ch. 12. Metal contaminants in New Zealand: sources, treatments, and effects on ecology and human health. Resolutionz Press, Christchurch, New Zealand.

Black, C., P. Ziemkiewicz and J. Skousen. 1999. Construction of a limestone leach bed and preliminary water quality results in Beaver Creek. *In*: Proceedings of the 20th Annual West Virginia Surface Mine Drainage Task Force. Morgantown, West Virginia. 13-14 April 1999.

Blumenstein, E.P. and J.J. Gusek. 2009. Overcoming the obstacles of operating a biochemical reactor and aerobic polishing cell year round in central Montana. pp. 107-129. *In*: Proceedings of the 2009 National Meeting of the American Society of Mining and Reclamation. Billings, Montana. 30 May-5 June 2009.

Blumenstein, E.P., J. Volberding and J.J. Gusek. 2008. Designing a biochemical reactor for selenium and thallium removal, from bench scale testing to pilot construction . pp. 148-179. *In*: Proceedings of the 2008 National Meeting of the American Society of Mining and Reclamation. Richmond, Virginia. 14-19 June 2008.

Bowden, L.I., K.L. Johnson, A.P. Jarvis, H. Robinson, N. Gazireh and P.L. Younger. 2006. The use of basic oxygen steel furnace slag (BOS) as a high surface area media for the removal of iron from circumneutral mine waters. pp. 234-246. *In*: Proceedings of the 7th International Conference on Acid Rock Drainage (ICARD). St. Louis, Missouri. 25-30 March 2006.

Boyle, R.W. 1965. Geology, Geochemistry, and Origin of the Lead-Zinc-Silver Deposits of the Keno Hill-Galena Hill area, Yukon Territory. Geological Survey of Canada Bulletin 111.

Brown, M., B. Barley and H.Wood (Eds.). 2002. Mine water treatment: technology, application and policy. 472 pp. IWA Publishing.

Buccambuso, E., L. Figueroa, J. Ranville, T. Wildeman and D. Reisman. 2007a. Microbial activityin the Peerless Jenny King sulphate reducing bioreactor system. pp. 109-122. *In*: Proceedings of the 2007 National Meeting of the American Society of Mining and Reclamation. Gillette, Wyoming. 2-7 June 2007.

Buccambuso, E., A. Ruhs, L. Figueroa, J.J. Gusek, T. Wildeman, M. Holmes and D. Reisman. 2007b. Ethanol-fed or solid-phase organic sulfate reducing bioreactors for the National Tunnel drainage, Clear Creek/Central City Superfund site? pp. 95-105. *In*: Proceedings of the 2007 National Meeting of the American Society of Mining and Reclamation. Gillette, Wyoming. 2-7 June 2007.

Buchman, M.F. 2008. NOAA Screening Quick Reference Tables. National Oceanic and Atmospheric Administration **(**NOAA) OR&R Report 08-1, Seattle WA, Office of Response and Restoration Division, National Oceanic and Atmospheric Administration. 34 pp.

Building Industry Authority. 2001. Approved Document for New Zealand Building Code Surface Water Clause E1.

Busler, S., C. Cooper, T. Danehy, D. Peart and M. Dunn. 2002. Visual demonstration of water distribution patterns in vertical flow systems. p. 1048. *In*: Proceedings of the 2002 National

Meeting of the American Society of Mining and Reclamation. Lexington, Kentucky. 9-13 June 2002.

Canadian Council of Ministers of the Environment. 2007. Canadian water quality guidelines for the protection of aquatic life: Summary table. Updated September, 2007. *In:* Canadian water quality guidelines, 1999, Canadian Council of Ministers of the Environment, Winnipeg.

Chang, I.S., P.K. Shin and B.H. Kim. 2000. Biological treatment of acid mine drainage under sulphate-reducing conditions with solid waste materials as substrate. Water Research. Vol. 34. pp. 1269-1277.

Chazarenc, F., M. Gerard and Y. Gontheir. 2003. Hydrodynamics of horizontal subsurface flow constructed wetlands. Ecological Engineering. Vol. 21. pp. 165-173.

Chen, H. and Cutright, T.J. 2003. Preliminary evaluation of microbially mediated precipitation of cadmium, chromium and nickel by rhizosphere consortium. Journal of Environmental Engineering. Vol. 129. pp. 4-9.

Christchurch City Council Waterways, Wetlands and Drainage Guide. 2003.

Cochrane, T.A., D. Wicke and A.D. O'Sullivan. Developing a public information and engagement portal of urban waterways with real-time monitoring and modelling. *In*: Proceedings of the International World Water Congress and Exhibition (International Water Association). Montreal, Canada. 19-24 September 2010.

Cocos, I.A., G.J. Zagury, B. Clement and R. Samson. 2002. Multiple factor design for reactive mixture selection for use in reactive walls in mine drainage treatment. Water Research. Vol. 36. pp. 167-177.

Cornell, R.M. and U. Schwertmann. 1996. The iron oxides: structure, properties, reactions, occurrences and uses. VCH, Weinham.

Cravotta III, C.A. 2002. New method to estimate size and longevity of anoxic limestone drains. pp. 1062-1066. *In*: Proceedings of the 2002 National Meeting of the American Society of Mining and Reclamation. Lexington, Kentucky. 9-13 June 2002.

Cravotta III, C.A. 2003. Size and performance of anoxic limestone drains to neutralize acidic mine drainagee. Journal of Environmental Quality. Vol. 32(4). pp. 1277-1289.

Cravotta II, C.A. 2007. Passive aerobic treatment of net-alkaline, iron-laden drainage from a flooded underground anthracite mine, Pennsyslvania, USA. Mine Water and the Environment. Vol. 26(3). pp. 128-149.

Cravotta III, C.A. and M.K. Trahan. 1999. Limestone drains to increase pH and remove dissolved metals from acidic mine drainage. Applied Geochemistry. Vol. 14. pp. 581-606.

Cravotta III, C.A. and C.S. Kirby. 2004. Acidity and alkalinity in mine drainage: practical considerations. pp. 334-365. *In*: Proceedings of the 2004 National Meeting of the American Society of Mining and Reclamation and the 25th West Virginia Surface Mine Drainage Task Force. Morgantown, West Virginia. 18-22 April 2004.

Cravotta III, C.A., S.J. Ward, D.J. Koury and R.D. Koch. 2004. Optimization of limestone drains for long-term treatment of mine drainage, Swatara Creek Basin, Schuylkill County, PA. pp. 366-411. *In*: Proceedings of the 2004 National Meeting of the American Society of Mining and Reclamation and the 25th West Virginia Surface Mine Drainage Task Force. Morgantown, West Virginia. 18-22 April 2004.

Cravotta II, C.A. and S.J. Ward. 2008. Downflow Limestone Beds for Treatment of Net-Acidic, Oxic, Iron-Laden Drainage form a Flooded Anthracite Mine, Pennsylvania, USA: 1. Field Evaluation. Mine Water and the Environment. Vol. 27(2). pp. 67-85.

Crites, R. and G. Tchobanoglous. 1998. Small and decentralized wastewater management systems. 1104 pp. McGraw-Hill, New York.

Crohn, D.M., N.C. Ruud, J.G. Decruyenaere and D.B. Carlon. 2005. Goodness-of-fit test for modeling tracer breakthrough curves in wetlands. Journal of Environmental Engineering. Vol. 131. pp. 242-251.

Cubillas, P., S. Köhler, M. Prieto, C. Chaïrat and E.H. Oelkers. 2005. Experimental determination of the dissolution rates of calcite, aragonite, and bivalves. Chemical Geology. Vol. 216. pp. 59-77.

Czepiel, P.M., J.H. Shorter, B. Mosher, E. Allwine, J.B. McManus, R.C. Harriss, C.E. Kolb and B.K. Lamb. 2003. The influence of atmospheric pressure on landfill methane emissions. Waste Management. Vol. 23. pp. 593-598.

Das, B.M. 1998. Principles of Geotechnical Engineering. 712 pp. 4th Ed. PWS, Boston.

Davies-McConchie, F., D. McConchie, M. Clark, C. Lin, S. Pope and T. Ryffel. 2002. A new approach to the treatment and management of sulphidic mine tailings, waste rock and acid mine drainage. New Zealand Mining. Vol. 31. pp. 7-16.

Davis, M.L. and D.A. Cornwell. 1991. Introduction to Environmental Engineering. 822 pp. 2nd Ed. McGraw-Hill Inc., New York.

de Joux, A. 2003. Geochemical investigation and computer modeling of acid mine drainage, Sullivan Mine, Denniston Plateau, West Coast. 261 pp. M.Sc. Thesis in Geology. University of Canterbury. Christchurch, New Zealand.

Demchak, J., T. Morrow and J. Skousen. 2001. Treatment of acid mine drainage by four vertical-flow wetlands in Pennsylvania. Geochemistry: Exploration Environment Analysis. Vol. 1. pp. 71-80.

Denholm, C.F., T.P. Danehy, M.H. Dunn and S.L. Busler. 2003. Horizontal flow limestone bed: an effective and valuable passive treatment system component for Mn removal and alkalinity generation. pp. 228-230. *In*: Proceedings of the 2003 Meeting of the American Society of Mining and Reclamation and the 9th Billings Land Reclamation Symposium. Billings, Montana. 3-6 June 2003.

Denholm, C., T. Danehy, S. Busler, R. Dolence and M. Dunn. 2008. Sustainable passive treatment of mine drainage: Demonstration of manganese resource recovery (a preliminary case study). pp. 285-297. *In*: Proceedings of the 2008 National Meeting of the American Society of Mining and Reclamation. Richmond, Virginia. 14-19 June 2008.

Doshi, S.M. 2006. Bioremediation of acid mine drainage using sulfate-reducing bacteria. 65 pp. U.S. Environmental Protection Agency. Office of Solid Waste and Emergency Response and Office of Superfund Remediation and Technology Innovation.

Dvorak, D.H, R.S. Hedin, H.M. Edenborn and P.E. McIntire. 1992. Treatment of metal contaminated water using bacterial sulfate reduction: results from Pilot-scale reactors. Biotechnology and Bioengineering. Vol. 40. pp. 609-616.

Dzombak D.A. and F.M.M. Morel. 1990. Surface complexation modelling: hydrous ferric oxide. Wiley, New York.

Elliott, P., S. Ragusa and D. Catcheside. 1998. Growth of sulfate-reducing bacteria under acidic conditions in an upflow anaerobic bioreactor as a treatment system for acid mine drainage. Water Research. Vol. 32. pp. 3724-3730.

ERMITE Consortium. 2004. Mining Impacts on the Fresh Water Environment: Technical and Managerial Guidelines for Catchment Scale Management. 80 pp. European Commission 5th Framework RTD Project no. EVK1-CT-2000-00078 "Environmental Regulation of Mine Waters in the European Union" (ERMITE). University of Newcastle Upon Tyne, Newcastle Upon Tyne, UK.

European Commission. 2000. Directive 2000/60/EC of the European Parliament and of the Council establishing a framework for the Community action in the field of water policy, Official Journal of the European Communities, L 327/1, 72 pp.

European Commission. 2006. Directive 2000/60/EC of the European Parliament and of the Council on the management of waste from the extractive industries, Official Journal of the European Communities, L 102, 11.4.2006, pp. 15-34.

Faulkner, B.B. and J.G. Skousen. 1995. Effects of land reclamation and passive treatment systems on improving water quality. Green Lands. Vol. 25. pp. 34-40.

FLIR Systems, Inc. 2007. Reduce greenhouse gas emissions with this infrared camera. Chemical Engineering Progress. May 2007. pp. 26.

Figueroa, L., A. Miller, M. Zaluski and D. Bless. 2007. Evaluation of a two-stage passive treatment approach for mining influenced waters. pp. 238-247. *In*: Proceedings of the 2007 National Meeting of the American Society of Mining and Reclamation. Gillette, Wyoming. 2-7 June 2007.

Ford, K.L. 2003. Passive treatment systems for acid mine drainage. Technical Note 409. BLM/ST/ST-02/001+3596. Bureau of Land Management Web-based report available online at http://www.blm.gov/nstc/library/techno2.htm.

Freeze, R.A. and J.A. Cherry. 1979. Groundwater. 604 pp. Prentice-Hall, Englewood Cliffs.

Fumoto, T. and H. Sverdrup. 2001. Implementation of sulfate adsorption in the SAFE model. Journal of Environmental Quality. Vol. 30(1). pp. 45-57.

Garrett, W.E., A.A.Bartolucci, R.R. Pitt and M.E. Vermace. 2002. Recirculating-reducing and alkalinity producing system (ReRAPS) for the treatment of acidic coal pile runoff. pp. 539-557.

In: Proceedings of the 2002 National Meeting of the American Society of Mining and Reclamation. Lexington, Kentucky. 9-13 June 2002.

Gerth, J. 1990. Unit-cell dimentsions of pure and trace metal-associated goethites. Geochim. Cosmochim. Acta 54. pp. 363-371.

Gibert, O., J. de Pablo, J.L. Cortina and C. Ayora. 2002. Treatment of acid mine drainage by sulphate-reducing bacteria using reactive barriers: a review from laboratory to full-scale experiments. Reviews in Environmental Science and Biotechnology. Vol. 1. pp. 327-333.

Gibert, O., J. de Pablo, J.L. Cortina and C. Ayora. 2003. Evaluation of municipal compost/limestone/iron mixtures as filling material for permeable reactive barriers for *in-situ* acid mine drainage treatment. Journal of Chemical Technology and Biotechnology. Vol. 78. pp. 489-496.

Gibert, O., J. de Pablo, J.L. Cortina and C. Ayora. 2004. Chemical characterization of natural organic substrates for biological mitigation of acid mine drainage. Water Research. Vol. 38. pp. 4186-4196.

Gibert, O., J. de Pablo, J.L. Cortina and C. Ayora. 2005a. Municipal compost-based mixture for acid mine drainage bioremediation: metal retention mechanisms. Applied Geochemistry. Vol. 20. pp. 1648-1657.

Gibert, O., J. de Pablo, J.L. Cortina and C. Ayora. 2005b. Sorption studies of Zn (II) and Cu (II) onto vegetal compost used on reactive mixtures for *in-situ* treatment of acid mine drainage. Water Research. Vol. 39. pp. 2827-2838.

Glombitza, F. 2001. Treatment of acid lignite mine flooding water by means of microbial sulfate reduction. Waste Management. Vol. 21. pp. 197-203.

Gulliver, J.S., J.R. Thene and A.J. Rindels. 1990. Indexing gas transfer in self-aerated flows. Journal of Environmental Engineering. Vol. 116(3). pp. 503-523.

Gusek, J.J. 2002. Sulfate-reducing bioreactor design and operating issues: is this the passive treatment technology for your mine drainage? 13 pp. *In*: Proceedings of the 2002 National Association of Abandoned Mine Land Programs Annual Conference. Park City, Utah. 15-18 September 2002.

Gusek, J.J. 2004. Scaling up design challenges for large scale sulfate reducing bioreactors. pp. 752-765. *In*: Proceedings of the 2004 National Meeting of the American Society of Mining and Reclamation and the 25th West Virginia Surface Mine Drainage Task Force. Morgantown, West Virginia. 18-22 April 2004.

Gusek, J.J. 2009a. A periodic table of passive treatment for mining influenced water. Reclamation Matters. Spring 2009. pp. 22-27.

Gusek, J.J. 2009b. A periodic table of passive treatment for mining influenced water. pp. 550-562. *In*: Proceedings of the 2009 National Meeting of the American Society of Mining and Reclamation. Billings, Montana. 30 May-5 June 2009.

Gusek, J.J. and T.R. Wildeman. 2002. Passive treatment of aluminum-bearing acid rock drainage. 9 pp. Presented at the 23rd Annual West Virginia Surface Mine Drainage Task Force Symposium. Morgantown, West Virginia. 16-17 April 2002.

Gusek, J.J., T. Rutkowski, E. Blumenstein and B. Shipley. 2008. pp. 424-441. Two-year sulfate reducing bioreactor pilot test results at the Golinski Mine, California. *In*: Proceedings of the 2008 National Meeting of the American Society of Mining and Reclamation. Richmond, Virginia. 14-19 June 2008.

Hach Company. 2003. Hach Water Quality Analysis Handbook. 2003. 4th Ed. Rev.2. 1268 pp.

Hallberg, K.B. and D.B. Johnson. 2005. Biological manganese removal from acid mine drainage in constructed wetlands and prototype bioreactors. Science of the Total Environment. Vol. 338. pp. 115-124.

Harding, J.S. 2005. Impacts of metals and mining on stream communities. *In*: Moore, T.A., A. Black, J.A. Centeno, J.S. Harding and D.A. Trumm. (Eds.). Ch. 17. Metal contaminants in New Zealand: sources, treatments, and effects on ecology and human health. pp. 343-357. Resolutionz Press, Christchurch, New Zealand.

Harding, J.S. and I. Boothryd. 2004. Impacts of Mining. *In*: Harding, J., C. Pearson, B.Sorrell and P. Mosley. (Eds.). Ch. 36. Freshwaters of New Zealand, pp. 16.1-16.10. New Zealand Hydrological Society and New Zealand Limnological Society, Christchurch, New Zealand.

Harden, H.S., J.P. Chanton, J.B. Rose, D.E. John and M.E. Hooks. Comparison of sulfur hexafluoride, fluorescein and rhodamine dyes and the bacteriophage PRD-1 in tracing subsurface flow. Journal of Hydrology. Vol. 277. pp. 100-115.

Hedin, R.S. 1999. Recovery of iron oxides from polluted coal mine drainage. Patent No. 5,954,969. U.S. Patent and Trademark Office, Washington D.C.

Hedin, R.S. 2003. Recovery of marketable iron oxide from mine drainage. Land Contamination and Reclamation. Vol. 11(2). pp. 93-97.

Hedin, R.S. 2006a. Sustainable mine drainage treatment through the passive production of saleable iron oxide solids. pp. 764-773. *In*: Proceedings of the 7th International Conference on Acid Rock Drainage (ICARD). St. Louis, Missouri. 25-30 March 2006.

Hedin, R.S. 2006b. The use of measured and calculated acidity values to improve the quality of mine drainage datasets. Mine Water and the Environment. Vol. 25(3). pp. 146-152.

Hedin, R.S. 2008a. Effective passive treatment of a large flow of alkaline Fe-containing mine water. pp. 465-486. *In*: Proceedings of the 2008 National Meeting of the American Society of Mining and Reclamation. Richmond, Virginia. 14-19 June 2008.

Hedin, R.S. 2008b. Iron removal by a passive system treating alkaline coal mine drainage. Mine Water and the Environment. Vol. 27(4). pp. 200-209.

Hedin, R.S., R.W. Nairn and R.L.P. Kleinmann. 1994a. Passive treatment of coal mine drainage. U.S. Department of the Interior. Bureau of Mines. Information Circular 9389. 35 pp.

Hedin, R.S., G.R. Watzlaf and R.W. Nairn. 1994b. Passive treatment of acid mine drainage with limestone. Journal of Environmental Quality. Vol. 23. pp. 1338-1345.

Hedwin Corporation. 2007. Cubitainer® combination package. Baltimore, Maryland. http://www.hedwin.com/library /pdfs/cubitainer_info.pdf. 3 pp.

Hemsi, P.S., C.D. Shackelford and L.A. Figueroa. 2005. Modeling the influence of decomposing organic solids on sulfate reduction rates for iron precipitation. Environmental Science and Technology. Vol. 39. pp. 3215-3225.

Hemsi, P.S., C.D. Shackelford and L.A. Figueroa. 2010. Calibration of reactive transport models for remediation of mine drainage in solid-substrate bio-columns. Journal of Environmental Engineering. Vol. 136(9). pp. 914-925.

Herschy, R.W. 1999. Hydrometry: principles and practices. 376 pp. 2nd Ed. John Wiley, Chichester.

Holland, J.F., J.F. Martin, T. Granata, V. Bouchard, M. Quigley and L. Brown. 2004. Effects of wetland depth and flow rate on residence time distribution characteristics. Ecological Engineering. Vol. 23. pp. 189-203.

Huntsman, B.E., J.G. Solch and P.M. Erickson. 1978. Utilization of Sphagnum species dominated bog for coal acid mine drainage abatement. p. 322. *In*: Proceedings of the 91st Annual Meeting of the Geological Society of America. Toronto, Ontario, Canada.

Hutchinson R. and R.W. Nairn. 2005. Determining hydraulic conductivities in a vertical flow system. pp. 504-511. *In*: Proceedings of the 2005 National Meeting of the American Society of Mining and Reclamation. Breckenridge, Colorado. 19-23 June 2005.

Hutchinson, J. and A.D. O'Sullivan. 2008. Scanning electron microscopy of substrates from bioengineered treatment reactors; elucidating the black box. Unpublished Report. Department of Civil and Natural Resources Engineering. University of Canterbury. (aisling.osullivan@canterbury.ac.nz). 26 pp.

Ingvorsen, K., M.Y. Nielsen and C. Joulian. 2003. Kinetics of bacterial sulfate reduction in an activated sludge plant. FEMS Microbiology Ecology. Vol 46. pp. 129-137.

International Organisation for Standardization (ISO) 1438. 2008. Hydrometry - Open channel flow measurement using thin-plate weirs.

Jack, G. 2006. Assessment of Coal Mining Waste Rock Capping Materials and Engineered Landform Sediment Yield Analysis. Unpublished Report. Department of Civil and Natural Resources Engineering. University of Canterbury. (tom.cochrane@canterbury.ac.nz). 122 pp.

James, T.I.. 2003. Water quality of streams draining various coal measures in the North-Central West Coast. *In*: Proceedings of the Australasian Institute of Mining and Metallurgy New Zealand Branch 36th Annual Conference. Greymouth, New Zealand. 3-5 September 2003.

Jarvis, A.P. and P.L. Younger. 2001. Passive treatment of ferrugious mine waters using high surface area media. Water Research. Vol. 35 pp. 3643-3648.

Johnson, K.L. 2002. Manganese in mine water and its removal by passive treatment. PhD Thesis. Department of Civil Engineering, University of Newcastle. 260 pp.

Johnson, K.L. 2003. Enhanced *in-situ* bioremediation technique for manganese removal from mine waters. 4 pp. CL:AIRE Research Bulletin.

Johnson, R.A. 2005. Miller and Freund's probability and statistics for engineers. 642 pp. 7th Ed. Pearson Prentice Hall, Upper Saddle River.

Johnson, D.B. and K.B. Hallberg. 2005. Acid mine drainage remediation options: a review: Science of the Total Environment. Vol. 338. pp. 3-14.

Jong, T. and D.L. Parry. 2004. Adsorption of Pb(II), Cu(II), Cd(II), Zn(II), Ni(II), Fe(II) and As(V) on bacterially produced metal sulfides. Journal of Colloid and Interface Science. Vol. 275. pp. 61-71.

Jong, T. and D.L. Parry. 2006. Microbial sulfate reduction under sequentially acidic conditions in an upflow anaerobic packed bed bioreactor. Water Research. Vol. 40. pp. 2561-2571.

Kadlec, R.H. 2003. Effects of pollutant speciation in treatment wetlands design. Ecological Engineering. Vol. 20. pp. 1-16.

Kadlec, R.H., W. Bastiens, and D.T. Urban. 1993. Hydrological design of for water surface treatment wetlands. pp. 77-86. *In:* Moshira, G.A. (Ed.). Constructed Wetlands for Water Quality Improvement. CRC Press, Boca Raton, Florida.

Kadlec, R.H. and R.L. Knight. 1996. Treatment Wetlands. 893 pp. CRC Press LLC, Boca Raton.

Kadlec, R.H. and S.D. Wallace. 2009. Treatment Wetlands. 2nd ed. 1016 pp. CRC Press LLC, Boca Raton.

Kairies, C.L., R.C. Capo and G.R. Watzlaf. 2005. Chemical and physical properties of iron hydroxide precipitates associated with passively treated coal mine drainage in the Bituminous Region of Pennsylvania and Virginia. Applied Geochemistry. Vol. 20. pp. 1445-1460.

Kaksonen, A.H., J.J. Plumb, P.D. Franzmann, and J.A. Puhakka. 2004. Simple organic electron donors support diverse sulfate-reducing communities in fluidized-bed reactors treating acidic metal- and sulfate-containing wastewater. FEMS Microbiology Ecology. Vol. 47. pp. 279-289.

Keller, C.H. and J.S. Bays. 2001. Tracer studies in treatment wetlands. pp. 173-182. *In*: Treatment Wetlands for Water Quality Improvement: Quebec 2000 Conference Proceedings. Quebec, Canada. 6-12 August 2000.

Kepler, D.A. and E.C. McCleary. 1997. Passive aluminum treatment success. *In*: Proceedings of the 18th Annual West Virginia Surface Mine Drainage Task Force. Morgantown, West Virginia. 15-16 April 1997.

Kirby, C.S., H.M. Thomas, G. Southman and R. Donald. 1999. Relative contributions of abiotic and biological factors in Fe(II) oxidation in mine drainage. Applied Geochemistry. Vol. 14. pp. 511-530.

Kleinmann, R.L.P and D.A. Crerar. 1979. Thiobacillus ferrooxidands and the formation of acidity in simulated coal mine environments. Geomicrobiology. Vol. 1. pp. 373-388.

Knauer, K., T. Jabusch and L. Sigg. 1999. Manganese uptake and Mn(II) oxidation by the alga *Scenedesmus subspicatus*. Aquatic Sciences. Vol. 61. pp. 44-58.

Koduri, S. and B.D. Barkdoll. 2003. Evaluation of oxygen transfer at stepped cascade aerators. *In*: Conference Proceedings of World Water & Environmental Resources Congress 2003 and Related Symposia. Philadelphia, Pennsylvania.

Kolmert, A., T. Henrysson, R. Hallberg and B. Mattiasson. 1997. Optimization of sulphide production in an anaerobic continuous biofilms process with sulfate-reducing bacteria. Biotechnology Letters. Vol. 19. pp. 971-975.

Korte, K.M., C.E. Newcombe, and R.A. Brennan. 2008. Evaluation of three different purities of crab-shell for the remediation of mine impacted water. pp. 510-524. *In*: Proceedings of the 2008 National Meeting of the American Society of Mining and Reclamation. Richmond, Virginia. 14-19 June 2008.

Labar, J.A. and R.W. Nairn. 2009. Evaluation of first 1.5 years of operation of a passive treatment system in SE Oklahoma. pp. 693-708. *In*: Proceedings of the 2009 National Meeting of the American Society of Mining and Reclamation. Billings, Montana. 30 May-5 June 2009.

Labar, J.A., R.W. Nairn and G.A. Canty. 2008. Generation of 400-500 Mg/L Alkalinity in a vertical anoxic limestone drain. pp. 551-563. *In*: Proceedings of the 2008 National Meeting of the American Society of Mining and Reclamation. Richmond, Virginia. 14-19 June 2008.

Lapointe, F., K. Fytas and D. McConchie. 2006. Efficiency of Bauxsol^{TM} in permeable reactive barriers to treat acid rock drainage. Mine Water and the Environment. Vol. 25. pp. 37-44.

Lasorso, D., G. Patrick and C. Patterson. 2009. Protocol considerations to improve the reliability of data collection in a radio telemetry system. pp. 2220-2235. *In:* Proceedings of the World Environmental and Water Resources Congress. Kansas City, Missouri. 19-21 May 2009.

Ledin, M. and K. Pedersen. 1996. The environmental impact of mine wastes – roles of microorganisms and their significance in treatment of mine wastes. Earth-Science Reviews. Vol. 41. pp. 67-108.

Lee, G., J.M. Bigham and G. Faure. 2002. Removal of trace metals by coprecipitation with Fe, Al and Mn from natural waers contaminated with acid mine drainage in the Ducktown Mining District, Tennessee. Applied Geochemistry. Vol 17. pp. 569-581.

Lee, S., Q. Xu, M. Booth, T.G. Townsend, P. Chadik and G. Bitton. 2006. Reduced sulfur compounds in gas from construction and demolition debris landfills. Waste Management. Vol. 26. pp. 526-533.

Levenspiel, O. 1999. Chemical reaction engineering. 668 pp. John Wiley & Sons, Inc., New York.

Levenspiel, O and W.K. Smith. 1957. Notes on the diffusion-type model for the longitudinal mixing of fluids in flow. Chemical Engineering Science. Vol. 6. pp. 227-233.

Lin, A.Y.C, J.F. Debroux, J.A. Cunningham and M. Reinhard. 2003. Comparison of rhodamine WT and bromide in the determination of hydraulic characteristics of constructed wetlands. Ecological Engineering. Vol. 20. pp. 75-88.

Lindsay, P., M. Kingsbury, and M. Pizey. 2003. Impact of mining the Lower Ngakawau River. Not paginated. *In*: Proceedings of the 36th Annual Australasian Institute of Mining and Metallurgy New Zealand Branch Conference. (Greymouth. 3-5 September 2003).

Lloyd, J.R., D.A. Klessa, D.L. Parry, P. Buck and N.L. Brown. 2004. Stimulation of microbial sulphate reduction in a constructed wetland: microbiological and geochemical analysis. Water Research. Vol. 38. pp. 1822-1830.

Lo, Y.M.-C and X.-Y Yang. 1998. Removal and redistribution of metals from contaminated soils by a sequential extraction method. Waste Management. Vol. 18. pp. 1-7.

Logan, M.V., D. Ahmann and L. Figueroa. 2003. Assessment of microbial activity in anaerobic columns treating synthetic mine drainage. pp. 658-678. *In*: Proceedings of the 2003 National Meeting of the American Society of Mining and Reclamation and the 9th Billings Land Reclamation Symposium. Billings, Montana. 3-6 June 2003.

Logan, M.V., Reardon, K.F., L.A. Figueroa, J.E.T. McLain and D.M. Ahmann. 2005. Microbial community activities during establishment, performance, and decline of bench-scale passive treatment systems for mine drainage. Water Research. Vol. 39. pp. 4537-4551.

Lowson, R.T. 1982. Aqueous oxidation of pyrite by molecular oxygen. Chemical Reviews. Vol. 82(5). pp. 461-497.

Lung, E.H. 2009. Ensuring water quality: let the fishes tell you if your water is safe. Innovation. Vol. 9. pp. 46-47.

Lyew, D. and Sheppard, J.D. 1997. Effects of physical parameters of a gravel bed on the activity of sulfate-reducing bacteria in the presence of acid mine drainage. Journal of Chemical Technology and Biotechnology. Vol. 70. pp. 223-230.

Mackenzie, A. 2010. Characterization of Drainage Chemistry in Fanny Creek Catchment and Optimal Passive AMD Treatment Options for Fanny Creek. MS Dissertation. University of Canterbury.

Map Data Sciences PtyLtd, PSMA. Various Google Earth Images. 2009.

Marsili-Libelli, S. and N. Checchi. 2005. Identification of dynamic models for horizontal subsurface constructed wetlands. Ecological Modelling. Vol. 187. pp. 201-218.

Martinez, C.J. and W.R. Wise. 2003. Hydraulic Analysis of Orlando Easterly Wetland. Journal of Environmental Engineering. Vol. 129. pp. 553-560.

McCloskey, A.L., B. Stasney, J. Wright, J.L. Conca, N. Yancey, N. Lewis and H. Joyce. 2006. Comparison of Apatite II™ treatment systems at two mines for metals removal. pp. 846-848. *In*: Proceedings of the 7th International Conference on Acid Rock Drainage (ICARD). St. Louis, Missouri. 25-30 March 2006.

Means, B., B. McKenzie and T. Hilton. 2003. A computer-based model for estimating mine drainage treatment costs. *In*: Proceeding of the 24th Annual West Virginia Surface Mine Drainage Task Force Symposium. Morgantown West Virginia.

Means, B. and T. Hilton. 2004. Comparison of three methods to measure acidity of coal-mine drainage. pp. 1249-1277. *In*: Proceedings of the 2004 National Meeting of the American Society of Mining and Reclamation and the 25th West Virginia Surface Mine Drainage Task Force. Morgantown, West Virginia. 18-22 April 2004.

Meyer, M.L. and G.M. Huey. 2006. Telemetric system for hydrology and water quality monitoring in watersheds of Northern New Mexico, USA. Environmental Monitoring and Assessment. Vol. 116. pp. 9-19.

Miller, A., L. Figueroa and T. Wildeman. Mechanisms of nickel and zinc removal in oxic limestone systems and the application to metal mine drainages. pp. 1302-1313. *In*: Proceedings of the 7th International Conference on Acid Rock Drainage (ICARD). St. Louis, Missouri. 25-30 March 2006.

Ministry for the Environment. 1991. The Resource Management Act. www.mfe.govt.nz/rma/index.html. 1 October 2010.

Mukhopadhyay, B., L. Bastias and A. Mukhopadhyay. 2007. Limestone drain design parameters for acid rock drainage mitigation. Mine Water and the Environment. Vol. 26. pp. 29-45.

Nagpal, S., S. Chuichulcherm, A. Livingston and L. Peeva. 2000. Ethanol utilization by sulfate-reducing bacteria: An experimental and modeling study. Biotechnology and Bioengineering. Vol. 70. pp. 533-543.

Nairn, R.W. and R.S. Hedin. 1993. Contaminant removal capabilities of wetlands constructed to treat coal mine drainage. pp. 187-195. *In*: G.A. Moshiri (Ed). Constructed wetlands for water quality improvement. Lewis Publishers, Boca Raton.

Nairn, R.W., T. Beisel, R.C. Thomas, J.A. Labar, K.A. Strevett, D. Fuller, W.H. Strosnider, W.J. Andrews, J. Bays and R.C. Knox. 2009. Challenges in design and construction of a large multi-cell passive treatment system for ferruginous lead-zinc mine waters. pp. 871-892. *In*: Proceedings of the 2009 National Meeting of the American Society of Mining and Reclamation. Billings, Montana. 30 May-5 June 2009.

Neculita, C.M., G.J. Zagury and B. Bussiere. 2007. Passive treatment of acid mine drainage in bioreactors using sulfate-reducing bacteria: critical review and research needs. Journal of Environmental Quality. Vol. 36. pp. 1-16.

Neeper, D.A. and P. Stauffer. 2005. Unidirectional gas flow in soil porosity resulting from barometric pressure cycles. Journal of Contaminant Hydrogeology. Vol. 78. pp. 281-289.

Nelson, D.J., T.C. Rains and J.A. Norris. 1966. High-purity calcium carbonate in freshwater clam shell. Science. Vol. 152(3727). pp. 1368-1370.

New Zealand Seafood Industry Training Organisation (SITO) (2006) Biology of the New Zealand Greenshell™ Mussel. Unit Standard 16340v2. 40 pp.

Newcombe, C.E. and R.A. Brennan. 2009. Chitin as a fractional amendment to compost to enhance the efficiency of MIW treatment: longevity tests in continuous flow columns. pp. 871-892. *In*:

Proceedings of the 2009 National Meeting of the American Society of Mining and Reclamation. Billings, Montana. 30 May-5 June 2009.

Newcombe, C.E. and R.A. Brennan. 2008. Chitin as a fractional amendment to spent mushroom compost to enhance the efficiency and effectiveness of treatment of mine impacted water. p. 738. *In*: Proceedings of the 2008 National Meeting of the American Society of Mining and Reclamation. Richmond, Virginia. 14-19 June 2008.

Newman, N.A. 1988. Mineral matter in coal of the West Coast, South Island, New Zealand. Unpublished PhD thesis. University of Canterbury, Christchurch, New Zealand.

Niyogi D. and J. Harding. 2007. Coal mine drainage: complex effects on streams. The New Zealand Wastewater Association Journal. Vol. 152. pp. 50-53.

O'Halloran K., J. Cavanagh, J.S. Harding. 2008. Response of a New Zealand mayfly (*Deleatidium spp.*) to acid mine drainage: implications for mine remediation. Environmental Toxicology and Chemistry. Vol. 27(5). pp. 1135-1140.

O'Sullivan, A.D. 2005. Passive treatment technologies for managing metal mine waster: lessons learnt from global applications. *In*: Metal contaminants in New Zealand, (Eds.) Moore, T.A., A. Black, J.A. Centeno, J.S. Harding, and D.A. Trumm. Ch.14. pp. 279-299. Resolutionz Press, Christchurch, New Zealand.

Okabe, S., P.H. Nielsen and W.G. Characklis. 1992. Factors affecting microbial sulfate reduction by *Desulfovibrio desulfuricans* in continuous culture: Limiting nutrients and sulfide concentration. Biotechnolgy and Bioengineering. Vol. 40. pp. 725-734.

Pahler, J., R. Walker, T. Rutkowski and J. Gusek. 2007. Passive removal of selenium from gravel pit seepage using selenium reducing bioreactors. pp. 589-601. *In*: Proceedings of the 2007 National Meeting of the American Society of Mining and Reclamation. Gillette, Wyoming. 2-7 June 2007.

Panuvatvanich, A., T. Koottatep and D. Koné. 2009. Hydraulic behaviour of vertical-flow constructed wetland under different operating conditions. Environmental Technology. Vol. 30(10). pp. 1031-1040.

Pattrick, J. 2004. Heart of Coal. 333 pp. Black Swan Press.

Pearson, F.H. and A.J. McDonnell. 1975. Use of crushed limestone to neutralize acid wastes. Proceedings Paper 11131 in the Journal of Environmental Engineering Division, American Society of Civil Engineering. Vol. 101. pp. 139-158.

Pennsylvania Department of Environmental Protection. 1999. The science of acid mine drainage and passive treatment. Publication 5400-BK-DEP2365. Harrisburg, PA.

Pereyra, L.P., R. Hanson, S. Hiibel, A. Pruden and K.F. Reardon. 2005. Comparison of inocula applied in the remediation of acid mine drainage by sulfate reduction. pp. 894-903. *In*: Proceedings of the 2005 National Meeting of the American Society of Mining and Reclamation. Breckenridge, Colorado. 19-23 June 2005.

Perez-Lopez, R., J.M. Nieto and G.R. Almodovar. 2007. Utilization of fly ash to improve the quality of the acid mine drainage generated by oxidation of a sulphide-rich mining waste: column experiments. Chemosphere. Vol. 67(2007). pp. 1637-1646.

Personn, J.S., N.L.G. Somes and T.H.F. Wong. 1999. Hydraulics efficiency of constructed wetlands and ponds. Water Science and the Environment. Vol. 40. pp. 291-300.

PIMS nw. 2007. www.pimsnw.com/HowApatiteIIworksPaper30.pdf. 14 December 2007.

PIRAMID Consortium. 2003. Engineering guidelines for the passive remediation of acidic and/or metalliferous mine drainage and similar wastewaters. 166 pp. European Commission 5th Framework RTD Project no. EVK!-CT-1999-000021 "Passive in-situ remediation of acidic mine / industrial drainage" (PIRAMID). University of Newcastle Upon Tyne, Newcastle Upon Tyne, UK.

Place, D.L., L. Figueroa, T. Wildeman and D. Reisman. 2006. Characterizing and tracking reactive mixture alterations: new tools for passive treatment system design and monitoring. pp. 1605-1619. *In*: Proceedings of the 7th International Conference on Acid Rock Drainage (ICARD). St. Louis, Missouri. 25-30 March 2006.

Pope, J., N. Newman and D. Craw. 2006. Coal mine drainage geochemistry, West Coast, South Island – a preliminary water quality hazard model. 12 pp. *In*: Proceedings of the 39th Annual New Zealand Branch Australasian Institute of Mining and Metallurgy (AusIMM) Conference. Waihi, New Zealand. 29 August-1 September 2006.

Pope, J., N. Newman, D. Craw, D. Trumm and R. Rait. 2010. Factors that influence coal mine drainage chemistry, West Coast, South Island, New Zealand. New Zealand Journal of Geology and Geophysics. Vol. 53(2). pp. 115-128.

Prieto, M.V., S.R. Hiibel, L.P. Pereyra, A. Pruden, K.F. Reardon and D. Reisman. 2008. Effect of organic substrate composition on microbial community structure of pilot-scale biochemical reactors treating mining influenced water. pp. 878-891. *In*: Proceedings of the 2007 National Meeting of the American Society of Mining and Reclamation. Gillette, Wyoming. 2-7 June 2007.

Pruden, A., H.H. Hong, L.Y. Inman, M.V. Logan, C. Sans, D. Ahmann, L.A. Figueroa and K.F. Reardon. 2005. Microbial characterization of sulfate-reducing columns remediating acid mine drainage. pp. 935-944. *In*: Proceedings of the 2005 National Meeting of the American Society of Mining and Reclamation. Breckenridge, Colorado. 19-23 June 2005.

Pruden, A., L.P. Pereyra, S.R. Hiibel, L.Y. Inman, N. Kashani, K.F. Reardon and D. Reisman. 2006. Microbiology of sulfate-reducing passive treatment systems. pp. 1620-1631. *In*: Proceedings of the 7th International Conference on Acid Rock Drainage (ICARD). St. Louis, Missouri. 25-30 March 2006.

Reinertsen, S.A., L.F. Elliot, V.L. Cochran and G.S. Campbell. 1984. Role of available carbon and nitrogen in determining the rate of wheat straw decomposition. Soil Biology and Biochemistry. Vol. 16. pp. 459-464.

Reis, M.A.M., J.S. Almeida, P.C. Lemos and M.J.T. Carrondo. 1992. Effect of hydrogen sulfide on growth of sulfate-reducing bacteria. Biotechnology and Bioengineering. Vol. 40. pp. 593-600.

Reisman, D., T. Rutkowski, P. Smart, J. Gusek and M. Sieczkowski. 2009. Passive treatment and monitoring at the Standard Mine Superfund Site, Crested Butte, Co. pp. 1107-1128. *In*: Proceedings of the 2009 National Meeting of the American Society of Mining and Reclamation. Billings, Montana. 30 May-5 June 2009.

Reisman, D., T. Rutkowski, P. Smart and J. Gusek. 2008. The construction and instrumentation of a pilot treatment system at the Standard Mine Superfund Site, Crested Butte, Co. pp. 892-909. *In*: Proceedings of the 2008 National Meeting of the American Society of Mining and Reclamation. Richmond, Virginia. 14-19 June 2008.

RJ Hill Laboratories Limited. 2009. Environmental Division Catalogue. Version 6.0.

Robinson-Lora, M.A. and R.A. Brennan. 2008. Evaluating crab-shell chitin, lactate and spent mushroom compost for acid mine drainage remediation in central Pennsylvania. pp. 911-926. *In*: Proceedings of the 2008 National Meeting of the American Society of Mining and Reclamation. Richmond, Virginia. 14-19 June 2008.

Robinson-Lora, M.A. and R.A. Brennan. 2009. Efficient metal removal and neutralization of acid mine drainage by crab-shell chitin under batch and continuous-flow conditions. Bioresource Technology. Vol. 100(2009). pp. 5063-5071.

Robinson-Lora, M.A. and R.A. Brennan. 2010. Chitin complex for the remediation of mine impacted water: Geochemistry of metal removal and comparison with other common substrates. Applied Geochemistry. Vol. 25(3). pp. 336-344.

Rose, A.W. 2004. Vertical flow systems – effects of time and acidity relations. pp. 1595-1616. *In*: Proceedings of the 2004 National Meeting of the American Society of Mining and Reclamation and the 25th West Virginia Surface Mine Drainage Task Force. Morgantown, West Virginia. 18-22 April 2004.

Rose, A.W. 2006. Long-term performance of vertical flow ponds: an update. pp. 1704-1716. *In*: Proceedings of the 7th International Conference on Acid Rock Drainage (ICARD). St. Louis, Missouri. 25-30 March 2006.

Rose, A.W. 2007. Modeling the controls on acidity removal in vertical flow ponds. pp. 692-705. *In*: Proceedings of the 2007 National Meeting of the American Society of Mining and Reclamation. Gillette, Wyoming. 2-7 June 2007.

Rose, A.W. and C.A. Cravotta III. 1998. Geochemistry of coal mine drainage. *In*: Brady, K.B.C., M.W. Smith, and J. Schueck (Eds.). Coal mine drainage prediction and pollution prevention in Pennsylvania. pp. 1-1 to 1-22. Pennsylvania Department of Environmental Protection (Harrisburg, PA).

Rose, S. and A.M. Ghazi. 1998. Experimental study of the stability of metals associated with iron oxyhydroxides precipitated in acid mine drainage. Environmental Geology. Vol. 36. pp. 364-370.

Rose, A.W. and J.M. Dietz. 2002. Case studies of passive treatment systems: vertical flow systems. pp. 776-797. *In*: Proceedings of the 2002 National Meeting of the American Society of Mining and Reclamation. Lexington, Kentucky. 9-12 June 2002.

Rose, A.W., P.J. Shah and B. Means. 2003. Case studies of limestone-bed passive systems for manganese removal from acid mine drainage. pp. 1059-1078. *In*: Proceedings of the 2003 Meeting of the American Society of Mining and Reclamation and the 9th Billings Land Reclamation Symposium. Billings, Montana. 3-6 June 2003.

Ross, C.S., R.B. Verburg, B. Stasney and L. McCloskey. 2006. Effective passive treatment of mine effluent using a phosphate reactive medium. pp. 1728-1752. *In*: Proceedings of the 7th International Conference on Acid Rock Drainage (ICARD). St. Louis, Missouri. 25-30 March 2006.

Ross, J.A., C.L. Bayer, R.P. Socha, C.S. Sochor, C.B. Fliermans, P.C. McKinsey, M.R. Millings, M.A. Phifer, K.R. Powell, S.M. Serkiz, F.C. Sappington and C.E. Turick. 2003. Evaluation of natural and *in-situ* remediation technologies for a coal-related metals plume. *In*: Proceedings of the WM '03 Conference. Tucson, Arizona. 23-27 February 2003.

Rousch, J.M. and M.R. Sommerfeld. 1999. Effect of manganese and nickel on growth of selected algae in pH buffered medium. Water Research. Vol. 33. pp. 2448-2454.

Ruiz, A., L. Figueroa, M. Zaluski and D. Bless. 2008. Substrate degradation and metal removal performance of a 1,500-gallon sulfate reducing bioreactor for mining-influenced water treatment. pp. 950-968. *In*: Proceedings of the 2008 National Meeting of the American Society of Mining and Reclamation. Richmond, Virginia. 14-19 June 2008.

Sabolewski, A. http://technology.infomine.com/enviromine/wetlands/Welcome.htm. 30 November 2007.

Sapsford, D.J., A. Barnes, M. Dey, K.P. Williams, A. Jarvis, P. Younger and L. Liang. 2006. Iron and manganese removal in a vertical flow reactor for passive treatment of mine water. pp. 1831-1843. *In*: Proceedings of the 7th International Conference on Acid Rock Drainage (ICARD). St. Louis, Missouri. 25-30 March 2006.

Sapsford, D., A. Barnes, M. Dey, K. Williams, A. Jarvis and P. Younger. 2007. Low footprint passive mine water treatment: field demonstration and application. Mine Water and the Environment. Vol. 26. pp. 243-250.

Schmid, B.H., M.A. Hengl and U. Stephen. 2004a. Salinity-induced density stratification in near-laminar open-channel flows. Journal of Hydraulic Engineering. Vol. 130. pp. 1206-1210.

Schmid, B.H., M.A. Hengl and U. Stephen. 2004b. Salt tracer experiments in constructed wetland ponds with emergent vegetation: laboratory study on the formation of density layers and its influence on breakthrough curve analysis. Water Research. Vol. 38. pp. 2095-2102.

Schwager, A. and M. Boller. 1997. Transport phenomena in intermittent filters. Water Science and Technology. Vol. 35. 13-20.

Sheoran, A.S. 2005. Performance of a natural wetland treating acid mine drainage in arid conditions. Mine Water and the Environment. Vol. 24. pp. 150-154.

Sheoran, A.S. and S. Bhandari. 2005. Treatment of mine water by a microbial mat: bench-scale experiments. Mine Water and the Environment. Vol. 24. pp. 38-42.

Sheoran, A.S. and V. Sheoran. 2006. Heavy metal removal mechanism of acid mine drainage in wetlands: a critical review. Minerals Engineering. Vol. 19. pp. 105-116.

Shepherd, H.L., G. Tchobanoglous and M.E. Grismer. 2001. Time-dependent retardation model for chemical oxygen demand removal in a subsurface-flow constructed wetland for winery wastewater treatment. Water Environment Research. Vol. 73. pp. 597-606.

Sikora, F.J., L.L. Behrends, G.A. Brodie and H.N. Taylor. 2000. Design criteria and required chemistry for removing manganese in acid mine drainage using subsurface flow wetlands. Water Environment Research. Vol. 72. pp. 536-544.

Simmons, J., P. Ziemkiewicz, and D.C. Black. 2002. Use of steel slag leach beds for the treatment of acid mine drainage: the McCarty highwall project. pp. 527-538. *In*: Proceedings of the 2002 National Meeting of the American Society of Mining and Reclamation. Lexington, Kentucky. 9-13 June 2002.

Singer, P.C. and W. Stumm. 1970. Acid mine drainage: the rate limiting step. Science. Vol.167. pp. 1121-1123.

Skousen, J.G. 1996. Acid mine drainage. *In*: Skousen, J. and P. Ziemkiewicz (Eds.), Acid mine drainage control and treatment. National Mine Reclamation Center, West Virginia University, pp. 9-12. Originally published in 1995 in Green Lands, 25 (2), pp. 52-55.

Skousen, J.G. 2006. Overview of passive systems for treating acid mine drainage. www.wvu.edu/~agexten/landrec/passtrt/passtrt.htm. 10 April 2006.

Skousen, J.G. and P. Ziemkiewicz. 2005. Performance of 116 passive treatment systems for acid mine drainage. pp. 1100-1133. *In*: Proceedings of the 2005 National Meeting of the American Society of Mining and Reclamation. Breckenridge, Colorado. 19-23 June 2005.

Smart, P., D. Reisman, J. Gusek and E. Hathaway. 2008. Case studies – bench scale biochemical reactor results from two sites at the Elizabeth Mine, Vermont. pp. 1017-1038. *In*: Proceedings of the 2008 National Meeting of the American Society of Mining and Reclamation. Richmond, Virginia. 14-19 June 2008.

Snoeyink, V.L. and D. Jenkins. 1980. Water Chemistry. 463 pp. John Wiley and Sons, New York.

Solid Energy New Zealand Limited. 2007. http://www.coalnz.com/mines-stockton.htm. 7 November 2007.

Solid Energy New Zealand Limited. 2005. http://www.coalnz.com. 6 October 2005.

Solid Energy New Zealand Limited. 2007. http://www.solidenergy.co.nz. 10 November 2007.

Spangler, K, L. Figueroa and B. Honeyman. 2008. Ironing out your system: removal of ferrihydrite precipitates from mining influenced water pipelines. pp. 1070-1084. *In*: Proceedings of the 2008 National M R.H. Kadlec, M.M. Gibbs, J.P. Sukias and M.L. Nguyen. 2002. Nitrogen processing

gradients in subsurgace-flow treatment wetlands: Influent wastewater characteristics. Ecological Engineering. Vol. 18. pp. 499-520.

Tchobanoglous, G. and E.D. Schroeder. 1985. Water quality: characteristics, modeling and modification. 780 pp. Prentice Hall.

Tchobanoglous, G., R. Crites, R.A. Gearheart and S.C. Reed. 2000. A review of treatment kinetics for constructed wetlands. *In:* Proceedings of Disinfection 2000: Disinfection of Wastes in the New Millennium. Water Environment Federation. New Orleans, Louisiana. 15-18 March 2000.

Tchobanoglous, G., F.L. Burton and D.H. Stensel. 2003. Wastewater Engineering: Treatment and Reuse. 1819 pp. 4th Ed. McGaw-Hill, Boston.

Thibodeaux, L.J. 1996. Environmental Chemodynamics. 593 pp. 2nd Ed. John Wiley & Sons, Inc., New York.

Thomas, R.C. and C.S. Romanek. 2002a. Acid rock drainage in a vertical flow wetland I: acidity neutralization and alkalinity generation. pp. 723-751. *In*: Proceedings of the 2002 National Meeting of the American Society of Mining and Reclamation. Lexington, Kentucky. 9-13 June 2002.

Thomas, R.C. and C.S. Romanek. 2002b. Passive treatment of low-pH, ferric-iron dominated acid rock drainage in a vertical flow wetland II: metal removal. pp. 752-775. *In*: Proceedings of the 2002 National Meeting of the American Society of Mining and Reclamation. Lexington, Kentucky. 9-13 June 2002.

Thompson, D.N., R.L. Sayer and K.S. Noah. 2000. Sawdust-supported passive bioremediation of western United States acid rock drainage in engineered wetland systems. Minerals & Metallurgical Processing. Vol. 17. pp. 96-104.

Trumm, D.A. 2006a. Acid Rock Drainage Rehabilitation. Non paginated. *In*: Multiple Authors. Objective 3. West Coast coal and gold mine drainage workshop. Westport, New Zealand. 4 May 2006.

Trumm, D.A. 2006b. Herbert Stream AMD Remediation – Preliminary Conceptual Design. 15 pp. CRL Ref: 06-41031.

Trumm, D.A. 2007a. Acid Mine Drainage in New Zealand. Reclamation Matters. Issue 1. pp. 23-28.

Trumm, D.A. 2007b. Selection of AMD treatment systems: flow chart for New Zealand conditions. 5 pp. *In*: Proceedings of Proceedings of the 40th Annual New Zealand Branch Australasian Institute of Mining and Metallurgy (AusIMM) Conference. Christchurch, New Zealand. 13-15 August 2007.

Trumm, D.A. 2008. Selection of active treatment systems for acid mine drainage. pp. 563-575. *In*: Proceedings of the 2008 Meeting of the New Zealand Branch of the Australasian Institute of Mining and Metallurgy. Wellington, New Zealand. 31 August-3 September 2008.

Trumm, D.A. 2010. Selection of active and passive treatment systems for AMD-flow charts for New Zealand conditions. New Zealand Journal of Geology and Geophysics. Vol. 53(2). 195-210.

Trumm, D.A., A. Black, K. Gordon. 2003. Remediation strategies for acid mine drainage at Sullivan Mine, West Coast, New Zealand. pp. 325-337. *In*: Proceedings of the 36th Annual Australasian Institute of Mining and Metallurgy (AusIMM) Conference. Greymouth, New Zealand. 3-5 September 2003.

Trumm, D.A., A. Black, K. Gordon, J. Canach, K. O' Halloran, and A. de Joux. 2005. Acid mine drainage assessment and remediation at an abandoned west coast coal mine. pp. 317-340. *In*: Moore, T.A., A. Black, J.A. Centeno, J.S. Harding, J.S. and D.A. Trumm (Eds.). Ch. 16. Metal contaminants in New Zealand: sources, treatments, and effects on ecology and human health. Resolutionz Press, Christchurch, New Zealand.

Trumm, D.A., M. Watts and P. Gunn. 2006. AMD treatment in New Zealand – use of small-scale passive systems. pp. 2142-2158. *In*: Proceedings of the 7th International Conference on Acid Rock Drainage (ICARD). St. Louis, Missouri. 25-30 March 2006.

Trumm, D.A., Lindsay, P. and Watts, M. 2007. Acid mine drainage treatment at Herbert Stream, Stockton. 5 pp. *In*: Proceedings of Proceedings of the 40th Annual New Zealand Branch Australasian Institute of Mining and Metallurgy (AusIMM) Conference. Christchurch, New Zealand. 13-15 August 2007.

Trumm, D.A., M. Watts, J. Pope and P. Lindsay. 2008. Using pilot trials to test geochemical treatment of acid mine drainage on Stockton Plateau. New Zealand Journal of Geology and Geophysics. Vol. 51. pp. 175-186.

Trumm, D.A. and M. Watts. 2010. AMD treatment in New Zealand: use of small-scale passive treatment systems. New Zealand Journal of Geology and Geophysics. Vol. 53(2). 227-237.

Tsukamoto, T.K., H.A. Killion and G.C. Miller. 2004. Column experiments for microbialtreatment of acid mine drainage: low-temperature, low pH and matrix investigations. Water Research. Vol. 38. pp. 1405-1418.

Turner D. and D. McCoy. 1993. Anoxic alkaline drain treatment system, low cost acid mine drainage treatment alternative. pp. 73-75. *In*: Proceedings of the National Symposium on Mining. Lexington, Kentucky.

UK Environment Agency. 2008. Environmental quality standards for list 2 dangerous substances (response to EC dangerous substances directive 76/464/EEC). Bristol.

U.S. Code of Federal Regulations. 2008a. 40 CFR Part 434 – Coal mining point source category BPT, BAT, BCT limitations and new source performance standards. Accessed July 7, 2008 at http://ecfr.gpoaccess.gov/cgi/t/text/text-idx?c=ecfr&tpl=%2Findex.tpl

U.S. Code of Federal Regulations. 2008b. 40 CFR Parts 100 - 135 (or United States Code 33. pp. 1251-1376). The clean water act of 1977.

U.S. Department of the Interior Office of Surface Mining Appalachian Region. 2010. AMDTreat. http://amd.osmre.gov/. 18 September 2010.

U.S. Environmental Protection Agency (EPA). 2002. Methods for measuring the acute toxicity of effluents and receiving waters to freshwater and marine organisms. 5th ed. Office of Water. 266 pp.

U.S. Environmental Protection Agency (EPA). 2006. National Recommended Water Quality Criteria. Office of Water and Office of Science and Technology. 24 pp.

U.S. Environmental Protection Agency (EPA). 2008. Mining operations as nonpoint source pollution. http://www.epa.gov/reg3wapd/nps/mining/index.htm. 11 August 2008.

Utgikar, V.P., S.M. Harmon, N. Chaudhary, H.H. Tabak, R. Govind and J.R. Haines. 2002. Inhibition of sulfate-reducing bacteria by metal sulfide formation in bioremediation of acid mine drainage. Environmental Toxicology. Vol. 17. pp. 40-48.

Venot, C., L. Figueroa, R.A. Brennan, T.R. Wildeman, D. Reisman and M. Sieczkowski. 2008a. Comparing chitin and organic substrates on the national tunnel waters in Blackhawk, Colorado for manganese removal. pp. 1352-1366. *In*: Proceedings of the 2008 National Meeting of the American Society of Mining and Reclamation. Richmond, Virginia. 14-19 June 2008.

Venot, C., L. Figueroa, T.R. Wildeman, D. Reisman and M. Holmes. 2008b. Pilot-scale evaluation of solid and liquid phase organic substates used in biochemical reactors for the treatment of mining influenced water. pp. 1332-1351. *In*: Proceedings of the 2008 National Meeting of the American Society of Mining and Reclamation. Richmond, Virginia. 14-19 June 2008.

Waters , J.C., S. Santomartino, M. Cramer, N. Murphy and J.R. Taylor. 2003. Acid rock drainage treatment technologies-Identifying appropriate solutions. pp. 831-843. *In*: Proceedings of the 6th International Conference on Acid Rock Drainage (ICARD). Cairns, Australia. 12-18 July 2003.

Watzlaf G.R. and R.S. Hedin. 1993. A method for predicting the alkalinity generated by anoxic limestone drains. *In*: Proceedings of Fourteenth Annual West Virginia Surface Mine Drainage Task Force Symposium. Morgantown, West Virginia.

Watzlaf, G., Schroeder, K., Kleinmann, R., Kairies, C. and Nairn, R. 2004. The passive treatment of coal mine drainage. 72 pp. Information Circular. National Energy Technology Laboratory, US Department of Energy.

Waybrant, K.R., D.W. Blowes and C.J. Ptacek. 1998. Selection of reactive mixtures for use in permeable reactive walls for treatment of mine drainage. Environmental Science and Technology. Vol. 32. pp. 1972-1979.

Weaver, R.W., M.C. Stecher and K.J. McInnes. 2003. Water flow patterns in subsurface flow constructed wetlands designed for on-site domestic wastewater treatment. Environmental Technology. Vol. 24. pp. 77-86.

Webb, J.S., S. McGinness and H.M. Lappin-Scott. 1998. Metal removal by sulphate-reducing bacteria from natural and constructed wetlands. Journal of Applied Microbiology. Vol. 84. pp. 240-248.

Weber, P.A. 2003. Geochemical investigations of neutralising reactions associated with acid rock drainage: Prediction, mechanisms and new tools for management. PhD Dissertation. University of South Australia.

Weber, W.J. 2001. Environmental Systems and Processes: Principles, Modeling, and Design. 556 pp. John Wiley & Sons, New York.

Weber, P.A., W.M. Skinner, J.B. Hughes, P. Lindsay and T.A. Moore. 2006. Sources of Ni in coal mine acid rock drainage, West Coast, New Zealand. International Journal of Coal Geology. Vol. 67(2006). pp. 214-220.

Weber, W.J. and F.A. DiGiano. 1996. Process Dynamics in Environmental Systems. 950 pp. John Wiley & Sons, New York.

Wieder, R.K. and G.E. Lang. 1982. Modification of acid mine drainage by a freshwater wetland. *In*: Proceedings of the Symposium on Wetlands of the Unglaciated Appalachian Region. Morganstown, West Virginia.

Wildeman, T.R. and R. Schiermund. 2004. Mining influenced waters: their chemistry and methods of treatment. pp. 2001-2013. *In*: Proceedings of the 2004 National Meeting of the American Society of Mining and Reclamation and the 25th West Virginia Surface Mine Drainage Task Force. Morgantown, West Virginia. 18-22 April 2004.

Wildeman, T.R., J.J. Gusek and J. Higgins. 2006. Passive treatment of mine influenced waters. *In*: Course Material for the ARD Treatment Short Course presented at the 7th International Conference on Acid Rock Drainage (ICARD). St. Louis, Missouri. 25-30 March 2006.

Winterbourn, M.J., W.F. McDiffett and S.J. Eppley. 2000. Aluminium and iron burdens of aquatic biota in New Zealand Streams contaminated by acid mine drainage: effect of trophic level. Science of the Total Environment. Vol. 254. pp. 45-54.

World Health Organization (WHO). 2008. Guidelines for drinking-water quality incorporating 1st and 2nd addenda, Vol. 1, Recommendations. 3rd edition. Geneva.

Xiuqing, L., Z. Dehao and T. Tao. 2009. Study of Flow Pattern of Vertical Flow Constructed Wetlands by Reaction Theory. *In:* Proceedings of the 3rd International Conference on Bioinformatics and Biomedical Engineering. Beijing, China. 11-13 June 2009.

Younger, P., Banwart, S., and Hedin, R., 2002. Mine water: hydrology, pollution, remediation. 442 pp. Kluwer Academic, London.

YSI Inc. 1999. YSI model 55 handheld dissolved oxygen and temperature system operations manual. 22 pp.

Zagury, G.J., V.I. Kulnieks and C.M. Neculita. 2006. Characterization and reactivity assessment of organic substrates for sulphate-reducing bacteria in acid mine drainage treatment. Chemosphere. Vol. 64. pp. 944-954.

Zanker, H., W. Richter and G. Hüttig. 2003. Scavenging and immobilization of trace contaminants by colloids in the waters of abandoned ore mines. Colloids and Surfaces. Vol. 217. pp. 21-31.

Ziemkiewicz, P.F., J.G. Skousen and R. Lovett. 1994. Open limestone channels for treating acid mine drainage: a new look at an old idea. Green Lands. Vol 24. pp. 36-41.

Ziemkiewicz, P.F., J.G. Skousen, D.L. Brant, P.L. Sterner and R.J. Lovett. 1997. Acid mine drainage treatment with armored limestone in open limestone channels. Journal of Environmental Quality. Vol. 26. pp. 560-569.

Ziemkiewicz, P.F., J.G. Skousen and J. Simmons. 2003. Long-term performance of passive acid mine drainage treatment systems. Mine Water and the Environment. Vol. 22. pp. 118-129.

Zipper, C.E. and J.G. Skousen. 2010. Influent water quality affect performance of passive treatment systems for acid mine drainage. Mine Water and the Environment. Vol. 29(2). pp. 135-143.